

(1000)  
9 B  
No. 525-D

REPORT PAPERS IN—

analytical methods

economic geology

engineering geology

geochemistry

geochronology

geophysics

ground water

hydrologic instrumentation

marine geology

mineralogy

ore deposits

paleontology

petrology

quaternary geology

quality of water

stratigraphy

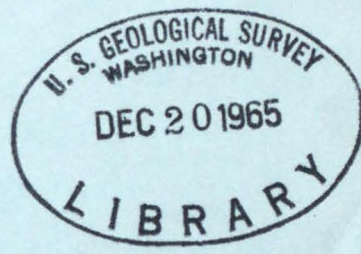
structural geology

surface water



# GEOLOGICAL SURVEY RESEARCH 1965

## Chapter D



M.S.

gB  
no. 525-D

# GEOLOGICAL SURVEY RESEARCH 1965

## Chapter D

U.S.  
GEOLOGICAL SURVEY PROFESSIONAL PAPER 525-D

*Scientific notes and summaries of investigations by members of the Conservation, Geologic, and Water Resources Divisions in geology, hydrology, and related fields*



---

UNITED STATES GOVERNMENT PRINTING OFFICE, WASHINGTON: 1965

UNITED STATES DEPARTMENT OF THE INTERIOR

STEWART L. UDALL, Secretary

GEOLOGICAL SURVEY

William T. Pecora, Director

# CONTENTS

## GEOLOGIC STUDIES

### Geochronology

	Page
Implications of new radiometric ages in eastern Connecticut and Massachusetts, by Robert Zartman, George Snyder, T. W. Stern, R. F. Marvin, and R. C. Bucknam.....	D1
Reconnaissance of mineral ages of plutons in Elko County, Nev., and vicinity, by R. R. Coats, R. F. Marvin, and T. W. Stern.....	11
Jurassic plutonism in the Cook Inlet region, Alaska, by R. L. Detterman, B. L. Reed, and M. A. Lanphere.....	16
Age and distribution of sedimentary zircon as a guide to provenance, by R. S. Houston and J. F. Murphy.....	22
Carboniferous isotopic age of the metamorphism of the Salmon Hornblende Schist and Abrams Mica Schist, southern Klamath Mountains, Calif., by M. A. Lanphere and W. P. Irwin.....	27
Radiocarbon dates from Iliamna Lake, Alaska, by R. L. Detterman, B. L. Reed, and Meyer Rubin.....	34

### Mineralogy and petrology

Magnetic spherules, colored corundum, and other unusual constituents of a heavy beach sand, Martha's Vineyard, Mass., by C. A. Kaye and M. E. Mrose.....	37
Zeolitic authigenesis of tuffs in the Ricardo Formation, Kern County, southern California, by R. A. Sheppard and A. J. Gude 3d.....	44
Thorium-bearing microcline-rich rocks in the southern Caballo Mountains, Sierra County, N. Mex., by M. H. Staatz, J. W. Adams, and N. M. Conklin.....	48
Volcanic origin of flint clay in the Fire Clay coal bed, Breathitt Formation, eastern Kentucky, by V. M. Seiders.....	52
Prehnite and hydrogarnet(?) in Precambrian rocks near Boulder, Colo., by C. T. Wrucke.....	55

### Geochemistry

Geochemical prospecting in the Browns Canyon fluor spar district, Chaffee County, Colo., by R. E. Van Alstine.....	59
Heat and free energy of formation of herzenbergite, troilite, magnesite, and rhodochrosite calculated from equilibrium data, by R. A. Robie.....	65
Extractable organic material in nonmarine and marine shales of Cretaceous age, by H. A. Tourtelot and I. C. Frost.....	73
Composition of magnetite as related to type of occurrence, by Michael Fleischer.....	82

### Geophysics

Seismic study of crustal structure in the Southern Rocky Mountains, by W. H. Jackson and L. C. Pakiser.....	85
Thermal features at Mount Rainier, Wash., as revealed by infrared surveys, by R. M. Moxham, D. R. Crandell, and W. E. Marlatt.....	93
Seismic investigations in the Harwich and Dennis quadrangles, Cape Code, Mass., by R. N. Oldale and C. R. Tuttle.....	101

### Structural geology

Evidence of large strike-slip displacement along a fault in the southern Salinas Valley, Calif., by D. L. Durham.....	106
---	-----

### Stratigraphy and paleontology

Upper Precambrian and Paleozoic stratigraphy and structure of the Neptune Range, Antarctica, by D. L. Schmidt, P. L. Williams, W. H. Nelson, and J. R. Ege.....	112
Occurrence and stratigraphic significance of <i>Oldhamia</i> , a Cambrian trace fossil, in east-central Alaska, by Michael Churkin, Jr., and E. E. Brabb.....	120
Late Devonian and Early Mississippian age of the Woodford Shale in Oklahoma, as determined from conodonts, by W. H. Hass and J. W. Huddle.....	125
Gray Bull and Lysite faunal zones of the Willwood Formation in the Tatman Mountain area, Bighorn Basin, Wyo., by W. L. Rohrer and C. L. Gazin.....	133
Tongues of the Green River and Wasatch Formations in the southeastern part of the Green River Basin, Wyo., by W. C. Culbertson.....	139

### Economic geology

Possible buried mineralized areas in Nye and Esmeralda Counties, Nev., by R. E. Anderson, E. B. Ekren, and D. L. Healey.....	144
Outlook for resumption of diatomite mining in southern Maryland and eastern Virginia, by M. M. Knechtel and J. W. Hosterman.....	151
Evaluation of the Martinsburg Shale and two younger formations as sources of lightweight aggregate in the Delaware River area, Pennsylvania-New Jersey, by A. A. Drake, Jr., M. V. Denny, and H. P. Hamlin.....	156
Lithium-bearing bentonite deposit, Yavapai County, Ariz., by J. J. Norton.....	163

	Page
<b>Pleistocene geology</b>	
Subsurface stratigraphy of glacial drift at Anchorage, Alaska, by F. W. Trainer and R. M. Waller.....	D167
<b>Marine geology</b>	
Basins of the Gulf of Maine, by Elazar Uchupi.....	175
<b>Analytical methods</b>	
Automatic sample changer and controller for an X-ray quantometer, by Leonard Shapiro and Camillo Massoni.....	178
Selective removal of $Po^{210}$ from aged radium standards, by K. W. Edwards.....	184
Use of bathocuproine in the quantitative determination of copper in soils, sediments, and rocks, by G. A. Nowlan.....	189
Use of arsenazo III in determination of thorium in rocks and minerals, by Irving May and L. B. Jenkins.....	192
<b>HYDROLOGIC STUDIES</b>	
<b>Surface water</b>	
Changes in character of unit hydrographs, Sharon Creek, Calif., after suburban development, by J. R. Crippen.....	196
A method of estimating mean runoff from ungaged basins in mountainous regions, by H. C. Riggs and D. O. Moore....	199
<b>Ground water</b>	
Relation of permeability to particle size in a glacial-outwash aquifer at Piketon, Ohio, by S. E. Norris and R. E. Fidler..	203
<b>Relation between ground water and surface water</b>	
Computation of ground-water discharge to streams during floods, or to individual reaches during base flow, by use of specific conductance, by G. R. Kunkle.....	207
Relation of ground-water inflow and of bank and channel storage to streamflow pickup in the Santa Fe River, Fla., by W. E. Clark.....	211
<b>Quality of water</b>	
Changes in quality of water in the Passaic River at Little Falls, N. J., as shown by long-term data, by P. W. Anderson and S. D. Faust.....	214
Chemical distinction between ground water of four sedimentary units on the Kitsap Peninsula and adjacent islands, Washington, by A. S. Van Denburgh.....	219
<b>Hydrologic instrumentation</b>	
Multiple hydrologic-parameter recording on a digital recorder, by R. N. Cherry.....	222
Effects of sample and fluorometer-compartment temperatures on fluorometer readings, by Bernard Dunn and D. E. Vaupel.....	225

## INDEXES

<b>Subject</b> .....	229
<b>Author</b> .....	231

## GEOLOGICAL SURVEY RESEARCH 1965

---

This collection of 43 short papers is the third published chapter of Geological Survey Research 1965. The papers report on scientific and economic results of current work by members of the Conservation, Geologic, and Water Resources Divisions of the U.S. Geological Survey.

Chapter A, to be published later in the year, will present a summary of significant results of work done during fiscal year 1965, together with lists of investigations in progress, reports published, cooperating agencies, and Geological Survey offices.

Geological Survey Research 1965 is the sixth volume of the annual series Geological Survey Research. The five volumes already published are listed below, with their series designations.

- Geological Survey Research 1960—Prof. Paper 400
- Geological Survey Research 1961—Prof. Paper 424
- Geological Survey Research 1962—Prof. Paper 450
- Geological Survey Research 1963—Prof. Paper 475
- Geological Survey Research 1964—Prof. Paper 501

Geological Survey of Canada  
Department of Energy, Mines and Technical Surveys  
Ottawa, Ontario K1A 0H8

Geological Survey of Canada  
Department of Energy, Mines and Technical Surveys  
Ottawa, Ontario K1A 0H8

## GEOLOGICAL SURVEY RESEARCH 1983

The purpose of this report is to provide a summary of the research activities of the Geological Survey of Canada for the year 1983. The report covers the work of the various research units and is intended for the general public and the scientific community.

The Geological Survey of Canada is a government agency that is responsible for the collection, interpretation and dissemination of geological information. The survey's research activities are carried out in a number of different areas, including:

- Basic geological research
- Applied geological research
- Environmental geology
- Geomatics
- Paleontology
- Petrology
- Stratigraphy
- Structural geology
- Tectonics
- Volcanology

The research activities of the Geological Survey of Canada are carried out in a number of different ways, including:

- Fieldwork
- Laboratory work
- Theoretical work
- Interdisciplinary work

The research activities of the Geological Survey of Canada are carried out in a number of different ways, including:

- Fieldwork
- Laboratory work
- Theoretical work
- Interdisciplinary work

The research activities of the Geological Survey of Canada are carried out in a number of different ways, including:

- Fieldwork
- Laboratory work
- Theoretical work
- Interdisciplinary work

The research activities of the Geological Survey of Canada are carried out in a number of different ways, including:

- Fieldwork
- Laboratory work
- Theoretical work
- Interdisciplinary work

## IMPLICATIONS OF NEW RADIOMETRIC AGES IN EASTERN CONNECTICUT AND MASSACHUSETTS

By ROBERT ZARTMAN,<sup>1</sup> GEORGE SNYDER,<sup>1</sup> THOMAS W. STERN,<sup>2</sup>  
RICHARD F. MARVIN,<sup>1</sup> and ROBERT C. BUCKNAM,<sup>1</sup>

<sup>1</sup> Denver, Colo., <sup>2</sup> Washington, D.C.

*Work done in cooperation with the Connecticut Geological  
and Natural History Survey*

*Abstract.*—New Rb-Sr, K-Ar, U-Th-Pb, and Pb-a radiometric ages are presented for granitic and pegmatitic rocks and minerals from eastern Connecticut and Massachusetts. Synthesis of these radiometric data with the field geology indicates that, in eastern Connecticut: (1) the Tatnic Hill Formation (as well as equivalents and underlying rocks including the Quinebaug Formation) is probably Middle Ordovician or older; (2) the Scotland Schist and Hebron Formation are Early Devonian or older; (3) the Canterbury Gneiss, a related quartz monzonite dike, and the gabbro of Lebanon were intruded during the Acadian orogeny in Early Devonian time; (4) older pegmatites have been intruded over a time span ranging from possibly Middle Ordovician to Middle Devonian; (5) the area was regionally dynamothermally metamorphosed in the Acadian (Devonian) and thermally re-metamorphosed in the Alleghenian (Permian) orogenies; and (6) younger pegmatites were intruded in the Permian. In eastern Massachusetts, the nonporphyritic Ayer Granite at Millstone Hill was intruded in Late Devonian or Early Mississippian time, implying either that the Worcester Formation lies unconformably above the Ayer Granite, or that the Worcester coal-mine fossils are not Pennsylvanian as reported.

### SUMMARY OF PREVIOUS GEOLOGIC AND RADIOMETRIC WORK

Fossils have never been found in the medium to high-grade metasedimentary rocks covering most of eastern Connecticut. Ages assigned to these rocks have heretofore been based on an imperfect knowledge of the stratigraphic section, correlation of this section with distant fossil localities to the north, and radiometric ages of minerals in pegmatites near Middletown, which are of limited applicability to the rest of the section. Radiometric work before 1952 has been

summarized by Rodgers (1952). More recent age determinations have been summarized by Goldsmith (1964), Faul (1954), and Brookins and Hurley (1965).

Before 1955 the geology of east-central Connecticut was known only from a few small-scale studies that have been summarized by Rodgers and others (1956). Since 1955, detailed mapping on 7½-minute quadrangle bases has been undertaken by the U.S. Geological Survey and the Connecticut Geological and Natural History Survey. This recent work has been summarized by Goldsmith (1963, 1964). The geology of the area pertinent to this report is shown on figure 1.

Lower and middle Paleozoic fossiliferous rocks with a possible bearing on eastern Connecticut geology are present at many outcrops in Massachusetts, Vermont, New Hampshire, and Maine. Equivalents of the upper Lower Silurian Clough Formation, Middle Silurian Fitch Formation, and Lower Devonian Littleton Formation have been recognized in the western part of eastern Connecticut (Rodgers and others, 1959, p. 9), and this section has been correlated (Rodgers and Rosenfeld *in* Rodgers and others, 1959; Dixon and others, 1963) with a section of similar lithologies in the central part of eastern Connecticut. By this correlation the Scotland Schist would be equivalent to the Littleton Formation.

The Scotland Schist has also been correlated with the Worcester Formation of south-central Massachusetts, which appears to lie on strike with the Scotland Schist. Pennsylvanian (Pottsville) fossiliferous rocks have been reported from one outcrop of Worcester Formation in the vicinity of Worcester, Massachusetts,



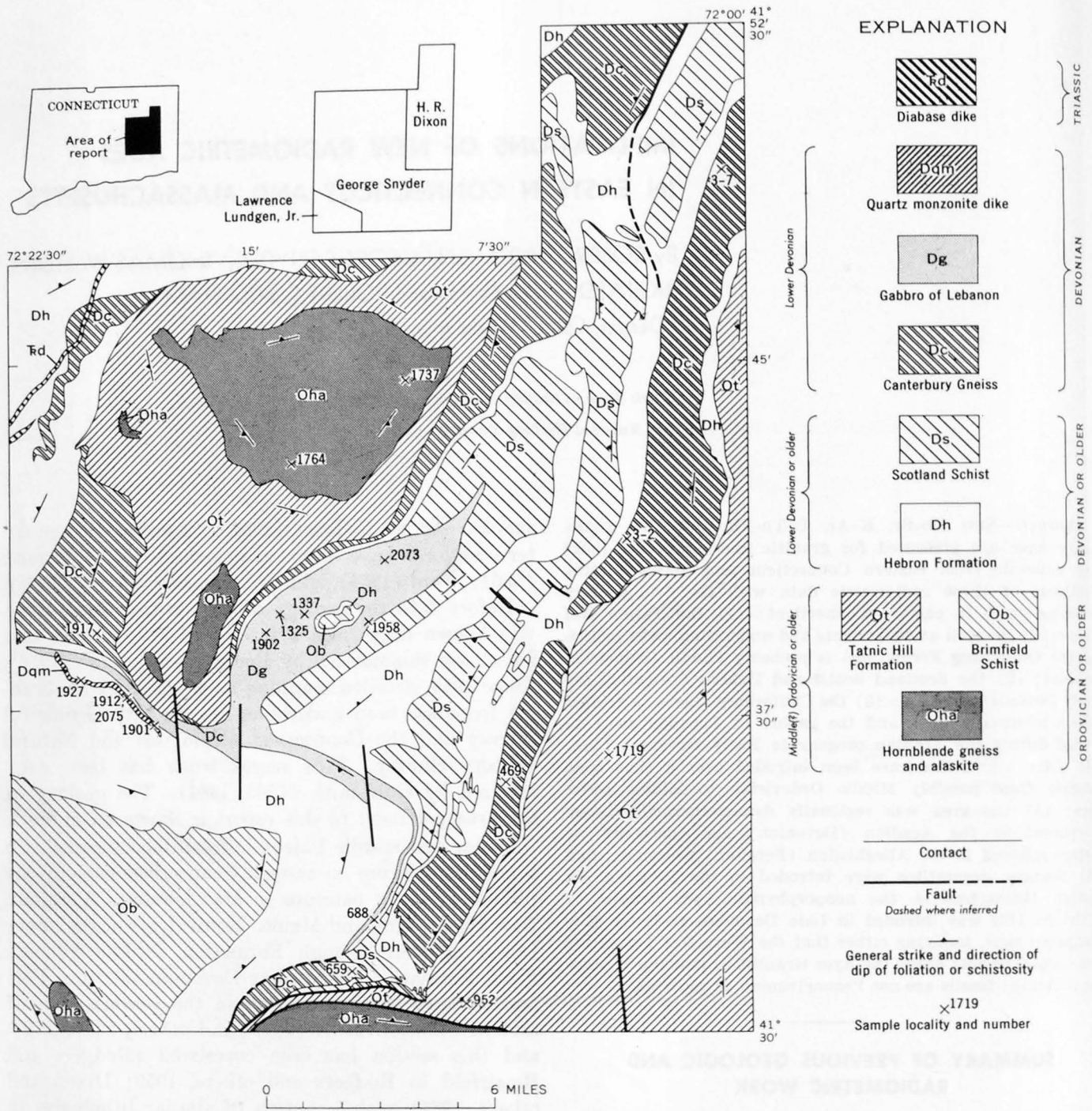


FIGURE 1.—Generalized geologic map of east-central Connecticut, showing localities of dated samples. Pegmatites are too small to distinguish at this scale. Canterbury Gneiss includes Eastford Granite Gneiss of Rodgers and others (1956) along north edge of map. Hornblende gneiss includes Quinebaug Formation (Dixon, 1964) and Middletown Gneiss (Lundgren, 1965). Alaskite includes Willimantic Gneiss (Snyder, 1964b) and Monson Gneiss (Lundgren, 1965).

## DESCRIPTION AND LOCATION OF SAMPLE LOCALITIES IN CONNECTICUT (SHOWN ON FIGURE 1)

[Mineral modifiers are given in order of decreasing abundance]

## Foliated pegmatites:

952. Microcline-quartz-oligoclase-biotite pegmatite cutting Fly Pond Member of Tatnic Hill Formation. Outcrop 0.45 mile N. 30° W. of Leffingwell School, southeast ninth, Fitchville quadrangle.
1337. Oligoclase-orthoclase-quartz-muscovite-biotite pegmatite cutting mafic hornblende gabbro. Northeast corner of large quarry on south side of Owunnegunset Hill half a mile by dirt road from State Route 89, southwest ninth, Willimantic quadrangle.
1719. Microcline perthite-quartz-oligoclase-biotite pegmatite cutting Fly Pond Member of Tatnic Hill Formation. Scotland Road cut above Shetucket River 0.15 mile northwest of Cote Pond, north-central ninth, Norwich quadrangle.
1902. Oligoclase-quartz-microcline-muscovite pegmatite cutting hornblende-biotite gabbro. State Route 87 cut 0.3 mile northwest of intersection with Oliver Road, southwest ninth, Willimantic quadrangle.

## Canterbury Gneiss:

469. Gray oligoclase-quartz-microcline-biotite gneiss. Ledge at 300 feet elevation 0.45 mile S. 48° W. from summit of Hearststone Hill, northwest ninth, Norwich quadrangle.
659. Gray microcline-quartz-oligoclase-biotite-muscovite gneiss. Ledge 0.5 mile east of State Route 163 and 0.1 mile northwest of hairpin curve of Round Brook, south-central ninth, Fitchville quadrangle.
1917. Gray oligoclase-quartz-microcline-biotite-muscovite gneiss. Ledge 650 feet south of summit of 672-foot hill, Wells Woods, southwest ninth, Columbia quadrangle.
- 3-2. Gray oligoclase-quartz-microcline-biotite gneiss. Old quarry exposure about 0.5 mile west of Little River and Fort Ned Pond and 0.25 mile east of Hanover Road, central ninth, Scotland quadrangle.
- 3-7. Gray quartz-oligoclase-microcline-biotite gneiss. Old quarry exposure in southwest Pomfret about 1,000 feet south of Carter Road, east-central ninth, Hampton quadrangle.

## Gabbro of Lebanon:

688. Speckled black labradorite-hornblende-biotite-quartz gabbro gneiss. Parson Brook exposure 0.5 mile north of Scott Hill road, central ninth, Fitchville quadrangle.
1325. Black bytownite-hornblende-biotite-quartz gabbro. Outcrop on 490-foot knoll on south side of Commons Hill 0.5 mile west of State Route 89, southwest ninth, Willimantic quadrangle.
1958. Gray microcline-biotite-quartz-andesine gneiss, granite phase of gabbro. Ledge on south side of Pigeon Swamp 0.35 mile north of Babcock Hill Road, south-central ninth, Willimantic quadrangle.
2073. Dark-green hornblende-bytownite mafic gabbro. Outcrop in small draw on north side of summit of Obwebetuck Hill, central ninth, Willimantic quadrangle.

## Quartz monzonite dike:

1901. Light-gray oligoclase-microcline-quartz-muscovite gneiss with minor garnet. Ledge 0.15 mile southwest of Brewster Pond, north-central ninth, Colchester quadrangle.
1912. Light-gray oligoclase-microcline-quartz-muscovite gneiss with minor biotite and garnet. Ledge 500 feet north-east of State Route 207, 900 feet north northwest of intersection with Levita Road, south-central ninth, Columbia quadrangle.
1927. Light-gray oligoclase-microcline-quartz-muscovite-garnet gneiss. Outcrop 400 feet east of railroad and 1,000 feet south of State Route 207, southwest ninth, Columbia quadrangle.
2075. Light-gray microcline-quartz-oligoclase-muscovite-biotite gneiss with minor garnet. Small quarry exposure 100 feet west of sample 1912, south-central ninth, Columbia quadrangle.

## Nonfoliated pegmatite and carbonatite vein:

1764. Cleavelandite-microcline-quartz-muscovite pegmatite cutting Quinebaug Formation. Blasted ledge 100 feet north of U.S. Route 6 near Stop and Shop store in western part of city of Willimantic, northwest ninth, Willimantic quadrangle.

1737. Coarse calcite-biotite vein cutting Quinebaug Formation. Large quarry exposure 200 feet northwest of U.S. Route 6 on east side of Windham Airport, north-central ninth, Willimantic quadrangle.

## SAMPLE LOCALITIES IN MASSACHUSETTS (NOT SHOWN ON FIGURE 1)

- Ayer Granite (Emerson, 1917) (nonporphyritic, at Millstone Hill):
1105. Gray granular albite-microcline perthite-quartz-muscovite-biotite-garnet gneiss. Field outcrop 0.35 mile west of summit of Wigwam Hill and 0.25 mile southwest of Worcester coal mine, southeast ninth, Worcester North quadrangle.
1709. Gray granular microcline perthite-quartz-albite-muscovite-biotite gneiss. Large quarry exposure on east side of Millstone Hill 0.15 mile northwest of State hospital, southeast ninth, Worcester North quadrangle.
1710. Gray granular quartz-albite-microcline perthite-muscovite-biotite-garnet gneiss. Large quarry exposure on top of Millstone Hill, southeast ninth, Worcester North quadrangle.
- Ayer Granite (Emerson, 1917) (porphyritic):
- N-A1. Gray quartz-oligoclase-microcline-biotite porphyritic gneiss. Exposure north of Wataquodock Road 0.17 mile east-southeast of Bolton Station, east-central ninth, Clinton quadrangle.
- 1+86. Gray quartz-oligoclase-microcline-biotite porphyritic gneiss. 1,086 feet east of west end of Wachusett-Marlboro tunnel, 400 feet beneath Carville Basin, south-central ninth, Clinton quadrangle.
- 4+08. Gray quartz-oligoclase-microcline-biotite porphyritic gneiss. 4,008 feet east of west end of Wachusett-Marlboro tunnel, 400 feet beneath northwest edge of Rattlesnake Hill, south-central ninth, Clinton quadrangle.

(for example, White, 1912), but the areal extent of these rocks near Worcester has never been accurately known. However, previous lead- $\alpha$  ages from metamorphic zircons and monazites have dated metasedimentary rocks (including Scotland Schist) in east-central Connecticut as pre-Pennsylvanian (Snyder, 1964a).

The Canterbury Gneiss of eastern Connecticut, which intrudes Scotland Schist, has long been thought to be correlative with the Ayer Granite of Emerson (1917) in eastern Massachusetts (Foye, 1949, p. 54, 55; Rodgers and others, 1959, p. 47). Such Ayer has been thought to have a syntectonic intrusive relation to the Worcester Formation, but it includes at least two varieties, nonporphyritic and porphyritic, which are lithologically quite distinct and which may have slightly different ages. Perry and Emerson (1903, p. 58-60, 65) reported inclusions of dark phyllite of the Worcester Formation in the nonporphyritic Ayer Granite at Millstone Hill within half a mile of the fossiliferous mica schist at the Worcester coal mine. Hansen (1956, p. 48) reported xenoliths, probably derived from the Worcester Formation, in the porphyritic facies of the Ayer. On these bases the Ayer has been assigned to the "late Paleozoic (?)" (Hansen, 1956, pl. 1, p. 45) and to the "post-Carboniferous" (Foye, 1949, pl. 1, p. 55).

In eastern Connecticut the relation between the large bodies of Canterbury Gneiss and the body of gabbro near Lebanon is not clear, but the gabbro is thought to

postdate the Canterbury because of apparent cross-cutting relations on the northwest side of the gabbro (fig. 1). A quartz monzonite dike near the western part of the gabbro is compositionally similar to the Canterbury Gneiss but mineralogically distinct and separable from it; this dike, 4 miles long and as much as 200 yards wide, cuts the gabbro (fig. 1), and contains inclusions or schlieren of gabbro.

In east-central Connecticut all the metasedimentary rocks, above-mentioned granites, gabbro, and many older pegmatites were regionally dynamothermally metamorphosed to at least staurolite grade and subsequently intruded by a set of lithologically distinct un-sheared pegmatites. These un-sheared pegmatites have previously been assigned to the Permian(?) (Snyder, 1964b) on the basis of the radiometric ages for the Middletown pegmatites (Baadsgaard and others, 1957; Brookins and Hurley, 1965; Eckelmann and Kulp, 1957; Henry Faul in U.S. Geol. Survey, 1960, p. A29; Powell and others, 1957; Rodgers, 1952; Stugard, 1958; Wasserburg and Hayden, 1955).

The present radiometric study deals with mineral separates and rock splits from the gabbro, dynamothermally metamorphosed and un-sheared pegmatites, Canterbury Gneiss, and related quartz monzonite dike (all eastern Connecticut), and Ayer Granite (eastern Massachusetts).

#### ANALYTICAL PROCEDURES AND DATA

Procedures for the potassium-argon and rubidium-strontium analyses are similar to those described previously (Goldich and others, 1961; Zartman, 1964). Mineral separates were at least 98 percent pure. The analytical data and resultant ages are given in tables 1 to 3.

Potassium analyses were made by flame photometry using lithium as an internal standard. Radiogenic argon was extracted from the mineral sample by direct fusion in a closed vacuum system and then determined quantitatively by isotope-dilution techniques. The overall analytical error for the potassium-argon determinations is approximately  $\pm 5$  percent of the calculated age.

Samples for total-rock rubidium-strontium analysis were always large compared to the grain-size of the rock, and were carefully split and pulverized to -100 mesh to assure homogeneity. The precision uncertainty in determinations of rubidium and strontium concentrations is approximately  $\pm 2$  percent, and of isotopic composition of strontium is  $\pm 0.4$  percent. All strontium data have been normalized to a  $\text{Sr}^{86}/\text{Sr}^{88}$  ratio of 0.1194. The error assigned to the age represents the most unfavorable conjunction of parent and daughter isotope uncertainties. The theory of the

TABLE 1.—Potassium-argon ages of minerals from eastern Connecticut and Massachusetts

[Analysts: R. F. Marvin, H. H. Thomas, Paul Elmore, and Harald Mehnert]

Sample		K <sub>2</sub> O (percent)	*Ar <sup>40</sup> (ppm)	Percentage of Ar <sup>40</sup> of radiogenic origin	Age (m.y.) <sup>1</sup>
No.	Type				
<b>Gabbro of Lebanon</b>					
688----	Hornblende---	0.45	0.0101	89	343 ± 17
1325----	Biotite-----	8.08	.123	97	240 ± 12
2073----	Hornblende---	.24	.00432	77	285 ± 14
1958----	Biotite-----	9.59	.142	95	234 ± 12
<b>Foliated pegmatites (cutting gabbro)</b>					
1337----	Muscovite----	6.80	0.105	93	244 ± 12
1337----	Biotite-----	7.71	.115	96	236 ± 12
1902----	Muscovite----	9.44	.145	93	244 ± 12
1902----	Biotite-----	5.26	.0755	92	228 ± 11
<b>Quartz monzonite dike (cutting gabbro)</b>					
2075----	Muscovite----	10.54	0.160	93	240 ± 12
<b>Carbonate vein</b>					
1737----	Biotite-----	9.08	0.145	95	252 ± 13
<b>Ayer Granite</b>					
1709----	Muscovite----	10.36	0.160	94	245 ± 12
N-A1----	Biotite-----	8.02	.127	97	250 ± 13

<sup>1</sup> Decay constants:  $\lambda_{\beta} = 4.72 \times 10^{-10} \text{ yr}^{-1}$ ,  $\lambda_{\alpha} = 0.585 \times 10^{-10} \text{ yr}^{-1}$ ;  $\text{K}^{40}/\text{K} = 0.0122$  weight percent.

rubidium-strontium isotopic relations which led to the development of the isochron age concept (Compston-Jeffery model) has been described by Compston and Jeffery (1959), Compston and others (1960), Nicolayson (1961), Allsopp (1961), and Lanphere and others (1963). In a cogenetic suite of rocks, which remain closed systems to strontium and rubidium and which had the same initial strontium isotopic composition but different Rb/Sr ratios, the  $\text{Rb}^{87}$  in each rock will decay to  $\text{Sr}^{87}$ . When the isotopic ratios for several rocks are plotted on a  $\text{Rb}^{87}/\text{Sr}^{86}$  versus  $\text{Sr}^{87}/\text{Sr}^{86}$  diagram, they will fall along a line the slope of which is  $(e\lambda t - 1)$ , where  $\lambda$  is the decay constant for  $\text{Rb}^{87}$ , and  $t$  is the age of the suite of rocks. The isochron ages given in this paper were calculated by use of the least-square equations, and the uncertainties in age and initial isotopic composition represent the standard errors of estimate. With the exception of the Canterbury Gneiss total-rock isochron, the initial  $\text{Sr}^{87}/\text{Sr}^{86}$  ratio is given only to the nearest 0.005 because the highly radiogenic nature of the samples does not permit an accurate determination of this ratio. The error in fitting the isochron to the data is commensurate with that of the analytical uncertainty and suggests that no natural scatter of a larger magnitude is present.

Reconnaissance lead-alpha ages were determined for the samples given in table 4. Standard analytical

TABLE 2.—Rubidium-strontium ages of minerals from eastern Connecticut and Massachusetts

[Analyst: Robert Zartman]

Sample		Rb <sup>87</sup> (ppm)	Sr <sub>N</sub> (ppm)	*Sr <sup>87</sup> (ppm)	Percent- age of Sr <sup>87</sup> of radio- genic origin	Age (m.y.) <sup>1</sup>
No.	Type					
<b>Gabbro of Lebanon</b>						
688	Biotite	67.6	49.7	0.194	5.4	195 ± 40
1325	do	84.7	94.8	.251	3.7	195 ± 60
1958	do	108.4	21.2	.355	19.5	220 ± 15
<b>Foliated pegmatites (cutting gabbro)</b>						
1337	Muscovite	77.5	84.5	0.347	5.6	300 ± 55
1337	Biotite	217.8	25.7	.694	28.1	215 ± 15
1902	Muscovite	140.2	62.4	.579	11.9	280 ± 30
1902	Biotite	201.1	20.0	.639	31.7	215 ± 15
<b>Nonfoliated pegmatite</b>						
1764	Muscovite	782.5	4.7	2.841	89.7	245 ± 10
<b>Carbonatite vein</b>						
1737	Biotite	111.2	17.9	0.352	22.2	215 ± 15
<b>Ayer Granite</b>						
1709	Muscovite	531.7	4.8	2.805	89.4	360 ± 10

<sup>1</sup> Decay constant:  $\lambda_{87} = 1.47 \times 10^{-11}$  yr<sup>-1</sup>; initial Sr<sup>87</sup>/Sr<sup>86</sup> assumed to be 0.706.

techniques (Gottfried and others, 1959; Rose and Stern, 1960) were used. The zircon from sample 1719 was analyzed isotopically as well as by the lead-alpha method, and these data are presented in table 5.

### INTERPRETATION OF DATA

Although the lead-alpha results on zircon and monazite from foliated pegmatites in the Fly Pond Member of the Tatnic Hill Formation are suggestive only of a middle to early Paleozoic age for this rock, a uranium-thorium-lead isotopic analysis on one of the zircons permits a more restrictive age assignment. The isotopic ages obtained for sample 1719 are somewhat discordant, and additional analyses are desirable; however, both episodic and continuous diffusion models indicate an age of greater than 500 million years (Middle Ordovician or older) as does the Pb<sup>207</sup>/Pb<sup>206</sup> age by itself, for this single zircon. As this age would be older than Acadian, and the host pegmatite contains the large uncrushed feldspars and quartz of a typical syntectonic Acadian pegmatite (L. R. Page, oral communication, 1964), this anomaly is resolvable only if: (1) a pegmatite intruded before the Acadian were remobilized in the Acadian metamorphism while retaining its original zircon, or (2) the zircons are xenocrysts obtained from the country rock. In case 1 the

TABLE 3.—Rubidium-strontium total rock and mineral isochron ages of rocks from eastern Connecticut and Massachusetts

[Analyst: Robert Zartman]

Sample		Rb (ppm)	Sr (ppm)	Rb <sup>87</sup> Sr <sup>86</sup>	Sr <sup>87</sup> Sr <sup>86</sup>	Age (m.y.) <sup>1</sup>
No.	Type					
<b>Quartz monzonite dike</b>						
2075	Total rock	328	35.4	26.8	0.848	405 ± 20
1912	do	333	12.0	80.5	1.210	
1927	do	180	50.3	10.4	.779	
1901	do	330	24.0	39.8	.913	
<b>Quartz monzonite dike (mineral)</b>						
2075	Muscovite	785	4.62	492	2.807	285 ± 15
2075	Microcline	701	57.1	35.5	.872	
2075	Total rock	328	35.4	26.8	.848	
<b>Canterbury Gneiss</b>						
659	Total rock	224	111.4	5.83	0.738	405 ± 20
1917	do	202	76.3	7.68	.753	
3-2	do	141	159.7	2.56	.721	
3-7	do	175	65.9	7.70	.750	
<b>Ayer Granite</b>						
1709	Total rock	328	14.5	65.8	1.036	345 ± 15
1105	do	312	19.2	47.1	.939	
1710	do	386	14.2	78.8	1.100	

<sup>1</sup> Decay constant:  $\lambda_{87} = 1.47 \times 10^{-11}$  yr<sup>-1</sup>; ages calculated from least-squares equations. See graphical representation of these data on figure 2.

TABLE 4.—Lead-alpha ages of minerals from eastern Connecticut and Massachusetts

[Alpha-activity measurements by T. W. Stern; spectrographic analysis of lead by N. B. Sheffey]

Sample		Alpha/mg-hr	Pb (ppm)	Age (m.y.) <sup>1</sup>
No.	Type			
<b>Foliated pegmatites (in Fly Pond Member of Tatnic Hill Formation)</b>				
1719	Zircon	434	90	500 ± 60
1719	Monazite	6,832	990	300 ± 40
952	do	7,124	1,025	300 ± 40
<b>Canterbury Gneiss</b>				
469	Zircon	621	74	290 ± 30
<b>Ayer Granite</b>				
4+08	Zircon	510	112	520 ± 60
1+86	do	619	107	420 ± 50
N-Al	do	573	98	410 ± 50

<sup>1</sup> Ages were calculated using the following equations:(1)  $t = c \text{ lead}/\alpha$ , where  $c$ , a constant based upon an assumed Th/U ratio of 1, equals 2,485, and(2)  $t_0 = t - 1/2kt^2$ , where $k = \text{constant equal to } 1.56 \times 10^{-4}$ , $t = \text{approximate age in millions of years}$ , $t_0 = \text{age in millions of years, corrected for decay of parent}$ ,

lead = lead content in parts per million, and

alpha = alpha activity in alpha/mg-hr.

TABLE 5.—Uranium-thorium-lead isotopic ages of sample-1719 zircon from a foliated pegmatite in the Fly Pond Member of the Tatnic Hill Formation

[Analysts: T. W. Stern and Marcia Newell]

Concentration (ppm)			Isotopic composition of lead (atom percent)			
U	Th	Pb	Pb <sup>204</sup>	Pb <sup>206</sup>	Pb <sup>207</sup>	Pb <sup>208</sup>
1,382	112.9	74.5	0.047	89.39	5.84	4.72
Age (m.y.)						
Pb <sup>206</sup> /U <sup>238</sup>	Pb <sup>207</sup> /U <sup>235</sup>		Pb <sup>207</sup> /Pb <sup>206</sup>	Pb <sup>208</sup> /Th <sup>232</sup>		
350 ± 15	374 ± 20		520 ± 70	434 ± 25		

Composition of common lead used for correction: 206/204=18.5, 207/204=15.7, 208/204=38.4.

zircon age would reflect the age of the original pegmatite, and would be a minimum age for the sediments intruded. In case 2 the zircon age would also be greater than the age of the present pegmatite body and would be a minimum age for the surrounding sediments if the zircons were derived locally and were metamorphic rather than detrital. Although the calc-silicate rocks of the Fly Pond Member have only scant zircon, the metashales of the Tatnic Hill Formation both above and below the Fly Pond Member contain abundant zircon in this area. The large size, euhedral shape, and uniform, unzoned appearance of this zircon in rocks whose original grain size was much smaller suggests that if the pegmatitic zircon is xenocrystic it was originally metamorphic rather than detrital. Alternatively, it may be possible that the zircon is pegmatitic and that this uncrushed pegmatite has escaped Acadian metamorphism and is really Middle Ordovician or older. In any case, it seems probable that the isotopic age of this zircon establishes a minimum age of Middle Ordovician or older for the surrounding Tatnic Hill Formation and its equivalents.

The oldest total-rock rubidium-strontium ages determined in this study are 405 ± 20 m.y. (fig. 2) for the Canterbury Gneiss and a related quartz monzonite dike. If these rocks have remained closed systems since their emplacement, a Silurian or Early Devonian age is indicated by these data on radioactivity. A lead-alpha age of a zircon from the Canterbury Gneiss is somewhat younger, but, because of the inherent uncertainty in this method, the age is not inconsistent with the better rubidium-strontium total-rock data. If relations between the gabbro of Lebanon and the Canterbury Gneiss (see p. D3) are correctly interpreted, the age of the gabbro is also Silurian or Early Devonian; however, a pre-Canterbury Gneiss age is not precluded by the rather obscure field data. If the Canterbury Gneiss intrudes the gabbro, no maximum age is established for the gabbro from the radiometric work, but field relations with the Scotland Schist would indicate

a maximum age of Early Devonian for the gabbro if present stratigraphic correlations are correct.

With the exception of the zircon age discussed above, all mineral ages from this area are younger than the total-rock rubidium-strontium ages of the Canterbury Gneiss and the quartz monzonite dike. Analysis of sample 2075 of the quartz monzonite dike gives a mineral isochron age of 285 ± 15 m.y. (fig. 2), which is due, presumably, to a metamorphic effect. Potassium-argon and rubidium-strontium mineral ages ranging from 343 to 195 m.y. also could reflect this tectonism, which is recorded in a lowered apparent age measured on older rocks, the intrusion of nonfoliated pegmatites, and the emplacement of carbonatite veins. It is likewise possible that the micas from the nonfoliated pegmatites and carbonatite veins show a metamorphic and not an intrusive age, but correlation with the more thoroughly dated Middletown area suggests that this was a time of actual pegmatite emplacement. The exact extent and nature of the metamorphism are not well understood, but the grouping of potassium-argon mica ages at about 240 m.y. suggests a culmination during Permian time. Similar or younger potassium-argon mica ages have been found throughout Rhode Island and eastern Massachusetts regardless of the stratigraphic age of the rock (see Goldsmith, 1964; also Fairbairn and others, 1960, table 1, p. 8), suggesting that a rather widespread area has been affected by a Permian metamorphism. No visible evidence of this pervasive event appears to be recorded in the dated minerals of the older rocks of eastern Connecticut. Causes of this apparent Permian radiometric age could have been (1) Permian uplift and erosion of rocks heated in the Acadian, with consequent Permian cooling of the pertinent rocks; (2) dynamic metamorphism and mylonitization such as evidenced along the Honey Hill thrust fault (Lundgren and others, 1958); or (3) late retrogressive alteration (Snyder, 1961). The only igneous rocks of this age in this general area are nonfoliated pegmatites and rather small, localized bodies of the Pennsylvanian or younger Westerly Granite and the Upper or post-Pennsylvanian Narragansett Pier Granite (Nichols, 1956; Quinn and others, 1957; Moore, 1959).

The somewhat higher potassium-argon hornblende and rubidium-strontium muscovite ages from the gabbro of Lebanon and the foliated pegmatites, respectively, may indicate a partial retention of daughter products, hence a closer approach to the original age. In the case of the hornblende this could represent either an incomplete degassing of the original hornblende or the effect of a mixture of two generations of hornblende. On the other hand, the rubidium-stron-

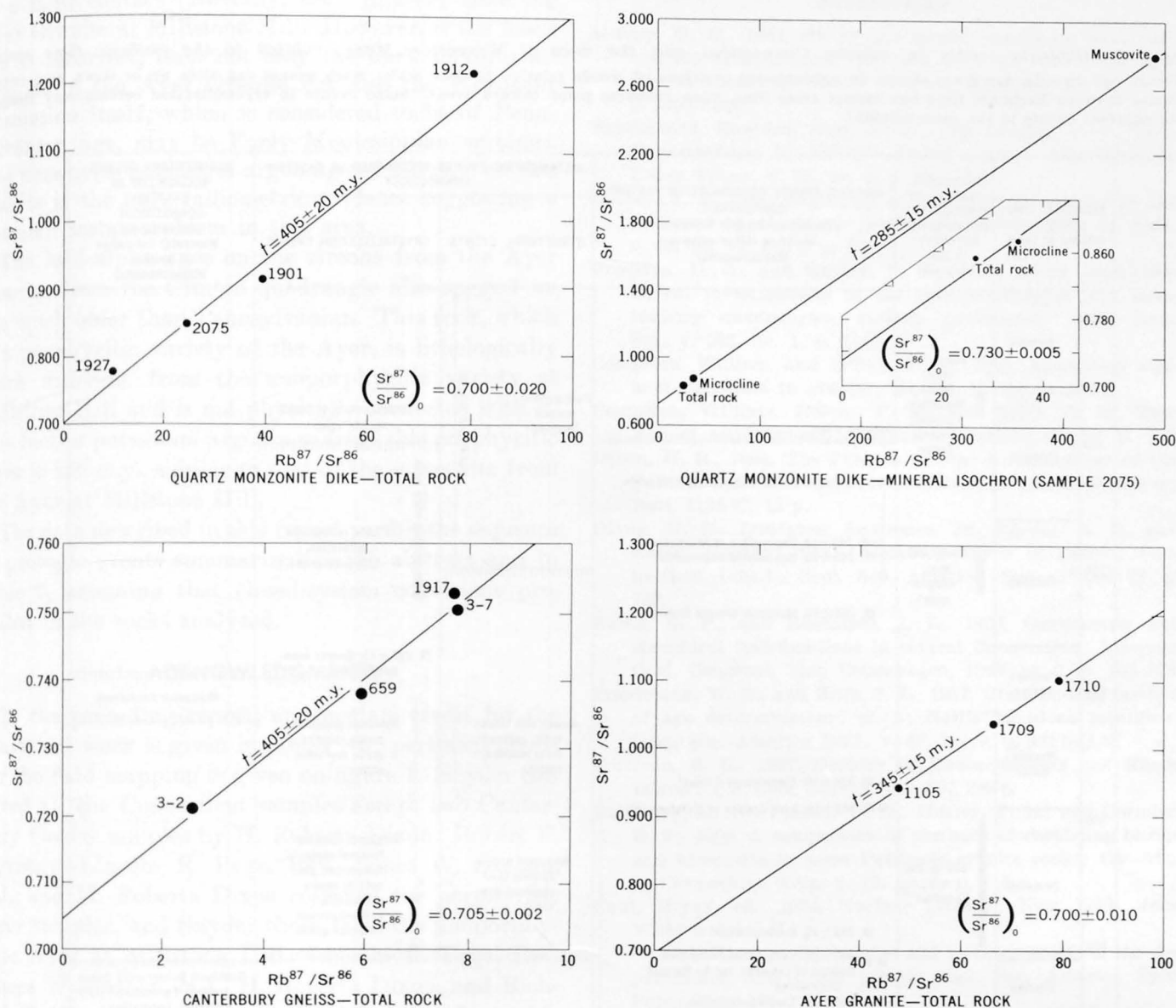


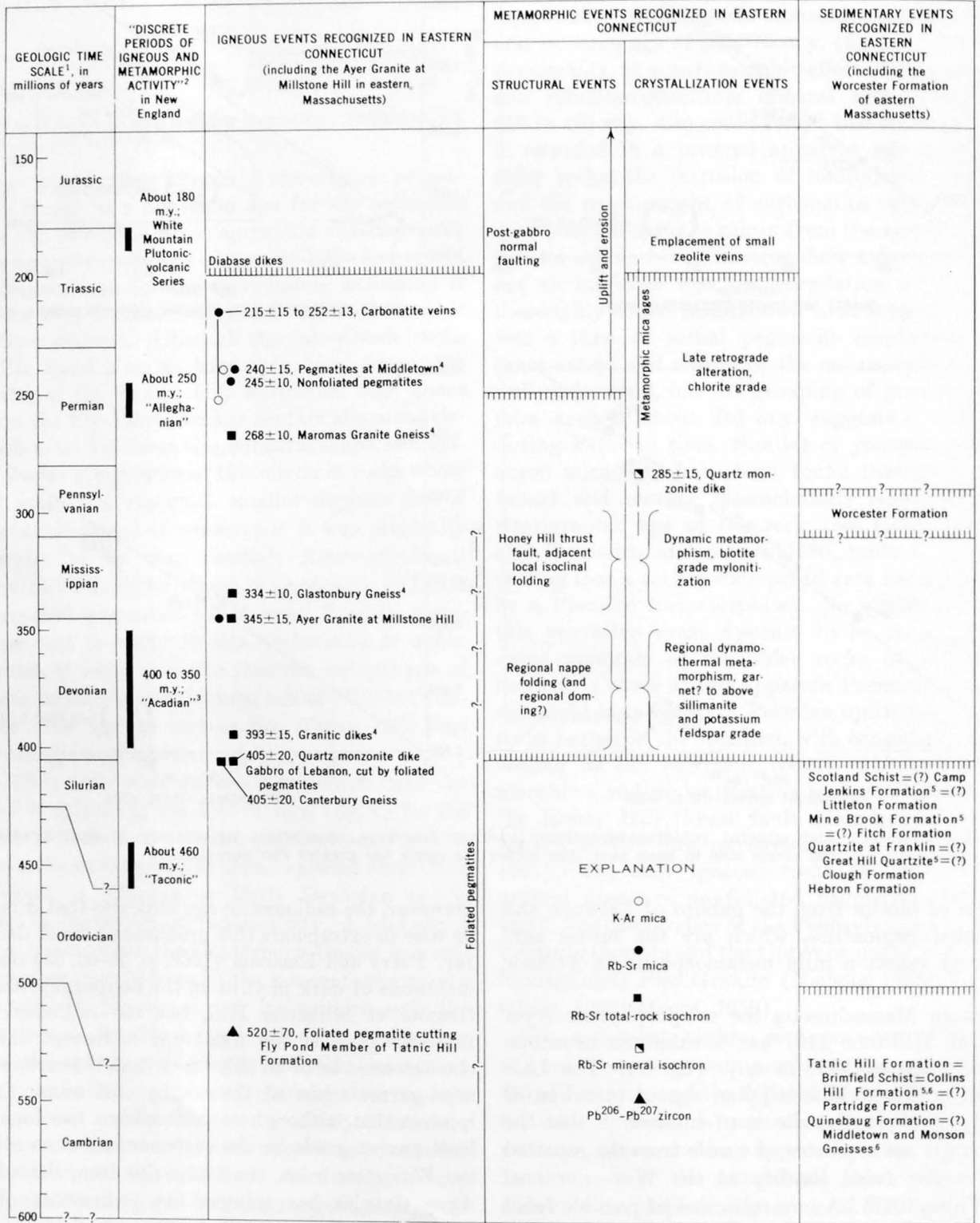
FIGURE 2.—Total-rock and mineral rubidium-strontium isochron diagrams. Analytical uncertainty is approximated by the circle size in each plot—the larger the circle the greater the uncertainty.

tium ages of biotite from the gabbro of Lebanon and the foliated pegmatites, which are the lowest ages found, may reflect a mild metamorphism in Triassic time.

In eastern Massachusetts the nonporphyritic Ayer Granite at Millstone Hill has a rubidium-strontium whole-rock age of  $345 \pm 15$  m.y. (fig. 2). The Late Devonian or Early Mississippian age of intrusion of this body of Ayer Granite is of interest in that the granite crops out a quarter of a mile from the reported Pennsylvanian fossil locality at the Worcester coal mine (White, 1912). A new collection of possible fossil plant remains from this area does not dispute this age (James M. Schopf, written communications, 1962).

However, the radiometric age indicates that it may not be wise to extrapolate this problematic fossil date very far. Perry and Emerson (1903, p. 58–60, 65) observed inclusions of dark phyllite in the nonporphyritic Ayer Granite at Millstone Hill, but the radiometric age indicates that, if the fossil age is correct, these inclusions must be of an older rock than the carbonaceous mica-garnet schist at the nearby coal mine. It is of interest that, although metamorphism has been of at least garnet grade in the carbonaceous mica schist at the Worcester mine, the muscovite from the adjacent Ayer Granite has retained its indications of Late Devonian or Early Mississippian rubidium-strontium age. Possibly the carbonaceous mica schist is separated

TABLE 6.—Geologic events in eastern Connecticut and the area of Worcester, Mass., related to the geologic time scale [Events not directly dated are shown by approximate positions of words relative to time scale. Such events can slide up or down respective columns between hachured lines but cannot cross lines when hachures point toward event. Some events in crystallization column may merge with adjacent events in the same column]



by a fault contact (Novotny, 1961, p. D49) from the Ayer Granite at Millstone Hill. However, if the fossil age is incorrect, then not only the dark phyllite inclusions in the Ayer Granite but also the Worcester Formation itself, which is considered to be of Pennsylvanian age, may be Early Mississippian or older. The muscovite potassium-argon age of 245 m.y. on this granite is the only radiometric evidence suggesting a Permian metamorphism in this area.

The lead-alpha ages on the zircons from the Ayer Granite from the Clinton quadrangle also suggest an age much older than Pennsylvanian. This rock, which is a porphyritic variety of the Ayer, is lithologically much different from the nonporphyritic variety at Millstone Hill and is not physically connected with it. The biotite potassium-argon age from this porphyritic Ayer is 250 m.y., similar to that of the muscovite from the Ayer at Millstone Hill.

The data described in this report permit the sequence of geologic events summarized in the abstract and in table 6, assuming that closed-system conditions prevailed in the rocks analyzed.

#### ACKNOWLEDGMENTS

In the preceding report, appropriate credit for the analytical work is given in tables 1-5; pertinent credit for the field mapping is given on figure 1. Snyder collected all the Connecticut samples except two Canterbury Gneiss samples by H. Roberta Dixon. Robert F. Novotny, Lincoln R. Page, Rev. James W. Skehan, S.J., and H. Roberta Dixon collected the porphyritic Ayer samples, and Snyder those from the nonporphyritic Ayer at Millstone Hill. Lincoln R. Page, Rev. James W. Skehan, S.J., H. Roberta Dixon, and Richard Goldsmith made the new collections of possible fossil plant remains from the Worcester mine. Bucknam and Snyder did most of the mineral-separation work.

<sup>1</sup> Geologic time scale on left from Kulp (1961); Ordovician boundaries on right from Poole and others (1963) whose data ". . . provide a minimum date of 480 million years for the end of the late Middle Ordovician." (But see Rickard, 1964a; Poole and others, 1964; Rickard, 1964b.)

<sup>2</sup> Terminology in this column from Faul (1961); bars from Faul and others (1963, fig. 4, p. 17).

<sup>3</sup> On the basis of paleontologic evidence from New York to the Gaspé Peninsula, Boucot (1958) considers the Acadian orogeny ". . . to begin in late Early and early Middle Devonian time. . ."

<sup>4</sup> Data on intrusive igneous rocks from Brookins and Hurley (1965). Ages recalculated to Rb<sup>87</sup> half-life used by Kulp (1961) and this paper.

<sup>5</sup> Nomenclature from Eaton and Rosenfeld (1960).

<sup>6</sup> Brookins and Hurley (1965) report rubidium-strontium total-rock isochrons on these metasedimentary formations (recalculated to Rb<sup>87</sup> half-life used by Kulp, 1961, and this paper), as follows: Collins Hill Formation, 367±40 m.y.; Middletown Gneiss, 414±15 m.y.; Monson gneiss, 444±15 m.y.

#### REFERENCES

- Allsopp, H. H., 1961, Rb-Sr age measurements on total rock and separated-mineral fractions from the Old Granite of central Transvaal: *Jour. Geophys. Research*, v. 66, no. 5, p. 1499-1508.
- Baadsgaard, Haefdon, Nier, A.O.C., and Goldich, S. S., 1957, Investigations in Ar<sup>40</sup>-K<sup>40</sup> dating [abs.]: *Am. Geophys. Union Trans.*, v. 38, no. 3, p. 385-386.
- Boucot, A. J., 1958, Beginning of the Acadian orogeny in the northern Appalachians [abs.]: *Geol. Soc. America Bull.*, v. 69, no. 12, pt. 2, p. 1537.
- Brookins, D. G., and Hurley, P. M., 1965, Rb-Sr geochronological investigations in the Middle Haddam and Glastonbury quadrangles, eastern Connecticut: *Am. Jour. Sci.*, v. 263, no. 1, p. 1-16.
- Compston, William, and Jeffery, P. M., 1959, Anomalous common strontium in granite: *Nature*, v. 184, p. 1792.
- Compston, William, Jeffery, P. M., and Riley, G. H., 1960, Age of emplacement of granites: *Nature*, v. 186, p. 702.
- Dixon, H. R., 1964, The Putnam Group; a redefinition of the Putnam Gneiss of eastern Connecticut: *U.S. Geol. Survey Bull.* 1194-C, 12 p.
- Dixon, H. R., Lundgren, Lawrence, Jr., Snyder, G. L., and Eaton, Gordon, 1963, Colchester nappe of eastern Connecticut [abs.]: *Geol. Soc. America, Spec. Paper* 73, p. 139.
- Eaton, G. P., and Rosenfeld, J. L., 1960, Gravimetric and structural investigations in central Connecticut: *Internat. Geol. Congress, 21st, Copenhagen, 1960, pt. 2, p. 168-178.*
- Eckelmann, W. R., and Kulp, J. L., 1957, Uranium-lead method of age determination; pt. 2; North American localities: *Geol. Soc. America Bull.*, v. 68, no. 9, p. 1117-1140.
- Emerson, B. K., 1917, Geology of Massachusetts and Rhode Island: *U.S. Geol. Survey Bull.* 597, 289 p.
- Fairbairn, H. W., Pinson, W. H., Hurley, P. M., and Cormier, R. F., 1960, A comparison of the ages of coexisting biotite and muscovite in some Paleozoic granite rocks: *Geochim. et Cosmochim. Acta*, v. 19, no. 1, p. 7-9.
- Faul, Henry, ed., 1954, *Nuclear geology*: New York, John Wiley & Sons, 414 p.
- 1961, History of intrusion and metamorphism in the Appalachians and Urals [abs.]: *Geol. Soc. America Spec. Paper* 68, p. 176.
- Faul, Henry, Stern, T. W., Thomas, H. H., and Elmore, P. L. D., 1963, Ages of intrusion and metamorphism in the northern Appalachians: *Am. Jour. Sci.*, v. 261, no. 1, p. 1-19.
- Foye, W. G., 1949, The geology of eastern Connecticut: *Connecticut Geol. Nat. History Survey Bull.* 74, 95 p.
- Goldich, S. S., Nier, A. O. C., Baadsgaard, Haefdon, Hoffman, J. H., and Krueger, H. W., 1961, The Precambrian geology and geochronology of Minnesota: *Minnesota Geol. Survey Bull.* 41, 193 p.
- Goldsmith, Richard, 1963, Geologic sketch map of eastern Connecticut: *U.S. Geol. Survey open-file report*, Nov. 15, 1963, 1 map and 1 cross section.
- 1964, Geologic map of New England; 1. General geology; 2. Metamorphic zones; and 3. Radiometric ages: *U.S. Geol. Survey open-file report*, Feb. 5, 1964, 3 maps and 4 pages of references.
- Gottfried, David, Jaffe, H. W., and Senftle, F. E., 1959, Evaluation of the lead-alpha (Larsen) method for determining ages of igneous rocks: *U.S. Geol. Survey Bull.* 1097-A, p. 1-63.



- Hansen, W. R., 1956, Geology and mineral resources of the Hudson and Maynard quadrangles, Massachusetts: U.S. Geol. Survey Bull. 1038, 104 p.
- Kulp, J. L., 1961, Geologic time scale: *Science*, v. 133, no. 3459, p. 1105-1114.
- Lanphere, M. A., Wasserburg, G. J., Albee, A. L., and Tilton, G. R., 1963, Redistribution of strontium and rubidium isotopes during metamorphism, World Beater complex, Panamint Range, California *in* Isotopic and cosmic chemistry, Urey volume: Amsterdam, North-Holland Publishing Co., 553 p.
- Lundgren, Lawrence, Jr., 1965, The bedrock geology of the Hamburg quadrangle: Connecticut Geol. Nat. History Survey Quad. Rept. [In press]
- Lundgren, Lawrence, Jr., Goldsmith, Richard, and Snyder, G. L., 1958, Major thrust fault in southeastern Connecticut [abs.]: *Geol. Soc. America Bull.*, v. 69, no. 12, pt. 2, p. 1606.
- Moore, G. E., Jr., 1959, Bedrock geology of the Carolina and Quonochontaug quadrangles, Rhode Island: U.S. Geol. Survey Geol. Quad. Map, GQ-117.
- Nichols, D. R., 1956, Bedrock geology of the Narragansett Pier quadrangle, Rhode Island: U.S. Geol. Survey Geol. Quad. Map, GQ-91.
- Nicolaysen, L. O., 1961, Graphic interpretation of discordant age measurements on metamorphic rocks: *New York Acad. Sci. Annals*, v. 91, p. 198.
- Novotny, R. F., 1961, A regional fault in east-central Massachusetts and southern New Hampshire: Art. 311 *in* U.S. Geol. Survey Prof. Paper 424-D, p. D48-D49.
- Perry, J. H., and Emerson, B. K., 1903, The geology of Worcester, Massachusetts: Worcester, Mass., Worcester Nat. History Soc., 166 p.
- Poole, W. H., Béland, Jacques, and Wanless, R. K., 1963, Minimum age of Middle Ordovician rocks in southern Quebec: *Geol. Soc. America Bull.*, v. 74, no. 8, p. 1063-1066.
- 1964, Minimum age of Middle Ordovician rocks in southern Quebec; Reply: *Geol. Soc. America Bull.*, v. 75, no. 9, p. 911.
- Powell, R. M., Pinson, W. H., Jr., Fairbairn, H. W., and Cormier, R. F., 1957, Test of the half-life of  $Rb^{87}$  [abs.]: *Geol. Soc. America Bull.*, v. 68, no. 12, pt. 2, p. 1782-1783.
- Quinn, A. W., Jaffe, H. W., Smith, W. L., and Waring, C. L., 1957, Lead-alpha ages of Rhode Island granitic rocks compared to their geologic ages: *Am. Jour. Sci.*, v. 255, p. 547-560.
- Rickard, M. J., 1964a, Minimum age of Middle Ordovician rocks in southern Quebec; discussion: *Geol. Soc. America Bull.*, v. 75, no. 9, p. 909.
- 1964b, Minimum age of Middle Ordovician rocks in southern Quebec; discussion of reply: *Geol. Soc. America Bull.*, v. 75, no. 9, p. 913, 914.
- Rodgers, John, 1952, Absolute ages of radioactive minerals from the Appalachian region: *Am. Jour. Sci.*, v. 250, no. 6, p. 411-427.
- Rodgers, John, Gates, R. M., Cameron, E. N., and Ross, R. J., Jr., 1956, A preliminary geological map of Connecticut: Connecticut Geol. Nat. History Survey, scale 1:253,440.
- Rodgers, John, Gates, R. M., and Rosenfeld, J. L., 1959, Explanatory text for preliminary geological map of Connecticut, 1956: Connecticut Geol. Nat. History Survey Bull. 84, 64 p.
- Rose, Harry, Jr., and Stern, Thomas, 1960, Spectrochemical determinations of lead in zircon for lead-alpha age measurements: *Am. Mineralogist*, v. 45, p. 1234-1256.
- Snyder, G. L., 1961, Bedrock geology of the Norwich quadrangle, Connecticut: U.S. Geol. Survey Geol. Quad. Map, GQ-144.
- 1964a, Petrochemistry and bedrock geology of the Fitchville quadrangle, Connecticut: U.S. Geol. Survey Bull. 1161-I, 63 p.
- 1964b, Bedrock geology of the Willimantic quadrangle, Connecticut: U.S. Geol. Survey Geol. Quad. Map, GQ-335.
- Stugard, Frederick, Jr., 1958, Pegmatites of the Middletown area, Connecticut: U.S. Geol. Survey Bull. 1042-Q, p. 613-683 [1959].
- U.S. Geological Survey, 1960, Geological Survey Research 1960, synopsis of geologic results: U.S. Geol. Survey Prof. Paper 400-A, 136 p.
- Wasserburg, G. J., and Hayden, R. J., 1955,  $Ar^{40}$ - $K^{40}$  dating: *Geochim. et Cosmochim. Acta*, v. 7, nos. 1-2, p. 51-60.
- White, C. D., 1912, Age of the Worcester phyllite: *Washington Acad. Sci. Jour.*, v. 2, no. 5, p. 114-118.
- Zartman, R. E., 1964, A geochronologic study of the Lone Grove pluton from the Llano uplift, Texas: *Jour. Petrology*, v. 5, no. 3, p. 359-408.



## RECONNAISSANCE OF MINERAL AGES OF PLUTONS IN ELKO COUNTY, NEVADA, AND VICINITY

By R. R. COATS, R. F. MARVIN, and T. W. STERN,  
Menlo Park, Calif., Denver, Colo., Washington, D.C.

*Abstract.*—The small and scattered plutons of silicic rock in Elko County, northeastern Nevada, and vicinity have long been known to be post-Paleozoic and pre-late-Tertiary. Nine pairs of K-Ar and Pb-a dates from 9 plutons give generally reasonable agreement and fall into 3 age groups: Middle Jurassic, Late Cretaceous, and Oligocene. Cretaceous plutons generally lie north of Jurassic ones, an arrangement analogous to that in the Sierra Nevada; two Tertiary granodiorite plutons were apparently intruded along inferred major transverse faults.

In Elko County, the northeasternmost county in Nevada, and in adjacent Idaho and Utah, widely scattered and relatively small plutons of silicic rock intrude rocks as young as late Paleozoic and are overlain by rocks, mostly volcanic, that can be dated paleontologically as late Miocene. Somewhat older volcanic rocks, perhaps as old as late Eocene, are present in some places, but reliable ages have not, to our knowledge, been obtained for these rocks where they are in actual contact with the intrusives.

As a result of the paucity of direct paleontologic evidence for the dating of the intrusives, they have in the past been assigned ages based mostly on analogy or petrographic resemblance with rocks from other generally distant areas where ages are better known. As will be shown, the blanket age assignments made on this basis are in part correct. We have not yet found any petrographic criteria that will afford a definite basis for age assignment in this area.

### PREVIOUS WORK

Nolan (written communication, 1933) assigned a Cretaceous age to the granites in the Mountain City quadrangle because of their evident relation to the Idaho batholith. Later, Nolan (1943, p. 163) in a paper written in 1938, suggested the possibility that emplacement of the stocks in the Basin and Range

province "occurred at different times from the late Lower Jurassic into the Tertiary period."

In the first edition of the Tectonic Map of the United States (King and others, 1944) all the intrusives of Elko County, except the Cretaceous Mountain City pluton, are shown as Tertiary. The basis for this assignment is not known, but probably this decision represents an extrapolation from Utah areas, and the extension to other plutons of the Tertiary age assigned to the Harrison Pass granite by Sharp (1942).

In a reconnaissance map of Elko County (Granger and others, 1957, p. 16 and pl. 1) the major period of granitic intrusion was assigned to the Cretaceous; all the plutons here reported were shown on the map by Granger and others as Jurassic or Cretaceous.

A later edition of the Tectonic Map of the United States (Cohee and others, 1961) shows all the intrusives in northern Elko County as Mesozoic, except the stock in the Elk Mountains; the intrusives of southern Elko County are shown as Tertiary.

In a recent summary (Gilluly, 1963) a map of the Phanerozoic granitic rocks of the Western United States indicates only middle Tertiary ages for plutons in Elko County.

### PRESENT WORK

#### The plutons

As indicated by the map (fig. 1), the plutons of Elko County, Nev., are all relatively small in exposed area. Only three would qualify as batholiths by the Daly definition: the Bruneau River pluton, the Contact pluton, and the Ruby Mountains (Harrison Pass) pluton.

All the plutons have nearly directionless textures in the localities sampled; two of the plutons, the Bearpaw Mountain and the one just west of it (Hicks Mountain), have phases that show a small degree of cata-

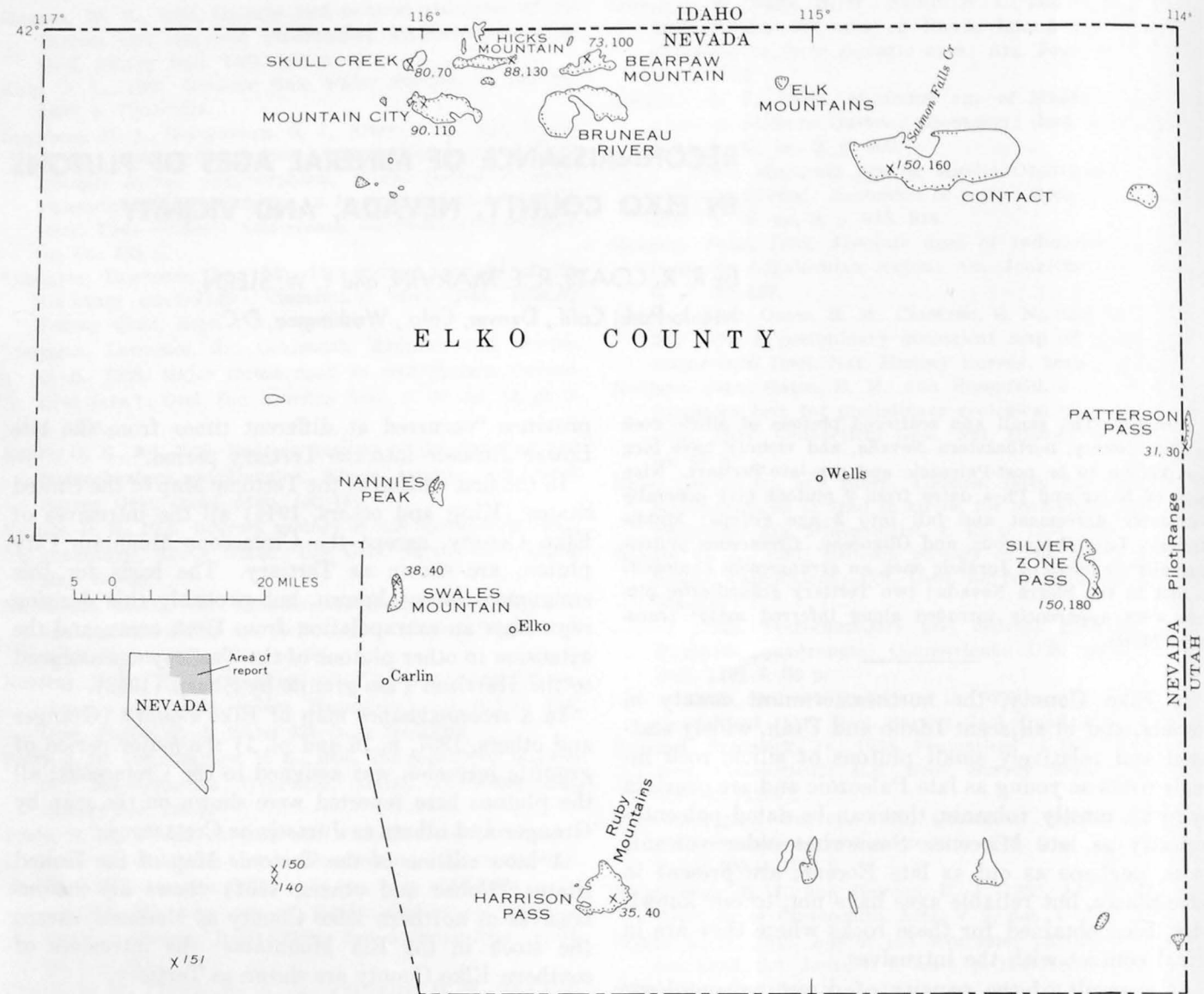


FIGURE 1.—Map of Elko County, Nev., and vicinity, showing plutons (names in capital letters), sample localities (X), and mineral ages (in millions of years). Italic numbers, K-Ar age; other numbers, Pb-a age. Intrusive contacts are distinguished by dots along contact, on plutonic side. The ages in the area west of southern Elko County were furnished by Harold Masursky and L. J. P. Muffler.

clasis and foliation, suggesting that these bodies are synorogenic. The boundaries indicated on the map are only in part intrusive contacts; the intrusive contacts have been differentiated from fault contacts and overlap contacts of younger rocks by a line of dots on the intrusive side of the contact, in order to permit the reader to infer the original shape of the body at the outcrop level. Most of the intrusives in the southern part of the county appear to be fairly equidimensional, but the rest commonly display a pronounced tendency toward an east-west elongation. This is probably a reflection of an east-west tectonic trend, recognized by Butler (Butler and others, 1920) in the Raft River Mountains, east of the northeastern corner

of Elko County, and by Nolan (1943, p. 177) in the pre-Tertiary rocks of the Mountain City area. Two other plutons, (1) the pluton north of Patterson Pass, in the Pilot Range, on the Nevada-Utah border (D. M. Blue<sup>1</sup>), and (2) the Swales Mountain pluton, have a generally north-south elongation, which appears to be structurally controlled.

All the samples examined, except the one from Swales Mountain, are medium to coarse grained (1-mm to 1-cm grain size), locally with coarser 2-cm K-

<sup>1</sup> D. M. Blue, 1960, Geology and ore deposits of the Lucin mining district, Box Elder County, Utah, and Elko County, Nevada: Utah Univ., M.S. thesis.

feldspar phenocrysts. The Swales Mountain sample is a granodiorite porphyry with an aphanitic groundmass. All contain biotite and minor hornblende; the Silver Zone Pass pluton has small amounts of pale diopsidic pyroxene. The samples of the coarser plutons examined are all granodiorite according to the nomenclature of Johannsen; some are quartz monzonite or dellenite, if one wishes to use the nomenclature of

Williams, Turner, and Gilbert. Apatite, zircon, and, commonly, sphene and magnetite are accessories.

### Age results

The age results are shown in the accompanying table, and the results, including the uncertainties of the analytical methods, are summarized graphically on figure 2. All the K-Ar ages were determined on biotite; all the Pb- $\alpha$  ages were determined on zircon.

Sample numbers, sample localities, analytical data, and mineral ages of coexistent minerals from plutons in Elko County, Nev., and vicinity

[Analysts: Pb determinations, Harold Westley; K-Ar determinations, H. H. Thomas, R. F. Marvin, Paul Elmore, H. Smith]

Field No.	Lab. No.	Zircons			Biotite					
		$\alpha$ /mg-hr	Pb (ppm) <sup>1</sup>	Calculated age <sup>2</sup> (m.y.)	K <sub>2</sub> O (percent)	K <sup>40</sup> (ppm)	*Ar <sup>40</sup> (ppm)	Ar <sup>40</sup> (percent radiogenic)	*Ar <sup>40</sup> /K <sup>40</sup>	Age <sup>3</sup> (m.y.)
57NC89	270	714	32.5	110 ± 20	9.03	9.15	0.0494	95	0.00540	90
59NC57	271	303	20.1	160 ± 20	7.84	7.94	.0735	96	.00926	152
59NC59	272	335	25.2	180 ± 20	9.29	9.41	.0848	95	.00901	148
60NC175		341	10	70 ± 20	8.56	8.67	.0419	71	.00483	81
62NC142	269	1306	21	40 ± 10	8.44	8.55	.0172	80	.00201	34
63NC20	426	767	30	100 ± 20	9.04	9.16	.0400	73	.00437	73
63NC40	427	256	14	130 ± 20	8.28	8.39	.0444	92	.00529	88
63NC86	428	338	5.5	40 ± 10	8.29	8.40	.0189	84	.00225	38
63NC106	429	610	7.8	30 ± 10	8.20	8.31	.0152	82	.00183	31

Description of samples and location of sample sites:

57NC89. Biotite granodiorite, Mountain City quadrangle, 1,500 ft south of Indian reservation boundary, on State Highway 11A.

59NC57. Hornblende biotite granodiorite, U.S. Highway 93, near Contact, just south of crossing of Salmon Falls Creek.

59NC59. Pyroxene-hornblende-biotite granodiorite, U.S. Highway 40, Silver Zone Pass, Nev., at underpass.

60NC175. Biotite granodiorite, Skull Creek. Owyhee quadrangle, Nevada (east zone), coordinates N. 2,612,500, E. 381,000.

62NC142. Biotite granodiorite, east of Harrison Pass, Ruby Mountains, Nevada (east zone), coordinates N. 2,026,300, E. 526,300.

63NC20. Biotite granodiorite, Bearpaw Mountain pluton, SE $\frac{1}{4}$ NE $\frac{1}{4}$ SE $\frac{1}{4}$  sec. 20, T. 47 N., R. 57 E. Mount Diablo base line and meridian.

63NC40. Biotite granodiorite, McDonald Creek, highway cut, Nevada (east zone), coordinates N. 2,612,550, E. 449,550.

63NC86. Biotite granodiorite porphyry, east face Swales Mountain, NE $\frac{1}{4}$ SE $\frac{1}{4}$ NE $\frac{1}{4}$  sec. 7, T. 55 N., R. 53 E. MDBM.

63NC106. Biotite granodiorite, west side Patterson Pass, Pilot Range, SE $\frac{1}{4}$  sec. 33, T. 6 N., R. 19 W. Salt Lake base line and meridian. Box Elder County, Utah.

\*Radiogenic.

<sup>1</sup>Lead determinations in duplicate except as noted.

<sup>2</sup>Lead- $\alpha$  ages were calculated from the following equation:  $t = C \text{ Pb}/\alpha$ , where  $t$  is the calculated age in millions of years,  $C$  is a constant based on the U/Th ratio, Pb is the lead content in parts per million, and  $\alpha$  is the alpha counts per milligram per hour. The following constants were used: Assumed U/Th ratio=1.0;  $C=2485$ . Age is rounded off to nearest 10 m.y. The error quoted here is that due only to uncertainties in the analytical techniques.

<sup>3</sup>Overall analytical error is approximately  $\pm 5$  percent of the quoted age value for K-Ar ages.

Decay constants:  $K^{40}\lambda_e = 0.585 \times 10^{-10}/\text{yr.}$ ;  $\lambda_\delta = 4.72 \times 10^{-10}/\text{yr.}$ . Abundance:  $K^{40} = 1.22 \times 10^{-4} \text{ g/g K.}$

Potassium determinations made with a Perkin-Elmer flame photometer with Li internal standard; argon by isotope-dilution techniques.

<sup>4</sup>Single lead determination.

Although all 18 mineral ages are of a reconnaissance nature and no single age can be accepted with complete certainty, figure 2 shows the K-Ar ages, with which the Pb- $\alpha$  ages are reasonably consistent, grouped as follows: 30 to 40 million years, 69 to 92 m.y., and 141 to 160 m.y. The precision of the determinations does not warrant any attempt to assign precise geologic ages to these plutons, but grossly considered, they were emplaced during the middle Jurassic, Late Cretaceous, and Oligocene. The good to fair agreement between K-Ar and Pb- $\alpha$  ages indicates that subsequent regional tectonic events were not sufficiently intense to cause radical degassing of the biotites after their initial crystallization.

### GEOLOGIC SIGNIFICANCE

The concentration of the Cretaceous plutons in the northern part of the county, north and west of the

plutons of middle Jurassic age, suggests the possibility of a geographic distribution with respect to age, similar to that in the central Sierra Nevada and Inyo Mountains, Calif., where a central zone of Cretaceous plutons is flanked on the east by a belt of Jurassic plutons (Kistler and others, 1965; Hurley and others, 1965). In northeastern Nevada this flanking belt of Jurassic plutons could be projected to the southwest of Elko County, where a Jurassic age of 151 m.y. (K-Ar determination by Garniss Curtiss) is reported by Gilluly and Masursky (1965) for a pluton in the Cortez quadrangle. Two ages of  $140 \pm 10$  and 150 m.y. (K-Ar analysis by neutron activation by R. L. Armstrong) are reported for two plutons in the Frenchie Creek quadrangle (Muffler, 1946). One of these plutons cuts Jurassic volcanic rocks and is overlain by the Lower Cretaceous Newark Canyon Formation, according to Muffler (oral communication, 1965).

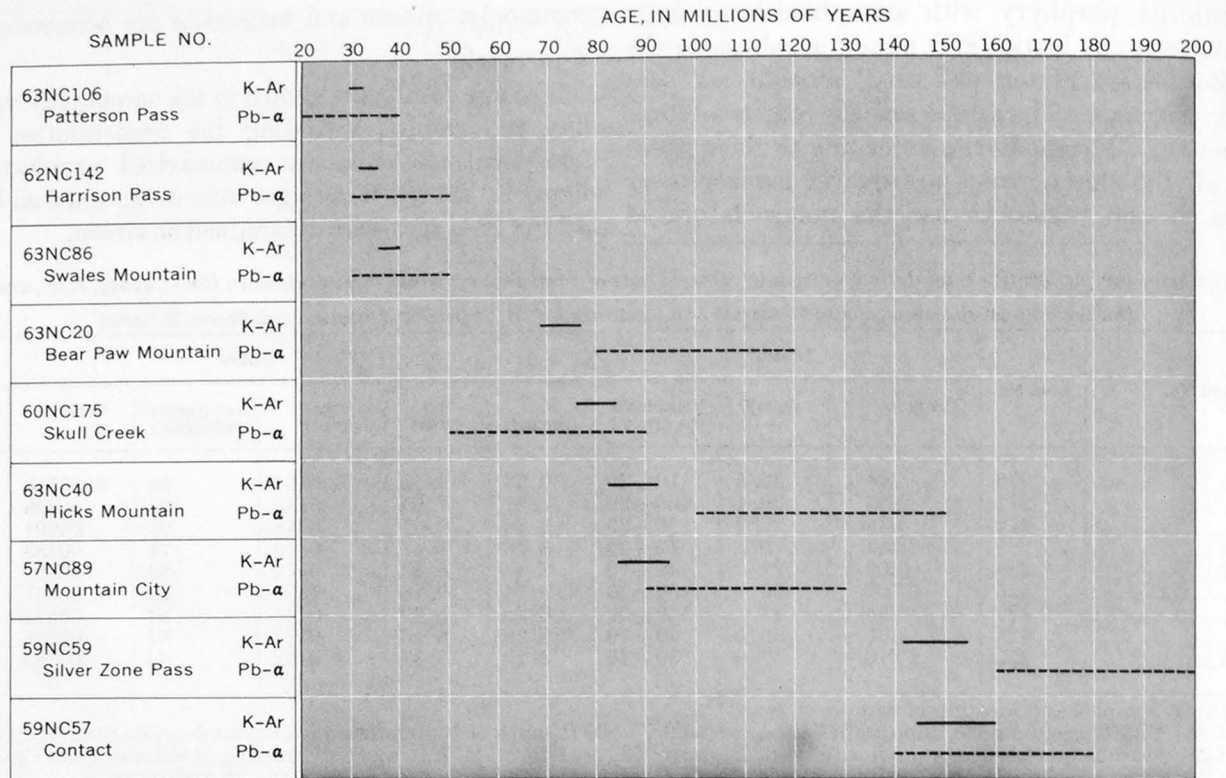


FIGURE 2.—K-Ar ages of biotite and Pb- $\alpha$  ages of zircon from nine plutons in Elko County, Nev., and vicinity.

The reason for the somewhat greater disagreement between K-Ar and Pb- $\alpha$  ages from the two plutons in the extreme northern part of the county is not clear. This could be random error, or the effect of subsequent intrusion or tectonism in promoting slight argon loss from the biotite, or possibly contamination by older zircon. Further determinations would be needed to support any of the above suggestions.

The two coarse-grained plutons (Harrison Pass and Patterson Pass) from which Tertiary ages have been obtained are probably situated on pregranitic transverse dislocations of considerable magnitude. In the Pilot Range, D. M. Blue<sup>2</sup> has recognized this same relation between location of a pluton and pregranitic transverse faulting. This relation is also suspected from the geologic map (Sharp, 1942) of the southern Ruby Mountains, where there is a strong contrast in grade of metamorphism and style of deformation between the highly deformed metamorphic rocks north of Harrison Pass (Sharp, 1942; Keith Howard, oral communication, 1963) and the less deformed and less metamorphosed Paleozoic rocks to the south.

The contrast in texture between the Swales Mountain

pluton and the other two Tertiary plutons is marked. It is possible that the coarser intrusives have been much more deeply eroded than the granodiorite porphyry of Swales Mountain. A corollary would seem to be that the rates of uplift and erosion of the Ruby Mountains and the Pilot Range have been higher than those of Swales Mountain. The Ruby and Pilot Ranges are among the highest ranges in this part of the Great Basin.

#### REFERENCES

- Butler, B. S., Loughlin, G. F., Heikes, V. C., and others, 1920, The ore deposits of Utah: U.S. Geol. Survey Prof. Paper 111, 672 p.
- Cohee, G. V., chm., and others, 1961, Tectonic map of the United States, exclusive of Alaska and Hawaii; U.S. Geol. Survey and Am. Assoc. Petroleum Geologists, scale 1:2,500,000.
- Gilluly, James, 1963, The tectonic evolution of the western United States: Geol. Soc. London Quart. Jour., v. 119, pt. 2, p. 133-174.
- Gilluly, James, and Masursky, Harold, 1965, Geology and ore deposits of the Cortez quadrangle, Nevada: U.S. Geol. Survey Bull. 1175. [In press]
- Granger, A. E., Bell, M. M., Simmons, G. C., and Lee, Florence, 1957, Geology and mineral resources of Elko County, Nevada: Nevada Bur. Mines Bull. 54, 190 p.

<sup>2</sup> See footnote 1 on p. D12.

- Hurley, P. M., Bateman, P. C., Fairbairn, H. W., and Pinson, W. H., Jr., 1965, Investigation of initial  $Sr^{87}$ - $Sr^{86}$  ratios in the Sierra Nevada plutonic province: *Geol. Soc. America Bull.*, v. 76, p. 165-174.
- King, P. B., and others, 1944, Tectonic map of the United States, 1944: *Am. Assoc. Petroleum Geologists*, scale 1:2,500,000.
- Kistler, R. W., Bateman, P. C., and Brannock, W. W., 1965, Isotopic ages of minerals from granitic rocks of the cen-

- tral Sierra Nevada and Inyo Mountains, California: *Geol. Soc. America Bull.*, v. 76, p. 155-164.
- Muffer, L. J. P., 1964, Geology of the Frenchie Creek quadrangle, Nevada: *U.S. Geol. Survey Bull.* 1179, 99 p. [1965]
- Nolan, T. B., 1943, The Basin and Range province in Utah, Nevada, and California: *U.S. Geol. Survey Prof. Paper* 197-D, p. 141-196.
- Sharp, R. P., 1942, Stratigraphy and structure of the southern Ruby Mountains, Nevada: *Geol. Soc. America Bull.*, v. 53, no. 5, p. 647-690.



## JURASSIC PLUTONISM IN THE COOK INLET REGION, ALASKA

By ROBERT L. DETTERMAN, BRUCE L. REED,  
and MARVIN A. LANPHERE, Menlo Park, Calif.

*Abstract.*—Potassium-argon determinations on hornblende and biotite indicate an age of 170 m.y. for emplacement of the Aleutian Range batholith; geologic mapping suggests emplacement between Early Jurassic and early Middle Jurassic time. The age of this batholith agrees closely with the age of the Kosina batholith in the Talkeetna Mountains about 250 miles to the northeast.

A nearly complete Jurassic section in south-central and southwestern Alaska stratigraphically brackets plutonic rocks that occur in a belt extending from the Talkeetna Mountains to the Alaska Peninsula. The stratigraphic data combined with isotopic ages provide the basis for a tie between the stratigraphic and radioactivity time scales. In the eastern Talkeetna Mountains, Grantz and others (1963) reported a tie between the Toarcian-Oxfordian interval (and perhaps the Early-Middle Jurassic boundary) on the stratigraphic time scale and 160–165 million years on the radioactivity time scale (Kulp, 1961). Potassium-argon ages of hornblende and biotite are herein reported for 3 samples from a stratigraphically bracketed pluton on the west side of Cook Inlet (fig. 1), about 250 miles southwest of the eastern Talkeetna Mountains. The ages obtained indicate that emplacement of granitic rocks was practically synchronous for the two areas.

### GEOLOGIC SETTING OF THE ALEUTIAN RANGE BATHOLITH

Reconnaissance studies were made on parts of the Aleutian Range batholith by Martin and Katz (1912, p. 74–77), who reported that the pluton is mainly hornblende granite but also includes various kinds of granodiorite and quartz diorite. Juhle (1955, p. 42–59) mapped the eastern margin of the batholith between Chinitna Bay and Tuxedni Bay. He reported that the margin consists dominantly of hornblende quartz diorite which grades westward into biotite-muscovite granodiorite, and that stocks of quartz mon-

zonite intrude the quartz diorite. More detailed current work in the Iliamna area (Detterman and Reed, 1964) has shown the batholith to be a composite body consisting of hornblende quartz diorite, hornblende-biotite quartz diorite, biotite-hornblende quartz diorite, and biotite quartz diorite. Phases of granodiorite, quartz monzonite, and granite are present locally.

The lower stratigraphic limit for the emplacement of the Aleutian Range batholith is set by the Talkeetna Formation of Early Jurassic age (fig. 2). The Talkeetna Formation is widespread in the Cook Inlet region and consists of 6,000 to 9,000 feet of predominantly volcanic rocks with a few interbedded sedimentary rocks. The lower part of the formation as exposed in the mapped area (fig. 1) is intruded by the Aleutian Range batholith near the head of Chinitna Bay. In nearby exposures the lower part of the Talkeetna Formation disconformably overlies beds of Late Triassic (Norian) age. Rocks lithologically similar to the Talkeetna are intruded by the batholith near sample site X<sup>2</sup> at Tuxedni Bay. Fossils have not been found in the Talkeetna Formation west of Cook Inlet, but the formation is correlated on the basis of lithology with rocks in the Talkeetna Mountains that contain a Lower Jurassic fauna (Grantz and others, 1963).

A definite upper stratigraphic limit for emplacement of the Aleutian Range batholith is established by the Chisik Conglomerate Member, the basal member of the Naknek Formation of Late Jurassic age. The Chisik Conglomerate Member contains abundant fresh-appearing granitic cobbles and boulders that are petrographically similar to the rocks of the Aleutian Range batholith. A rapid southeastward thinning of the conglomerate accompanied by a corresponding decrease in size of clasts, plus relict conglomerate-filled stream channels that cut into the underlying rocks, indicates a nearby northwestern source of the granitic detritus. The conglomerate lenses out laterally into sandstone and siltstone between Chisik Island and Iniskin Bay,

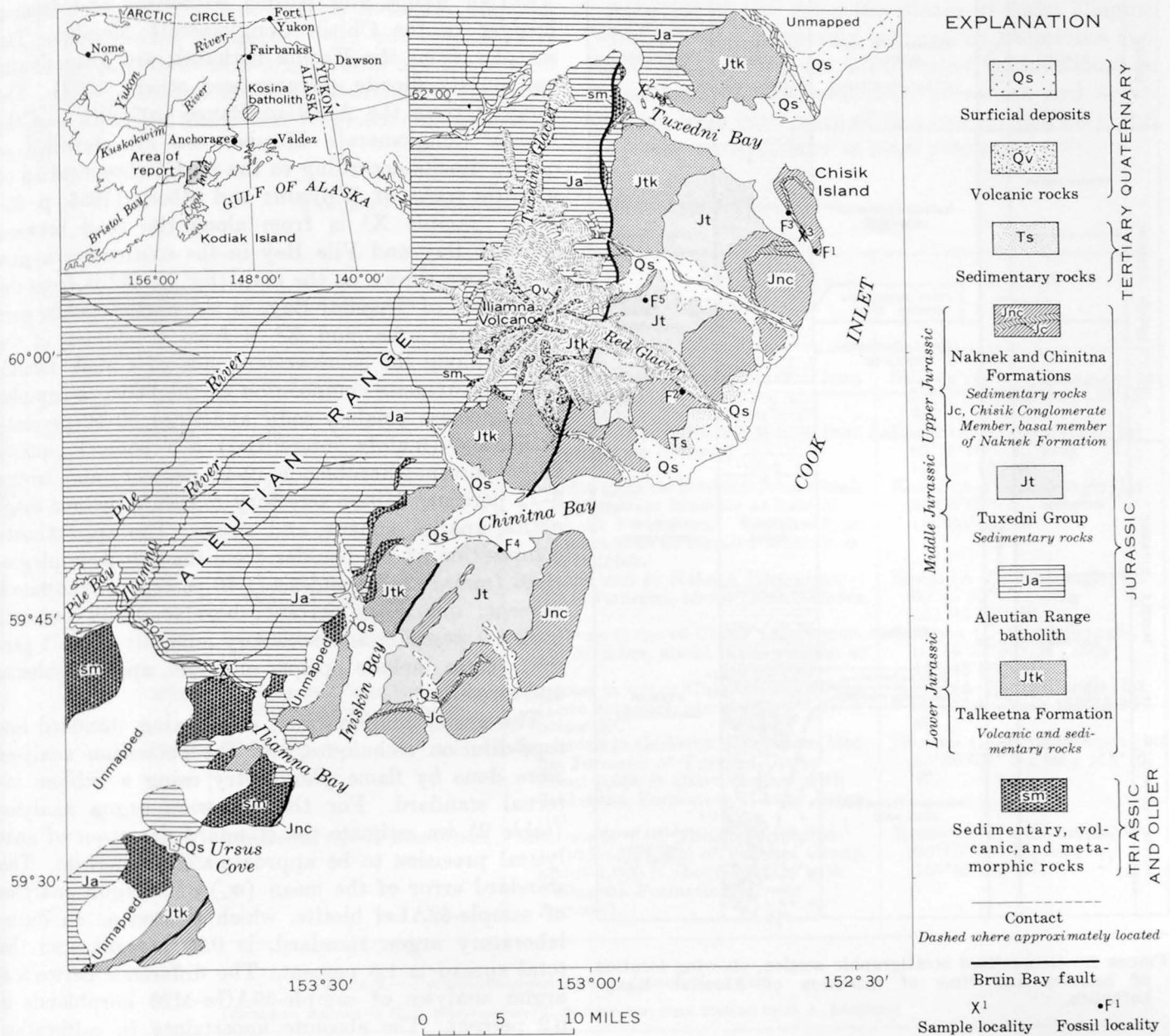


FIGURE 1.—Generalized geologic map of part of the Cook Inlet region, Alaska, showing location of sample and fossil localities.

and the sandstone facies contains a fauna characterized by *Cardioceras* sp. (locality F<sup>2</sup> in figs. 1 and 2 and table 1) of early Oxfordian age. The Chisik is overlain by fossiliferous siltstone beds in the Naknek Formation (locality F<sup>1</sup>) and is underlain by fossiliferous siltstone beds in the Chinitna Formation (locality F<sup>3</sup>). Naknek siltstone (F<sup>1</sup>) contains *Buchia* sp. and *Perisphinctes* sp. of late Oxfordian to early Kimmeridgian age, and the siltstone in the Chinitna Formation (F<sup>3</sup>) contains *Phylloceras* (*Partschiceras*) sp. (Imlay, 1953, p. 73), of middle to late Callovian age.

A more restrictive time of emplacement for the batholith is suggested by field evidence west of Cook

Inlet. Arkosic sandstone near the base of the Red Glacier Formation (fig. 2) and a few granitic clasts from the overlying Gaikema Sandstone both of Middle Jurassic (Bajocian) age, and parts of the Tuxedni Group (Detterman, 1963) suggest that the batholith was partly unroofed by Bajocian time. We cannot say unequivocally that the granitic detritus from the Red Glacier Formation and Gaikema Sandstone was derived from the Aleutian Range batholith, but there is no evidence of a pre-Jurassic granitic source in southwestern Alaska. Fossils in the Red Glacier Formation includes *Tmetoceras* sp., *Erycites* sp., *Pseudodolloceras* sp., *Emilea* sp., and *Sonninia* sp., all of early to middle



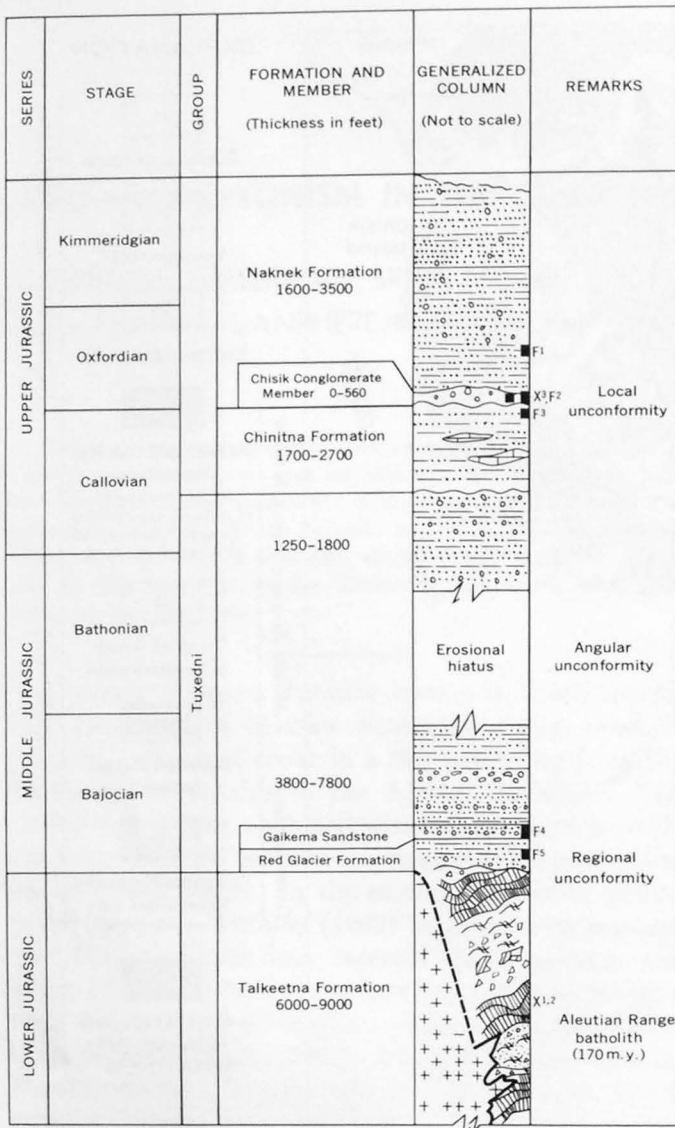


FIGURE 2.—Generalized stratigraphic section, showing location of samples and time of intrusion of Aleutian Range batholith.

Bajocian age (Imley, 1964, p. B6-B11). A specimen of *Tmetoceras regleyi* Dumortier (F<sup>5</sup>) was found in a siltstone of the Red Glacier Formation which overlies the arkosic sandstone within 1,000 feet of the unconformity between the Tuxedni Group and the underlying Talkeetna Formation (figs. 1 and 2). This unconformity marked the end of Early Jurassic volcanism and the beginning of marine sedimentary deposition. Stratigraphic relations suggest also that the Aleutian Range batholith was emplaced during this tectonic event.

#### ANALYTICAL RESULTS

Potassium-argon ages were determined for hornblende and biotite separated from samples of the

Aleutian Range and Kosina batholiths and from a boulder in the Chisik Conglomerate Member. The samples from the Kosina batholith are granodiorite and quartz diorite (Grantz and others, 1963). The samples from the Aleutian Range batholith and the Chisik Conglomerate Member are all classified as quartz diorite according to the modal classification of granitic rocks of Williams and others (1954, p. 93-148). Sample X<sup>1</sup> is from along the road between Iliamna Bay and Pile Bay in the southwestern part of the area shown on the map (fig. 1), X<sup>2</sup> is from the north side of Tuxedni Bay, in the northeastern part of the map area, and X<sup>3</sup> is from a boulder in the Chisik along the southwestern side of Chisik Island. The approximate composition of the bedrock samples is plagioclase (mainly sodic andesine) 30-50 percent; orthoclase (mainly interstitial) 5-8 percent; quartz 20-35 percent; hornblende 12-25 percent; and biotite 6-12 percent. Minor accessory minerals include magnetite, apatite, sphene, and zircon. The approximate composition of the boulder from the Chisik is plagioclase (mainly sodic andesine) 40 percent; orthoclase 8 percent; quartz 32 percent; hornblende 12 percent; biotite 7 percent; and accessory minerals about 1 percent (these include opaque minerals, apatite, sphene, and zircon).

The argon analyses were made using standard isotope-dilution techniques, and the potassium analyses were done by flame photometry using a lithium internal standard. For the potassium-argon analyses (table 2) we estimate the standard deviation of analytical precision to be approximately 4 percent. The standard error of the mean ( $\sigma_x$ ) of 9 argon analyses of sample-62ALel biotite, which is used as an intralaboratory argon standard, is 0.20 percent, and the total spread is 1.6 percent. The difference between 2 argon analyses of sample-59AGz-M26 hornblende is 0.2 percent. The absolute uncertainty in calibration of the Ar<sup>38</sup> tracer is considered to be less than 1 percent. Replicate potassium analyses of intralaboratory standard minerals give standard errors of the mean ( $\sigma_x$ ) of 0.39 percent for 12 analyses of a biotite (7.71 percent K<sub>2</sub>O) and 0.41 percent for 10 analyses of a hornblende (0.493 percent K<sub>2</sub>O). On the basis of these data we assign an analytical uncertainty of  $\pm 6$  million years to the potassium-argon ages reported in this paper (table 2).

As part of our investigation, fragments of two of the bedrock samples from the Kosina batholith collected by Arthur Grantz were crushed; hornblende was separated from one sample and hornblende and biotite were separated from the other sample. The ages previously reported (Evernden and others, 1961; Grantz

and others, 1963) for biotite from these two samples are shown in table 2 together with our results. The 3 ages for sample-59AGz-M26 biotite are the results of analyses, made in 3 different laboratories, of biotite concentrated from 3 different fragments of the granodiorite.

Ages for biotite from the pluton at Lake Iliamna (62ALe1) were previously reported by Detterman and Reed (1964). However, these earlier values should be disregarded because additional potassium and argon analyses have been made of this biotite (62ALe1), and the value reported here is more precise.

TABLE 1.—Location and source of samples dated and of fossils

[Fossils identified by Ralph W. Imlay]

Loc. on figures 1 and 2 and table 2	Field No. or U.S. Geol. Survey Mesozoic locality No.	Rock type or fossil	Source	Locality
X <sup>1</sup>	62ALe1	Quartz diorite	Aleutian Range batholith, 2,000 ft from its contact.	Iliamna (D-2) quadrangle; lat 59°42'05" N., long 153°42' W.
X <sup>2</sup>	62ALe5	do	Aleutian Range batholith, ½ mile from its southeast contact.	Kenai (A-8) quadrangle; lat 60°15'10" N., long 152°53'10" W.
X <sup>3</sup>	62ALe6e	do	Rounded granitic boulders from Chisik Conglomerate Member at base of Naknek Formation. Boulders from about middle of member where it is 560 ft thick.	Kenai (A-7) quadrangle; lat 60°06'50" N., long 152°35'05" W.
F <sup>1</sup>	22667	<i>Buchia</i> cf. <i>B. concentrica</i> Lahusen <i>Perisphinctes</i> sp.	Siltstone unit in Naknek Formation (Late Jurassic), about 1,000 ft above X <sup>3</sup> .	Kenai (A-7) quadrangle; lat 60°05'50" N., long 152°33'55" W.
F <sup>2</sup>	22701	<i>Cardioceras martini</i> Reeside	Sandstone facies of Chisik Conglomerate Member, about same position as X <sup>3</sup> .	Seldovia (D-8) quadrangle; lat 59°57'50" N., long 152°48'50" W.
F <sup>3</sup>	22668	<i>Phylloceras (Partschiceras) subobtusiforme</i> Pompeckj.	Siltstone in upper Chinitna Formation (Late Jurassic), about 350-400 ft below X <sup>3</sup> .	Kenai (A-7) quadrangle; lat 60°07' N., long 152°35'30" W.
F <sup>4</sup>	19961	<i>Witchellia</i> sp.	Sandstone in Gaikema Sandstone (Middle Jurassic) of Tuxedni Group, about 5,000 ft above contact with Talkeetna Formation (Lower Jurassic).	Iliamna (D-1) quadrangle; lat 59°49'05" N., long 153°10' W.
F <sup>5</sup>	24335	<i>Tmetoceras regleyi</i> Dumortier	Siltstone in Red Glacier Formation (Middle Jurassic) of Tuxedni Group, about 1,000 ft above contact with Talkeetna Formation (Lower Jurassic).	Kenai (A-8) quadrangle; lat 60°13'15" N., long 152°53'20" W.

TABLE 2.—Potassium-argon ages and analytical data

[Potassium analyses by H. C. Whitehead and L. B. Schlocker; argon analyses by M. A. Lanphere]

Field No.	Loc. on fig. 1	Mineral	K <sub>2</sub> O analyses (percent)	Average K <sub>2</sub> O (percent)	Ar <sup>40</sup> <sub>rad</sub> (10 <sup>-10</sup> moles/g)	$\frac{Ar^{40}_{rad}}{Ar^{40}_{total}}$	Apparent age (m.y.)
62ALe1 (Aleutian Range batholith).	{ X <sup>1</sup>	Biotite	8.75, 8.77, 8.83	8.78	<sup>1</sup> 21.56	0.82-0.96	160
		Hornblende	0.952, 0.951	.952	2.469	.77	168
62ALe5 (Aleutian Range batholith).	{ X <sup>2</sup>	Biotite	5.59, 5.63	5.61	14.75	.68	170
		Hornblende	0.473, 0.475	.474	1.229	.58	168
62ALe6e (Chisik Conglomerate).	{ X <sup>3</sup>	Biotite	5.64, 5.75	5.70	13.43	.83	153
		Hornblende	0.714, 0.715	.714	1.708	.74	156
		Biotite	4.33, 4.37	4.35	11.12	.82	166
		do					
59AGz-M26 (Kosina batholith).	{	do					<sup>3</sup> 157
		Hornblende	0.498, 0.501	.500	1.227	.68	159
		do			1.225	.77	159
59AGz-M58 (Kosina batholith).	{	Biotite					<sup>3</sup> 170
		Hornblende	0.399, 0.408	.404	.7627	.69	163

Decay constants for K<sup>40</sup>:  $\lambda_e = 0.585 \times 10^{-10}$  year<sup>-1</sup>;  $\lambda_\beta = 4.72 \times 10^{-10}$  year<sup>-1</sup>.  
Atomic abundance of K<sup>40</sup> =  $1.19 \times 10^{-4}$ .

<sup>1</sup> Mean value of nine Ar determinations.  $\sigma_x = 0.20$  percent.

<sup>2</sup> Evernden and others (1961).

<sup>3</sup> Grantz and others (1963). Age recalculated with the decay constants used in this paper.

All the potassium-argon ages of bedrock samples from the Aleutian Range and Kosina batholiths agree within the analytical uncertainty referred to above. The mean of 4 mineral ages from outcrop samples of the Aleutian Range batholith is 166 m.y., and the mean of 4 mineral ages from outcrop samples of the Kosina batholith (using the mean of the 3 different results reported for sample-59AGz-M26 biotite as a single mineral age) is 164 m.y. The mean of all of the available potassium-argon ages from these batholiths is 165 m.y. However, our data on reproducibility suggest that the scatter in results is not due to analytical uncertainty, but probably reflects differences in the cooling history of the samples analyzed or a slight loss of radiogenic argon since the minerals crystallized. In discussing the results we assume that the potassium-argon ages are minimum ages because there is no evidence that hornblende or biotite from granitic rocks incorporate significant amounts of radiogenic argon during crystallization. Therefore, we consider the higher apparent ages to be the most reliable estimate of the time of emplacement of these plutonic masses, and suggest a probable age of 170 m.y. for the emplacement of the Aleutian Range and Kosina batholiths.

#### DISCUSSION OF RESULTS

There are no significant differences in the ages of minerals from the Kosina and Aleutian Range batholiths, and we interpret these results to indicate generally synchronous emplacement of the two batholiths. As stated earlier we assume that the potassium-argon ages are minimum values, but we also believe that the ages reported by Grantz and others (1963) and by us closely approximate the age of emplacement of the Aleutian Range and Kosina batholiths. The most compelling evidence supporting this interpretation is the pattern of concordant ages obtained on coexisting hornblende and biotite, which contrasts with discordant ages that commonly are obtained where postcooling thermal metamorphism has affected plutonic rocks. For example, in the Sierra Nevada batholith of California, which had a complex intrusive and cooling history, hornblende and biotite from the older plutonic units yield grossly discordant ages (Kistler and others, 1965, p. 91-92). On the basis of the concordant hornblende-biotite ages from the Aleutian Range and Kosina batholiths we infer that the parts of the batholiths studied reflect a simple history of emplacement and crystallization and that the hornblende and biotite ages approximate the time of crystallization.

The apparent ages of hornblende and biotite from the quartz diorite boulder in the Chisik Conglomerate Member are significantly less than the apparent ages of minerals from outcrop samples of the Aleutian Range batholith. Grantz and others (1963) reported the same type of difference between the ages of biotite from granitic boulders in the Naknek Formation and from outcrop samples of the Kosina batholith. All the outcrop samples were collected within half a mile of the border of the plutons. If the boulders also were derived from the marginal portions of the batholiths, the difference in age between outcrop samples and boulders suggests that loss of radiogenic argon may have occurred during erosion, transportation, and deposition of the boulders. But, if the boulders were derived from the interior of the plutons, the age discrepancy may reflect differences in cooling history of the plutons. Analysis of samples from interior portions of the plutons may yield additional information on this discrepancy.

The data obtained by Grantz and others (1963) for the Kosina batholith and by us for the Aleutian Range batholith indicate a generally synchronous emplacement of the granitic rocks for the two widely separated areas. The accumulated stratigraphic evidence also indicates that this emplacement occurred during the Toarcian-Oxfordian interval and that it may have occurred at the Early-Middle Jurassic boundary.

#### REFERENCES

- Detterman, R. L., 1963, Revised stratigraphic nomenclature and age of the Tuxedni Group in the Cook Inlet region, Alaska: Art. 68 in U.S. Geol. Survey Prof. Paper 475-C, p. C30-C34.
- Detterman, R. L., and Reed, B. L., 1964, Preliminary geologic map of the Iliamna Quadrangle: U.S. Geol. Survey Misc. Geol. Inv. Map I-407, scale 1:250,000.
- Evernden, J. F., Curtis, G. H., Obradovich, J. D., and Kistler, R. W., 1961, On the evaluation of glauconite and illite for dating sedimentary rocks by the potassium-argon method: *Geochim. et Cosmochim. Acta*, v. 23, p. 78-99.
- Grantz, Arthur, Thomas, Herman, Stern, T. W., and Sheffey, N. B., 1963, Potassium-argon and lead-alpha ages for stratigraphically bracketed plutonic rocks in the Talkeetna Mountains, Alaska: Art. 16 in U.S. Geol. Survey Prof. Paper 475-B, p. B56-B59.
- Imlay, R. W., 1953, Callovian (Jurassic) ammonites from the United States and Alaska, pt. 2. Alaska Peninsula and Cook Inlet regions: U.S. Geol. Survey Prof. Paper 249-B, p. 41-108.
- , 1964, Middle Bajocian ammonites from the Cook Inlet region, Alaska: U.S. Geol. Survey Prof. Paper 418-B, 61 p., 29 pls.
- Juhle, R. W., 1955, Iliamna Volcano and its basement: U.S. Geol. Survey open-file report, April 27, 1955, 74 p.

Kistler, R. W., Bateman, P. C., and Brannock, W. W., 1965, Isotopic ages of minerals from granitic rocks of the central Sierra Nevada and Inyo Mountains, California: Geol. Soc. America Bull., v. 76, p. 155-164.

Kulp, J. L., 1961, Geologic time scale: Science, v. 133, no. 3459, p. 1105-1114.

Martin, G. C., and Katz, F. J., 1912, A geologic reconnaissance of the Iliamna region, Alaska: U.S. Geol. Survey Bull. 485, 138 p.

Williams, Howell, Turner, F. J., and Gilbert, C. M., 1954, Petrography, an introduction to the study of rocks in thin sections: San Francisco, W. H. Freeman and Co., 406 p.



## AGE AND DISTRIBUTION OF SEDIMENTARY ZIRCON AS A GUIDE TO PROVENANCE

By ROBERT S. HOUSTON and JOHN F. MURPHY,  
Laramie, Wyo., Denver, Colo.

*Work done in cooperation with the Geological Survey of Wyoming*

*Abstract.*—Two distinct varieties of zircon were handpicked from Upper Cretaceous black sandstone deposits in Wyoming and dated by the lead-alpha method as  $80 \pm 15$  and  $770 \pm 80$  million years. Based on the principle that an unmetamorphosed sedimentary rock can be no older than the youngest zircon it contains, the younger zircon provides a limiting age of 95 million years for the base of the Upper Cretaceous Frontier Formation. The older zircon is a well-rounded, apparently much-reworked variety of Precambrian age. The regional distribution of the zircon and the age of the younger zircon suggest a source to the northwest, presumably the Idaho batholith or related extrusive rocks.

Zircon is one of the most abundant and universal minerals in sedimentary heavy-mineral suites and has long been considered a useful mineral in stratigraphic and provenance studies. Many attempts have been made, with varying success, to correlate zircon found in sedimentary rocks with that in possible source areas by utilizing such properties as shape, color, length-width ratio, and index of refraction. Whereas these studies have provided indirect methods of determining the source areas of zircon contained in sedimentary rocks, very few attempts have been made to determine source areas by the more direct method of correlating the lead-alpha age of zircon in sedimentary rocks with that of likely source areas. The present study is similar in many respects to that of Carroll and others (1957) on the heavy minerals of the Precambrian Ocoee Series but is more limited in its scope and objectives.

Almost all the lead-alpha age determinations made of zircon to date have been of zircon contained in igneous and metamorphic rocks. This is understandable inasmuch as these determinations provide a direct age of the host rock if the history of metamorphism

or intrusive activity has not been overly complex. Age determinations of zircon in sedimentary rocks, however, provide only an intermediate or average age of the total zircon content, which may be from many source rocks of widely divergent ages. As the actual age of the zircon is not modified by metamorphism or other events that affect normal sedimentary rocks, the sedimentary host rock can be no older than the youngest zircon that it contains. If the total zircon content includes several recognizable varieties, each of which may represent a different source, and if age determinations can be made of the individual varieties, then the probable error is reduced considerably and the age of the youngest variety of zircon will be closer to the true age of the sedimentary host.

Although the effect of analytical errors on the measured lead-alpha age can be reasonably assessed, the uncertainty growing out of the field and laboratory "sampling" cannot be evaluated unless a number of zircon samples from different localities are available for analysis. In the studies here described, only single samples of each type of zircon could be obtained, owing to the time consumed in tedious handpicking.

A study of many black sandstone deposits of known Late Cretaceous age in Wyoming (fig. 1) by Houston and Murphy (1962) has suggested the possible usefulness of dated zircon in sedimentary and stratigraphic investigations. The black sandstone deposits, which are ancient beach placers, contain as much as 80 percent common heavy minerals (Houston and Murphy, 1962, p. 27). Included in the heavy-mineral concentrations are two distinctive varieties of zircon; one is euhedral and colorless, and the other is well rounded and pinkish violet (fig. 2).



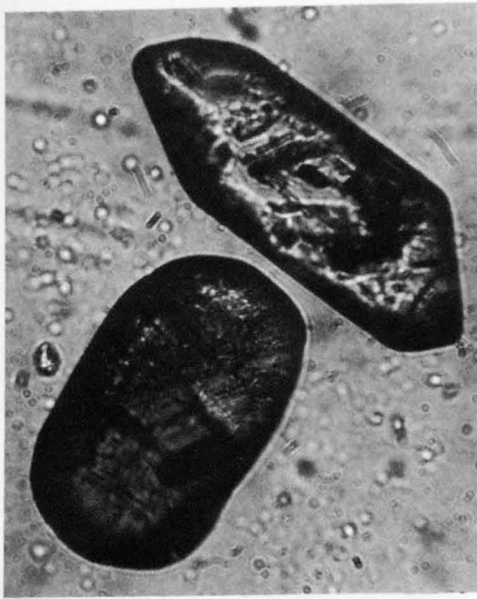


FIGURE 2.—Examples of euhedral colorless zircon (upper right) and well-rounded pinkish-violet zircon (lower left) in black sandstone deposits. Ordinary light.  $\times 200$ .

minerals. Except for the shape and color of the two zircon varieties, the physical properties are virtually identical. The total zircon content of each sample can be readily extracted by standard methods of mineral separation, but the two varieties can be separated only by handpicking. Two such samples, one representing each zircon variety, were subsequently dated by the lead-alpha method and are reported here. Great care was used in the physical extraction of each variety. The sample of the rounded pinkish-violet variety is from a black sandstone deposit at the base of the Upper Cretaceous Rock Springs Formation on Red Creek (No. 1, fig. 1), in sec. 22, T. 12 N., R. 105 W., Sweetwater County, Wyo. The euhedral colorless variety is from a deposit in the lower part of the Upper Cretaceous Frontier Formation at Cumberland Gap (No. 2, fig. 1) in sec. 18, T. 18 N., R. 116 W., Uinta County, Wyo. The lead-alpha ages are given in table 1.

TABLE 1.—Lead-alpha age of sedimentary zircon in black sandstone of Cretaceous age in Wyoming

Variety of zircon	Mesh size	a/mg-hr	Lead (ppm)	Lead-alpha age (millions of years <sup>1</sup> )
Pinkish violet	—100+400	115 <sup>2</sup>	38 <sup>3</sup>	770 $\pm$ 80
Colorless	—100+400	173 <sup>4</sup>	5.4 <sup>5</sup>	80 $\pm$ 15

<sup>1</sup> Lead-alpha ages (rounded off to nearest 10 million years) were calculated from the following equations (Gottfried and others, 1959, p. 19):

(1) For ages 0-200 m.y.:  $t = C \text{ Pb}/a$ , where  $t$  is the calculated age in millions of years,  $C$  is a constant based upon the U/Th ratio and has a value of 2,485, Pb is the lead content in parts per million, and  $a$  is the alpha count per milligram per hour; and

(2) For ages 200-1,700 m.y.:  $T = t - \frac{1}{2} kt^2$ , where  $T$  is the age in millions of years corrected for decay of uranium and thorium, and  $k$  is a decay constant based upon the U/Th ratio and has a value of  $1.56 \times 10^{-4}$ . U/Th ratio assumed to be 1.0.

<sup>2</sup> Alpha-activity measurements by H. W. Jaffe.

<sup>3</sup> Lead analysis by C. L. Waring and H. W. Worthing.

<sup>4</sup> Alpha-activity measurements by T. W. Stern.

<sup>5</sup> Lead analysis by Harold Westley.

On consideration of the above limits of error of the lead-alpha determination for the colorless variety it seems probable that the age of the Frontier Formation is no greater than 95 million years. This figure agrees very well with the presently used (Kulp, 1961) 63- to 135-million-year age range of the Cretaceous Period. Cobban and Reeside (1952) have shown that the Frontier Formation in Wyoming is the basal unit of the Late Cretaceous Epoch and, hence, the dated zircon in its lower part affords a maximum age for the Late Cretaceous in this area.

It is generally recognized that the source of Cretaceous clastic sediments in this region lay to the west along the margin of the Rocky Mountain geosyncline (Gilluly, 1963, p. 146). Within this vast source area the Idaho batholith, or its related volcanic rocks, is postulated to have provided the euhedral colorless zircon that is so common in the black sandstone deposits. The zircon was probably transported east and south to the Late Cretaceous sea by streams that had eroded batholithic rocks at their breakwaters or by air currents laden with pyroclastic ejecta associated with the batholith. This contention is compatible with the investigations of Larsen and others (1958, p. 54), who determined the ages of 16 zircon samples from many parts of the Idaho batholith as ranging from 94 to 135 million years. They conclude that the batholith is early Late Cretaceous in age and that it was intruded in a short time, not more than a few million years.

Table 2 shows that the percentage of the colorless zircon increases northward, in the general direction of the Idaho batholith and, conversely, it decreases southward. The source area or areas for the older well-rounded pink-violet zircon is not determined, but the shape of the zircon suggests a complex history involving many cycles of erosion, transport and redeposition since removal from its original Precambrian parent rock.

In the deposits of New Mexico and Arizona, there is a marked reversal in the trend of zircon distribution, as shown in table 2, and the euhedral colorless variety is relatively abundant. This is believed to indicate detritus from a source area other than the Idaho batholith, but probably one of Mesozoic age. Such a hypothesis for explaining the distribution of the euhedral zircon of presumed Mesozoic age is in general agreement with the distribution of major centers of plutonic activity in the Western United States during middle and early Late Cretaceous time as discussed by Gilluly (1965, p. 16, and fig. 5).

The New Mexico and Arizona black sandstone deposits, as well as those in southwestern Colorado and Utah, contain significant percentages of pinkish-violet

TABLE 2.—Regional distribution of zircon varieties

Region	Number of deposits sampled	Number of samples	Total zircon grains <sup>1</sup> counted	Average within region and range (in parentheses) of individual samples (volume percent)			Ratio of euhedral colorless to well-rounded pink-violet
				Euhedral colorless	Well-rounded pink-violet	Euhedral pink-violet	
Montana	3	3	370	78 (72-79)	22 (21-28)	0	2.81
Northern Wyoming	5	24	3,067	49 (16-54)	51 (46-84)	0	.96
Southern Wyoming	7	18	2,516	45 (27-82)	55 (18-73)	0	.82
Northern Colorado	1	2	142	25 (11-39)	75 (61-89)	0	.33
Southwestern Colorado and southeastern Utah	2	4	1,088	7 (0-25)	86 (25-91)	7 (0-40)	.08
Northwestern New Mexico and northeastern Arizona	9	10	1,000	41 (36-74)	32 (9-48)	27 (0-50)	1.25

<sup>1</sup> Only 115-, 170-, and 250-mesh sizes were counted, but these included virtually all zircon in samples.

zircon that is conspicuously euhedral (table 2). It is generally assumed that pinkish-violet zircon is derived from rocks of Precambrian age (Hutton, 1950, p. 700; H. W. Jaffe, written communication, 1956). If this is true, then the euhedral shapes of the New Mexico and Arizona pinkish-violet zircon would suggest a more direct derivation from Precambrian rocks with little or no reworking.

In the black sandstone deposits of Wyoming the well-rounded pinkish-violet (Precambrian) zircon is more abundant relative to euhedral colorless zircon in the younger of the Upper Cretaceous deposits, and less abundant in the older deposits (fig. 3). This can be interpreted as indicating that during the early part of the Late Cretaceous orogeny the younger igneous rocks provided a major part of the detritus, either by erosion of the Idaho batholith or by associated volcanism. As

uplift continued, older rocks were probably exposed to erosion and the zircon from the batholith was diluted with the older pinkish-violet variety.

The foregoing demonstrates only one way in which the lead-alpha ages of sedimentary zircon can be used in geologic studies. Conceivably, there are many more, particularly when age data are used in conjunction with data gained by the more conventional techniques employed in stratigraphic and sedimentation studies. It should be noted, however, that aside from the limits of interpretation already mentioned regarding sedimentary zircon, the lead-alpha method of age determination has, in itself, several possible sources of error which should be considered before any precise conclusions are attempted. Critical evaluations as to the limitations of the method have been discussed by Gottfried and others (1959) and by Stern and Rose (1961).

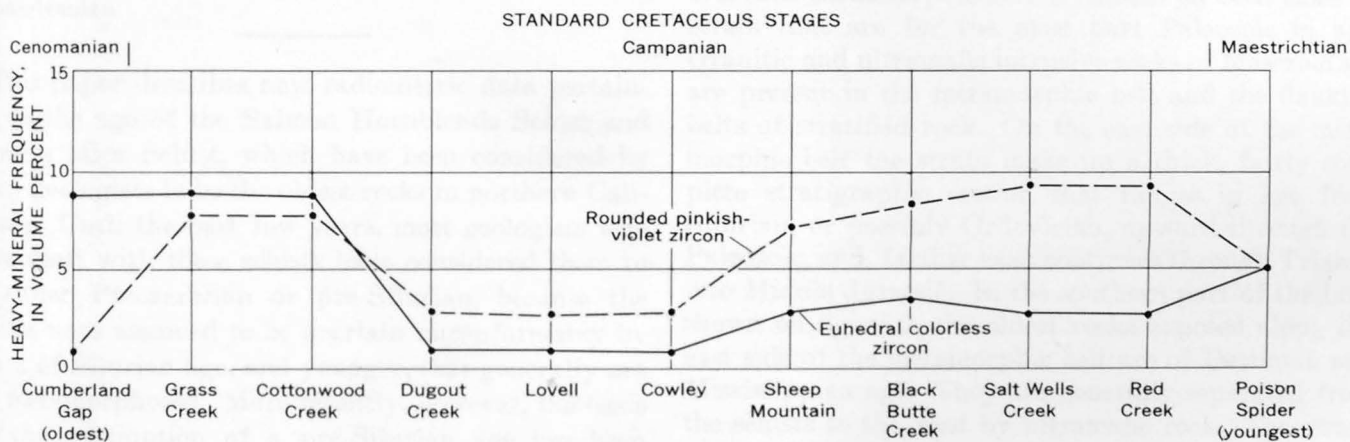


FIGURE 3.—Relative distribution of zircon varieties in black sandstone deposits of Wyoming. Deposits are arranged diagrammatically in order of decreasing stratigraphic age from left to right. Location of deposits shown on figure 1.

## REFERENCES

- Carroll, Dorothy, Neuman, R. B., and Jaffe, H. W., 1957, Heavy minerals in arenaceous beds in parts of Ocoee Series, Great Smoky Mountains, Tennessee: *Am. Jour. Sci.*, v. 255, no. 3, p. 175-193.
- Cobban, W. A., and Reeside, J. B., Jr., 1952, Frontier Formation, Wyoming and adjacent areas: *Am. Assoc. Petroleum Geologists Bull.*, v. 36, p. 1913-1961.
- Gilluly, James, 1963, The tectonic evolution of the western United States: *Geol. Soc. London Quart. Jour.*, v. 119, p. 133-174.



- Gilluly, James, 1965, Volcanism, tectonism, and plutonism in the western United States: Geol. Soc. America Special Paper 80, p. 1-69.
- Gottfried, David, Jaffe, H. W., and Senftle, F. E., 1959, Evaluation of the lead-alpha (Larsen) method for determining ages of igneous rocks: U.S. Geol. Survey Bull. 1097-A, p. 1-63.
- Houston, R. S., and Murphy, J. F., 1962, Titaniferous black sandstone deposits of Wyoming: Wyoming Geol. Survey Bull. 49, p. 1-120.
- Hutton, C. O., 1950, Studies of heavy detrital minerals: Geol. Soc. America Bull., v. 61, p. 635-716.
- Kulp, J. L., 1961, Geologic time scale: Science, v. 133, no. 3459, p. 1111.
- Larsen, E. S., Jr., Gottfried, David, Jaffe, H. W., and Waring, C. L., 1958, Lead-alpha ages of the Mesozoic batholiths of western North America: U.S. Geol. Survey Bull. 1070-B, p. 35-62.
- Stern, T. W., and Rose, H. J., Jr., 1961, New results from lead-alpha age measurements: Am. Mineralogist, v. 46, p. 606-612.



## CARBONIFEROUS ISOTOPIC AGE OF THE METAMORPHISM OF THE SALMON HORNBLENDE SCHIST AND ABRAMS MICA SCHIST, SOUTHERN KLAMATH MOUNTAINS, CALIFORNIA

By MARVIN A. LANPHERE and WILLIAM P. IRWIN,  
Menlo Park, Calif.

*Prepared in cooperation with the California Division of Mines and Geology*

*Abstract.*—Potassium-argon ages ranging from  $270 \pm 10$  to  $329 \pm 13$  m.y. were obtained on hornblende from the Salmon Hornblende Schist and on muscovite from the Abrams Mica Schist in the southern part of the Klamath Mountains. These ages suggest that the metamorphic event that produced the schists took place during the Carboniferous. Two younger ages obtained on the schists probably reflect the thermal effects of Nevadan plutons. Mineral ages from one of these plutons, the Shasta Bally batholith, range from 127 to 132 m.y. The isotopic data make it possible to consider certain Paleozoic strata exposed east of the metamorphic belt as protoliths of the schists. The apparent age of metamorphism indicated by the isotopic data coincides in northern California and Oregon with a possible period of uplift during the Carboniferous and with an interruption of normal marine deposition during the Pennsylvanian.

This paper describes new radiometric data pertaining to the age of the Salmon Hornblende Schist and Abrams Mica Schist, which have been considered by many geologists to be the oldest rocks in northern California. Until the past few years, most geologists who have dealt with these schists have considered them to be either Precambrian or pre-Silurian, because the schists were assumed to be overlain unconformably by strata of Silurian age, and younger, that generally are not metamorphosed. More recently, however, the basis for the assumption of a pre-Silurian age has been recognized as incorrect, and it has become increasingly clear that the problem of the age of the schist is not likely to be resolved solely by application of normal field methods of stratigraphy. Thus the application of a supplementary technique such as radiometric dating should prove fruitful, at least to the extent of assign-

ing a minimum age to the metamorphism that produced the schists.

The Salmon and Abrams Schists were named by Hershey (1901) and are the principal rocks of the central metamorphic belt (Irwin, 1960a) of the Klamath Mountains (fig. 1). The Salmon consists principally of hornblende schist and gneiss that are thought to be metamorphosed volcanic rocks. The Abrams is chiefly micaceous quartz schist and marble, and is thought to be metasedimentary. The central metamorphic belt is approximately 10 miles wide and trends nearly north-south for about 90 miles in a broad, westward-bulging arc. The metamorphic belt is flanked on both sides by strata that are for the most part Paleozoic in age. Granitic and ultramafic intrusive rocks of Mesozoic age are present in the metamorphic belt and the flanking belts of stratified rock. On the east side of the metamorphic belt the strata make up a thick, fairly complete stratigraphic section that ranges in age from Silurian, or possibly Ordovician, upward through the Paleozoic, and, farther east, continues through Triassic into Middle Jurassic. In the southern part of the belt, shown on figure 2, the oldest rocks exposed along the east side of the metamorphic belt are of Devonian and Mississippian age. They are generally separated from the schists to the west by ultramafic rock. The strata west of the schist belt are structurally complex and less well known than those to the east of the belt. Near the schist they seem chiefly Permian in the latitude of figure 2, and may be Triassic along the northern part of the belt.

Unequivocal evidence for the age of the schists has not been found, although until recently they have been

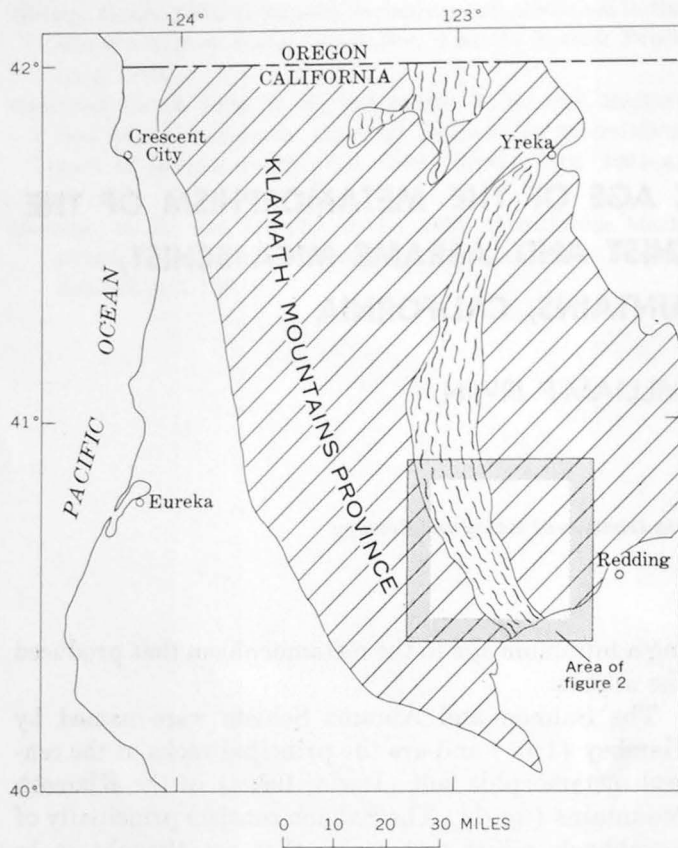


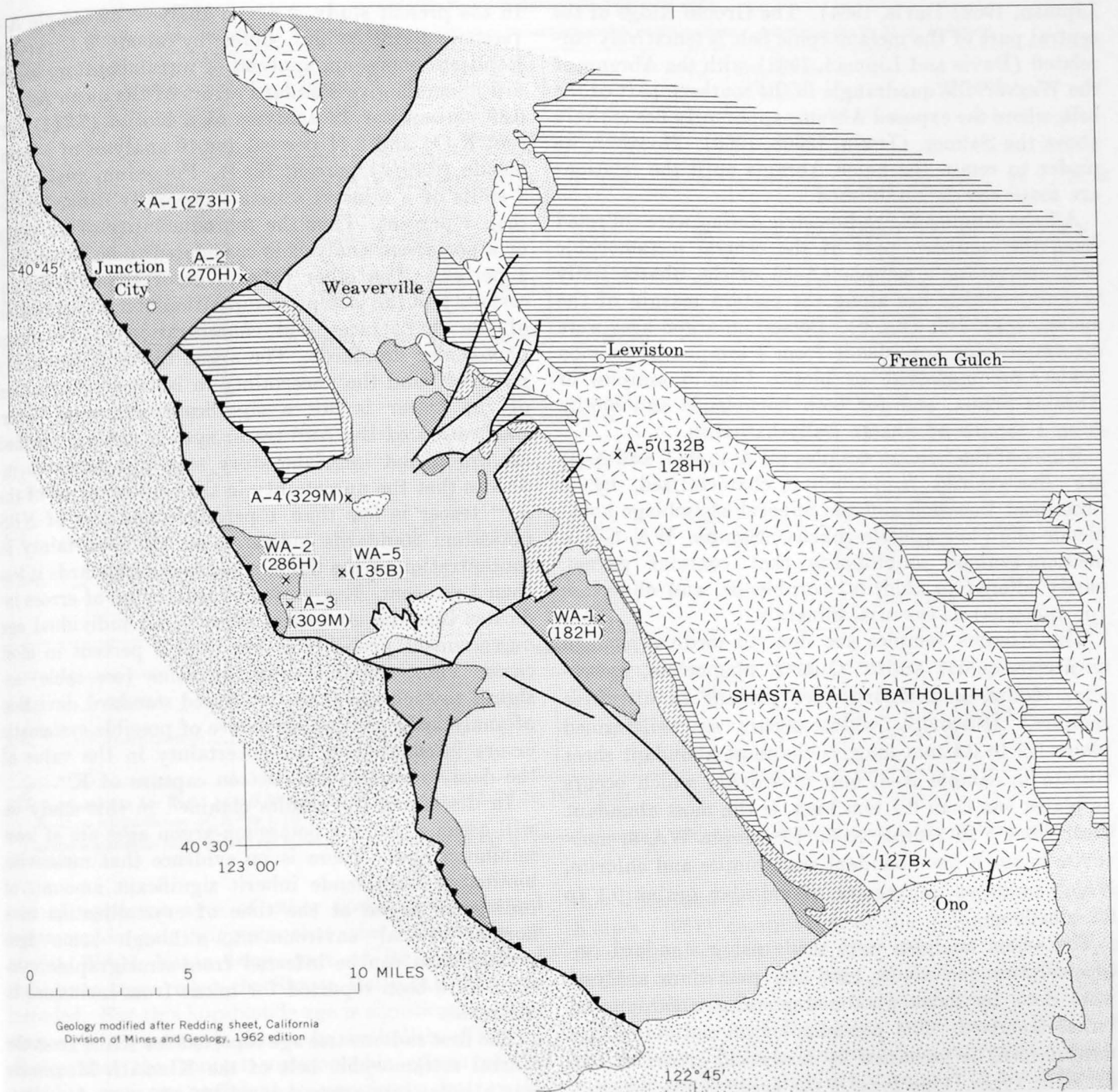
FIGURE 1.—Map of part of northwestern California, showing the Klamath Mountains province (diagonal pattern) and the area of figure 2. The central belt of metamorphic rocks and area of related rocks are indicated by schist pattern.

considered distinctly older than other formations of northwestern California. Hershey (1901) considered the schists to be pre-Devonian, favoring an Algonkian age. He thought the adjacent so-called Devonian-Carboniferous rocks were deposited unconformably on the schists. He discussed but rejected the idea that the schists could be metamorphic equivalents of the adjacent Paleozoic strata. Later, Diller (1922) and Hinds (1933) also thought that the schists were overlain unconformably by the Paleozoic strata, some of which were then known to be Silurian in age, and they considered the schists to be certainly pre-Silurian and probably Precambrian.

During a reconnaissance of the Klamath Mountains, Irwin (1960a) noted the linear tectonic aspect of the metamorphic belt, and nowhere was the so-called unconformable relation between the schists and Paleozoic strata seen. The Paleozoic strata to the west seemed clearly in fault contact with the schists, as noted by Hershey (1906), and the boundary between the schists and Paleozoic strata to the east was the locus of ultramafic and granitic intrusions. Irwin favored a

modification of the idea conceived but rejected by Hershey (1901) that the schists are metamorphic equivalents of adjacent Paleozoic formations. An isolated patch of Paleozoic strata (Bragdon Formation) lying within the central metamorphic belt in the Weaverville quadrangle seemed to offer the possibility of establishing whether the Paleozoic strata actually were deposited on the schists, but here, too, the Paleozoic strata proved to be either in fault contact with the schists or separated from the schist by ultramafic rock (Irwin, 1963). It appeared that not only are the Paleozoic strata to the west in fault contact with the schists, but that the Paleozoic strata east of the schists are separated from the schists essentially everywhere by a sheet of ultramafic rock. The ultramafic sheet was postulated to be emplaced along a regional fault along which the Paleozoic strata were thrust westward over the schist (Irwin and Lipman, 1962). Due to the fault-bounded character of the central metamorphic belt, early statements regarding unconformable stratigraphic relations between the schists and Paleozoic strata seem unfounded.

Further complications in the problem of the age of the schists have been pointed up by studies in the central part of the metamorphic belt, where the Abrams Mica Schist is separated from that in the southern part of the belt by a broad area of Salmon Hornblende Schist. Davis and Lipman (1962) have shown that the Abrams in the central part of the belt occurs both above and below the Salmon. They recommended that the name Abrams be abandoned, and that the names Grouse Ridge and Stuart Fork Formations be substituted for the metasedimentary rocks lying above and below the Salmon, respectively. They consider the Salmon Hornblende Schist and their Grouse Ridge Formation, the part of the Abrams that structurally overlies the Salmon, to have shared a similar history of metamorphism under conditions of the almandine-amphibolite facies. Their Stuart Fork Formation, the part of Abrams that underlies the Salmon, was metamorphosed under conditions of the greenschist facies and is overthrust to the west by the Salmon and Grouse Ridge (Davis and Lipman, 1962; Davis, 1965). Incomplete retrograde metamorphism of the Grouse Ridge occurred either during the same metamorphism that developed the greenschist mineral assemblage of the Stuart Fork Formation (Davis and Lipman, 1962), or while the higher grade metamorphic rocks were already lying over the greenschist facies rocks during the waning stages of this metamorphic event (Late? Jurassic) (Davis, 1965). The Stuart Fork Formation is correlated with strata of the Paleozoic and Triassic belt adjacent to the west (Davis and



Geology modified after Redding sheet, California Division of Mines and Geology, 1962 edition

EXPLANATION





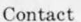


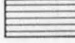

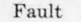
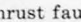
- |  |   |   |   |   |
|--|---|---|---|---|
|  |  |    |  |  |
| Detrital rocks of Cenozoic age   | Granitic rocks of Late Jurassic (Nevadan) age                                       | Chiefly sedimentary and volcanic rocks of the western Paleozoic and Triassic belt   | Abrams Mica Schist  | Contact   |
|  |  |    |  |  |
| Marine detrital rocks of Cretaceous age  | Ultramafic rocks  | Chiefly Bragdon Formation (Mississippian) and Copley Greenstone (Devonian?). Metamorphosed where adjacent to granitic rocks | Salmon Hornblende Schist  | Fault   |
|  |   |   |   |  |
|  |   |   |   | Thrust fault<br><i>Sawteeth on upper plate</i>  |

FIGURE 2.—Geologic map of part of southern Klamath Mountains, Calif. X, sample locality. Potassium-argon ages, in millions of years, are in parentheses following the sample numbers, except for the locality near Ono, which is from Curtis and others (1958); letter following age indicates mineral analyzed (H, hornblende; B, biotite; M, muscovite).

Lipman, 1962; Davis, 1964). The Grouse Ridge of the central part of the metamorphic belt is tentatively correlated (Davis and Lipman, 1962) with the Abrams of the Weaverville quadrangle in the southern part of the belt, where the exposed Abrams apparently lies entirely above the Salmon (Irwin, 1960b, 1963). However, we prefer to retain the name Abrams until the relations are more clearly established.

All the samples for radiometric dating were collected from the southern part of the central metamorphic belt, except for a sample (A-5) of the Shasta Bally batholith which lies along the eastern margin of the metamorphic belt (fig. 2). Potassium-argon ages were determined for hornblende from 4 samples of Salmon Schist, for muscovite or biotite from 3 samples of Abrams Schist, and for both hornblende and biotite from 1 sample of Shasta Bally batholith.

Three of the Salmon samples (WA-2, A-1, and A-2) are fine-grained amphibolite characterized by a prominent lineation and the mineral assemblage hornblende-oligoclase-epidote-sphene. Sample WA-1 is a medium-grained amphibolite that contains garnet, partly altered to chlorite, hornblende, and oligoclase (or andesine) as essential minerals.

The Abrams samples are fine- to medium-grained micaceous quartz schist. Quartz, plagioclase, muscovite, biotite, and chlorite are present in all three samples. Muscovite, which occurs as well-formed plates 0.2 to 0.4 mm long, is the most abundant sheet silicate in sample A-4, and muscovite, which occurs as plates less than 0.1 mm long, is the most abundant sheet silicate in sample A-3. In sample WA-5, muscovite is much less abundant than biotite and chlorite, which occur as aggregates of acicular grains 0.1 to 0.2 mm long.

The argon analyses were made using standard isotope-dilution techniques, and the potassium analyses were done by flame photometry using a lithium internal standard. The precision of an individual age measurement is governed by analytical errors of two different types. One type is the error in the determination of the potassium and argon contents of a mineral (or rock) that is caused by inhomogeneity of the mineral separate and scatter of the data obtained on the mass spectrometric and flame photometric analyses. The results of replicate (repeated) analyses of pure mineral separates give an estimate of the analytical errors that may be expected in an individual analysis. In the U.S. Geological Survey laboratory in Menlo Park, 12 analyses of a biotite that is used as an intralaboratory standard give a standard error of the mean ( $\sigma_x$ ) of 0.18 percent and a total spread of 1.6 percent.

In the present study, 2 argon analyses of sample A-4 (accompanying table) differ by about 0.1 percent. Replicate potassium analyses of intralaboratory standard minerals give standard errors of the mean ( $\sigma_x$ ) of 0.39 percent for 12 analyses of a biotite (7.7(1) percent  $K_2O$ ) and 0.41 percent for 10 analyses of a hornblende (0.49(3) percent  $K_2O$ ). Potassium analyses of 2 splits of a mineral separate generally differ by less than 2 percent. Thus the reproducibility of an argon or a potassium analysis is considered to be better than 1 percent. The other type of error comes from uncertainty in the isotopic composition and concentration of the  $Ar^{38}$  tracer and concentration of the flame photometer standards. The argon tracer is essentially pure  $Ar^{38}$  and the uncertainty in isotopic composition of the tracer is not a significant source of error. Calibration of the  $Ar^{38}$  tracer system against purified air argon and interlaboratory standard minerals indicates that the uncertainty in the concentration of the  $Ar^{38}$  tracer is less than 1 percent. Analyses of NBS potassium standards indicate that the uncertainty in concentration of the flame photometer standards is less than 1 percent. Evaluation of both types of errors indicates that the analytical error in an individual age measurement probably is less than 4 percent in most cases. Thus, the plus-or-minus value (see table) assigned to each age is the estimated standard deviation of analytical precision, exclusive of possible systematic errors introduced by an uncertainty in the value of the decay constant for electron capture of  $K^{40}$ .

In discussing the results obtained in this study we will assume that the potassium-argon ages are at least minimum ages. There is no evidence that muscovite, biotite, or hornblende inherit significant amounts of radiogenic argon at the time of crystallization in a normal crustal environment, although some ages greater than can be inferred from stratigraphic relations have been reported for micas from inclusions in diatremes.

The first radiometric age reported for schist from the central metamorphic belt of the Klamath Mountains was a potassium-argon age of  $190 \pm 10$  m.y. for hornblende from the Salmon Schist in the Weaverville quadrangle (Irwin, 1963). Additional analytical work on this sample (WA-1 in table) showed that the original potassium analysis was in error. The age of sample WA-1, based on 3 potassium analyses which are in good agreement, is 182 m.y., and the previously reported age for this sample should be disregarded. The sample was collected approximately 1 mile from the Shasta Bally batholith, and this locality may lie within the zone of contact heating that surrounded the batholith. The pat-

*Potassium-argon ages and analytical data*

[Potassium analyses by H. C. Whitehead and L. B. Schlocker; parentheses enclose uncertain digits. Argon analyses by M. A. Lanphere]

Field No.	Mineral	K <sub>2</sub> O analyses (percent)	Average K <sub>2</sub> O (percent)	Ar <sup>40</sup> <sub>rad</sub> (10 <sup>-10</sup> moles/gm)	Ar <sup>40</sup> <sub>rad</sub> /Ar <sup>40</sup> <sub>total</sub>	Apparent age (millions of years)	Location <sup>1</sup>
<b>Salmon Hornblende Schist</b>							
WA-1	Hornblende	0. 22, 0. 22(4), 0. 22(4)	0. 22(3)	0. 7198	0. 30	182 ± 10	SW <sup>1</sup> / <sub>4</sub> sec. 29, T. 32 N., R. 8 W. 40°35'45" N.; 122°48'00" W.
WA-2	do	0. 35, 0. 35(5)	. 35(3)	1. 613	. 63	286 ± 12	Center W <sup>1</sup> / <sub>2</sub> sec. 23, T. 32 N., R. 10 W. 40°37'00" N.; 122°58'30" W.
A-1	do	0. 33(6), 0. 32(7)	. 33(2)	1. 440	. 81	273 ± 11	NE <sup>1</sup> / <sub>4</sub> sec. 25, T. 34 N., R. 11 W. 40°46'45" N.; 123°02'45" W.
A-2	do	0. 39(9), 0. 39(8)	. 39(8)	1. 706	. 87	270 ± 10	SE <sup>1</sup> / <sub>4</sub> sec. 4, T. 33 N., R. 10 W. 40°44'30" N.; 122°59'45" W.
<b>Abrams Mica Schist</b>							
A-3	Muscovite	7. 0(6), 7. 1(4)	7. 1(0)	35. 17	0. 95	309 ± 12	NW <sup>1</sup> / <sub>4</sub> sec. 26, T. 32 N., R. 10 W. 40°36'15" N.; 122°58'30" W.
A-4	do	7. 2(8), 7. 1(9)	7. 2(4)	38. 42 38. 39	. 98 . 87	329 ± 13 329 ± 13	SE cor. sec. 1, T. 32 N., R. 10 W. 40°39'00" N.; 122°56'30" W.
WA-5	Biotite	1. 6(8), 1. 6(4)	1. 6(6)	3. 440	. 82	135 ± 5	NE <sup>1</sup> / <sub>4</sub> sec. 24, T. 32 N., R. 10 W. 40°37'00" N.; 122°56'45" W.
<b>Shasta Bally batholith</b>							
A-5	Biotite	8. 3(1), 8. 4(5), 8. 5(2), 8. 4(7)	8. 4(4)	17. 12	0. 96	132 ± 5	N <sup>1</sup> / <sub>2</sub> NE <sup>1</sup> / <sub>4</sub> sec. 5, T. 32 N., R. 8 W. 40°40'00" N.; 122°47'15" W.
A-5	Hornblende	0. 47(4), 0. 46(5), 0. 47(4) 0. 46(7)	. 47(0)	. 9172	. 69	128 ± 5	

Decay constants for K<sup>40</sup>: λ<sub>ε</sub> = 0.585 × 10<sup>-10</sup> year<sup>-1</sup>; λ<sub>β</sub> = 4. 72 × 10<sup>-10</sup> year<sup>-1</sup>  
Atomic abundance of K<sup>40</sup> = 1.19 × 10<sup>-4</sup>.<sup>1</sup> Locations of samples based on land net shown on U.S. Geological Survey Weaverville quadrangle, 1950, scale 1:62,500, except sample A-1 from Helena quadrangle, 1951, scale 1:62,500.

tern of apparent ages of other rocks in the central metamorphic belt suggests that the hornblende in sample WA-1 lost a large part of its accumulated radiogenic argon when the Shasta Bally batholith was intruded. But this hornblende age is significantly older than ages of minerals from the batholith. This indicates that the contact metamorphic effects of the batholith were not sufficient to completely destroy the "memory" of an older age; that is, the primary age of metamorphism of the Salmon Schist.

Ages ranging from 270 m.y. to 329 m.y. were obtained from schist samples collected several miles from the nearest pluton. Ages of the 3 hornblendes (WA-2, A-1, and A-2) from the Salmon Schist are in good agreement and give a mean age of 276 m.y. Ages of 309 m.y. and 329 m.y. for 2 muscovites (A-3 and A-4) from the Abrams Schist agree within analytical uncertainty. The muscovite and hornblende ages differ by more than analytical uncertainty, but the reason for

this difference is not known. However, according to Kulp's (1961) compilation of the geologic time scale, these ages suggest that the Abrams and Salmon Schists of the southern part of the metamorphic belt were produced during the Carboniferous.

The 135 m.y. age for biotite from sample WA-5 of the Abrams Schist is considered to represent a metamorphic overprint that is not related to the primary metamorphism of the schists. Biotite is known to be sensitive to thermal metamorphism, and we believe that this sample lost its accumulated radiogenic argon at the time that the Shasta Bally batholith and related plutons were emplaced. The age for the biotite is in good agreement with ages obtained from these intrusive rocks. The ages of 128 m.y. and 132 m.y. for hornblende and biotite, respectively, from a sample of granodiorite (A-5) from the northern part of the Shasta Bally batholith (fig. 1) are in excellent agreement with an age of 127 ± 4 m.y. (recalculated using

presently accepted decay constants) determined by Curtis and others (1958) for biotite from quartz diorite from the southern part of the batholith. Potassium-argon age ranging from 127 m.y. to 133 m.y. have been measured on biotite from other plutons in the central and northern parts of the metamorphic belt (Davis, 1963). Most geologists consider that these intrusive rocks were emplaced during the Nevadan orogeny. The biotite in sample WA-5 may have been formed during the Nevadan, but it seems more likely that this biotite lost its accumulated radiogenic argon during that orogeny.

The radiometric data are considered to indicate minimum ages for the metamorphic event that formed the schists. One might postulate that the Salmon and Abrams were formed during an ancient metamorphic event, perhaps during the Precambrian, and that the Carboniferous age suggested by the isotopic data results from a loss of argon during a later orogeny such as the Nevadan (Late Jurassic). However, the 3 concordant ages of hornblende from the Salmon indicate the likelihood of a real metamorphic episode at approximately 280 m.y., not an accidental concordance of hybrid ages. The potassium content of these three hornblendes differs by about 20 percent, and in order for the ages to be hybrid, and still be concordant, a mechanism would be required to remove argon from each hornblende in amounts proportional to its potassium content. Such a mechanism seems unlikely.

If the schists were formed during the Carboniferous, it is reasonable to look to some of the Carboniferous and older strata east of the metamorphic belt for a suitable protolith, and to search for supplementary evidence of an orogenic episode during that period. Of the exposed Paleozoic strata, only the Copley Greenstone (Devonian?) has the right age, correct lithology, and sufficient thickness and lateral extent to be considered a protolith of the Salmon Schist. The choice of formations that might serve as protoliths for the Abrams of the southern part of the metamorphic belt is not as narrow as for the Salmon, and more than one formation might be included. Strata that apparently are suitable as protoliths for the Abrams of the southern part of the belt, and for the schist overlying the Salmon in the central and northern parts, occur stratigraphically both above and below the Copley Greenstone. Those above the Copley include the Kennett (Devonian), Bragdon (Mississippian), and Baird (Mississippian) Formations, and are exposed in the latitudes of the southern and central parts of the metamorphic belt. Those below the Copley include the Duzel (Ordovician?) and Gazelle (Silurian) Forma-

tions, and are exposed only along the northern part of the belt.

The isotopic data indicate a Carboniferous age for the metamorphism that formed the Abrams and Salmon Schists of the southern part of the metamorphic belt. Metasedimentary rocks that underlie the Salmon in the central part of the belt have been correlated with strata to the west that include upper Paleozoic and Triassic units (Davis and Lipman, 1962; Davis, 1964b). If this correlation is correct, these metasedimentary rocks must be younger and not equivalent to the Abrams of the southern part of the belt.

The possibility of the schists being metamorphic equivalents of Carboniferous and older strata exposed to the east of the metamorphic belt should not be discounted because of the abrupt transition between the two terranes. As mentioned earlier, the two terranes are now separated by an ultramafic sheet and are thought to have been brought into present juxtaposition by the Paleozoic strata being thrust westward over the schists (Irwin and Lipman, 1962).

There are certain anomalies in the Carboniferous portion of the Paleozoic section that might relate to the age of metamorphism indicated by the isotopic data. In the Klamath Mountains, sparse Early Pennsylvanian strata have been recognized only recently, despite the fact that all other systems from Silurian through Jurassic are well represented east of the central metamorphic belt by thick marine deposits. Skinner and Wilde (1965) identified fusulinids of probable Early Pennsylvanian age in the uppermost part of the Baird, but state that a faunal hiatus between the Baird and McCloud Limestone (Permian) may represent most of Pennsylvanian time. Although they saw little or no physical evidence of a break between the Baird and McCloud, much of the McCloud is engulfed in mafic quartz diorite (Albers and Robertson, 1961), and, as pointed out by Albers (oral communication, 1965), the Baird and older strata are more highly deformed and intruded by dikes and sills than are the Permian and younger strata to the east. The upturned edges of the Baird and McCloud follow the same gross regional trend, but the boundary between them might actually be a surface of major unconformity when viewed normal to the regional trend. Further evidence of orogeny during the Carboniferous is seen where coarse conglomerate and grit totaling hundreds of feet in thickness constitute much of the upper part of the Mississippian (Bragdon Formation) that underlies the Baird. In the Suplee area of east-central Oregon, which lies along a projection of the Klamath Mountains, the Spotted Ridge Formation includes plant-bearing sandstones and mudstones that are land-laid,

and Pennsylvanian in age, in an otherwise marine Paleozoic section (Merriam and Berthiaume, 1943; Mamay and Read, 1956). Thus, in the California-Oregon region there is a suggestion of uplift during the Carboniferous and an interruption of normal marine deposition during the Pennsylvanian.

#### REFERENCES

- Albers, J. P., and Roberston, J. F., 1961, Geology and ore deposits of East Shasta copper-zinc district, Shasta County, California: U.S. Geol. Survey Prof. Paper 338, 107 p.
- Curtis, G. H., Evernden, J. H., and Lipson, J. I., 1958, Age determination of some granitic rocks in California by the potassium-argon method: California Div. Mines Spec. Rept. 54, 16 p.
- Davis, G. A., 1963, Structure and mode of emplacement of Caribou Mountain pluton, Klamath Mountains, California: Geol. Soc. America Bull., v. 74, p. 331-348.
- 1964, Correlation of Stuart Fork Formation with rocks of the western Paleozoic and Triassic belt, Klamath Mountains, California [abs.]: Am. Assoc. Petroleum Geologists, Pacific Sec., 99th Ann. Mtg., Los Angeles, Calif., 1964, program, p. 42-43.
- 1965, Regional Mesozoic thrusting in the south-central Klamath Mountains of California [abs.]: Geol. Soc. America Spec. Rept. 82, p. 248.
- Davis, G. A., and Lipman, P. W., 1962, Revised structural sequence of pre-Cretaceous metamorphic rocks in the southern Klamath Mountains, California: Geol. Soc. America Bull., v. 73, p. 1547-1552.
- Diller, J. S., 1922, Chromite in the Klamath Mountains, California and Oregon: U.S. Geol. Survey Bull. 725, p. 1-35.
- Hershey, O. H., 1901, Metamorphic formations of northwestern California: Am. Geologist, v. 27, p. 225-245.
- 1906, Some western Klamath stratigraphy: Am. Jour. Sci., ser. 4, v. 21, p. 58-66.
- Hinds, N. E. A., 1933, Geologic formations of the Redding-Weaverville districts, northern California: California Div. Mines 29th Rept. of State Mineralogist, v. 29, nos. 1-2, p. 77-122.
- Irwin, W. P. 1960a, Geologic reconnaissance of the northern Coast Ranges and Klamath Mountains, California, with a summary of the mineral resources: California Div. Mines Bull. 179, 80 p.
- 1960b, Relations between Abrams Mica Schist and Salmon Hornblende Schist in Weaverville quadrangle, California: Art. 147 in U.S. Geol. Survey Prof. Paper 400-B, p. B315-B316.
- 1963, Preliminary geologic map of the Weaverville quadrangle, California: U.S. Geol. Survey Min. Inv. Field Studies Map MF-275.
- Irwin, W. P., and Lipman, P. W., 1962, A regional ultramafic sheet in eastern Klamath Mountains, California: Art. 67 in U.S. Geol. Survey Prof. Paper 450-C, p. C18-C21.
- Kulp, J. L., 1961, Geologic time scale: Science, v. 133, no. 3459, p. 1105-1114.
- Mamay, S. H., and Read, C. B., 1956, Additions to the flora of the Spotted Ridge Formation in central Oregon: U.S. Geol. Survey Prof. Paper 274-I, p. 211-226.
- Merriam, C. W., and Berthiaume, S. A., 1943, Late Paleozoic formations of central Oregon: Geol. Soc. America Bull., v. 54, no. 2, p. 145-171.
- Skinner, J. W., and Wilde, G. L., 1965, Permian biostratigraphy and fusulinid faunas of the Shasta Lake area, northern California: California Div. Mines and Geology. [In press]





## RADIOCARBON DATES FROM ILIAMNA LAKE, ALASKA

By ROBERT L. DETTERMAN, BRUCE L. REED; and MEYER RUBIN,  
Menlo Park, Calif.; Washington, D.C.

*Abstract.*—A radiocarbon date of  $8,520 \pm 350$  years Before Present from a lacustrine sand deposit in a terrace at the west end of Iliamna Lake establishes a minimum age for the second major advance of the Brooks Lake Glaciation. The advance must be considerably older than 8,520 years, as other terraces are cut into the moraine as much as 49 feet above the dated terrace.

Iliamna Lake, Alaska (fig. 1), is one of many large lakes in southern and southwestern Alaska that occupy basins enclosed by moraines of Wisconsin age. Muller<sup>1</sup>

<sup>1</sup>E. H. Muller, 1952, The glacial geology of the Naknek district, the Bristol Bay region, Alaska: Illinois Univ., thesis, 97 p.; microfilm copy available from University Microfilms, Inc, Ann Arbor, Mich.

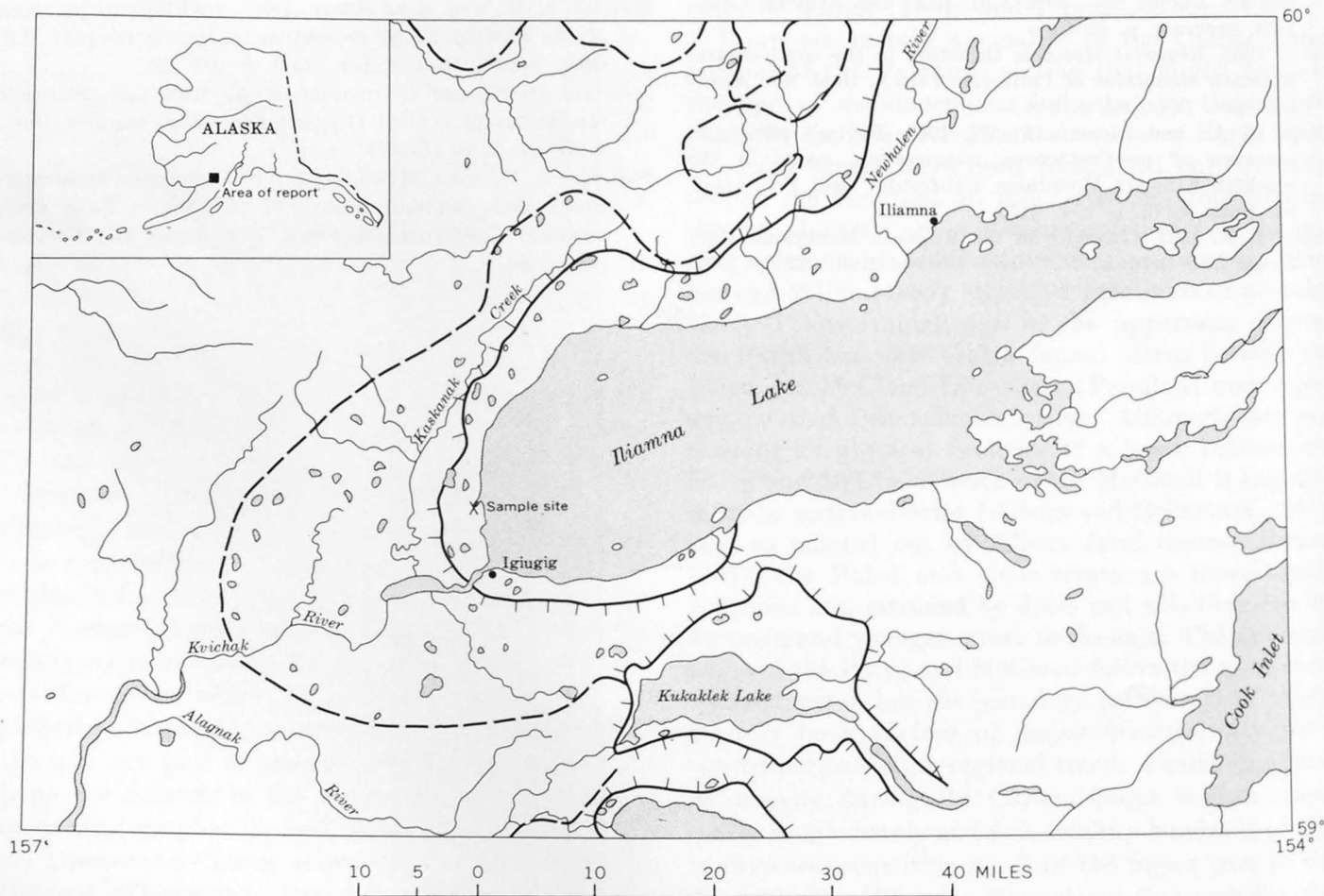


FIGURE 1.—Maximum extent of the Brooks Lake Glaciation in the Iliamna Lake region, Alaska. Dashed line, extent of first major glacial advance; glaciated area lies on the east side of line. Hachured line, extent of second major glacial advance; glaciated area lies opposite the hachured side of line.

U.S. GEOL. SURVEY PROF. PAPER 525-D, PAGES D34-D36

(1953) named the glacial episode during which these lake-enclosing moraines were built the Brooks Lake Glaciation. In the Iliamna Lake area the Brooks Lake Glaciation, as mapped by Detterman and Reed, is recorded by moraines of 4, or possibly 5, major advances that were separated by several minor periods of recession and readvance. The major advances of the Brooks Lake Glaciation probably correspond to the advances of the Naptowne Glaciation as distinguished by Karlstrom (1957; 1964, p. 56-57; Karlstrom and others, 1964).

The moraine of the second major advance of the Brooks Lake Glaciation (fig. 1) encloses the basin of the modern Iliamna Lake. A prominent wave-cut terrace is present on the inner side of this moraine. The altitude of this terrace is about 127 feet above mean sea level; that of the present lake surface is 47 feet. A series of younger terraces with beach ridges and escarpments is present between the 127-foot level and the present lake.

The dates presented herein, the first from the Iliamna Lake area, are from deposits at an altitude of about 78 feet in a terrace that has several beach ridges and a lakeward escarpment. Silt deposits and oriented lakes now occupy a former lagoon on the terrace. Locally, sand dunes obscure the beach ridges and escarpment.

Two pits (fig. 2) were excavated in an area of generally stabilized sand dunes that now is covered by a sparse stand of spruce and brush. The pits, about 20 feet apart, both struck the white volcanic ash layer shown just above zone 3 in figure 2. The sediments penetrated are interpreted as being in part lacustrine and in part eolian. The upper 54 inches, considered to be an eolian deposit, includes dated zones 4 (200±200 years old) and 3 (400±200 years old). The sand is light tan, unstratified, and has well-frosted grains; minor silt is present. Zone 4 has many pieces of rotted wood, some of which are carbonized, probably as a result of a forest fire. Zone 3 is an organic layer containing many carbonized small seed pods, small twigs, and grass(?); it is overlain by the thin bed of white volcanic ash.

Material in the interval between zones 3 and 2b may be either eolian or lacustrine; some of the sand grains are frosted, but many are not, and there is more silt mixed with the sand than is present above zone 3. Zone 2a and b (1,980±250 years old) appears to be in a lacustrine deposit and probably marks the highest stand of water on this terrace; it is composed of 2 layers of organic material about 6 inches apart, separated by sand. The organic material is concentrated in the troughs of probable oscillation ripples.

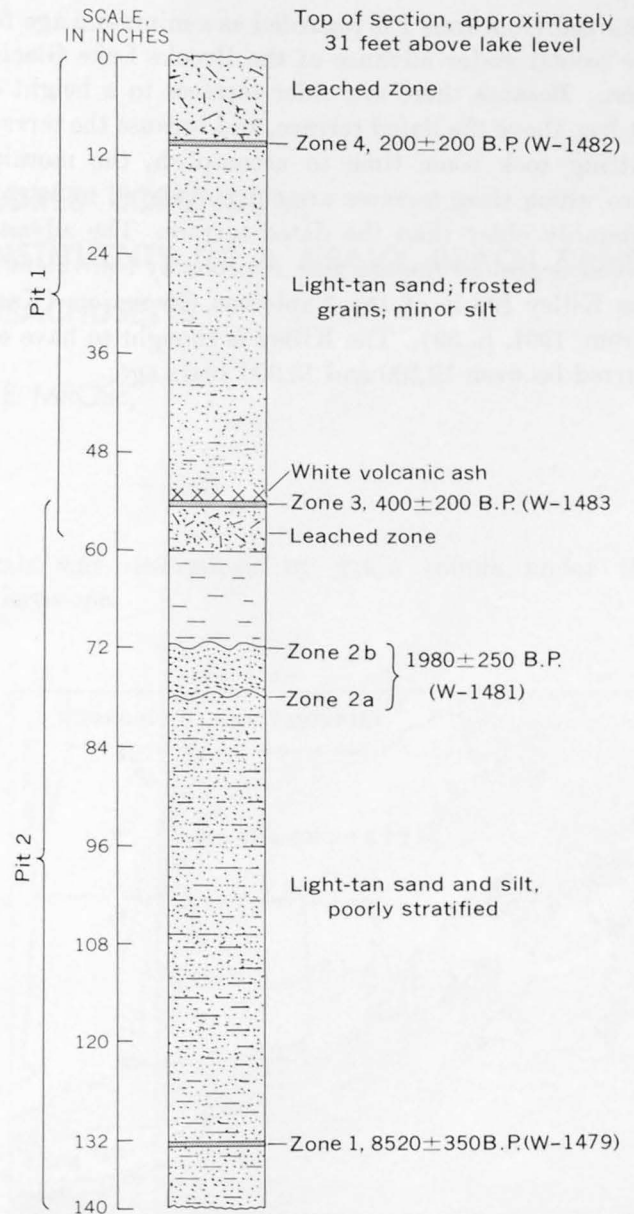


FIGURE 2.—Stratigraphic section in two pits in lake terrace at Iliamna Lake, Alaska. Numbers in parentheses are numbers of samples on which age determinations were made by Rubin at the U.S. Geological Survey radiocarbon laboratory, Washington, D.C. B.P., years Before Present (that is, before A.D. 1950).

The paucity of frosted sand grains and the presence of what are probably oscillation ripple marks suggest water rather than the wind as the agent of deposition. Sand below zone 2a is poorly stratified, finer grained, and contains more silt than the overlying units; it is of probable lacustrine origin. The unit appears to lack depositional breaks, and probably marks a prolonged stand of the lake at this level. Zone 1 is thin (0.25-0.75 in.) and contains very fine organic material without identifiable plant remains. The age (8,520±350 years)

obtained from zone 1 is regarded as a minimum age for the second major advance of the Brooks Lake Glaciation. Because there are older terraces to a height of 49 feet above the dated terrace, and because the terrace cutting took some time to accomplish, the moraine into which these terraces are cut is believed to be considerably older than the dated terrace. The advance which deposited the moraine is probably equivalent to the Killey Stade of the Naptowne Glaciation (Karlstrom, 1964, p. 59). The Killey is thought to have occurred between 12,500 and 19,000 years ago.

#### REFERENCES

- Karlstrom, T. N. V., 1957, Tentative correlation of Alaskan glacial sequence, 1956: *Science*, v. 125, no. 3237, p. 73-74.
- 1964, Quaternary geology of the Kenai lowland and glacial history of the Cook Inlet region, Alaska: U.S. Geol. Survey Prof. Paper 443, 69 p.
- Karlstrom, T. N. V., and others, 1964, Surficial geology of Alaska: U.S. Geol. Survey Misc. Geol. Inv. Map I-357, 2 sheets.
- Muller, E. H., 1953, Northern Alaska Peninsula and eastern Kilbuck Mountains, Alaska, *in* Péwé, T. I., and others, Multiple glaciation in Alaska, a progress report: U.S. Geol. Survey Circ. 289, p. 2-3.



## MAGNETIC SPHERULES, COLORED CORUNDUM, AND OTHER UNUSUAL CONSTITUENTS OF A HEAVY BEACH SAND, MARTHA'S VINEYARD, MASSACHUSETTS

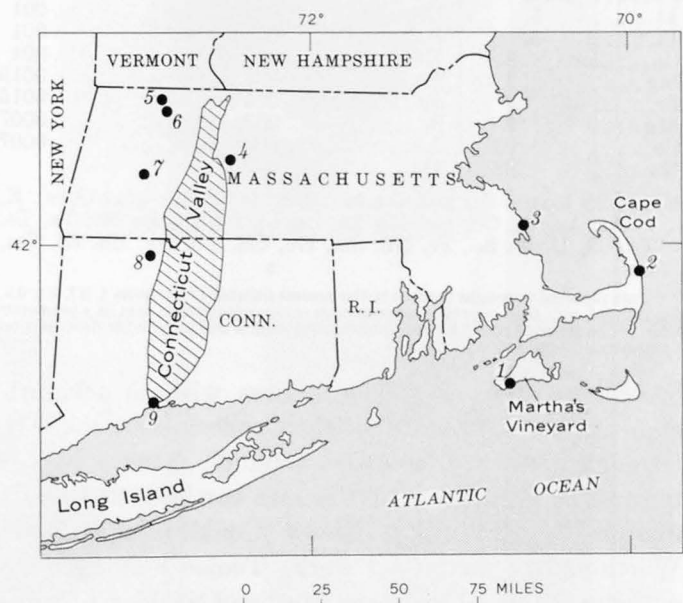
By CLIFFORD A. KAYE and MARY E. MROSE,  
Boston, Mass., Washington, D.C.

**Abstract.**—Naturally concentrated heavy beach sand from western Martha's Vineyard contains small quantities of magnetic spherules, red and blue corundum, gahnite, native copper, and gold. Except for larger average size, the magnetic spherules are similar to those considered to be of extraterrestrial origin. Their composition is maghemite and magnetite. Surfaces and shapes are varied and reflect crystal-line structure. Colored corundum, gahnite, and native copper are known to occur in the rocks of western Massachusetts and Connecticut and the grains may have been transported by glacial ice from there to the southeastern part of Massachusetts.

Concentrations of dark, heavy sand are formed sporadically throughout the year on several beaches of Martha's Vineyard, an island lying 5 miles south of Cape Cod, Mass. (fig. 1). Examination of samples of naturally concentrated heavy sand from the beach at the western end of the sea cliff known as Nasha-quitsa showed the presence of several unusual minerals, rare or unreported in New England, as well as magnetic spherules.

The samples were taken from dark, heavy sand, a few inches to several feet thick, that overlies a coarse cobbly substratum. The sand is very uniform medium grained ( $M_{50}=0.32$  mm,  $S_o=1.18$ ; Trask, 1930). The heavy minerals are dominantly garnet, staurolite, magnetite, and ilmenite (table 1). The percentage of quartz, feldspar, and other light minerals varies, with the sample, from 5 to 11 percent of the total weight. In order to estimate the concentration of some of the rarer minerals, the sand was separated into magnetic fractions using the Franz Isodynamic Separator. Grains were identified petrographically, and the rarer minerals were also determined by X-ray diffraction techniques. The concentration of more abundant min-

erals was determined by grain counts under the microscope.



- |   |                 |
|---|-----------------|
| 1. Nashaquitsa beach,<br>Martha's Vineyard. | 5. Rowe.        |
| 2. Nauset beach, Cape Cod.                  | 6. Charlemont.  |
| 3. Fieldston beach.                         | 7. Chester.     |
| 4. Pelham.                                  | 8. Barkhamsted. |
|   | 9. New Haven.   |

FIGURE 1.—Location map of southern New England, showing outline of the Triassic basin (diagonal pattern) of the Connecticut Valley.

A semiquantitative spectrographic analysis was obtained on a small sample of the beach sand (table 2). The composition is relatively high in the rare-earth elements, cerium and yttrium, and in vanadium, zirconium, and titanium.

TABLE 1.—*Heavy minerals in sand at Nashaquitsa beach*

[Percent by volume of total sample]

Garnet:		Epidote, yellow to	
Pink (almandite)-----	23	green-----	1.0-0.1
Brown (spessartite)---	18	Tourmaline, black,	
Red brown (spes-		brown-----	1.0-0.1
sartite)-----	5	Amphiboles-----	1.0-0.1
Colorless, purple, and		Rutile:	
clouded (alman-		Red to silver-----	1.0-0.1
dite)-----	3	Jet black-----	1.0-0.1
Staurolite-----	20	Sillimanite-----	1.0-0.1
Magnetite-----	8	Kyanite-----	1.0-0.1
Ilmenite-----	7	Andalusite-----	Tr.
Goethite, pseudomor-		Biotite-----	Tr.
phous after glau-		Gahnite-----	Tr.
conite-----	2	Corundum, red, blue---	Tr.
Glauconite-----	1	Monazite-----	Tr.
Zircon:		Topaz-----	Tr.
Colorless prisms-----	2	Copper-----	Tr.
Opaque brown-----	1.0-0.1	Gold-----	Tr.
		Magnetic spherules---	Tr.

TABLE 2.—*Semiquantitative spectrographic analysis of heavy beach sand, Nashaquitsa, Martha's Vineyard*<sup>1</sup>

[Analyst, Helen W. Worthing]

Si-----	>10.	V-----	0.03	Pb-----	0.002
Fe-----	>10.	Y-----	.03	Ba-----	.001
Al-----	5.	Cr-----	.02	Mo-----	.001
Ti-----	5.	B-----	.01	Ni-----	.001
Ca-----	.3	Hf-----	.005	Sr-----	.001
Mg-----	.3	Nb-----	.005	Be-----	.0015
Zr-----	.3	Sn-----	.005	Co-----	.0015
Mn-----	.2	Sc-----	.003	Ag-----	.0007
Ce-----	.05	Yb-----	.003	Cu-----	.0007
Na-----	.05	Ga-----	.002		

Elements looked for but not found in detectable quantities: K, P, As, Au, Bi, Cd, Ge, Hg, In, La, Li, Pd, Pt, Re, Sb, Ta, Te, Th, Tl, U, W, Zn, Pr, Nd, Sm, Eu, Gd, Tb, Dy, Ho, Er, Tm, Lu.

<sup>1</sup> Data reported in weight percent to the nearest number in the series 1, 0.7, 0.5, 0.3, 0.2, 0.15, 0.1, etc.; these represent approximate midpoints of group data on a geometric scale. The assigned group for semiquantitative results will include the quantitative value about 30 percent of the time.

*Acknowledgments.*—The writers wish to acknowledge the help of several of their colleagues in the U.S. Geological Survey, notably: John W. Adams, for his interest in the source of the rare earths in the sand; Joseph W. Budinsky, Nancy Conklin, and Helen Worthing for analytical work; Tomas Feininger for noticing the first blue corundum; and Sheldon Shapiro for collecting several sand samples. In addition, Prof. Clifford Frondel, Harvard University, made available samples of gahnite from the collection of Harvard University; Prof. C. S. Hurlbut, Jr., Harvard University, identified the blue corundum by X-ray diffraction; and Prof. Frances W. Wright, Smithsonian Astrophysical Observatory, Harvard University, furnished electron-probe analyses of a magnetic spherule.

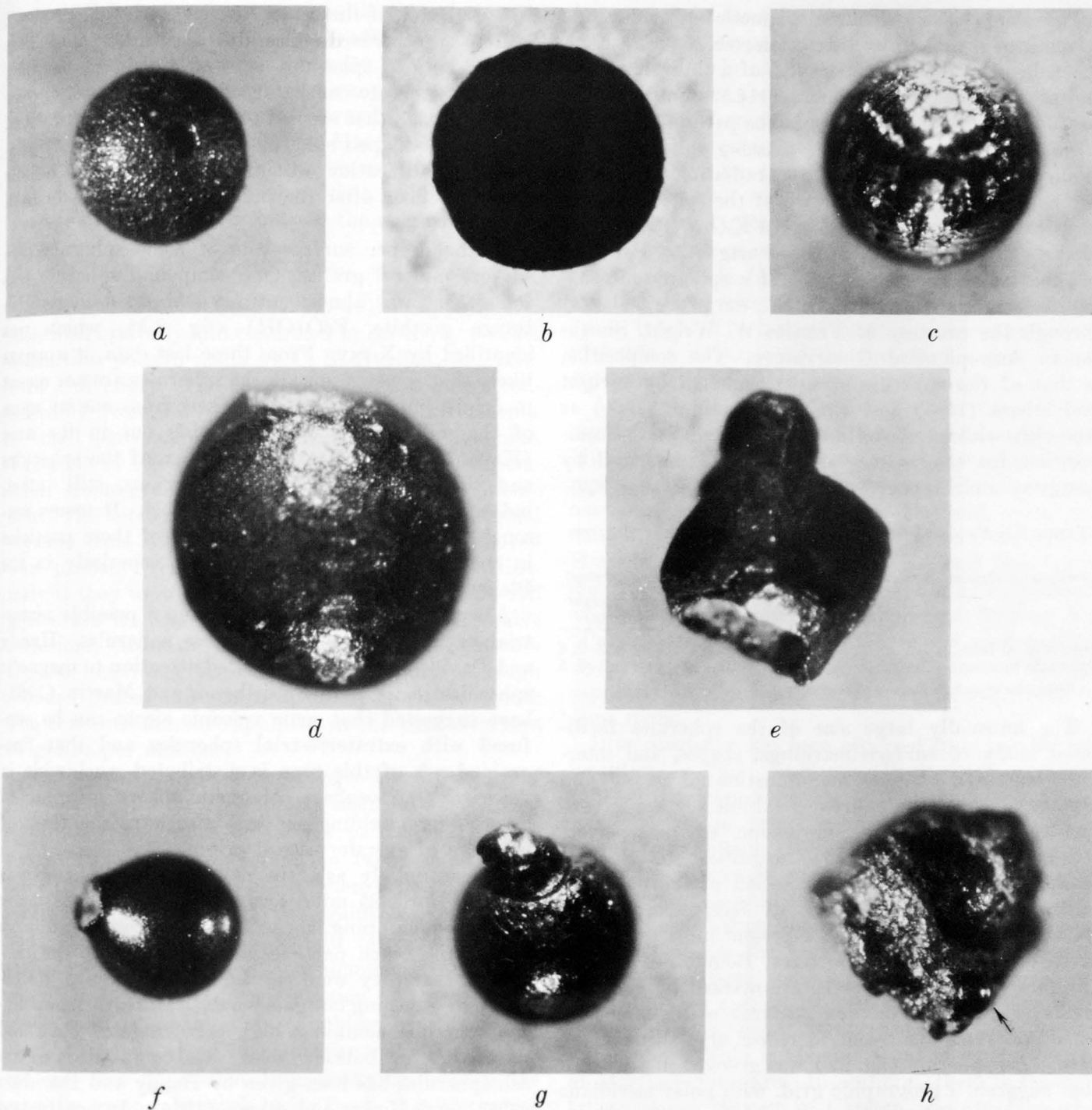
### MAGNETIC SPHERULES

Strongly magnetic grains of striking sphericity and polish (fig. 2) are very sparsely distributed in the beach sand. The concentration of spherules in the samples examined was not greater than 3 grains per

million and probably less. A total of 22 spherules was separated by scanning the strongly magnetic (separated by hand magnet) fraction of the sand. The near-perfect sphericity of the grains was sufficiently distinctive in comparison to even the best rounded magnetite grains to permit the spherules to be easily noticed while scanning. The high polish of most of them gave them the appearance of minute steel ball bearings. This, too, is in sharp contrast to the duller luster of even well-polished magnetite grains.

The spherules resemble the magnetic spherules that have provoked considerable interest in recent years because of their probable meteoric origin (for example, Cassidy and others, 1964; Crozier, 1960, 1962; Hodge and Wright, 1964; Hodge and others, 1964; Wright and others, 1963). These particles are generally thought to represent cosmic dust and ablation droplets that have been stripped from meteoroids falling through the earth's atmosphere. The beach-sand spherules resemble those described as being of extraterrestrial origin, except that the beach-sand spherules are exceptionally large. The largest found measured 660 $\mu$  in diameter (fig. 2, *d*) and the smallest 200 $\mu$ ; the large majority are between 300 $\mu$  and 400 $\mu$  in diameter. Spherules collected from the atmosphere, polar ice, and from older sediments are generally less than 100 $\mu$  and rarely as large as 230 $\mu$  (Crozier, 1960, 1962; Hodge and others, 1964; Langway and Marvin, 1964; Thiel and Schmidt, 1961; Wright and others, 1963). Assuming that the beach-sand spherules were sorted from an original spherule population whose average size was the same as that described from other localities, one can explain this concentration of the very rare large grains by the same process that concentrated the uniform heavy beach sand—the dynamic sorting action of the surf. The beach sand is made up of particles with an extremely small weight range. In surf-sorting, lighter particles are winnowed out and carried off the beach by the backwash, and heavier particles are not carried up onto the beach face at all. The heavy sand therefore represents a concentration of grains that originally may have been only very minor components of their respective sedimentary complexes. It is, therefore, most probable that for every large spherule in the beach sand, a considerable number of smaller congeners were winnowed out and carried away by the swash of the surf.

Six of the spherules were placed in bromoform (specific gravity, 2.85) and all sank rapidly. The bulk density therefore probably exceeded 3.0 in spite of the hollow centers that some of the spherules are known to have. Langway and Marvin (1964) give 4.54 as the average bulk density of their Greenland spherules.



- a.* Rough granular texture, deep pit.  
*b.* Silhouette of a spherule showing surface irregularities.  
*c.* Polycrystalline pattern on surface of spherule.  
*d.* Oval shape and faceted surface. Facets are crystal faces of maghemite.  
*e.* Compound spherule, larger one has beaker shape.  
*f.* Very highly polished spherule, part of a compound spherule. This spherule consists of a thin, frag-

- ile outer shell over a polyhedral interior mass.  
*g.* Broken compound spherule. The irregular interior of smaller member still adheres and the attachment collar of outer shell of smaller spherule can be seen.  
*h.* Compound spherule embedded in a hard matrix of goethite. Only part of the highly polished smaller twin is clear on photograph (arrow).

FIGURE 2.—Magnetic spherules from Nashaquitza beach sand, showing variations in shape, structure, and surface texture.

The composition of three magnetic spherules was determined by X-ray diffraction techniques. Each spherule was mounted at the end of a thin glass fiber and placed in a powder camera (114.59 mm diameter) so that only the spherule was in the path of the X-ray beam. X-ray patterns of the rotating spherules were taken in manganese-filtered iron radiation. The powder patterns obtained from two of the spherules were identical to that of maghemite,  $\gamma\text{-Fe}_2\text{O}_3$ . The pattern of the third spherule was that of magnetite,  $\text{FeFe}_2\text{O}_4$ .

The surface and the interior of a spherule measuring  $200\mu$  were analyzed by the electron probe (table 3) through the courtesy of Frances W. Wright, Smithsonian Astrophysical Observatory. The composition is that of the spherule group designated by Wright and others (1963) and Hodge and others (1964) as iron-rich without nickel and is the same as the composition for some Greenland spherules described by Langway and Marvin (1964).

TABLE 3.—*Electron-probe analyses of a  $200\mu$  spherule from Nashaquitsa beach sand*

[Analysis by Advanced Metals Research Corp., S. H. Moll, laboratory supervisor]

	Fe (weight percent)	Mn (weight percent)
Spherule surface.....	68-73	1 0. 2-0. 4
Spherule interior.....	68-73	1 0. 1-0. 5

<sup>1</sup> Remainder of analysis assumed to be oxygen.

The unusually large size of the spherules facilitated study of surface markings, shapes, and internal structures. Under magnification of  $\times 45$  and greater, most of the spherules exhibit surface irregularities that mar the impression of near-perfect sphericity conveyed by low magnification. Surface markings are mostly the expression of the polycrystalline structure and consist of facets, ridges, and striations. Facets appear to represent individual magnetite or maghemite crystal faces. Boundaries between adjoining facets, or crystals, are marked by very low crests or ridges. Complex patterns of striations on some spherules also seem to reflect crystalline structure. One spherule (fig. 2,c) was grooved in a pattern that suggests a geographic grid, with polar meridians and parallels of latitude.

Most spherules have one or more very deep to shallow pits on the surface and some have bulges and blisters. Several spherules are compound, consisting of small spherules attached to larger. Many spherules show by remnant collars and pits that they, too, were originally parts of twins that had broken apart. The spherules are relatively fragile. One that broke in half when pressed and two others that had been ground halfway through after being embedded in hardened Canada balsam showed hollow spherical interiors.

The diameter of the central cavity varied from about half to two-thirds the diameter of the spherule. Two partly broken spherules showed a rather complex internal structure consisting of a thin outer shell over an inner mass that seemed to have a polyhedral form. One beaker-shaped spherule was found (fig. 2,e) suggesting solidification either before a complete bubble had formed or after the bubble had in some fashion burst.

In the deeper surface pits of some spherules are silt-size mineral grains. One compound spherule was found that was almost entirely embedded in reddish brown goethite,  $\text{FeO(OH)}$  (fig. 2,h), which was identified by X-ray. From these last data, it appears likely that some, if not all, the spherules are not recent in origin but have been reworked from one or more of the sedimentary units cropping out in the area (Kaye, 1964a, 1964b). The fragility of the spherules and the presence of compound grains, still intact, indicates only slight littoral transport. It seems reasonable therefore to seek the source of these particles in the immediately adjoining cliff, especially in the Pleistocene marine clay and sand.

A word should be said concerning a possible terrestrial or artificial origin for these spherules. Handy and Davidson (1953) have called attention to magnetic spherules in fly ash. Fredriksson and Martin (1963) have suggested that some volcanic ejecta can be confused with extraterrestrial spherules and that fine-grained ash of this type is distributed worldwide in the earth's atmosphere. Magnetic spherules produced by welding (welding spatter) also have the form of particles of extraterrestrial origin.

Concerning fly ash, the closest city and source is New Bedford, 25 miles away, and the beach is many miles from shipping lanes. The high density and large size of the beach particles seem to preclude the possibility that they were carried this far in the atmosphere by anything but gale winds. Moreover, most fly-ash spherules contain a high percentage of glass and have very low bulk densities. The composition of fly-ash spherules has been given by Handy and Davidson (1953) and Hodge and others (1964). In contrast to the simple iron oxide composition of the beach-sand spherules, their data show substantial amounts of Si, Al, and other elements characteristic of coal ash.

Similar reasoning points to the improbability of the beach-sand spherules being of volcanic or welding origin. The large size and density of the beach spherules and the remoteness of the locality from active volcanism would seem to eliminate airborne volcanic ash as a possible source. In addition, studies by Hodge and Wright (1964) of magnetic volcanic-dust particles

show that the composition is not unlike that of volcanic ash and rocks in general with a substantial content of Si, Al, and other elements. As for welding spatter, it reflects the relatively complex composition of welding rods and the alloying additives in steel (Wright and others, 1963; Langway and Marvin, 1964). Furthermore X-ray diffraction analyses reported by Langway and Marvin (1964) show that welding spatter consists of elemental Fe and not the magnetic oxides.

### CORUNDUM

*Blue corundum*,  $Al_2O_3$ , (*sapphire*).—Sapphire was identified optically and confirmed by an X-ray powder diffraction pattern made by C. S. Hurlbut, Jr., Harvard University. The color of the grains varies considerably from very deep to very light ultramarine. A small percentage of grains are light indigo blue. Variation in color within a single grain is not uncommon. Some grains are colorless, with spots of intense blue. The intensity of color is such that the original crystals from which most of the grains were derived were probably very dark blue to nearly black, particularly if they were larger than about one-half inch. All grains are transparent, clear, and without noticeable inclusions. Most of the grains are angular to subangular and range between 0.3 and 0.6 mm, although rounded grains and grains up to 1.4 mm were found. The concentration of sapphires in the sand averages 25 grains per million.

*Red corundum*,  $Al_2O_3$ , (*ruby*).—Identification of ruby was established by optical means and confirmed by an X-ray powder diffraction pattern. The color ranges from moderately light to fairly intense carmine red. Unlike the sapphires, there is no color variation within single grains. The grains are transparent and clear although some contain fairly large black inclusions. Judging from their abundance in the non-magnetic fraction, the concentration of rubies in the beach sand is greater than sapphires by a factor of about 3; that is, about 75 grains per million. One does not get this impression from scanning because the sapphire grains are much easier to see than the rubies midst the predominating population of pink and red garnets.

Colored corundums have been found in beach sand by Kaye in several other beaches in southeastern Massachusetts. Blue corundum was found in a heavy beach sand at Fieldston (3 on fig. 1), northeast of Plymouth, and several grains of red corundum were found in samples of heavy sand from the beach at Nauset, in eastern Cape Cod (2 on fig. 1). The distribution is therefore fairly widespread. The imme-

diately source of the mineral is undoubtedly the Pleistocene deposits cropping out in the cliffs and in the area immediately offshore, where sand can be worked and carried onto the beach by waves. In addition, both Miocene and Cretaceous sediments crop out on western Martha's Vineyard within a mile or two of Nasha-quitsa beach. An unsuccessful attempt was made to determine which stratigraphic unit in western Martha's Vineyard (Kaye, 1964a, 1964b) contributed the colored corundum to the sand. Heavy-mineral separations were made from sand washed from samples of each of the sedimentary units in the cliff at Nasha-quitsa beach. The lack of success in this enterprise is probably a reflection of the very high degree of concentration that the beach sand represents.

Although blue corundum is not unusual as a detrital mineral in sands, the red variety is considerably rarer. Milner and others (1962) state that it has never been reported. Red corundum, as far as the writers know, has never been reported in New England, either as a detrital mineral or in place as a rock constituent. However, it is not unusual for red and blue corundum to occur together in rock deposits, as for example, at Warwick, N.Y., and at Franklin and Newton, N.J. (Palache and others, 1944). There is a good possibility, therefore, that the rubies and some, if not all, sapphires in the beach sands are derived from the same rocks.

Blue corundum has been reported from two bedrock localities in New England (Pratt, 1906). Adams (1870) and later Emerson (1898, 1917) described a small deposit of colorless corundum with deep-blue spots from Pelham, Mass. (4 on fig. 1), about 110 miles due northwest of western Martha's Vineyard. Furthermore, several other contact-metamorphic deposits of the Pelham type have been described (Emerson, 1917) from the same area, although corundum is not listed from these localities. Emerson (1902) also described a small deposit of blue-black to dark-blue corundum from Barkhamsted in northwestern Connecticut. This is about 120 miles west-northwest of Martha's Vineyard. In addition, there is the well-known emery deposit in Chester, western Massachusetts (7 on fig. 1), about 140 miles from Martha's Vineyard. The color of the very fine-grained corundum from this sizeable deposit has been variously described as bronzy (Emerson, 1917) and blue black to black (Pratt, 1906). Any or all of these deposits may conceivably have supplied the corundum of the beach sand. However, it is also possible that some or all of the beach-sand corundum comes from as yet undiscovered deposits located somewhat closer to Martha's Vineyard.



**GAHNITE,  $ZnAl_2O_4$** 

Subrounded to well-rounded frosted to clear grains of striking blue-green color were determined by X-ray powder pattern to be the zinc spinel, gahnite. The color ranges from very light to deep blue-green and, making allowances for the surface frosting, the grains are transparent and clear. The concentration is about 250 grains per million.

Gahnite has been reported (Morrill and Chaffee, 1957; Morrill and others, 1958) from one locality in central Vermont, the Taggart mine, which is about 200 miles north-northwest of Martha's Vineyard, and from several localities in southwestern Maine, about 200 miles east-northeast of Martha's Vineyard. Closer to Martha's Vineyard, and a much more likely source, is the occurrence of gahnite in the Hawley Schist in the vicinity of Rowe and Charlemont (5 and 6 on fig. 1) in northwestern Massachusetts (Dana, 1887; Flint, 1908). This is about 140 miles from Martha's Vineyard and in the same northwest azimuth as Pelham, Mass. In the Rowe-Charlemont area, crystals up to 5 inches across are associated with pyrite in chlorite and sericite schist. The gahnite of the beach sand was compared with samples from both Rowe and Charlemont in the mineral collection of Harvard University. Quarter-inch crystals from both localities are opaque black to greenish black. When crushed to sand-size fragments the gahnite from Charlemont is indistinguishable from the beach-sand gahnite under the petrographic microscope as to color, clarity, and general absence of inclusions. The index of refraction of gahnite from both places is the same ( $n=1.802$ ). On the other hand, gahnite from Rowe is more bluish, contains abundant minute inclusions, and has a somewhat higher index of refraction ( $n=1.808$ ). Although the evidence does not preclude an origin less distant from Martha's Vineyard, the presence of other minerals in the sand with known occurrences in western Massachusetts increases the probability that the beach-sand gahnites do come from the belt of Hawley Schist in the vicinity of Charlemont.

**GOLD**

Several grains of gold were found in the sand during scanning. Additional grains were found in non-magnetic separates. The highest concentration noted was about 5 grains per million.

**NATIVE COPPER**

Two rounded, irregular-shaped blue-green grains resembling turquois were noted while scanning. The largest grain was 1.4 mm in length. Under the micro-

scope the blue-green material was seen to be a surface coating over a hard core. The surface coating was found by X-ray powder analysis to consist of a mixture of the mineral paratacamite,  $Cu_2(OH)_3Cl$ , and lesser amounts of the monoclinic modification of gerhardtite,  $Cu_2(NO_3)(OH)_3$ . The core consists of elemental copper and some cuprite,  $Cu_2O$ .

It is of course possible that this copper is from man-made material and represents pieces of electric wire, copper rods, and so forth. However, this seems less probable than a natural occurrence. Palache and others (1944, p. 101) report copper from the Triassic sandstones and basalts of Massachusetts and Connecticut and masses of copper, up to 200 pounds in weight, in the glacial drift near New Haven (9 on fig. 1). As the colored corundum and gahnite of the beach sand probably came from the borders of the Connecticut Valley in western Massachusetts, it seems more reasonable for the copper to have come from there than for it to be an adventitious artifact. The reasoning on which this judgment is based is that the constant on-beach-off-beach movement of sand combined with the longshore transport, that is characteristic of the wave-swept beach at Nashaquitsa, has the effect of rapidly dispersing to an extremely dilute concentration any fragmented contamination (such as a mass of wire broken down by corrosion to sand-size particles). The probability of finding two grains in a grab sample taken from the face of the beach in the deserted winter season seems small indeed.

**REFERENCES**

- Adams, J. H., 1870, Notice of asbestos and corundum with other minerals at Pelham, Mass.: *Am. Jour. Sci.*, ser. 2, v. 49, p. 271-272.
- Cassidy, W. A., and others, 1964, Cosmic dust: *New York Acad. Sci. Ann.*, v. 119, 368 p.
- Crozier, W. D., 1960, Black, magnetic spherules in sediments: *Jour. Geophys. Research*, v. 65, p. 2971-2977.
- 1962, Five years of continuous collection of black, magnetic spherules from the atmosphere: *Jour. Geophys. Research*, v. 67, p. 2543-2548.
- Dana, A. G., 1887, On the gahnite of Rowe, Mass.: *Am. Jour. Sci.*, ser. 3, v. 29, p. 455-456.
- Emerson, B. K., 1898, Geology of old Hampshire County, Mass. comprising Franklin, Hampshire, and Hampden Counties: *U.S. Geol. Survey Mon.* 29, 790 p.
- 1902, Note on corundum and a graphitic essonite from Barkhamsted, Conn.: *Am. Jour. Sci.*, ser. 4, v. 14, p. 234-236.
- 1917, Geology of Massachusetts and Rhode Island: *U.S. Geol. Survey Bull.* 597, 289 p.
- Flint, G. M., 1908, Gahnite from Charlemont, Mass.: *Am. Jour. Sci.*, ser. 4, v. 26, p. 584.
- Fredriksson, K., and Martin, L. R., 1963, The origin of black spherules found in Pacific islands, deep-sea sediments, and Antarctic ice: *Geochim. Cosmochim. Acta*, v. 27, p. 245-248.

- Handy, R. L., and Davidson, D. T., 1953, On the curious resemblance between fly ash and meteoritic dust: *Iowa Acad. Sci., Proc.* v. 60, p. 373-379.
- Hodge, P. W., and Wright, F. W., 1964, Studies of particles for extraterrestrial origin, pt. 2—A comparison of microscopic spherules of meteoritic and volcanic origin: *Jour. Geophys. Research*, v. 69, p. 2449-2454.
- Hodge, P. W., Wright, F. W., and Langway, C. C., Jr., 1964, Studies of particles for extraterrestrial origin, pt. 3—Analyses of dust particles from polar ice deposits: *Jour. Geophys. Research*, v. 69, p. 2919-2931.
- Kaye, C. A., 1964a, Upper Cretaceous to Recent stratigraphy of Martha's Vineyard, Mass. [abs.]: *Geol. Soc. America Spec. Paper* 76, p. 91.
- 1964b, Outline of Pleistocene geology of Martha's Vineyard, Massachusetts, in *Geological Survey Research 1964*: U.S. Geol. Survey Prof. Paper 501-C, p. C134-C139.
- Langway, C. C., Jr., and Marvin, U. B., 1964, Some characteristics of black spherules: *New York Acad. Sci. Ann.*, v. 119, p. 205-223.
- Milner, H. B., Ward, A. M., and Higham, Frank, 1962. *Sedimentary petrography*, 4th ed.: New York, The Macmillan Co., v. 2, 715 p.
- Morrill, Philip, and Chaffee, R. G., 1957, Vermont mines and mineral localities, pt. 1—Southern Vermont: Hanover, N. H., Dartmouth Coll. Mus., 43 p.
- Morrill, Philip, and others, 1958, Maine mines and minerals, western Maine: Naples, Maine, Dilligham Nat. History Mus., 80 p.
- Palache, Charles, Berman, Harry, and Frondel, Clifford, 1944, The system of mineralogy of James Dwight Dana and Edward Salisbury Dana, Yale University 1837-1892, 7th ed., v. 1—Elements, sulfides, sulfosalts, oxides: New York, John Wiley and Sons, Inc., 834 p.
- Pratt, J. H., 1906, Corundum and its occurrence and distribution in the United States: *U.S. Geol. Survey Bull.* 269, 175 p.
- Thiel, Edward, and Schmidt, R. A., 1961, Spherules from the Antarctic ice cap: *Jour. Geophys. Research*, v. 66, p. 307-310.
- Trask, P. D., 1930, Mechanical analysis of sediments by centrifuge: *Econ. Geology*, v. 25, p. 581-599.
- Wright, F. W., Hodge, P. W., and Langway, C. C., Jr., 1963, Studies of particles for extraterrestrial origin, pt. 1—Chemical analyses of 118 particles: *Jour. Geophys. Research*, v. 68, p. 5575-5587.



## ZEOLITIC AUTHIGENESIS OF TUFFS IN THE RICARDO FORMATION, KERN COUNTY, SOUTHERN CALIFORNIA

By RICHARD A. SHEPPARD and ARTHUR J. GUDE 3d,  
Denver, Colo.

*Abstract.*—Vitric tuffs in the Ricardo Formation of the El Paso Mountains are altered to clinoptilolite, opal, and (or) montmorillonite. The pattern of alteration indicates that the alteration was accomplished by subsurface meteoric water after the formation was tilted northwestward. A comparison of chemical analyses indicates that the formation of clinoptilolite from rhyolitic glass involves mainly gains of  $H_2O$  and  $CaO$  and losses of  $SiO_2$  and  $K_2O$ .

The Ricardo Formation of Pliocene age is well exposed in the El Paso Mountains of south-central California, where it consists mainly of fluvatile and lacustrine sedimentary rocks. Lava flows and volcanic breccias are locally common, particularly in the lower half of the formation. The formation has a maximum thickness of 7,000 feet and dips  $15^\circ$  to  $20^\circ$  N.W. (Dibblee, 1952). Near the middle of the formation in member 4 of Dibblee (1952) are several well-bedded units of white to light-gray tuff. The thickest and most continuous of these tuffs has been mined for pumicite on the west side of Last Chance Canyon (Chesterman, 1956, p. 68) where it is free of alteration. Only this conspicuous tuff was examined in detail. The other tuffaceous units, stratigraphically below and above this tuff, were examined in a reconnaissance fashion.

Excellent exposures of the conspicuous tuff along the east face of Red Buttes (fig. 1) afford the opportunity to study the stages of alteration from freshest glass to complete replacement of vitric material by clinoptilolite and other diagenetic silicates. Analysis 1 (table 1) shows that even the freshest glass contains 5.96 weight percent total water and indicates that the glass has undergone much hydration. The individual authigenic silicate minerals cannot be identified in the field because of their very fine crystallinity. X-ray diffractometer analyses of bulk samples supplemented by thin-section examination were utilized in this study.

The authigenic silicate minerals can be readily identified from the diffractometer pattern (fig. 2).

The fresh tuff is white to light gray and 6 to 22 feet thick. It consists of individual beds that range from thin laminae to beds 30 inches thick. Crossbedding and channeling are locally present. The beds are generally fine grained, friable, and consist mainly of vitric material and 3 to 10 percent fragmental crystals of sanidine, plagioclase ( $An_{14-16}$ ), quartz, and biotite. All these crystals are presumably pyrogenic. The vitric particles are mainly shards but include some small angular fragments of long-tube pumice. An analysis

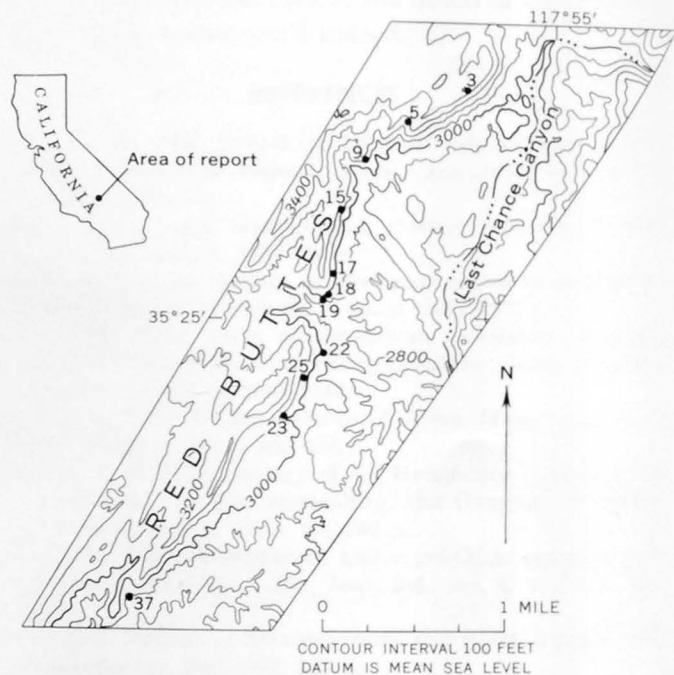


FIGURE 1.—Index map of Red Buttes area, Kern County, showing sampled localities (dots). X-ray analysis of samples given in table 2.

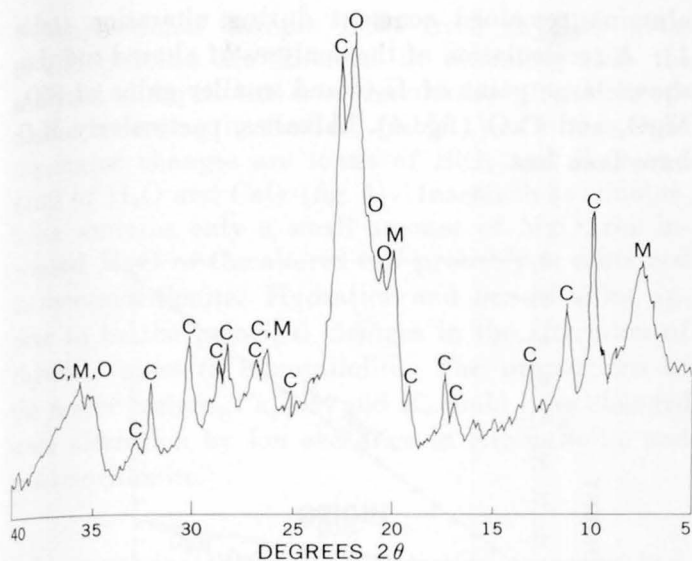


FIGURE 2.—Diffractometer pattern of altered tuff, showing principal authigenic silicate minerals. All diffractometer patterns of opal show peaks at 4.36A, 4.22A, 4.10A, and 2.52A. Radiation is  $\text{CuK}\alpha$  ( $\lambda=1.5417\text{A}$ ). C, clinoptilolite; M, montmorillonite; O, opal.

(table 1, No. 1) of the fresh tuff shows that it is rhyolitic in composition.

#### DESCRIPTION OF ALTERED TUFF

Altered tuff is readily distinguished from fresh tuff in the field. The altered tuff has a conchoidal fracture (fig. 3), earthy rather than vitreous luster, and greater hardness. Color is the least distinguishing feature, but generally the zeolitized tuff is white or very light pink. The vitroclastic texture and primary sedimentary structures are well preserved, although no glass remains. Pyrogenic crystals in the tuff are unaltered. Thin lenses and irregular segregations of light-gray opal or opal-rich tuff occur in the upper and lower parts of altered tuff. The lenses are sub-parallel to bedding and have irregular, gradational contacts.

The transition between fresh tuff and completely altered tuff is gradational through a vertical distance of approximately 250 feet. Table 2 shows the vertical variation in authigenic silicate minerals from fresh vitric tuff to completely altered tuff. The completely altered tuff consists mainly of clinoptilolite, but the less altered tuff generally consists of varying amounts of clinoptilolite, opal, montmorillonite, and relict glass. The upper and lower stratigraphic parts of the tuff are generally more altered than the middle part. Where alteration is only slight, the middle part is unaltered. Even though the tuff is slightly altered at an elevation of 3,165 feet, the alteration is not obvious in outcrop except at elevations lower than 3,000 feet.

TABLE 1.—Chemical analyses and chemical comparison of fresh tuff, altered tuff, and clinoptilolite

Constituent	Analysis (weight percent)										
	1		2			3			4		
	a	a	b	c	a	b	c	a	b	c	
$\text{SiO}_2$ .....	72.49	68.98	73.77	+1.28	68.92	74.10	+1.61	68.11	65.15	-7.34	
$\text{Al}_2\text{O}_3$ .....	11.87	11.10	11.87	.00	11.04	11.87	.00	12.41	11.87	.00	
$\text{Fe}_2\text{O}_3$ .....	.63	.97	1.04	+.41	.95	1.02	+.39	.77	.74	+.11	
$\text{FeO}$ .....	.14	.04	.04	-.10	.04	.04	-.10	.00	.00	-.14	
$\text{MgO}$ .....	.13	1.37	1.46	+1.33	1.51	1.62	+1.49	.19	.18	+.05	
$\text{CaO}$ .....	.57	.94	1.00	+.43	1.10	1.18	+.61	1.78	1.70	+1.13	
$\text{Na}_2\text{O}$ .....	2.46	1.75	1.87	-.59	1.46	1.57	-.89	2.39	2.29	-.17	
$\text{K}_2\text{O}$ .....	5.39	1.77	1.89	-3.50	1.54	1.66	-3.73	3.86	3.69	-1.70	
$\text{H}_2\text{O}^+$ .....	5.44	4.83	5.16	-.28	4.70	5.05	-.39	5.01	4.79	-.65	
$\text{H}_2\text{O}^-$ .....	.52	7.67	8.20	+7.68	8.23	8.85	+8.33	4.84	4.63	+4.11	
$\text{TiO}_2$ .....	.12	.14	.15	+.03	.14	.15	+.03	.03	.03	-.09	
$\text{P}_2\text{O}_5$ .....	.02	.03	.03	+.01	.03	.03	+.01	.02	.02	.00	
$\text{MnO}$ .....	.05	.14	.15	+.10	.10	.11	+.06	.01	.01	-.04	
$\text{CO}_2$ .....	.01	.02	.02	+.01	.00	.00	-.01	.....	.....	.....	
Cl.....	.06	.01	.01	-.05	.01	.01	-.05	.....	.....	.....	
F.....	.03	.04	.04	+.01	.05	.05	+.02	.....	.....	.....	
Total.....	99.93	99.80	106.70	+6.77	99.82	107.31	+7.38	99.42	95.10	-4.73	

1. Fresh vitric tuff; serial No. D100515. Analyst: E. S. Daniels. Mineralogy: glass ( $n=1.497$ ) and approximately 4 percent crystals (sanidine, plagioclase, quartz, and biotite). Locality: No. 3 (fig. 1), SE $\frac{1}{4}$ SW $\frac{1}{4}$  sec. 5, T. 29 S., R. 38 E., Kern County, Calif.
  2. Altered tuff, middle part; serial No. D100516. Analyst: E. S. Daniels. Mineralogy: clinoptilolite, 30 percent; opal, 20 percent; montmorillonite, 30 percent; glass, 20 percent. Locality: No. 19 (fig. 1), NW $\frac{1}{4}$ NE $\frac{1}{4}$  sec. 18, T. 29 S., R. 38 E., Kern County, Calif.
  3. Altered tuff, upper part; serial No. D100517. Analyst: E. S. Daniels. Mineralogy: clinoptilolite, 30 percent; opal, 20 percent; montmorillonite, 40 percent; glass, 10 percent. Locality: No. 19 (fig. 1), NW $\frac{1}{4}$ NE $\frac{1}{4}$  sec. 18, T. 29 S., R. 38 E., Kern County, Calif.
  4. Clinoptilolite; serial No. D100245. Analyst: E. L. Munson. Separated from altered vitric tuff of member 2 of Dibblee (1952). Locality: NW $\frac{1}{4}$ SE $\frac{1}{4}$  sec. 17, T. 29 S., R. 38 E., Kern County, Calif. (Sheppard and others, 1965).
- a. Uncorrected analysis.  
b. Recalculated, assuming  $\text{Al}_2\text{O}_3$  content of analysis 1a.  
c. Gains (+) and losses (-) in weight percent; differences between "b" and analysis 1a, assuming no gain or loss of  $\text{Al}_2\text{O}_3$ .

TABLE 2.—Mineralogic composition of tuff estimated from X-ray diffractometer patterns

Sample (fig. 1)	Elevation (feet above sea level)	X-ray analysis (parts of ten)			
		Glass	Clinoptilolite	Opal	Montmorillonite
3-----	3,480	10	-----	-----	-----
5-----	3,265	10	-----	-----	-----
9-----	3,165	9	Tr.	1	Tr.
15-----	3,120	9	1	-----	Tr.
23-----	3,090	10	-----	-----	-----
25-----	3,040	9	Tr.	1	Tr.
17-----	3,025	8	1	1	Tr.
22-----	2,995	Tr.	7	-----	3
18 (upper part)-----	2,945	2	5	3	2
18 (middle part)-----	2,945	7	2	1	Tr.
18 (lower part)-----	2,945	3	6	1	Tr.
19 (upper part)-----	2,910	1	3	2	4
19 (middle part)-----	2,910	2	3	2	3
37-----	2,865	-----	8	2	Tr.

Thin-section examination of altered tuff shows that clinoptilolite occurs as pseudomorphs of the larger vitric particles and in the finely crystalline matrix associated with montmorillonite and presumably opal. Each pseudomorph consists of many randomly oriented prismatic or tabular crystals of clinoptilolite. Petrographic study of fresh tuff indicates that the finely crystalline matrix of altered tuff originally consisted of fine vitric material. The vitroclastic texture of the matrix apparently was not preserved by the authi-



FIGURE 3.—Altered tuff, showing conchoidal fracture. Bedding dips toward left of photograph.

genic minerals. Fresh glass, when present, generally is found only in the interiors of the larger particles. The birefringence of clinoptilolite is very low, and the mean refractive index ranges from 1.475 to 1.479 ( $\pm 0.001$ ).

Montmorillonite occurs in the matrix and as a thin film surrounding shards pseudomorphed by clinoptilolite. These occurrences suggest that the montmorillonite formed early, assuming it was derived directly from glass.

Reconnaissance of other tuffaceous units in the Ricardo Formation, both stratigraphically below and above this tuff, shows that in general the pattern of alteration is similar to that described above. Tuffaceous units throughout the formation are generally fresh above an elevation of 3,000 feet but altered below that elevation. The "surface" separating the two phases apparently is uneven, however, and has a local relief of at least 500 feet. For example, a lapilli tuff stratigraphically lower in the section and exposed along the south side of Last Chance Canyon in the NW1/4 sec. 9, T. 29 S., R. 38 E., has been altered to clinoptilolite, opal, and montmorillonite at an elevation of 3,530 feet.

#### CHEMICAL CHANGES IN ZEOLITIC ALTERATION

Chemical analyses of fresh and altered tuff are given in table 1. Analyses 2 and 3 are of altered tuff that consists of clinoptilolite, opal, montmorillonite, and relict glass. Analysis 4 is of a relatively pure clinoptilolite that was separated from an altered tuff in the lower part of the section by a heavy-liquid mixture of bromoform and *n,n*-dimethylformamide (Sheppard and others, 1965).

Approximate changes in chemical composition from fresh to altered tuff are inferred by assuming that

alumina remained constant during alteration (table 1). A recalculation of the analyses of altered tuff then shows large gains of  $H_2O$  and smaller gains of  $SiO_2$ ,  $MgO$ , and  $CaO$  (fig. 4). Alkalies, particularly  $K_2O$ , have been lost.

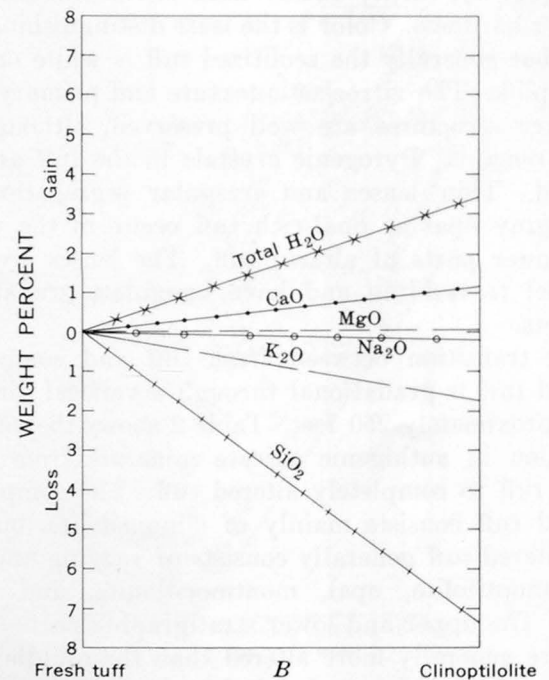
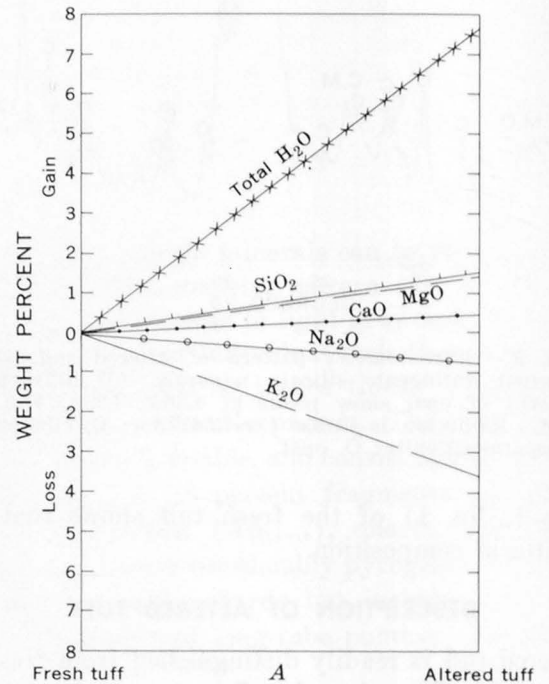


FIGURE 4.—Chemical comparison between A, fresh tuff and altered tuff and B, fresh tuff and clinoptilolite. Altered tuff is average of analyses 2 and 3, table 1; clinoptilolite, analysis 4, table 1.

Compositional changes from fresh rhyolitic glass to clinoptilolite are inferred by assuming that the analyzed clinoptilolite is representative of the clinoptilolite occurring in the tuff (table 1). On this basis the major changes are losses of  $\text{SiO}_2$  and  $\text{K}_2\text{O}$  and gains of  $\text{H}_2\text{O}$  and  $\text{CaO}$  (fig. 4). Inasmuch as clinoptilolite contains only a small amount of  $\text{MgO}$ , the increased  $\text{MgO}$  of the altered tuff probably is contained in montmorillonite. Hydration and loss of silica appear to be the principal changes in the alteration of rhyolitic glass to clinoptilolite. The proportions of the major cations, Ca, Na, and K, could have changed since alteration by ion exchange in clinoptilolite and montmorillonite.

#### ORIGIN

Inasmuch as the zeolitic alteration transects bedding, the alteration probably occurred after the Ricardo Formation was tilted. The surface separating fresh glass from zeolitized glass is nearly horizontal although locally uneven. There is no evidence to indicate that hydrothermal solutions were responsible for the alteration. Typical hydrothermal minerals such as alunite, kaolinite, and fluorite are absent. The regional extent of the alteration and its restriction to lower elevations is strong evidence against hydrothermal alteration. Authigenic minerals are not localized within or along fractures as might be expected if the tuffs were hydrothermally altered. Evidently the differences in chemical composition and mineralogy of tuffs above and below the nearly horizontal surface were produced by subsurface water. The preexisting topography during alteration probably controlled the configuration of the surface, but data are lacking as to the nature of the topography. The unevenness of

the surface may be in part due to local variations in impermeability.

Studies of Quaternary lakes (Hay and Moiola, 1964) and experimental work (Hemley, 1961) indicate that zeolites form in an environment of moderate to high pH and high salinity. Hay (1963, p. 239-244) proposed solution and hydrolysis of vitric material by subsurface water to account for the zeolitic diagenesis of tuff and claystone in the lower part of the Tertiary John Day Formation in central Oregon. A similar mechanism probably accounts for the zeolization of tuffs in the Ricardo Formation. The subsurface water which originated as meteoric water increased in pH and concentration of alkalis as it moved downward through the formation. The early alteration of rhyolitic glass to montmorillonite also would increase the pH and salinity of the water, thereby providing a chemical environment more favorable for the formation of zeolites (Hay, 1963, p. 240).

#### REFERENCES

- Chesterman, C. W., 1956, Pumice, pumicite, and volcanic cinders in California: California Div. Mines Bull. 174, p. 3-97.
- Dibblee, T. W., Jr., 1952, Geology of the Saltdale quadrangle, California: California Div. Mines Bull. 160, p. 7-43.
- Hay, R. L., 1963, Stratigraphy and zeolitic diagenesis of the John Day Formation of Oregon: California Univ. Pubs. Geol. Sciences, v. 42, p. 199-262.
- Hay, R. L., and Moiola, R. J., 1964, Authigenic silicate minerals in three desert lakes of eastern California [abs.]: Geol. Soc. America Spec. Paper 76, p. 76.
- Hemley, J. J., 1961, Alteration studies in the systems  $\text{Na}_2\text{O}-\text{Al}_2\text{O}_3-\text{SiO}_2-\text{H}_2\text{O}$  and  $\text{K}_2\text{O}-\text{Al}_2\text{O}_3-\text{SiO}_2-\text{H}_2\text{O}$  [abs.]: Geol. Soc. America Spec. Paper 68, p. 196.
- Sheppard, R. A., Gude, A. J., 3d, and Munson, E. L., 1965, Chemical composition of diagenetic zeolites from tuffaceous rocks of the Mojave Desert and vicinity, California: Am. Mineralogist, v. 50, p. 244-249.



## THORIUM-BEARING MICROCLINE-RICH ROCKS IN THE SOUTHERN CABALLO MOUNTAINS, SIERRA COUNTY, NEW MEXICO

By MORTIMER H. STAATZ, JOHN W. ADAMS,  
and NANCY M. CONKLIN, Denver, Colo.

*Abstract.*—Anomalously radioactive rocks, consisting chiefly of brick-red microcline, are found as elongate bodies as much as 300 feet long in quartz monzonite in the southern Caballo Mountains. These rocks, believed to be comparable in origin to fenites, are thought to have been produced by the reaction of alkalic solutions on the quartz monzonite. The solutions probably originated with unspecified alkalic rocks located at some unknown depth or distance from the microcline-rich bodies. Most of the radioactivity of the microcline-rich bodies is due to thorium contained in thorite. Uranium is present locally in uranophane, and the rare-earth fluorocarbonate, bastnaesite, was found in one deposit.

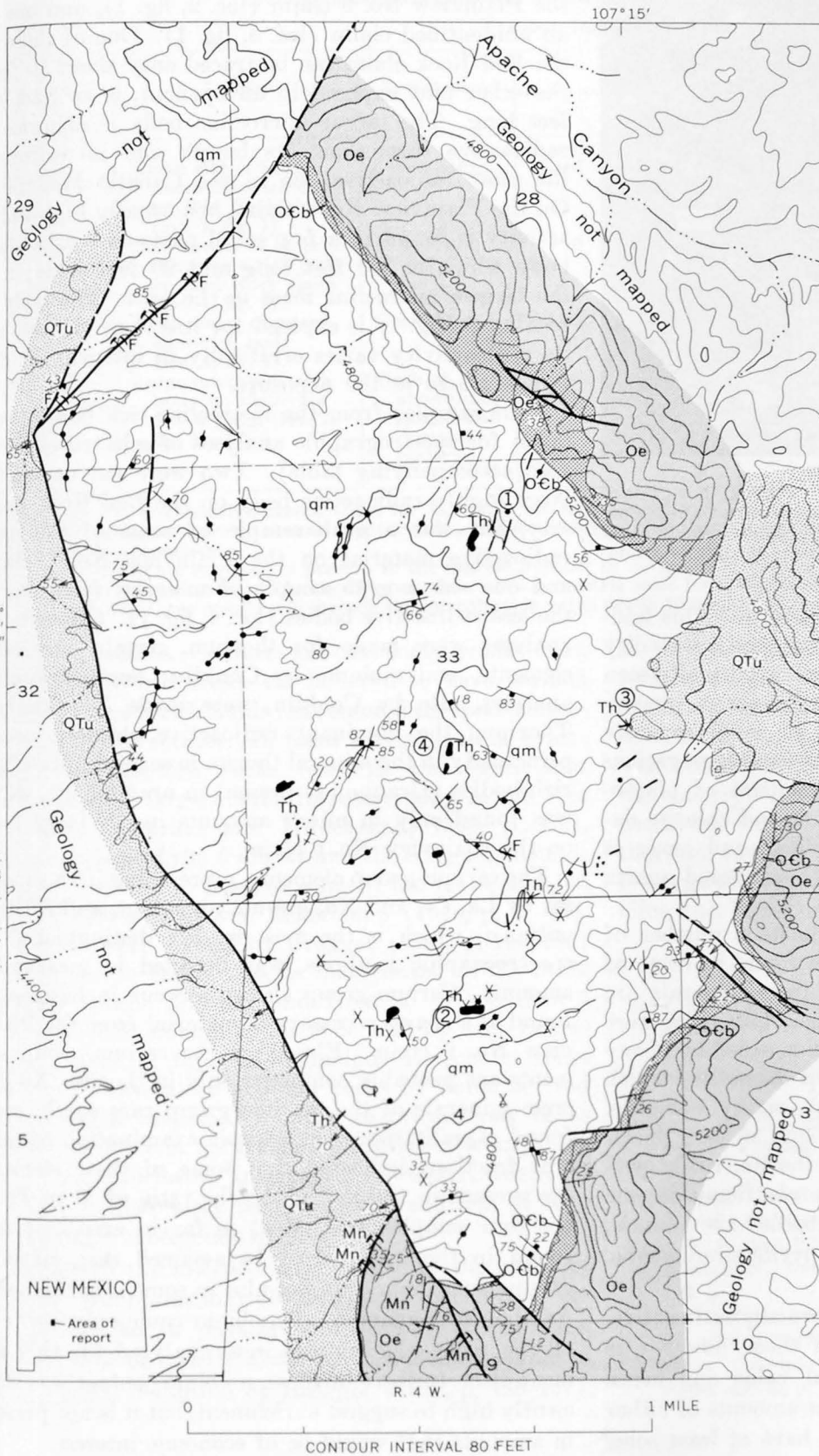
Radioactive syenite dikes containing thorium and uranium were reported by Boyd and Wolfe (1953, p. 141) in the southern Caballo Mountains. As this type of thorium occurrence appeared unique, Staatz and Adams visited this area in September 1964 and studied and mapped the deposits (fig. 1). Samples were taken of the deposits for thin sections, spectrographic analyses, and mineralogic examination. Subsequent study of these materials and their occurrence has led us to the conclusion that these so-called "syenite dikes" are really metasomatic bodies composed chiefly of microcline.

These unusual microcline-rich bodies occur within an area of about 3 square miles in the southern part of the Caballo Mountains (fig. 1). The center of this area is approximately  $2\frac{1}{2}$  miles southeast of the Caballo dam. More than 45 such bodies were noted in this area. They occur in a coarse-grained quartz monzonite that is cut by many irregular dikes of fine-grained quartz monzonite and small dikes of perthite-quartz pegmatite. Two small diabase dikes also occur in the mapped area (fig. 1). These rocks, all of probable Precambrian age, are bounded on the northeast and southeast side by the Bliss Sandstone of Cambrian

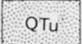
and Ordovician age and the El Paso Formation of Ordovician age (fig. 1). The stratigraphy of the Paleozoic rocks of this area is described by Kelly and Silver (1952, p. 33-56). To the east and west the Precambrian rocks are bounded by clastic rocks of Tertiary and Quaternary age.

The microcline-rich bodies are elongate and range from a few feet to 300 feet in length and from less than an inch to 20 feet in width. Although from the surface, many appear to be dikelike, exposures of several of these bodies in small cuts indicate that some are pipelike in shape. These bodies trend N.  $10^{\circ}$  E. to N.  $85^{\circ}$  E.; in the northern part of the area they trend generally north-northeast and in the southern part generally east-northeast (fig. 1). Dips are commonly steep. Where the contacts occur along small shears, they are sharp (fig. 2), but in most places they are irregular, and small apophyses into the quartz monzonite are common. Many of the contacts between the microcline masses and quartz monzonite are gradational and the texture of the quartz monzonite can be traced into the marginal part of the feldspar-rich bodies.

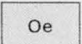
The composition of the microcline-rich bodies varies considerably in detail, depending on the completeness of the metasomatism of the country rock, which is a fine- and coarse-grained quartz monzonite consisting principally of microcline, plagioclase, and quartz. The two feldspars are approximately equal in abundance. Mafic minerals make up from about 1 to 20 percent of the rock, and the principal mafic mineral is chlorite; muscovite, biotite, and sphene occur in minor amounts. In most places during metasomatism these minerals were replaced or partly replaced by a turbid brick-red microcline whose turbidity and color are caused by many tiny specks of included hematite. The micro-




EXPLANATION

- 


Undifferentiated alluvium, sandstone, siltstone, and shale


TERTIARY AND QUATERNARY
- 


El Paso Formation

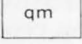
ORDOVICIAN
- 

Bliss Sandstone

CAMBRIAN AND ORDOVICIAN
- 

Microcline-rich rocks
- 

Diabase dike
- 


Pegmatite
- 

Quartz monzonite

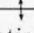
Coarse-grained quartz monzonite cut by irregular dikes of fine-grained quartz monzonite

PRECAMBRIAN

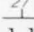
- Contact

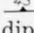
Dashed where approximately located
- 

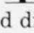
Fault, showing dip


Dashed where approximately located
- 

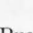
Anticline

Showing trace of axial plane
- 

Strike and dip of beds
- 

Strike and dip of foliation
- 

Strike and dip of joint
- 

Mine
- 

Prospect
- F, fluorite

Th, thorium

Mn, manganese
- ②

Locality number referred to in text

FIGURE 1.—Geologic map of the thorium district in the southern Caballo Mountains, Sierra County, N. Mex. Geology by M. H. Staatz and J. W. Adams, 1964. Base from U.S. Geological Survey topographic quadrangle maps. Datum is mean sea level.



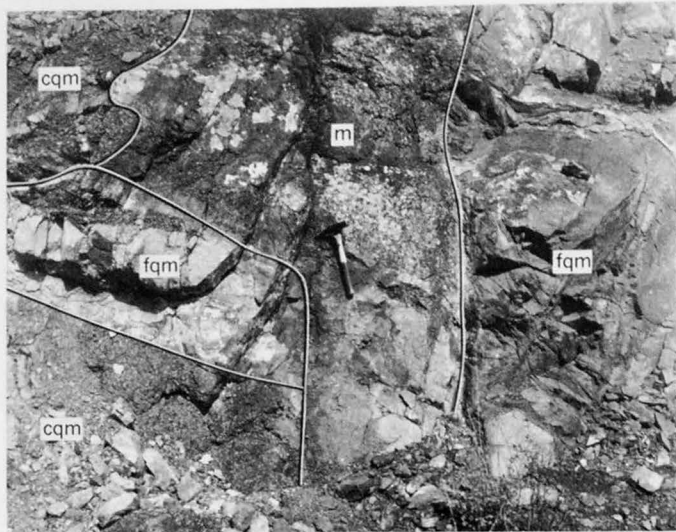


FIGURE 2.—Microcline-rich body (m) cutting fine-grained (fqm) and coarse-grained (cqm) quartz monzonite. Contact on right of the feldspar-rich body follows small shear and is sharp and fairly straight: contact on left is gradational and irregular.

cline has highly irregular grain boundaries. This feldspar is identified by its X-ray pattern, as the turbidity masks most of the crosshatch twinning normally seen in microcline. In a few places, however, a quartz-chlorite rock is produced either as small separate bodies in the quartz monzonite or as local segregations in the microcline-rich rock. The amount of plagioclase, microcline, and original quartz and chlorite depends on the degree of metasomatism, and hence is greater adjacent to the contact with unaltered quartz monzonite.

In addition to feldspar and chlorite a number of erratically distributed minerals are found in some of these microcline bodies. Most of these minerals are not recognizable in hand specimen, but they were recovered in mineral separates and identified by X-ray diffraction. The most abundant is hematite, which occurs both as specularite and as earthy hematite. Magnetite and limonite are also found in most specimens. Less common minerals are thorite, rutile, yellow muscovite, and apatite. Minerals found in one or only a few of the microcline bodies are anatase, barite, bastnaesite, calcite, fluorite, pyrite, uranophane, and zircon.

All the microcline bodies are abnormally radioactive. The radioactivity value of most of them, however, is only several times the background value and hence the bodies contain only insignificant amounts of either thorium or uranium. Four bodies have at least some parts in which the radioactivity value is greater than 40 times the background value. Two of these bodies are on the Red Rock claim (locality 1, fig. 1), one on

the Plainview No. 6 claim (loc. 2, fig. 1), and one on an unidentified claim (loc. 3, fig. 1). One of those on the Red Rock claim can be traced only about 10 feet; the other one, exposed in an open-cut, is at least 130 feet long. The larger microcline body is abnormally radioactive throughout its length and is uniformly the most radioactive one in the Caballo Mountains. On the Plainview No. 6 claim, abnormally high radioactivity is found in a few small parts of a microcline body which is 300 feet long and 20 feet wide; it is the largest microcline mass in the area. The body at locality 3 (fig. 1) is exposed for less than 10 feet, and its radioactivity varies erratically in intensity at different places in the exposure.

Four samples from the microcline-rich bodies were taken for spectrographic analyses of selected elements (see accompanying table). Two were cut across the large highly radioactive body on the Red Rock property, one was a grab sample of some of the more radioactive material on the Plainview No. 6 claim, and one was a grab sample of material from one of the less radioactive bodies (loc. 4, fig. 1). Quantitative analyses were made for thorium, certain rare-earth elements, and niobium by Conklin; semiquantitative analyses, also by Conklin, were made for uranium. Thorium, the dominant radioactive element, occurs principally in the mineral thorite in several microcline-rich bodies. Uranium is present in uranophane, which was found only in minor amounts in the large body on the Plainview No. 6 claim.

The cerium-group elements, represented in the analyses by La, Ce, and Nd, are not abundant, and of these only La, which is the most readily distinguished by spectrographic methods, was detected in measurable amounts. Cerium-group elements occur in bastnaesite found as a sparse accessory in material from the Plainview No. 6 claim. Elsewhere the cerium-group elements are probably contained only in thorite. No discrete minerals of the yttrium-group rare earths were found. Qualitative spectroscopic examination of mineral fractions indicated that some of these elements are present in thorite, but as the ratio of Y to Th in the four samples (see table) is far in excess of that found in thorite, it must be assumed that yttrium-group elements are present also in some other mineral. As abnormal amounts of niobium commonly occur in alkalic rocks, the samples were analyzed for this element also. In three of these, niobium content was sufficiently high to suggest enrichment, but it is not present in amounts that would be of economic interest.

From our investigation of these radioactive microcline-rich bodies we conclude that they are not intrusive syenites, but rather are metasomatically altered

*Spectrographic analyses of microcline-rich bodies from the Caballo Mountains*

[Analyst, Nancy Conklin]

Sample No.	Location	Type of sample	Minor elements (weight percent)							
			Th	La	Ce	Nd	Yb	Y	Nb	U
RR-1-64-----	North end of large microcline-rich body on Red Rock claim (loc. 1, fig. 1).	6-inch chip----	0.44	0.012	<0.05	<0.05	0.011	0.11	0.013	0.03
RR-2-64-----	Near center of large microcline-rich body on Red Rock claim (loc. 1, fig. 1).	15-inch chip---	.16	<.007	<.05	<.05	.0060	.040	.011	0
RR-5-64-----	Near center of microcline-rich body (loc. 4, fig. 1).	Grab-----	<.05	<.007	<.05	<.05	.0024	.016	.0022	0
RR-6-64-----	Large microcline-rich body on Plainview No. 6 claim (loc. 2, fig. 1).	Grab of abnormally radioactive dump material.	.086	.017	<.05	<.05	.0052	.037	.0081	.07

All analyses are quantitative except those for U, which are semiquantitative.

Quantitative analyses have an overall accuracy of  $\pm 15$  percent except that they are less accurate near limits of detection, where only one digit is reported

Uranium analyses are reported in percent to the nearest number in the series 1, 0.7, 0.5, 0.3, 0.2, 0.15, and 0.1, and so forth, which represent approximate midpoints of group data on a geometric scale for a 6-step method of analysis. The assigned group or midpoint for these results will include the quantitative value about 30 percent of the time.

quartz monzonite. Contacts are commonly gradational, and these hybrid rocks are believed to have formed from potassium-rich fluids that entered the quartz monzonite along fractures. In hand specimen these brick-red microcline-rich rocks resemble the fenite that surrounds the large alkalic intrusive body in the Wet Mountains (Parker and Hildebrand, 1963, p. E9). The turbidity of the feldspar and the irregular boundaries are similar to those of some of the fenite at Alnö Island described by von Eckermann (1948, p. 27-43).

Fenites were defined by Brögger (1921, p. 156-166) as leucocratic contact rocks that consist of 70 to 90 percent alkalic feldspar and from 25 to less than 5 percent mafic minerals. As redefined by von Eckermann (1948, p. 13), fenites include all contact rocks formed by alteration of older rocks by fluids derived from alkalic magmas. Fenites, therefore, may be as highly variable in nature as the wallrocks from which they were formed. In general, however, fenite is formed from country rock by major addition of  $K_2O$  and a major subtraction of  $SiO_2$ .

Although the microcline-rich rocks of the southern Caballo Mountains may closely resemble known fenites of some areas in physical and chemical appearance, they cannot be strictly classified as fenite according to the original definition by Brögger (1921, p. 156-157),

as they are not in contact with alkalic rocks. The lack of alkalic rock outcrops in the small area of Precambrian terrane in the southern Caballo Mountains does not mean, however, that some hidden alkalic body was not the source of the fluids which reacted with the country rock to form microcline-rich bodies. Furthermore, as alkalic rocks commonly have a high thorium, rare-earth, and niobium content, another tie is suggested between an alkalic source and the microcline-rich bodies of the Caballo Mountains.

## REFERENCES

- Boyd, F. S., and Wolfe, H. D., 1953, Recent investigations of radioactive occurrences in Sierra, Doña Ana, and Hidalgo Counties, New Mexico, in *New Mexico Geol. Soc. Guidebook 4th Field Conf., southwestern New Mexico*: p. 141-142.
- Brögger, W. C., 1921, *Die Eruptivgesteine des Kristianiagebietes*: Vidensk. Selsk. Kristiania Skr., 1920, v. 2, no. 9, 408 p.
- Eckermann, Harry, von, 1948, The alkaline district of Alnö Island: *Sveriges Geol. Undersökning, ser. Ca, no. 36*, 176 p.
- Kelly, V. C., and Silver, Caswell, 1952, *Geology of the Caballo Mountains*: New Mexico Univ. Pubs. in Geology, no. 4, 286 p.
- Parker, R. L., and Hildebrand, F. A., 1963, Preliminary report on alkalic intrusive rocks in the northern Wet Mountains, Colorado: Art. 181 in *U.S. Geol. Survey Prof. Paper 450-E*, p. E8-E10.



## VOLCANIC ORIGIN OF FLINT CLAY IN THE FIRE CLAY COAL BED, BREATHITT FORMATION, EASTERN KENTUCKY

By VICTOR M. SEIDERS, San Juan, P.R.

*Work done in cooperation with the Kentucky Geological Survey*

**Abstract.**—The flint-clay parting of the Fire Clay coal bed in the Breathitt Formation of eastern Kentucky is composed chiefly of kaolinite and sparse angular grains of quartz and sanidine. The mineralogy and texture indicate that the rock formed by alteration of volcanic ash in a coal swamp.

The Fire Clay coal bed in the Breathitt Formation of Pennsylvanian age contains a thin but persistent parting of flint clay. This parting is very extensive in eastern Kentucky, and also occurs in correlative beds in Tennessee, Virginia, and West Virginia (Huddle and Patterson, 1961, p. 1646). Near Hazard, Ky., where the flint clay was examined by the writer, it is generally 3 to 4 inches thick, rarely as much as 8 inches thick, and throughout eastern Kentucky is reported to be between 0 and 8 inches thick. It may occur immediately above, below, or within the coal bed but generally occurs within the lower third of the bed (Huddle and Paterson, 1961, p. 1646). Locally the flint clay is absent where the coal bed is present, and in some areas both flint clay and coal are absent. The writer has found flint clay only where it is associated with coal or carbonaceous shale. The flint clay is light to dark gray, locally brownish gray, and commonly shows a slightly mottled appearance on fresh surfaces. The rock has a Mohs scale hardness of about 3 and breaks readily with a hackly to conchoidal fracture. It is nonfissile and generally shows no conspicuous bedding features except for rare well-graded 1/8- to 1-inch beds of silt- to fine-sand-size material. Well-preserved imprints of plant leaves, stems, and roots are abundant.

### PETROGRAPHY

In thin section the rock is seen to be composed of 0.5 to 4 percent of 0.1- to 0.5-mm grains of quartz and

sanidine in a groundmass of clay minerals. The quartz is unstrained and includes both sharply angular fragments and grains with crystal faces. Some grains have the smooth embayments and rounded corners (fig. 1) which are characteristic of volcanic quartz (Williams and others, 1954, fig. 50 B-C). Sanidine (small  $2V(-)$ ) occurs as irregular grains and well-formed lath-shaped crystals, some of which show 001 cleavage. Most grains are clear and unaltered, but some are partly to completely replaced by fine-grained kaolinite.

The clay mineral of a typical sample of flint clay was identified by P. D. Blackmon, U.S. Geological Survey, by X-ray diffraction as kaolinite. An unusual sample, notably softer than the normal flint clay, was found by H. A. Tourtelot, U.S. Geological Survey, to

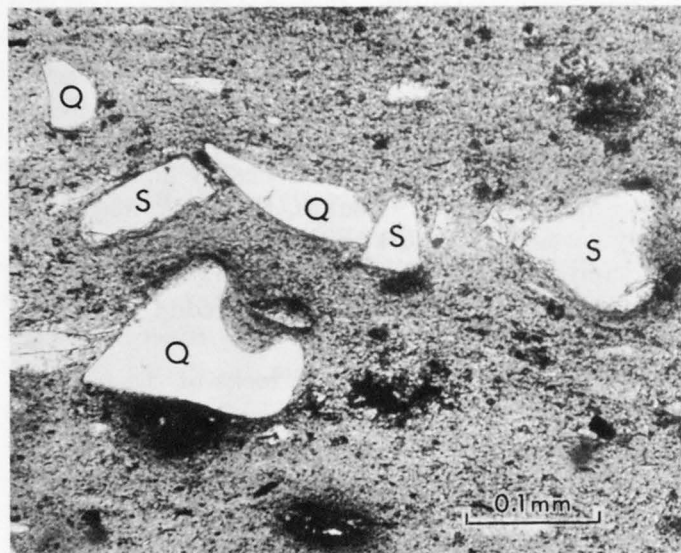


FIGURE 1.—Photomicrograph of flint clay, showing sanidine (S) and angular and embayed quartz grains (Q). Ordinary light.

contain illite and mixed-layer illite-montmorillonite in addition to kaolinite.

Examination of heavy minerals from one sample of flint clay by P. D. Blackmon showed only anatase, zircon, and rutile. Both rounded and euhedral zircon are present. Carbonaceous matter is present in variable amounts in most thin sections as irregular streaks or in well-preserved plant forms.

In thin sections of some samples the clay groundmass is uniformly cryptocrystalline to microcrystalline and appears nearly isotropic under crossed nicols. Other samples contain abundant angular to rounded globules of cryptocrystalline to coarsely crystalline kaolinite (fig. 2). In the groundmass of some samples are a few small vermicular crystals of kaolinite showing a good cleavage perpendicular to the direction of elongation. Such crystals are common in flint clays, and Stach (1950, p. 43-45) has suggested that they form directly by the alteration of feldspar. The origin of the vermicular kaolinite crystals in the Fire Clay flint clay is not known, but they do not seem to have formed directly from sanidine, because in all examples of partly altered sanidine the kaolinite is finely granular rather than vermicular.

#### ORIGIN

The origin of the flint-clay parting in the Fire Clay coal bed has puzzled geologists for many years because this thin uniform widely distributed bed contrasts sharply with the variable, discontinuous nature of most other sedimentary units of the coal measures. Although conclusive evidence was lacking, Ashley (1928, p. 63) was the first to suggest a volcanic origin; Huddle and Patterson (1961, p. 1646-1647) have shown that the wide distribution and unique character of the flint clay require an unusual origin. The Fire Clay flint clay, along with similar rocks from many parts of the world, was examined in polished section by Hoehne (1957), who believed that the quartz grains formed in place and concluded that these rocks originated by the alteration of clastic nonvolcanic parent sediments.

The volcanic origin of the Fire Clay flint clay is indicated by the presence of clearly clastic grains of sanidine and embayed quartz and the absence of any obviously nonvolcanic debris except carbonaceous matter. In specimens containing kaolinite globules, the poor sorting, the angularity of the quartz, sanidine, and some kaolinite grains, and the local presence of graded beds are all consistent with an origin as a water-laid tuff. The fact that the globules have been completely converted to kaolinite, whereas the quartz and sanidine have not, suggests that the globules origi-

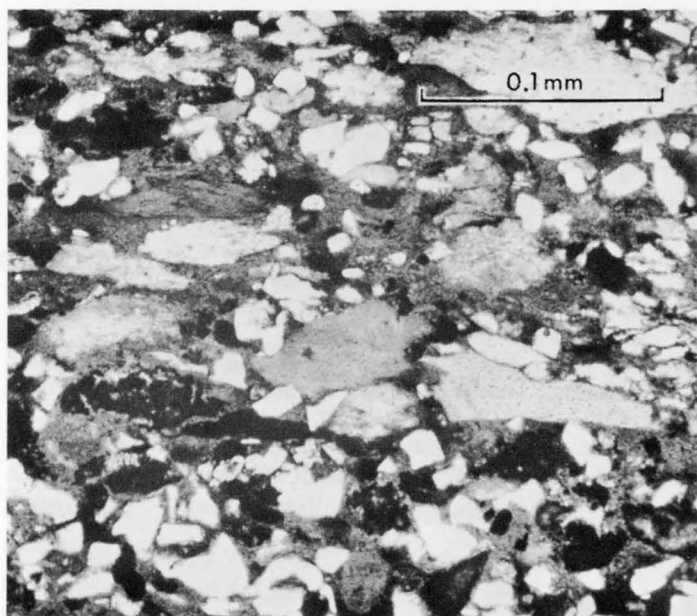


FIGURE 2.—Photomicrograph of flint clay, showing turbid kaolinite globules and clear quartz and sanidine grains.

nally were composed of very unstable material, probably volcanic glass.

Mineralogically, plastic underclay differs from flint clay in that it is richer in clay minerals other than kaolinite. According to some authors (Keller and others, 1954; Huddle and Patterson, 1961) both plastic clay and flint clay form by the in-place alteration of sediments in an acid environment, and flint clay represents the more advanced stage of such alteration. Huddle and Patterson (1961, p. 1655) also point out that although detrital feldspar is common in plastic underclay it generally is not preserved in flint clay. The presence of sanidine in the flint clay of the Fire Clay coal bed, therefore, seems anomalous. The explanation probably lies in the nature of the original materials; the alteration to flint clay was probably achieved because of the highly unstable nature of the original volcanic glass. Environmental conditions may have been no more severe than those which would produce plastic clay from a nonvitric sediment.

The angularity of most grains and the presence of the very delicate kaolinite "worms" indicate that the Fire Clay ash fall was altered to flint clay in place and cannot have originated by deposition of clay minerals derived from an intensively weathered source area as suggested by Schultz (1958) for many plastic underclays.

No other North American flint clay has been demonstrated to have formed from volcanic ash, but Francis (1961) has described kaolinitized tuff beds from the Carboniferous of Scotland that are very similar to the Fire Clay flint clay. He was able to recognize

all stages of alteration from volcanic glass to kaolinite and to trace the altered tuff beds into a nearby volcanic source area. The tonstein beds of western Europe (Stach, 1950; Scheere, 1957) are also very similar, but opinion is divided as to whether they formed from volcanic ash.

#### REFERENCES

- Ashley, G. H., 1928, Bituminous coal fields of Pennsylvania, pt. I: Pennsylvania Topog. and Geol. Survey, ser. 4, Bull. M-6, 241 p.
- Francis, E. H., 1961, Thin beds of graded kaolinized tuff and tuffaceous siltstone in the Carboniferous of Fife: Great Britain Geol. Survey Bull 17, p. 191-219.
- Hoehne, K., 1957, Tonstein in Kohlenflözen der Oststaaten von Nordamerika and Ostaustralien: Chemie der Erde, v. 19, p. 111-129.
- Huddle, J. W., and Patterson, S. H., 1961, Origin of Pennsylvanian underclay and related seat rocks: Geol. Soc. America Bull., v. 72, p. 1643-1660.
- Keller, W. D., Wescott, J. F., and Bledsoe, A. O., 1954, The origin of Missouri fire clays, in Swineford, Ada, ed., Clays and clay minerals: Second Natl. Conf. Clays and Clay Minerals Proc., Natl. Acad. Sci. - Natl. Research Council Pub 327, p. 7-46.
- Scheere, J., 1957, La petrologie des tonstein du Houiller belge: Soc belge geologie, paleontologie, et hydrologie Bull., v. 66, p. 300-317.
- Schultz, L. C., 1958, Petrology of underclays: Geol. Soc. America Bull., v. 363-402.
- Stach, E., 1950, Volcanic ash in coal swamps: Gulckauf, v. 86, p. 41-50. [In German.]
- Williams, Howell, Turner, F. J., and Gilbert, C. M., 1954, Petrography: San Francisco, Freeman and Co., 406 p.



## PREHNITE AND HYDROGARNET(?) IN PRECAMBRIAN ROCKS NEAR BOULDER, COLORADO

By CHESTER T. WRUCKE, Denver, Colo.

**Abstract.**—Prehnite and a hydrogarnet(?) occur as accessory minerals in several rocks of Precambrian age that crop out near Boulder, Colo. The principal host for these minerals is the Boulder Creek batholith, but gabbroic and dioritic masses intruded by the batholith also contain them. Both minerals form small lens-shaped masses in biotite. Prehnite is interpreted as having crystallized from CaO-rich deuteritic solutions that originated in the Boulder Creek batholith, but a metamorphic origin is possible. The hydrogarnet(?) may have formed from the prehnite later in the deuteritic period.

Prehnite and a mineral tentatively identified as a hydrogarnet occur as late accessory constituents in rocks of Precambrian age that crop out on the east flank of the Front Range near Boulder, Colo. (fig. 1). These rocks are the Boulder Creek Granodiorite (Lovering and Goddard, 1950; Wells and others, 1964) and rocks of gabbroic to dioritic composition intruded by the granodiorite and labelled "metagabbro" on figure 1. The prehnite and hydrogarnet form small lens-shaped masses in biotite, a somewhat unusual occurrence, as is the presence of hydrogarnet in a granitic rock. These minerals may have crystallized from deuteritic solutions that originated in the granodiorite, but a metamorphic origin is possible.

The lens-shaped aggregates of prehnite average about 0.04 by 0.35 mm in size. These lenses commonly comprise several thin gently curving bands. Biotite lamellae generally pass smoothly around the lenses as though the growing prehnite had pushed them aside (fig. 2). Moreover, optical directions in the host and in the outer parts of the lenses suggest epitaxial growth of prehnite on biotite.

Identification of the prehnite was made from X-ray powder patterns (by Theodore Botinelly) and from optical data. Measurements of the optic axial angle were made on a universal stage; indices were determined by using a spindle stage and central masking

techniques (Cherkasov, 1957). Several grains from the metagabbro show the following optical properties:

$$\begin{aligned} n_x &= 1.614 \text{ to } 1.617 \pm 0.001 & n_z - n_x &= 0.026 \\ n_y &= 1.621 \text{ to } 1.624 \pm 0.001 & 2V_z &= 58^\circ \text{ to } 61^\circ \\ n_z &= 1.640 \text{ to } 1.643 \pm 0.003 \end{aligned}$$

The range of the optic axial angle is slightly lower than usually reported for prehnite (Deer and others, 1962). Interference colors in standard thin sections

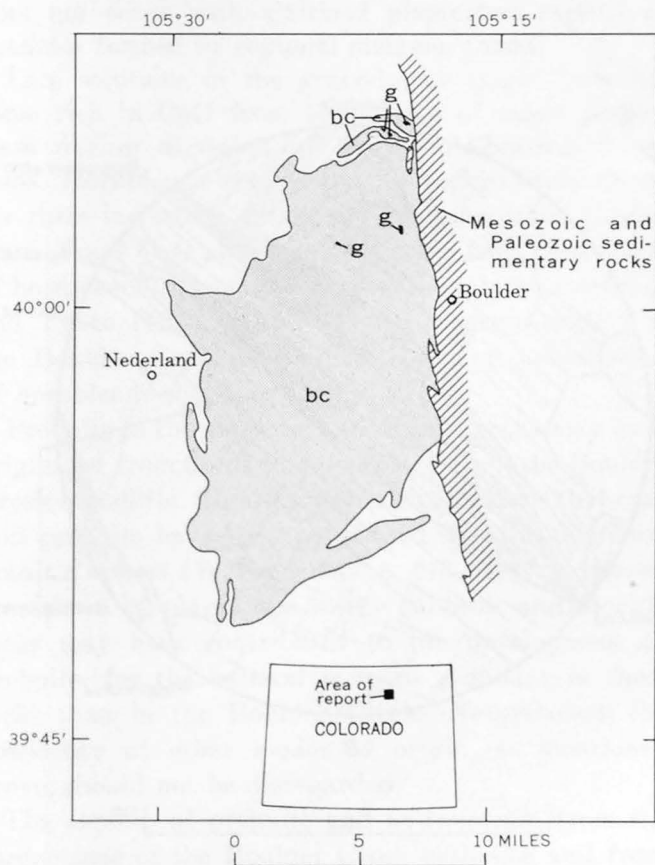


FIGURE 1.—Geologic sketch map of part of north-central Colorado, showing location of the Boulder Creek batholith. *g*, metagabbro (Precambrian); *bc*, Boulder Creek Granodiorite and related granitic rocks (Precambrian).

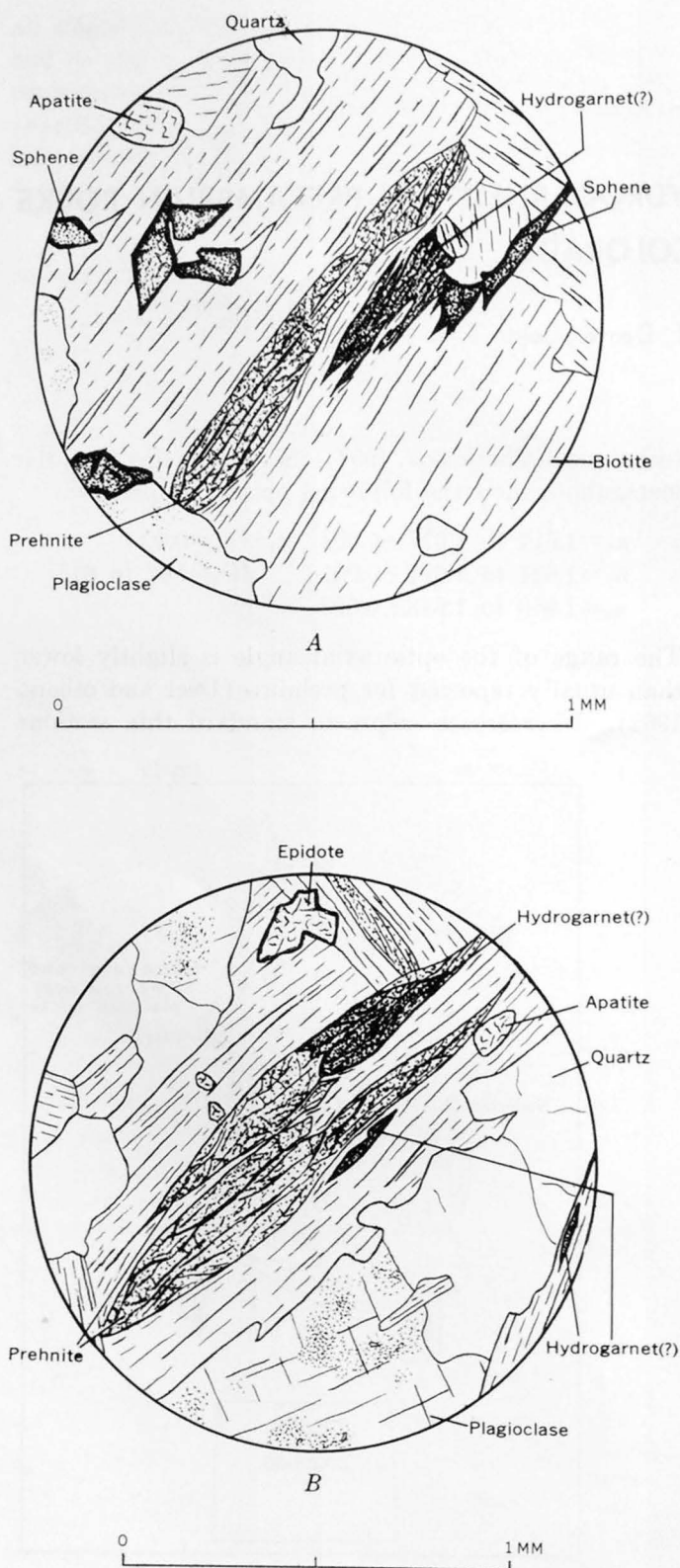


FIGURE 2.—Thin-section sketches of Boulder Creek Granodiorite. A, Prehnite and hydrogarnet(?) in biotite. B, Prehnite partly replaced by hydrogarnet(?). Plagioclase is partly sericitized.

commonly do not exceed first-order red. Some grains show fine grid-twin lamellae resembling those of microcline, and these grains commonly have anomalous blue interference colors. A "bow-tie" structure occurs in some aggregates. In thin section, prehnite from either the metagabbro or the Boulder Creek Granodiorite is colorless; in hand specimen it is white.

The name "hydrogarnet" is used here as a general term for hydroxyl-bearing garnets. The hydrogarnet reported here was determined (by F. A. Hildebrand from a specimen collected in the Boulder Creek batholith) to have the structure of the garnet and a cell edge of  $12.00 \pm 0.01 \text{ \AA}$ . In thin section the mineral is colorless to very pale brown and generally turbid; in reflected light it is silvery white. Most grains have a refractive index ranging from 1.793 to 1.798; a few grains have an index as low as 1.790, and some as high as 1.802. A small percentage of the grains have an index slightly above 1.802, the index of the highest immersion oil used. All grains are anisotropic; under crossed nicols the grains appear mottled in shades of dark to light gray, resulting from the myriad of tiny interlocking grains that form the hydrogarnet masses. The refractive index is too high for hydrogrossular, the commonly reported hydrogarnet, but the color and birefringence and the large cell edge otherwise suggest a hydrogarnet. The data suggest that the hydrogarnet may be a hydroxyl-bearing member of the grossularite-andradite series, but positive identification must await a chemical analysis.

Hydrogarnet in the Boulder, Colo., area occurs within prehnite lenses and as separate masses (fig. 2B). It forms pseudomorphs after prehnite, as indicated by its occurrence in lenses having the same general size and shape, fracture pattern, and granular appearance as the prehnite.

#### PETROLOGY OF THE HOST ROCKS

Study of the eastern half of the Boulder Creek batholith, a synkinematic pluton composed mainly of Boulder Creek Granodiorite, indicates that prehnite and hydrogarnet are rather evenly distributed in the central part of the body. Each of these minerals forms about 0.3 percent of the rock, as determined from examination of about 100 specimens, but preliminary study reveals that they are slightly more abundant in reaction zones around some hornblende-bearing inclusions. Neither mineral occurs at the periphery of the batholith within 1 mile of the contact. Prehnite not

associated with biotite occurs in a few veinlets  $\frac{1}{2}$  mm wide at one place in the batholith.

The central part of the Boulder Creek batholith in the area studied ranges in composition from quartz diorite to quartz monzonite but has an average composition of granodiorite. Some local variation in composition resulted from digestion of biotite- and hornblende-bearing inclusions. Most exposures exhibit a weak to moderately strong foliation. Plagioclase ( $An_{28-32}$ ) is weakly zoned to unzoned. Microcline locally forms phenocrysts as much as 2 inches long. Greenish-brown biotite is the principal varietal mineral, but green hornblende occurs in varietal amounts locally and especially in the vicinity of hornblende-bearing inclusions. Accessory minerals in addition to prehnite and hydrogarnet include hornblende, allanite, epidote, sphene, apatite, zircon, and magnetite.

The border zone of the batholith, in contrast to the central part, generally exhibits a strong foliation and contains brown biotite similar to that in the metasedimentary country rock. Prehnite and hydrogarnet do not occur in this rock.

The prehnite- and hydrogarnet-bearing central part of the batholith is interpreted as being of igneous origin, whereas the minerals of the border zone are thought to have recrystallized during metamorphism synchronous with emplacement of the granodiorite and during a postgranodiorite deformation.

The gabbroic and dioritic rocks form irregular bodies, generally a few hundred feet across, within and adjacent to the Boulder Creek batholith. They have been metamorphosed by the Boulder Creek batholith. Prehnite constitutes 1.5 to 3.0 percent of these rocks, but hydrogarnet occurs only in trace amounts. The gabbroic masses occur at the margin of the batholith and consist principally of calcic labradorite, cummingtonite, hornblende, and biotite. The dioritic bodies in the interior of the batholith also contain hornblende and biotite, but cummingtonite is sparse and the plagioclase is no more calcic than andesine. This rock is thought to be a strongly metamorphosed equivalent of the gabbroic material, for both have similar texture and little or no foliation, but it might have formed from hornblende gneiss. Quartz occurs in varietal or accessory amounts in both rocks, and accessory minerals include epidote, sphene, apatite, and magnetite.

Precambrian deformation during and subsequent to emplacement of the Boulder Creek Granodiorite had little effect on the gabbroic and dioritic masses.

## ORIGIN OF PREHNITE AND HYDROGARNET

The restriction of prehnite and hydrogarnet to the central undeformed part of the Boulder Creek batholith and to the adjacent and included gabbroic and dioritic masses suggests that these minerals formed by igneous processes related to the Boulder Creek batholith. A deuteritic origin would account for this restricted occurrence and for the fairly even distribution of the minerals. Moreover, crystallization from late solutions would have allowed prehnite to grow at favorable structural sites in biotite. However, additional evidence of deuteritic processes was not found, and the relation of prehnite and hydrogarnet to epidote, another late mineral of uncertain origin common in the Boulder Creek batholith, was not determined. The possibility that the prehnite and hydrogarnet formed by other processes, perhaps under low-grade metamorphic conditions, should not be excluded, because the Precambrian rocks of the Front Range have had a complex history not fully understood. Nevertheless, compelling evidence of a metamorphic origin of these minerals was not found, and it may be significant that the prehnite does not occur with albitized plagioclase typical of prehnite formed by regional metamorphism.

Late solutions in the granodiorite might have become rich in CaO from breakdown of calcic plagioclase during digestion of hornblende-bearing inclusions. Hornblende-bearing country rock, a likely source for these inclusions, commonly contains calcic plagioclase. Some CaO also may have come from conversion of hornblende to biotite, a process thought by Lovering and Tweto (1953, p. 15) to have occurred widely in the Boulder Creek Granodiorite during assimilation of hornblende schist.

Prehnite in the gabbroic and dioritic rocks may have originated from fluids that emanated from the Boulder Creek batholith. Significantly, many gabbros that contain prehnite have been penetrated by solutions from granitic masses (Watson, 1942, p. 643-644). However, breakdown of plagioclase in the gabbroic and dioritic rocks may have contributed to the development of prehnite, for the mineral is more abundant in these rocks than in the Boulder Creek. Nevertheless, the possibility of other modes of origin, as mentioned above, should not be disregarded.

The absence of prehnite and hydrogarnet from the border zone of the Boulder Creek batholith and from the adjacent metasedimentary country rock indicates either that these minerals were obliterated in them



during penetrative deformation or that they never existed in those rocks.

The hydrogarnet may have formed from prehnite. Fyfe and others (1958, p. 168-169) have shown that hydrogarnet can form from glass of prehnite composition at pressures—and to a lesser extent temperatures—lower than those in the stability range of prehnite.

#### REFERENCES

Cherkasov, Yu. A., 1957, [Application of "focal screening" to measurement of indices of refraction by the immersion method] [in Russian], in *Sovremennii metodi mineralogich, issled. gornikh porod, rud, i mineralov*: Gosudar. Nauch-Tekh. Izdat. Lt. po Geol. i Okh., Moscow, p. 184-207. (English translation in *Internat. Geol. Rev.*, v. 2, 1960, p. 218-235).

Deer, W. A., Howie, R. A., and Zussman, J., 1962, *Rock forming minerals*, v. 3, sheet silicates: New York, John Wiley and Sons, Inc., 270 p.

Fyfe, W. S., Turner, F. J., and Verhoogen, John, 1958, *Metamorphic reactions and metamorphic facies*: Geol. Soc. America Mem. 73, 259 p.

Lovering, T. S., and Goddard, E. N., 1950, *Geology and ore deposits of the Front Range, Colorado*: U.S. Geol. Survey Prof. Paper 223, 319 p. [1951].

Lovering, T. S., and Tweto, Ogden, 1953, *Geology and ore deposits of the Boulder County tungsten district, Colorado*: U.S. Geol. Survey Prof. Paper 245, 199 p. [1954].

Watson, K. D., 1942, *Zoisite-prehnite alteration of gabbro*: *Am. Mineralogist*, v. 27, p. 638-645.

Wells, J. D., Sheridan, D. M., and Albee, A. L., 1964, *Relationship of Precambrian quartzite-schist sequence along Coal Creek to Idaho Springs Formation, Front Range, Colorado*: U.S. Geol. Survey Prof. Paper 454-O, p. 01-025.



## GEOCHEMICAL PROSPECTING IN THE BROWNS CANYON FLUORSPAR DISTRICT, CHAFFEE COUNTY, COLORADO

By RALPH E. VAN ALSTINE, Washington, D.C.

*Work done in cooperation with the Colorado Mining Industrial Development Board*

*Abstract.*—In the Browns Canyon district, geochemical prospecting investigations revealed abnormal fluorine concentrations in residual soil directly above and downslope from a fluor spar vein, and in alluvium downstream from the vein. The largest anomalies are approximately 6 to 20 times the background in the soil and 3 times the background in the alluvium. Fluorine contents of soil near a concealed fault are too low to suggest the presence of an underlying fluor spar deposit. Although geochemical prospecting methods have been reported as not especially suited for locating fluor spar deposits directly, fluorine actually can be a favorable indicator element for this purpose.

Geochemical anomalies based upon 44 fluorine analyses resulting from investigations in the Browns Canyon district show that fluorine is a favorable indicator element in both residual soil and alluvium derived partly from the fluor spar deposits. Fluorite apparently has a lower mobility in residual soils and alluvium than previously recognized, and additional geochemical prospecting work in fluor spar districts might reveal significant anomalies that will lead to the discovery of ore bodies.

Various opinions have been expressed on the value of geochemical prospecting methods in finding fluor spar deposits. Geochemical methods are regarded (Grogan, 1964) as not especially adapted to locating fluor spar deposits directly by searching for anomalous concentrations of fluorine. On the other hand, Hawkes and Webb (1962, p. 365) stated that the fluorine content of soils may be useful as a guide in locating fluor spar deposits. This conclusion, however, was based mainly on the results of an extensive geochemical study of residual soil above bedding-replacement and vein deposits in the Illinois-Kentucky district by Nackowski<sup>1</sup>

(1957, p. 378), who actually concluded that in that district "fluorine is technically unsuited as an indicator element for preliminary fluor spar exploration." Evidently the topography, climate, or geologic environment in this area was unfavorable for fluorine to be highly concentrated in the soil. His auger samples consisted mainly of residual soil beneath about 20 feet of loess; the soil overlies fluor spar ore in limestones, shales, and sandstones in a maturely dissected plateau area where the annual precipitation is about 46 inches. The reported small positive fluorine anomalies there amounted to only 21 percent above background for the bedding-replacement deposits and 54 percent above background over a vein deposit where the background value was 0.065 percent fluorine. Some later auger drilling and geochemical investigations in the district revealed areas with 2-fold and 3-fold anomalies, based on a background value of about 0.035 percent fluorine, which were diamond drilled and found to contain fluorite-bearing calcite veinlets and no minable bodies of fluor spar.

Similarly alluvium has not been regarded as useful in prospecting for fluor spar. According to Grogan (1960, p. 375), fluor spar does not last long in the beds of streams because of its softness and extreme cleavability, and ordinarily cannot be traced by panning.

Special thanks are due Lyman C. Huff, of the U.S. Geological Survey, for help in collecting the samples and for preparing them for analysis.

### LOCATION AND GEOLOGIC SETTING

The Browns Canyon fluor spar district is in the Poncha Springs quadrangle, Chaffee County, Colo., about 100 miles southwest of Denver and about 8 miles northwest of Salida. It extends west from the Ar-

<sup>1</sup>M. O. Nackowski, 1952, Geochemical prospecting applied to the Illinois-Kentucky fluor spar area: Missouri Univ. Ph.D. thesis, 144 p.

kansas River and is readily accessible from U.S. Highway 285. The terrain is mountainous, and the steep southwest-facing slope in the area under investigation has only a thin soil. The altitude of the principal deposits ranges from 7,360 to 7,720 feet. The annual precipitation is less than 10 inches, and vegetation is sparse.

The fluor spar deposits shown in figure 1 occur chiefly as epithermal veins along a steeply dipping, northwest-trending normal fault zone between Tertiary rhyolitic welded tuff and Precambrian banded gneiss, hornblende gneiss, and gneissic quartz monzonite; most of the other faults are not known to contain commercial deposits of fluor spar. The veins generally show abrupt slickensided walls with silicification and slight replacement of wallrock by fluorite. The Precambrian rocks strike northeast and dip steeply northwest and southeast, whereas the rhyolitic welded tuff strikes northwest and dips gently southwest. A black vitrophyric welded tuff near the base of the rhyolitic welded tuff was dated by the K-Ar method (analysts H. H. Thomas, R. F. Marvin, P. L. D. Elmore, and H. Smith, of the U.S. Geological Survey); because biotite and the glassy matrix each showed the age to be 34 million years ( $\pm 3$  m.y.), these volcanic rocks are regarded as Oligocene.

The district yielded about 130,000 short tons of fluor spar concentrates between 1929 and 1949. Although the deposits are not now being mined, they constitute a resource of more than a million tons of fluor spar containing more than 15 percent  $\text{CaF}_2$  (Van Alstine, in U.S. Geol. Survey, 1964, p. A10-A11). The maximum thickness of the veins is about 40 feet, and the  $\text{CaF}_2$  content ranges from 15 to 75 percent. The fault zone mentioned above is mineralized with fine-grained fluorite and chalcedonic quartz almost continuously for nearly 3,000 feet in secs. 34 and 27, T. 51 N., R. 8 E. To the northwest, in sec. 28, this fault zone contains fluor spar, as revealed in drilling, and is joined by two other faults that have yielded commercial fluor spar. Most of the geochemical investigations were made in these three sections of land along the principal mineralized structure, in order to test the usefulness of the fluorine content of residual soil and alluvium as an indicator in prospecting for fluor spar deposits.

**FLUORINE IN THE RESIDUAL SOIL**

Thirty samples consisting largely of residual soil were collected from depths of about 6 inches along traverses made from northeast to southwest, crossing the main vein at right angles in order to include background and anomalous samples. The samples were

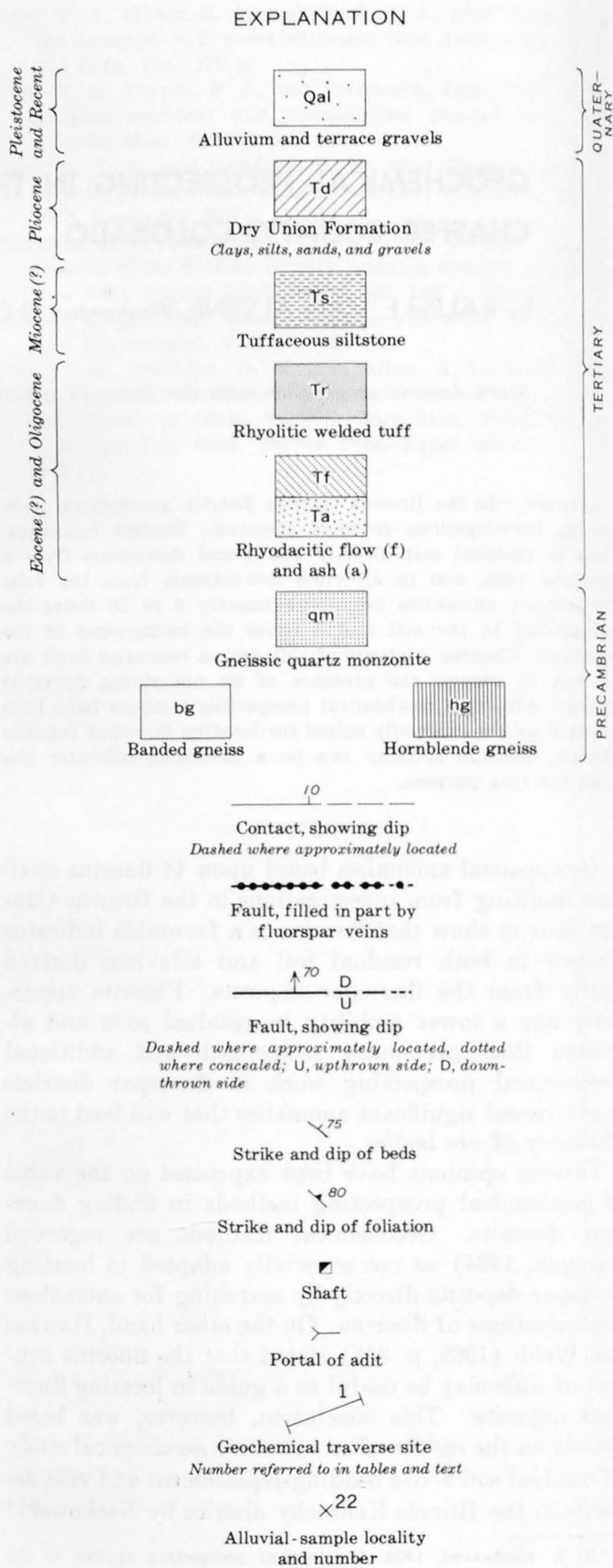


FIGURE 1.—EXPLANATION.

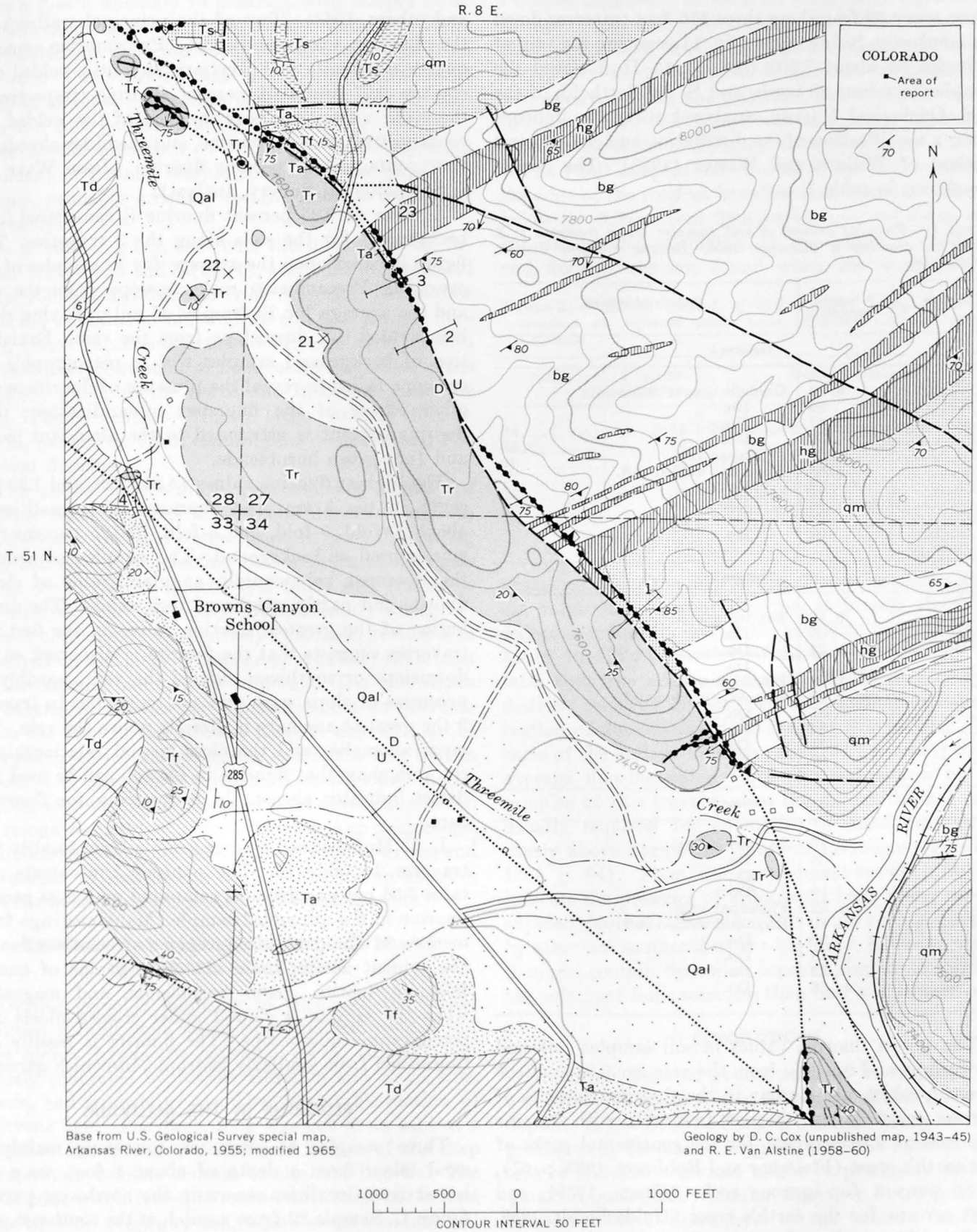


FIGURE 1.—Geologic map of part of the Browns Canyon fluorspar district, Chaffee County, Colo.

taken every 50 feet along three 450-foot traverses down the southwest-facing slope (fig. 1), crossing the vein at altitudes of about 7,700 feet. L. C. Huff sieved the samples to minus-80 mesh, and S. M. Berthold, of the U.S. Geological Survey, analyzed them for fluorine, using a modification of the distillation and colorimetric method of Willard and Winter (1933). The results are shown in table 1.

TABLE 1.—Fluorine content of soil samples along traverses 1, 2, and 3, crossing a fluor spar vein, Browns Canyon district, Colorado

Sample	F (weight percent)	Underlying bedrock
<b>Traverse 1</b>		
31	0.29	Gneissic quartz monzonite.
32	.54	Do.
33	.47	Do.
34	.39	Do.
35	.58	Fluorspar vein.
36	4.84	Rhyolitic welded tuff.
37	.32	Do.
38	.18	Do.
39	.20	Do.
40	.08	Do.
<b>Traverse 2</b>		
1	0.18	Banded gneiss.
2	.08	Do.
3	.24	Do.
4	.18	Do.
5	2.28	Fluorspar vein.
6	2.00	Rhyolitic welded tuff.
7	.87	Do.
8	.36	Do.
9	.25	Do.
10	.37	Do.
<b>Traverse 3</b>		
11	0.10	Banded gneiss.
12	.06	Do.
13	.06	Do.
14	.10	Do.
15	1.52	Fluorspar vein.
16	.40	Rhyolitic welded tuff.
17	.50	Do.
18	.13	Do.
19	.32	Do.
20	.56	Do.

The lowest fluorine values in soil samples collected downslope and upslope from the vein are 0.08 and 0.06 percent, which are similar to the fluorine contents of certain rocks. They compare favorably with fluorine contents of 0.065 percent for the continental rocks of the earth's crust (Fleischer and Robinson, 1963, p. 67), 0.066 percent for igneous rocks (Green, 1959), and 0.08 percent for the earth's crust (Goldschmidt, 1958, p. 74). The median fluorine value of more than 170 samples of silicic glassy volcanic rocks in the Western States is 520 parts per million, or 0.052 percent (Coats

and others, 1963). Two of the principal wallrocks in the Browns Canyon district, Precambrian gneissic quartz monzonite and Tertiary rhyolitic welded tuff, contain 0.07 and 0.04 percent fluorine, respectively; the black vitrophyre near the base of the welded tuff contains 0.08 percent fluorine, and the older rhyodacite flow contains 0.11 percent fluorine (Jesse Warr, Jr., U.S. Geological Survey, analyst).

A value of 0.25 percent fluorine is considered to be background for the soils along the 3 traverses. This figure is based upon the average for 12 samples of soil overlying Precambrian rocks upslope from the vein and the average for 12 samples of soil overlying rhyolitic welded tuff downslope from the vein. Examination of background samples with a petrographic microscope failed to reveal the presence of fluorite or any other effects of the fluor spar mineralization; their fluorine content is attributed to the abundant biotite and (or) green hornblende.

The highest fluorine values (4.84, 2.28, and 1.52 percent) in the 3 traverses represent abnormalities of about 20-fold, 9-fold, and 6-fold, if 0.25 percent fluorine is used as background. The samples adjacent to the fluor spar vein contain angular grains of clastic fluorite and partly weathered rock debris. The distribution of the greatest fluorine values in the first two traverses suggests that the fluorite is dispersed on the downslope or southwest side of the vein, possibly by processes of slope wash and soil creep, but in traverse 3 the greatest anomaly is directly above the vein. The large anomalies and the close spatial relationship to the vein show that fluorine in the soil can be used as a direct indicator element in prospecting for fluor spar here.

L. C. Huff panned a large sample from locality 5 of traverse 2 (table 1). The panning concentrate contains 3.56 percent fluorine, compared with 2.28 percent fluorine in the unpanned sample. Many cleavage fragments and fine-grained aggregates of colorless fluorite are evident among more abundant grains of quartz, feldspar, biotite, green hornblende, and magnetite, when the sample is viewed under crossed nicols of a petrographic microscope. The fluorite is readily distinguished from similarly isotropic, brownish garnet.

#### FLUORINE IN THE ALLUVIUM

Three samples of alluvium, consisting mainly of sand taken from a depth of about 1 foot, were collected from localities shown in the northwest part of figure 1. Sample 22 from a gulch at the southeast edge of sec. 28, T. 51 N., R. 8 E., about 900 feet downstream from the outcropping fluor spar vein, contains 0.16 percent fluorine and grains of fluorite. This value repre-

sents a 3-fold anomaly in contrast with sample 23 of the alluvium containing 0.05 percent fluorine and no visible fluorite, collected about 300 feet upstream from the vein. Concentrates that Huff panned from large samples at these 2 localities contain 0.94 percent fluorine and 0.39 percent fluorine, respectively; biotite or green hornblende, both of which are relatively more abundant in panned sample 23 than in the unpanned sample, probably accounts for the fluorine content of this sample.

In a smaller gulch that cuts the fluor spar vein between traverses 2 and 3 (fig. 1), alluvium was collected about 700 feet downstream from the vein. The sample (No. 21) contains visible fluorite and 0.30 percent fluorine, which represents a 6-fold increase over the 0.05 percent fluorine content of fluorite-free alluvium in the adjacent gulch to the north and upstream from the vein. The concentrates from a large quantity of sample 21, panned by Huff, contain fluorite grains and 1.38 percent fluorine.

The above results imply geochemically significant fluorine concentrations in alluvium downstream from the fluor spar vein and suggest that, in general, panning may be helpful in detecting the presence of fluor spar veins. Even though fluorite is a fairly soft (hardness 4) mineral that commonly breaks readily along excellent cleavage, it is relatively insoluble, resistant to weathering, and heavier (sp gr approx 3.2) than most of the common nonmetallic minerals. The persistence of fluorite in gulches for short distances downstream from the vein in the Browns Canyon district may be due partly to its fine grain size and to the fact that in places it is intergrown with hard chalcedonic quartz. In districts where fluorite persists in alluvium and can be recognized readily under a hand lens or microscope, examination of panned concentrates from alluvium and estimation of the fluorite content may be an effective and cheap way to prospect for fluor spar deposits.

#### GEOCHEMICAL RECONNAISSANCE OVER AN UNEXPOSED FAULT ZONE

During geologic mapping in this area the writer mapped a fault zone separating rhyolitic welded tuff and older rhyodacitic volcanic rocks (fig. 1), but largely concealed by Recent alluvium and clays, silts, sands, and gravels of the Dry Union Formation of Pliocene age. The fault zone was cut in an adit at a fluor spar mine, near the southeast corner of the map area, where veinlets contain calcite and fluorite. The fault zone was inferred to extend northwest to the west edge of U.S. Highway 285, where seven residual soil samples were collected from south to north (traverse 4, fig. 1). At this locality the fault zone is covered by

Pliocene sediments between an outcrop of rhyodacitic volcanic rocks and an outcrop of rhyolitic welded tuff about 200 feet to the north. The rhyodacitic volcanics are locally whitened, altered, and cut by veinlets of chalcedony, calcite, and gypsum; the rhyolitic welded tuff is silicified. Fluorite, however, was not observed in the volcanic rocks or Pliocene sediments here.

The 7 soil samples collected at 50-foot intervals near the edge of the roadcut have fluorine contents (table 2) below the 0.25-percent fluorine background value used for delineating anomalies in the other 3 traverses, and fluorite was not found when the samples were

TABLE 2.—Fluorine content of soil samples along traverse 4, crossing an inferred fault zone, Browns Canyon district, Colorado

Sample	F (weight percent)	Underlying material
24-----	0.16	Rhyodacitic volcanic rocks.
25-----	.16	Do.
26-----	.15	Pliocene sediments.
27-----	.16	Do.
28-----	.21	Do.
29-----	.18	Rhyolitic welded tuff.
30-----	.12	Do.

examined under the microscope. Nevertheless the highest value, 0.21 percent fluorine, is in soil above the Pliocene sediments and at the probable location of the fault. Possibly deposition of the sediments, which was later than the mineralization in the Browns Canyon district, removed or obscured any anomalous concentration of fluorite along the fault at this locality. The ratio of the highest fluorine value (0.21 percent) to the average fluorine value (0.16 percent) shown by the samples of this traverse does not exceed the 2/1 ratio usually required for anomalies to stand out significantly above normal background variations (Hawkes, 1959, p. 64). Thus, the geochemical traverse fails to indicate the presence of a fluor spar body along the unexposed fault at this site. This fault zone is covered by alluvium southeast of the highway, however, where it might contain fluor spar deposits similar to those in the principal fault zone less than half a mile northeast.

#### CONCLUSIONS

Abnormal fluorine concentrations in residual soil and alluvium are spatially related to sizable fluor spar deposits in the Browns Canyon district. Study of these geochemical anomalies suggests that the fluorine content of soil and alluvium might be profitably investigated in geologically similar fluor spar districts of the Western States. Since most of the western fluor spar deposits are epithermal, Tertiary in age, and lacking in sulfides of metals commonly useful for geochemical

or geophysical prospecting, the direct search for fluorine anomalies might be useful in preliminary exploration work. Caution should be exercised in interpreting analytical results in any areas where beds of fluorine-bearing phosphate rock or the use of phosphatic fertilizers may have caused abnormal fluorine concentrations that are unrelated to fluorspar deposits.

#### REFERENCES

- Coats, R. R., Goss, W. D., and Rader, L. F., 1963, Distribution of fluorine in unaltered silicic volcanic rocks of the western conterminous United States: *Econ. Geology*, v. 58, p. 941-951.
- Fleischer, Michael, and Robinson, W. O., 1963, Some problems of the geochemistry of fluorine, in *Studies in analytical chemistry*: Royal Soc. Canada Spec. Pub. 6, Univ. Toronto Press, p. 58-75.
- Goldschmidt, V. M., 1958, *Geochemistry*: London, Oxford Univ. Press.
- Green, Jack, 1959, Geochemical table of the elements for 1959: *Geol. Soc. America Bull.*, v. 70, p. 1144.
- Grogan, R. M., 1960, Fluorspar and cryolite, in *Industrial Minerals and Rocks*, 3d ed.: Am. Inst. Mining Metall. Petroleum Engineers, p. 363-382.
- 1964, Finding sources of fluorine [abs.]: *Mining Eng.*, v. 16, no. 1, p. 65.
- Hawkes, H. E., 1959, Geochemical prospecting, in Abelson, P. H., ed., *Researches in geochemistry*: New York, John Wiley and Sons, Inc., 511 p.
- Hawkes, H. E., and Webb, J. S., 1962, *Geochemistry in mineral exploration*: New York, Harper and Row, 401 p.
- Nackowski, M. O., 1957, Geochemical prospecting applied to the Illinois-Kentucky fluorspar area [abs.], in Erikson, J. E., *Geochemical prospecting abstracts, July 1952-December 1954*: U.S. Geol. Survey Bull. 1000-G, p. 357-395.
- U.S. Geological Survey, 1964, *Geological Survey Research 1964*: U.S. Geol. Survey Prof. Paper 501-A, 367 p.
- Willard, H. H., and Winter, O. B., 1933, Volumetric method for determination of fluorine: *Indus. Eng. Chemistry, Anal. Ed.*, v. 5, p. 7-10.



## HEAT AND FREE ENERGY OF FORMATION OF HERZENBERGITE, TROILITE, MAGNESITE, AND RHODOCHROSITE CALCULATED FROM EQUILIBRIUM DATA

By RICHARD A. ROBIE, Silver Spring, Md.

*Abstract.*—Improved values for the heat of formation of herzenbergite (SnS), troilite (FeS), magnesite (MgCO<sub>3</sub>), and rhodochrosite (MnCO<sub>3</sub>) have been calculated from high-temperature equilibrium data using “third law” methods. The new values for  $\Delta H_f^{\circ, 298.15}$  are: SnS =  $-25,350 \pm 150$  cal mole<sup>-1</sup>, FeS =  $-24,015 \pm 300$  cal mole<sup>-1</sup>, MgCO<sub>3</sub> =  $-28,230 \pm 200$  cal mole<sup>-1</sup>, and MnCO<sub>3</sub> =  $-26,420 \pm 150$  cal mole<sup>-1</sup>. For the carbonates these values refer to formation from the oxides.

Values for the entropy of rhodochrosite (MnCO<sub>3</sub>) and siderite (FeCO<sub>3</sub>)  $S_{298.15}^{\circ}$  have been corrected to include the contribution due to antiferromagnetic ordering at temperatures below 50°K. The corrected values for  $S_{298.15}^{\circ}$  are: MnCO<sub>3</sub> =  $23.9 \pm 0.5$  cal mole<sup>-1</sup> deg<sup>-1</sup>, and FeCO<sub>3</sub> =  $25.1 \pm 0.6$  cal mole<sup>-1</sup> deg<sup>-1</sup>. The free energies of formation from the elements,  $\Delta G_f^{\circ, 298.15}$  are: SnS =  $-24,875 \pm 200$  cal, and FeS =  $-24,095 \pm 400$  cal. The free energies of formation for the carbonates from the oxides are: MnCO<sub>3</sub> =  $-14,064 \pm 300$  cal, and MgCO<sub>3</sub> =  $-15,764 \pm 270$  cal.

During the course of preparation of a set of tables of thermodynamic data for minerals by Robie (1962), several sets of high-temperature equilibrium data were examined in order to compare their internal consistency and agreement with calorimetric results or conversely to utilize the equilibrium measurements to obtain a “best value” for the heat or free energy of formation. It is believed that these calculations should be recorded since the resultant heats of formation differ by up to 2,000 calories from the values listed in the standard source for such data (Rossini and others, 1952), and also because the methods used for treating the equilibrium data offer a more critical test of the correctness of the equilibrium measurements than the usual calculation of  $\Delta H$  from the slope of the equilibrium curve (that is, using the van't Hoff equation or “second law” methods). The treatment of the data used in the subsequent calculations is based on the use of the Gibbs free-energy function (for example, Darken and Gurry, 1953; Lewis and Randall, 1961). This function is defined by the relation

$$\frac{G_T^{\circ} - H_{298.15}^{\circ}}{T} = \frac{H_T^{\circ} - H_{298.15}^{\circ}}{T} - S_T^{\circ}, \quad (1)$$

where  $G$ ,  $H$ ,  $S$ , and  $T$  are respectively the Gibbs free-energy, enthalpy, entropy, and temperature in degrees Kelvin, and the small circle superscript indicates that the element or compound is in its standard state, which for a condensed phase is 1 atmosphere pressure at any temperature. For a gas the standard state is the ideal gas at 1 atmosphere. It should be emphasized that the Gibbs function is determined only from specific-heat data, usually the most accurate of the data used in a thermodynamic calculation, and that it is a slowly varying function of temperature.

In equation 1 we have adopted 298.15°K (25.0°C) as our reference temperature. This is only as a convenience. Provided we had values of

$$H_T^{\circ} - H_0^{\circ} = \int_0^T C_p dT \quad (2)$$

for all phases, where  $C_p$  is the heat capacity at constant pressure, we could have equally well used 0°K as the reference temperature and the Gibbs function would have become

$$\frac{G_T^{\circ} - H_0^{\circ}}{T} = \frac{H_T^{\circ} - H_0^{\circ}}{T} - S_T^{\circ}, \quad (3)$$

the form most frequently encountered in thermodynamic properties of gases calculated from spectroscopic data. Using the Gibbs function the standard free-energy change at any temperature may be written as

$$\Delta G_T^{\circ} = \Delta H_{298.15}^{\circ} + T \Delta \left[ \frac{G_T^{\circ} - H_{298.15}^{\circ}}{T} \right]. \quad (4)$$

Since the free-energy change for a reaction is directly related to the thermodynamic equilibrium-constant or activity-product  $K$ , by the relation



$$\Delta G_T^\circ = RT \ln K, \quad (5)$$

and where  $R$  is the gas constant,  $1.9873 \text{ cal mole}^{-1} \text{ deg}^{-1}$ , equation 4 may be rewritten as

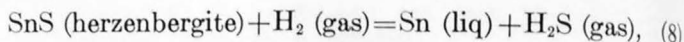
$$-RT \ln K = \Delta H_{298.15}^\circ + T \Delta \left[ \frac{G_T^\circ - H_{298.15}^\circ}{T} \right] \quad (6)$$

or

$$-\frac{\Delta H_{298.15}^\circ}{T} = R \ln K + \Delta \left[ \frac{G_T^\circ - H_{298.15}^\circ}{T} \right]. \quad (7)$$

For a reaction involving pure solids (and (or) liquids) and gases at pressures sufficiently low such that the activities of the condensed phases can be taken as unity and the gases may be assumed to behave ideally, the equilibrium-constant  $K$  can be written in terms of the pressures.

As a specific example we consider the reduction of herzenbergite by  $\text{H}_2$ ,



for which the equilibrium-constant  $K_P$  may be written as

$$K_P = P_{\text{H}_2\text{S}}/P_{\text{H}_2}. \quad (9)$$

Substituting equation 9 into 7 gives

$$-\frac{\Delta H_{298.15}^\circ}{T} = R \ln P_{\text{H}_2\text{S}}/P_{\text{H}_2} + \Delta \left[ \frac{G_T^\circ - H_{298.15}^\circ}{T} \right]. \quad (10)$$

The thermodynamic functions necessary for this and the subsequent calculations of this paper are shown in table 1.

TABLE 1.—Summary of thermodynamic properties

	$\Delta H_{f,298.15}^\circ$		Gibbs free-energy function $-(G_T^\circ - H_{298.15}^\circ)/T$ (cal mole <sup>-1</sup> deg <sup>-1</sup> )										Reference	
	Elements (cal mole <sup>-1</sup> )	Oxides (cal mole <sup>-1</sup> )	<sup>1</sup> 298.15	400	500	600	700	800	900	1,000	1,100	1,200		1,300
Fe.....			6.52 ±.03	6.76	7.24	7.79	8.36	8.94	9.52	10.10	10.69	11.28	11.84	Hultgren and others (1963).
H <sub>2</sub> .....			31.208 ±.01	31.480	31.995	32.573	33.153	33.715	34.250	34.758	35.240	35.696	36.130	Stull and others (1964).
H <sub>2</sub> S.....	-4,815±100		49.152 ±.03	49.476	50.100	50.814	51.546	52.270	52.974	53.654	54.311	54.944	55.553	Do.
FeS.....	-24,015±300		14.42 ±.03	14.95	16.32	17.86	19.35	20.72	21.98	23.16	24.24	25.25	26.21	Coughlin (1950).
MgO.....	<sup>2</sup> -143,800±100	0	6.44 ±.03	6.81	7.54	8.39	9.27	10.14	10.98	11.78	12.55	13.29	-----	Grønvdal and others (1959).
MnO.....	<sup>2</sup> -92,050±110	0	14.27 ±.10	14.70	15.53	16.48	17.44	18.38	19.29	20.15	20.97	21.76	-----	Barron and Douglas (1953).
CO <sub>2</sub> .....	-94,054±30	0	51.072 ±.05	51.434	52.148	52.981	53.845	54.706	55.546	56.359	57.143	57.896	-----	Vietor and Douglas (1963).
MgCO <sub>3</sub> .....	-266,084±300	<sup>3</sup> -28,230±200	15.70 ±.20	16.48	18.01	19.83	21.74	23.66	25.55	27.38	29.15	30.85	-----	Kelley (1960).
MnCO <sub>3</sub> .....	-212,524±300	<sup>3</sup> -26,420±150	23.9 ±.5	24.72	26.34	28.24	30.24	32.22	34.17	36.05	37.86	-----	Kelley and King (1961).	
SnS.....	<sup>3</sup> -25,349±150		18.36 ±.20	18.82	19.71	20.73	21.78	22.81	23.82	24.79	25.72	26.85	-----	Kelley (1960).
S <sub>2</sub> .....	30,840±150		54.510 ±.03	54.819	55.416	56.094	56.783	57.455	58.099	58.712	59.294	59.846	60.371	King and Todd (1953).
Sn.....			12.32 ±.06	12.58	13.08	14.18	15.16	16.01	16.77	17.45	-----	-----	-----	Orr and Christensen (1958).
														Stull and others (1964).
														Hultgren and others (1963).

<sup>1</sup> Note that  $S_{298.15}^\circ = -(G_T^\circ - H_{298.15}^\circ)/T$  at 298.15°K.

<sup>3</sup> Coughlin (1954).

<sup>2</sup> This paper.

### HERZENBERGITE

Richards (1955) has studied this equilibrium between 773° and 948°K and, using an estimated entropy for SnS (herzenbergite) and some questionable high-temperature heat-content measurements on SnS, calculated  $\Delta H_{298.15}^\circ = 19,549 \pm 1,100$  cal for the heat of this reaction. After Richards' measurements were made, accurate low-temperature heat-capacity and high-temperature heat-content data became available for SnS (King and Todd, 1953; Orr and Christensen, 1958). These data were used to obtain the free-energy functions in table 1.

We have recalculated the experimental data of Richards using the newer calorimetrically determined values for  $(G_T^\circ - H_{298.15}^\circ)/T$  for SnS by using equation 10. The results are shown in table 2. Combining

the mean value of  $\Delta H_{298.15}^\circ$  for this equilibrium, 20,534 ± 56 cal,<sup>1</sup> with the adopted values of  $\Delta H_{f,298.15}^\circ$  for H<sub>2</sub>S, gives -25,349 cal for the standard heat of formation,  $\Delta H_{f,298.15}^\circ$ , of herzenbergite from white tin and orthorhombic sulfur. It is believed that this value is accurate to ±150 cal, but it should be checked by HCl-solution calorimetry. Using the entropies at 298.15°K for tin and orthorhombic sulfur gives -24,875 ± 200 cal for the free energy of formation,  $\Delta G_{f,298.15}^\circ$ .

The measurements of Sudo (1951) on this same equilibrium are less extensive, and although they show general agreement with the above calculation, his data (Sudo's average value 20,938 cal) do show a

<sup>1</sup> The uncertainties listed with derived values of  $\Delta H^\circ$  are those recommended by Rossini (1956); that is,  $2\sqrt{\sum(x_i - \bar{x})^2/n(n-1)}$  where  $x_i$  is the value of an individual measurement,  $\bar{x}$  is the arithmetic mean of all the measurements, and  $n$  is the number of measurements.

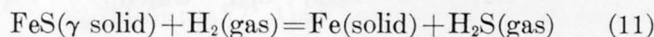
TABLE 2.—Calculation of the heat of the reaction  $\text{SnS} + \text{H}_2 = \text{Sn} + \text{H}_2\text{S}$  from the equilibrium data of Richards (1955)

$T$ (degrees K)	$\log P_{\text{H}_2\text{S}}/P_{\text{H}_2}$	$R \ln K$ (cal deg <sup>-1</sup> )	$\Delta \left[ \frac{G_T^\circ - H_{298.15}^\circ}{T} \right]$ (cal deg <sup>-1</sup> )	$\Delta H_{298.15}^\circ$ (cal)
773	-3.208	-14.679	-11.768	20,443
790	-2.983	-13.650	-11.760	20,074
800	-3.019	-13.814	-11.755	20,455
813	-3.015	-13.796	-11.750	20,769
833	-2.876	-13.160	-11.734	20,737
843	-2.818	-12.895	-11.727	20,756
848	-2.733	-12.506	-11.721	20,544
858	-2.695	-12.332	-11.714	20,631
873	-2.550	-11.668	-11.701	20,401
898	-2.425	-11.096	-11.676	20,449
923	-2.330	-10.662	-11.650	20,594
948	-2.199	-10.062	-11.619	20,554
Mean				20,534 ± 56

definite trend of  $\Delta H_{298.15}^\circ$  with the temperature of measurement and will therefore not be considered further. The values for  $\Delta H^\circ$  and  $\Delta G^\circ$  of formation of SnS given above supersede those in Rossini and others (1952), which were based on poorly reproducible electrochemical-cell data.

### TROILITE

Cox and others (1949), Sudo (1950), Alcock and Richardson (1951), and Rosenqvist (1954) have studied the reaction



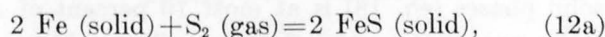
at temperatures between 773° and 1,260°K. The last three investigations paid particular attention to the elimination of thermal segregation in the  $\text{H}_2\text{S}/\text{H}_2$  gas mixture (Soret effect), an effect which caused much of the earlier  $\text{H}_2$  reduction equilibrium studies on sulfides to be unreliable.

The experimental gas ratios of Sudo (1950) and Rosenqvist (1954) were treated by the method implicit in equation 7. The difference in the free-energy functions for the products and reactants  $\Delta \left[ \frac{G_T^\circ - H_{298.15}^\circ}{T} \right]$  were obtained from table 1. The results of these calculations are given in tables 3 and 4. The mean value for the heat of reaction 11, obtained by averaging the data in tables 3 and 4, is  $19,437 \pm 200$  cal.

Unfortunately Alcock and Richardson (1951) did not list their experimental data but instead gave the equation

$$\Delta G_{720^\circ-1261^\circ\text{K}}^\circ = -71,820 + 25.12T \text{ cal} \quad (12)$$

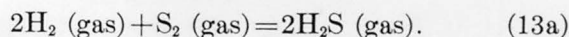
for the free-energy change for the reaction



which they obtained from their measurements together with the equation

$$\Delta G_T^\circ = -38,810 + 15.41T \log T - 2.065 \times 10^{-3}T^2 - 25.02T \text{ cal} \quad (13)$$

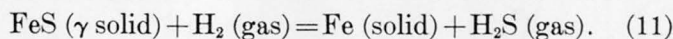
given by Kelley (1937) for the reaction



Combining the two equations yields

$$\Delta G_T^\circ = 16,505 + 7.705T \log T - 1.033 \times 10^{-3}T^2 - 25.07T \text{ cal} \quad (13b)$$

for the equilibrium



The experimental data of Rosenqvist and Sudo and points calculated from equation 13b are shown on figure 1. The solid line is a least-squares fit to these equilibrium data and weights Alcock and Richardson's data in proportion to the number of their observations.

Very recently Adami and King (1964) determined the heat of formation of FeS (troilite) by HCl-solution calorimetry. Their sample was prepared by the reaction of  $\text{Fe}_2\text{O}_3$  with a  $\text{CO}_2\text{-CS}_2$  gas stream at 750° to 800°C. Their value of  $\Delta H_{f,298.15}^\circ$  for FeS,  $-23,810 \pm$

TABLE 3.—Calculation of the heat of the reaction  $\text{FeS} + \text{H}_2 = \text{Fe} + \text{H}_2\text{S}$  from the equilibrium data of Rosenqvist (1954)

$T$ (degrees K)	$P_{\text{H}_2\text{S}}/P_{\text{H}_2}$ $\times 10^2$	$\log P_{\text{H}_2\text{S}}/P_{\text{H}_2}$	$\Delta \left[ \frac{G_T^\circ - H_{298.15}^\circ}{T} \right]$ (cal deg <sup>-1</sup> )	$R \ln K$ (cal deg <sup>-1</sup> )	$\Delta H_{298.15}^\circ$ (cal)
773	0.015	-3.824	-6.942	-17.498	18,892
973	.073	-3.137	-5.937	-14.354	19,743
1,173	.333	-2.478	-5.340	-11.339	19,564
1,073	.183	-2.738	-5.599	-12.529	19,451
973	.089	-3.051	-5.937	-13.961	19,361
873	.043	-3.366	-6.385	-15.402	19,020
1,073	.189	-2.724	-5.599	-12.465	19,383
1,261	.524	-2.281	-5.143	-10.437	19,646
1,068	.170	-2.770	-5.612	-12.675	19,531
968	.092	-3.036	-5.958	-13.892	19,215
1,257	.529	-2.277	-5.150	-10.419	19,570
1,173	.318	-2.498	-5.340	-11.430	19,671
1,261	.58	-2.224	-5.143	-10.177	19,318
Mean					19,413 ± 140

TABLE 4.—Calculation of the heat of reaction  $\text{FeS} + \text{H}_2 = \text{Fe} + \text{H}_2\text{S}$  from the equilibrium data of Sudo (1950)

$T$ (degrees K)	$P_{\text{H}_2\text{S}}/P_{\text{H}_2}$	$\log P_{\text{H}_2\text{S}}/P_{\text{H}_2}$	$\Delta \left[ \frac{G_T^\circ - H_{298.15}^\circ}{T} \right]$ (cal deg <sup>-1</sup> )	$R \ln K$ (cal deg <sup>-1</sup> )	$\Delta H_{298.15}^\circ$ (cal)
1,048	0.00145	-2.839	-5.673	-12.991	19,560
1,068	.00181	-2.742	-5.612	-12.547	19,394
1,097	.00220	-2.658	-5.530	-12.162	19,408
1,145	.00263	-2.580	-5.405	-11.806	19,706
Mean					19,517 ± 150

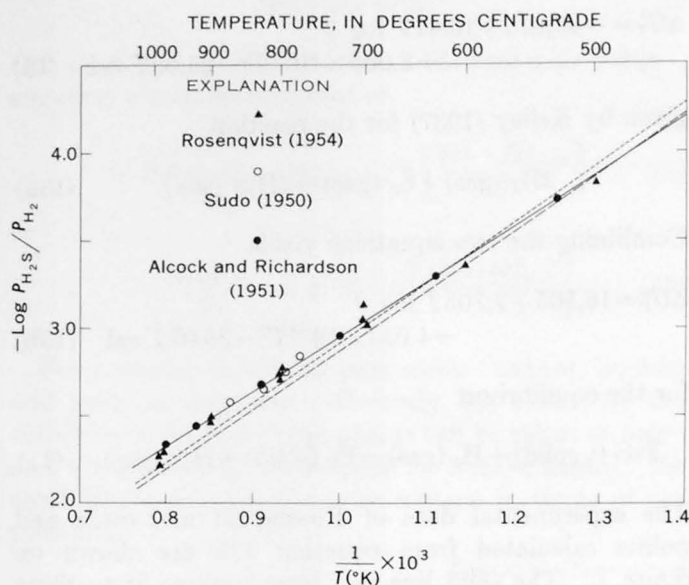


FIGURE 1.—Equilibrium data and calculated equilibrium curves for the reaction  $\text{FeS} + \text{H}_2 \rightleftharpoons \text{Fe} + \text{H}_2\text{S}$ . Least-squares fit to the equilibrium measurements is shown by solid line. Curve defined by short dashes is based upon a  $\Delta H_{298.15}^\circ$  of 19,200 cal, together with  $(G_T^\circ - H_{298.15}^\circ)/T$  functions of table 1. Curve defined by long dashes is based upon the calorimetric  $\Delta H_{298.15}^\circ$  of 18,985 cal, together with  $(G_T^\circ - H_{298.15}^\circ)/T$  functions given in table 1.

240 cal, combined with the heat of formation of  $\text{H}_2\text{S}$  in table 1, gives for reaction 11,  $\Delta H_{298.15}^\circ = 18,985 \pm 300$  cal. This value for  $\Delta H_{298.15}^\circ$  and the  $(G_T^\circ - H_{298.15}^\circ)/T$  data in table 1 were used to calculate the curve defined by the long dashes in figure 1.

Although the agreement is satisfactory, there exists a small but real systematic discrepancy between the equilibrium data (solid line on fig. 1) and the curve calculated entirely from calorimetric measurements (long-dashed curve). Inasmuch as the equilibrium studies used three distinct methods for obtaining  $P_{\text{H}_2\text{S}}/P_{\text{H}_2}$  and yet show excellent agreement, they are probably free of systematic error. Furthermore no value of  $\Delta H_{298.15}^\circ$  for reaction 11 can be chosen that, combined with the free-energy functions of table 1, will lead to the experimental curve. This strongly suggests that the error lies in the  $(G_T^\circ - H_{298.15}^\circ)/T$  data.

The thermodynamic functions for  $\text{H}_2$  and  $\text{H}_2\text{S}$  are based on a combination of spectroscopic and calorimetric data and are probably accurate to 0.05 percent. The values used for iron are based on two sets of modern measurements which show excellent agreement. The data for FeS at high temperature are based on Coughlin's (1950) measurements for which the sample composition was actually a pyrrhotite of composition  $\text{FeS}_{1.02}$ . We therefore suspect that the principal source of the discrepancy between the equilibrium measurements and the curve calculated from calorimetric data is due to the high-temperature heat-capacity data for FeS.

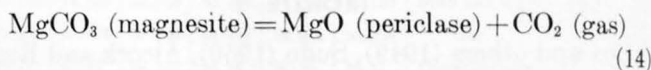
Furthermore we suspect that the method used by Adami and King to prepare their sample of FeS may have resulted in a material containing some residual iron oxides or possibly, as Grønvdal and others (1959) have suggested, a sulfur rich pyrrhotite.

A  $\Delta H_{298.15}^\circ$  of 19,200 cal for reaction 11 together with the  $(G_T^\circ - H_{298.15}^\circ)/T$  functions of table 1 were used to calculate the short-dashed curve of figure 1. This curve does the least damage to all the experimental data and would lead to  $\Delta H_{f,298.15}^\circ = -24,015$  cal, and  $\Delta G_{f,298.15}^\circ = -24,095$  cal for troilite, which we adopt as our best value. The uncertainties associated with these values should be less than  $\pm 350$  cal.

## MAGNESITE

For equilibrium measurements at higher pressures we can no longer assume that the activities of the solid phases are unity nor can we neglect the deviation of the gas phase from ideal behavior. In order to illustrate this we shall examine the decomposition of magnesite.

For the reaction



at equilibrium:

$$\Delta G_{P,T} = 0 = G_{\text{MgO}} + G_{\text{CO}_2} - G_{\text{MgCO}_3}, \quad (15)$$

$$\Delta G_{P,T} = \Delta G_T^\circ + (G_{P,T} - G_T^\circ)_{\text{MgO}} + (G_{P,T} - G_T^\circ)_{\text{CO}_2} - (G_{P,T} - G_T^\circ)_{\text{MgCO}_3}, \quad (16)$$

and

$$\Delta G_{T,P} = \Delta G_T^\circ + \int_0^P (V_{\text{MgO}} - V_{\text{MgCO}_3})_T dP + RT \ln f_{\text{CO}_2}. \quad (17)$$

In the above,  $V$  is the molar volume and  $f$  is the fugacity. Since data are not available to completely specify the change in volume with pressure and temperature for the solid phases, we shall approximate the integral in equation 17 by

$$\int_0^P (V_{\text{MgO}} - V_{\text{MgCO}_3})_T dP \approx \int_0^P (V_{\text{MgO}}^\circ - V_{\text{MgCO}_3}^\circ)_{298.15} dP = (P-1)\Delta V_{298.15}^\circ. \quad (18)$$

That is to say, we assume that  $\Delta V$  for the solid phases is independent of pressure and temperature. This approximation introduces very little error. The term due to the change in free energy with pressure for the solid phases (eq. 18) is at most 10 percent of  $\Delta G_T^\circ$  for the range of pressures that we will consider (that is, up to 2,000 atmospheres) and  $\Delta V(P,T)$  will change only slightly with pressure. This approximation would not

of course be justified for a reaction involving only solids.

Using the Gibbs function and the approximation (eq. 18) we can rewrite equation 17 as

$$\Delta G_{T,P} = \Delta H_{298.15}^{\circ} + T \Delta \left[ \frac{G_T^{\circ} - H_{298.15}^{\circ}}{T} \right] + (P-1) \Delta V_{298.15}^{\circ} + RT \ln f_{\text{CO}_2}, \quad (19)$$

or since we wish to obtain the heat of formation of  $\text{MgCO}_3$  from the equilibrium data,

$$-\frac{\Delta H_{298.15}^{\circ}}{T} = \Delta \left[ \frac{G_T^{\circ} - H_{298.15}^{\circ}}{T} \right] + \frac{(P-1) \Delta V^{\circ}}{T} \text{ (solid phases)} + R \ln f_{\text{CO}_2}. \quad (20)$$

We will use the magnesite decomposition measurements of Marc and Simek (1913) and of Harker and Tuttle (1955). These data were recently subjected to a similar treatment by Stout and Robie (1963) who gave only their result, 28,170 cal. These authors, however, did not have access to the recent accurate high-temperature  $C_p$  data of Victor and Douglas (1963) and of Pankratz and Kelley (1963) for periclase. The recalculation of the experimental data is summarized in tables 5 and 6. The required thermal data are taken from table 1 and Price's (1955)  $\text{CO}_2$  tables. The pressures (measured by Marc and Simek) are low enough so that we may neglect the  $(P-1)\Delta V$  term for the solids and also the difference between  $P_{\text{CO}_2}$  and  $f_{\text{CO}_2}$ . The results given in tables 5 and 6 for  $\Delta H_{298.15}^{\circ}$  show no appreciable trend from data extending over a range of 450°K and 2,000 atmospheres  $\text{CO}_2$  pressure. This is fairly conclusive proof of the essential correctness of the equilibrium data and the derived values of  $\Delta H_{298.15}^{\circ}$ . The average of all data in the 2 sets is  $28,230 \pm 200$  cal. Combining this value of  $\Delta H_{298.15}^{\circ}$  with the entropies in table 1, we get  $\Delta G_{T,298.15}^{\circ} = 15,764 \pm 270$  cal for the decomposition of magnesite to  $\text{CO}_2$  and periclase.

It is of interest to compare the calorimetric and equilibrium decomposition data on  $\text{MgCO}_3$  with solubility measurements. Yanat'eva (1954) measured the solubility of magnesite in  $\text{H}_2\text{O}$  under a fixed pressure of



This result, together with the well-established carbonic acid equilibrium data (Rossini and others, 1952;

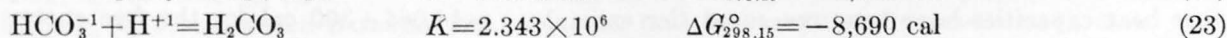
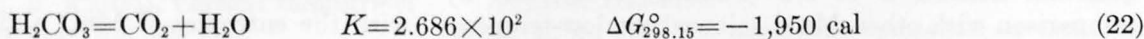


TABLE 5.—Heat of decomposition of  $\text{MgCO}_3$  based on data of Marc and Simek (1913)

$T$ (degrees K)	$P_{\text{CO}_2}$ (atm)	$\Delta \left[ \frac{G_T^{\circ} - H_{298.15}^{\circ}}{T} \right]$ (cal deg <sup>-1</sup> )	$R \ln f_{\text{CO}_2}$ (cal deg <sup>-1</sup> )	$\frac{\Delta H_{298.15}^{\circ}}{T}$ (cal deg <sup>-1</sup> )	$\Delta H_{298.15}^{\circ}$ (cal)
671.5	0.825	-41.425	-0.382	41.807	28,073
694.9	1.380	-41.382	.640	40.742	28,311
697.9	1.650	-41.377	.955	40.382	28,183
699.9	1.856	-41.372	1.229	40.143	28,096
702.3	1.730	-41.368	1.089	40.279	28,288
705.1	1.816	-41.363	1.185	40.178	28,330
711.1	3.277	-41.353	2.359	38.994	27,729
713.8	3.362	-41.347	2.410	38.937	27,793
713.9	3.059	-41.347	2.222	39.125	27,931
715.7	3.153	-41.343	2.282	39.061	27,956
716.7	2.900	-41.339	2.116	39.223	28,111
724.5	3.118	-41.327	2.260	39.067	28,304
725.6	3.874	-41.325	2.691	38.634	28,033
729.9	3.517	-41.318	2.499	38.819	28,334
743.2	4.391	-41.292	2.940	38.352	28,503
746.9	4.578	-41.285	3.023	38.262	28,578
754.3	6.162	-41.270	3.613	37.657	28,405
762.5	6.904	-41.255	3.839	37.416	28,530
763.9	6.943	-41.251	3.851	37.400	28,570
770.6	10.560	-41.238	4.638	36.600	28,204
770.6	9.201	-41.238	4.410	36.828	28,380
775.7	9.200	-41.229	4.410	36.819	28,560
782.1	11.169	-41.217	4.795	36.422	28,486
782.3	11.064	-41.216	4.777	36.439	28,506
Mean	-----	-----	-----	-----	28,258 ±100

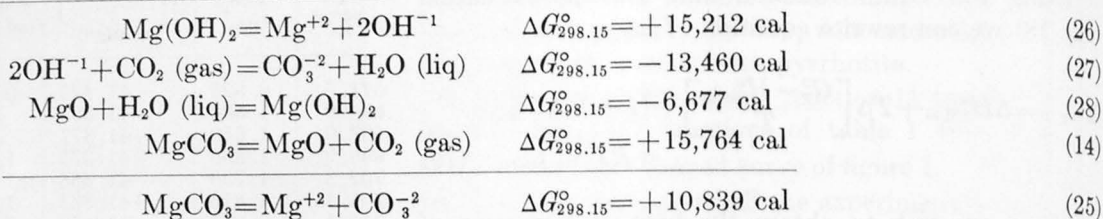
TABLE 6.—Heat of decomposition of  $\text{MgCO}_3$  from data of Harker and Tuttle (1955)

$T$ (degrees K)	$P_{\text{CO}_2}$ (atm)	$\Delta \left[ \frac{G_T^{\circ} - H_{298.15}^{\circ}}{T} \right]$ (cal deg <sup>-1</sup> )	$R \ln f_{\text{CO}_2}$ (cal deg <sup>-1</sup> )	$\frac{(P-1)\Delta V_{298.15}^{\circ}}{T}$ (cal deg <sup>-1</sup> )	$\frac{\Delta H_{298.15}^{\circ}}{T}$ (cal deg <sup>-1</sup> )	$\Delta H_{298.15}^{\circ}$ (cal)
873.2	61	-41.035	8.201	<sup>1</sup> -0.028	32.862	28,695
1,013.2	680	-40.735	13.393	-.274	27.616	27,980
1,083.2	1,361	-40.585	15.171	-.513	25.927	28,084
1,108.2	1,939	-40.532	16.197	-.714	25.049	27,759
1,123.2	2,041	-40.500	16.350	-.742	24.892	27,958
Mean	-----	-----	-----	-----	-----	28,095 ±320

<sup>1</sup> Molar volume data from Robie and Bethke (1962).

1 atmosphere  $\text{CO}_2$ . From her results Stout and Robie (1963) calculated the thermodynamic equilibrium constant (that is, activity product) for the reaction

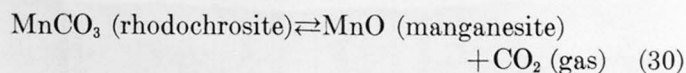
This result may be compared with the value based on the heat and free energy of formation of  $\text{MgCO}_3$  derived from the decomposition data using the following sequence of reactions:



The agreement is satisfactory but may be fortuitous in view of the recent work of Hostetler (1963b) on the complexing of  $\text{MgCO}_3$  in aqueous solution. In this calculation we have used Hostetler's (1963a)  $\text{Mg(OH)}_2$  solubility constant,  $K=3.07 \times 10^{-11}$ , and data from Rossini and others (1952) to obtain the  $\Delta G$ 's for reactions 26 and 27. The solubility results were *not* used in arriving at our "best values" of  $\Delta H_f^{\circ}$  and  $\Delta G_f^{\circ}$  for  $\text{MgCO}_3$ . The calculation has been included to illustrate one of the several reaction schemes that may be used in comparing decomposition results with the solubility measurements.

#### RHODOCHROSITE

Goldsmith and Graf (1957) have studied the decomposition of rhodochrosite,



between 650° and 1,050°K. Their data have been treated in the same fashion as was done with Harker and Tuttle's results on  $\text{MgCO}_3$ . Before proceeding with the calculation, however, it will be necessary to correct the entropy of  $\text{MnCO}_3$  given in the standard references (Rossini and others, 1952; Kelley and King, 1961). The value for  $S_{298.15}^{\circ}$  of rhodochrosite given in Rossini and in Kelley and King is based on heat-capacity measurements by Anderson (1934) between 50° and 300°K. Anderson extrapolated his  $C_p$  data to 0°K utilizing an empirical sum of Debye and Einstein specific-heat functions in order to obtain the entropy at 298.15°K. This procedure is valid for diamagnetic compounds if it can be assumed that no solid-state transition exists below the lowest temperature for which  $C_p$  was measured, a usually safe assumption. However,  $\text{Mn}^{+2}$  is a paramagnetic ion with a spin quantum number  $J$  of 5/2 (Pauling, 1960), and by comparison with other  $\text{Mn}^{+2}$  salts whose low-temperature heat capacities have been measured (for example,  $\text{MnF}_2$ ,  $\text{MnCl}_2$ ,  $\text{MnO}$ ,  $\text{MnBr}_2$ ,  $\text{Mn}_2\text{SiO}_4$ ) it is reasonable to assume that  $\text{MnCO}_3$  would exhibit an anomaly in the specific heat (due to the ordering of the unpaired electron spins) at some temperature below 50°K.

The elementary model of this ordering process for transition ion salts leads to a change in entropy of  $R \ln (2J+1)$  (Van Vleck, 1932) in passing from the ordered spin state at 0°K to the disordered state  $T \gg T_N$  where  $T_N$  is the Néel or ordering temperature. This term is an additional contribution to the entropy over and above that due to the lattice vibrations alone. We have assumed that Anderson's extrapolation represents a reasonable approximation for the lattice contribution to the entropy below 50°K and have added  $0.95 R \ln 6 = 3.38 \text{ cal mole}^{-1} \text{ deg}^{-1}$  to his value of  $20.5 \text{ cal mole}^{-1} \text{ deg}^{-1}$ , giving  $23.9 \pm 0.5 \text{ cal mole}^{-1} \text{ deg}^{-1}$  as the correct entropy of  $\text{MnCO}_3$  at 298.15°K. Justification for this correction is provided by recent heat-capacity measurements by Kalinkina (1962). His data show a large anomaly in the specific heats of  $\text{MnCO}_3$  and  $\text{FeCO}_3$  in the neighborhood of 30°K.

A similar situation exists with respect to Anderson's value of  $S_{298.15}^{\circ}$  for  $\text{FeCO}_3$ . In the case of  $\text{Fe}^{+2}$   $J$  is 2 and we should add a maximum of  $R \ln 5 = 3.20 \text{ cal mole}^{-1} \text{ deg}^{-1}$ . However, Anderson's lowest temperature heat capacity measurement at 54°K probably included some of the magnetic contribution, so we have added only  $0.9 R \ln 5$  to Anderson's value  $22.4 \pm .4 \text{ cal mole}^{-1} \text{ deg}^{-1}$ . We estimate the entropy of siderite at  $S_{298.15}^{\circ}$  as  $25.1 \pm 0.6 \text{ cal mole}^{-1} \text{ deg}^{-1}$ .

The corrected entropy of  $\text{MnCO}_3$  was combined with data listed in Kelley (1960) to give the free-energy functions for  $\text{MnCO}_3$  listed in table 1. The results of the calculations on the equilibrium data are given in table 7. The mean value for the heat of formation,  $\Delta H_{f, 298.15}^{\circ}$ , of rhodochrosite from  $\text{MnO}$  and  $\text{CO}_2$  is  $-26,420 \pm 150 \text{ cal mole}^{-1}$ . If we had not made the above correction to the entropy, the values of  $\Delta H_{f, 298.15}^{\circ}$  would have shown a trend with temperature of 1,400 cal and we would have probably concluded that Goldsmith and Graf's measurements represented non-equilibrium results. This heat of formation together with the entropies of  $\text{MnO}$  and  $\text{CO}_2$  gives  $\Delta G_{f, 298.15}^{\circ} = -14,064 \pm 300 \text{ cal}$  for the free energy of formation of rhodochrosite from the oxides. The free energy of formation from the elements obtained from these data is  $\Delta G_{f, 298.15}^{\circ} = -195,040 \text{ cal}$  and is in fair agreement with that obtained by Garrels and others (1960),

TABLE 7.—Calculation of the heat of the reaction  $\text{MnCO}_3 = \text{MnO} + \text{CO}_2$  from equilibrium data of Goldsmith and Graf (1957)

$T$ (degrees K)	$P_{\text{CO}_2}$ (atm)	$\Delta \left[ \frac{G_T^\circ - H_{298.15}^\circ}{T} \right]$ (cal deg <sup>-1</sup> )	$\frac{(P-1)\Delta V_{298.15}^\circ}{T}$ (cal deg <sup>-1</sup> )	$f_{\text{CO}_2}$ (atm)	$R \ln f_{\text{CO}_2}$ (cal deg <sup>-1</sup> )	$\Delta H_{298.15}$ (cal)
649----	1	-41.141	<sup>1</sup> 0.000	1	0.0	26,700
783----	34	-40.898	-.018	34	7.008	26,550
836----	102	-40.797	-.052	105	9.249	26,418
908----	345	-40.651	-.164	391	11.902	26,253
959----	672	-40.546	-.303	834	13.367	26,355
1,012----	1360	-40.433	-.581	2075	15.178	26,146
1,050----	1970	-40.357	-.811	(3000)	15.910	26,521
Mean----						26,420 ± 150

<sup>1</sup> Molar volume data from Robie and Bethke (1962).

$\Delta G_{T, 298.15}^\circ = -195,700$  cal, from solubility measurements on natural rhodochrosite.

### SUMMARY

In the foregoing discussion we have tried to demonstrate the usefulness of the Gibbs function,  $(G_T^\circ - H_{298}^\circ)/T$ , in obtaining the heat of a reaction from equilibrium data. The resultant values of  $\Delta H_T^\circ$  are listed in table 1 along with necessary auxiliary data. These values are recommended as the best presently available for FeS, SnS, MgCO<sub>3</sub>, and MnCO<sub>3</sub>.

### REFERENCES

- Adami, L. H., and King, E. G., 1964, Heats and free energies of formation of sulfides of manganese, iron, zinc, and cadmium: U.S. Bur. Mines, Rept. Inv. 6495, 10 p.
- Alcock, C. B., and Richardson, F. O., 1951, Thermodynamics of ferrous sulfide: *Nature*, v. 168, no. 4276, p. 661-662.
- Anderson, C. T., 1934, The heat capacities of magnesium, zinc, lead, manganese and iron carbonates at low temperatures: *Am. Chem. Soc. Jour.*, v. 56, p. 849-851.
- Barron, T. H. K., Berg, W. T., and Morrison, J. A., 1959, On the heat capacity of crystalline magnesium oxide: *Royal Soc. [Great Britain] Proc. A.*, v. 250, p. 70-83.
- Coughlin, J. P., 1950, High-temperature heat contents of manganese sulfide, ferrous sulfide and pyrite: *Am. Chem. Soc. Jour.*, v. 72, p. 5445-5447.
- 1954, Contributions to the data on theoretical metallurgy, XII. Heats and free energies of formation of inorganic oxides: U.S. Bur. Mines Bull. 542, 80 p.
- Cox, E. M., Bachelier, M. C., Nachtrieb, N. H., and Skapski, A. S., 1949, The influence of temperature on the affinity of sulfur for copper, manganese and iron: *Am. Inst. Mining and Metall. Engineers Trans.*, v. 185, p. 27-31.
- Darken, L. S., and Gurry, R. W., 1953, Physical chemistry of metals: New York, McGraw-Hill, 535 p.
- Garrels, R. M., Thompson, M. E., and Siever, Raymond, 1960, Stability of some carbonates at 25°C and one atmosphere total pressure: *Am. Jour. Sci.*, v. 258, p. 402-418.
- Goldsmith, J. R., and Graf, D. L., 1957, The system CaO-

MnO-CO<sub>2</sub>: *Geochim. et Cosmochim. Acta*, v. 11, no. 4, p. 310-333.

- Grønvold, Fredrik, Westrum, E. F., Jr., and Chou, C., 1959, The heat capacities and thermodynamic properties of the pyrrhotites FeS and Fe<sub>0.87</sub>S from 5 to 300°K: *Jour. Chem. Physics*, v. 30, no. 2, p. 528-531.
- Harker, R. I., and Tuttle, O. F., 1955, Studies in the system CaO-MgO-CO<sub>2</sub>, pt. I. The thermal dissociation of calcite, dolomite, and magnesite: *Am. Jour. Sci.*, v. 253, p. 209-224.
- Harned, H. S., and Owen, B. B., 1958, The physical chemistry of electrolytic solutions: New York, Reinhold Pub. Corp., 803 p.
- Hostetler, P. B., 1963a, The stability and surface energy of brucite in water at 25°C: *Am. Jour. Sci.*, v. 261, p. 238-258.
- 1963b, Complexing of magnesium with bicarbonate: *Jour. Phys. Chemistry*, v. 67, p. 720-721.
- Hultgren, Ralph, Orr, R. L., Anderson, P. D., and Kelley, K. K., 1963, Selected values of thermodynamic properties of metals and alloys: New York, John Wiley and Sons, 963 p.
- Kalinkina, I. N., 1962, Magnitiaya teployemkost' antiferromagnitnykh karbonatov Co, Ni, Mn, Fe: *Zh. Eksperim. i. teor. Fiz.*, v. 43, p. 2028-2037.
- Kelley, K. K., 1937, Contributions to the data on theoretical metallurgy, VII. The thermodynamic properties of sulfur and its inorganic compounds: U.S. Bur. Mines Bull. 406, 154 p.
- 1960, Contributions to the data on theoretical metallurgy, XIII. High temperature heat-content, heat-capacity and entropy data for the elements and inorganic compounds: U.S. Bur. Mines Bull. 584, 232 p.
- Kelley, K. K., and King, E. G., 1961, Contributions to the data on theoretical metallurgy, XIV. Entropies of the elements and inorganic compounds: U.S. Bur. Mines Bull. 592, 149 p.
- King, E. G., and Todd, S. S., 1953, Heat capacities at low temperatures and entropies at 298.15°K of stannic and stannous sulfides: *Am. Chem. Soc. Jour.*, v. 75, p. 3023.
- Lewis, G. N., and Randall, Merle, 1961, Thermodynamics, 2nd ed., revised by Pitzer, K. S., and Brewer, Leo, New York, McGraw-Hill, 723 p.
- Marc, R., and Simek, A., 1913, Über die thermische dissoziation des magnesiumkarbonats: *Zietschr. anorg. Chem.*, v. 82, p. 17-49.
- Orr, R. L., and Christensen, A. U., 1958, High temperature heat contents of stannous and stannic sulfides: *Jour. Phys. Chemistry*, v. 62, p. 124-125.
- Pankratz, L. B., and Kelley, K. K., 1963, Thermodynamic data for magnesium oxide (periclase): U.S. Bur. Mines Rept. Inv. 6295, 5 p.
- Pauling, Linus, 1960, The nature of the chemical bond, 3rd ed.: Ithaca, N.Y., Cornell Univ. Press, 644 p.
- Price, Donna, 1955, Thermodynamic functions for carbon dioxide: *Indus. and Eng. Chemistry*, v. 47, p. 1649-1652.
- Richards, A. W., 1955, The heat and free energy of formation and vaporization of stannous sulfide: *Faraday Soc. Trans.*, v. 51, p. 1193-1197.
- Robie, R. A., 1962, Thermodynamic properties of minerals: U.S. Geol. Survey TEI-816 (open-file rept), 31 p.
- Robie, R. A., and Bethke, P. M., 1962, Molar volumes and densities of minerals: U.S. Geol. Survey TEI-822 (open-file rept), 30 p.

- Rosenqvist, Terkel, 1954, A thermodynamic study of the iron, cobalt, and nickel sulfides: *Iron and Steel Inst. Jour.*, v. 176, p. 37-57.
- Rossini, F. D., and others, 1952, Selected values of chemical thermodynamic properties: U.S. Natl. Bur. Standards, Circ. 500, 1268 p.
- Rossini, F. D., 1956, Assignment of uncertainties to thermochemical data, in *Experimental thermochemistry*, v. 1, p. 319: New York, Interscience, p. 297-326.
- Stout, J. W., and Robie, R. A., 1963, Heat capacity from 11 to 300°K, entropy and heat of formation of dolomite: *Jour. Phys. Chemistry*, v. 67, p. 2248-2252.
- Stull, D. R., and others, 1964, JANAF thermochemical tables: Midland, Mich., Dow Chem. Co.
- Sudo, Kingo, 1950, Fundamental researches on smelting of sulfide ores, II. On the equilibrium reduction of solid ferrous sulfide by hydrogen gas: *Tohoku Univ. Research Inst., Sci. Repts.*, ser. A, v. 2, p. 312-330.
- Sudo, Kingo, 1951, Fundamental researches on smelting of sulfide ores, IX. On the equilibrium in the reduction of sulfur in molten tin by hydrogen gas: *Tohoku Univ. Research Inst., Sci. Repts.*, ser. A, v. 3, p. 356-363.
- Van Vleck, J. H., 1932, The theory of electric and magnetic susceptibilities: Oxford, Oxford Univ. Press, 384 p.
- Victor, A. C., and Douglas, T. B., 1963, Thermodynamic properties of magnesium oxide and beryllium oxide from 298 to 1200°K: U.S. Natl. Bur. Standards Jour. Research, v. 67A, p. 325-329.
- Yanat'eva, O. K., 1954, O rastvorimosti dolomita v vode v prisutstvii uglekisloty: *Izvest. Akad. Nauk. S.S.S.R. Otdel. Khim. Nauk*, p. 1119-1120.



## EXTRACTABLE ORGANIC MATERIAL IN NONMARINE AND MARINE SHALES OF CRETACEOUS AGE

By H. A. TOURTELOT and I. C. FROST, Denver, Colo.

*Abstract.*—Organic material extracted from 5 samples of nonmarine carbonaceous shale, 10 samples of marine black shale, and 3 samples of marine marlstone, all from the Pierre Shale and equivalent stratigraphic units of Late Cretaceous age, was separated with activated silica gel and solvents into fractions interpreted as saturated hydrocarbons, aromatic hydrocarbons, and nonhydrocarbons. Organic-carbon content of the samples extracted ranges from 0.53 percent to 17.3 percent; only 1 sample contained less than 2 percent organic carbon. Extractable organic material ranges from 0.008 to 0.355 percent of the sample and is roughly proportional to the organic-carbon content of the samples. The ratio between saturated and aromatic hydrocarbon fractions is more than 1, except for one sample, and tends to be inversely proportional to the organic-carbon content. The data on extractable material do not distinguish between shale and marlstone of marine and nonmarine origin. Comparison of the data on the samples of Cretaceous age with published data on samples of a wide range of ages and geologic histories suggests that postdepositional reactions increase the proportion of saturated and aromatic hydrocarbons compared to nonhydrocarbons.

Data from solvent-extraction analyses of 5 samples of nonmarine carbonaceous shale, 10 samples of marine black shale, and 3 samples of marine marlstone from the Pierre Shale and equivalent rocks of Late Cretaceous age provide a basis for comparison of the composition of rocks of marine and nonmarine origin. A sample of the nonmarine Green River Formation of Eocene age provided by K. E. Stanfield, U.S. Bureau of Mines, and one of the marine Chattanooga Shale of Devonian and Mississippian (?) age furnished by V. E. Swanson, also were analysed. These data are compared with those from other sediments and sedimentary rocks. The samples of Cretaceous age were collected from outcrops by H. A. Tourtelot, J. R. Gill, and L. G. Schultz in the course of the geochemical investigations of the Pierre Shale (Tourtelot, 1962; Tourtelot and others, 1960). The extraction analyses were made by I. C. Frost and J. A. Thomas. We have benefited greatly from consultation with W. S. Ferguson and D.

R. Baker, Marathon Oil Co., Denver Research Laboratory, and from their advice at many stages in the analytical work and consideration of the data.

### ANALYSES

The extraction of organic material with organic solvents from rocks and sediments is an empirical procedure. Such factors as the weight of sample in relation to volume of solvent, the grain size to which the sample is crushed or ground, and the length of time during which the sample is extracted, as well as the solvents used, also can affect the results materially. Data obtained in one study cannot be compared confidently with data from another because of differences in analytical procedures. Most previous work has been done with solvents made up of mixtures of 70 to 90 percent benzene with 10 to 20 percent methanol (or ethanol) or of 70 percent benzene with 15 percent ethanol and 15 percent acetone. Ferguson (1962, p. 1615) reviewed the general problem of extracting hydrocarbons from rocks and found benzene to be fully effective. He pointed out that mixtures involving polar solvents such as methanol and acetone extract larger amounts of nonhydrocarbon organic material which tend to interfere with chromatographic separations (Ferguson, 1962, p. 1616). The methods used by Ferguson have been adopted without much modification because the Pierre Shale here described and the Pennsylvanian Cherokee Shale studied by Ferguson are generally similar in gross composition and were deposited under similar conditions; as a result, comparisons between them would be of interest.

Crushed and ground portions of each sample were pulverized in a hammer mill. Generally, 500 grams of the pulverized samples was extracted with approximately 2,000 milliliters of redistilled reagent-grade benzene. The extractions were made in large Soxhlet extractors. Bright copper strips were added to the



flask containing benzene to react with and precipitate any extracted sulfur. The extraction was continued for 3 working days to give approximately 75 extraction cycles in a total of 24 hours. The benzene extract was then concentrated by distillation to less than 500 ml, and then filtered through a fine fritted-glass filter to remove any copper sulfide, shale dust, or filter fibers in the extract. This filtered extract was made to exactly 500 ml.

Duplicate aliquots of the filtered benzene extract were evaporated to constant weight under slight vacuum. The residues were then treated separately with 30 ml of cyclohexane and transferred to silica-gel columns for chromatographic separations. Three separate fractions of the benzene extracts were obtained as follows: (1) a fraction eluted by cyclohexane, interpreted to represent the saturated hydrocarbons; (2) a fraction eluted by benzene, interpreted as aromatic hydrocarbons; and (3) a fraction, which included polar compounds, eluted by a 50-percent mixture of benzene-methanol. The solvents were removed from the eluted fractions by distillation at 55°C under vacuum, and the residues were taken to constant weight. Oxidation of the extracted organic material and the fractions was avoided or minimized by carrying out concentration in vacuum or under an atmosphere of nitrogen. The figures reported as nonhydrocarbons included the amounts of polar compounds eluted by the benzene-methanol mixture, the amounts of material retained on the silica-gel column, and any manipulation losses. Even though these figures for nonhydrocarbons thus include unrecovered material, it is convenient to speak of them in the following discussions as if they represented an actual compositional entity.

The chromatographic columns were 10 mm in inside diameter and were packed with 2 layers of silica gel. The lower layer consisted of approximately 15 cm of 60-mesh gel that had been boiled in concentrated HNO<sub>3</sub>, washed, and dried at 225°C. The upper layer consisted of 12 cm of 40–60-mesh acid-treated gel. (See Ferguson, 1962, p. 1614, for further details.)

All reagents were run as blanks to assure no contamination, and all weighings were double checked. Generally, very close agreement was obtained between duplicate determinations. Samples that had the larger amounts of extractable organic material had less percentage variation than samples yielding little extractable organic material.

### GEOLOGIC SETTING

The geologic setting and large-scale depositional pattern of the Pierre Shale and equivalent stratigraphic units, and the history of organic matter within

this depositional pattern, have been described by Tourtelot (1962, 1964). Part of the organic matter produced by land plants in the western source area was deposited under nonmarine conditions, chiefly on flood plains adjacent to the shoreline of the Pierre Sea. Locally, coal beds were formed, but most of the organic matter deposited under nonmarine conditions was incorporated in what are now beds of brown carbonaceous shale. Much organic matter produced on land was swept across the coastal plain into the sea where it was mixed with at least some organic matter produced in the sea. The mixture of organic matter and clay was deposited on the sea floor. Most of these marine shales contain enough organic matter to fall into the general class called black shales.

### SAMPLES AND ANALYTICAL DATA

Samples and analytical data are listed in the accompanying table in order of decreasing content of organic carbon. All samples, except one of marine shale, contain more than 2 percent organic carbon.

The samples of nonmarine carbonaceous shale are from nonmarine formations in Wyoming and Montana that are equivalent in age to about the lower third of the Pierre Shale along the Missouri River in South Dakota (see Gill and Cobban, 1961). All but one of the samples of shale of marine origin are from the lowermost part of the Pierre Shale in Wyoming, North Dakota, and South Dakota. The sample of marine Bearpaw Shale is from Montana and is younger than the sample of the nonmarine Judith River Formation, but older than the three samples of marlstone from the Mobridge Member of the Pierre Shale from South Dakota and Nebraska. The localities where the samples were collected are indicated on figure 1.

A sample of the Chattanooga Shale and one from the Green River Formation also were included in the study to provide extraction data on these two well-known examples of marine and nonmarine organic-rich shales, respectively.

The number of samples of rocks of Cretaceous age is too small for averages of the different kinds of data in the table to be meaningful. The overlap of values between the groups having different origins is evident. The total extractable organic material and the nonhydrocarbon portion of this material are roughly proportional to the amount of organic carbon in the samples. The hydrocarbon portion of the extractable material, however, as well as the amount of saturated and aromatic hydrocarbons making up the hydrocarbon portion show no evident relation to the other analytical data or geologic parameters.

[Extraction analyses by I. C. Frost and J. A. Thomas. Solvent-extractable nonhydrocarbons include material not removable from chromatographic column. Organic carbon determined by I. C. Frost by gasometric method (Rader and Grimaldi, 1961, p. A33-A39)]

Sample No.	Location						Description		Organic carbon (weight percent)	Solvent-extractable material (weight percent of shale)				
	Section		Township	Range	County	State	Formation	Member		Total	Saturated hydrocarbon	Aromatic hydrocarbon	Total hydrocarbon	Non-hydrocarbon
	Subdivision	No.												
<b>NONMARINE</b>														
<b>Carbonaceous shale</b>														
298356	SE $\frac{1}{4}$ SE $\frac{1}{4}$	5	38 N.	78 W.	Natrona	Wyo.	Mesaverde	Parkman Sandstone	17.3	0.355	0.0335	0.0240	0.0575	0.2975
298452	NW $\frac{1}{4}$	26	24 N.	17 E.	Blaine	Mont.	Judith River		5.76	.128	.0105	.0035	.0140	.1140
298425	SW $\frac{1}{4}$ NE $\frac{1}{4}$ SW $\frac{1}{4}$	35	2 S.	22 E.	Carbon	do.	Eagle Sandstone		4.29	.051	.0170	.0065	.0235	.0275
298395	SW $\frac{1}{4}$ SE $\frac{1}{4}$ NW $\frac{1}{4}$	4	14 N.	31 E.	Garfield	do.	Judith River		3.48	.068	.0165	.0115	.0280	.0400
298354	CNW $\frac{1}{4}$	25	39 N.	78 E.	Natrona	Wyo.	Mesaverde	Teapot Sandstone	2.33	.048	.0150	.0035	.0185	.0295
<b>MARINE</b>														
<b>Black shale</b>														
259549	NW $\frac{1}{4}$ NE $\frac{1}{4}$	17	104 N.	71 W.	Lyman	S. Dak.	Pierre Shale	Sharon Springs	8.5	0.140	0.0100	0.0045	0.0145	0.1255
259582	SW $\frac{1}{4}$ NE $\frac{1}{4}$	23	38 N.	62 W.	Niobrara	Wyo.	do.	do.	6.5	.138	.0260	.0275	.0535	.0845
259591	NE $\frac{1}{4}$ NE $\frac{1}{4}$	35	12 N.	2 E.	Butte	S. Dak.	do.	Mitten Black Shale	5.7	.081	.0220	.0060	.0280	.0530
259527	SW $\frac{1}{4}$	25	161 N.	57 W.	Cavalier	N. Dak.	do.	Pembina	5.6	.063	.0185	.0080	.0265	.0365
259561		36	94 N.	64 W.	Charles Mix	S. Dak.	do.	Sharon Springs	5.4	.052	.0130	.0040	.0170	.0350
259526	SE $\frac{1}{4}$ SE $\frac{1}{4}$	118	163 N.	57 W.	Cavalier	N. Dak.	do.	Pembina	4.8	.057	.0315	.0035	.0350	.0220
259573	NE $\frac{1}{4}$ NE $\frac{1}{4}$	31	7 S.	7 E.	Fall River	S. Dak.	do.	Gammon Ferruginous	3.3	.028	.0125	.0035	.0160	.0120
259563	NE $\frac{1}{4}$	17	93 N.	56 W.	Yankton	do.	do.	Sharon Springs	3.1	.081	.0455	.0040	.0495	.0315
259571	SW $\frac{1}{4}$ NW $\frac{1}{4}$	32	7 S.	7 E.	Fall River	do.	do.	do.	2.5	.046	.0150	.0095	.0245	.0215
298491	NW $\frac{1}{4}$ NW $\frac{1}{4}$	3	36 N.	8 W.	Glacier	Mont.	Bearpaw Shale		.53	.011	.0060	.0010	.0070	.0040
<b>MARLSTONE</b>														
259556	SW $\frac{1}{4}$ SW $\frac{1}{4}$	18	96 N.	67 W.	Gregory	S. Dak.	Pierre Shale	Mobridge	2.9	0.055	0.0345	0.0035	0.0380	0.0170
259553	SE $\frac{1}{4}$ SW $\frac{1}{4}$	21	106 N.	73 W.	Lyman	do.	do.	do.	2.6	.008	.0040	.0010	.0050	.0030
259562	NE $\frac{1}{4}$	24	30 N.	7 W.	Knox	Neb.	do.	do.	2.5	.030	.0080	.0040	.0120	.0180
<b>OTHER SHALES</b>														
D-115183 <sup>1</sup>		12	6 S.	95 W.	Garfield	Colo.	Green River	Parachute Creek Mahogany zone	14.1	1.650	0.3000	0.2840	0.5840	1.0660
D-112453 <sup>2</sup>					DeKalb	Tenn.	Chattanooga Shale	Gassaway	13.0	.285	.0515	.1695	.2210	0.0640

<sup>1</sup> Average mine-run shale from the Bureau of Mines Demonstration Mine near Rifle, Colo. See Stanfield and others (1951, "composite sample," p. 4, tables 6, 15-20) for data on properties and composition of a sample of similar but not identical shale.<sup>2</sup> Adit, about 1 mi southwest on old Tennessee Route 26 (now a boat-landing road) from point where it joins Route 26 at top of descent to east end of Sligo Bridge. See Bates and Strahl (1957) for data on mineralogy of shale from the same locality.

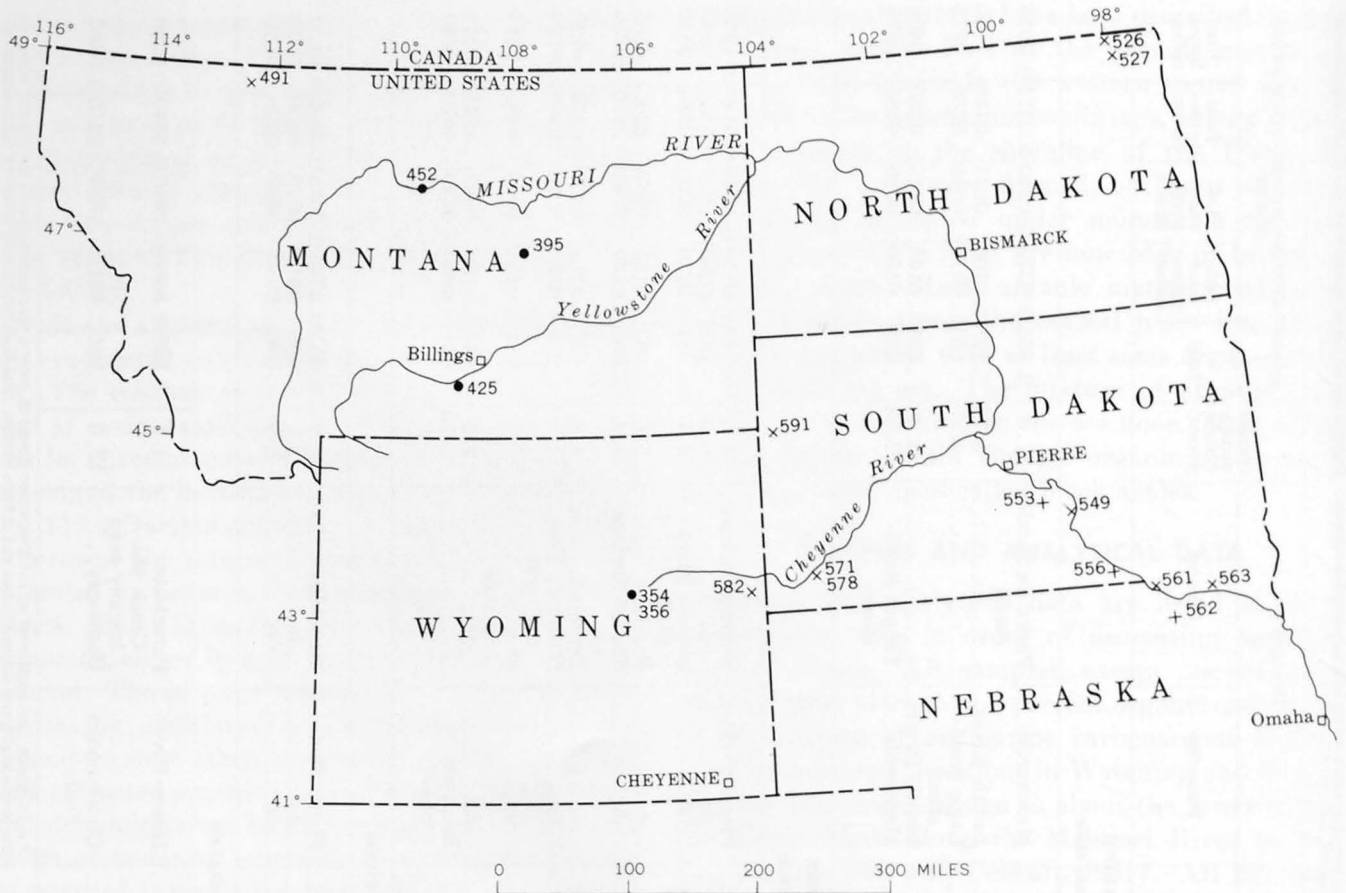


FIGURE 1.—Location of samples. Symbols: ●, nonmarine carbonaceous shale; ×, marine black shale; +, marine marlstone. Sample numbers are last three figures of sample numbers used in the table.

Breger and others (1960) and Breger and Brown (1962, 1963) reported that the nonsoluble organic matter, or kerogen, in three of these black-shale samples (259549, 259563, 259582) from the Pierre is compositionally and structurally similar to lignite or subbituminous coal and hence is predominantly humic in nature. The hydrogen content of the organic isolates (on a moisture- and ash-free basis) of these three samples (I. A. Breger and J. C. Chandler, oral communication, May 1960) increases from east to west, as shown below:

	Eastern-most sample (259563)	Intermedi-ate sample (259549)	Western-most sample (259582)
Hydrogen (weight percent)-----	4.5	5.7	6.7

<sup>1</sup> Calculated from original analysis to eliminate pyrite sulfur on assumption that the organic matter contains 5 percent sulfur on a moisture- and ash-free basis.

The increase correlates with increasing distance from the eastern shoreline of the Pierre Sea and was attributed to increased contributions of marine organic detritus. It is not certain that much if any of the organic matter was derived from the land behind that shoreline (Tourtelot, 1964). The contributions of marine organic detritus probably were small since the

hydrogen amounts for the presumably mixed marine and terrigenous organic matter are not greatly different from the 5.5 percent for terrigenous humic material cited by Breger and Brown (1962).

#### HYDROCARBON FRACTIONS AND NONHYDROCARBONS

Figure 2 shows the data on saturated hydrocarbons, aromatic hydrocarbons, and nonhydrocarbons plotted on a triangular diagram, along with similar data reported in the literature. The samples of Cretaceous age, as a group, are characterized by relatively low proportions of aromatic hydrocarbons and a wide range of proportions between the saturated hydrocarbons and the nonhydrocarbons that make up the bulk of the extractable organic matter. Nonhydrocarbons amount to more than half of the extractable organic matter in six of the marine samples and in all of the nonmarine samples of Cretaceous age, as well as of the shale sample from the Green River Formation. The extractable organic matter of the remaining seven marine Cretaceous samples consists of less than half nonhydrocarbons, and more than a third saturated

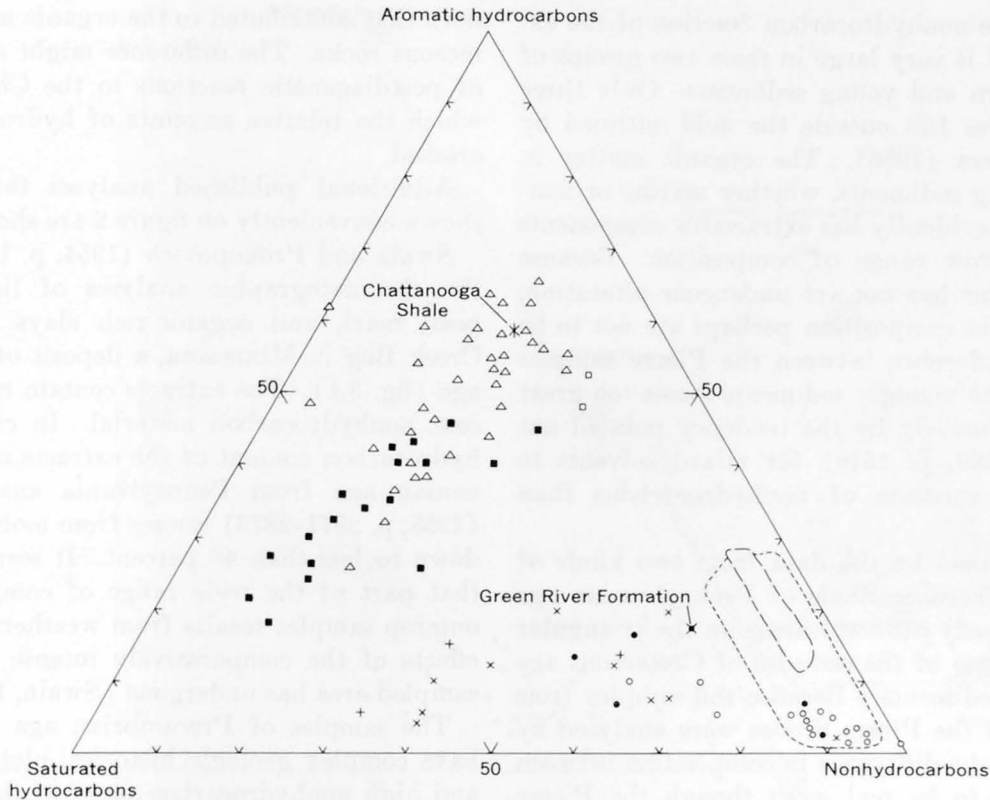


FIGURE 2.—Proportional composition of solvent-extractable material from shale, marlstone, clay, and marine mud. Symbols: ●, Cretaceous nonmarine carbonaceous shale; ×, Cretaceous marine black shale; +, Cretaceous marine marlstone; ○, Recent clays (Smith, 1954, p. 396, 398, 399); □, coal from Pennsylvanian Cherokee Shale; ■, marine black shale from Cherokee Shale; △, marine gray shale from Pennsylvanian Cherokee Shale (data on Cherokee Shale from D. B. Baker, written communication, September 1964). Area enclosed by short-dashed line, soils; area enclosed by long-dashed line, marine muds (Stevens and others, 1956, p. 980).

hydrocarbons. The extractable material in the Cretaceous marlstones is similar to that in both marine and nonmarine shales. Although the marine Cretaceous samples form a diffuse group on the diagram toward high proportions of saturated hydrocarbons, the overlapping of data on marine and nonmarine samples toward a high content of nonhydrocarbons makes it clear that these data cannot be used to distinguish these organic-rich rocks of marine and nonmarine origin. The extracts from the marlstones are not distinguishable from those from the shales.

The samples of Cretaceous age are outcrop samples, and some organic compounds have undoubtedly been removed during weathering. Baker (1962, p. 1638–1639) investigated the difference between outcrop and core samples of equivalent rock types of the Cherokee Shale and found that outcrop samples of gray shale and black shale probably had lost about half of their original hydrocarbon content; both saturated and aromatic hydrocarbons were affected about equally, as the saturated-aromatic hydrocarbon ratios of the outcrop and core samples were not greatly different. No com-

parable data are available for the Cretaceous samples, but some allowance must be made for loss of hydrocarbons on weathering, and Baker's data serve as a guide. If the amounts of hydrocarbons reported in the table are doubled, the points on figure 2 would be shifted away from the nonhydrocarbon corner a maximum distance of about 20 percent nonhydrocarbon. None of the points that represent Cretaceous samples would be shifted into the areas covered for the gray and black shales of the Cherokee Shale.

#### COMPARISONS WITH PUBLISHED DATA

The composition of the extractable organic material in Recent clays, which include the silty clay and clay samples from the Pelican Island, La., core (Smith, 1954, p. 396) and other modern sediments (Smith, 1954, p. 398 and 399) is shown in figure 2, as well as the general fields representing the composition of the extractable material in samples of soils and modern marine muds (Stevens and others, 1956, p. 980). Mixtures of benzene and methanol were used in both of

these studies. The nonhydrocarbon fraction of the extractable material is very large in these two groups of samples of modern and young sediments. Only three of Smith's samples fall outside the field outlined by Stevens and others (1956). The organic matter in modern and young sediments, whether marine or non-marine in origin, evidently has extractable components with a very narrow range of composition. Because this organic matter has not yet undergone alteration, large differences in composition perhaps are not to be expected. The difference between the Pierre samples as a group and the younger sediments seems too great to be caused exclusively by the tendency pointed out by Ferguson (1962, p. 1616) for mixed solvents to dissolve greater amounts of nonhydrocarbons than benzene alone.

The fields outlined by the data from two kinds of shale from the Cherokee Shale of Pennsylvanian age occupy conspicuously different areas on the triangular diagram from those of the samples of Cretaceous age or the younger sediments. Because the samples from the Cherokee and the Pierre Shales were analysed by the same method the difference in composition between them is believed to be real, even though the Pierre samples are from weathered rock.

The gray shales are interpreted by Baker (1962, p. 1628) as having been deposited under nearshore shallow marine conditions. The black shales also are marine in origin but were deposited under conditions that were different in the sense that either much more organic matter was produced in the environment and delivered there from other sources or that more of the organic matter was preserved. The two kinds of shale seem remarkably similar in proportions of hydrocarbons and nonhydrocarbons, although many of the samples of gray shale have a greater proportion of aromatic hydrocarbons, and about half the samples of black shale tend to have a greater proportion of saturated hydrocarbons. This similarity in composition seems to imply that the extractable material in these two kinds of shale was produced from very similar kinds of organic matter incorporated in the sediments, and that the diagenetic and postdiagenetic history of the two kinds of shale also has been similar.

The difference in composition of total extractable material between the Cherokee Shale and the Pierre samples may be due to primary differences in the composition of the organic matter produced in Pennsylvanian time and in Cretaceous and younger time. The Pennsylvanian flora, being made up chiefly of pteridophytic plants, may have had a composition that yielded greater amounts of hydrocarbons, compared to extractable nonhydrocarbons, than the relatively modern

flora that contributed to the organic matter in the Cretaceous rocks. The difference might also be the result of postdiagenetic reactions in the Cherokee Shale by which the relative amounts of hydrocarbons were increased.

Additional published analyses that could not be shown conveniently on figure 2 are shown on figure 3.

Swain and Prokopovich (1954, p. 1189) reported on the chromatographic analyses of lipoid extracts of peat, marl, and organic-rich clays from the Cedar Creek Bog in Minnesota, a deposit of late Pleistocene age (fig. 3A). The extracts contain more than 70 percent nonhydrocarbon material. In contrast, the nonhydrocarbon content of the extracts of samples of Devonian age from Pennsylvania analysed by Swain (1958, p. 2871-2873) ranges from more than 90 percent down to less than 40 percent. It seems possible to us that part of the wide range of composition of these outcrop samples results from weathering and from the effects of the comparatively intense folding that the sampled area has undergone (Swain, 1958, p. 2859).

The samples of Precambrian age (fig. 3A), which have complex geologic histories, plot in both the low and high nonhydrocarbon parts of the diagram. This scatter seems expectable, and the fact that any of these rocks have extracts of low hydrocarbon content seems to be the most important. Shimada (1963) analysed sediments and rocks of a wide range of origin, age, and geologic history (fig. 3B). A decrease in nonhydrocarbon content of the extracts with increasing age of the rock is a conspicuous feature of his data.

Despite many uncertainties in the data, a general conclusion is that solvent extracts of older rocks are likely to have a lower nonhydrocarbon content than those of young sediments, even though the extracts of some older rocks contain as much nonhydrocarbon material as the younger ones. With respect to the general geochemistry of organic material, it is perhaps more noteworthy that the extracts of all the modern sediments consist predominantly of nonhydrocarbon material. This implies that the lower nonhydrocarbon content of the extracts of many older rocks is the result of processes acting after those rocks were deposited as sediments rather than being a function of their original composition. The high ratios of odd- to even-carbon-number *n*-paraffins in Recent sediments compared to the low ratios in ancient shales reported by Bray and Evans (1961, p. 12-13) also indicate a difference in composition that seems primarily time dependent. Erdman (1961) emphasizes that reactions must take place in aquatic sediments after the end of the life processes of the plants and animals yielding the basic organic matter. Part of the reactions involved

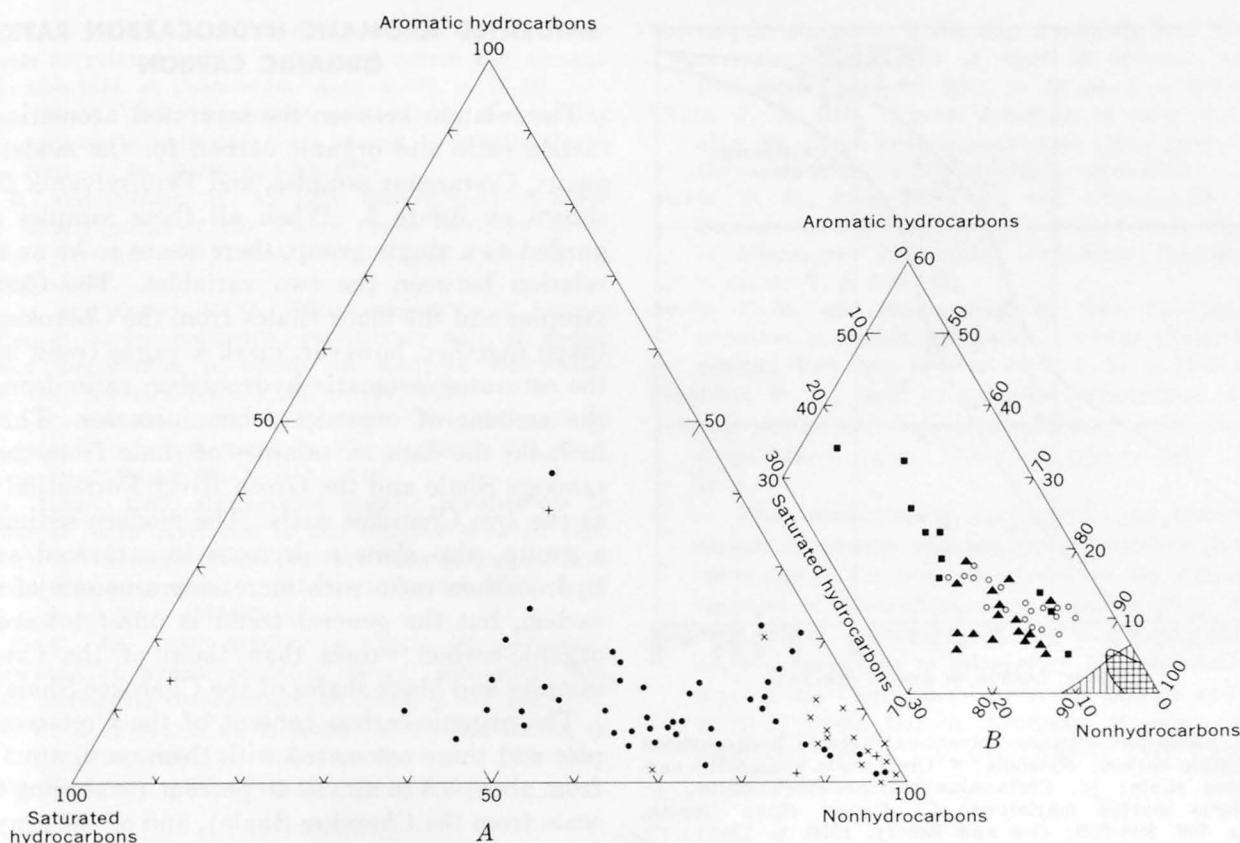


FIGURE 3.—Proportional composition of solvent-extractable material from a bog deposit, shale and other consolidated rocks, marine sediments, lake deposits, and brackish-water deposits. A.  $\times$ , Cedar Creek Bog of late Pleistocene age (Swain and Prokopovich, 1954, p. 1189);  $\bullet$ , shale of Devonian age (Swain, 1958, p. 2871–2873);  $+$ , rocks of Precambrian age (Swain and others, 1958, p. 180). B.  $\circ$ , rocks of Neogene (Miocene?) age (Shimada, 1963, p. 455);  $\blacktriangle$ , modern marine sediments (Shimada, 1963, p. 443);  $\blacksquare$ , rocks of Permian or Triassic age (Shimada, 1963, p. 462); vertical-lined area, lake deposits of Pliocene and Pleistocene age (Shimada, 1963, p. 458); crosshatched area, modern brackish-water lake deposits (Shimada, 1963, p. 436).

seems to be suggested by Erdman's (1961, p. 21, 24) finding of greater amounts of aromatic hydrocarbons in ancient sediments than in younger ones.

#### TOTAL HYDROCARBONS AND ORGANIC CARBON

The amount of total hydrocarbons (saturated plus aromatic compounds) extracted from the Cretaceous samples is very roughly proportional to the organic-carbon content of the samples. This relation is shown on figure 4, which also shows some of the data from Baker's similar diagram (Baker, 1962, p. 1637). The data for the Cretaceous samples do not indicate differences between samples of marine origin and those of nonmarine origin. The data generally plot below the field outlined by Baker, perhaps as a result of the loss of hydrocarbons by weathering of the Cretaceous shales. If the hydrocarbon content of the Cretaceous shales is doubled to allow for the order of magnitude of loss from weathering found by Baker (1962, p. 1638–1639), 11 of the 18 points for Cretaceous samples plot within the field outlined by Baker and at posi-

tions intermediate between those of his gray shales and those of his black shales.

Baker (1962, p. 1638) points out that a higher carbon values on his diagram, there appears to be a general leveling out in the amount of hydrocarbons extracted from the samples. He suggests that this may indicate that the samples with larger organic-carbon content contain relatively more humic organic matter that was not particularly appropriate for the generation of large amounts of hydrocarbons (Baker, 1962, p. 1638). (See also Breger and Brown, 1962, p. 223–224.) The black shales, however, must contain more of the hydrocarbon-producing organic matter (nonhumic material) than the gray shales, as yields of hydrocarbons are larger in the black shales. That this hydrocarbon-producing organic matter is very similar in the two shales is suggested by the data on figure 2. It cannot be inferred that the hydrocarbon-producing matter was specifically of marine origin, as the data on the marine samples and the coals from the Cherokee Shale and the nonmarine Cretaceous samples do not differ significantly.

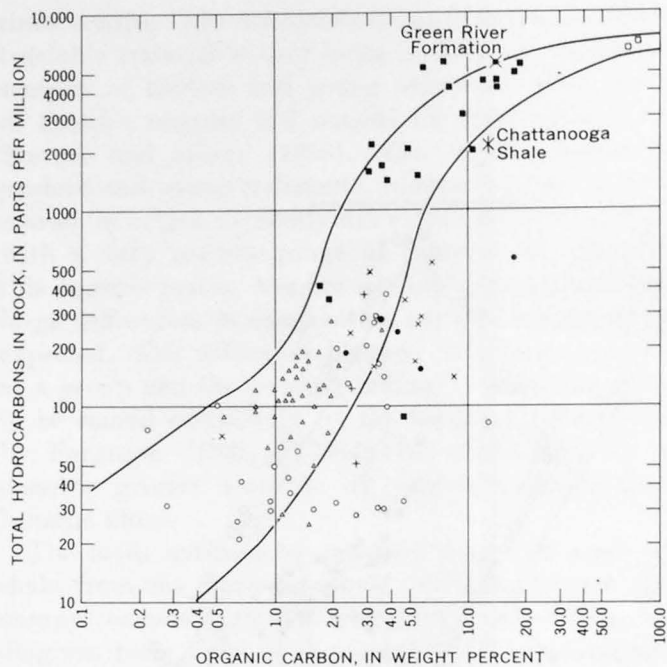


FIGURE 4.—Relation between solvent-extractable hydrocarbons and organic carbon. Symbols: ●, Cretaceous nonmarine carbonaceous shale; ×, Cretaceous marine black shale; +, Cretaceous marine marlstone; ○, Recent clays (Smith, 1954, p. 396, 398-399; Orr and Emery, 1956, p. 1251); □, ■, Δ, coal, black shale, and gray shale, respectively, from the Pennsylvanian Cherokee Shale. Samples studied by Baker (1962, p. 1637) fall in the field outlined between the two curves.

## SATURATED AROMATIC HYDROCARBON RATIO AND ORGANIC CARBON

The relation between the saturated/aromatic hydrocarbon ratio and organic carbon for the modern sediments, Cretaceous samples, and Pennsylvania shales is shown on figure 5. When all these samples are regarded as a single group, there seems to be no marked relation between the two variables. The Cretaceous samples and the black shales from the Cherokee Shale, taken together, however, mark a vague trend in which the saturated/aromatic hydrocarbon ratio decreases as the amount of organic carbon increases. This trend includes the data on samples of shale from the Chattanooga Shale and the Green River Formation as well as the two Cherokee coals. The modern sediments, as a group, also show a decrease in saturated/aromatic hydrocarbon ratio with increasing amounts of organic carbon, but the general trend is offset toward lower organic-carbon values than those of the Cretaceous samples and black shales of the Cherokee Shale.

The organic-carbon content of the Cretaceous samples and those associated with them on figure 5 ranges from about 0.5 to almost 20 percent (excluding the two coals from the Cherokee Shale), and of the gray shales from the Cherokee Shale and the younger samples, from about 0.2 to 4 percent. The ranges of the saturated/aromatic hydrocarbon ratio for these two groups of samples also are similar. When the overlap of these data is considered, it is surprising that the two groups should be separated so sharply on a diagram of this kind. No consistency is evident with respect to either geologic or geochemical parameters associated with the samples.

## REFERENCES

- Baker, D. R., 1962, Organic geochemistry of Cherokee group in southeastern Kansas and northeastern Oklahoma: *Am. Assoc. Petroleum Geologists Bull.*, v. 46, no. 9, p. 1621-1642.
- Bates, T. F., and Strahl, E. O., 1957, Mineralogy, petrography, and radioactivity of representative samples of Chattanooga Shale: *Geol. Soc. America Bull.*, v. 68, no. 10, p. 1305-1314.
- Bray, E. E., and Evans, E. D., 1961, Distribution of n-paraffins as a clue to recognition of source beds: *Geochim. et Cosmochim. Acta*, v. 22, p. 2-15.
- Breger, I. A., and Brown, Andrew, 1962, Kerogen in the Chattanooga Shale: *Science*, v. 137, no. 3525, p. 221-224.
- , 1963, Distribution and types of organic matter in a barred marine basin: *New York Acad. Sci. Trans.*, v. 25, no. 7, serial II, p. 741-755.
- Breger, I. A., Tourtelot, H. A., and Chandler, J. C., 1960, Geochemistry of kerogen from the Sharon Springs member of the Pierre shale [abs.]: *Geol. Soc. America Bull.*, v. 71, no. 12, pt. 2, p. 1832.

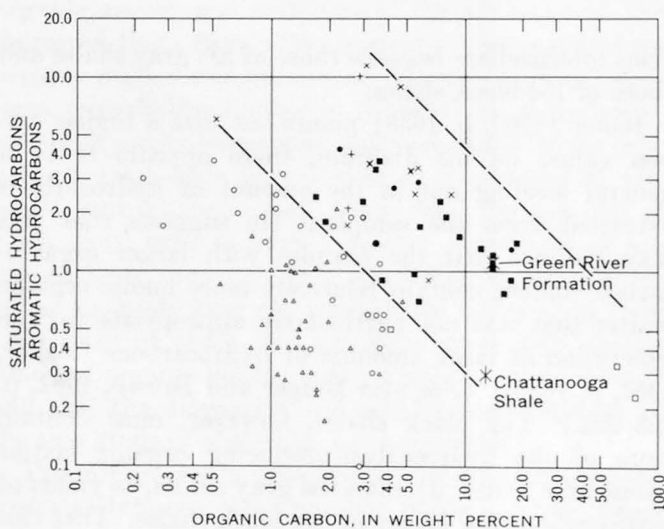


FIGURE 5.—Relation between saturated/aromatic hydrocarbon ratio and organic carbon. Symbols are same as those used in figure 2. Dashed lines show vague trend of decrease in saturated/aromatic hydrocarbon ratio with increase in organic carbon in Cretaceous samples and black shales from the Cherokee Shale.

- Erdman, J. G., 1961, Some chemical aspects of petroleum genesis as related to the problem of source bed recognition: *Geochim. et Cosmochim. Acta*, v. 22, p. 16-36.
- Ferguson, W. S., 1962, Analytical problems in determining hydrocarbons in sediments: *Am. Assoc. Petroleum Geologists Bull.*, v. 46, no. 9, p. 1613-1620.
- Gill, J. R., and Cobban, W. A., 1961, Stratigraphy of lower and middle parts of the Pierre shale, northern Great Plains: Art. 352 in *U.S. Geol. Survey Prof. Paper 424-D*, p. D185-D191.
- Orr, W. L., and Emery, K. O., 1956, Composition of organic matter in marine sediments; preliminary data on hydrocarbon distribution in basins off southern California: *Geol. Soc. America Bull.*, v. 67, p. 1247-1258.
- Rader, L. F., and Grimaldi, F. S., 1961, Chemical analyses for selected minor elements in Pierre shale: *U.S. Geol. Survey Prof. Paper 391-A*, p. A1-A45.
- Shimada, Ikuro, 1963, Extractable organic constituents in sediments, with reference to the relation between composition of the chromatographic fractions in extracts and depositional environment: *Tohoku Univ. Sci. Repts.*, ser. III, v. 8, no. 3, p. 421-482.
- Smith, P. V., Jr., 1954, Studies on origin of petroleum; occurrence of hydrocarbons in recent sediments: *Am. Assoc. Petroleum Geologists*, v. 38, no. 3, p. 377-404.
- Stanfield, K. E., Frost, I. C., McAuley, W. S., and Smith, H. N., 1951, Properties of Colorado oil shale: *U.S. Bur. Mines Rept. Inv. 4825*, 27 p., 20 tables, 9 figs.
- Stevens, N. P., Bray, E. E., and Evans, E. D., 1956, Hydrocarbons in sediments of Gulf of Mexico: *Am. Assoc. Petroleum Geologists Bull.*, v. 40, no. 5, p. 975-983.
- Swain, F. M., 1958, Organic materials of early Middle Devonian, Mt. Union area, Pennsylvania: *Am. Assoc. Petroleum Geologists Bull.*, v. 42, no. 12, p. 2858-2891.
- Swain, F. M., Blumentals, A., and Prokopovich, N., 1958, Bituminous and other organic substances in Precambrian of Minnesota: *Am. Assoc. Petroleum Geologists Bull.*, v. 42, no. 1, p. 173-189.
- Swain, F. M., and Prokopovich, N., 1954, Stratigraphic distribution of lipid substances in Cedar Creek Bog, Minnesota: *Geol. Soc. America Bull.*, v. 65, p. 1183-1198.
- Tourtelot, H. A., 1962, Preliminary investigation of the geologic setting and chemical composition of the Pierre Shale, Great Plains region: *U.S. Geol. Survey Prof. Paper 390*, 74 p.
- 1964, Minor-element composition and organic carbon content of marine and nonmarine shales of Late Cretaceous age in the western interior of the United States: *Geochim. et Cosmochim. Acta*, v. 28, no. 10, p. 1579-1604.
- Tourtelot, H. A., Schultz, L. G., and Gill, J. R., 1960, Stratigraphic variations in mineralogy and chemical composition of the Pierre shale in South Dakota and adjacent parts of North Dakota, Nebraska, Wyoming, and Montana: Art. 205 in *U.S. Geol. Survey Prof. Paper 400-B*, p. B447-B452.





## COMPOSITION OF MAGNETITE AS RELATED TO TYPE OF OCCURRENCE

By MICHAEL FLEISCHER, Washington, D.C.

*Abstract.*—Compilation of 12 analyses of magnetite from veins in basaltic trap rock shows a characteristic high MgO content, indicative of samples representing the greater part of the isomorphous series magnetite-magnesioferrite. Many samples are probably magnesioferrite rather than magnetite, and are characterized by having a much lower content of TiO<sub>2</sub> than igneous magnetite from diabase and basalt. Eleven analyses of magnetite from alkalic rocks and carbonatite show a generally high content of MgO, Al<sub>2</sub>O<sub>3</sub>, and MnO; the composition of these samples is such that they should contain exsolved hercynite or spinel. The analyses compiled were relatively few in number and were representative of rocks from only certain areas. Further study of such magnetite from many other, widely scattered localities is needed to test whether or not the compositional peculiarities noted are broadly characteristic of the genetic types.

Some years ago attention was called (Fleischer, 1953), to the fact that few analyses had been made of pure magnetite of known paragenesis, but that the few good analyses available suggested some relation between the type of occurrence of the magnetite and its composition. During the intervening years, dozens of new analyses have been published, especially of titaniferous magnetite, many on samples that had been studied optically. These have been recently summarized by Buddington and Lindsley (1964). The purpose of the present note is to call attention to the composition of magnetite from two types of occurrences on which little has been published in English: (1) magnetite from veins and ore bodies associated with trap rock, and (2) magnetite from alkalic rocks. A recent review (Sergeeva and Grudev, 1964) discusses the first of these types in part, but not the second. The data here assembled indicate a distinct relation between the type of occurrence and the composition of the magnetite; it is hoped that further study of material from other localities will be stimulated by this note.

## MAGNETITE FROM VEINS ASSOCIATED WITH TRAP ROCK

All the analyses available of magnetite from veins associated with trap rock are from two areas, Nova

Scotia and the Siberian platform. The deposits in Nova Scotia have been described by Hornor (1939); the large commercial deposits of the Tungusk syncline, Siberia, have been described by Sobolev (1935) and by Pavlov (1961). Twelve analyses of magnetite of this type are given in table 1; dozens of analyses from Siberia are listed by Pavlov, and the 10 given in table 1 were chosen to show the range of composition, using analyses with low content of SiO<sub>2</sub> (admixed serpentine, diopside, and other silicates) and P<sub>2</sub>O<sub>5</sub> (admixed apatite).

The results of the analyses suggest a solid-solution series ranging from nearly pure Fe<sub>3</sub>O<sub>4</sub> to ferroan magnesioferrites;<sup>1</sup> the rocks analyzed are generally quite low in TiO<sub>2</sub>, and contain some Al<sub>2</sub>O<sub>3</sub> and about 0.2 percent MnO. The content of MgO in many magnetites from the associated veins is much higher than that reported in analyses of "igneous" magnetite present as disseminated grains and segregations in basaltic and diabasic rocks themselves. The content of TiO<sub>2</sub> (less than 1 percent) is far lower than the 10–20 percent of TiO<sub>2</sub> normally found in the magnetite of basalt and diabase, where it is commonly present as a solid solution of magnetite with ulvöspinel, or as exsolved ulvöspinel or ilmenite. Vanadium and manganese, when determined, appear to be present in approximately the amounts usually found in magnetite from basalt and diabase.

Pavlov and his coworkers consider the Siberian deposits to be of hydrothermal origin and to have been formed from solutions containing much H<sub>2</sub>O, Cl, and P<sub>2</sub>O<sub>5</sub>. The constituents of the magnetite were transported as chlorides, the chlorine having been acquired by reaction with salt-bearing Lower Cambrian strata known to exist in the area; it is suggested that the presence of these rock-salt strata may account for the large deposits of magnetite, and that the lack of salt helps explain their absence in otherwise similar areas

<sup>1</sup> In the Russian literature, the term "magnomagnetite" is used for both magnesian magnetite and ferroan magnesioferrite. The usage is undesirable.

TABLE 1.—Analyses of the magnetite-magnesioferrite series from veins in diabase and basaltic rocks

[Tr., trace]

	A	1	2	3	4	5	6	7	8	B	9	10	11	12	C
Fe <sub>2</sub> O <sub>3</sub> -----	68.97	72.72	66.30	70.64	63.85	62.41	68.11	62.45	71.30	74.01	69.50	66.22	69.96	67.02	79.84
Al <sub>2</sub> O <sub>3</sub> -----		1.26	1.70		3.75	4.13	1.79	6.42			1.43	3.80	3.46	6.85	
TiO <sub>2</sub> -----		.21	.17	.24	.40	Tr.	.38	.50			.76		.33	.60	
FeO-----	31.03	23.28	28.52	26.13	25.42	23.14	23.49	17.43	20.80	16.65	16.00	16.35	11.92	10.85	
MgO-----		.80	1.12	2.97	3.89	4.20	5.30	5.98	6.42	9.34	9.40	11.74	13.00	13.83	20.16
MnO-----		.22	.21	Tr.	.26	.20	.26	.24	.03		.12				
CaO-----		.16	.64		.59	1.71	1.00	2.36	Tr.		.04				
SiO <sub>2</sub> -----		1.00	1.32	.03	2.20	2.53	.10	2.96	1.40		1.06	2.25	1.32	.98	
V <sub>2</sub> O <sub>5</sub> -----								.20			.67				
P <sub>2</sub> O <sub>5</sub> -----		.01	.26			.85		1.47	Tr.						
H <sub>2</sub> O-----		.38									.70				
CO <sub>2</sub> -----								.52							
Total-----	100.00	100.04	100.24	100.01	100.36	99.17	100.43	100.53	99.95	100.00	99.68	100.36	99.99	100.13	100.00
Specific gravity-----			4.9	5.067							4.76		4.67	4.55	

A. Theoretical composition, Fe<sub>3</sub>O<sub>4</sub>.

1-2 Pavlov (1961):

1. Chernorechensk deposit.

2. Region of the Kureiki River; P. S. Lazarevich, analyst.

3. Harrington (1907), crystals from veins in trap rocks; Annapolis County, Nova Scotia.

4-7 Pavlov (1961):

4. Region of the Severnaya River; K. P. Sokovaya, analyst.

5. Calcite-magnetite vein; Korshunovsk deposit; R. E. Yakubovich, analyst.

6. Region of Anakit River; K. P. Sokovaya, analyst.

7. Radiating-fibrous; Korshunovsk deposit; R. E. Yakubovich, analyst.

8. Hornor (1939), zoned crystals from veins in Triassic basalt near Lakeville, Nova Scotia; R. B. Ellestad, analyst.

B. Theoretical composition, (Mg,Fe)Fe<sub>2</sub>O<sub>4</sub> with MgO:FeO=1:1.

9-12 Pavlov (1961):

9. Columnar ore, Kamyshev Baikitik deposit; T. M. Miguushina, analyst.

10. Vein ore, Krasnoyarsk deposit; O. P. Ostrogorskaya, analyst.

11 and 12. Magnetite-calcite ore, dense, acicular; Ilimpei River; Z. V. Vasil'eva, analyst.

C. Theoretical composition, MgFe<sub>2</sub>O<sub>4</sub>.

The analyses from Pavlov are all from the Siberian platform; many others not shown here are available. Two others are given in Sobolev (1935).

of trap rocks elsewhere in the world. These authors further relate the magnesium content of the magnetite to the depth of formation, with low-magnesium magnetite formed at depth (low O<sub>2</sub> potential), and magnesioferrite formed under near-surface conditions where most of the iron was in the ferric condition (Pavlov, 1961, Pavlov and Chupryna, 1955; Pavlov and Yanchenko, 1959).

The mechanism of transport as chlorides does not, however, explain why these magnetites are so low in TiO<sub>2</sub>; the data of Buddington and Lindsley (1964) suggest that they were formed at low temperatures. The need is clear for further study of the composition and mode of transport of magnetite in similar occurrences elsewhere and for analyses of co-existing magnetite (or magnesioferrite) and ilmenite from such veins.

### MAGNETITE FROM ALKALIC ROCKS AND CARBONATITE

In table 2 are assembled 11 analyses, all that could be found of "magnetite" from alkalic rocks and carbonatite. These are mostly very high in Al<sub>2</sub>O<sub>3</sub>, MgO, and MnO content, so much so that calculations of the theoretical "molecules" present show large amounts of either spinel, MgAl<sub>2</sub>O<sub>4</sub>, or of hercynite, FeAl<sub>2</sub>O<sub>4</sub>.

According to the data of Turnock and Eugster (1962), material of compositions such as those in table 2 should have unmixed on cooling to magnetite plus hercynite. Unfortunately, optical study of these samples is not recorded; however, Dr. D. P. Gold, of Pennsylvania State University (written communication, Jan. 1965), informs me that magnetite from the Oka district, Quebec (analyses 9-11 in table 2) shows exsolution lamellae of hercynite on the (100) planes of magnetite. It should be noted also that the material of analyses 1 and 8 of table 2 represented single crystals, both showing the trapezohedron [311], uncommon for magnetite.

The analyses in table 2 show that magnetite from a single locality may vary appreciably in composition. Spectrographic analyses of seven samples from Magnet Cove, Arkansas, given by Erickson and Blade (1963, p. 76), show that the composition varies considerably, with only those from carbonatite and jacupirangite being high in Mg (>10 percent), whereas all the samples are high in Mn (0.5-2.7 percent).

More analyses of magnetite from alkalic rocks and carbonatites from other areas are needed; careful attention to the paragenesis, optical study, and X-ray data on such material is needed to explain the observed chemical variation.

TABLE 2.—Analyses of "magnetite" from alkalic and related rocks

[Tr., trace]

	1	2	3	4	5	6	7	8	9	10	11
Fe <sub>2</sub> O <sub>3</sub> -----	59.01	46.95	57.11	61.95	62.39	88.41	67.94	59.71	54.30	56.98	64.28
Al <sub>2</sub> O <sub>3</sub> -----	10.37	15.14	3.62	6.57	6.80	6.85	.07	.62	5.17	7.25	.15
TiO <sub>2</sub> -----	2.40	5.01	6.98	1.31	4.70	4.08	1.76	5.32	3.18	3.85	3.71
FeO-----	16.82	26.58	21.83	18.72	23.24	-----	26.95	22.70	17.23	21.60	24.52
MgO-----	9.47	5.83	7.18	6.74	2.59	4.57	.15	3.24	5.42	3.91	0.60
MnO-----	2.10	-----	1.82	3.40	-----	Tr.	2.19	8.46	5.36	1.49	3.71
CaO-----	-----	.11	.94	-----	-----	-----	.30	-----	1.83	1.54	1.58
SiO <sub>2</sub> -----	-----	.13	.38	<sup>1</sup> 1.10	.34	-----	.65	.16	7.45	2.21	.83
H <sub>2</sub> O-----	-----	-----	-----	-----	-----	-----	.38	-----	-----	-----	-----
Others-----	-----	-----	<sup>2</sup> .11	-----	-----	-----	-----	-----	<sup>3</sup> .47	<sup>3</sup> .39	<sup>3</sup> .31
Total-----	100.17	99.75	99.97	99.79	100.06	103.91	100.39	100.21	100.41	99.22	99.69
Specific gravity-----	4.558	-----	-----	-----	-----	-----	5.093	4.913	-----	-----	-----

1. Harrington (1907), crystals showing {311}; Magnet Cove, Ark.
2. Newhouse and Glass (1936); Magnet Cove, Ark.; M. G. Keyes, analyst.
3. Basta (1957); Magnet Cove, Ark.; H. B. Milner, analyst.
- 4-5 H $\ddot{u}$ gel (1924); Kaiserstuhl, Baden, Germany.
  4. Schelingen.
  5. Vogtsburg.
6. Knop (1877), inclusions in sanidine-hauyne phonolite; Horberig, Kaiserstuhl.

<sup>1</sup> Insoluble.<sup>2</sup> V<sub>2</sub>O<sub>5</sub>, 0.10; Cr<sub>2</sub>O<sub>3</sub>, 0.01 percent.<sup>3</sup> P<sub>2</sub>O<sub>5</sub>.

7. Morozewicz (1930, p. 365); mariupolite, Mariupol, Ukraine.
8. Harrington (1907), crystals showing {311}, apparently in crystalline limestone; St. Joseph du Lac, Quebec. D. P. Gold (oral communication, Jan. 1965) states that this sample was probably from the Oka complex.
- 9-11 D. P. Gold (written communication, 1965); Oka complex, Quebec; analyst H. Soutar.
  9. Monticellite-calcite rock.
  10. Okaite, Dufresne Hill.
  11. Soda pyroxene-magnetite-pyroxchlore-calcite rock.

## REFERENCES

- Basta, E. Z., 1957, Accurate determination of the cell dimensions of magnetite: *Mineralog. Mag.*, v. 31, p. 431-442.
- Buddington, A. F., and Lindsley, D. H., 1964, iron-titanium oxide minerals and synthetic equivalents: *Jour. Petrology*, v. 5, p. 310-357.
- Erickson, R. L., and Blade, L. V., 1963, Geochemistry and petrology of the alkalic igneous complex at Magnet Cove, Arkansas: U.S. Geol. Survey Prof. Paper 425, 95 p.
- Fleischer, Michael, 1953, Some problems of chemical mineralogy: *Am. Mineralogist*, v. 38, p. 149-162.
- Gold, D. P., 1965, Petrology of the alkaline igneous rocks of Oka and St. Hilaire, Quebec: [In press].
- Harrington, B. J., 1907, Isomorphism as illustrated by certain varieties of magnetite: *Mineralog. Mag.*, v. 14, p. 373-377.
- Hornor, A. P., Jr., 1939, Magnetite and hematite veins in Triassic lavas of Nova Scotia: *Econ. Geology*, v. 34, p. 921-930.
- H $\ddot{u}$ gel, E., 1924, [Abstract of dissertation presented at Univ. of Freiburg in 1912]: *Zeitschr. Kristallographie*, v. 60, p. 334.
- Knopf, A., 1877, Ueber den Schorlomit vom Kaiserstuhl: *Zeitschr. Kristallographie*, v. 1, p. 58-64.
- Morozewicz, J., 1930, Der Mariupolit und seine Blutsverwandten: *Tschermaks mineralog. petrog. Mitt.*, v. 40, p. 335-436.
- Newhouse, W. E., and Glass, J. P., 1936, Some physical properties of certain iron oxides: *Econ. Geology*, v. 31, p. 699-711.
- Pavlov, N. V., 1961, Magnomagnetite deposits of the region of the Tungussk synclinal platform: *Akad. Nauk SSSR, Trudy Inst. Geol. Rudnykh Mestorozhd., Petrog., Mineral., i Geokhim.*, no. 52, p. 1-224 [In Russian].
- Pavlov, N. V., and Chuprynina, I. I., 1955, Magnomagnetites as indicators of depth of mineralization: *Akad. Nauk SSSR, Doklady*, v. 104, p. 298-301 [In Russian].
- Pavlov, N. V., and Yanchenko, M. T., 1959, Some new data on magnomagnetite: *Geol. Rudnykh Mestorozhdenii 1959*, no. 2, p. 74-80 [In Russian].
- Sergeeva, N. E., and Grudev, A. P., 1964, The chemical composition of magnetite: *Vestnik Moscow. Univ., ser. IV, Geol.*, 1964, no. 4, p. 27-36 [In Russian].
- Sobolev, Vladimir, 1935, The iron ore deposits of the Ilimpia River, eastern Siberia: *Econ. Geology*, v. 30, p. 783-791.
- Turnock, A. C., and Eugster, H. P., 1962, Fe-Al oxides; phase relationships below 1000°C: *Jour. Petrology*, v. 3, p. 533-565.



## SEISMIC STUDY OF CRUSTAL STRUCTURE IN THE SOUTHERN ROCKY MOUNTAINS

By W. H. JACKSON and L. C. PAKISER, Denver, Colo.

*Abstract.*—Two underground mining blasts of 25,500 pounds and 416,235 pounds of explosives, detonated at Climax, Colo., on May 21 and 23, 1964, were recorded at 17 locations in the Front Range uplift of the Southern Rocky Mountains at distances ranging from 25 to 360 km north of the shotpoint. Strong secondary events recorded at distances ranging from 119 to 192 km from the shotpoint were identified as reflections from the Mohorovicic discontinuity and from an intermediate layer in the crust. An analysis of both reflected and refracted events suggests that the crustal thickness north of Climax is approximately 54 km and that it decreases abruptly by about 15 km in the area directly east of the Uinta Mountains. Comparison of crustal models in the different geologic and physiographic provinces of the Far West indicates that isostatic compensation is related primarily to density variations in the upper mantle and only secondarily to variations in crustal thickness.

Two large underground mining blasts were detonated by the Climax Molybdenum Co. at Climax, Colo., on May 21 and 23, 1964. The first blast, which will be designated "Climax 1," consisted of a series of delayed explosions of various sized charges totaling approximately 25,500 pounds. The second blast, designated "Climax 2," was produced by an explosion of 416,235 pounds of explosives in two adjacent tunnels; the charge was so detonated as to result in a practically instantaneous blast. The size and location of these blasts provided an exceptional opportunity to make a reconnaissance study of crustal structure in the Southern Rocky Mountains, using the Climax-1 blast for recording at distances of 200 kilometers and less and Climax 2 at distances greater than 200 km.

Recordings of the two blasts were made by the U. S. Geological Survey at 17 locations in the Front Range uplift of the Southern Rocky Mountains at distances ranging from 25 to 360 km north of Climax (fig. 1). The Colorado School of Mines (CSM) recorded the Climax-2 blast at a site 64 km north of Climax. This larger blast was also recorded at three

VELA UNIFORM fixed seismograph stations in the Rocky Mountain region.

The time instant of each blast was determined by recording the surge of current through the firing line and the time of detonation of a blasting cap identical to those used in the mine. Absolute timing was accomplished by recording radio timing signals from National Bureau of Standards Station WWV. Back-

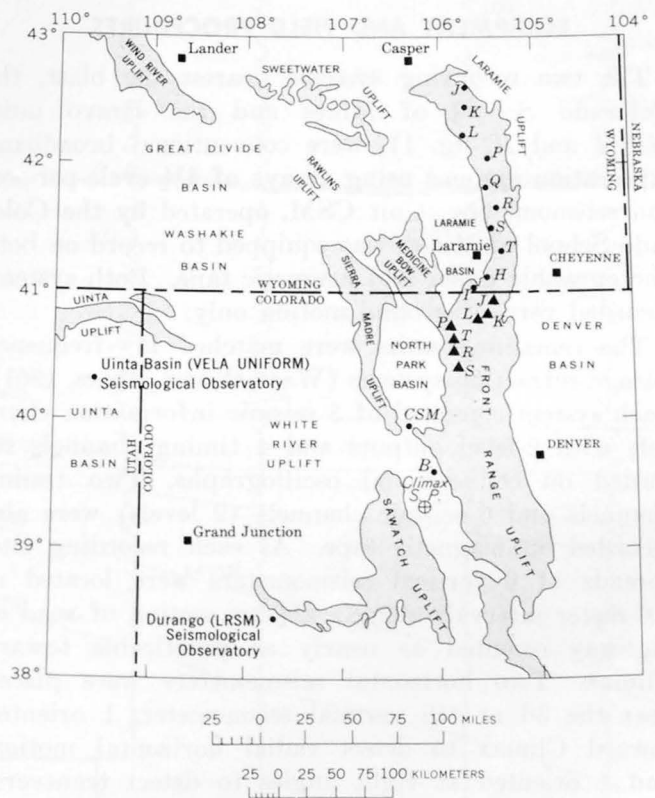


FIGURE 1.—Index map of parts of Colorado, Wyoming, and Utah, showing shotpoint and recording locations. The Raton long-range seismic-measurements (LRSM) observatory is to the south, off the map. Solid triangles, Climax-1 recording locations of units R, S, T, and so forth; dots, Climax-2 recording locations; Climax S.P., Climax shotpoint. Unit India (I) recorded both shots at the same location.

up timing was obtained by recording timing pulses from an electronic chronometer and a coded tone from a portable communications station located near the Climax mine. These timing signals were also recorded by all recording units.

Coordinates of both blasts were: lat  $39^{\circ}22.25'N.$ , long  $106^{\circ}10.06'W.$  The origin time for Climax 1 was  $22^h34^m33.105^s$  G.m.t., and for Climax 2  $21^h44^m59.124^s$  G.m.t.

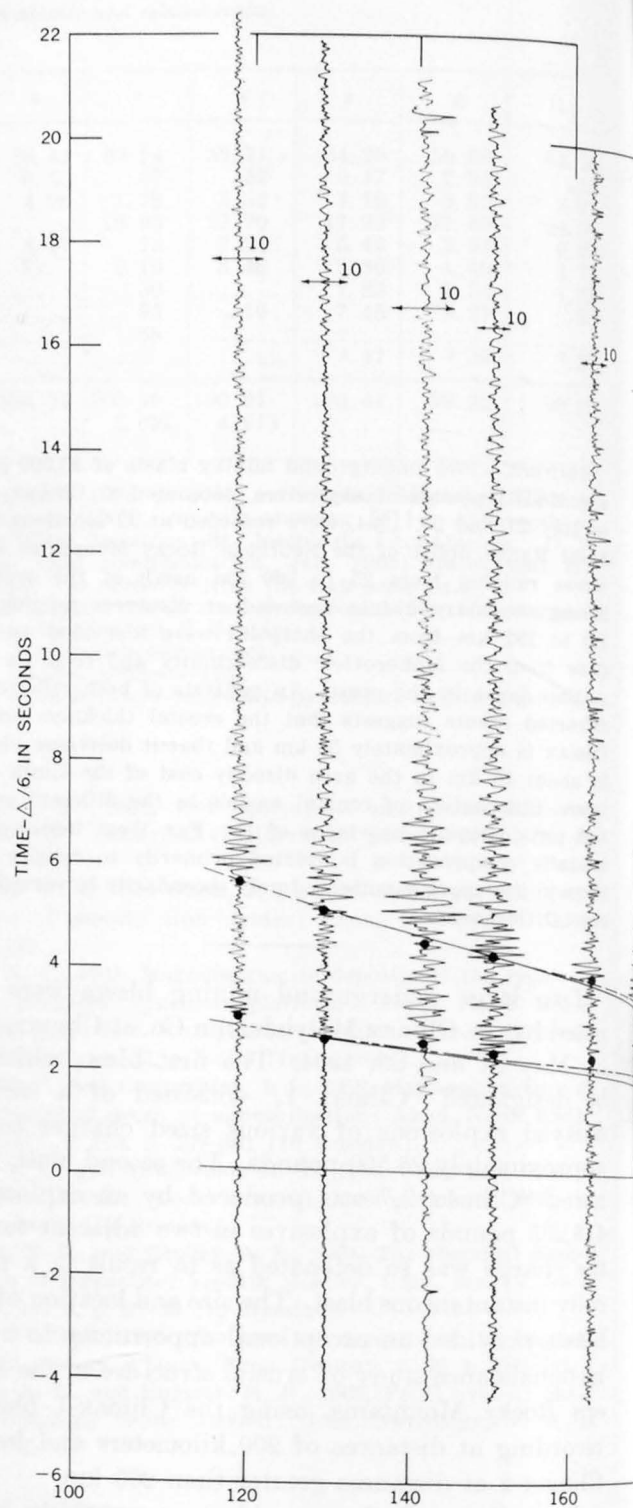
*Acknowledgments.*—We wish to express our appreciation to Dr. Stewart R. Wallace, Chief Geologist, and to Mr. James Ludwig, Mine Superintendent, of the Climax Molybdenum Co., Climax, Colo., for their cooperation in making this study possible. We also wish to thank Professor John Hollister of the Colorado School of Mines for recording the Climax-2 blast and making the seismogram available for this study. Arrival times for the Raton, N. Mex., Durango, Colo., and Uinta Basin Seismological Observatory, Vernal, Utah, were obtained from the U. S. Air Force Technical Applications Center.

#### EQUIPMENT AND FIELD PROCEDURES

The two recording systems nearest the blast, the Colorado School of Mines and the Bravo units (CSM and B, fig. 1), were conventional broadband exploration systems using arrays of  $4\frac{1}{2}$ -cycle-per-second seismometers. Unit CSM, operated by the Colorado School of Mines, was equipped to record on both photographic paper and magnetic tape. Both systems recorded vertical ground motion only.

The remaining units were matched low-frequency seismic-refraction systems (Warrick and others, 1961). Each system consisted of 8 seismic information channels with 2-level outputs and 4 timing channels recorded on conventional oscillographs. Two timing channels and 6 seismic channels (2 levels) were also recorded on magnetic tape. At each recording site, spreads of 6 vertical seismometers were located at 500-meter intervals along a  $2\frac{1}{2}$ -km section of road or highway oriented as nearly as practicable toward Climax. Two horizontal seismometers were placed near the 3d or 4th vertical seismometer, 1 oriented toward Climax to detect radial horizontal motion, and 1 oriented at right angles to detect transverse motion. All seismometers had a natural period of 1 second. The field method used was described in more detail by Jackson and others (1963).

The recording distances were determined by plotting locations of the recording spreads on the best available U. S. Geological Survey topographic maps, establishing the coordinates of the end seismometers, and computing the distances from the seismometers



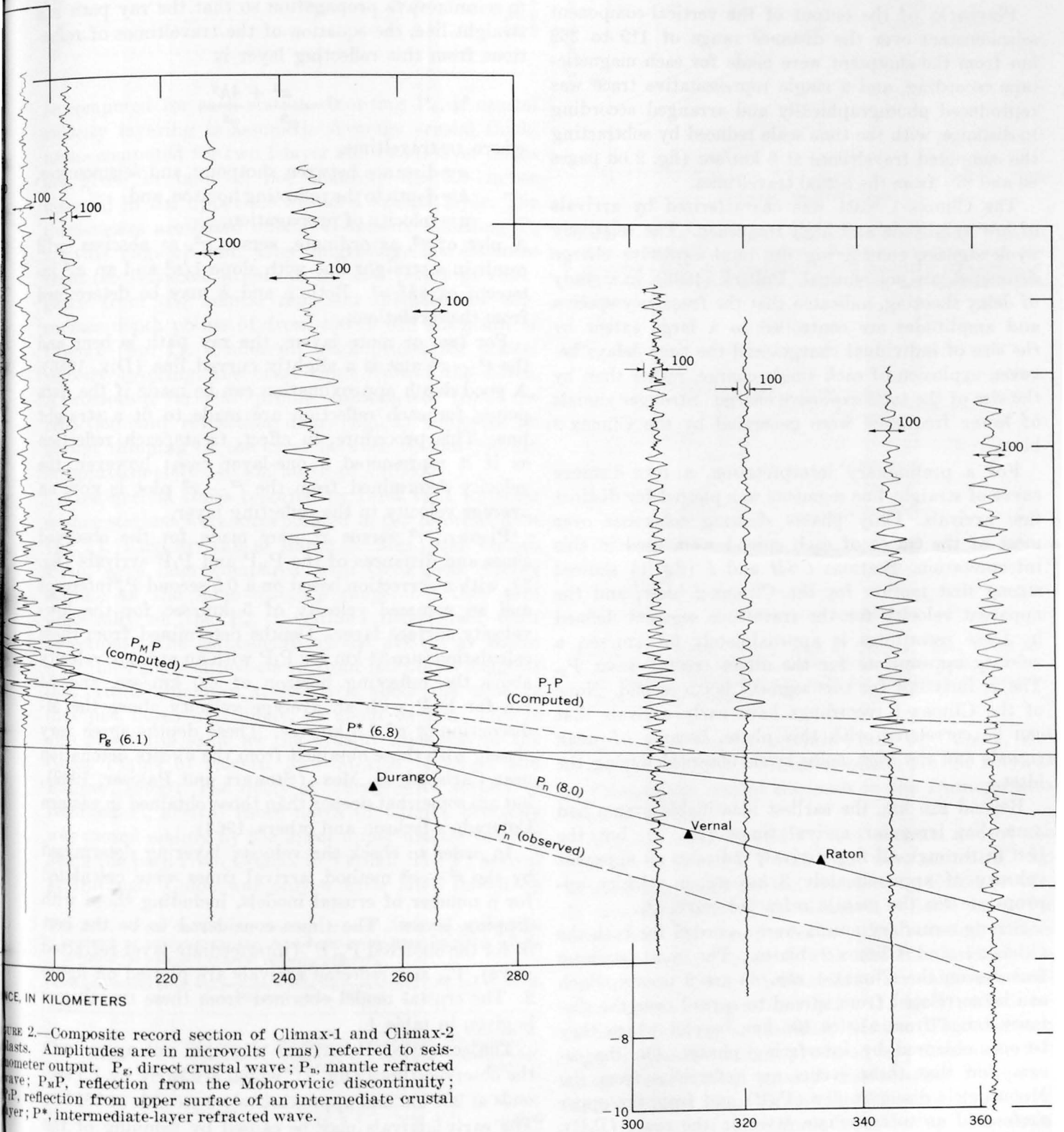


FIGURE 2.—Composite record section of Climax-1 and Climax-2 stations. Amplitudes are in microvolts (rms) referred to seismometer output.  $P_g$ , direct crustal wave;  $P_n$ , mantle refracted wave;  $P_M P$ , reflection from the Mohorovicic discontinuity;  $P_I P$ , reflection from upper surface of an intermediate crustal layer;  $P^*$ , intermediate-layer refracted wave.

to the shotpoint according to the method of Richter (1958). Errors in computed distances are less than 1 km.

### RESULTS

Playbacks of the output of the vertical-component seismometers over the distance range of 119 to 362 km from the shotpoint were made for each magnetic-tape recording, and a single representative trace was reproduced photographically and arranged according to distance, with the time scale reduced by subtracting the computed traveltimes at 6 km/sec (fig. 2 on pages 86 and 87) from the actual traveltimes.

The Climax-1 blast was characterized by arrivals of low amplitude and high frequency. The relatively weak signals, considering the total explosive charge detonated, are not unusual. Pollack (1963), in a study of delay shooting, indicated that the frequency spectra and amplitudes are controlled to a large extent by the size of individual charges and the time delays between explosion of each single charge, rather than by the size of the total explosive charge. Stronger signals of lower frequency were generated by the Climax-2 blast.

For a preliminary interpretation, a time-distance curve of straight-line segments was plotted for distinct first arrivals. Only phases showing coherence over most of the traces of each spread were used in this interpretation. Stations *CSM* and *I* (fig. 1) showed strong first motion for the Climax-2 blast, and the apparent velocity for the traveltime segment defined by these recordings is approximately 6.1 km/sec, a velocity appropriate for the direct crustal wave,  $P_g$ . The  $x_0$  intercept for this segment is 0.5 second. None of the Climax-1 recordings have early arrivals that can be correlated with this phase, because of weak signals and the high noise levels observed during the blast.

Beyond 225 km, the earliest identifiable events had somewhat irregular arrival times (fig. 2), but the best fit through all first arrivals indicates an apparent velocity of approximately 8 km/sec, a velocity appropriate for the mantle refracted wave,  $P_n$ .

Strong secondary events were recorded for both the Climax-1 and Climax-2 blasts. The most striking features on the Climax-1 records are 2 events which can be correlated from spread to spread over the distance range from 119 to 192 km, beyond which they become obscured by interfering phases. On the assumption that these events are reflections from the Mohorovicic discontinuity ( $P_M P$ ) and from the upper surface of an intermediate layer in the crust ( $P_I P$ ), an approximate crustal model may be computed using the  $t^2 - x^2$  method (Dix, 1955).

The  $t^2 - x^2$  method, briefly, is explained by considering a simple one-layer case with plane, horizontal boundaries. If the medium between the surface and the reflecting boundary is homogeneous and isotropic to seismic-wave propagation so that the ray path is a straight line, the equation of the traveltimes of reflections from this reflecting layer is

$$t^2 = \frac{x^2}{v^2} + \frac{4h^2}{v^2},$$

where  $t$  = traveltime,

$x$  = distance between shotpoint and seismometer,

$h$  = depth to the reflecting horizon, and

$v$  = velocity of propagation.

A plot of  $t^2$ , as ordinate, versus  $x^2$ , as abscissa, will result in a straight line with slope  $1/v^2$  and an  $x_0^2$  intercept of  $4h^2/v^2$ . Both  $v$  and  $h$  may be determined from these relations.

For two or more layers, the ray path is bent and the  $t^2 - x^2$  plot is a slightly curved line (Dix, 1955). A good depth approximation can be made if the data points for each reflection are made to fit a straight line. This procedure, in effect, treats each reflection as if it represented a one-layer case; however, the velocity determined from the  $t^2 - x^2$  plot is now an average velocity to the reflecting layer.

Plots of  $t^2$  versus  $x^2$  were made for the observed times and distances of the  $P_M P$  and  $P_I P$  arrivals (fig. 3), with a correction based on a 0.5-second  $P_g$  intercept and an assumed velocity of 5 km/sec for the low-velocity surface layer. Depths determined from these calculations are 34 km for  $P_I P$  with an average velocity above the reflecting horizon of 6.0 km/sec, and 54 km for  $P_M P$  with an average velocity above the M-discontinuity of 6.6 km/sec. These depths agree very closely with those obtained from the GNOME detonation near Carlsbad, N. Mex. (Stewart and Pakiser, 1962), but are somewhat deeper than those obtained in eastern Colorado (Jackson and others, 1963).

In order to check the velocity layering determined by the  $t^2 - x^2$  method, arrival times were calculated for a number of crustal models, including those with dipping layers. The times considered to be the best fit for the observed  $P_g$ ,  $P^*$  (intermediate-layer refracted wave),  $P_n$ , and reflected arrivals are plotted on figure 2. The crustal model obtained from these traveltimes is given in table 1.

The computed  $P_n$  arrival times do not agree with the observed times (fig. 2), which are early by 1.3 seconds at 227 km and approximately 2 seconds at 362 km. The early arrivals may be caused by thinning of the crust to the north. By use of delay-time methods (Pakiser and Black, 1957) the crustal thickness may

TABLE 1.—Preferred crustal model, Climax, Colo., area

Velocity (km/sec)	Layer thickness (km)	Depth to bottom of layer (km)
5.0	2.3	2.3
6.1	31.7	34.0
6.8	19.8	53.8
8.0		

be computed for each station recording  $P_n$ , if crustal velocity layering is assumed. Average crustal thicknesses computed for two 1-layer and two 2-layer crusts are given in table 2, not counting the 5.0-km/sec material in the upper 2.3 km as a crustal layer. The thicknesses are based on the 7 stations recording  $P_n$  arrivals (fig. 2) and, after migrating, the distances from the refracted events to the last points of emergence from the mantle represent distances of subsurface depth points of from 190 to 310 km north of Climax (fig. 1). Under all assumptions for crustal velocity layering, the crust thins toward the north. A composite crustal profile constructed from the reflection and refraction data (fig. 4) indicates an abrupt thinning of the crust between 90 and 190 km or approximately 140 km north of Climax.

First-arrival times reported by three VELA UNIFORM seismic stations were incorporated in the recorded data (fig. 2). First arrivals at Raton, N. Mex., and Vernal, Utah, were later compared with Geological Survey stations in the same distance range, but they plot practically on the  $P_n$  traveltimes determined from reflections. The coincidence of the arrival at Raton with the  $P_n$  traveltime curve from reflections suggests that crustal thickness at Raton is about the same as that just north of Climax, or about 54 km. This is also about the same as the crustal thickness in the Great Plains of eastern New Mexico (Stewart and Pakiser, 1962). The delay at Vernal with respect to recorded  $P_n$  arrival times north of Climax probably was caused mainly by the lower upper-mantle velocity along the path from Climax to Vernal. The  $P_n$  arrival at Durango, Colo., was only a little later (about 1/2

TABLE 2.—Four models for average crustal thickness of northern segment of seismic profile, based on delay-time analysis of  $P_n$  arrivals for selected crustal velocity layering

[All crustal models given will produce, within the experimental error, the  $P_n$  traveltimes observed beyond 220 km]

Model	Average thickness of 6.1-km/sec layer plus 5.0-km/sec layer	Average thickness of 6.8-km/sec layer (km)	Average total crustal thickness (km)	Variation of thickness from average (km)
1	18.6	19.8	38.4	± 2.0
2	23.5	13.2	36.7	± 2.3
3	33.0	0.0	33.0	± 2.5
4	2.3	42.1	44.4	± 2.7

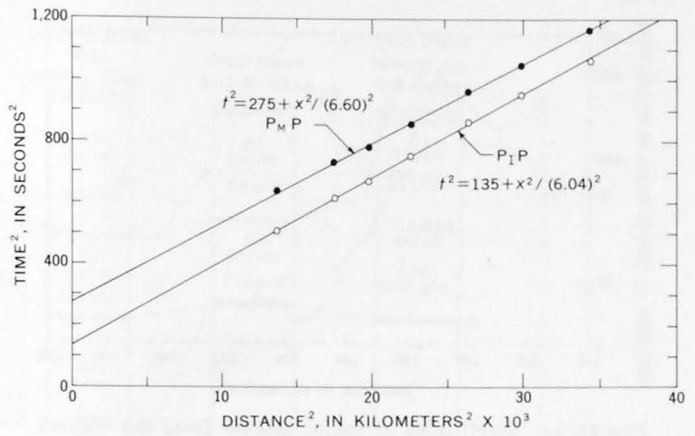


FIGURE 3.— $t^2 - x^2$  plot of  $P_M P$  and  $P_I P$  reflections of the Climax-1 shot,  $t$ , traveltime;  $x$ , distance between shotpoint and seismometer;  $P_M P$ , reflection from the Mohorovicic discontinuity;  $P_I P$ , reflection from upper surface of an intermediate crustal layer.

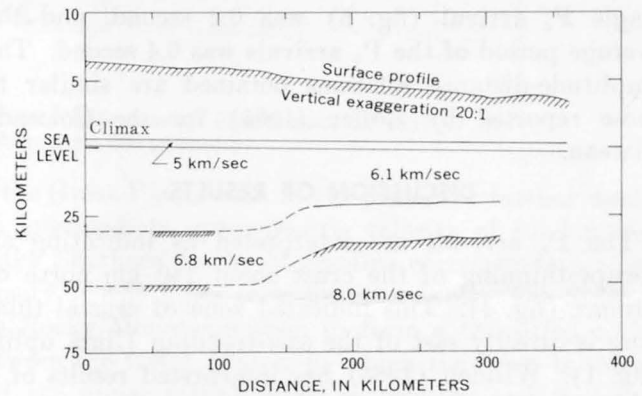


FIGURE 4.—Crustal profile north of Climax, Colo., based on  $P_n$  delay times and the assumptions of the second model of table 2. Hachures are only for emphasis of certain parts of the profile.

second) than the  $P_n$  arrivals north of Climax, and if crustal and upper-mantle velocities are the same as at Climax, the crustal thickness in the Durango area is about 41 km.

Amplitudes of  $P_g$  and  $P_n$  first arrivals and of the first few cycles of  $P_I P$  and  $P_M P$  were estimated (fig. 5) according to the method described by Eaton (1963). It was very difficult to obtain a reliable basis for comparing the amplitudes of the reflected phases recorded from Climax 1 with the first arrivals recorded from Climax 2. Secondary arrivals were compared on recording at unit India ( $I$ , fig. 1), which recorded both blasts at the same location. These arrivals suggest that Climax 2 produced approximately 100 times more vertical ground displacement for correlatable phases than Climax 1. Climax-1 amplitudes were normalized to Climax 2 by using this ratio. Average periods of  $P_I P$  and  $P_M P$  arrivals from Climax 1 were approximately 0.1 second. The period of the



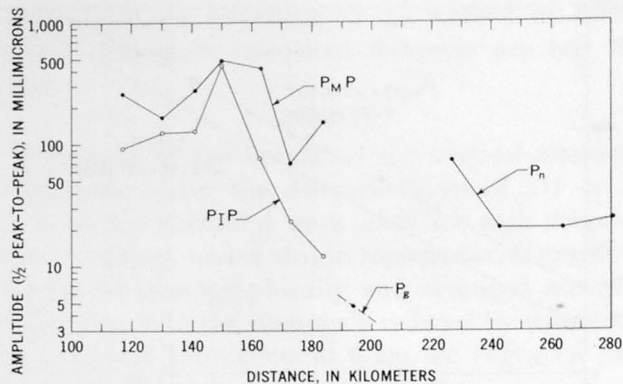


FIGURE 5.—Amplitudes of major phases from the Climax 1 and Climax 2 shots,  $P_M P$  and  $P_I P$ , from Climax 1, are shown as 100 times the observed amplitudes in order to normalize the shot sizes.  $P_g$  and  $P_n$  are from Climax 2.  $P_g$ , direct crustal wave;  $P_n$ , mantle refracted wave;  $P_M P$ , reflection from the Mohorovicic discontinuity;  $P_I P$ , reflection from upper surface of an intermediate crustal layer.

single  $P_g$  arrival (fig. 5) was 0.2 second, and the average period of the  $P_n$  arrivals was 0.4 second. The amplitude-distance relations obtained are similar to those reported by Roller (1965) for the Colorado Plateau.

#### DISCUSSION OF RESULTS

The  $P_n$  arrivals are interpreted as indicating an abrupt thinning of the crust about 140 km north of Climax (fig. 4). This indicated zone of crustal thinning is directly east of the east-trending Uinta uplift (fig. 1). Willden (1965) has interpreted results of a reversed refraction profile extending from American Falls Reservoir, Idaho, to Flaming Gorge Reservoir, Utah, to indicate a total crustal thickness of about 35 km at Flaming Gorge Reservoir, which lies on the north flank of the Uinta uplift. Willden's interpreted crustal thickness is within a few kilometers of the crustal thickness of the northern segment analyzed in this study, except for the last model of table 2, in which it is assumed that practically the entire crust is made up of material having a velocity of 6.8 km/sec. We therefore suggest a zone of crustal instability involving an abrupt change in crustal thickness in the Southern Rocky Mountains along an eastward extension of the Uinta uplift.

Some ideas concerning the relations of crustal and upper-mantle structure and the nature of isostatic compensation in the different geologic and physiographic provinces of the Western United States can be obtained by comparing the results for the Southern Rocky Mountains reported in this paper with results previously reported for the Basin and Range (Eaton, 1963), Colorado Plateaus (Roller, 1965), Middle Rocky Mountains (Willden, 1965), and Great

Plains provinces (Jackson and others, 1963; Stewart and Pakiser, 1962). To do this a crustal and upper-mantle section which extends from Eureka, Nev., through Hanksville, Utah, Flaming Gorge Reservoir, Utah, Climax, Colo., and eastern Colorado, to eastern New Mexico (fig. 6) was plotted. This section (fig. 7) reveals the following general relations:

(1) The crust is from 35 to 40 km thick in the Basin and Range province, the Colorado Plateaus, and the Middle Rocky Mountains, and distinctly thicker, about 50 km thick, in the area of the highest peaks of the Southern Rocky Mountains and in the Great Plains.

(2) Isostatic compensation is related primarily to density variations in the upper mantle and only secondarily to variations in crustal thickness.

(3) There is no pronounced crustal root under the Southern Rocky Mountains.

The density distribution in the upper mantle required to maintain isostatic equilibrium from the eastern New Mexico section of the Great Plains (taken as the standard) to the high mountains and plateaus farther west has been estimated (fig. 7). Densities corresponding to the various crustal and upper-mantle velocities were taken from the empirical velocity-density relations of Nafe and Drake (Talwani and others, 1959). If 8.2 km/sec and 3.43 grams per cubic centimeter are assumed to be the standard mantle velocity

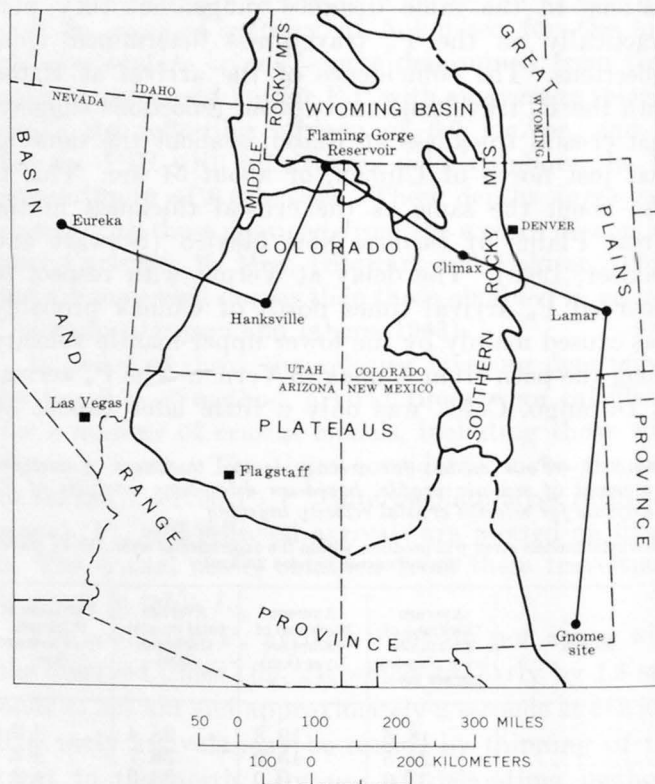


FIGURE 6.—Line of section shown in figure 7.

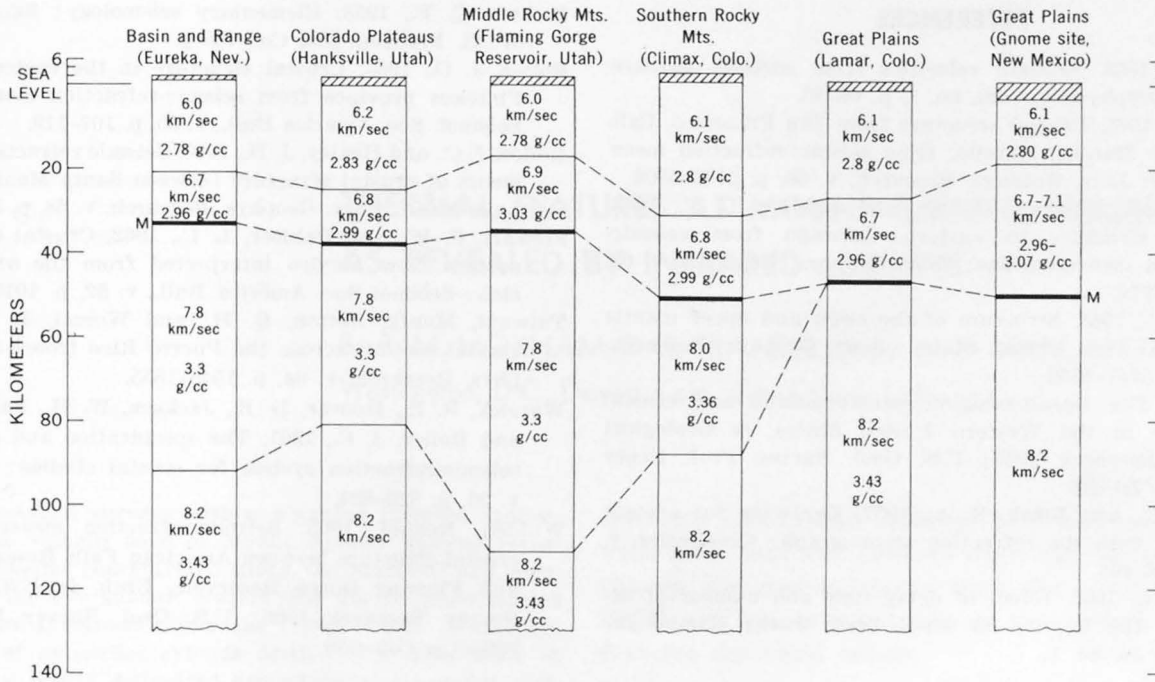


FIGURE 7.—Approximate crustal and upper mantle velocity and density distribution in part of the Western United States. M, Mohorovicic discontinuity.

and density, respectively, isostatic compensation requires that:

(1) Mantle material of velocity 7.8 km/sec and density 3.3 g per cc extends to depths of about 80 to 110 km in the Basin and Range province at Eureka, the Colorado Plateaus at Hanksville, and the Middle Rocky Mountains at Flaming Gorge Reservoir (fig. 7).

(2) Mantle material of velocity 8.0 km/sec and density 3.36 g per cc extends to a depth of about 90 km in the Southern Rocky Mountains at Climax.

(3) Contradictory results are obtained in attempting to determine the nature of isostatic compensation from the Great Plains of eastern New Mexico to the Great Plains of eastern Colorado if the upper-mantle velocity at Lamar, in eastern Colorado, is 8.0 km/sec as reported (Jackson and others, 1963) and the corresponding density is 3.36 g per cc. The contradiction virtually disappears, however, if the upper-mantle velocity and density are assumed to be the same in eastern Colorado and eastern New Mexico. The two crustal models under that assumption are isostatically compensated within 1/2 of 1 percent.

Only the upper-mantle velocity of 7.8 km/sec in the Basin and Range province, the Colorado Plateaus, and the Middle Rocky Mountains can be regarded as well established. The upper-mantle velocities in the Southern Rocky Mountains and the Great Plains are based on unreversed profiles. Nevertheless, isostatic considerations require that the upper-mantle density (and presumably velocity) must be significantly higher

in the Great Plains than in the provinces farther west. An intermediate upper-mantle velocity of 8.0 km/sec in the Southern Rocky Mountains corresponding to a density of 3.36 g per cc seems reasonable. The Southern Rocky Mountains seem to form a transition zone between the Great Plains, in which the crust is thick and the upper mantle high in velocity and density, and the provinces farther west, in which the crust is relatively thin and the upper mantle low in velocity and density. The relations depicted in the section (fig. 7) are consistent with those presented by Pakiser (1963, 1965).

Of course, the variations with depth of upper-mantle velocities and densities may be gradual rather than abrupt, but an upper-mantle velocity and density distribution like that of figure 7 seems to be required by the seismic evidence and considerations of isostasy.

The conclusions for the Southern Rocky Mountains presented above are based largely on the identification of reflections (P<sub>i</sub>P) from the upper surface of the intermediate crustal layer and reflections (P<sub>M</sub>P) from the Mohorovicic discontinuity. A rapid and relatively inexpensive method of mapping crustal structure using wide-angle reflections is now being tested in an experimental field program by the Geological Survey. Such wide-angle reflections have been shown to be useful in studying crustal structure in the Basin and Range province (Roller and Healy, 1963; Eaton, 1963).

## REFERENCES

- Dix, C. H., 1955, Seismic velocities from surface measurements: *Geophysics*, v. 20, no. 1, p. 68-86.
- Eaton, J. P., 1963, Crustal structure from San Francisco, California, to Eureka, Nevada, from seismic-refraction measurements: *Jour. Geophys. Research*, v. 66, p. 5789-5806.
- Jackson, W. H., Stewart, S. W., and Pakiser, L. C., 1963, Crustal structure in eastern Colorado from seismic-refraction measurements: *Jour. Geophys. Research*, v. 68, p. 5767-5776.
- Pakiser, L. C., 1963, Structure of the crust and upper mantle in the Western United States: *Jour. Geophys. Research*, v. 68, p. 5747-5756.
- 1965, The Basalt-eclogite transformation and crustal structure in the Western United States, in *Geological Survey Research 1965*: U.S. Geol. Survey Prof. Paper 525-B, p. B1-B8.
- Pakiser, L. C., and Black, R. A., 1957, Exploring for ancient channels with the refraction seismograph: *Geophysics*, v. 23, p. 388-405.
- Pollack, H. N., 1963, Effect of delay time and number of delays on the spectra of ripple-fired shots: *Earthquake Notes*, v. 34, no. 1.
- Richter, C. F., 1958, *Elementary seismology*: San Francisco, W. H. Freeman and Co., 768 p.
- Roller, J. C., 1965, Crustal structure in the eastern Colorado Plateaus province from seismic-refraction measurements: *Seismol. Soc. America Bull.*, v. 55, p. 107-119.
- Roller, J. C., and Healey, J. H., 1963, Seismic refraction measurements of crustal structure between Santa Monica Bay and Lake Mead: *Jour. Geophys. Research*, v. 68, p. 5837-5849.
- Stewart, S. W., and Pakiser, L. C., 1962, Crustal structure in eastern New Mexico interpreted from the GNOME explosion: *Seismol. Soc. America Bull.*, v. 52, p. 1017-1030.
- Talwani, Manik, Sutton, G. H., and Worzel, J. L., 1959, A crustal section across the Puerto Rico trench: *Jour. Geophys. Research*, v. 64, p. 1545-1555.
- Warrick, R. E., Hoover, D. B., Jackson, W. H., Pakiser, L. C., and Roller, J. C., 1961, The specification and testing of a seismic-refraction system for crustal studies: *Geophysics*, v. 26, p. 820-824.
- Willden, Ronald, 1965, Seismic-refraction measurements of crustal structure between American Falls Reservoir, Idaho, and Flaming Gorge Reservoir, Utah, in *U.S. Geological Survey Research 1965*: U.S. Geol. Survey Prof. Paper 525-C, p. C44-C50.



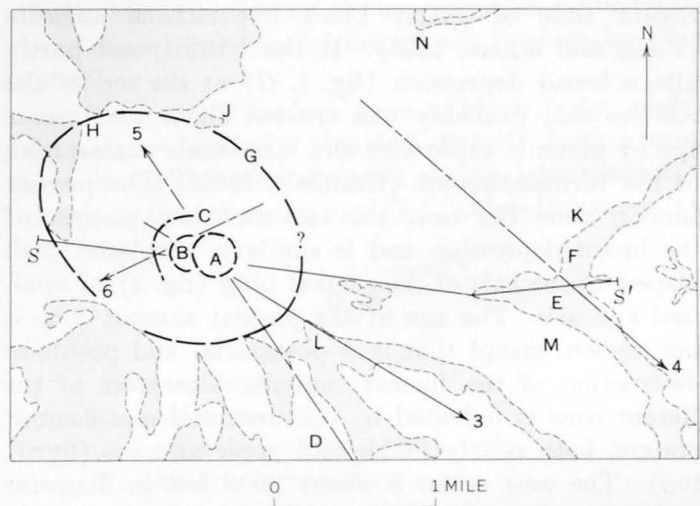
## THERMAL FEATURES AT MOUNT RAINIER, WASHINGTON, AS REVEALED BY INFRARED SURVEYS

By R. M. MOXHAM, D. R. CRANDELL, and W. E. MARLATT,<sup>1</sup>  
 Washington, D.C., Denver, Colo., Fort Collins, Colo.

*Abstract.*—Aerial surveys with a scanning infrared radiometer over the summit cone of Mount Rainier volcano reveal thermal anomalies concentrated along the northern and western rims of the two summit craters that are no doubt related to well-known fumaroles along the crater walls. A complex reticulation of anomalies extends down the western flank of the cone to a poorly delineated arc which may coincide with a concentric structural element of the volcano. The present summit craters are offset toward the southeast of the axis of the volcano's central plug. The thermal anomalies lie in a similarly oriented pattern, but temperatures generally increase with distance from the axis of the central plug. Highest temperatures are associated with the youngest (east) crater, most distant from the central plug, while lower temperatures are found with older volcanic features. Maximum ground temperature of 33°C (integrated over a 3° field of view) was recorded with a fixed-field radiometer in 3 flights over the summit.

In December 1963 a series of very large rockfalls and avalanches originated at Little Tahoma Peak, on the east flank of Mount Rainier (fig. 1). A large scar was thereby created on the northwest-facing wall of Little Tahoma, and rock debris was strewn for several miles northeast, down the surface of Emmons Glacier. Plumes of what appeared to be steam issuing from the base of the rockfall scar at Little Tahoma were observed by D. R. Crandell on July 9, 1964, but inaccessibility prevented closer inspection. To verify the possibility of an unusual source of heat at this locality, aerial surveys with a scanning infrared radiometer, provided by the U. S. Forest Service, were made by Moxham and Crandell at midafternoon, September 3, and at early dawn, September 4, 1964, at Little Tahoma Peak and at several other places on Mount Rainier, including the summit. It was subsequently learned that on July 11, 1964, W. E. Marlatt had made visible-

spectrum albedo and infrared radiation measurements with fixed-field radiometers over the summit craters; though his measurements were for other purposes,<sup>2</sup> the results are included here as they relate to thermal features described below.



- A, East summit crater.
- B, West summit crater.
- C, Arcuate pattern of thermal anomalies.
- D, Nisqually Glacier.
- E, Little Tahoma Peak.
- F, Rockfall scar.
- G, Approximate location of rim of original summit depression.
- H, Liberty Cap.
- J, Russell Cliff.
- K, Emmons Glacier.
- L, Gibraltar Rock.
- M, Ingraham Glacier.
- N, Steamboat Prow.
- 3, Approximate flight path used in making the fixed-field-radiometer records (fig. 3).
- 4, 5, 6, Approximate centerlines of infrared images.
- S-S', Trace of geologic section.

FIGURE 1.—Map of the Mount Rainier summit area. Rock outcrops (approximate configuration) are shown by stipple pattern. The summit of Mount Rainier, at 14,410 feet, is on the west rim of the east crater.

<sup>1</sup> Colorado State University.

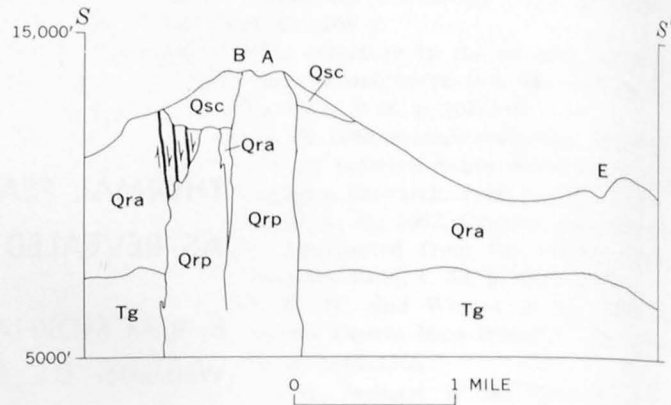
<sup>2</sup> Research flights conducted under NASA contract NASY-147.

*Acknowledgments.*—We are grateful for the generous cooperation of the U. S. Forest Service Northern Forest Fire Laboratory, Missoula, Mont., and to Stanley N. Hirsch of that organization, who made this work possible by providing the aircraft equipped with an infrared scanner. Particular thanks are due to Robert A. Cook, who operated the infrared scanner, and to Eldon Down, who piloted the aircraft. We are also pleased to acknowledge the assistance provided by the National Park Service and the staff at Mount Rainier National Park. Dr. Maynard M. Miller, Michigan State University, generously supplied information on his temperature measurements. Aaron C. Waters, University of California (Santa Barbara), and Richard S. Fiske and William A. Fischer, U. S. Geological Survey, made helpful comments on the manuscript.

### GEOLOGY OF THE SUMMIT CONE

The summit of Mount Rainier is formed by a small Recent cone of glassy black hypersthene andesite (Fiske and others, 1963). It lies within, and partly fills, a broad depression (fig. 1, *G*) at the top of the volcano that probably was created about 5,000 years ago by phreatic explosions and large-scale avalanching of the former summit (Crandell, 1963). The present summit cone lies near the east-southeast margin of the broad depression and is similarly displaced with respect to the axis of the central plug (fig. 2) of opalized andesite. The age of the present summit cone is not known, except that it is postglacial and postdates destruction of the former summit. The crest of the Recent cone is indented by the west and east summit craters, both nearly filled with snow and ice (fig. 6, top). The west crater is about 1,000 feet in diameter and is overlapped on its eastern edge by a slightly higher, younger crater about 1,300 feet in diameter, the rim of which is tilted to the east. Rocks exposed in the wall of this crater consist of a series of superposed lava flows that are hydrothermally altered in part along the north quadrant of the crater rim.

Heated rock and jets of steam help keep the rims of both craters mostly bare of snow during the summer months. Abnormal temperatures on Mount Rainier were first suggested in a story told by a Yakima Indian named Saluskin, who guided two men to the base of the mountain in about 1854. The two men set out to climb to the summit of the volcano one morning, and returned the same evening. According to Saluskin (*in* Haines, 1962, p. 17), they told him that there was “. . . ice all over top, lake in center and smoke or steam coming out all around like sweat-house.”



- Qsc, Postglacial lavas of the present summit cone.
- Qra, Andesitic lavas of Mount Rainier.
- Qrp, Central plug of opalized andesite.
- Tg, Rocks of the Tatoosh pluton.
- A, East summit crater.
- B, West summit crater.
- E, Little Tahoma Peak.

FIGURE 2.—Geologic section S-S', showing the upper part of Mount Rainier. (After Fiske and others, 1963.)

Verification of the observation of steam at the summit was made in 1870, when Hazard Stevens (1876) and P. B. Van Trump made the first authenticated summit climb. They walked over the flank of the summit cone and crossed the snow-filled west crater, noting sulfurous fumes and numerous steam jets issuing from crevices in the rock along the northern rim of the crater. Stevens and Van Trump spent the night in a cave melted into the ice along the crater wall, and next day discovered the east crater, along the northern side of which they also noted jets of steam.

Hack (1912) mentioned that the ground on the east crater rim was too hot locally to provide a comfortable resting place, and Sanders (1915) reported that the inner walls of the craters were quite warm in places. The rim of the east crater is 50 to 100 feet above the snow-filled crater floor. The crater probably is not filled to the brim with snow and ice because of constant melting along the sides and possibly at the base of the crater. Flett (1912) stated that a member of a climbing party descended about 85 feet into one of the ice caves along the rim of the east crater. From this point, he threw stones farther down into the cave, and splashes could be heard as the stones fell into a body of water. Hack and Flett both pointed out that the thermal region at the summit extends northward beyond the rims of the two craters, into the saddle between the summit cone and the ridge between Liberty Cap and Russell Cliff (fig. 1). Flett (1912), noted that

On the northwest slope of the small [west] crater the steam has melted all the snow off so that there can be no [ice] caves formed on the outside of the rim for the space of a quarter of a mile. All around the rim of the large [east]

crater are found large dome-shaped caves where the ice is melted by the slumbering heat beneath. These caves do not extend far on the outside on the south. On the north side the heat is so intense that the snow is melted off for a long distance down toward North Park [Grand Park]. The hottest caves are found on the northeast slope of Crater Peak [the summit cone]. In one of these ice-water was boiled in exactly three minutes. The steam comes quite fast, at fixed intervals like the breathing of a large animal.

Temperature measurements on the ground were made in 1959 by M. M. Miller. He reported (Miller, 1961, and written communication, Nov. 17, 1964) that the temperature in the ice in the west crater, near the summit, was  $-7^{\circ}$  to  $-10^{\circ}\text{C}$ . In the rock surrounding the crater, temperatures of approximately  $79^{\circ}\text{C}$  were found in fumarole zones; where no fumarolic activity was noted, the rock surface was at  $0^{\circ}\text{C}$ .

On the south flank of the mountain, a climbing party in 1956 noted a feature that was interpreted to be of thermal origin on Ingraham Glacier near Gibraltar Rock (memorandum dated July 23, 1956, from District Ranger Louis G. Kirk to Park Naturalist). The surface of the glacier was indented by a pit about 30 feet in diameter and 30 feet deep, which was floored with bare rock. Although no water vapor could be seen, a strong odor of sulfur came from the pit. More recently, steam issued under high pressure from a vent at the southern end of Gibraltar Rock throughout the summer of 1961, according to L. G. Jerstad, a summit guide (written communication, Sept. 16, 1964). A party of ski mountaineers, on March 7, 1965, sighted a steam jet at 11,500 feet elevation, west of Kautz Glacier (Danès, 1965). (This location is about 1 mile west of *D* on fig. 1.) The steam was not seen the following day and no further activity in this area has been reported.

### INSTRUMENTATION

A detailed description of the scanning radiometer is given elsewhere (Fischer and others, 1964). In the present survey, the sensing element was an indium antimonide (InSb) detector, operated at  $77^{\circ}\text{K}$ . At this temperature, the detector response extends from  $\approx 1$  to 6 microns and peaks near  $5\mu$ , in an atmospheric window. A  $4.5\text{--}5.5\mu$  band-pass interference filter was placed in the optical path to minimize reflected solar radiation. By means of a rotating  $45^{\circ}$  mirror the radiometer scans a path along the ground perpendicular to the aircraft flight direction. Forward motion of the aircraft provides a progression of contiguous scans. The radiant flux falling upon the detector creates an electrical signal which modulates a light beam focused upon a photographic film. Motion of the light beam across the film in the  $x$  direction is coordinated with the rotation of the scanning mirror;

exposure of the film in the  $y$  direction is coordinated with the relative terrain motion beneath the aircraft by means of the film-transport mechanism. A film image of the terrain is thereby created, with a gray scale the tone of which is a measure of the radiant flux passing through the entrance aperture—the higher the intensity, the lighter the tone.

The fixed-field infrared radiometer was a Barnes Engineering Co. Model IT-2. The instrument has a field of view that subtends an arc of approximately  $3^{\circ}$ . A flake thermistor operated at ambient temperature is the sensing element. Filters (InSb and Irtran-2) in the optical path limit response of the instrument to the  $8\text{--}13\mu$  atmospheric-window region. The radiometer operates in a conventional chopped-radiation mode as the detector views alternately the external unknown source and an internal black-body reference. A continuous readout on a strip-chart recorder (fig. 3) is provided. The apparent temperature of a source within the field of view is determined by calibration against the internal black-body reference source. Additional information on the accuracy and measurement precision of this type of instrument is given by Clark (1964).

If the earth's surface were a black body, surface temperature could be obtained directly from a measurement of the radiance with an ideal radiometer, as shown by the following modified Stefan-Boltzman law:

$$W_{\lambda_{0-\infty}} = \epsilon\sigma T^4,$$

where

$\lambda$  = wavelength,

$W$  = radiance,

$\epsilon$  = emissivity = 1 for a black body,

$T$  = absolute temperature, and

$\sigma$  = constant.

Emissivities of the various surface materials in the report area are uncertain but doubtless quite high. Buettner and others (1965) give values of 0.95 and 0.89 respectively for rough basalt and dunite (at  $50^{\circ}\text{C}$ ); clean ice and snow have values of  $>0.95$  (Dorsey, 1940). The apparent temperature of the terrain indicated by the fixed-field radiometer will be about 5 percent less than true surface temperature where  $\epsilon = 0.85$ . (Reflection from the sky background, reflected solar radiation, and atmospheric-transmission loss in the  $8\text{--}14\mu$  region are considered negligible.)

The gray scale of the scanning radiometer image similarly depicts surface radiance (and apparent temperatures), but in this instrument there is no internal black-body calibration. The image is further degraded

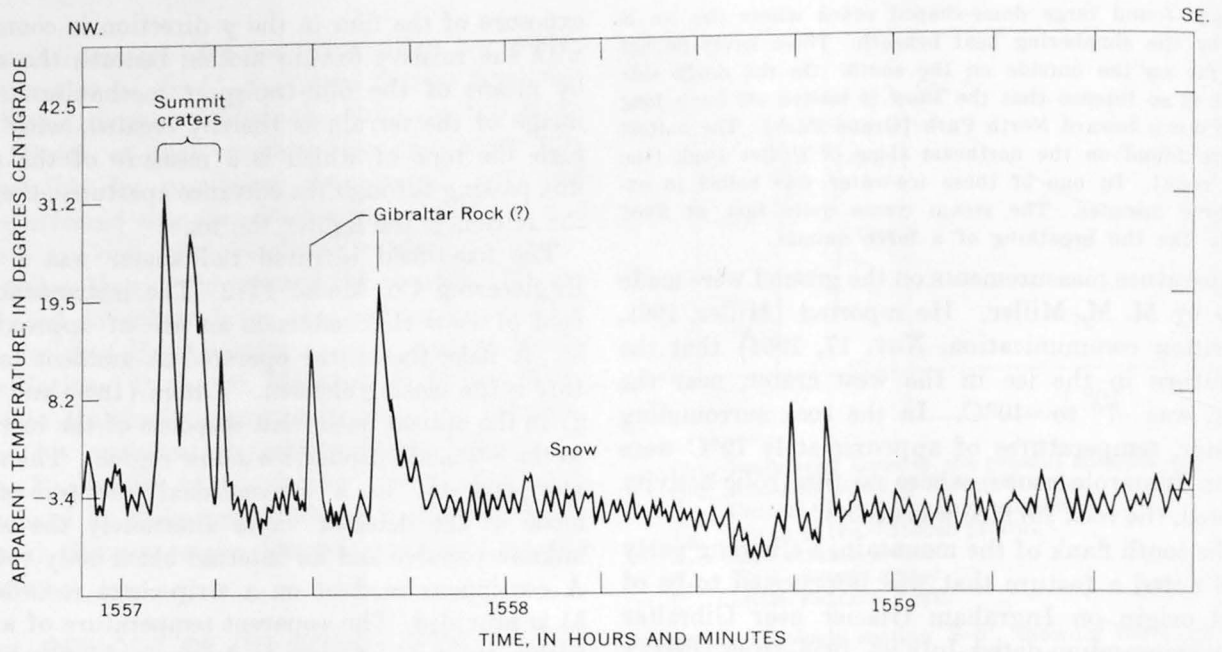


FIGURE 3.—Record of airborne fixed-field radiometer traverse across summit (flight 3). Time 1557 (P.d.t.), July 11, 1964; altitude 14,800 feet. Approximate location of flight 3 is shown on figure 1.

by atmospheric-transmission losses as the scan range increases toward the horizon. The gray scale is therefore best regarded as a relative measure of surface radiance.

Some geometric distortion is evident in the scanner images, resulting from a mismatch between aircraft velocity and film transport. Such distortion, present in figures 5 and 6, accounts for the disparity between the true shapes of the craters revealed by aerial photography and the shapes of their infrared images.

**RESULTS OF THE AERIAL SURVEYS**

Three flights with the fixed-field radiometer were flown over the summit of Mount Rainier, but as there was no means of recording the flight path, considerable uncertainty exists as to the locations on the summit of the points of maximum temperature. The record for flight 3 is shown on figure 3; the data for all three flights are summarized below:

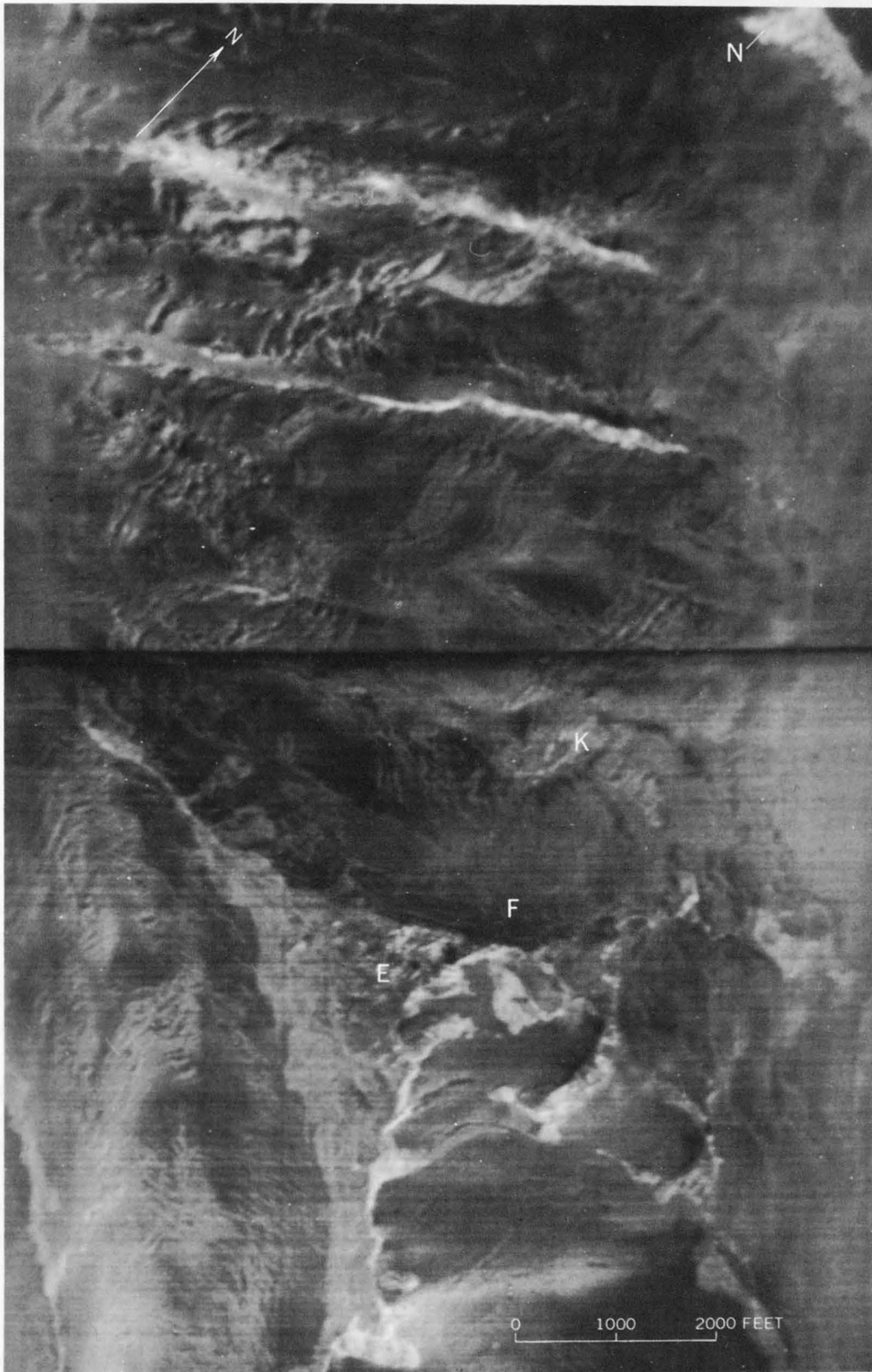
Flight	Time (P.d.t.)	Altitude (feet)	Apparent snow temperature (degrees C)	Maximum apparent rock temperature (degrees C)
1-----	1551	15,200	-6	+13
2-----	1554	15,100	-6	+22
3-----	1557	14,800	-5	+33

Air temperature=0°C (at 14,000 ft)  
 Total incoming radiation at top of aircraft=1.7 langley/min  
 Wind velocity ≈ 10 knots

The radiometer temperatures, compared to Miller's ground measurements reported on an earlier page, are considerably lower than the ground temperatures

of the fumaroles and higher than those of the adjacent rock outcrops. The radiometer's field of view of about 3° would cover an area on the ground of from about 40 feet (flight 1) to 20 feet (flight 3) in diameter. We can only surmise that the high-temperature fumaroles, if indeed they were "seen," did not fully cover the field of view, and that the recorded temperatures represent an integration of the fumaroles and the adjacent outcrops. The double peak at Gibraltar Rock (if we have correctly identified this location) probably results from snow or glacier ice separating two outcrops.

Infrared images of the summit and south flank of Mount Rainier were obtained at early dawn, September 4, 1964. The sky was light but the sun had not yet risen. At this hour the western slopes of the summit were deeply shaded. Little Tahoma Peak and vicinity are shown in figure 4. The rock outcrops, as expected, show higher apparent temperatures than do the glaciers and snow-filled basins. Some of the steep, east-facing rock slopes are warmer than adjacent rock outcrops, perhaps due to solar heating or reflection, but the thermal pattern at Little Tahoma seems similar to that elsewhere in the image. If any unusual thermal activity was associated with the December 1963 rockfall, it either had no recognizable surface manifestation at the time of this survey or it was not sufficiently large to be detected. As there was no unexplainable increase in the discharge of the stream draining Emmons Glacier following the rockfall, there

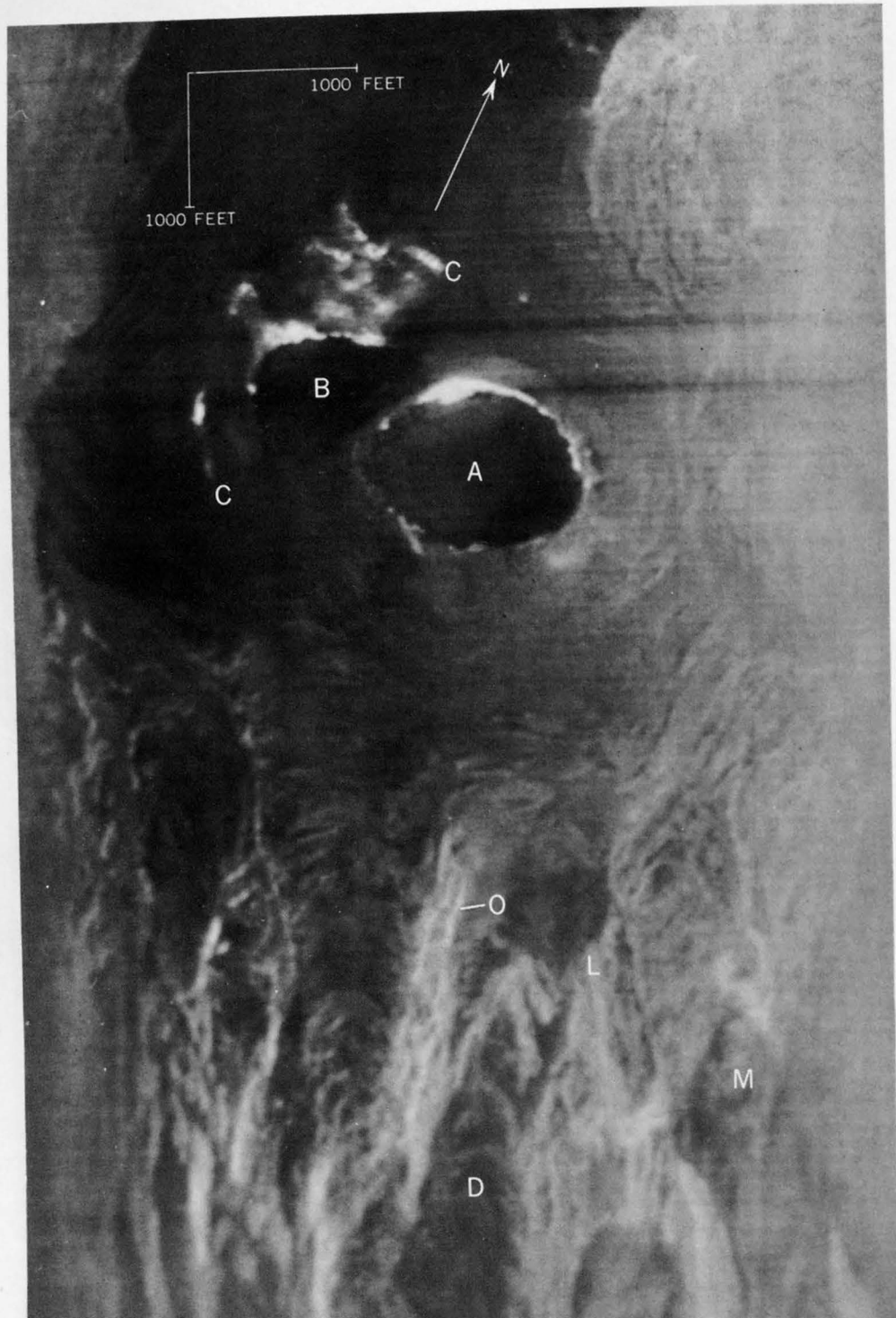


E, Little Tahoma Peak.  
F, Rockfall scar.

K, Emmons Glacier.  
N, Steamboat Prow.

FIGURE 4.—Infrared image of Little Tahoma Peak and Emmons Glacier. Time 0725 P.d.t., Sept. 4, 1964; altitude 12,000 feet. Scale is approximate. Black streak indicates data missing at film stoppage.





- |  |  |
|--|--|
| A, East summit crater.                   | L, Gibraltar Rock.   |
| B, West summit crater.                   | M, Ingraham Glacier.   |
| C, Arcuate pattern of thermal anomalies. | O, Long, narrow areas of slightly higher apparent temperature. |
| D, Nisqually Glacier.                    |  |

FIGURE 5.—Infrared image of the summit area of Mount Rainier. Time, 0700 P.d.t., Sept. 4, 1964; altitude, 16,000 feet. Scales indicate approximate geometric distortion caused by mismatch between aircraft velocity and film transport.

seems no compelling reason to attribute the fall to thermal activity.

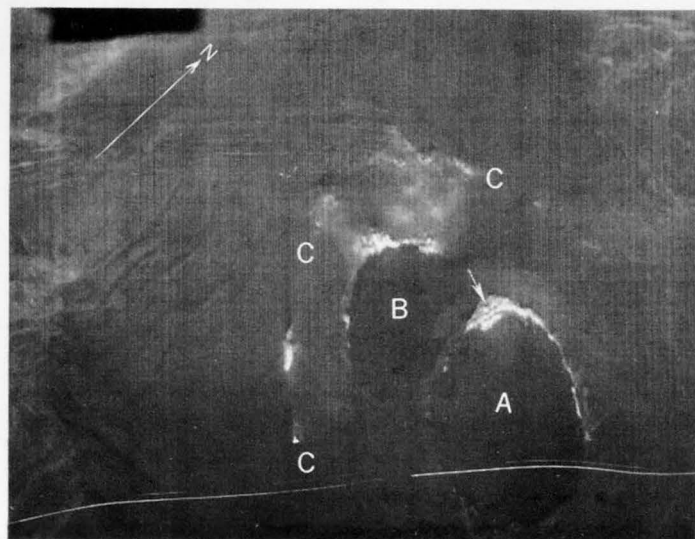
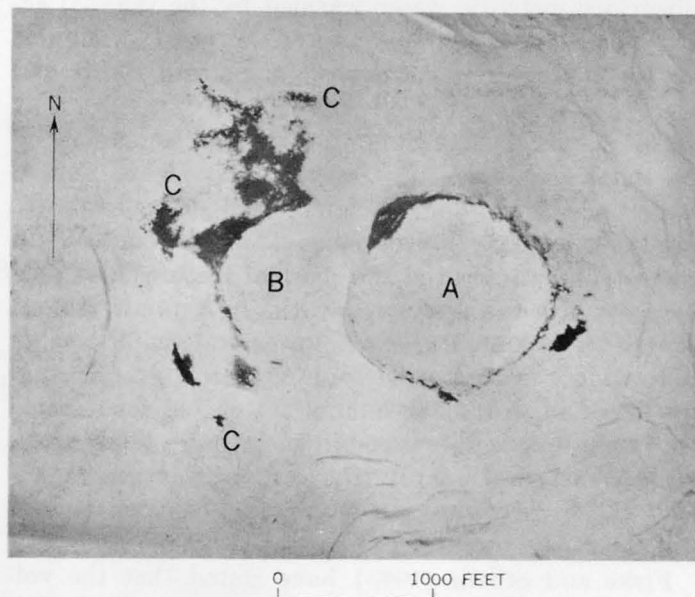
Between Little Tahoma Peak and Steamboat Prow, several rock ridges, on radii from the summit of Mount Rainier, protrude through Emmons Glacier. In the upper half of the infrared image (fig. 4) there are at least two northeast-trending narrow bands of higher apparent temperature coinciding with these ridges, that contrast rather markedly in tone from adjacent rock and snow. By inspection, the thermal patterns here seem somewhat more intense than those associated with other outcrops on the image. Radial dikes have been mentioned by earlier workers and several were mapped elsewhere on the mountain, but none have been previously noted in this area. The radial thermal patterns may correlate with some compositional variant but we cannot tell whether the higher radiance denotes any abnormal thermal gradient.

In the summit area of Mount Rainier, the infrared imagery (fig. 5) shows, on the lower slopes (around the edges of the image), easily discernible gray-tone differences between rock outcrops and the surrounding glaciers and snow, similar to figure 4. In the exposed ridges adjacent to Nisqually Glacier there are long narrow bands of slightly higher apparent temperatures, generally along radii from the summit (for example, *O*, fig. 5) similar to those on figure 4. We could find no outstanding thermal features in the infrared image that correlate with the thermal activity reported at Ingraham Glacier and Gibraltar Rock.

At the summit there are additional thermal features, much greater in intensity (that is, whiter on the image), which evidently relate to the abnormal thermal activity described by the earlier geologic investigators. The highest apparent temperatures were recorded along a narrow arc coinciding with the northwestern rim of the east summit crater (fig. 6, bottom). Toward the northwest end of the arc, the thermal pattern widens and apparently bifurcates southwestward, resulting in at least four separate thermal lineaments within the crater wall (arrow, fig. 6). The separate lineaments do not show clearly on figure 6, but are evident on other images not included here.

A similar arcuate thermal pattern occurs on the northwest quadrant of the west-summit crater rim, and a complex reticulation of anomalies extends down the northwest slope from the west-summit crater, coinciding with the bare outcrops in this area. Without

detailed examination of the outcrops we can only speculate that these rocks have some more or less direct



A, East summit crater.  
B, West summit crater.  
C, Arcuate pattern of thermal anomalies.

FIGURE 6.—Aerial photograph (top) and infrared image (bottom) of crater area of Mount Rainier. Aerial photograph taken Sept. 16, 1960. Infrared image: Time 0630 P.d.t., Sept. 4, 1964; altitude 16,000 feet; white streak is an emulsion scratch; arrow indicates thermal lineaments within the crater wall; scale indicates approximate geometric distortion caused by mismatch between aircraft velocity and film transport.

subsurface connection with a primary heat source; or perhaps heat is being transferred down the slope by subsurface meteoric water warmed by the thermal activity in the west summit crater. There is a similar but much less distinct downslope pattern north and east of the east summit crater.

The downslope extent of the thermal anomalies on the northwest flank of the summit cone is limited rather markedly along a fairly well defined arc (C, fig. 1) which may reflect some structural control. In geometric configuration the thermal features along arc C resemble those associated with the summit craters, though the temperatures are lower and the anomalies more widely scattered. There is little topographic suggestion of a third, older summit crater, but the thermal arc raises this remote possibility. A more likely cause could be ascribed simply to a concentric fracture system which provides pathways for convective heat transfer.

Fiske and others (1963) have stated that the volcano's central axis and presumably the central plug are northwest of the summit craters. The location of the thermal patterns at the summit, with maximum intensities consistently in the northwest quadrants, further suggests the possibility that the volcano's plug (and presumed primary source of heat at depth) is centered northwest of the present summit. Apparent temperatures, on the other hand, increase in the opposite direction; that is, the highest values are associated with the east summit crater, farthest from the central plug axis. This corresponds, perhaps coincidentally, with the relative ages of the features. According to data obtained with the scanning radiometer, the highest apparent temperatures and most well defined peripheral arc are associated with the northwest side of the youngest (east) crater, which lies farthest from

the axis of the central plug. The west crater shows somewhat lower apparent temperature and is less well defined than the east crater. Anomalies of the lowest apparent temperatures are scattered along a very indistinct arc but closest to the axis of the central plug.

## REFERENCES

- Buettner, K. J. K., Kern, C. D., and Cronin, J. F., 1965, The consequences of terrestrial surface infrared emissivity: Michigan Univ., Third Symposium on Remote Sensing of Environment, Proc., pub. 4864-9—, p. 549-561.
- Clark, John (chm.), 1964, Techniques for infrared survey of sea temperature: U.S. Bur. Sport Fisheries and Wildlife Circ. 202, Sandy Hook Marine Lab., 142 p.
- Crandell, D. R., 1963, Paradise debris flow at Mount Rainier, Washington: Art. 36 in U.S. Geol. Survey Prof. Paper 475-B, p. B135-B139.
- Daněš, Z. F., 1965, A new steam vent on Mt. Rainier, Washington: Jour. Geophys. Research, v. 70, no. 8, p. 2003.
- Dorsey, E. N., 1940, Properties of ordinary water-substance: New York, Reinhold Pub. Co., Am. Chem. Soc. Series, no. 81, p. 493-494.
- Fischer, W. A., Moxham, R. M., Polcyn, Fabian, and Landis, G. H., 1964, Infrared surveys of Hawaiian volcanoes: Science, v. 146, no. 3645, p. 733-742.
- Fiske, R. S., Hopson, C. A., and Waters, A. C., 1963, Geology of Mount Rainier National Park: U.S. Geol. Survey Prof. Paper 444, 93 p.
- Flett, J. B., 1912, The thermal caves [of Mount Rainier]: The Mountaineer, v. 5, p. 58-60.
- Hack, E. M., 1912, The ascent of Mt. Rainier: The Mountaineer, v. 5, p. 28-36.
- Haines, A. L., 1962, Mountain fever; historic conquests of Rainier: Portland, Oreg., Oregon Hist. Soc., 255 p.
- Miller, M. M., 1961, Wind, sky and ice report from Project Crater, 1959-1960, in Harvard Mountaineering: Cambridge, Mass., The Harvard Mountaineering Club, no. 15.
- Sanders, E. J., 1915, The geological story of Mount Rainier: The Mountaineer, v. 8, p. 67-72.
- Stevens, Hazard, 1876, The ascent of Mount Tahoma: Atlantic Monthly, Nov., p. 511-530.



## SEISMIC INVESTIGATIONS IN THE HARWICH AND DENNIS QUADRANGLES, CAPE COD, MASSACHUSETTS

By R. N. OLDALE and C. R. TUTTLE, Boston, Mass.

*Work done in cooperation with the Massachusetts Department of Public Works and the Bureau of Public Roads, U.S. Department of Commerce*

**Abstract.**—Subsurface data in the Harwich and Dennis quadrangles indicate that the top of the basement ranges from 180 to at least 555 feet below sea level. The basement, composed of crystalline rock of pre-Mesozoic age, is locally overlain by compact till a few tens of feet to 375 feet thick. Stratified drift 115 to 480 feet thick overlies the till. Valleys of Cretaceous(?) age cut the basement and indicate a change in relative sea level of at least 600 feet. The deepest of these valleys is filled in part by the till.

Seismic studies in the Harwich and Dennis quadrangles (fig. 1) show that three seismic layers, defined by their compressional-wave velocities, overlie a crystalline basement. These layers have been correlated with stratified drift and till identified in three boreholes located in the Harwich quadrangle. The boreholes were drilled through unconsolidated Pleistocene deposits into pre-Mesozoic basement rocks. The basement surface ranges from 180 to 555 feet below sea level and forms part of a poorly defined ridge that extends from the western end of Cape Cod to Chatham. The maximum depths below sea level occur in valleys, thought to be of Cretaceous age, cut into the basement.

The seismic data used in this report were obtained from surveys made in 1947 and 1948 by Rev. Daniel Linehan, S. J., and between 1951 and 1962 by members of the U.S. Geological Survey. Seismic studies were made in 1951 by Robert Hazelwood and in 1952 by Raymond Miller. Surveys were made in 1957 by the authors, and in 1962 by the authors and several other members of the U.S. Geological Survey as part of a seismic seminar. The authors wish to acknowledge the work of L. W. Currier, who until 1960 directed the seismic investigations in this area.

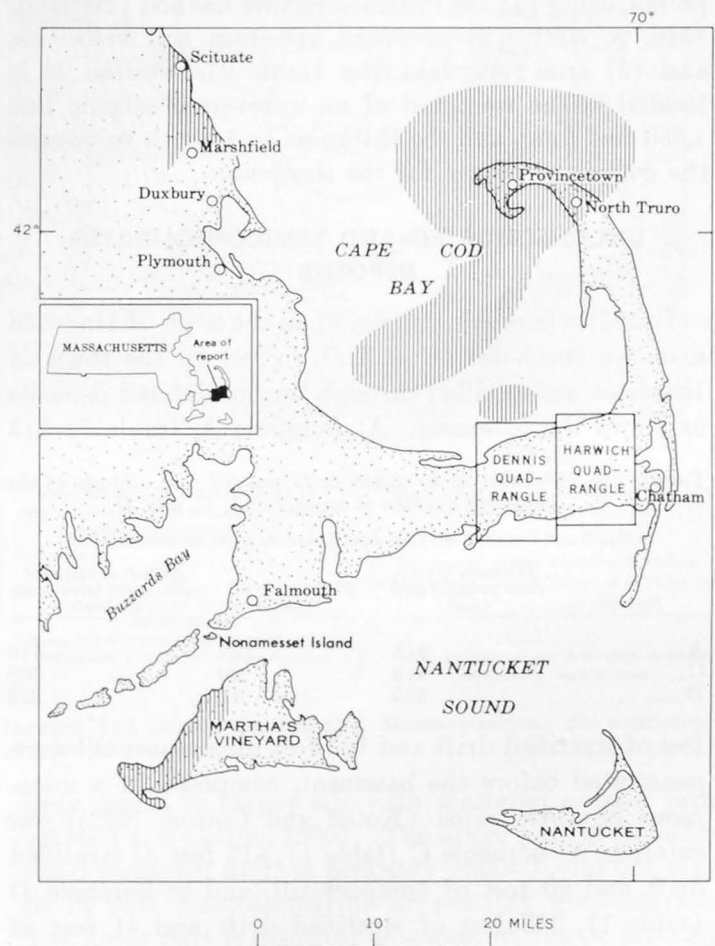


FIGURE 1.—Index map of Cape Cod, Mass., showing the location of the Harwich and Dennis quadrangles. Vertical pattern, areas where sediments of possible Tertiary and Mesozoic age are known to occur or are inferred to occur from borehole and seismic data.

**METHODS OF STUDY**

All seismic traverses were of the in-line refraction type. Those before 1962 utilized a single 12-channel portable seismograph and ranged from 1,100 to 2,400 feet in length. Successive explosions of 15 to 150 pounds of dynamite at a single shot location were used with geophone spreads of approximately 500 to 1,000 feet at increasing distances from the shotpoint. In 1962, seismic traverses 2,100 feet long were made by using two 12-channel refraction seismographs, each with a set of 12 geophones recording half the traverse.

Seismograms and traveltime curves obtained by previous workers were examined by the authors and in some cases reinterpreted. The seismic stations shown in figure 2 are located at the center of the seismic lines. The thickness and depth values given for the station are the average of the values computed for the shotpoints, using (1) the critical-distance method (Heiland, 1940, p. 508), (2) recorded apparent soil velocities, and (3) true rock velocities (table 2). Station 20 is located at the west end of an unreversed seismic line 1,650 feet long, and the thickness and depth values are the computed values for the shotpoint.

**UNCONSOLIDATED AND SEMICONSOLIDATED DEPOSITS**

In 1961 a borehole (A, fig. 2) in the town of Harwich and two boreholes (C and D, fig. 2) in the town of Brewster were drilled through unconsolidated deposits and into the basement. At borehole A (table 1) 313

TABLE 1.—*Thickness of stratified drift and till and altitude of the basement surface at boreholes A, C, and D*

[Koteff and Cotton, 1962; Carl Koteff, written communication, 1964]

Borehole	Thickness of saturated stratified drift (feet)	Thickness of till (feet)	Altitude of basement surface (feet below mean sea level)
A-----	313	122	-416
C-----	413	20	-368
D-----	355	41	-326

feet of stratified drift and 122 feet of compact till were penetrated before the basement, composed of a micaeous phyllitic schist (Koteff and Cotton, 1962), was entered. At borehole C (table 1), 413 feet of stratified drift and 20 feet of compact till, and at borehole D (table 1), 355 feet of stratified drift and 41 feet of compact till, were found above the basement, which is composed of granite gneiss (Carl Koteff, written communication, 1962). The compressional-wave velocities measured near the boreholes have been correlated with the stratified drift, till, and basement rocks. At the remaining seismic stations, similar compressional-wave velocities are assumed to represent the materials identi-

fied in the boreholes. Using this assumption, the distribution and thickness of the stratified drift and till and the depth of the basement surface within the quadrangles have been determined.

At 22 seismic stations an uppermost seismic layer ( $L^1$ ), 10 to 100 feet thick, with velocities of 1,200 to 3,100 feet per second was recorded (table 2). The base

TABLE 2.—*Thickness of unconsolidated layers, and depth, altitude, and true velocity of the basement rocks at 45 seismic stations in the Harwich and Dennis quadrangles*

Traverse	Thickness of unconsolidated layers (feet)			Depth to basement (feet)	Altitude of basement surface below mean sea level (feet)	True velocity in basement rocks (feet per second) $\frac{2(V^*zV^2)}{V^*+V^2}$
	$L^1$	$L^2$	$L^3$			
1 <sup>1</sup> -----	20	230	55	305	-255	18,700
2-----	15	340	190	545	-500	20,400
3-----	20	220	375	615	-555	20,800
4-----	10	250	310	570	-530	19,100
5-----	20	265	305	590	-540	21,500
6 <sup>1</sup> -----	15	295	150	460	-440	21,500
7-----	-----	195	350	545	-540	17,800
8 <sup>1</sup> -----	-----	370	-----	370	-325	16,300
9-----	100	350	-----	450	-330	15,500
10-----	85	370	-----	455	-335	18,000
11-----	85	270	-----	355	-255	18,300
12-----	-----	430	-----	430	-340	22,500
13-----	55	475	-----	530	-440	17,200
14-----	-----	395	-----	395	-355	17,700
15-----	-----	465	-----	465	-395	22,000
16-----	45	345	-----	390	-320	15,000
17-----	( <sup>2</sup> )	( <sup>2</sup> )	( <sup>2</sup> )	365	-315	( <sup>2</sup> )
18 <sup>1</sup> -----	35	210	185	430	-360	21,200
19-----	20	410	-----	430	-370	14,100
20-----	-----	450	-----	450	-395	18,000
21-----	-----	480	-----	480	-420	18,200
22-----	15	440	-----	455	-415	14,500
23-----	20	390	-----	410	-375	17,500
24-----	20	405	-----	425	-365	14,500
25-----	-----	275	-----	275	-270	16,600
26 <sup>1</sup> -----	35	80	140	255	-180	18,600
27 <sup>1</sup> -----	25	310	-----	335	-280	20,700
28-----	-----	320	-----	320	-270	17,100
29 <sup>1</sup> -----	-----	325	-----	325	-285	19,500
20 <sup>1</sup> -----	-----	210	-----	210	-205	15,400
31 <sup>1</sup> -----	-----	375	-----	375	-360	16,900
32-----	-----	375	-----	375	-370	15,900
33-----	-----	305	-----	305	-285	21,300
34-----	-----	310	-----	310	-290	18,400
35-----	-----	300	-----	300	-275	20,500
36-----	-----	315	-----	315	-280	19,300
37-----	25	275	-----	300	-255	17,200
38-----	25	290	-----	315	-265	18,100
39-----	-----	365	-----	365	-315	18,000
40-----	-----	305	-----	305	-265	16,400
41-----	-----	325	-----	325	-285	16,200
42-----	40	295	-----	335	-285	18,400
43-----	-----	265	-----	265	-260	17,700
44-----	-----	320	-----	320	-270	17,500
45-----	20	315	-----	335	-295	20,100

<sup>1</sup> Seismic record not available; data taken from traveltime curve.

<sup>2</sup> No data for thickness of layers or true rock velocity.

of this seismic layer is at or near the water table determined from the altitude of lakes or ponds near the seismic station; therefore the layer is the unsaturated part of the stratified drift. The  $L^1$  layer was not recorded where the water table is within a few feet of the top of the ground or where the geophone interval

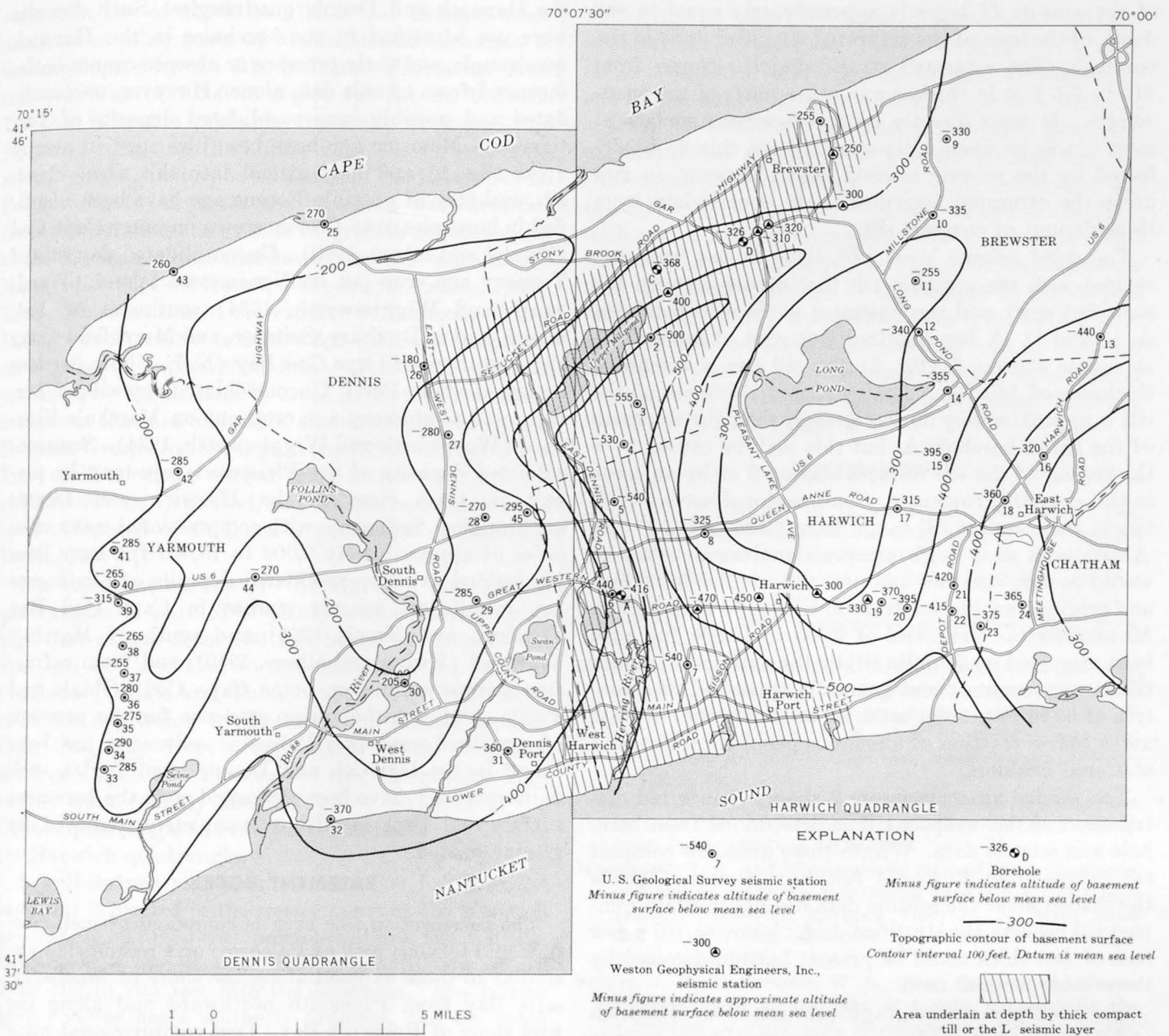


FIGURE 2.—Topographic map of the basement surface in the Harwich and Dennis quadrangles, Massachusetts. All altitudes of basement surface are given in feet below mean sea level.

used was too long to record an unsaturated zone a few tens of feet thick.

The second seismic layer ( $L^2$ , table 2) has been correlated with the saturated stratified drift identified in boreholes A, C, and D. Near the boreholes this layer has a velocity of approximately 5,000 feet per second. Therefore, at all other seismic stations, velocities of 4,600 to 5,600 fps are interpreted to be recorded from saturated stratified drift somewhat similar to the material described from borehole A. The saturated stratified drift at borehole A is composed of 160 feet of fine sand with scattered coarser beds and 153 feet of bluish-

gray coarse to clayey silt with scattered coarser beds (Koteff and Cotton, 1962). The upper part of the saturated stratified drift is probably glaciofluvial but may be in part glaciolacustrine or possibly glaciomarine. The lower part is probably glaciolacustrine or possibly glaciomarine. The coarser beds are sand and gravel. No interbedded till layers were recognized (Carl Koteff, oral communication, 1964). The base of the  $L^2$  seismic layer is interpreted to be equivalent to the contact between the saturated stratified drift and the underlying till, as at station 6, a few hundred feet west of borehole A, where the computed depth to the base

of the seismic  $L^2$  layer is approximately equal to the depth of the base of the saturated stratified drift in the borehole. The saturated stratified drift ranges from 115 to 475 feet in thickness in other parts of the quadrangle. It rests directly on the basement surface at most places or upon a layer of till too thin to be detected by the seismic method used; however, in two areas the saturated stratified drift is underlain by a thick deposit of compact till.

The third seismic layer ( $L^3$ , table 2) has been correlated with the compact till that occurs between the stratified drift and the basement surface in boreholes A, C, and D. A few hundred feet west of borehole A at seismic station 6 (fig. 2) the till has a computed thickness of 150 feet. The computed thickness of the till is approximately 30 feet greater than the thickness of the till at borehole A, but this may be caused by a thickening of the till towards station 6 or by an error in the computed thickness. Compressional-wave velocities in the compact till range from 6,400 to 11,500 fps. A till with such high compressional-wave velocities would be very compact and probably similar in texture and origin to subglacial drumlin till found elsewhere in Massachusetts. Velocities of 6,000 to 10,000 fps have been measured on drumlin till by the authors. Drumlin till is very compact and generally composed of a matrix of 60 to 70 percent sand, 30 to 40 percent silt-clay, and a coarse fraction of numerous pebbles, cobbles, and scattered boulders.

The shaded areas on figure 2 show the inferred distribution of the compact till as determined from borehole and seismic data. Within these areas the compact till ranges from 20 to 375 feet in thickness. Outside the shaded areas the seismic data did not indicate compact till beneath the stratified drift; however, till a few tens of feet thick could be present but not detected by the seismic method used.

The Pleistocene stratigraphic section in the Harwich and Dennis quadrangles, as determined from seismic and borehole data, is made up of thick stratified drift composed of fluvial and lacustrine and (or) marine deposits overlying a locally thick deposit of compact till of probable subglacial origin. Such a relation suggests that the glacial deposits in this area were laid down during a single major glaciation. However, the multiple drifts found on Martha's Vineyard, approximately 30 miles to the southwest, indicate that more than one glaciation reached this area, and that the compact till beneath the stratified drift may be a complex deposit of several till sheets laid down at different times.

Unconsolidated and semiconsolidated deposits older than Pleistocene may be present beneath the drift in

the Harwich and Dennis quadrangles. Such deposits were not identified in the boreholes in the Harwich quadrangle, and their presence or absence cannot be determined from seismic data alone. However, unconsolidated and possibly semiconsolidated deposits of Tertiary and Mesozoic age have been identified in nearby areas (fig. 1) and may extend into this area. Sand, silt, and clay of possible Eocene age have been identified in boreholes near Provincetown on outer Cape Cod (Zeigler and others, 1960). Unconsolidated deposits of Tertiary age crop out on Nonamesset Island (Woodworth and Wigglesworth, 1934) southwest of Falmouth, and at Duxbury, Scituate, and Marshfield along the west shore of Cape Cod Bay (N. E. Chute, written communication, 1964). Unconsolidated deposits of Tertiary and Cretaceous age crop out on Martha's Vineyard (Woodworth and Wigglesworth, 1934). Semiconsolidated deposits of pre-Pleistocene age may be present in areas close to the Harwich and Dennis quadrangles. Sediments with compressional-wave velocities of approximately 9,000 to 13,000 fps have been interpreted as semiconsolidated deposits of Cretaceous age in offshore seismic studies in Cape Cod Bay (Hoskins and Knott, 1961) and south of Martha's Vineyard (Ewing and others, 1950), and from refraction seismic studies on outer Cape Cod (Oldale and Tuttle, 1964). Although no evidence for the presence of pre-Pleistocene-post-Paleozoic sediments has been found in the Harwich and Dennis quadrangles, such sediments may have been deposited over the basement surface and later mostly, or completely, removed by glacial erosion.

#### BASEMENT ROCKS

The basement in this area is composed of metamorphic and igneous rock of Paleozoic or Precambrian age similar to those exposed along the shore of Massachusetts Bay from Plymouth northward and along the west shore of Buzzards Bay. True compressional-wave velocities computed for the basement rocks range from 14,100 to 22,000 fps. Velocities in this range are comparable to those measured by the authors in areas underlain by igneous and metamorphic rocks in other parts of Massachusetts. There appears to be no systematic variation between true rock velocities measured along different azimuths, as the average of the velocities measured in an east-west direction differed by only 1,300 fps from the average of the velocities measured in a north-south direction. The basement rocks were identified in borehole A as a micaceous phyllitic schist similar to the Rhode Island Formation of Pennsylvanian age (Koteff and Cotton, 1962). Seismic measurements in the vicinity of this borehole gave true

rock velocities of 17,800 to 21,500 fps. Seismic measurements in other parts of Massachusetts underlain at shallow depths by the Rhode Island Formation show true velocities of 7,200 to 20,800 fps for the bedrock. The low velocities probably represent weathered and fractured rock, and the higher velocities unweathered, more highly metamorphosed facies of the Rhode Island Formation. In Brewster the basement was identified from the boreholes as granite or granite gneiss similar to the Dedham Granodiorite exposed in southeastern Massachusetts (Carl Koteff, oral communication, 1962). True rock velocities in the vicinity of boreholes C and D range from 18,000 to 20,000 fps (Weston Geophysical Engineers, unpublished data). True rock velocities measured by the authors in areas in southeastern Massachusetts that are underlain at shallow depths by the Dedham Granodiorite range from 11,900 to 16,000 fps. True rock velocities ranged from 12,150 to 17,750 fps at Falmouth on Cape Cod, and the basement is thought to be composed of Dedham Granodiorite (Oldale and Tuttle, 1964).

The basement surface in the Harwich and Dennis quadrangles is part of a poorly defined topographic high that ranges from 100 feet below sea level at the west end of Cape Cod to 300 feet below sea level at Chatham (Oldale and Tuttle, 1964). This high separates the depression in the basement surface beneath Cape Cod Bay from deeper parts of the basement south of Cape Cod. The crest of this topographic high ranges from roughly 200 feet below sea level in the Dennis quadrangle to nearly 300 feet below sea level in the Harwich quadrangle.

A well-defined valley cut at least 300 feet into the basement is located in the western part of the Harwich quadrangle. Three other possible valleys, less well defined because of sparse seismic coverage, may be cut from 100 to 200 feet into the basement. The largest buried valley has a southerly gradient, and the other valleys may have been tributary to the largest. These

valleys are at least Pleistocene in age and are thought to be as old as Cretaceous. They are thought to be similar to the buried valley, located between Provincetown and North Truro on outer Cape Cod, cut to a depth of at least 900 feet below sea level and filled in part with unconsolidated sediments of possible Eocene age and semiconsolidated sediments of possible Cretaceous age (Oldale and Tuttle, 1964). If the valleys in the Harwich and Dennis quadrangles were at one time filled with marine sediments of Tertiary and Cretaceous age then the present altitude of the bottom of the deepest valley suggests (1) that relative sea level during part of Cretaceous or pre-Cretaceous time was at least 600 feet below present sea level, and (2) that sediments of Tertiary and Cretaceous age were deposited during a rise in relative sea level.

#### REFERENCES

- Ewing, W. M., Worzel, J. L., Steenland, N. C., and Press, Frank, 1950, Geophysical investigations in the emerged and submerged Atlantic Coastal Plain, pt. V, Woods Hole, New York, and Cape May sections: *Geol. Soc. America Bull.*, v. 61, p. 877-892.
- Heiland, C. G., 1940, Geophysical exploration: New York, Prentice-Hall, 1013 p.
- Hoskins, Hartley, and Knott, S. T., 1961, Geophysical investigation of Cape Cod Bay, Massachusetts, using the continuous seismic profiler: *Jour. Geology*, v. 69, p. 330-340.
- Koteff, Carl, and Cotton, J. E., 1962, Preliminary results of recent deep drilling on Cape Cod, Massachusetts: *Science*, v. 137, p. 34.
- Oldale, R. N., and Tuttle, C. R., 1964, Seismic investigations on Cape Cod, Massachusetts: Art. 145 in *U.S. Geol. Survey Prof. Paper 475-D*, p. D118-D122.
- Woodworth, J. B., and Wigglesworth, Edward, 1934, Geography and geology of the region including Cape Cod, the Elizabeth Islands, Nantucket, Martha's Vineyard, No Mans Land and Block Island: *Harvard Coll., Mus. Comp. Zoology Mem.*, v. 52, 322 p.
- Zeigler, J. M., Hoffmeister, W. S., Geise, Graham, and Tasha, Herman, 1960, A discovery of Eocene sediments in the subsurface of Cape Cod, Massachusetts: *Science*, v. 132, p. 1397-1398.





## EVIDENCE OF LARGE STRIKE-SLIP DISPLACEMENT ALONG A FAULT IN THE SOUTHERN SALINAS VALLEY, CALIFORNIA

By DAVID L. DURHAM, Menlo Park, Calif.

*Abstract.*—Offset of the limits of deposition of the Pancho Rico and Santa Margarita Formations along a fault in the southern Salinas Valley indicates right-lateral strike-slip displacement of at least 11 miles. The faulting explains the juxtaposition of contemporaneous but unlike sequences of upper Miocene and Pliocene strata exposed near the Nacimiento River. It occurred after deposition of at least part of the Paso Robles Formation of Pliocene and Pleistocene(?) age.

The southern Salinas Valley lies in the Coast Ranges between the San Andreas and Nacimiento fault zones (fig. 1). The basement complex of granitic and associated metamorphic rocks is mantled by sedimentary rocks and contrasts markedly with the Franciscan terranes northeast of the San Andreas and southwest of the Nacimiento fault zones. Although many investigators, including Hill and Dibblee (1953) and Crowell (1962), have cited evidence of strike-slip movement along the San Andreas, only a few have suggested this sort of displacement on faults in the nearby Salinas Valley. Kilkenny (1948, p. 2264) inferred that movement on two faults in the southern Salinas Valley had a "strong horizontal component," but gave no supporting evidence. Hill and Dibblee (1953, p. 454-455) also suggested that some faults in the Salinas Valley are probably characterized by major right-lateral components of displacement, but mentioned as evidence only the approximate parallelism of the faults to the San Andreas. Gribi (1963, p. 23) stated that lateral faults apparently "control the orientation of folds" in some places in the Salinas Valley, but pointed out that the similarity of strata as old as early Miocene across a fault that he cited as an example precludes lateral offset greater than about 2,000 feet. The purpose of this paper is to present evidence of right-lateral strike-slip displacement of several miles along a fault in the southern Salinas Valley.

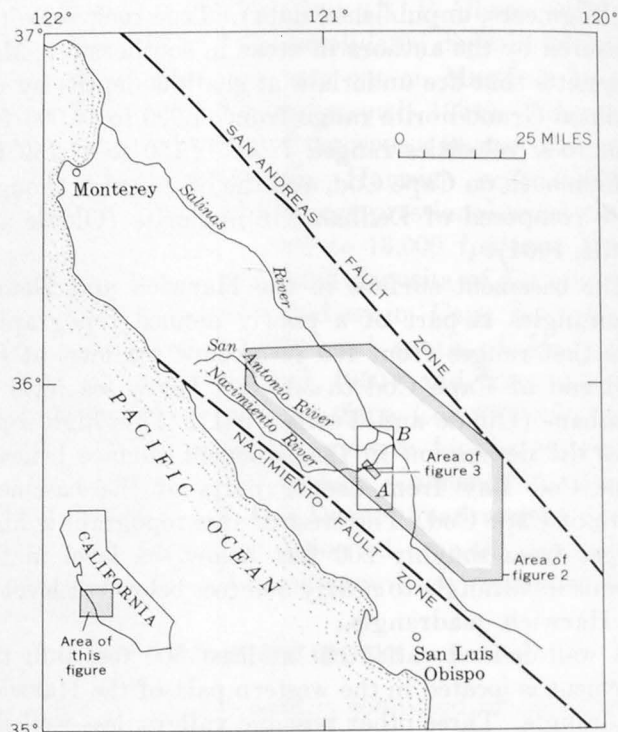


FIGURE 1.—Index map showing southern Salinas Valley area, California. A, Adelaida quadrangle. B, Bradley quadrangle.

### REGIONAL STRATIGRAPHIC RELATIONS

The Santa Margarita Formation is, in effect, a lenticular sandstone unit that directly overlies or intertongues with the upper part of the Monterey Shale (Durham and Addicott, 1964, p. 4). It commonly contains marine fossils indicative of late Miocene age. Near Indian Creek (fig. 2) it includes all of the upper Miocene marine strata that overlie middle Miocene beds of the Monterey Shale (Bramlette, 1946, pl. 2). It thins to the north, where it overlies upper Miocene beds of the Monterey Shale that are the lateral age equivalents of the lower part of the Santa Margarita

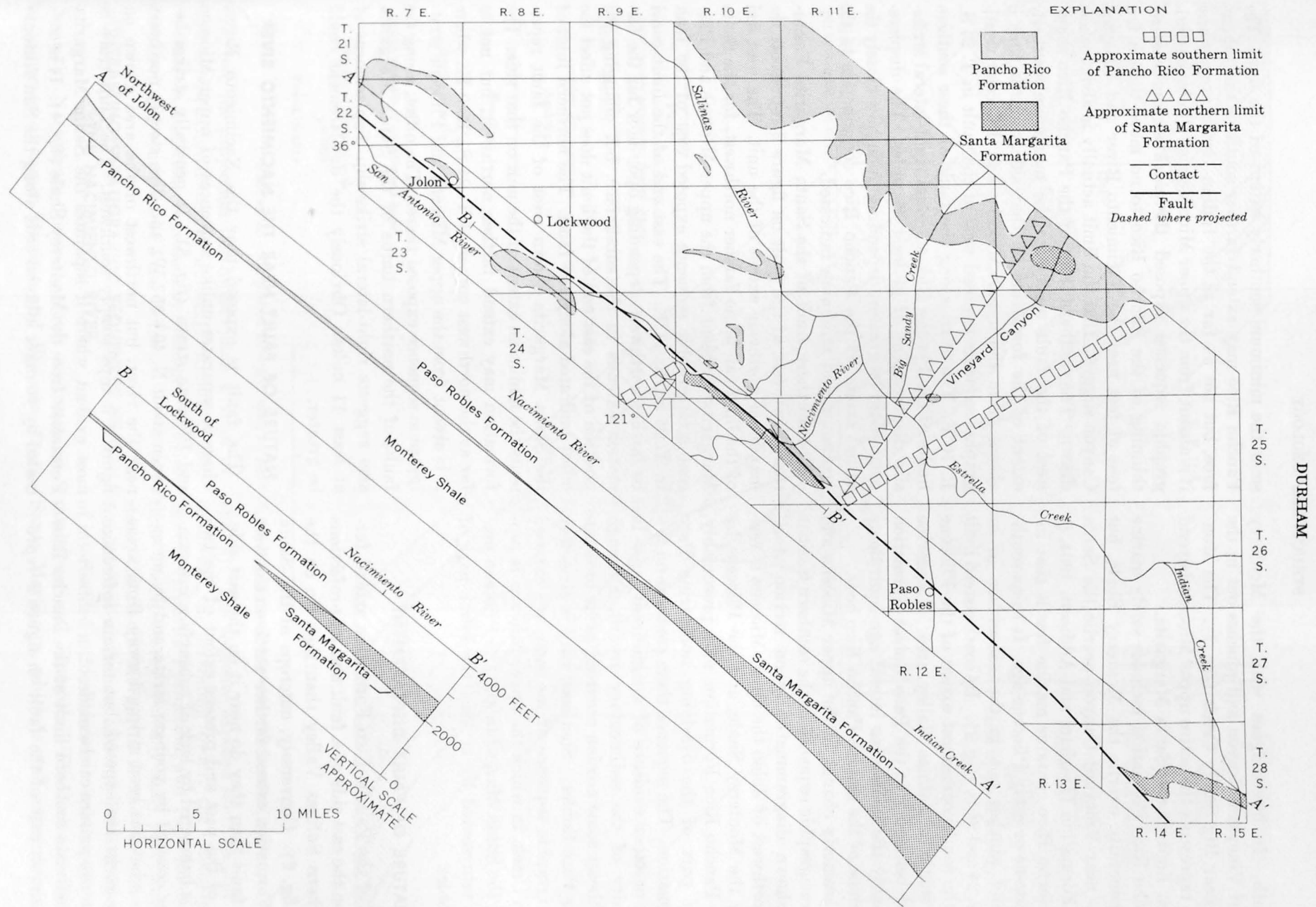


FIGURE 2.—Map showing outcrops of the Santa Margarita and Pancho Rico Formations in the southern Salinas Valley, the approximate limits of deposition of the formations, and the inferred offset of these limits along a fault. Longitudinal sections parallel to the fault show diagrammatically the stratigraphic relations and lateral variation of the Monterey Shale and Santa Margarita, Pancho Rico, and Paso Robles Formations in the area.

farther south. It intertongues with the Monterey northwest of Vineyard Canyon and pinches out in the subsurface near Big Sandy Creek (fig. 2). The Monterey Shale represents the entire upper Miocene beyond the northern limit of the Santa Margarita.

The Pancho Rico Formation includes sandy marine beds that generally overlie the Monterey Shale, but that locally near Vineyard Canyon overlie the Santa Margarita Formation (Durham and Addicott, 1964, p. 4). The Pancho Rico contains marine fossils that indicate a Pliocene or early Pliocene age. It thins southeastward and pinches out in the subsurface in or beyond Tps. 24 and 25 S. (fig. 2). Its southeastern limit represents the southeasternmost extent of the Pliocene sea in the southern Salinas Valley area. Nonmarine beds beyond belonging to the Paso Robles Formation are presumably the nonmarine lateral age equivalents of at least some of the marine Pancho Rico beds.

The southeasterly change in the upper Miocene and Pliocene stratigraphic sequence in the southern Salinas Valley is shown diagrammatically on section A-A' (fig. 2). Northwest of Jolon the upper Miocene is represented by the Monterey Shale, and the Pliocene by the marine Pancho Rico Formation, and, presumably, by at least part of the overlying nonmarine Paso Robles Formation. The sequence there contains no unconformity or other evidence of a significant lapse in the continuity of the sedimentary record, although farther southeast some erosion occurred prior to deposition of the Paso Robles. Southeastward it gives way to the stratigraphic sequence of the same age exposed near Indian Creek, in which the upper Miocene is represented by the Santa Margarita and the Pliocene presumably is represented by at least the lower part of the Paso Robles.

#### NATURE OF FAULT DISPLACEMENT

Outcrops of the Pancho Rico Formation extend farther south on the east side of a fault and its projections in the southern Salinas Valley than they do on the west side (fig. 2). Conversely, outcrops of the Santa Margarita Formation extend farther north on the west side of the fault than they do near it on the east side. Knowledge of the past and present extent of the two formations is hampered by lack of subsurface information in areas covered by younger strata and by uncertainty as to what has been stripped away from areas where older rocks are exposed, but certain inferences based on outcrop pattern can be made.

The approximate southern limit of the Pancho Rico Formation shown east of the fault on figure 2 repre-

sents the minimum southerly extent of the unit. The Pancho Rico may extend farther south in the subsurface, but not as far as the Indian Creek area, where it is absent from the upper Miocene and Pliocene stratigraphic sequence exposed there. The southeasterly thinning of the Pancho Rico to no more than a few tens of feet near the Nacimiento River and Vineyard Canyon suggests that the limit actually is about where drawn. The southern limit of the Pancho Rico shown west of the fault represents the maximum southerly extent of the formation on that side, for the unit is absent from the upper Miocene and Pliocene stratigraphic sequence exposed west of the fault in T. 24 S., R. 10 E. The offset along the fault of these southern limits of the Pancho Rico suggests right-lateral strike-slip displacement of at least 11 miles. The displacement could be greater, depending upon how closely the actual extent of the Pancho Rico corresponds to the maximum and minimum indicated.

The northern limit of the Santa Margarita Formation shown east of the fault on figure 2 represents the maximum northerly extent of the unit. The west end of the limit can be no farther northwest, for the Santa Margarita is absent from the upper Miocene and Pliocene stratigraphic sequence exposed east of the fault in T. 25 S., R. 11 E. The east end of the limit could be farther northwest, depending upon how far the formation extends in the subsurface, but changing the position of the east end of the limit does not affect the offset indicated along the fault. The northern limit of the Santa Margarita shown west of the fault represents the minimum extent of the unit on that side. The formation may extend farther northwest, but not as far as the northwest corner of T. 24 S., R. 9 E., where it is absent from the upper Miocene and Pliocene stratigraphic sequence exposed there. The offset, along the fault, of the northern limits of the Santa Margarita also suggests right-lateral strike-slip displacement of at least 11 miles. Obviously the displacement could be greater.

#### NATURE OF FAULT NEAR THE NACIMIENTO RIVER

The fault is exposed near the Nacimiento River, where it separates unlike sequences of upper Miocene and Pliocene strata (fig. 3). It generally strikes between about N. 40°-55° W., and dips steeply northeast near the river, but northwest of the area shown on figure 3 it dips steeply southwest. The fault trace is most evident where it separates the Santa Margarita Formation from the Monterey Shale (fig. 4). It is concealed by younger alluvial beds along the San Antonio

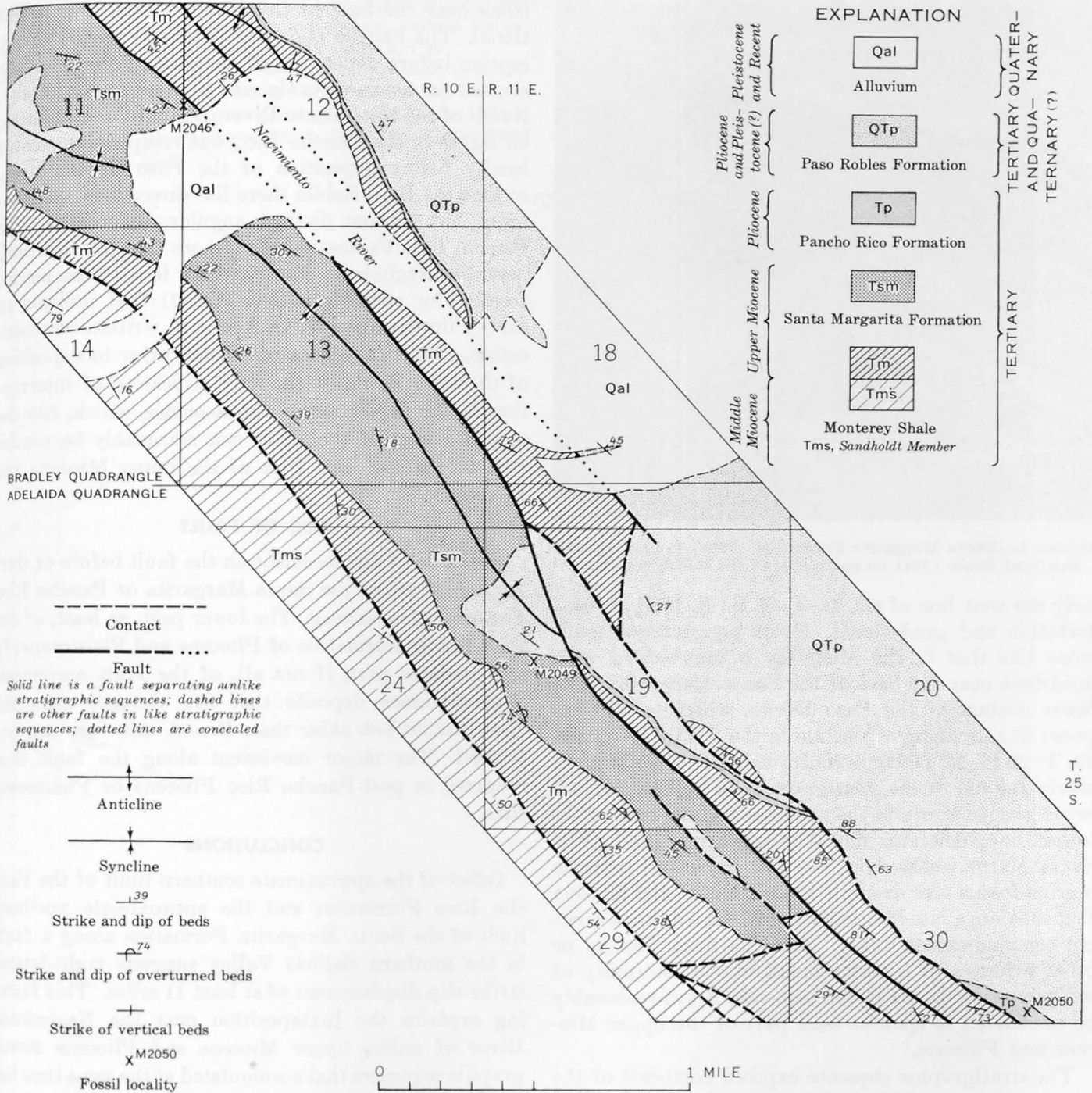


FIGURE 3.—Simplified geologic map of part of the Bradley and Adelaida quadrangles.

River, but its projection northwest joins a zone of faults exposed northwest of Jolon (Durham, 1965). The trace is likewise concealed by younger alluvial strata near and southeast of Paso Robles.

**CONTRASTING STRATIGRAPHIC SEQUENCES NEAR THE NACIMIENTO RIVER**

Near the Nacimiento River the fault separates unlike sequences of upper Miocene and Pliocene strata

(fig. 3). The sequence exposed southwest of the fault comprises, in ascending order, the Monterey Shale, Santa Margarita Formation, and Paso Robles Formation. The Monterey is chiefly shaly porcelaneous mudstone, the Santa Margarita is fine- to coarse-grained fossiliferous sandstone, and the Paso Robles consists of interbedded unfossiliferous conglomerate, sandstone, mudstone, and limestone. The lower contact of the Santa Margarita, which is well exposed in a roadcut

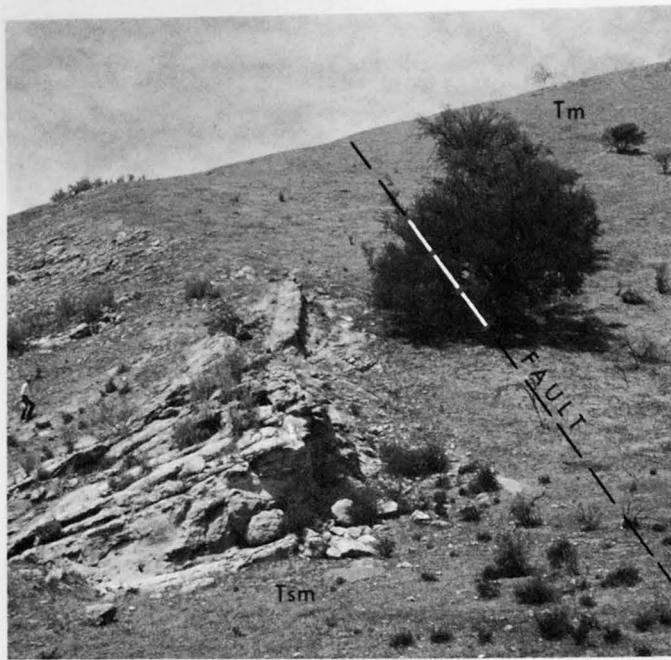


FIGURE 4.—Santa Margarita Formation (Tsm) faulted against Monterey Shale (Tm) on north side of the Nacimiento River.

near the west line of sec. 13, T. 25 S., R. 10 E., is conformable and gradational. Some porcelaneous mudstone like that in the Monterey is interbedded with sandstone near the base of the Santa Margarita. The lower contact of the Paso Robles, which is well exposed in cuts along a pipeline in the SW $\frac{1}{4}$ NW $\frac{1}{4}$  sec. 19, T. 25 S., R. 11 E., is conformable and distinct. It marks the top of the stratigraphically highest fossiliferous marine strata in the sequence and the base of the lowest conglomeratic fluvialite-appearing beds. The Santa Margarita is about 500 feet thick and contains marine fossils (for example at locs. M2046 and M2049) that indicate a late Miocene age (W. O. Addicott, written communication, 1964). Since no unconformity or other evidence of a major break in the continuity of sedimentation occurs in the sequence, it can reasonably be considered to span at least part of the upper Miocene and Pliocene.

The stratigraphic sequence exposed northeast of the fault near the Nacimiento River includes, in ascending order, the Monterey Shale, Pancho Rico Formation, and Paso Robles Formation. The Monterey is mainly shaly porcelanite and chert, but diatomaceous mudstone is common near the top. The Pancho Rico is mainly fine-grained sandstone that locally contains marine fossils. The Paso Robles is poorly sorted unfossiliferous conglomerate and sandstone. The lower contact of the Pancho Rico is conformable and, where rocks like those in the Monterey are interbedded with sand-

stone near the base of the Pancho Rico, it is gradational. The Pancho Rico was partly stripped away by erosion before deposition of the Paso Robles, but the contact is not noticeably an angular unconformity. North of the Nacimiento River, beyond the area shown on figure 3, the Pancho Rico was completely removed locally before deposition of the Paso Robles began, so that the Paso Robles there lies directly on the Monterey, but without distinct angular discordance. The Pancho Rico Formation is no more than 25 feet thick near the Nacimiento River, where it contains marine fossils (for example at loc. M2050) that indicate an early Pliocene age (W. O. Addicott, written communication, 1964). Evidence of erosion prior to deposition of the Paso Robles is the only indication of interruption in the deposition of the sequence, which, like the sequence west of the fault, can reasonably be considered to span at least part of the upper Miocene and Pliocene.

#### AGE OF FAULT

Evidence of displacement on the fault before or during deposition of the Santa Margarita or Pancho Rico Formations is lacking. The lower part, at least, of the Paso Robles Formation of Pliocene and Pleistocene(?) age predates part, if not all, of the fault movement. Stream-terrace deposits that are younger than the Paso Robles but older than Recent alluvium are unfaulted. The major movement along the fault thus occurred in post-Pancho Rico Pliocene or Pleistocene time.

#### CONCLUSIONS

Offset of the approximate southern limit of the Pancho Rico Formation and the approximate northern limit of the Santa Margarita Formation along a fault in the southern Salinas Valley suggests right-lateral strike-slip displacement of at least 11 miles. This faulting explains the juxtaposition near the Nacimiento River of unlike upper Miocene and Pliocene stratigraphic sequences that accumulated at the same time but under different circumstances in areas separated by several miles.

#### REFERENCES

- Bramlette, M. N., 1946, The Monterey formation of California and the origin of its siliceous rocks: U.S. Geol. Survey Prof. Paper 212, 57 p. [1947].
- Crowell, J. C., 1962, Displacement along the San Andreas fault, California: Geol. Soc. America Spec. Paper 71, 61 p.
- Durham, D. L., 1965, Geology of the Jolon and Williams Hill quadrangles, Monterey County, California: U.S. Geol. Survey Bull. 1181-Q, 27 p.

Durham, D. L., and Addicott, W. O., 1964, Upper Miocene and Pliocene marine stratigraphy in southern Salinas Valley, California: U.S. Geol. Survey Bull. 1194-E, 7 p.

Gabi, E. A., Jr., 1963, The Salinas basin oil province, in Guidebook to the geology of Salinas Valley and the San Andreas fault: Am. Assoc. Petroleum Geologists-Soc. Econ. Paleontologists and Mineralogists, Pacific Sec., Ann. Spring Field Trip 1963, p. 16-27.

Hill, M. L., and Dibblee, T. W., Jr., 1953, San Andreas, Garlock, and Big Pine faults, California—a study of the character, history, and tectonic significance of their displacements: Geol. Soc. America Bull., v. 64, no. 4, p. 443-458.

Kilkenny, J. E., 1948, Geology and exploration for oil in Salinas Valley, California: Am. Assoc. Petroleum Geologists Bull., v. 32, no. 12, p. 2254-2268.



## UPPER PRECAMBRIAN AND PALEOZOIC STRATIGRAPHY AND STRUCTURE OF THE NEPTUNE RANGE, ANTARCTICA

By DWIGHT L. SCHMIDT,<sup>1</sup> PAUL L. WILLIAMS,<sup>2</sup> WILLIS H. NELSON,<sup>3</sup> and JOHN R. EGE,<sup>2</sup>

<sup>1</sup> Washington, D.C., <sup>2</sup> Denver, Colo., <sup>3</sup> Menlo Park, Calif.

*Abstract.*—More than 30,000 feet of sedimentary and volcanic rocks is divided into the following 3 stratigraphic and structural units, in ascending order, bounded by major unconformities: (1) isoclinally folded eugeosynclinal sedimentary rocks of late Precambrian age; (2) limestone of Cambrian age, felsic volcanic rocks, and siltstones, all moderately folded and intruded by hypabyssal rhyolite; granite was emplaced during Late Cambrian or Early Ordovician time; and (3) gently folded clastic sedimentary rocks. All folds trend northerly, about parallel to the trend of the Neptune Range.

The Neptune Range constitutes the middle third of the Pensacola Mountains, which lie along the southeastern margin of the Filchner Ice Shelf between long 48° W. and 68° W. and lat 80° S. and 85° S. The Pensacola Mountains are a segment of the Transantarctic Mountains system which extends across the Antarctic continent from the Ross Sea to the Weddell Sea (fig. 1). Investigation of the Neptune Range during the 1963–64 field season was the second phase of a 3-year study of the Pensacola Mountains by the U.S. Geological Survey (for a brief account of the expedition, see Schmidt, 1964). The first phase was in the Patuxent Range of the southern Pensacola Mountains during the 1962–63 season (Schmidt and Ford, 1963). Neither the Patuxent Range nor the Neptune Range had been visited by man prior to the Survey study. The third phase will be in the northern Pensacola Mountains, where the northernmost area was examined by the IGY Ellsworth Station traverse party during 1957–58 (Aughenbaugh, 1961).

Geologic mapping in the Neptune Range covers about 2,000 square miles, of which about 20 percent is made up of snow-free nunataks and mountains with relief that ranges from several hundred to several thousand feet. An exceptionally complete record of late Precambrian and early Paleozoic geology is preserved in this area. This record is particularly valuable

because it is unusual to find so many sedimentary and igneous units, which have been involved in a long and complex orogenic history, so well exposed in snow-shrouded Antarctica.

This report is based on field observations by the authors and Walter W. Boyd, U.S. Geological Survey, and on preliminary petrographic examination of typical rock specimens by Nelson. Map control was provided by Donald C. Barnett and James R. Heiser, topographic engineers of the U.S. Geological Survey. We are indebted to the U.S. Navy for logistic support, and especially to Air Development Squadron Six for their readiness to fly across 1,200 formidable miles of ice and snow between the Neptune field camp and the staging base at McMurdo Station.

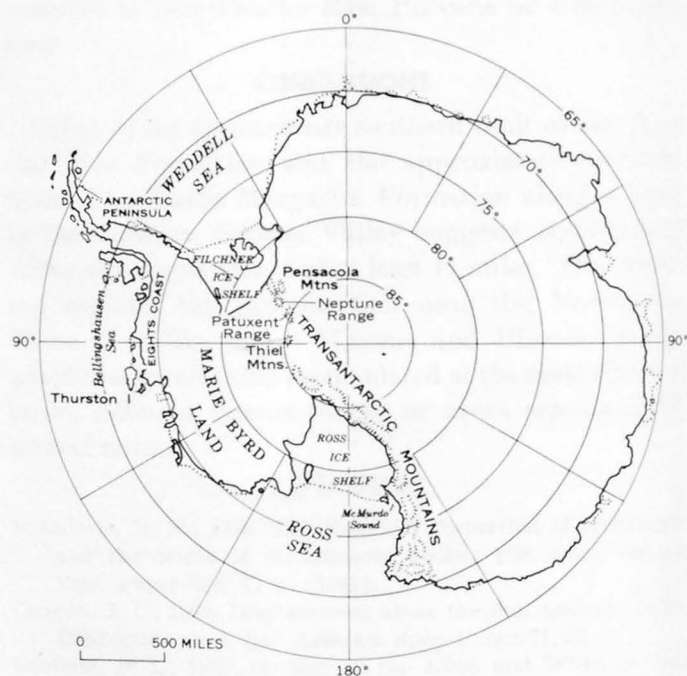


FIGURE 1.—Index map of Antarctica, showing location of the Neptune Range.

## STRATIGRAPHY

Ten sedimentary and volcanic rock formations have been mapped in the Neptune Range. The formations are formally named for geographic localities to which names have been assigned by the U.S. Board on Geographic Names. The geographic names and localities are well documented on unpublished maps of the Neptune Range and are shown on the locality map, figure 2, in this report.

The 10 formations are grouped in 3 stratigraphic sequences, each of which is bounded above by a major angular unconformity. The first sequence consists of a single formation which is estimated to be several tens of thousands of feet thick and is probably of late Precambrian age. The second sequence consists of 3 formations, has a total thickness as great as 3,000 feet, and is of earliest Paleozoic age. The third sequence consists of 6 formations with a total thickness of about 12,000 feet, and is pre-late Paleozoic in age (fig. 3).

## First sequence

The first and oldest sequence consists wholly of the Patuxent Formation, the type locality of which is in the Patuxent Range (Schmidt and others, 1964). The formation consists of interbedded argillaceous sandstone and slate. Pillow lavas and basalt flows are interlayered with the sedimentary rocks in the western part of the Neptune Range. Coarse-grained sandstone and intraformational conglomerate occur locally in discontinuous beds and lenses. The sedimentary rocks are typically grayish green, are well bedded and well indurated, and in many places consist of rhythmically layered sandstone and slate exhibiting graded bedding, load casts, current bedding, and channel fillings. The fine-grained constituents of the slate and the sandstone matrix consist predominantly of microscopic sericite, chlorite, and quartz; this composition suggests that the rocks were partially recrystallized in the chlorite zone of regional metamorphism.

The thickness of the Patuxent Formation in the Patuxent Range is estimated, on the basis of several thousand feet of structural relief and widespread areal distribution, to be several tens of thousands of feet. There is no reason to believe that the Patuxent Formation is any thinner in the Neptune Range. The full thickness of the formation is not shown in the stratigraphic column (fig. 3) because the thickness of the lower part of the formation is so poorly known, and because it is more important to show the upper part of the column with reasonable detail. Stratigraphic subdivision of the Patuxent in either range is difficult because distinctive marker beds have not been found. About 40 percent of the rock exposed in the Neptune

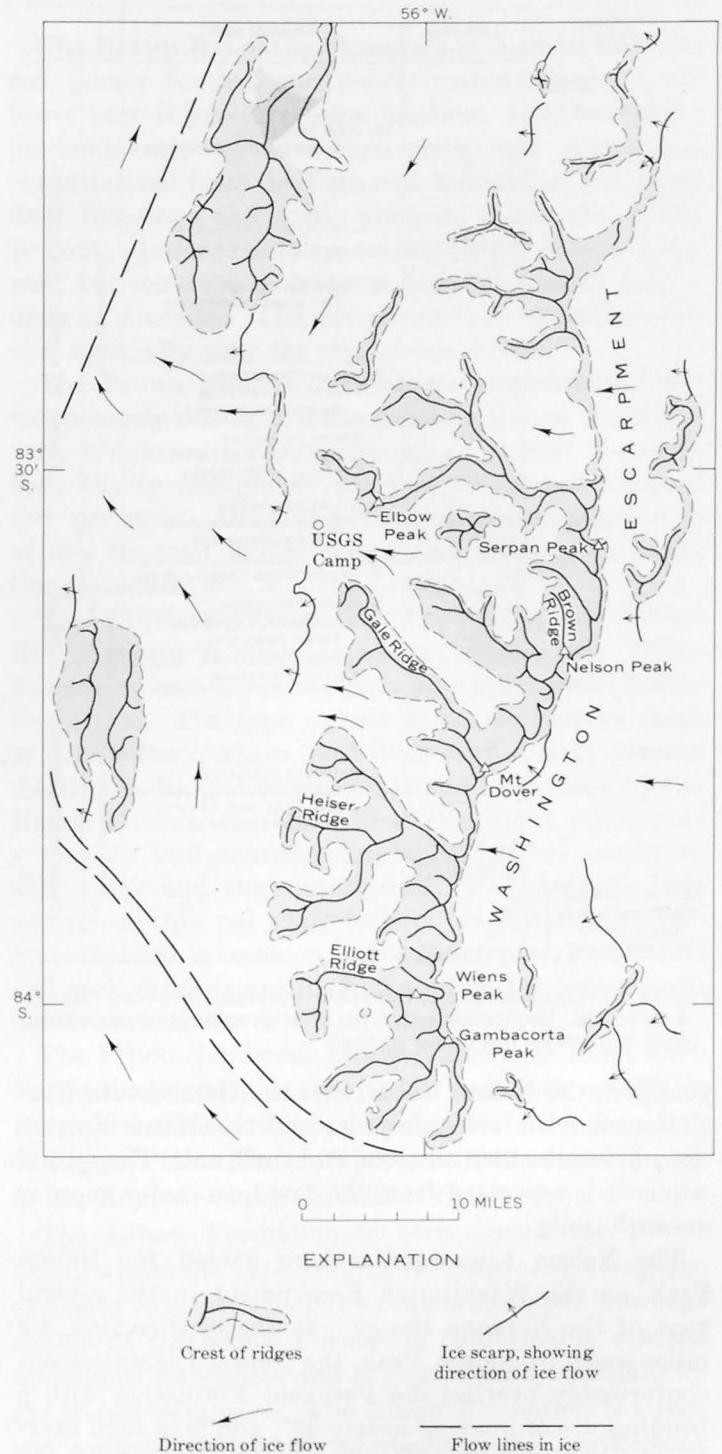


FIGURE 2.—Locality map of the Neptune Range, Antarctica. Mountain masses shown as shaded areas.

Range consists of the Patuxent Formation. The Patuxent is probably of late Precambrian age, and is unconformably overlain by limestone of Early Cambrian age.

## Second sequence

The second sequence consists of three newly named conformable formations which are, from oldest to



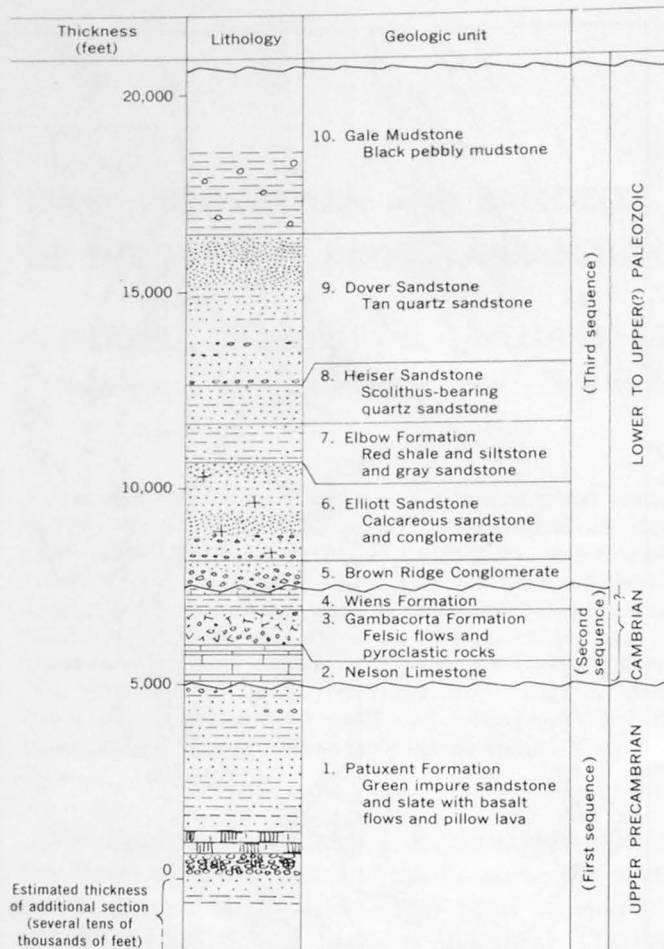


FIGURE 3.—Composite stratigraphic column, Neptune Range, Antarctica. Sequences refer to stratigraphic and structural rock sequences discussed in text.

youngest, the Nelson Limestone; the Gambacorta Formation, a felsic volcanic unit; and the Wiens Formation, an interbedded siltstone and shale unit. The second sequence is separated from the first by a major angular unconformity.

The Nelson Limestone is here named for Nelson Peak, on the Washington Escarpment in the central part of the Neptune Range. In the type section, 1.5 miles south of Nelson Peak, the Nelson Limestone unconformably overlies the Patuxent Formation with a bedding discordance of nearly 90°, and is in turn overlain by a felsic sill. The contact of the conformably overlying Gambacorta Formation is exposed on the northwest slope of Wiens Peak.

The Nelson Limestone consists of 5 members: (1) a basal red quartz-fragment conglomerate, 1 to 20 feet thick, which is composed largely of erosional detritus of the Patuxent Formation; (2) a local red-bed clastic succession which is as much as 60 feet thick; (3) a lower gray limestone, 200 to 300 feet thick, which consists of thin-bedded limestone containing interbedded

lamellae of limy shale; (4) a middle gray limestone, 200 to 300 feet thick, which consists of thick-bedded massive limestone; and (5) an upper gray limestone, about 100 to 150 feet thick, which consists of thin-bedded limestone and shaly limestone. The thin-bedded limestones, members 3 and 5, are commonly oolitic, pisolitic, and nodular. Member 4 is commonly bleached white by alteration that probably was associated with intrusion of hypabyssal rhyolite.

The Nelson Limestone is 600 to 800 feet thick, both in the type area and elsewhere in the Neptune Range. The formation makes up about 5 percent of the exposed rock in the Neptune Range.

The age of the Nelson Limestone is Middle Cambrian and possibly, in part, Early Cambrian. Three different faunal assemblages of trilobites and brachiopods from member 3 are of Middle Cambrian age, and one specimen from locally derived talus contains an archaeocyathid of probable Early Cambrian age (A. R. Palmer, written communication, Aug. 7, 1964). The Nelson Limestone is similar to an undated carbonate-rock unit in the Patuxent Mountains (Schmidt and others, 1964).

The Gambacorta Formation is here named for Gambacorta Peak, a rugged mountainous mass consisting of a complex pile of volcanic and hypabyssal rocks. A complete section of the Gambacorta has not been measured. The base and lower part are best exposed on the northwest slope of Wiens Peak, where intensely altered sandstones and conglomerates of volcanic detritus, about 300 feet thick, conformably overlie member 5 of the Nelson Limestone. The upper contact and upper part of the Gambacorta are typically exposed on the southeasternmost part of Elliott Ridge, where rhyolite flows about 200 feet thick are conformably overlain by the Wiens Formation. The Gambacorta Formation consists of interlayered dark-brown, red-brown, and light-green rhyolitic flows, volcanic breccias, pyroclastic deposits, and detrital sandstones and conglomerates; the detrital rocks are composed mostly of volcanic clasts. These units are variously and complexly interlayered and thicken toward the southeastern part of the Neptune Range. Most of the rocks have been intensely altered.

The Gambacorta Formation thins northward and northwestward, from a maximum thickness of more than 1,000 feet in the vicinity of Gambacorta Peak, and completely disappears within 10 to 15 miles. The volcanic rocks are not found in the northern and western parts of the range. About 5 percent of the exposed rock of the Neptune Range is underlain by the Gambacorta Formation. Fossils have not been found within the formation.

The Wiens Formation is here named for Wiens Peak, where the formation is well exposed along a ridge west of the summit. The type section is located on the southeasternmost part of Elliott Ridge, where the Wiens Formation conformably overlies the Gambacorta Formation and is disconformably overlain by the Elliott Sandstone. Elsewhere, the lower part of the Wiens intertongues with volcanic sedimentary rocks of the upper part of the Gambacorta Formation. The disconformity above the Wiens at the type section is only local; elsewhere, there is strong unconformity. The Wiens consists of interlayered green and red-brown thin-bedded shale, siltstone, and fine sandstone. Several thin-bedded gray oolitic limestone members occur in the section.

The Wiens Formation is less than 1,000 feet thick in the southern Neptune Range and does not occur in the northern part of the range. The formation makes up about 1 percent of the exposed rock of the range. Nondiagnostic fucoidal impressions are locally abundant on bedding planes of green shale and are the only evidence in it of former life.

### Third sequence

The third sequence consists of six newly named conformable formations which are, from oldest to youngest, the Brown Ridge Conglomerate, a massive basal conglomerate; the Elliott Sandstone, a calcareous sandstone and conglomerate; the Elbow Formation, a red-bed siltstone and shale; the Heiser and Dover Sandstones, quartzose sandstones; and the Gale Mudstone, a massive pebbly mudstone. The Gale Mudstone is the youngest sedimentary rock unit exposed in the Neptune Range. An angular unconformity separates the third and second sequences. Parts of the third sequence occur throughout the Neptune Range. The third sequence is younger than the Cambrian Nelson Limestone of the second sequence, but from regional considerations it is probably not younger than late Paleozoic. Fossils that can be dated have not been found in any of the formations of the third sequence.

The Brown Ridge Conglomerate is here named for Brown Ridge, where it is well exposed. The type section is along a ridge 2 miles southwest of the western end of Brown Ridge, where the conglomerate unconformably overlies a felsic sill and the Nelson Limestone. Elsewhere, the Brown Ridge most commonly unconformably overlies the Nelson Limestone or the Patuxent Formation. In the few exposures where it overlies the Gambacorta and Wiens Formations, the contact relation has been obscured by bedding-plane slippage. The Brown Ridge is overlain by the Elliott Sandstone throughout the Neptune Range.

The Brown Ridge Conglomerate is characteristically red, poorly bedded, and poorly sorted; however, the lower part is green at some localities. Cobbles consist predominantly of sandstone, slate, and vein-quartz clasts derived from the Patuxent Formation, but abundant limestone and felsic volcanic clasts are locally present. Larger clasts are commonly 3 inches in diameter, but some are as large as boulders several feet or more in diameter. The matrix contains abundant calcite, especially near the top of the section.

The Brown Ridge Conglomerate is distributed discontinuously throughout the Neptune Range. Its thickness, which reaches a maximum of several thousand feet, locally changes at the rate of several hundred feet per mile. About 2 percent of the exposed rock of the Neptune Range consists of the Brown Ridge Conglomerate.

The Elliott Sandstone is here named for Elliott Ridge, where it disconformably overlies the Wiens Formation and is conformably overlain by the Elbow Formation. The type section is on the eastern slope of Elbow Peak, where the Elliott conformably overlies the Brown Ridge Conglomerate and is overlain by the Elbow Formation. The Elliott Sandstone consists of a pink to buff coarse-grained crossbedded sandstone with thick and thin interbedded conglomeratic beds and minor thin red shaly beds in the lower half. Volcanic detritus is common in the lower part, and quartz and rock detritus are predominant in the upper part. Calcareous cement is characteristic.

The Elliott Sandstone probably averages about 2,500 feet in thickness; it is about 5,000 feet thick on Elliott Ridge and thins away completely about 10 miles north of Elbow Peak. About 20 percent of the exposed rock in the Neptune Range is Elliott Sandstone.

The Elbow Formation is here named for Elbow Peak, where the type section is designated along the east-west ridge on which the peak is situated. The type section of the Elbow Formation conformably overlies the Elliott Sandstone and is gradationally overlain by the Heiser Sandstone. The Elbow Formation is a red-bed unit consisting of interbedded red argillaceous siltstone and gray fine-grained quartzose sandstone in well-indurated layers 1 to 4 feet thick; the layers are made up of lamellae 1/16 to 1/4 inch thick. In overall color, about half the formation is red and half is light gray. The coarser grained layers are commonly mottled gray or gray with red specks. Crossbedding is abundant, and ripple-marked bedding planes are common. In some beds, mottled patterns perpendicular to the bedding disrupt bedding lamellae and are suggestive of animal burrowings.

The facies or character of the red beds changes laterally away from the type section, and the definition of the upper and lower contacts of the Elbow Formation in the southern Neptune Range has not been resolved.

The Elbow Formation is about 1,000 feet thick at the type section and thins toward the south and west; the thinning probably corresponds in part to a thickening of the Elliott Sandstone toward the south and west. The Elbow makes up about 2 percent of the exposed rock in the Neptune Range.

The Heiser Sandstone is here named for Heiser Ridge, where its type section, on the western end of the ridge, gradationally overlies the Elbow Formation and is conformably overlain by the Dover Sandstone. The Heiser consists of a light-green to brown quartzose sandstone which is moderately well bedded in beds 1 to 3 feet thick. The sandstone is characterized by the common occurrence of scolithus-like tubes of lighter colored quartzite set in a darker, less well indurated, encompassing sandstone. The tubes range from  $\frac{1}{4}$  to (rarely) 1 inch in diameter, are characteristically perpendicular to the bedding planes, and commonly extend through the thickness of only one bed. At several outcrops tubes about 1 inch in diameter occur randomly oriented on bedding planes. The scolithus-like tubes are indicative of ancient life.

The Heiser Sandstone is about 1,000 feet thick and underlies about 1 percent of the outcrop area in the Neptune Range.

The Dover Sandstone is here named for Mount Dover, on the eastern end of Gale Ridge. The type section is on the western end of Gale Ridge, where the Dover conformably overlies the Heiser Sandstone and is conformably overlain by the Gale Mudstone. The Dover Sandstone is a tan to white thick-bedded to massive medium- to coarse-grained sandstone. Individual beds are commonly coarsely crossbedded and are several feet to many tens of feet thick; where massive the sandstone is commonly friable, although many other beds consist of well-indurated quartzite. Scattered rounded pebbles of quartz occur in a few indistinct lenses of sandstone in the lower third of the section. Conglomerate beds are even less common. The basal part of the Dover consists of 3 distinctive zones: (1) a basal white conglomerate as much as 20 feet thick, containing 1 to 10 percent black pebbles and cobbles; (2) an overlying black-stained sandstone as much as 10 feet thick; and (3) an upper brown iron-stained sandstone, several feet to several hundred feet thick. The third zone is overlain by tan sandstone. Zones 1 and 2 are locally absent.

The type section of the Dover Sandstone is about 4,000 feet thick. The unit constitutes about 5 percent of the exposed rock in the Neptune Range.

The Gale Mudstone, the youngest bedrock formation in the Neptune Range, is here named for Gale Ridge. In its type section, on the westernmost end of the ridge, the formation conformably overlies the Dover Sandstone. The Gale Mudstone consists of a black homogeneous well-indurated mudstone containing scattered pebbles, cobbles, and boulders of granite, granitic gneiss, and the underlying sedimentary rocks. The clasts, which are scattered, constitute less than 1 percent of the whole rock. They are angular to subrounded; the larger ones average about 3 inches in diameter, and the largest are about 2 feet in diameter. Bedding or other sedimentary structures have not been found within the formation.

The Gale Mudstone is at least 1,000 feet thick and is probably thicker than 2,000 feet. It is well exposed in the west-central and northeastern parts of the Neptune Range. It extends in outcrops for 30 miles along the range and for about 30 miles across the range. Fragments of pebbly mudstone in recent moraine are thought to indicate that the areal extent of the formation is at least several times as large. The Gale probably constitutes about 1 percent of the exposed rock of the Neptune Range.

### IGNEOUS ROCKS

Six units of igneous rocks are mapped in the Neptune Range. Of these, two are stratigraphic units and have been briefly discussed. The four other units form hypabyssal sills and plugs and a large plutonic mass. The six units are listed below in their inferred chronologic order, beginning with the oldest:

1. Pillow lavas and basalt flows aggregating at least several thousand feet in thickness are interlayered with sandstone and slate of the Patuxent Formation in the western part of the Neptune Range. The age of the lavas and flows is the same as that of the enclosing Patuxent strata—probably late Precambrian.

2. Diabase intruded into the Patuxent Formation in the western part of the Neptune Range forms sills 5 feet to 1,000 feet thick which constitute as much as 30 percent of the exposed rock in some areas. The age of the diabase is uncertain, but the sills seem to have been folded at the time of the initial deformation of the Patuxent rocks and are tentatively considered to be of late Precambrian age.

3. Felsic rock in a sill, about 300 feet thick, and a plug, about 100 feet in diameter, was intruded into the Patuxent Formation in the western part of the Neptune Range. The felsic rock is younger than

the enclosing Patuxent rocks; and, because the rock is intensely deformed parallel to regional trends, it is at least older than the time of the folding of the second sequence.

4. Rhyolitic flows, volcanic breccias, and pyroclastic deposits of the Gambacorta Formation conformably overlie the Nelson Limestone of Cambrian age and are in turn truncated by the overlying unconformity in the Neptune Range.

5. Hypabyssal rhyolitic porphyry, in sills as much as a thousand feet thick and in irregular-shaped bodies as much as 5 miles across, intruded rocks as young as the Wiens Formation in the Neptune Range. The porphyry is younger than the Wiens Formation and older than the Brown Ridge Conglomerate which contains cobbles of the porphyry.

6. Coarse-grained biotite granite crops out on Serpan Peak on the Washington Escarpment. The distribution of granitic debris in Recent morainal deposits indicates that a large pluton underlies much of the snow- and ice-covered eastern part of the range. The granite was intruded into the Patuxent Formation, but in a zone several hundred feet wide the Patuxent rocks as well as the contact granite are intensely sheared along nearly vertical planes. The pluton therefore may have been uplifted to its present position along border faults. The granite is probably older than the Elliott Sandstone. A Rb-Sr whole-rock age of  $510 \pm 30$  million years (Z. E. Peterman, U.S. Geol. Survey, written communication, Nov. 27, 1964) for the granite indicates emplacement during the early Paleozoic, probably during Late Cambrian or Early Ordovician time. The nearest similar rock, the biotite granite of the Thiel Mountains, has been dated isotopically at about 500 m.y. (Aaron and Ford, 1964). The granite of the Neptune Range has been slightly metamorphosed since its emplacement, however, and its biotite has been largely altered to green biotite(?) which gives a K-Ar age of  $265 \pm 13$  m.y. (R. F. Marvin, U.S. Geol. Survey, written communication, Nov. 27, 1964).

## STRUCTURE

The 10 stratigraphic rock formations and 4 additional intrusive rock units of the Neptune Range are divided into 3 structural units bounded by the same angular unconformities that bound the 3 stratigraphic rock sequences. The oldest, the late Precambrian structural unit, is the most deformed. Each successively younger unit is less deformed (fig. 4).

### First structural unit

The first and oldest structural unit consists of the Patuxent Formation and the diabase occurring in the

Patuxent (igneous rock unit 2). Possibly the felsic rock (igneous rock unit 3) is also part of this oldest structural unit. The rocks of the unit are mostly isoclinally folded. In the eastern and central parts of the range a regional axial-plane cleavage commonly parallels bedding that is nearly vertical and strikes northerly. The isoclinally folded bedding and nearly vertical axial-plane cleavage are diagrammatically shown on figure 4. Fold axes plunge northerly or southerly; the average plunge is gentle to the south. In the western part of the range, folding is intense but commonly is not isoclinal; folds tend to be symmetrical, with steeply dipping limbs. Disharmonic folding is common where competent sandstone beds have resisted folding and interbedded slaty beds have yielded more easily to the folding.

### Second structural unit

The second structural unit consists of the Nelson Limestone of Cambrian age, the Gambacorta Formation, and the Wiens Formation, as well as the hypabyssal rhyolitic porphyry igneous rock (igneous rock unit 5) and the biotite granite (igneous rock unit 6). The sedimentary rocks of the second unit have been deformed into open sinuous folds. The larger folds tend to be symmetrical and to have a wavelength of about 3 miles. Some smaller subsidiary folds, however, are disharmonic, strongly asymmetrical, and locally overturned toward the west. Fold axes commonly trend northerly and plunge gently to the south, much as do those in the first structural unit. Axial-plane cleavage is not common, although slaty cleavage is developed in argillaceous beds in places of strongest deformation. Bedding-plane slippage during folding seems to have been the commonest way by which the rock responded to internal stresses.

### Third structural unit

The third and youngest structural unit in the Neptune Range consists of the third stratigraphic sequence. The rocks of the third unit have been gently deformed into broad folds trending northerly in the central part of the range. On the plateau of the eastern Neptune Range the rocks of the third unit dip gently toward the east, and in the northeastern part they are horizontal. In contrast, along a major structural discontinuity west of the central part of the range, the beds of the third unit are about vertical or are slightly overturned to the west. This structural discontinuity is probably a major fault zone, the nature of which is not satisfactorily known.

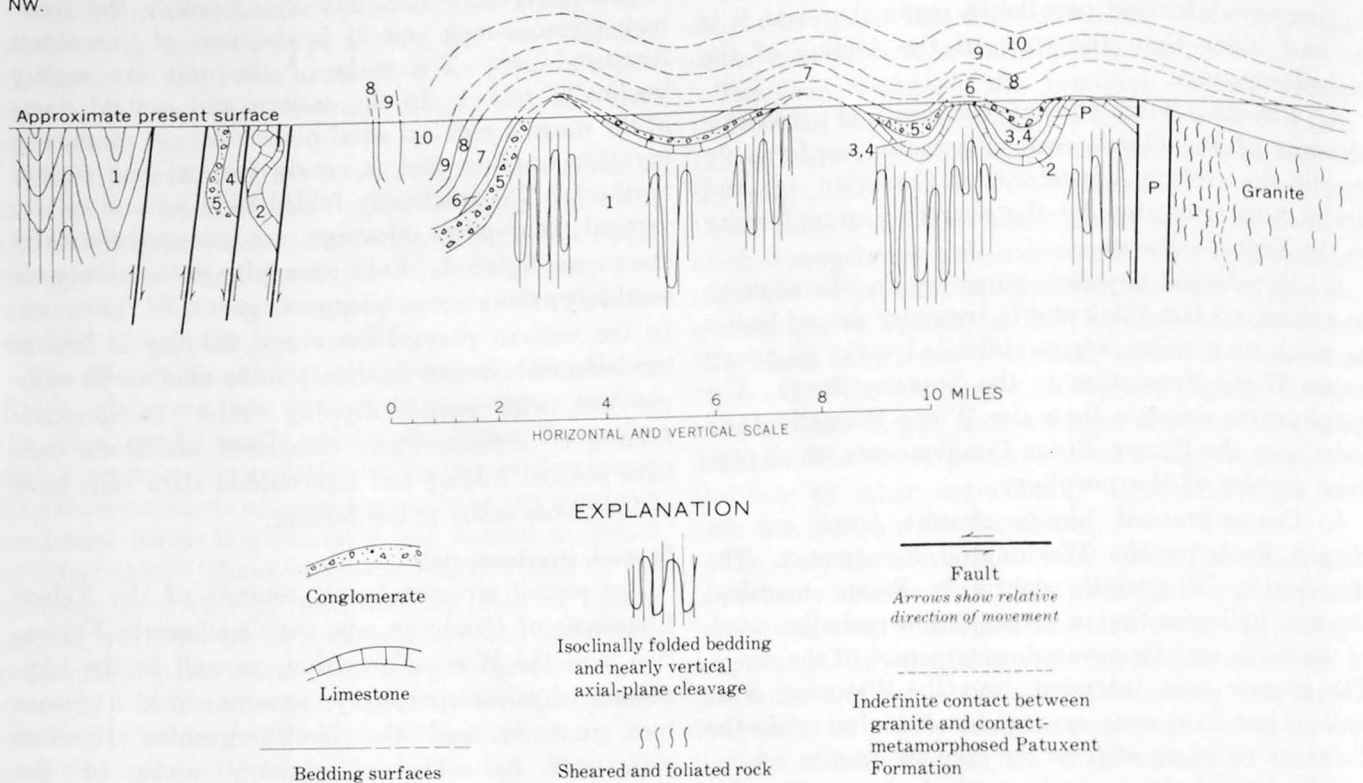


FIGURE 4.—Diagrammatic geologic section extending northwesterly across the Neptune Range, Antarctica. Numbers refer to rock units shown on figure 3; unit P is hypabyssal rhyolitic porphyry.

### GEOLOGIC HISTORY

The Pensacola Mountains area was part of a geosynclinal basin into which large quantities of terrigenous sediments were deposited during late Precambrian time. Interbedded pillow lavas and basalt flows indicate that volcanism occurred at times during the deposition. The injection of large amounts of diabase and minor amounts of felsic rock into the Patuxent strata as sills may have been closely associated with the outpourings of the basalt, or it may have occurred later and been associated with the first orogenic folding of the Patuxent rocks.

During the first and oldest orogeny recorded in the Neptune Range the Patuxent eugeosynclinal rocks were intensely deformed and uplifted. Extensive erosion of the deformed Patuxent rocks ended with marine transgression and the deposition of the Nelson Limestone during Cambrian time. Subsequent felsic volcanism, centered in the southern Neptune Range, is represented by the Gambacorta Formation. Deposition of siltstones and shales of the Wiens Formation ended the sedimentation of the second sequence.

The second orogeny caused moderately intensive folding of the rocks of the second structural unit. Rhyolitic porphyry and granite were intruded probably during the most active phase of the orogeny.

Volcanism represented by the Gambacorta Formation may have been an early expression of the onset of the second orogeny. The Rb-Sr whole-rock age of  $510 \pm 30$  m.y. for the granite near Serpan Peak probably dates a later part of the second orogeny.

The Brown Ridge Conglomerate, an orogenic deposit consisting of debris eroded from the uplifted fold mountains, initiated sedimentation of the third sequence. Detrital blocks of limestone several tens of feet across that occur in the conglomerate were deposited on a surface of rugged relief cut into the Nelson Limestone. The detrital sands and gravels comprising the lower part of the Elliott Sandstone suggest derivation from nearby mountains of moderate relief—possibly the same, but more subdued, mountains from which the Brown Ridge Conglomerate was derived. The red-bed siltstones and shales of the Elbow and the overlying quartz sandstones of the Heiser and Dover indicate the deposition of coarser, cleaner, better sorted, and more resistant detritus in a sedimentary environment of progressively higher energy. The sediment was probably derived from sources outside the Pensacola Mountains area. The apparently abrupt change to deposition of the dirty unsorted pebbly mudstone of the Gale Mudstone suggests a drastic environmental change. The origin

of the mudstone is uncertain. It has characteristics that elsewhere have been variously interpreted as those of a marine slump, a huge mudflow deposit, or a glaciomarine tillite.

During the third orogeny the rocks of the third structural unit were deformed by different amounts in different places. In the eastern part of the Neptune Range, folding was slight, but in the central part it was gentle to moderate. West of the central part of the range the entire sedimentary section was folded to nearly vertical or slightly overturned attitudes in part, perhaps, associated with faulting. It is possible that the K-Ar age of  $265 \pm 13$  m.y. for the altered biotite from the granite near Serpan Peak dates some part of the third orogeny.

The age and history of the rocks of the third structural unit are put in better perspective if additional information from the adjacent Patuxent Range is considered. A fourth stratigraphic sequence, which consists of well-bedded light-tan quartzose sandstone, siltstone, and shale, occurs in the Patuxent Range (Schmidt and others, 1964). This sequence contains interbedded carbonaceous beds with a Glossopterid flora, dated as Permian (Schopf, 1964). The sediments are correlative with part of the Beacon Sandstone of the Transantarctic Mountains in the Ross Sea area (Gunn and Warren, 1962). Igneous activity is recorded by diabase-forming sills in the Glossopterid-bearing sedimentary rocks. The diabase may be correlative with the Ferrar Dolerite of probable Jurassic age in the Ross Sea sector of the Transantarctic Mountains (McDougall, 1963, p. 1539).

This fourth sequence is inferred to make a fourth structural unit of flat-lying rocks that at one time covered the rocks which are now exposed in the Neptune Range, as well as those of the Patuxent

Range. This would indicate that the age of the rocks of the third structural unit in the Neptune Range is older than Permian and is in accord with the suggested isotopic age of late Carboniferous for the third orogeny.

Structures younger than those of the third orogeny have not been mapped, but epeirogenic crustal warping and faulting can be inferred. A large frontal fault with a displacement of several thousand feet probably separates the Pensacola Mountains from the rocks beneath the Filchner Ice Shelf. Relatively recent movement along this and related faults may account in part for the present altitude of the Pensacola Mountains.

#### REFERENCES

- Aaron, J. M., and Ford, A. B., 1964, Isotope age determinations in the Thiel Mountains, Antarctica [abs.]: Geol. Soc. America Spec. Paper 76, p. 1.
- Aughenbaugh, N. B., 1961, Preliminary report on the geology of the Dufek Massif: Am. Geogr. Soc., IGY Glaciological Rept., no. 4, p. 155-193.
- Gunn, B. M., and Warren, Guyon, 1962, Geology of Victoria Land between the Mawson and Mulock Glaciers, Antarctica: New Zealand Geol. Survey Bull. 71, 157 p.
- McDougall, Ian, 1963, Potassium-argon age measurements on dolerites from Antarctica and South Africa: Jour. Geophys. Research, v. 68, no. 5, p. 1535-1545.
- Schmidt, D. L., 1964, Geology of the Pensacola Mountains, U.S. Antarctic Research Program 64: U.S. Antarctic Projects Officer Bull., v. 5, no. 10, p. 98-101.
- Schmidt, D. L., Dover, J. H., Ford, A. B., and Brown, R. D., 1964, Geology of the Patuxent Mountains, in R. J. Adie, ed., Antarctic Geology: New York, John Wiley and Sons, p. 276-283.
- Schmidt, D. L., and Ford, A. B., 1963, U.S. Geological Survey in the Patuxent Mountains, Antarctica: U.S. Antarctic Projects Officer Bull., v. 4, no. 8, p. 20-24.
- Schopf, J. M., 1964, Paleobotanical studies in Antarctica [abs.]: Geol. Soc. America Spec. Paper 76, p. 317.



## OCCURRENCE AND STRATIGRAPHIC SIGNIFICANCE OF *OLDHAMIA*, A CAMBRIAN TRACE FOSSIL, IN EAST-CENTRAL ALASKA

By MICHAEL CHURKIN, JR., and EARL E. BRABB,  
Menlo Park, Calif.

**Abstract.**—Abundant specimens of *Oldhamia*, a fan-shaped trace fossil of probable Cambrian age, were found in the Charley River quadrangle, near the Alaska-Canada boundary. Although no other fossils have been found associated with *Oldhamia* there, the rocks in which it occurs can be correlated with an archaeocyathid-bearing unit of Early Cambrian age nearby. Assignment of this Alaskan *Oldhamia* to the Lower Cambrian is consistent with the Cambrian or possibly latest Precambrian age of *Oldhamia* in Europe and eastern North America. Occurrences of *Oldhamia* in the Mount Schwatka area and in the Crazy Mountains, about 180 and 100 miles, respectively, west of the Charley River quadrangle, suggest that rocks of Cambrian age, much older than previously reported, are probably present in the central interior of Alaska.

During mapping of the Charley River quadrangle (1:250,000) in east-central Alaska (Brabb and Churkin, 1964), abundant specimens of *Oldhamia*, a fan-shaped trace fossil<sup>1</sup> of probable Cambrian age, were found in rocks originally thought to be the Nation River Formation of Late Devonian age. Additional mapping and laboratory work indicated that the rocks containing *Oldhamia* are different from those of the Nation River Formation but are very similar both lithologically and in stratigraphic position to those bearing Lower Cambrian archaeocyathids in another part of the quadrangle. If this correlation is correct the areal extent inferred for Cambrian rocks in east-central Alaska is about doubled. Moreover, the earlier discovery by Mertie (1937) of a similar *Oldhamia* in the Mt. Schwatka area (locality 3, fig. 1), about 175 miles west of the mouth of the Nation River, suggests that the rocks there are much older than reported and that rocks of Cambrian age are probably present in the central interior of Alaska (fig. 1).

<sup>1</sup> A trace fossil is a sedimentary structure resulting from the activity of an animal moving on or in the sediment at the time of accumulation of the sediment. Trace fossils include tracks, burrows, feeding marks, and other traces (Simpson, 1957).

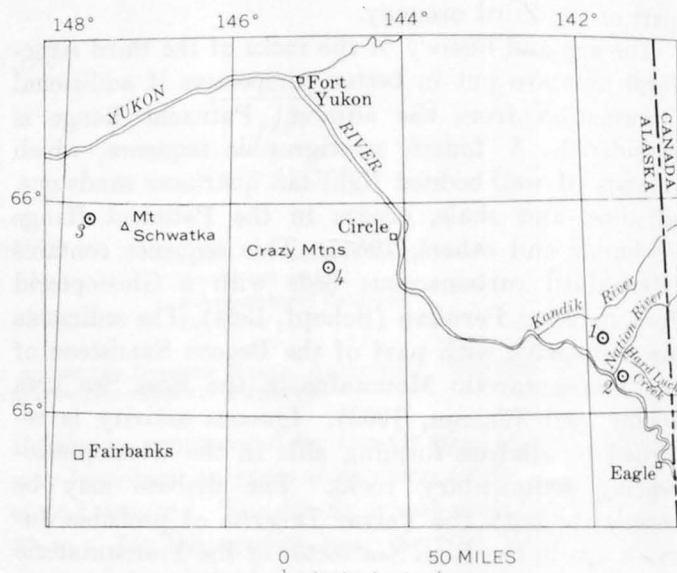


FIGURE 1.—Index map of central and east-central Alaska, showing numbered *Oldhamia* localities.

### OLDHAMIA FROM THE CHARLEY RIVER QUADRANGLE

The specimens of *Oldhamia* from the Charley River quadrangle were first identified by Preston E. Cloud, Jr., of the University of Minnesota (written communication, 1963). They consist of gently curved ridges and furrows  $\frac{1}{2}$  to 1 mm in width that radiate from centers to form fan-shaped impressions as much as 3 cm in diameter on bedding planes in quartzite and siltstone (fig. 2). Many of the specimens seem to cross each other, but this overlap is probably the result of imprints from one layer being preserved in the succeeding layer, as Ruedemann (1942a) pointed out in relating *Oldhamia* to worm trails. Each fan-shaped

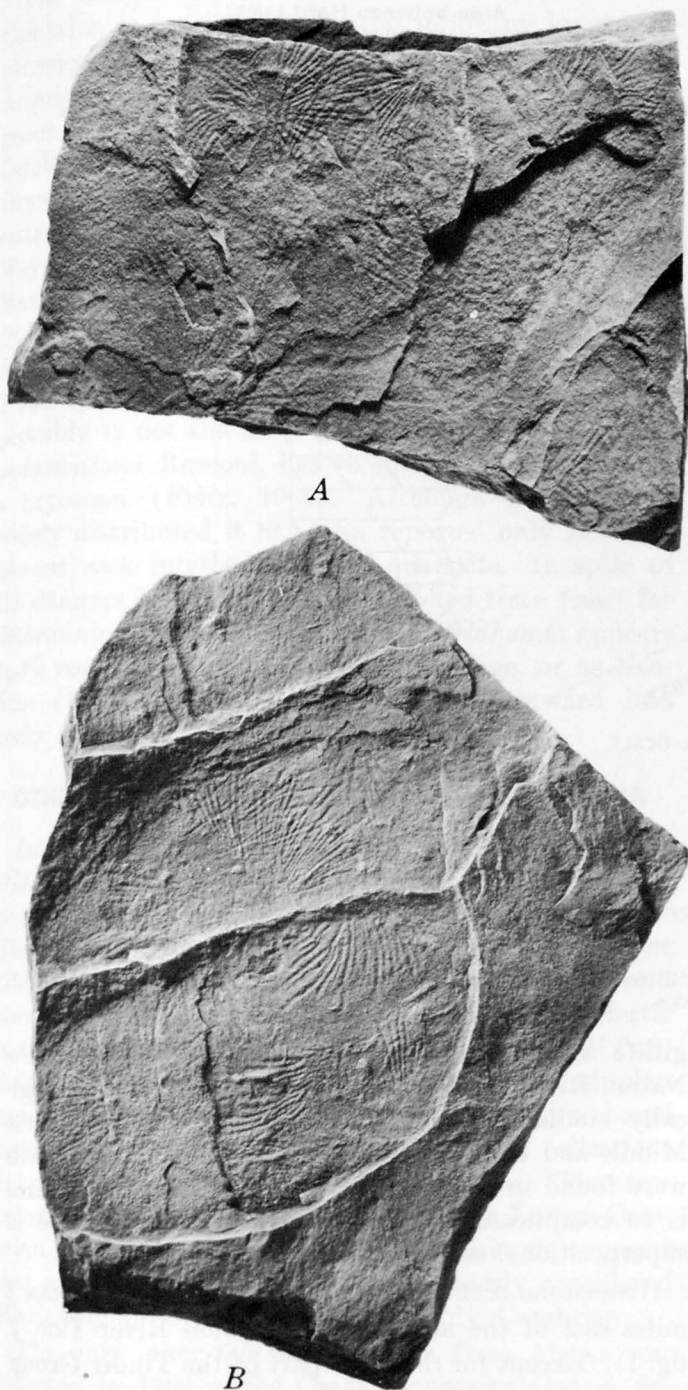


FIGURE 2.—*Oldhamia* from the area between the Kandik and Nation Rivers (loc. 1, fig. 1), Charley River quadrangle, east-central Alaska. A, USNM specimen 146373; natural size. B, USNM specimen 146374; natural size.

cluster of ridges in the Alaskan species seems to be disconnected from adjacent clusters, as it is in *Oldhamia radiata* Forbes (Ruedemann, 1942a, fig. 3, photographs 2 and 3) from Ireland and *Oldhamia smithi* Ruedemann (Neuman, 1962, fig. 2) from Maine. The arrangement of the fan-shaped clusters in an interconnected zigzag pattern, as in *Oldhamia antiqua*

Forbes (Ruedemann, 1942a, fig. 3, photograph 1) from Ireland or *Oldhamia occidentis* (Walcott) (Ruedemann, 1942a, fig. 3, photograph 4) from New York, was not found in the Alaskan material, but the close spacing and apparent overlap of specimens from successive sedimentary laminae has partly obscured their original pattern. The ridges and furrows of the *Oldhamia* from the Charley River quadrangle are more curved than those of *O. radiata* but seem identical to those of *O. smithi* and of the *Oldhamia* illustrated by Mertie (1937, pl. 9A) from Alaska.

All the specimens of *Oldhamia* found in the Charley River quadrangle are from two small areas of outcrop (locs. 1 and 2, fig. 1) of a distinctive formation of thinly interbedded and cross-laminated quartzite, quartzose siltstone, and silty argillite. The quartzitic layers are pale olive, and the fine-grained, more argillaceous interbeds are light olive gray. The distinct and very thin and laminated bedding, together with well-developed scour-and-fill structures and various small sole marks of undetermined origin, characterize this formation. White mica is usually abundant on the bedding planes, and in thin section abundant chloritic material, sericite, and strained quartz sand grains with well-developed quartz overgrowths collectively serve to distinguish the *Oldhamia*-bearing rocks from other formations in the Charley River quadrangle. In particular, the presence of white mica and abundant laminae and cross-laminae in the *Oldhamia*-bearing rocks, and the absence from these rocks of thick beds of chert-rich sandstone and chert-pebble conglomerate and of ubiquitous plant fragments, distinguish the *Oldhamia*-bearing rocks from those of the Nation River Formation.

#### CORRELATION AND AGE OF THE OLDHAMIA-BEARING ROCKS

Although no other fossils have been found at the two *Oldhamia* localities, the distinctive unit of argillite and quartzite in which *Oldhamia* occurs can be correlated (fig. 3) with a similar unit of Lower Cambrian argillite in a fossiliferous sequence exposed between Hard Luck Creek and the Yukon River, 10 to 25 miles east of the mouth of the Nation River. The unnamed argillite and quartzite unit in the fossiliferous sequence (Brabb and Churkin, 1964) contains archaeocyathids of Early Cambrian age, according to A. R. Palmer, of the U.S. Geological Survey (written communication, 1965), and is overlain by a limestone unit that contains, according to Palmer, trilobites of uppermost Cambrian age in its upper part and of Middle or possibly Lower Cambrian age in its lower



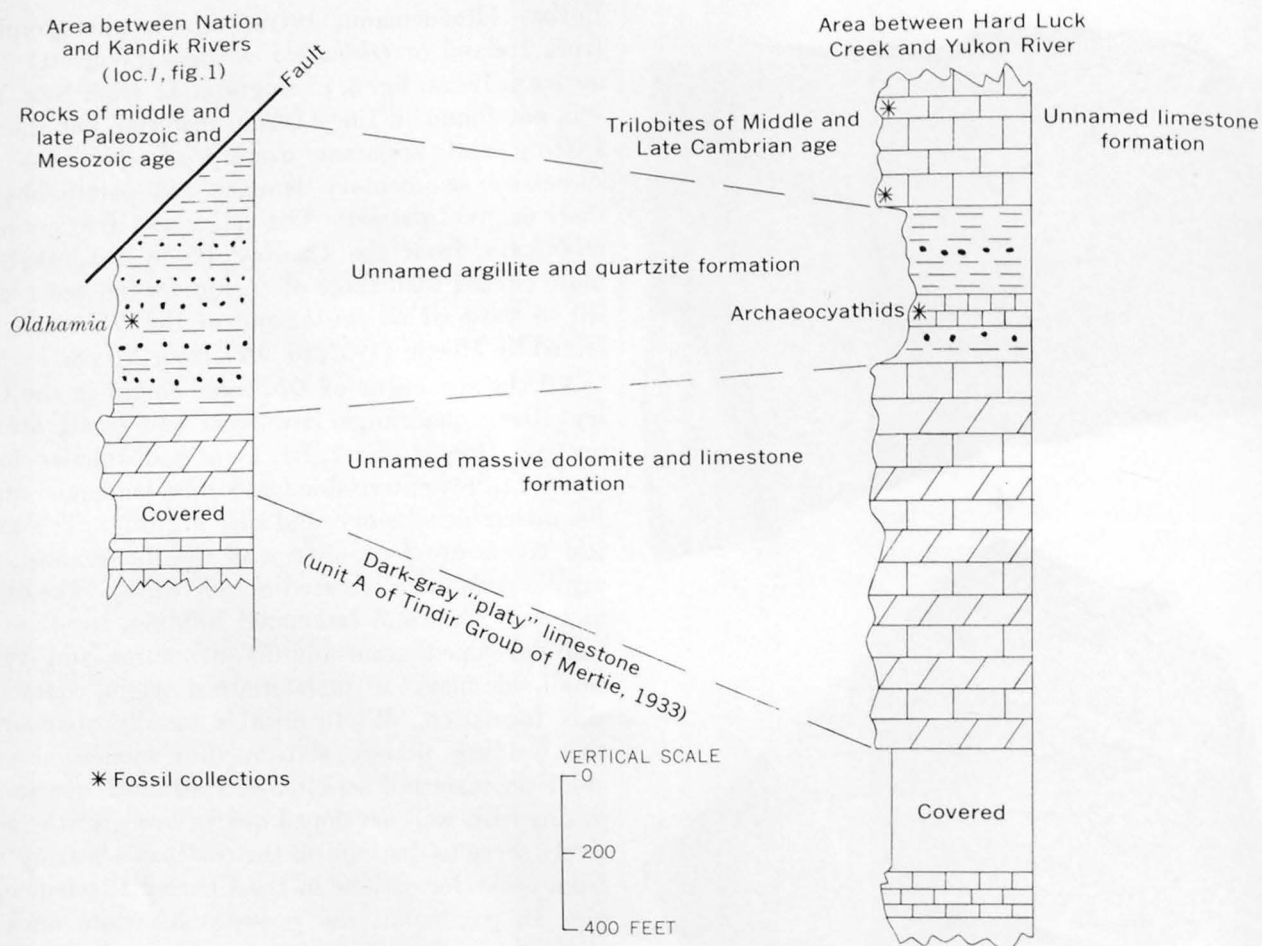


FIGURE 3.—Geologic sections showing the correlation of argillite and quartzite sequences in two areas of east-central Alaska.

part. It is underlain by an unnamed massive dolomite unit which in turn is underlain by dark-gray laminated and platy limestone characteristic of Mertie's (1933, p. 370-372) unit A of the Tindir Group of late Precambrian and Early Cambrian(?) age. This platy limestone is underlain by a succession of rocks characteristic of the older units of the Tindir Group. In the area between the Kandik and Nation Rivers (loc. 1, fig. 1), the *Oldhamia*-bearing argillite unit rests accordantly on a sequence of massive dolomite underlain by dark-gray platy limestone and older rocks of the Tindir Group similar to the sequence that underlies the archaeocyathid-bearing Lower Cambrian argillite in the area between Hard Luck Creek and the Yukon River. The upper part of the *Oldhamia*-bearing unit in the area between the Kandik and Nation Rivers is faulted against middle and upper Paleozoic and Mesozoic rocks, so that no direct correlation can be made with the Middle and Upper Cambrian limestone beds that overlie the Lower Cambrian argillite unit of the fossiliferous sequence. A limestone that seems to be stratigraphically above the *Oldhamia*-bearing ar-

gillite about 3 miles northeast of the mouth of the Nation River (just north of loc. 2, fig. 1) is lithologically similar to, and may be correlative with, the Middle and Upper Cambrian limestone; but no fossils were found in this unit, and the structure in the area is so complicated that the limestone may not be in superpositional sequence.

Greenstone occurs in the *Oldhamia*-bearing rocks 3 miles east of the mouth of the Nation River (loc. 2, fig. 1). Except for the older part of the Tindir Group, the only other greenstone known in the immediate area is in the argillite and quartzite formation exposed directly below fossiliferous Middle and Upper Cambrian limestone near the Alaska-Yukon boundary. This joint occurrence of greenstone in the two areas further supports the correlation of the enclosing argillite and quartzite.

In summary, similar lithology and similar sequence suggest that the *Oldhamia*-bearing rocks are correlative with Brabb and Churkin's (1964) unnamed argillite unit of Early Cambrian age.

The assignment of this *Oldhamia* to the Lower Cambrian is consistent with the following known occurrences of the genus in Europe and eastern North America: Cambrian of Ireland, the type area for the genus (Forbes, 1848-50); Nassau Formation of Early Cambrian age in eastern New York (Walcott, 1894); Grand Pitch Formation of Cambrian(?) age in northeastern Maine (Smith, 1928; Neuman, 1962); and Weymouth Formation of Early Cambrian age in Massachusetts (Howell, 1922). One of two species of *Oldhamia* reported in rocks of Ordovician age (*Oldhamia keithi* Ruedemann, 1942b, fig. 5, photographs 1 and 2) is substantially different in appearance and probably is not the same genus; the other, *Oldhamia pedemontana* Rusconi, has recently been shown to be a bryozoan (Fritz, 1965). Although *Oldhamia* is widely distributed it has been reported only in argillaceous rock interbedded with quartzite. In spite of the dangers of using a facies-restricted trace fossil for determining the age of a formation, *Oldhamia* appears to be restricted to rocks of Cambrian age, or as Neuman (1962) points out, may range downward into rocks as old as latest Precambrian.

#### OTHER OCCURRENCES OF OLDHAMIA IN ALASKA

In Alaska, trace fossils questionably assigned to *Oldhamia* had previously been found by Mertie (1937, p. 121, pl. 9A) near Mount Schwatka (loc. 3, fig. 1). These fossils have all the structural details of the *Oldhamia* found in the Charley River quadrangle, and they belong unquestionably to the same genus. Mertie included his *Oldhamia*-bearing rocks in a belt of "undifferentiated noncalcareous rocks of Mississippian age." The Mississippian age for these rocks was based mainly on a few widely scattered fossil collections from similar rocks in neighboring areas. The new occurrence of *Oldhamia* from probable Lower Cambrian rocks in the Charley River quadrangle suggests that at least some of the rocks previously considered Mississippian by Mertie are probably Cambrian.

The only other *Oldhamia* known from Alaska was collected in 1962 in the Crazy Mountains (loc. 4, fig. 1), 100 miles northwest of the mouth of the Nation River, by geologists of BP Exploration Co. (Alaska), Inc., who kindly loaned us the specimen (fig. 4). This *Oldhamia* is somewhat smaller and has correspondingly finer ridges and furrows than that from the Charley River quadrangle, but otherwise it has the same structure. The fossils were found in mudstone interbedded with quartzite that was originally mapped by Mertie (1937) as "undifferentiated noncalcareous rocks of Devonian age." The Devonian age was evidently based on a lithologic correlation inasmuch as

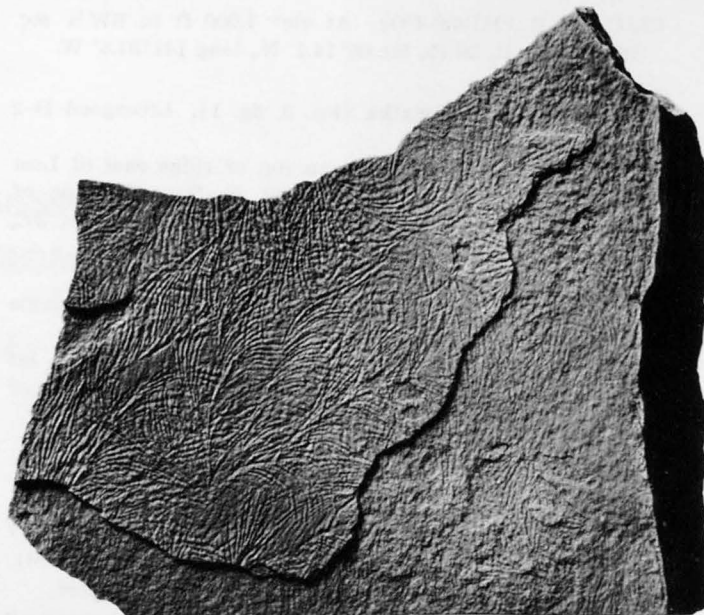


FIGURE 4.—*Oldhamia* from the Crazy Mountains (loc. 4, fig. 1) east-central Alaska. Specimen loaned by BP Exploration Co. (Alaska) Inc. Enlarged  $\times 1.5$ .

Mertie apparently did not find fossils in the area. The discovery of *Oldhamia* from the Crazy Mountains partly bridges the distance between the Mount Schwatka locality on the west and the Nation River area on the east and suggests that some of the rocks there are probably also Cambrian.

The geographic location of all known occurrences of *Oldhamia* is shown in the accompanying list.

#### Geographic location of *Oldhamia* collections in Alaska

Area between the Kandik and Nation Rivers, 10 miles north of the mouth of the Nation River (loc. 1, fig. 1). Charley River B-2 quadrangle (1:63,360):

62ACn 851<sup>1</sup> (M1024-CO).<sup>2</sup> From top of ridge at elev 3,000 ft in NE $\frac{1}{4}$  sec. 21, T. 6 N., R. 29 E., lat 65°20.2' N., long 141°46.0' W.

62ACn 891 (M1025-CO). NE $\frac{1}{4}$ SE $\frac{1}{4}$  sec. 21, T. 6 N., R. 29 E., lat 65°20.0' N., long 141°45.7' W.

62ACn 1081 (M1026-CO and USNM 146374,<sup>3</sup> see fig. 2B).

From top of ridge at elev 2,500 ft in NE $\frac{1}{4}$ NE $\frac{1}{4}$  sec. 30, T. 6 N., R. 29 E., lat 65°19.4' N., long 141°50.1' W.

63ACn 2091 (M1027-CO and USNM 146373, see fig. 2A).

From top of ridge at elev 2,500 ft in NE $\frac{1}{4}$ NE $\frac{1}{4}$  sec. 30, T. 6 N., R. 29 E., lat 65°19.4' N., long 141°50.1' W.

63ACn 2126 (M1028-CO). SW $\frac{1}{4}$ SW $\frac{1}{4}$  sec. 23, T. 6 N., R. 29 E., lat 65°19.7' N., long 141°43.4' W.

Area about 3 miles east of the mouth of the Nation River (loc. 2, fig. 1). Charley River A-2 quadrangle (1:63,360):

63ACn 2212 (M1029-CO). From top of ridge at elev 2,100 ft in NW $\frac{1}{4}$ NW $\frac{1}{4}$  sec. 32, T. 5 N., R. 30 E., lat 65°13.4' N., long 141°37.0' W.

<sup>1</sup> U.S. Geological Survey field locality number.

<sup>2</sup> U.S. Geological Survey fossil collection number.

<sup>3</sup> U.S. National Museum specimen number.

63AGs 344B (M1030-CO). At elev 1,000 ft in SW $\frac{1}{4}$  sec. 19, T. 5 N., R. 30 E., lat 65°14.7' N., long 141°37.6' W.

Vicinity of Mount Schwatka (loc. 3, fig. 1). Livengood D-2 quadrangle (1:63,360):

21AMt 152. At elev 3,000 ft on top of ridge east of Lost Creek. About 15.4 miles N. 39° E. from junction of Grouse and Bear Creeks. Collector, J. B. Mertie, Jr., 1921.

Crazy Mountains (loc. 4, fig. 1). Circle C-3 quadrangle (1:63,360):

Mountain crest 0.9 mile northeast of BM3728 (Craz), lat 65°43' N., long 145°4.3' W. Collected by geologists of BP Exploration Co. (Alaska) Inc. (fig. 4).

### REFERENCES

Brabb, E. E., and Churkin, Michael, Jr., 1964, Preliminary geologic map of the Charley River quadrangle (1:250,000), east-central Alaska: U.S. Geol. Survey open-file report.

Forbes, Edward, 1848-1850, On *Oldhamia*, a new genus of Silurian fossils: Jour. Geol. Soc. Dublin, v. 4, p. 20.

Fritz, M. A., 1965, Bryozoan fauna from the middle Ordovician of Mendoza, Argentina: Jour. Paleontology, v. 39, no. 1, p. 141-142.

Howell, B. F., 1922, *Oldhamia* in the Lower Cambrian of Massachusetts [abs.]: Geol. Soc. America Bull., v. 33, p. 198-199.

Mertie, J. B., Jr., 1933, The Tatonduk-Nation district: U.S. Geol. Survey Bull. 836, p. 347-443.

——— 1937, The Yukon-Tanana region, Alaska: U.S. Geol. Survey Bull. 872, 276 p.

Neuman, R. B., 1962, The Grand Pitch Formation—new name for the Grand Falls Formation (Cambrian?) in northeastern Maine: Am. Jour. Sci., v. 260, p. 794-797.

Ruedemann, Rudolf, 1942a, *Oldhamia* and the Rensselaer Grit problem: New York State Mus. Bull. 327, p. 5-17.

——— 1942b, Cambrian and Ordovician fossils: New York State Mus. Bull. 327, p. 19-32.

Simpson, Scott, 1957, On the trace-fossil *Chondrites*: Geol. Soc. London, Quart. Jour., v. 112, p. 475-499.

Smith, E. S. C., 1928, The Cambrian in northern Maine: Am. Jour. Sci., 5th ser., v. 15, p. 484-486.

Walcott, C. D., 1894, Discovery of the genus *Oldhamia* in America: U.S. Natl. Mus. Proc., v. 17, p. 313-315.



## LATE DEVONIAN AND EARLY MISSISSIPPIAN AGE OF THE WOODFORD SHALE IN OKLAHOMA, AS DETERMINED FROM CONODONTS

By WILBERT H. HASS<sup>1</sup> and JOHN W. HUDDLE,  
Washington, D.C.

**Abstract.**—Conodont collections from eight measured sections in Carter, Murray, Pontotoc, and Pittsburg Counties show that most of the Woodford Shale is Late Devonian in age, but that the uppermost part is Early Mississippian (Kinderhook). The Mississippian (Kinderhook) part of the Woodford Shale is generally less than 1 foot thick, but on Henryhouse Creek near Woodford, it is at least 10 feet thick. The oldest conodont fauna found in the base of the Woodford Shale is early Late Devonian in age.

Conodonts from the Woodford Shale have been described and figured by Cooper (1931a, b) and by Ellison (1950). Cooper correlated the Woodford Shale with the Chattanooga Shale and regarded both as Mississippian in age. Ellison determined the age of the Woodford Shale in the subsurface of western Texas and New Mexico as Late Devonian and found no evidence of a Mississippian age. Hass (1956b, p. 27–29), correlated the Upper Devonian and Mississippian parts of the Arkansas Novaculite with parts of the Woodford Shale on the basis of the conodont faunas.

The Woodford Shale of Oklahoma is considered to be partly of Late Devonian age and partly of Early Mississippian (Kinderhook) age. This conclusion is drawn from study of numerous conodonts present in collections obtained from measured sections located on Henryhouse Creek in Carter County; at Lake Classen in Murray County; at five places south of Ada in Pontotoc County (see fig. 1); and in the Ti Valley near Pinetop School, in Pittsburg County.

This paper is based on stratigraphic sections and collections of fossils made by Hass and H. D. Miser in 1949. Hass prepared the first draft of the report in 1952. Huddle subsequently prepared the paper for publication.

<sup>1</sup> Deceased, November 30, 1959.

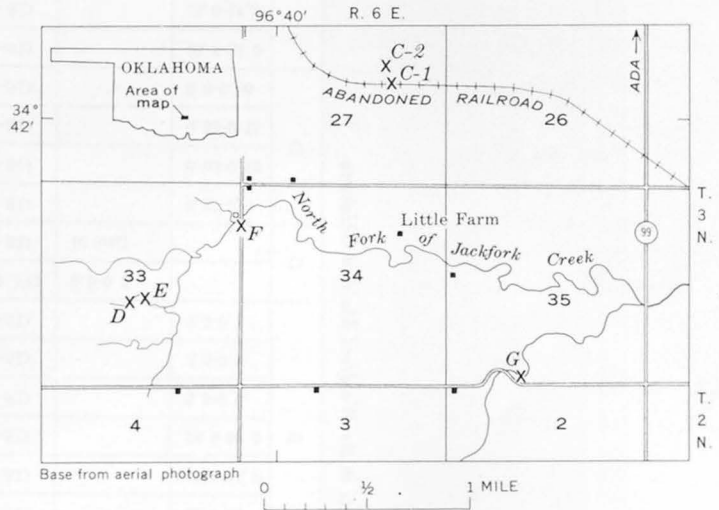


FIGURE 1.—Localities from which conodonts were collected in the Woodford Shale near Ada, Pontotoc County, Okla. Localities A, B, and H are outside the area of the map.

Conodonts are not abundant in the Woodford Shale and most of them in the collections studied are poorly preserved or are represented by molds. The most abundant forms are long-ranging bar-type conodonts, such as *Hindeodella*, but the conodont assemblage zones recognized by Hass (1951, 1956a, b) in the Arkansas Novaculite, and the black Chattanooga, Ohio, and New Albany Shales are present in the Woodford Shale. These zones were numbered by Hass (1956b) but are designated here by the name of a typical species. Many of the German conodont zones (Ziegler, 1962) have not been found in the black shales of central United States. Additional study of the conodont faunas of these black shales is needed to determine why some of the conodont zones are absent. Perhaps there are several unconformities within the black-shale formations. The conodont assemblages present in the Woodford Shale in age from Early Mississippian to early Late Devonian.



Early Late Devo- nian	Geographic Grid																												
	1	2	3	4	5	6	7	8	9	10	11	12	13	14	15	16	17	18	19	20	21	22	23	24	25	26	27	28	
	<i>Ancyrodella rotundiloba</i> (Bryant)																												
	<i>Neoprioniodus alata</i> (Hinde)																												
	<i>Polygnathus linguiformis</i> Hinde																												
	<i>pennata</i> Hinde																												
Long-ranging genera	<i>Bryantodus</i> sp.	X							X				X	X	X	X													
	<i>Euprioniodina</i> sp.	X	X				X					X	X	X	X						X	X							
	<i>Hibbardella</i> sp.	X													X	X	X							X	X				
	<i>Hindeodella</i> sp.	X	X				X			X	X	X	X	X			X	X			X	X		X	X				
	<i>Hindeodelloides</i> sp.		X									X	X											X	X				
	<i>Ligonodina</i> sp.	X	X				X					X	X	X	X			X	X	X	X		X	X					X
	<i>Lonchodina</i> sp.		X				X					X	X					X	X										X
	<i>Nothognathella</i> sp.																	X	X										
	<i>Ozarkodina</i> sp.	X										X	X		X	X								X	X				X
	<i>Polygnathus</i> sp.	X									X	X	X										X	X					X
<i>Spathognathodus</i> sp.		X									X	X		X	X								X	X				X	

- A. Henryhouse Creek, Carter County.
- B. Lake Classen, Murray County.
- C. Bushberg-Hannibal locality of Cooper (1939), Pontotoc County.
- D. At the head of a tributary to North Fork of Jackfork Creek, NE $\frac{1}{4}$ SW $\frac{1}{4}$  sec. 33, T. 3 N., R. 6 E., Pontotoc County.
- E. Bank of tributary to North Fork of Jackfork Creek, NW $\frac{1}{4}$ SW $\frac{1}{4}$  sec. 33, T. 3 N., R. 6 E., Pontotoc County.

- F. High ground just south of the North Fork of Jackfork Creek, NE $\frac{1}{4}$  sec. 33, T. 3 N., R. 6 E., Pontotoc County.
- G. Bank of South Fork of Jackfork Creek, SE $\frac{1}{4}$ SW $\frac{1}{4}$  sec. 35, T. 3 N., R. 6 E., Pontotoc County.
- H. Pinetop school area, NW $\frac{1}{4}$ NE $\frac{1}{4}$  sec. 3, T. 2 N., R. 15 E., Pittsburg County.  
 \* 0.0 to 0.5 feet above base of strata which directly overlie the Woodford Shale.

### STRATIGRAPHIC SETTING

The Woodford Shale is reported (Shannon, 1962, p. 19) to be more than 600 feet thick, but the sections from which conodonts were collected are all much thinner. The formation is principally grayish-black shale and, at some places (for example, at Lake Classen), greenish and brownish shale. On the south side of the Arbuckle Mountains and in the Ti Valley it contains numerous layers of interbedded chert which decrease in number and thickness northward. Phosphatic nodules are characteristic of the upper part of the Woodford at some localities.

### CONODONTS

#### Conodonts of Early Mississippian (Kinderhook) age

Conodonts indicating an Early Mississippian (Kinderhook) age were found near the top of the Woodford Shale on Henryhouse Creek, in the uppermost 0.3 foot of the formation at locality C, and in the uppermost 0.48 foot at locality G, and they may also be present in the slightly older beds at these localities. The genera and species on which the age designation is based are listed in the accompanying table. The generic assemblage *Elictognathus*, *Gnathodus*, *Pinacognathus*, *Pseudopolygnathus*, and *Siphonodella* found here indicates a Kinderhook age. A similar conodont fauna is also present in the upper part of the black-shale portion of the Chattanooga Shale (Devonian and Mississippian) of northeastern Oklahoma.

A collection of conodonts (USGS Colln. 21910-PC) from the basal 0.5 foot of the strata which directly overlie the Woodford Shale at locality H, near Pine-top School in Pittsburg County, contains an Early Mississippian (Kinderhook) fauna (see table). These beds were included in the Caney Shale by Hendricks and Gardner (Hendricks and others, 1947, p. 23). However, the presence in the collection of *Gnathodus punctatus* and *Siphonodella duplicata* var. B. suggests a Chouteau age. Those two species, as well as others mentioned in this report, have been figured by Hass (1951, p. 2530) and are not refigured here. These two conodonts have also been found in the topmost beds of the middle division of the Arkansas Novaculite at Caddo Gap, Montgomery County, Ark.; in the Chappel Limestone (Early Mississippian) of Texas; and in the Welden Limestone (Early Mississippian) and the topmost few tenths of a foot of the pre-Welden shaly interval at locality C, south of Ada, Pontotoc

County, Okla. It is suggested, therefore, that unit 11 of Hendricks and Gardner's section (*in* Hendricks and others, 1947, p. 23-24) should be regarded as a distinct and underlying stratigraphic unit rather than the basal beds of the Caney Shale (Late Mississippian).

#### Conodonts of Late Devonian age

Conodonts considered to be significant indicators of the Late Devonian are found throughout the major portion of the Woodford Shale. Several distinct faunal assemblages have been recognized. Most of the conodonts belong to one of the following genera indicative of the Devonian: *Ancyrodella*, *Ancyrognathus*, and *Palmatolepis*.

A few specimens of *Spathognathodus inornatus*, which is also characteristic of the Upper Devonian, have been found in the Woodford Shale in beds stratigraphically next beneath those containing conodonts of Kinderhook age. This species is also present (fig. 2) in the upper part of the Ohio Shale of Ohio and Kentucky (including the Cleveland Member of northern Ohio), in the very youngest beds of the Gassaway Member of the Chattanooga Shale of central Tennessee and adjacent States (Hass, 1956a), and in the basal bed of the Maury Formation (Early Mississippian) of north-central Tennessee. Specimens of *Spathiocaris* described by Cooper (1932) came from beds of the Woodford Shale in the Henryhouse Creek section that contain *Spathognathodus inornatus*.

Older beds of the Woodford Shale contain the *Palmatolepis glabra* assemblage, which includes the following: *Ancyrognathus bifurcata*, *Palmatodella delicatula*, *Palmatolepis perlobata*, *P. subperlobata*, *P. glabra*, *P. quadrantinodosa*, and *P. sp. A*. This assemblage, as represented in the Geological Survey's conodont collections, is represented in beds in the lower part of the Ohio Shale of Ohio and Kentucky (including the Huron Member of northern Ohio); in the Antrim Shale as exposed in the Paxton shale pit west of Alpena, Mich.; in much of the middle division of the New Albany Shale of Indiana; in a faunal zone present in all but the youngest beds of the Gassaway Member of the Chattanooga Shale of central Tennessee and adjacent States; and in a faunal zone of the middle division of the Arkansas Novaculite of Arkansas and Oklahoma which, at Caddo Gap, Montgomery County, Ark., is 46 to 140 feet below the top of the middle division of the Arkansas Novaculite. This same faunal assemblage is present the lower part of the Chattanooga Shale of northeastern Oklahoma.

Species characteristic of a still older portion of the Woodford Shale are *Ancyrognathus euglypheus*,

	ASSEMBLAGE ZONE	STATE					
		Oklahoma	Arkansas	Tennessee	Indiana	Ohio	
Lower Mississippian	<i>Siphonodella</i>			Upper	Maury Formation	Upper Division	
Upper Devonian	<i>Spathognathodus inornatus</i>		Arkansas Novaculite		Gassaway Member	Middle Division	Bedford Shale and upper (Cleveland Member) part of Ohio Shale
	<i>Palmatolepis glabra</i>	Woodford Shale		Middle			Chattanooga Shale
	<i>Palmatolepis subrecta</i>			Dowelltown Member		Lower Division	Olentangy Shale
	<i>Ancyrodella rotundiloba</i>						

FIGURE 2.—Occurrence of the Woodford Shale conodont assemblages in Oklahoma and other areas.

*Palmatolepis subrecta*, and *Palmatolepis unicornis*. The *Palmatolepis subrecta* assemblage (fig. 2) ranges throughout the Dowelltown Member of the Chattanooga Shale of central Tennessee and adjacent States (Hass, 1956a). *Ancyrognathus euglypheus* was described from the Olentangy Shale of Ohio, where it is associated with *Palmatolepis flabelliformis* (which may be conspecific with *P. subrecta*). *P. subrecta* is present in a faunal zone of the middle division of the Arkansas Novaculite located 184 feet below the top of the middle division. The conodonts that Ellison (1950) obtained from the subsurface in west Texas could be from beds correlated with this portion of the Woodford.

The conodont assemblage that includes *Ancyrodella rotundiloba* is present in the basal portion of the Woodford Shale at localities B, D, and E and is the same assemblage as that found in the basal sandstone of the Chattanooga Shale as exposed along the Eastern Highland Rim of central Tennessee, the lower part of the New Albany Shale of Indiana, and the Genesee Limestone Member of the Genesee Formation (Upper Devonian) of New York. The age of this conodont assemblage is early Late Devonian.

**OTHER FOSSILS**

Other fossils found in the Woodford shale include lingulas, orbiculoideas, arthropods (*Angustidontus* and *Spathiocaris*), fish scales, silicified wood (*Callixylon*), and spores (*Tasmanites*). Most of these are long-ranging forms and do not help much in dating the formation. *Angustidontus* was described by Cooper (1936) as the jaw of an actinopterygian fish, but Jean Berdan (written communication, 1964) regards these fossils as the rami of an arthropod. She has found similar rami in rocks of Silurian to Mississippian age. *Spathiocaris* has been reported only from Devonian formations. *Callixylon* is common at localities C through G in the *Palmatolepis glabra* zone. Hoskins and Cross (1952, p. 237) report that *Callixylon* ranges from Late Devonian to Early Mississippian.

**MEASURED SECTIONS**

**Locality A**

Along south bank of Henryhouse Creek near community of Woodford, Carter County. From Ardmore go north 11 miles on U.S. Highway 77 to State Highway 53; turn west on Highway 53, go 5.3 miles; turn north on farm road located just east of farm buildings;



follow road to Henryhouse Creek and outcrops of Woodford Shale.

Woodford Shale:

	Thickness (feet)	Distance of top above base of formation (feet)
Covered interval of undetermined thickness.		
Shale, grayish-black, interbedded with grayish-black chert beds as much as 0.25 foot thick. No phosphatic nodules in place-----	9.4	221.0
Shale, grayish-black, interbedded with grayish-black chert beds as much as 0.25 foot thick. Phosphatic nodules scattered throughout interval but especially abundant in zone 200 to 201 feet above the base of the Woodford Shale or 26 to 27 feet above the base of the interval. USGS Colln. 21906-PC, 7350-SD-----	36.6	211.6
Shale, grayish-black, interbedded with grayish-black chert beds as much as 0.25 foot thick. Chert beds predominant except in basal 10 feet. No phosphate nodules observed-----	46.0	175.0
Shale, grayish-black, interbedded with few grayish-black chert beds as much as 0.1 foot thick-----	36.0	129.0
Shale, grayish-black, interbedded with many grayish-black chert beds as much as 0.2 foot thick. USGS Colln. 7351-SD, 7352-SD-----	45.0	93.0
Chert, grayish-black, massive-----	.7	48.0
Shale, grayish-black, interbedded with some thin grayish-black chert beds. USGS Colln. 7353-SD-----	32.8	47.3
Shale, grayish-black, interbedded with some grayish-black chert beds as much as 0.25 foot thick. Interval also contains some greenish-gray mudstones, especially from 3.0 to 4.5 feet above the base of the interval. USGS Colln. 7354-SD, 7355-SD, and 7356-SD-----	13.5	14.5
Covered-----	1.0	1.0
Total-----	221.0	

Hunton Group.

Locality B

Lake Classen, Murray County, at YMCA camp along northeastern shore. Turn west off U.S. Highway 77 just south of bridge over Washita River; go 1.3 miles along secondary road to entrance to camp. Exposure is northwest of main building of camp.

Covered.

Woodford Shale:

	Thickness (feet)	Distance of top above base of formation (feet)
Shale, buff, light-tan to nearly white; interbeds that may be as much as 0.1 foot thick. USGS Colln. 7357-SD--	55.5	111.0
Shale, greenish- and brownish-gray; interbedded chert beds may be as much as 0.25 foot thick. USGS Colln. 7358-SD, 7359-SD, 7360-SD.	45.0	55.0

Woodford Shale—Continued

	Thickness (feet)	Distance of top above base of formation (feet)
Shale, greenish- and brownish-gray. No chert beds observed-----	4.0	10.5
Shale, predominantly greenish-gray; some brownish-gray beds. USGS Colln. 7361-SD, 7362-SD-----	6.4	6.5
Mudstone, greenish-gray, glauconitic. Contains bone fragments and chert pebbles as much as 0.05 foot in diameter. USGS Colln. 7363-SD---	.1	.1
Total-----	111.0	

Hunton Group.

Locality C

At and near type locality of Cooper's (1939) Bushberg-Hannibal conodont fauna, in Pontotoc County.

Locality C-1.—Cut on abandoned railroad in SE¼ SW¼NE¼ sec. 27, T. 3 N., R. 6 E. From business district in Ada, go south on State Highway 99 for 6.7 miles; west on graded county road for 1.3 miles to the Little farm. Outcrop is at north end of pasture across road from Little farmhouse.

	Thickness (feet)
Caney Shale.	
Welden Limestone-----	4.0
Pre-Welden Shale-----	1.8
Woodford Shale:	
Shale, grayish-black, thin-bedded; with few thin (0.05 foot thick) cherty beds. Phosphatic nodules scattered throughout interval. USGS Colln. 21907-PC. Exposed-----	1.0
Total-----	6.8

Locality C-2.—Exposures in cleared area 50 to 300 feet (estimated) northwest of west end of railroad cut at locality C-1. Entire exposure is in the Woodford Shale.

USGS Colln. 7367-SD. Estimated as 10 feet below top of Woodford Shale.

Locality D

At head of tributary to North Fork of Jackfork Creek, approximately 6 miles south of Ada, Pontotoc County, in creek bed in field; NE¼SW¼ sec. 33, T. 3 N., R. 6 E.

Covered.

Woodford Shale:

	Thickness (feet)	Distance of top above base of formation (feet)
Shale, grayish-black, brown, weathered. Phosphatic nodules present-----	0.70	1.6
Shale, grayish-black, tough. Phosphatic nodules present. USGS Colln. 7370-SD-----	.14	.90
Mudstone, dark-brown, iron oxide stained. Phosphatic nodules present.	.06	.76
Sandstone, greenish-brown, fine-grained, glauconitic; consists of rounded grains of quartz sand. Phosphatic nodules present. USGS Colln. 7371-SD----	.08	.70
Mudstone, light-gray, iron oxide stained, laminated, plastic. Phosphatic nodules present-----	.12	.62

	Thickness (feet)	Distance of top above base of formation (feet)
Woodford Shale—Continued		
Mudstone, brownish-black, laminated, friable.....	. 02	. 50
Mudstone, light-brown, iron oxide stained, plastic, laminated. Phosphatic nodules present.....	. 12	. 48
Mudstone, brownish-black.....	. 01	. 36
Sandstone, light-gray, chalky-white, porous, glauconitic; contains reworked silicified megafossils.....	. 10	. 35
Sandstone, dark-greenish-brown, glauconitic, fine-grained; consists chiefly of quartz sand grains.....	. 05	. 25
Mudstone, light-greenish-gray, friable. USGS Colln. 7373-SD.....	. 20	. 20
Total.....	1. 6	

Hunton Group.

Note: USGS Colln. 7372 collected from interval between 0.35 and 0.76 feet above base of formation.

Locality E

Bank of tributary to North Fork of Jackfork Creek, about 625 feet northeast and downstream from locality D; NW¼SE¼ sec. 33, T. 3 N., R. 6 E.

	Thickness (feet)	Distance of top above base of formation (feet)
Top of stream bank.		
Woodford Shale:		
Shale, grayish-black, weathering brownish; carbonaceous, numerous silicified logs of <i>Callixylon</i> , some logs in place. USGS Colln. 7374-SD, 7375-SD, 7376-SD, 7377-SD, 7378-SD.....	18. 00	22. 40
Mudstone, light-yellow-brown.....	. 04	4. 40
Shale, grayish-black, carbonaceous.....	1. 90	4. 36
Course of phosphatic nodules embedded in a greenish- and grayish-brown glauconitic sandy matrix.....	. 06	2. 46
Shale, grayish-black, carbonaceous, numerous spherical phosphatic nodules with diameters between 0.03 and 0.05 foot.....	1. 15	2. 40
Sandstone, greenish-gray, glauconitic; phosphatic nodules and reworked silicified megafossils present.....	. 40	1. 25
Covered.....	. 85	. 85
Total.....	22. 40	

Hunton Group.

Locality F

In a borrow pit along county road, on high ground just south of North Fork of Jackfork Creek, approximately 6 miles south of Ada, Pontotoc County; NE¼ sec. 33, T. 3 N., R. 6 E.

USGS Colln. 7379-SD. At road level. Estimated to be 10 to 12 feet below top of Woodford Shale.

Locality G

Along bank of South Fork of Jackfork Creek; SE¼SW¼ sec. 35, T. 3 N., R. 6 E. From Fittstown, Pontotoc County, go north on State Highway 99 for 4.7 miles; turn west onto county road and go approximately 0.6 mile. Exposure is on north side of road.

	Thickness (feet)	Distance of top above base of formation (feet)
Welden Limestone:		
Limestone, massive, ledge-forming.....	5. 7	21. 6
Pre-Welden shale (1.2 ft thick):		
Mudstone, greenish-gray; phosphatic nodules present throughout interval.....	. 6	15. 9
Mudstone, greenish-gray, sandy, phosphatic, laminated.....	. 6	15. 30
Woodford Shale (14.7 ft thick):		
Shale, grayish-black. USGS Colln. 21908-PC.....	. 08	14. 70
Chert, grayish-black.....	. 09	14. 62
Shale, grayish-black. USGS Colln. 21909-PC, 7380-SD.....	2. 0	14. 53
Mudstone, dark-gray, bedding contorted due to presence of irregularly shaped cherty masses. Contorted zones in section measure as much as 5 by 2.5 feet. Phosphatic nodules and persistent phosphatic beds as much as 0.12 foot thick present.....	2. 83	12. 53
Chert, persistent bed.....	. 5	9. 7
Shale, grayish-black, interbedded with dark-gray mudstones. Phosphatic nodules present. USGS Colln. 7381-SD.....	4. 0	9. 2
Iron sulfide, persistent bed.....	. 2	5. 2
Mudstone, dark-gray, somewhat contorted.....	5. 0	5. 0
Total.....	21. 6	

Bed of South Fork of Jackfork Creek.

Locality H

Near Pinetop School, Ti Valley, Pittsburg County, along small stream valley; NW¼NE¼ sec. 3, T. 2 N., R. 15 E. The following section is modified from Hendricks and others (1947, p. 23-24); the section was measured and described by Hendricks and L. S. Gardner. The fossil collections were made by Hass and Miser in 1949.

	Thickness (feet)	Distance of top above base of formation (feet)
Springer Formation.....	20. 0	
Caney Shale (514 ft thick):		
Units 2-10.....	505. 0	
Unit 11. Shale, greenish-gray, breaks into small angular fragments, contains conodonts and has abundant phosphate nodules and glauconite in a 6-inch zone at the base. USGS Colln. 21910-PC.....	9. 0	75. 5

	Thickness (feet)	Distance of top above base of formation (feet)
Woodford Shale (66.5 ft thick):		
Unit 12. Shale, black, hard, flaky, weathers gray, contains abundant phosphate nodules and conodonts---	2.5	66.5
Unit 13. Chert, black, in beds 1 to 4 inches thick, gritty. Contains partings of black paper shale, abundant round phosphate nodules and flattened discoidal phosphate nodules. USGS Colln. 7382-SD-----	32.0	64.0
Unit 14. Shale, hard, black, platy, cherty, in layers 1/16 to 1/4 inch thick, which contains some beds of blocky black chert about 4 inches thick. Weathers gray to white. USGS Colln. 7383-SD, 11092-PC-----	25.0	32.0
Unit 15. Chert breccia or conglomerate, white with some lenses of very fine grained crystalline limestone----	7.0	7.0
Pinetop Chert-----	60.0	
Total-----	660.5	

## REFERENCES

- Cooper, C. L., 1931a, Conodonts from the Arkansas Novaculite, Woodford formation, Ohio shale and Sunbury shale: *Jour. Paleontology*, v. 5, no. 2, p. 143-151.
- 1931b, New conodonts from the Woodford formation: *Jour. Paleontology*, v. 5, no. 3, p. 230-343.

- Cooper, C. L., 1932, A crustacean fauna from the Woodford formation of Oklahoma: *Jour. Paleontology*, v. 6, no. 4, p. 346-352.
- 1936, Actinopterygian jaws from the Mississippian black shales of the Mississippi valley: *Jour. Paleontology*, v. 10, no. 2, p. 92-94.
- 1939, Conodonts from a Bushberg-Hannibal horizon in Oklahoma: *Jour. Paleontology*, v. 13, no. 4, p. 379-422.
- Ellison, S. P., Jr., 1950, Subsurface Woodford black shale, west Texas and Southeast New Mexico: *Texas Univ. Bur. Econ. Geology Rept. Inv. 7*, 20 p.
- Hass, W. H., 1951, Age of the Arkansas novaculite: *Am. Assoc. Petroleum Geologists Bull.*, v. 35, no. 12, p. 2526-2541.
- 1956a, Age and correlation of the Chattanooga shale and the Maury formation: *U.S. Geol. Survey Prof. Paper 286*, 47 p.
- 1956b, Conodonts from the Arkansas novaculite, Stanley shale and Jackfork sandstone, in *Ardmore Geol. Soc. Guidebook Ouachita Mountains Field Conf.*, 1956: p. 25-33.
- Hendricks, T. A., and others, 1947, *Tulsa Geol. Soc. Guidebook Field Conf.*, May 8-10, 1947, Ouachita Mountains, Oklahoma: 56 p.
- Hoskins, J. H., and Cross, A. T., 1952, The petrification flora of the Devonian-Mississippian Black Shale: *The Paleobotanist*, v. 1, p. 215-238.
- Shannon, J. P., Jr., 1962, Hunton Group (Silurian-Devonian) and related strata in Oklahoma: *Am. Assoc. Petroleum Geologists Bull.*, v. 46, no. 1, p. 1-29.
- Ziegler, Willi, 1962, Taxionomie and Phylogenie Oberdevonischer Conodonten und ihre stratigraphische Bedeutung: *Hess. Landesamt Bodenforsch.*, v. 38, 166 p.



## GRAY BULL AND LYSITE FAUNAL ZONES OF THE WILLWOOD FORMATION IN THE TATMAN MOUNTAIN AREA, BIGHORN BASIN, WYOMING<sup>1</sup>

By W. L. ROHRER and C. L. GAZIN,<sup>2</sup>  
Denver, Colo., Washington, D.C.

*Abstract.*—Vertebrate fossils common to the Gray Bull and overlying Lysite faunal zones overlap in a mappable claystone bed in the lower Eocene Willwood Formation. The bed, which crops out over more than 70 square miles, is 2 to 10 feet thick and about 750 feet below the top of the Willwood. The claystone, herein identified as bed A, is a mollusk zonule that is considered to be a biostratigraphic and rock-stratigraphic unit. Fragmentary fossils found in the mollusk zonule include mammals, fish, alligators, crocodiles, turtles, clams, and snails. The mollusks are indicative of a fresh-water environment.

This report presents data for a more precise definition of the contact of the Gray Bull and Lysite faunal zones of the Willwood Formation than has been possible heretofore, and presents a fossil list and a map of fossil localities in the Willwood and Tatman Formations. It is based on numerous new collections of fossils from the lower Eocene Willwood Formation and the overlying lower Eocene Tatman Formation in the Tatman Mountain area, south of the Greybull River in the Bighorn Basin in Park and Big Horn Counties, northwestern Wyoming. The names of the Willwood faunal zones are used here in the biostratigraphic sense, following the usage of Van Houten (1944, p. 186, 187) and others.

The Willwood Formation has a maximum thickness of more than 2,000 feet, but only the upper 1,200 to 1,400 feet is exposed in the Tatman Mountain area (fig. 1). The Willwood consists mainly of variegated claystone but includes lenses of light-gray, buff-weathering sandstone. Some sandstone lenses are as much as 100 feet thick and extend a few miles along the outcrop. The upper 200 feet of the formation contains a few bentonite beds. The bentonite beds increase

in thickness and number from west to east, and there is a concomitant decrease in claystone and sandstone in the interval. Color bands in the Willwood tend to change or disappear along the outcrop. The Willwood is overlain by the Tatman Formation, the base of which is placed at the base of the lowest carbonaceous or lignitic shale.

Faunal zones of the "Bighorn Wasatch" (Wood and others, 1941) have been known for many years. Investigations by Van Houten (1944, 1945) resulted in the definition of the Willwood and Tatman Formations and in a compilation of the fossils recognized in the faunal zones of the Willwood Formation. According to Van Houten (1945, p. 426-433), the Willwood faunal zones, from bottom to top, are: Gray Bull, 2,000 feet thick; Lysite, 400 to 500 feet thick; and Lost Cabin, 325 feet thick. Each faunal zone is characterized by specific differences in certain of the genera common to more than one zone, and by the presence or absence of certain genera. In the Tatman Mountain area the Gray Bull beds contain *Homogalax*. The Lysite beds include *Heptodon* but not *Lambdaotherium* nor *Homogalax*. Both *Heptodon* and *Lambdaotherium* are present in the Lost Cabin beds, and the *Pelycodus-Nottharctus* sequence has by definition reached a more fully *Nottharctus* stage of development. Apparently no genera are restricted to the Lysite zone (Van Houten, 1944, p. 187).

In general, fossils are abundant in the upper 300 feet of the Gray Bull faunal zone, are common in the lower 300 feet of the Lysite zone, but are scarce in the Lost Cabin zone.

A widespread bed distinguished by its contained fauna, about 750 feet below the top of the Willwood Formation (Rohrer, 1964a, 1964b), is here called bed A. Although locally cut out along channels filled with sandstone, bed A is a mappable unit in most of the

<sup>1</sup> Published by permission of the Secretary of the Smithsonian Institution.

<sup>2</sup> U.S. National Museum. Research by Gazin on early Tertiary mammals is currently aided by a grant from the National Science Foundation.

Tatman Mountain area. Bed A is mainly purplish-maroon claystone, but locally it contains thin lenses of sandstone. The sandier parts of the bed are gray instead of maroon. Bed A is generally about 3 feet thick, but it ranges from 2 to 10 feet in thickness and contains gastropods, pelecypods, gar-pike scales, turtle-shell fragments, crocodilian bones and teeth, and mammalian fossils. Locally it is abundantly fossiliferous, although many outcrops have no fossils or are sparsely fossiliferous.

The sediments and animal assemblage in bed A are indicative of a stream, locally sluggish but having some current action. This is shown by the association of clams and snails found in the fine-grained sediments. The finding of fossil remains of gar pike and alligators or crocodiles, common carnivores or scavengers, with fragments of mammals is suggestive of watering holes along a stream frequented by land animals. It seems probable that the land animals, most of which were relatively small, were killed at the stream by the larger reptiles.

Fossil collections made in the Tatman Mountain area indicate that the Gray Bull and Lysite faunal zones overlap in bed A (fig. 1). This zonal overlap, a few feet thick, locates relatively precisely the boundary between the 2,000-foot Gray Bull zone below and the 400- to 500-foot Lysite zone above. Fossils below bed A are indicative of the Gray Bull zone. The Lysite and Lost Cabin faunal zones are not clearly separated in this area because of the paucity of diagnostic fossils in the upper strata of the Willwood. Bed A is a molluscan zonule that locally contains fragments of mammals, and it is both a biostratigraphic and rock-stratigraphic unit.

Figure 1 shows places where fossils were observed in the Willwood and Tatman Formations during mapping of the Tatman Mountain and Sheep Mountain quadrangles. Each of the invertebrate-fossil localities in the Willwood, with one exception, is in bed A. The exception is near locality 38 (fig. 1), where pelecypods and gastropods occur in material that may have been reworked during the Quaternary, but the material cannot be distinguished from the Willwood. Bed A is probably the same bed that Osborn (1929, p. 70) called the "chief faunal horizon of the Big Horn Wasatch" in the Buffalo Basin area (upper Dry Cottonwood Creek, sec. 20, 28, and 29, T. 50 N., R. 96 W.).

Mammals common to the Willwood sediments are the *Coryphodon*, a hippopotamuslike animal; *Homogalax*, an early tapiroid; and *Hyracotherium*, an early horse. Insectivores, carnivores, and other herbivores are also present. The list of fossils given below is numbered according to map locality (fig. 1). The fos-

sil mammals were identified by C. L. Gazin. Other animals were identified by members of the U.S. Geological Survey: the clams and snails by D. W. Taylor, the turtles and crocodilians by Nicholas Hotton III, and the fish by F. C. Whitmore, Jr. Forms marked with an asterisk (\*) were identified in the field by W. L. Rohrer.

Fossils from the Willwood and Tatman Formations, Tatman Mountain area, Wyoming

[All fossils are mammals unless otherwise noted. \*, field identification; †, reptile; ‡, fish]

Locality on figure 1	USGS Cenozoic locality	Fossil
1-----	-----	<i>Phenacodus</i> cf. <i>intermedius</i> .
2-----	22895	Fresh-water pelecypod <i>Plesielliptio priscus</i> (Meek and Hayden). <i>Coryphodon</i> sp. Undet. mammal. Gar pike. <i>Allognathosuchus</i> cf. <i>heterodon</i> †. Crocodile*, coprolite*, turtles*.
3-----	-----	<i>Coryphodon</i> sp. <i>Phenacodus</i> sp. <i>Hyracotherium</i> sp. Crocodiile.
4-----	-----	<i>Phenacodus copei</i> Granger.
5-----	-----	<i>Coryphodon</i> sp.
6-----	-----	<i>Coryphodon</i> sp. <i>Palaeosinopa</i> sp. <i>Hyracotherium</i> sp. <i>Allognathosuchus</i> cf. <i>heterodon</i> †. Crocodiile.
7-----	-----	<i>Palaeosinopa</i> cf. <i>veterrima</i> Matthew. <sup>1</sup>
8-----	-----	<i>Coryphodon</i> sp. <i>Pelycodus frugivorus</i> . cf. <i>Phenacodus vortmani</i> Cope.
9-----	-----	cf. <i>Hyracotherium</i> sp.
10-----	-----	<i>Hyracotherium</i> sp.
11-----	-----	<i>Homogalax</i> sp. <sup>1</sup>
12-----	-----	<i>Esthonyx bisulcatus</i> Cope. <i>Hyracotherium</i> sp. <i>Diacodexis metsiacus</i> (Cope). Turtle*, crocodile*.
14-----	-----	<i>Pelycodus</i> cf. <i>jarrovi</i> (Cope). <i>Pelycodus</i> ? sp. <i>Phenacodus brachypternus</i> Cope. <sup>1</sup> cf. <i>Phenacodus brachypternus</i> Cope. <i>Esthonyx bisulcatus</i> Cope. <i>Diacodexis metsiacus</i> (Cope). <i>Hyracotherium</i> sp. cf. <i>Homogalax</i> sp. <sup>1</sup> ? <i>Didymictis protenus</i> .
15-----	-----	<i>Coryphodon</i> sp. <i>Hyracotherium</i> sp.
16-----	22896	Fresh-water pelecypods: <i>Plesielliptio priscus</i> (Meek and Hayden). <i>wasatchensis</i> (Cockerell). Fresh-water gastropods: <i>Bellamyia</i> aff. <i>B. raynoldsana</i> (Meek and Hayden). <i>Pleurocera</i> aff. <i>P. tenera</i> (Hall).

<sup>1</sup> See footnote on p. D137.



## Fossils from the Willwood and Tatman Formations, Tatman Mountain area, Wyoming—Continued

Locality on figure 1	USGS Cenozoic locality	Fossil
16		<i>Hyracotherium</i> sp. Undet. mammal. Turtle*, crocodile*.
17		<i>Coryphodon</i> sp. <i>Pelycodus?</i> sp. Small creodont. Turtle*.
18		<i>Coryphodon</i> sp. Undet. smaller mammals and reptiles. Turtle*.
19		<i>Coryphodon</i> sp. Turtle*.
20		<i>Coryphodon</i> sp. <i>Hyracotherium</i> sp. <i>Heptodon</i> cf. <i>ventorum</i> (Cope). Undet. mammal. Gar pike.
21		<i>Coryphodon</i> sp.
22		<i>Coryphodon</i> sp. Turtle*, coprolite*. Undet. fresh-water pelecypods.
23		<i>Hyopsodus miticulus</i> (Cope). <sup>1</sup> <i>Hyracotherium</i> sp. Crocodile.
24		<i>Hyopsodus miticulus</i> (Cope). <sup>1</sup> <i>Hyracotherium</i> sp. <i>Homogalax?</i> sp. Small artiodactyl astragalus. <i>Coryphodon</i> *. Crocodile.
25		Fresh-water pelecypods*.
26		<i>Hyopsodus</i> cf. <i>miticulus</i> (Cope). <sup>1</sup>
27		<i>Coryphodon</i> *, turtle*, and crocodile*.
28	22897	Fresh-water pelecypods: <i>Plesielliptio priscus</i> (Meek and Hayden). <i>wasatchensis</i> (Cockerell). <i>Pelycodus</i> cf. <i>jarrovii</i> . <i>Anacodon</i> cf. <i>ursidens</i> (Cope). <i>Esthonyx bisulcatus</i> Cope. <i>Hyopsodus</i> cf. <i>miticulus</i> (Cope). <sup>1</sup> <i>Coryphodon</i> sp. <i>Allognathosuchus</i> cf. <i>heterodon</i> †. Crocodile.
29		Turtles*, <i>Coryphodon</i> *.
30		<i>Diacodon?</i> or <i>Palaictops?</i> sp. <i>Pelycodus</i> cf. <i>trigonodus</i> Matthew. <sup>1</sup> <i>Hyracotherium</i> sp.
31		<i>Hyracotherium</i> , either <i>H. angustidens</i> or <i>H. craspedotum</i> .
32		<i>Coryphodon</i> sp.
33		Fresh-water pelecypods* and gastropods*.
34	22898	Fresh-water pelecypods: <i>Plesielliptio priscus</i> (Meek and Hayden). <i>wasatchensis</i> (Cockerell). Fresh-water gastropods: <i>Bellamyia</i> aff. <i>B. raynoldsana</i> (Meek and Hayden).

## Fossils from the Willwood and Tatman Formations, Tatman Mountain area, Wyoming—Continued

Locality on figure 1	USGS Cenozoic locality	Fossil
		<i>Pleurocera</i> aff. <i>P. tenera</i> (Hall). <i>Coryphodon</i> sp. Gar pike*, crocodile*, turtle*, <i>Hyracotherium?</i> *
35		<i>Homogalax?</i> , <i>Coryphodon</i> *.
36		<i>Coryphodon</i> sp.
37		<i>Coryphodon?</i> sp. <i>Hyracotherium</i> sp. <i>Heptodon</i> sp. Crocodile. Undet. fish vertebra. Gar pike.
38		cf. <i>Didymictis protenus</i> (Cope).
39		<i>Coryphodon</i> sp. cf. <i>Homogalax</i> sp. <sup>1</sup> Crocodile.
40		<i>Pelycodus</i> sp. <i>Hyopsodus miticulus</i> (Cope). <sup>1</sup> <i>Homogalax</i> sp. <sup>1</sup> Crocodile. Aquatic emydid turtles of small to moderate size, a trionychid, and possibly other forms.
41		Crocodylian of proper size for <i>Allognathosuchus</i> †, but not certain. Turtles include probable emydid, more terrestrial form than at locality 48, or may be testudinid.
42		<i>Coryphodon</i> *.
43		Alligator*, turtle*, <i>Coryphodon</i> *.
44		<i>Hyracotherium</i> *.
45		<i>Esthonyx bisulcatus</i> Cope. cf. <i>Coryphodon</i> sp.
46		<i>Pelycodus?</i> sp. <i>Cynodontomys</i> sp. <i>Anacodon</i> cf. <i>ursidens</i> Cope. cf. <i>Didymictis protenus</i> (Cope). <i>Coryphodon</i> sp. <i>Phenacodus</i> sp. <i>Hyopsodus miticulus</i> (Cope). <sup>1</sup> <i>Hyracotherium</i> sp. <i>Heptodon?</i> sp. Crocodile.
		Turtles include large emydid, moderate-sized trionychid, and probably testudinid. Fresh-water pelecypods*.
47		<i>Hyracotherium</i> sp. cf. <i>Amyda</i> , aquatic soft-shell turtle; testudinid or possibly a terrestrial emydid.
48		cf. <i>Ectoganus</i> sp. cf. <i>Hyracotherium</i> sp. Crocodile. Large emydid turtle (aquatic) and small turtles, probably also emydid.
49		Large turtle, probably emydid.
50		<i>Coryphodon</i> *.
51		Crocodile*, turtle*.

<sup>1</sup> See footnote on p. D137.

## Fossils from the Willwood and Tatman Formations, Tatman Mountain area, Wyoming—Continued

Locality on figure 1	USGS Cenozoic locality	Fossil
52		<i>Hyopsodus miticulus</i> (Cope). <sup>1</sup> <i>Hyacotherium</i> sp. <i>Homogalax?</i> sp. <i>Diacodexis metsiacus</i> (Cope).
53		<i>Lepisosteus</i> †.
54	22904	Fresh-water gastropod <i>Bellamyia</i> cf. <i>B. paludinaeformis</i> (Hall).
55	22902	Fresh-water gastropod <i>Bellamyia</i> cf. <i>B. paludinaeformis</i> (Hall).
56	22903	Fresh-water pelecypod Unionidae?, indet. Fresh-water gastropod <i>Bellamyia</i> cf. <i>B. paludinaeformis</i> (Hall).
57	22906	Fresh-water gastropods: <i>Bellamyia</i> cf. <i>B. paludinaeformis</i> (Hall). <i>Pleurocera</i> aff. <i>P. tenera</i> (Hall).
58	22907	Fresh-water pelecypod <i>Sphaerium</i> .
59	22908	Fresh-water gastropod <i>Planorbina pseudoammonius</i> (Schlotheim). Percoidea †.
60	22901	Fresh-water gastropods: <i>Planorbina pseudoammonius</i> (Schlotheim). <i>Physa?</i>
61	22900	Fresh-water pelecypod Unionidae?, indet. Fresh-water gastropods: <i>Bellamyia</i> cf. <i>B. paludinaeformis</i> (Hall). <i>Planorbina pseudoammonius</i> (Schlotheim).
62	22899	Fresh-water pelecypods Unionidae?, two species. Fresh-water gastropod <i>Bellamyia</i> cf. <i>B. paludinaeformis</i> (Hall).

<sup>1</sup> These genera or species occurring in or below bed A have not been reported above the Gray Bull in the Bighorn Basin (Van Houten, 1945). Van Houten (1945, p. 450), however, reports *Pelycodus trigonodis* from only the lower and middle parts of the Gray Bull. The *P. trigonodis* specimen at locality 30 occurs only 250 feet below bed A, but it is referred to that species on the basis of size. The *Hyopsodus* cf. *miticulus* specimen at locality 26 is referred to the species also on the basis of size.

On the basis of the currently recognized vertical distribution of *Homogalax* and *Heptodon* locally, bed A may be interpreted as including an overlap of the Gray Bull and Lysite faunal zones. In this bed, *Heptodon*, suggestive of a Lysite age, was identified in the collection from locality 20 and tentatively recognized in the collection from locality 46. *Homogalax*, though found in younger beds in the Washakie Basin, appears to be restricted to the Gray Bull beds in the Bighorn Basin and has not been found in the typical Lysite of the Wind River Basin. It is evidently represented in the collection from localities 24 and 35 in bed A.

Recognition of *Hyopsodus miticulus* at several localities in bed A might appear from Van Houten's listing to present further evidence of the Gray Bull aspect of this level. The distinction of this species from later materials that have been called *Hyopsodus mentalis*

appears to be mainly a matter of size, but the frequency-distribution curves for tooth proportions of *H. miticulus* and *H. mentalis* overlap. This is particularly true when comparisons are made between Gray Bull and Lysite specimens, so that materials which have been called *Hyopsodus mentalis lysitensis* do not seem separable from the Gray Bull materials called *H. miticulus*. The speciation and morphology of *Hyopsodus* are currently under study by C. L. Gazin.

*Pelycodus* and *Notharctus* represent a continuous evolutionary line and are distinguished rather arbitrarily at a stage of development that is presumed to correspond to the change from Lysite to Lost Cabin. Bed A could not be definitely identified at locality 8, but the collection is approximately from that stratigraphic position. The specimen from locality 8 referred to *Pelycodus frugivorus* is rather *Notharctus*-like and might suggest recognition of this genus in beds rather earlier than Lost Cabin, but it is interpreted as a progressive variant in the *Pelycodus-Notharctus* sequence, much as Matthew (1915, p. 440) handled the later Gray Bull and Lysite materials that had been earlier included under *P. nuniensis* when that species was transferred by Osborn to *Notharctus*. A detailed review of the notharctids of Wasatchian provincial age of Wood and others (1941) is needed.

Nicholas Hotton III (written communication, May 22, 1962) reports that a true crocodile of modest size is present in the Willwood Formation, although most of the "crocodilian" material collected may pertain to the alligator genus *Allognathosuchus*. Mr. Hotton also reports that the groups of turtles break down generally into members of the families Trionychidae (soft-shell turtles) and Emydidae (pond turtles). The trionychids are water dependent as a family, and the emydids that are identifiable to family are more aquatic members of the group. Some of the sculpture on the fragments of trionychid turtles suggests that the genus represented is *Amyda*.

According to D. W. Taylor (written communication, May 3, 1962), the Willwood mollusks are species previously found in the formation, but the names have been changed. *Plesielliptio priscus* includes the species called *Unio clinopisthus* by Russell, *Bellamyia* aff. *B. raynoldsana* is *Viviparus wyomingensis* Russell, and *Pleurocera* aff. *P. tenera* is *Goniobasis carterii* Russell. These collections make up a large part of all known aquatic mollusks from the Willwood. They lived in perennial fresh water with some current action, probably a creek or river.

Taylor also reports that the Tatman molluscan assemblages are distinct from those in the Willwood For-



mation. *Pleurocera* aff. *P. tenera* in the Tatman is probably not the same *Pleurocera* that occurs in the Willwood. All the Tatman mollusks listed are characteristic of those in perennial bodies of fresh water, but they probably represent two different habitats. *Pleurocera*, *Bellamya*, and the pelecypods lived where some current action oxygenated the water, perhaps in a river or around the edges of a lake where there was wave action. The more thin shelled *Sphaerium* and *Planorbina* may have lived along the edges of a river or lake in quiet areas of less current.

Some fragments of fossil fish were collected from the Tatman Formation. F. C. Whitmore, Jr. (written communication, June 4, 1962), reports that one specimen is a tooth-bearing pharyngeal plate of a fish that probably belongs to the suborder Percoidea. The teeth on the pharyngeal plate are hemispherical and adapted to crushing. This fish was doubtless a bottom-living type that ate small mollusks. Another specimen is that of *Lepisosteus*, a gar pike. D. H. Dunkle (written communication, Feb. 5, 1963) identified a collection that contained two types of vertebrae, skull bones, ribs, and scale fragments of fresh-water teleostean fishes.

In summary, fossil vertebrates of the lower Eocene Willwood Formation, common to the Gray Bull and Lysite faunal zones, were found in a mappable claystone bed that is characterized by a molluscan fauna.

The claystone bed is about 750 feet below the top of the Willwood Formation and is within the stratigraphic range of the contact of the Gray Bull and Lysite faunal zones as determined by Van Houten. The claystone bed is considered a biostratigraphic and rock-stratigraphic unit that demarcates a time-stratigraphic boundary. This bed probably extends beyond the Tatman Mountain area; if so, it will be useful in separating the Gray Bull and Lysite faunal zones in adjacent areas.

#### REFERENCES

- Matthew, W. D., 1915, Entelonychia, Primates, Insectivora (part), pt. 4 in Matthew, W. D., and Granger, Walter, A revision of the Lower Eocene Wasatch and Wind River faunas: Am. Mus. Nat. History Bull., v. 34, p. 429-483.
- Osborn, H. F., 1929, The titanotheres of ancient Wyoming, Dakota, and Nebraska: U.S. Geol. Survey Mon. 55, 953 p.
- Rohrer, W. L., 1964a, Geology of the Sheep Mountain quadrangle, Wyoming: U.S. Geol. Survey Geol. Quad. Map GQ-310.
- 1964b, Geology of the Tatman Mountain quadrangle, Wyoming: U.S. Geol. Survey Geol. Quad. Map CQ-311.
- Van Houten, F. B., 1944, Stratigraphy of the Willwood and Tatman formations in northwestern Wyoming: Geol. Soc. America Bull., v. 55, no. 2, p. 165-210.
- 1945, Review of latest Paleocene and early Eocene mammalian fauna: Jour. Paleontology, v. 19, no. 5, p. 421-461.
- Wood, H. E., and others, 1941, Nomenclature and correlation of the North American continental Tertiary: Geol. Soc. America Bull., v. 52, no. 1, p. 1-48.



## TONGUES OF THE GREEN RIVER AND WASATCH FORMATIONS IN THE SOUTHEASTERN PART OF THE GREEN RIVER BASIN, WYOMING

By WILLIAM C. CULBERTSON, Denver, Colo.

*Abstract.*—The Luman Tongue of the Green River Formation and Niland Tongue of the Wasatch Formation, previously mapped only in the Washakie and Great Divide Basins, are here extended into the southeastern part of the Green River Basin. The Luman Tongue is 380 feet thick at the southeast corner of the basin; it thins northward and disappears about 30 miles to the north. The Niland Tongue is 280 feet thick at the southeast corner of the basin and thickens northward to a maximum of 455 feet at Sage Creek, about 13 miles to the northwest.

According to the latest geologic map of the Green River, Great Divide, and Washakie Basins (Bradley, 1961; 1964, pl. 1), the Luman and Tipton Tongues of the Green River Formation are present in the Great Divide and Washakie Basins, but only the Tipton is present in the Green River Basin. Recently several geologists (McGrew and Roehler, 1960; Bradley, 1964, p. 30; Love, 1964) have reported that beds equivalent to the Luman are present in the southeastern part of the Green River Basin. My investigation of these tongues began in 1962 as part of a project to evaluate oil shale and to map four 15-minute quadrangles southwest of Rock Springs, Wyo. Thanks are due H. Roehler and R. Wiegman for their helpful discussion of the problems involved.

### STRATIGRAPHY

In the Great Divide and Washakie Basins (fig. 1) the early Eocene Luman Tongue of the Green River Formation is a sequence of oil shale, sandstone, and clay shale 180–390 feet thick (Pipiringos, 1961). Overlying the Luman is the Niland Tongue of the Wasatch Formation, which consists of a sequence of clay shale, siltstone, and sandstone with beds of lignite and oil shale, 0–400 feet thick. The Niland, in turn, is overlain by the Tipton Tongue of the Green River Formation, which as redefined by Bradley (1964, p. 31) consists principally of low-grade oil shale and is about 180 feet thick.

In the southeastern part of the Green River Basin the Tipton Shale Member is a persistent, easily recognizable unit of oil shale 150–200 feet thick. The Tipton Shale is termed a member rather than a tongue in the Green River Basin because it is not separated from the main body of the Green River Formation by the Cathedral Bluffs Tongue of the Wasatch Formation, as it is in the Washakie and Great Divide Basins. The Tipton changes southward from a moderately rich dark-brown oil shale (locality 1) to a predominantly low-grade yellowish-brown or olive-gray oil shale (localities 4 and 5). Underlying the Tipton is the Wasatch Formation, which consists principally of lenticular beds of fine-grained massive friable sandstone, siltstone, mudstone, and clay shale. These rocks are for the most part brightly variegated, exhibiting shades of red, brown, purple, greenish gray, grayish orange, and olive gray.

In the vicinity of localities 3, 4, and 5 (fig. 1) the upper part of the Wasatch lacks red coloration, and contains many interbeds of oil shale, limestone, and lignite. The oil shale is yellowish-brown or olive-gray papery shale that at most places contains fossils of ostracodes, pelecypods, and a variety of gastropods. No assays of these oil-shale beds are available from cores or fresh outcrops, but these rocks resemble other oil shales whose known oil yield ranges from 5 to 15 gallons of oil per ton. The limestone beds are a few inches to 4 feet thick, and most contain such an abundant fauna of gastropods, pelecypods, and ostracodes that they are classifiable as coquina. The coquina occurs either as resistant ledge- or bench-forming beds, or as weak marly beds that crop out as a rubble of shells. At most places the coquina passes laterally from resistant ledge to nonresistant slope in a short distance. Locally the coquina grades into fossiliferous mudstone. The lignite beds are generally thin and highly weathered, and contain interbeds of shale, silt-

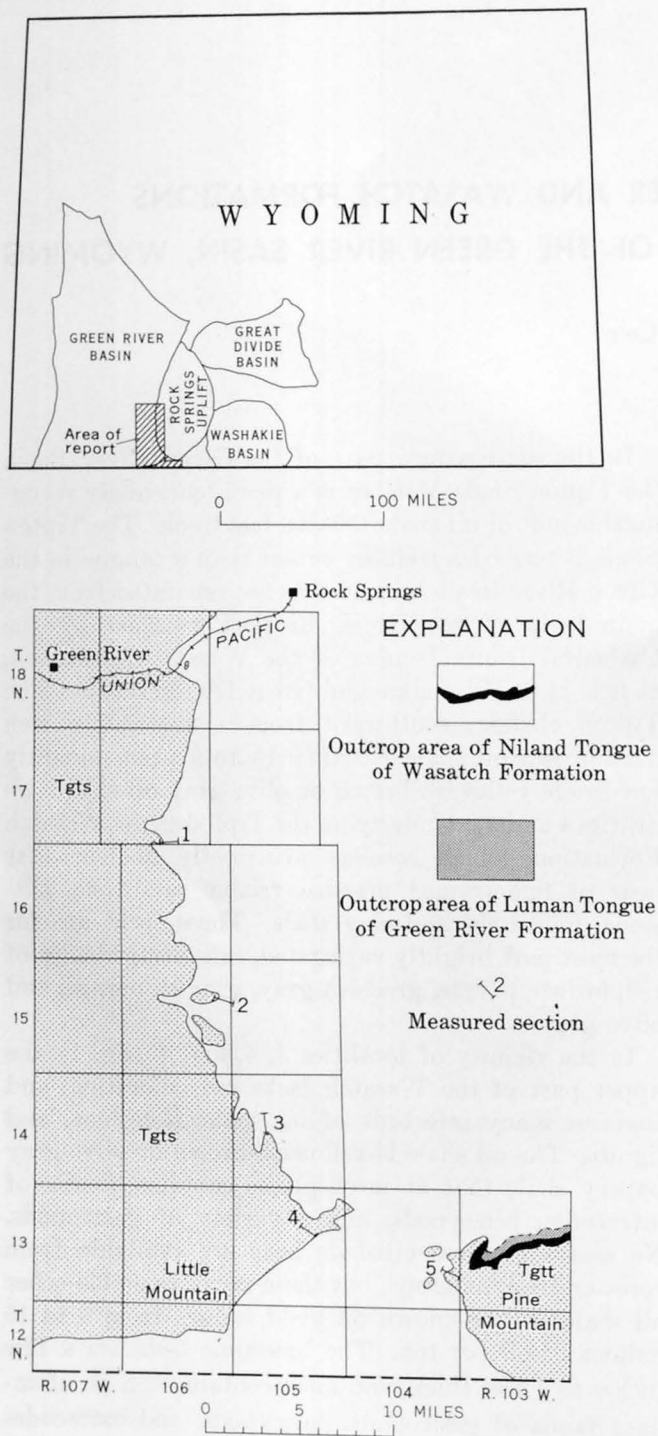


FIGURE 1.—Index maps showing location of area and location of measured sections. Area underlain by the Tipton Shale Member (Tgts) or the Tipton Tongue (Tgtt) of the Green River Formation shown by light stipple. Geology modified from Bradley (1964).

stone, and fossiliferous limestone. However, lignite beds are so numerous in the southern part of the area that at locality 5 (columnar section 5, fig. 2) a total of 22 feet of lignite is present; at locality 4, 31 feet; and at locality 3, 12 feet. At locality 5 an 18-foot bed

85 feet below the Tipton consists of 11 feet of lignite and 7 feet of shale and limestone.

The diversity of rock types in the upper part of the Wasatch in the southeastern part of the Green River Basin makes it difficult to determine what part, if any, should be assigned to the Luman Tongue of the Green River Formation. In a discussion of a similar problem in the northwest part of the Green River Basin, Oriol (1961) pointed out that some detrital rocks do not fit the original descriptions of either formation. In the original definition, Hayden (1869, p. 90-91) applied the name Wasatch to variegated sandstone and claystone in which some shade of red predominated; he applied the name Green River to "thinly laminated chalky shales" which locally include "combustible or petroleum shales." He stressed the peculiarly banded appearance of the Green River rocks. In this area (fig. 1) some of the sequences of sandstone and claystone locally lack the red coloration typical of the Wasatch, yet do not have laminae typical of the Green River. Some subsequent usage of Hayden's names stressed genesis; that is, rocks of lacustrine origin were assigned to the Green River and rocks of fluvial origin were assigned to the Wasatch. As Oriol further noted, this criterion becomes impractical where the rocks consist of sandstone and mudstone of undetermined origin. In this paper the name Wasatch Formation is applied to the typical red variegated rocks and to the non-red lignite-bearing sandstone and claystone that are otherwise lithologically similar to the Wasatch beds. The name Green River Formation is applied only to strata that consist predominantly of laminated or thin-bedded marlstone, oil shale, and limestone.

The section at locality 5 (fig. 2) was measured on Pine Mountain from the top of the uppermost red bed up to the base of a thick oil-shale sequence that is here considered to be the Tipton Tongue of the Green River Formation. Bradley (1961; 1964, pl. 1) showed the Luman and Niland Tongues pinching out about 3 miles northeast of locality 5 (fig. 1), and southwestward from there he placed the base of the Tipton Tongue at the base of the beds equivalent to the Luman. According to my observations, the Luman and Niland Tongues extend as far west as locality 5, and are interpreted as having been continuous westward to locality 4 (fig. 2). At locality 5 the upper 220 feet is assigned to the Niland Tongue of the Wasatch, and the underlying 180 feet is assigned to the Luman Tongue of the Green River Formation. According to Love (1964, pl. 1), the Luman thickens eastward from Pine Mountain by interfingering with the overlying Niland Tongue, and replaces the Niland about 16 miles east of locality 5.

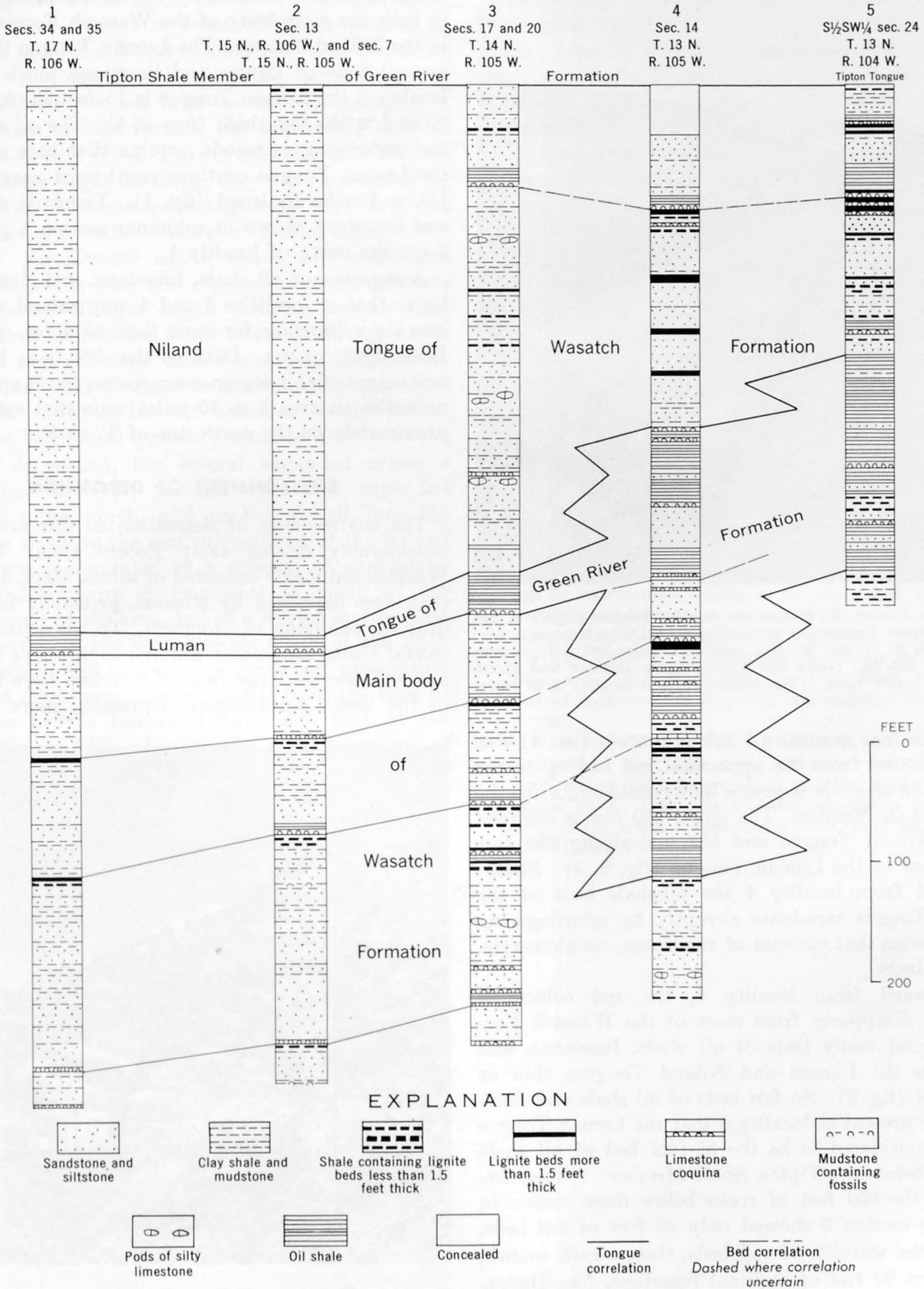


FIGURE 2.—Columnar sections showing tongues of the Wasatch and Green River Formations in the southeastern Green River Basin and on Pine Mountain, Wyo. Location of sections shown on figure 1.

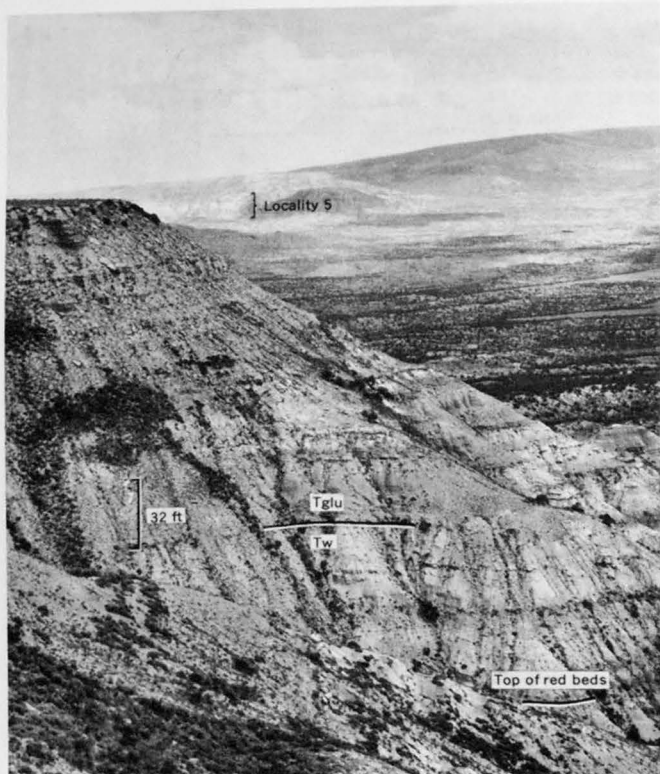


FIGURE 3.—Lower 190 feet of the Luman Tongue (Tglu) of the Green River Formation at locality 4 on Little Mountain, sec. 14, T. 13 N., R. 105 W. Top bench at upper left is limestone coquina 335 feet below the Tipton Shale Member and about 40 feet below road. Pine Mountain and locality 5 in background.

The 760-foot section on Little Mountain (loc. 4) was also measured from the uppermost red bed up to the base of the oil-shale sequence here considered to be the Tipton Shale Member. The upper 280 feet is assigned to the Niland Tongue and the underlying 380 feet is assigned to the Luman Tongue (fig. 2, 3). Southwestward from locality 4 the oil-shale beds of the Luman Tongue terminate abruptly by interfingering with a facies that consists of sandstone, conglomerate, and red beds.

Northward from locality 4, the red coloration abruptly disappears from most of the Wasatch Formation, and many beds of oil shale, limestone, and lignite in the Luman and Niland Tongues thin or pinch out (fig. 2). So few beds of oil shale and limestone are present at locality 3 that the Luman Tongue is here considered to be the 35-foot bed of oil shale 405 feet below the Tipton Shale Member. A measurement of the 600 feet of rocks below those shown in columnar section 3 showed only 20 feet of red beds. Despite the scarcity of red beds, these strata contain only about 20 feet of coquinal limestone, fossiliferous marlstones, or low-grade oil shale similar to the rocks in the Luman Tongue.

Northward from locality 3, red coloration appears in both the main body of the Wasatch Formation and in the Niland Tongue. The Luman Tongue thins, and several beds of lignite and limestone pinch out. At locality 2 the Luman Tongue is 15 feet thick, and the Niland is 455 feet thick (figs. 2, 4). The oil shale and the underlying ostracode coquina that here constitute the Luman Tongue continue northward nearly to the Union Pacific Railroad (fig. 1). The beds of lignite and limestone shown in columnar section 1 pinch out 5–6 miles north of locality 1.

A sequence of oil shale, limestone, and lignite similar to that at localities 3 and 4 may extend westward into the subsurface for more than 40 miles. (See also Love, 1964, pl. 1.) Data on the thickness, lithology, and extent of this sequence are sparse, but it apparently underlies an area 5 to 10 miles wide that centers approximately on the north line of T. 13 N.

### ENVIRONMENT OF DEPOSITION

The environment of deposition in this area varied considerably during early Eocene time. The first Wasatch sediments consisted of sands, clays, and muds that were deposited by streams, primarily in a well-drained, oxidizing environment. To the south the ancestral Uinta Mountains towered high above the area, and at intervals large fans of boulders were built out in the area. An elongate depression more than 40

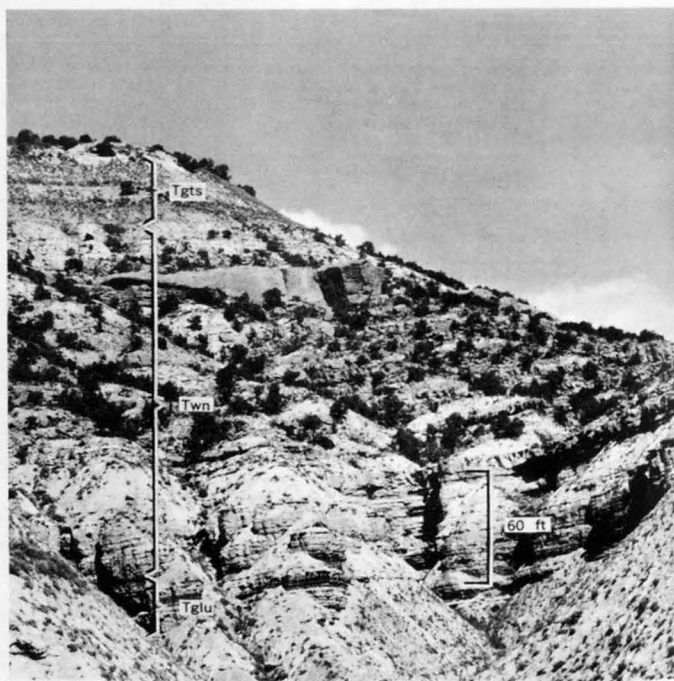


FIGURE 4.—The Luman Tongue (Tglu) and Tipton Shale Member (Tgts) of the Green River Formation and the Niland (Twn) Tongue of the Wasatch Formation at locality 2, north side of Sage Creek, NW ¼ sec. 13, T. 15 No., R. 105 W.

miles long and centering on the north line of T. 13 N. seems to have formed in front of the mountains at about this time. Sands, clays, and muds were deposited here, as elsewhere, but because the depression was poorly drained few red beds formed. Occasionally a small swamp or lake formed, but apparently each of these was quickly filled. During the late early Eocene, large swamps began to form; they were succeeded by a large lake. This abrupt change may have been due to the onset of a wetter climate or to more rapid downwarping. Fresh-water snails, clams, and ostracodes flourished in this lake, and deposition of the oil shale of the Luman Tongue began. During Luman time several lakes formed and, after intervals during which limestone and oil shale were deposited, disappeared. Swampy and fluvial conditions alternately prevailed during the intervals between episodes of lake formation. The lakes were probably confined chiefly to the elongate depression, but several expanded across a larger area for short periods. One lake expanded about 30 miles north, and probably well into the Washakie Basin to the east. Deposition of the Niland Tongue was inaugurated by a renewal of alternating fluvial and swampy environments in much of the southern part of the area, and of a fluvial environment in the north. In the area directly south of the Rock Springs uplift the lacustrine environment presumably continued on, almost uninterrupted, from the time of deposition of the Luman Tongue into that of the Tipton Tongue. Elsewhere in this area, deposition of the Niland Tongue was terminated by the growth of the large, stable Tipton lake, which eventually covered many thousands of square miles in the three-basin area (fig. 1).

Descriptions of the Luman and Niland Tongues by Pipiringos (1961) and Bradley (1964) indicate that a similar sequence of events also occurred at about the same time in the Washakie and Great Divide Basins. Whether the lakes in those basins were connected across or around the ancestral Rock Springs uplift with those in the southeastern Green River Basin is not known, but some of them may well have been. It is unlikely that any lakes extended into the northeastern Green River Basin, however, because no lake beds have been reported from the upper part of the Wasatch in that area.

#### REFERENCES

- Bradley, W. H., 1961, Geologic map of a part of southwestern Wyoming and adjacent states: U.S. Geol. Survey Misc. Geol. Inv. Map I-332.
- 1964, Geology of Green River Formation and associated Eocene rocks in southwestern Wyoming and adjacent parts of Colorado and Utah: U.S. Geol. Survey Prof. Paper 496-A, 86 p. [1965]
- Havden, F. V., 1869, Preliminary field report [3d ann.] of the U.S. Geological Survey of Colorado and New Mexico: Washington, Government Printing Office, 155 p.
- Love, J. D., 1964, Uraniferous phosphatic lake beds of Eocene age in intermontane basins of Wyoming and Utah: U.S. Geol. Survey Prof. Paper 474-E, 66 p.
- McGrew, P. O., and Roehler, H. W., 1960, Correlation of Tertiary units in southwestern Wyoming, *in* Wyoming Geol. Assoc. Guidebook 15th Ann. Field Conf., Overthrust belt of southwestern Wyoming and adjacent areas, 1960: p. 156.
- Oriel, S. S., 1961, Tongues of the Wasatch and Green River Formations, Fort Hill area, Wyoming: Art. 63 *in* U.S. Geol. Survey Prof. Paper 424-B, p. B151-B152.
- Pipiringos, G. N., 1961, Uranium-bearing coal in the central part of the Great Divide Basin: U.S. Geol. Survey Bull. 1099-A, 104 p.



## POSSIBLE BURIED MINERALIZED AREAS IN NYE AND ESERALDA COUNTIES, NEVADA

By R. E. ANDERSON, E. B. EKREN, and D. L. HEALEY,  
Denver, Colo.

*Work done in cooperation with the U.S. Atomic Energy Commission*

**Abstract.**—Recent geologic reconnaissance in the vicinity of Goldfield, Nev., has revealed the widespread occurrence of an upper Tertiary (Pliocene) ash-flow tuff sheet, the Thirsty Canyon Tuff, laid down on an erosional surface of considerable relief. Several topographically high areas that were not covered by the tuff sheet commonly contain hydrothermally altered and mineralized rock. At three localities adjacent to these areas it is likely that gold- and silver-bearing rock extends beneath, or lies in separate bodies beneath, the tuff or overlying alluvium. One of these localities is inferred from a gravity anomaly in Stonewall Flat.

Recent geologic reconnaissance in the vicinity of Goldfield, Nev., has revealed the widespread occurrence of an upper Tertiary (Pliocene) ash-flow tuff sheet called the Thirsty Canyon Tuff (Noble and others, 1964). At Goldfield the Spearhead Member (formerly called Spearhead Formation by Ransome, 1909, p. 71) of the Thirsty Canyon Tuff (Noble and others, 1964) is clearly younger than the gold- and silver-bearing veins and the major faulting of the area. Ransome (1909, p. 175) first recognized these relations, and later Searls (1948, p. 13) suggested that there may be ore under these younger strata.

### DISTRIBUTION OF THE THIRSTY CANYON TUFF

The Thirsty Canyon Tuff was deposited in low areas on an erosional surface of considerable topographic relief. Topographically high areas (fig. 1) such as the hills around Goldfield, the Cactus Range, Stonewall Mountain, Mount Helen, and the hills around Gold Crater, were not covered by the Thirsty Canyon Tuff. These areas of pre-Thirsty Canyon rocks contain the gold and silver deposits of the famous Goldfield district, as well as smaller deposits at Gold Crater, east of Gold Crater, and local areas along the western margin of the Cactus Range. At Goldfield, Gold Crater,

and east of Gold Crater the mineralized terrane abuts unmineralized Thirsty Canyon Tuff, but the Cactus Range is flanked on the west by Quaternary alluvium and colluvium through which the thinning margin of the sheet of Thirsty Canyon Tuff protrudes only locally. In a few places along the western margin of the Cactus Range unaltered Thirsty Canyon Tuff rests on hydrothermally altered Tertiary rocks. In most areas adjacent to the Cactus Range the surficial material, deposited on a gently sloping pediment surface, thickens gradually toward Stonewall Flat. If a concealed range-front fault (fig. 1) inferred from gravity data exists, an abrupt thickening of alluvium can be expected on the downthrown side, away from the Cactus Range. The Thirsty Canyon Tuff is probably buried by the Quaternary deposits throughout much of this area, as is inferred in figures 1 and 2.

It seems probable that the Thirsty Canyon Tuff and Quaternary surficial deposits conceal ore deposits that are extensions of known ore deposits and possibly also some totally separate, hitherto-unknown, ore deposits.

The Thirsty Canyon Tuff crops out discontinuously within an oval-shaped area that extends in a north-west direction from a point about 20 miles northeast of Beatty, Nev., to a point 7 miles north of Goldfield (fig. 2). The actual shape of the area of outcrop is not apparent in figure 2, as the patterned area on the figure shows both the outcrop and the inferred subsurface extent of the tuff. Geologic mapping in the northern half of the outcrop area (fig. 1) has shown that the Thirsty Canyon Tuff rests unconformably on Tertiary volcanic rocks and related intrusive rocks which are in part equivalent in age and rock type to the ore-bearing rocks in the Goldfield mining district.

## POTENTIAL GUIDES TO ORE

Geologic conditions that suggest favorable ground for buried mineral deposits can be inferred from the geologic environment in the Goldfield and Tonopah, Nev., mining districts. Ore in the Tonopah district, 26 miles north of Goldfield, has a gold-silver ratio of 1:100, and ore in the Goldfield district has a ratio of 3:1 (Bateman, 1950, p. 430, 459). Both areas are sites of extensive Tertiary intrusive and volcanic activity (Ransome, 1909; Nolan, 1935) and contain fault-controlled ore bodies and shoots that are modified locally by supergene processes. Replacement deposits in lava flows ranging in composition from rhyolite to andesite predominate at Tonopah, whereas most of the ore deposits at Goldfield are fissure fillings in andesite and dacite flows. Hypabyssal Tertiary intrusive bodies occur at both districts but are not considered to be the source of the mineralizing solutions. Alunitic alteration appears to be spatially and genetically related to ore deposition at Goldfield. Harvey and Vitaliano (1964) studied the wallrock alteration in the Goldfield district and found three principal zones of alteration. From the vein outward they are: (1) an alunite-quartz zone, (2) an argillic zone, which includes an illite-kaolinite subzone adjacent to the alunite-quartz zone and a montmorillonite subzone outward, and (3) a propylitic zone. In the Tonopah district, Nolan (1935, p. 11) recognized a central alteration zone characterized by a quartz-adularia-sericite mineral assemblage and a widespread chlorite-carbonate zone away from the central zone. These zones are superimposed on an earlier stage of wholesale albitization. Nolan's widespread chlorite-carbonate zone can be considered equivalent to a propylitic zone.

In the report area, the hydrothermally altered rocks in the Cactus Range and south of the Cactus Range (fig. 2) are all quite similar to altered rocks in the Tonopah and Goldfield districts. Mineralized veins (1) are fracture controlled in Tertiary igneous rocks; (2) show a preference for rocks of intermediate composition; (3) are accompanied by assemblages of secondary quartz, sericite, alunite, and kaolinite in various combinations, and (4) occur in terrane that is pervasively propylitized. The country rock adjacent to mineralized veins is generally bleached to pale pastel colors, is weakly pyritized, and locally intensely silicified. The primary mafic minerals and feldspars have commonly been replaced by secondary minerals.

## SUGGESTED AREAS FOR MINERAL EXPLORATION

On the basis of the foregoing observations and comparisons it is assumed that the search for concealed

mineral deposits in the Cactus Range and in the area south of the range should first be directed to areas adjacent to faulted terrane where flow rocks of intermediate composition and hypabyssal intrusive rocks are known or believed to occur. Three such areas in the mapped area are: (1) the east side of Stonewall Flat, (2) the area between Stonewall Mountain and Mount Helen, and (3) Stonewall Flat north of Stonewall Mountain.

The suggestion of a favorable area for buried mineral deposits on the east side of Stonewall Flat is based on (1) widespread occurrence of hydrothermally altered rock in the Cactus Range, which borders Stonewall Flat on the east, (2) occurrence of abundant large intrusive masses in the Cactus Range, and (3) the fact that the most productive mines along the range front are located at the margin of the valley alluvium and appear to have produced ore from faults in tuff.

The intrusive masses in the Cactus Range include several stocks and approximately 75 dikes and plugs ranging in composition from diorite to granite. These bodies are commonly bounded by faults that trend northwest and west; several have rather flat-lying roofs of ash-flow tuff and related tuffaceous sedimentary rocks. The country rock adjacent to the intrusive masses commonly is extensively altered, and in some places the intrusive masses themselves are pervasively altered. As an example, a quartz latite porphyry intrusive mass is eroded to a depth of about 400 feet along the road that leads from Cactus Spring to Goldfield (fig. 1). The intrusive mass contains horizontal zones of altered rocks. The lowest exposed zone contains propylitically altered rock in which biotite is chloritized and plagioclase is partially altered to albite, calcite, and sericite; alkali feldspar is largely unaffected. This rock grades upward through a zone of more intense argillic alteration in which plagioclase is completely altered and alkali feldspar is partially sericitized, leaving quartz as the only unaffected mineral. The uppermost zone is composed of intensely silicified quartz-sericitic rock that contains alunite and jarosite as determined by X-ray analysis. Locally the upper zone passes into the country rock of rhyolitic welded tuff, which commonly shows a reverse pattern of zoning away from the contact. The zones in the intrusive mass display color variations ranging from green gray and light brown upward through buff and pale orange to light gray in the intensely silicified rock. Where the quartz latite porphyry is unaltered in the northern part of the range it is medium gray and distinctly porphyritic.

Preliminary X-ray studies of altered rocks from several fault zones in the Cactus Range show sericitic



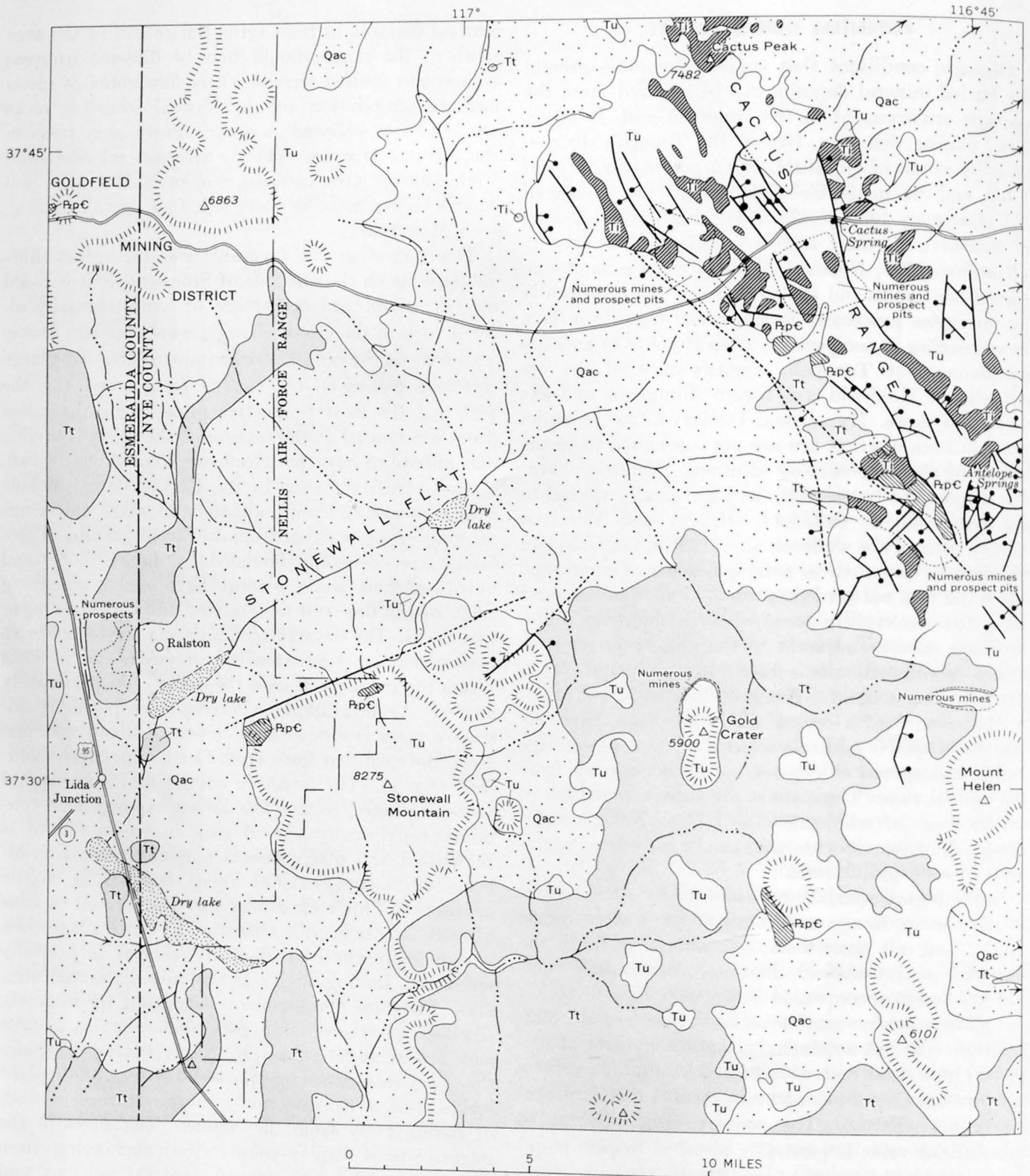


FIGURE 1.—Generalized geologic map of the Stonewall Mountain area, Nevada. Datum is mean sea level.

alteration and local development of jarosite and alunite. Silicified and kaolinized areas are also common. Most of the rocks in the Cactus Range show, in addition to fault-controlled hydrothermal alteration, the effects of pervasive propylitic alteration. This type of alteration results in partial or total alteration of plagioclase to albite, biotite to chlorite, and partial replacement of both phenocrysts and groundmass by carbonate (generally calcite), epidote, sericite, and magnetite.

It is not known to what distance the intrusive rocks or the hydrothermally altered rocks extend west of the Cactus Range beneath the Thirsty Canyon Tuff and superficial deposits, but the eastern part of Stonewall Flat appears favorable for the occurrence of altered and possibly mineralized rocks beneath the Thirsty Canyon Tuff and alluvium.

A second area of buried altered rocks seems likely under the Thirsty Canyon Tuff between Stonewall Mountain and Mount Helen and north of Mount Helen where isolated patches of altered Tertiary rhyolites, intermediate flow rocks, and tuffs are surrounded by the unaltered Thirsty Canyon Tuff (fig. 1). The general surface geology of the altered strata in this area is somewhat similar to the surface geology in the Goldfield area as described by Ransome (1909). Observations made at several abandoned mines and prospect pits indicate that the sulfide mineralization showed an affinity for hydrothermally altered rocks of intermediate composition. The area is characterized by

ridges of gray to red-gray dense silicified rocks that are bounded by valleys formed in light-gray, pink, and tan intensely argillized rock. Silicified and argillized rocks both contain pyrite and chalcocopyrite. The intensely altered areas about the Thirsty Canyon Tuff in numerous places and probably extend beneath the tuff.

The third possibly mineralized area is in Stonewall Flat north of Stonewall Mountain. The favorable location for prospecting in this area is delimited by a gravity high located about 12 miles southeast of the Goldfield mining district (fig. 3). Because of the alluvial cover this area has never been prospected. Thirsty Canyon Tuff probably extends beneath Quaternary alluvium and colluvium in Stonewall Flat, as inferred in figure 2.

A gravity high is located over the Goldfield mining district as well as over the smaller mining districts at Gold Crater, the Cactus Range, and south of the Cactus Range. Gravity lows are situated over the northeast part of Stonewall Mountain and Mount Helen, and neither of these areas contain known ore deposits. However, the presence of a gravity high is in itself no indication of the presence of ore. It can and commonly does reflect the thinning of relatively low density post-Mesozoic rocks over pre-Tertiary rocks of high density, or the juxtapositioning of rocks of these contrasting densities by faulting. Thus, the gravity high over the Goldfield district is in part at least the expression of a structural dome that brings pre-Tertiary rocks to the surface (Ransome, 1909, p. 76), and the gravity high over the Cactus Range is partly an expression of a northwest-trending raised structural block that also brings pre-Tertiary rocks to the surface. However, Tertiary lavas and intrusive masses of intermediate composition and propylitized tuffs have an average density greater than that of unaltered rhyolite and tuff (unpublished data, U.S. Geological Survey files, Denver, Colo.) and areas underlain by the former rocks can produce gravity highs. Part of each of the relative gravity highs within figure 3 is probably caused by density contrasts of this type.

The gravity high in Stonewall flat is located along a chain of gravity highs which together form a ridge extending from the Goldfield district southeast to the southeast corner of the map area (fig. 3).

A north-dipping fault scarp and a broad zone of fractured and altered rock on the north flank of Stonewall Mountain, and a broad zone of faulted and altered rock along the west side of the Cactus Range, together with steep gravity gradients in both areas, suggest that Stonewall Flat is in large part a structural basin. The Tertiary tuffs and flows that flank the southeast

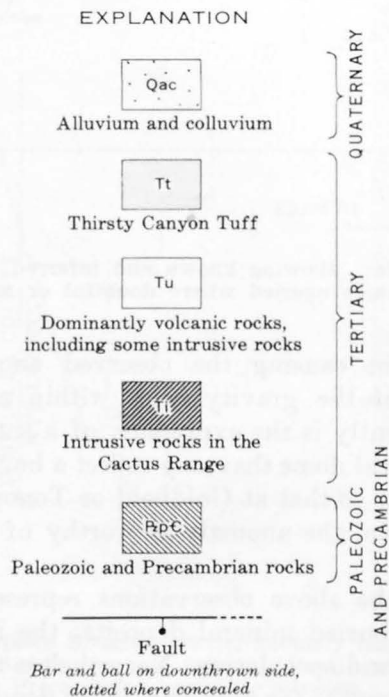


FIGURE 1.—EXPLANATION.

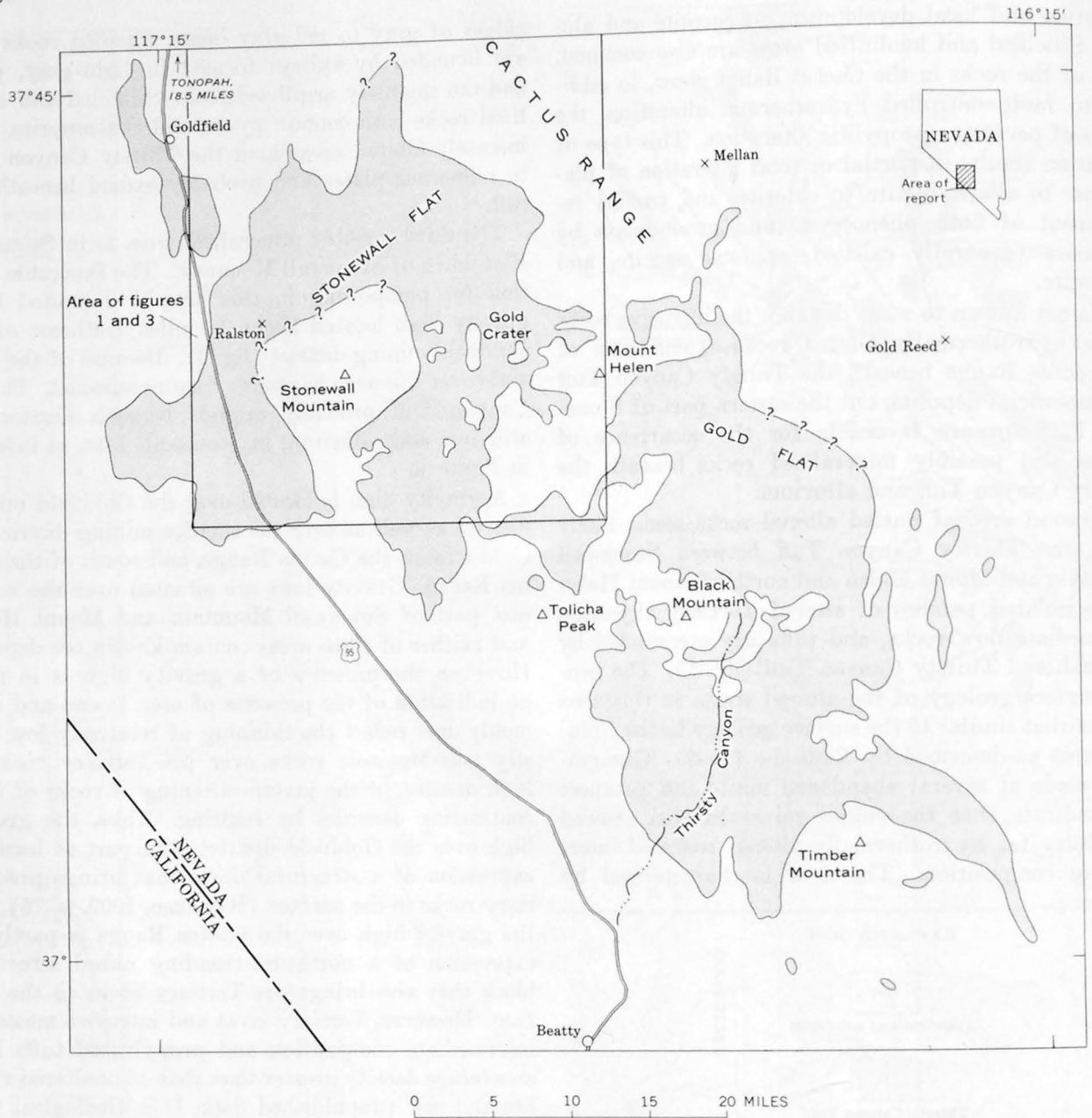


FIGURE 2.—Generalized map of parts of Nye and Esmeralda Counties, Nev., showing known and inferred surface and subsurface extent of Thirsty Canyon Tuff (patterned area). Contacts queried where doubtful or inferred. Area outside of figures 1 and 3 from Noble and others (1964).

side of the Goldfield district, to the northwest of Stonewall Flat, dip to the southeast and are unmineralized. If these dips are projected into Stonewall Flat one would expect a thickness of several thousand feet of Quaternary fill in the area where we see the gravity high; however, depth calculations based on an aeromagnetic survey over the Nellis Air Force Range indicate a depth of only 300 to 500 feet to the top of the rock causing this anomaly (G. W. Bath, written communication, 1964). Thus, the surface geology of the areas surrounding Stonewall Flat offers no clues either to the presence of a structural high or to the rock type

that could be causing the observed anomaly. The occurrence of the gravity high within a structural basin apparently is the expression of a somewhat isolated structural dome that may reflect a buried volcanic center similar to that at Goldfield or Tonopah. Whatever its origin, the anomaly is worthy of further investigation.

None of the above observations represent positive evidence of buried mineral deposits; the implications are tenuous and speculative. Nevertheless the area has sufficient potential for gold and silver deposits to warrant exploration by geophysical and geochemical meth-

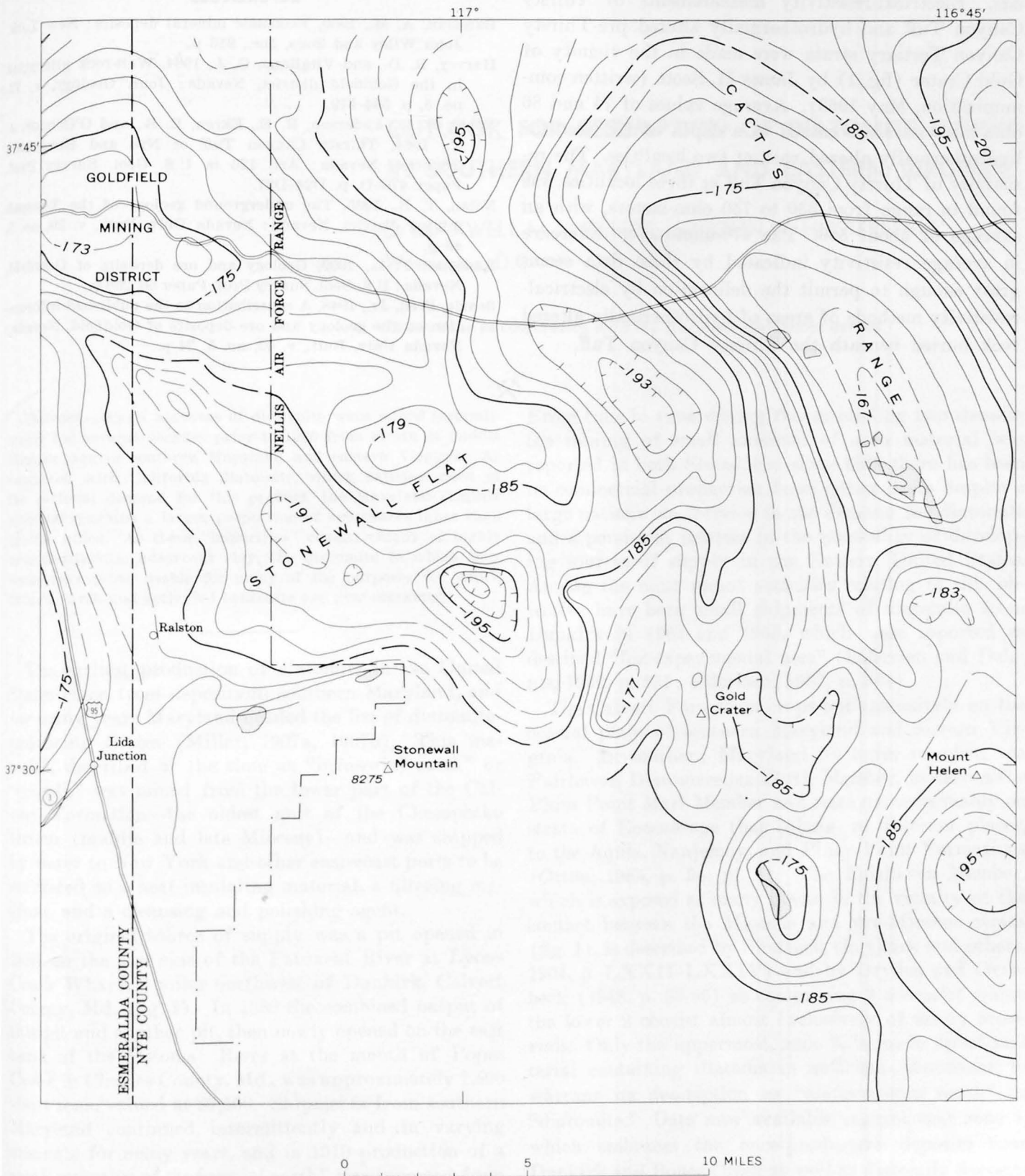


FIGURE 3.—Complete Bouguer gravity-anomaly map of Stonewall Flat and adjacent area, Nevada. Gravity contours dashed where approximate, contour interval 2 milligals; all numbers are negative. Gravity-low areas are hachured, and areas of Paleozoic and Precambrian rocks are stippled.

ods. Electrical-resistivity measurements of Thirsty Canyon Tuff and hydrothermally altered pre-Thirsty Canyon Tertiary strata were made in the vicinity of Gold Crater (fig. 1) by James H. Scott (written communication, May 1963). Average values of 74 and 86 ohm-meters were obtained to a depth of 200 feet for hydrothermally altered rock at two localities. The resistivity of Thirsty Canyon Tuff at three localities was found to range from 330 to 750 ohm-meters, with an average of about 550. The 470-ohm-meter difference in average resistivity indicated by these data seems great enough to permit the delineation by electrical-resistivity methods of areas of hydrothermally altered rock buried beneath the Thirsty Canyon Tuff.

## REFERENCES

- Bateman, A. M., 1950, *Economic mineral deposits*: New York, John Wiley and Sons, Inc., 916 p.
- Harvey, R. D., and Vitaliano, C. J., 1964, Wall-rock alteration in the Goldfield district, Nevada: *Jour. Geology*, v. 72, no. 5, p. 564-579.
- Noble, D. C., Anderson, R. E., Ekren, E. B., and O'Connor, J. T., 1964, Thirsty Canyon Tuff of Nye and Esmeralda Counties, Nevada: Art. 126 in *U.S. Geol. Survey Prof. Paper 475-D*, p. D24-D27.
- Nolan, T. B., 1935, The underground geology of the Tonopah mining district, Nevada: *Nevada Univ. Bull.*, v. 29, no. 5, 49 p.
- Ransome, F. L., 1909, *Geology and ore deposits of Goldfield, Nevada*: U.S. Geol. Survey Prof. Paper 66, 258 p.
- Searls, Fred, Jr., 1948, A contribution to the published information on the geology and ore deposits of Goldfield, Nevada: *Nevada Univ. Bull.*, v. 42, no. 5, 24 p.



## OUTLOOK FOR RESUMPTION OF DIATOMITE MINING IN SOUTHERN MARYLAND AND EASTERN VIRGINIA

By MAXWELL M. KNECHTEL and JOHN W. HOSTERMAN,  
Washington, D.C.

*Work done in cooperation with the Maryland Geological Survey*

*Abstract.*—Small amounts of diatomite were mined intermittently for several decades prior to 1930 from strata of middle Miocene age in southern Maryland and eastern Virginia. As compared with California diatomite, which satisfies most of the national demand for this product, the Maryland-Virginia material contains a larger proportion of substances other than opaline silica. As these "impurities" consist chiefly of highly montmorillonitic adsorbent clay, the diatomite in which they occur may prove usable for many of the purposes for which fuller's earth and activated bentonite are now marketed.

The earliest production of diatomite in the United States came from deposits in southern Maryland, and for many years Maryland headed the list of diatomite-producing States (Miller, 1907a, 1907b). This material, described at the time as "infusorial earth" or "tripoli," was mined from the lower part of the Calvert Formation—the oldest unit of the Chesapeake Group (middle and late Miocene)—and was shipped by water to New York and other east-coast ports to be marketed as a heat-insulating material, a filtering medium, and a cleansing and polishing agent.

The original source of supply was a pit opened in 1884 on the east side of the Patuxent River at Lyons Creek Wharf, 2 miles northwest of Dunkirk, Calvert County, Md. (fig. 1). In 1888 the combined output of this pit and another pit, then newly opened on the east bank of the Potomac River at the mouth of Popes Creek in Charles County, Md., was approximately 1,500 short tons, valued at \$7,500. Shipments from southern Maryland continued intermittently and in varying amounts for many years, and in 1910 production of a small quantity of "infusorial earth" was reported from stratigraphically equivalent deposits in Virginia.

From time to time during the succeeding two decades the mining of small amounts of such material was reported in both States, but since 1930 there has been no commercial production from either State despite a large nationwide increase in the demand for diatomite and a persistent interest in the possibility of developing sources of supply in the Eastern United States. Among the most recent activities relating to this objective have been small shipments of diatomite from Dunkirk in 1962 and 1963, which were reported as destined "for experimental uses" (Eilertsen and Dzienis, 1962, p. 531; Eilertsen, 1963, p. 534).

The Calvert Formation crops out extensively on the coastal plain of southern Maryland and eastern Virginia. In southern Maryland its lower member, the Fairhaven Diatomaceous Earth Member, underlies the Plum Point Marl Member and rests unconformably on strata of Eocene age that belong, in different places, to the Aquia, Nanjemoy, and Piney Point Formations (Otton, 1955, p. 94, pl. 1). The Fairhaven Member, which is exposed at many places in the vicinity of the contact between the Miocene and pre-Miocene strata (fig. 1), is described by Shattuck (in Clark and others, 1904, p. LXXII-LXXIV) and by Dryden and Overbeck (1948, p. 53-56) as comprising 3 zones, of which the lower 2 consist almost exclusively of sandy materials. Only the uppermost, zone 3, is made up of material containing diatoms in sufficient abundance to warrant its description as "diatomaceous earth" or "diatomite." Data now available suggest that zone 3, which embraces the once-productive deposits near Dunkirk and Popes Creek as well as diatomite deposits at and near the surface at many other sites in southern

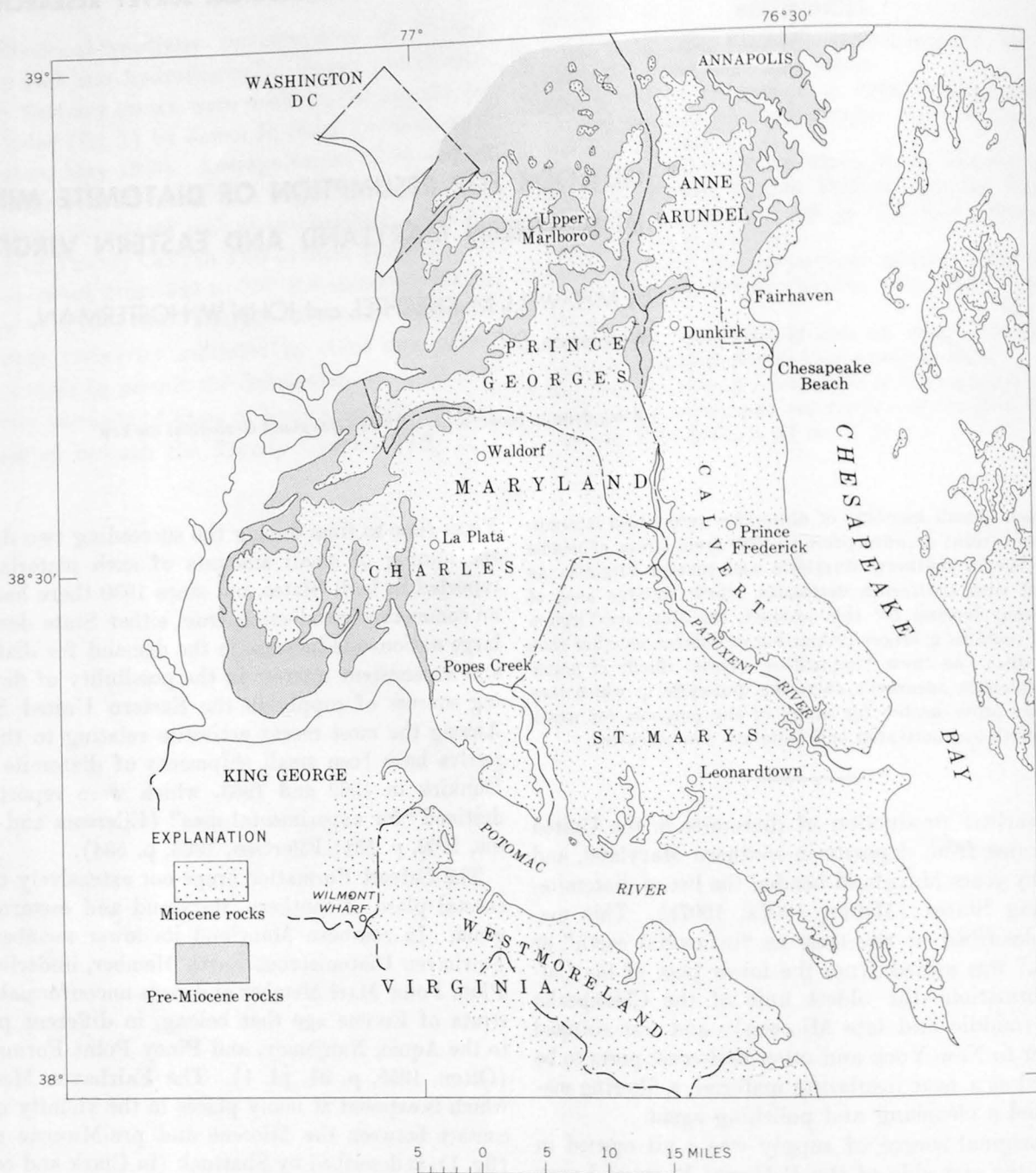


FIGURE 1.—Map showing areas in southern Maryland underlain by rocks of Miocene age (Chesapeake Group). Adapted from map by Shattuck (Clark and others, 1904, pl. 1).

Maryland and in Virginia, can still be considered a potential source of large supplies.

Though diatomite has been mined at only a few places in southern Maryland and eastern Virginia, closely comparable material is believed to be present in the Fairhaven Member throughout the large areas in which strata of the Miocene Series crop out (fig. 1). At many sites in the vicinity of the long, sinuous line of contact of the Miocene Series with older strata, and

in the outliers of that series near Upper Marlboro, such material is present at the surface or beneath overburden sufficiently thin to make strip mining possible. Farther southeastward, owing to the regional dip of the formations, the overburden is everywhere excessive.

The thickness of zone 3 is everywhere considerable, although much less than that of the vast deposits of late Miocene age from which large tonnages of diat-

omite are mined annually in the Lompoc district, Santa Barbara County, Calif. Shattuck (*in Clark and others, 1904, p. LXXXVI*) reported 60 feet of the material of zone 3 in the cliffs along the Chesapeake Bay shore at Fairhaven, Anne Arundel County, Md., and (p. LXXIV) 55 feet at Chesapeake Beach, Calvert County, Md. According to Dryden and Overbeck (1948, p. 54), zone 3 is 14 feet thick at Hollin Cliff, 8 miles southwest of Dunkirk, Calvert County; 8½ feet at Ferry Landing, 2 miles southwest of Dunkirk; 17 feet at Popes Creek, Charles County, Md.; 10 feet near Wilmot Landing [Wilmont Wharf], Va., on the north bank of the Rappahannock River, 2½ miles south of Rollins Fork, King George County, Va.; and (Dryden and Overbeck, 1948, p. 108) 60 feet in a well at Waldorf, Charles County, Md., wherein the top of zone 3 is reported to be 100 feet below the surface.

Specimens of the material of zone 3 are described by Shattuck (*in Clark and others, 1904, p. LXXIV*) as "very rich in diatomaceous matter, yielding more than 50 percent of diatoms" when analyzed mechanically. As exemplified in the chemical analyses in the accompanying table, however, the Maryland material contains insufficient silica and too much alumina to compare favorably, according to present standards, with diatomites typical of the California deposits.

*Analyses, in weight percent, of marine diatomite of Miocene age from deposits in Maryland and in California*

	Maryland <sup>1</sup>	California <sup>2</sup>
SiO <sub>2</sub> .....	79.55	89.70
Al <sub>2</sub> O <sub>3</sub> .....	8.18	3.72
Fe <sub>2</sub> O <sub>3</sub> .....	2.62	1.09
MgO.....	1.30	.65
CaO.....	.25	.35
Na <sub>2</sub> O+K <sub>2</sub> O.....	1.31	.82
TiO <sub>2</sub> .....	.70	.10
Ignition loss.....	5.80	3.70
	99.71	100.13

<sup>1</sup> Sample from zone 3, Fairhaven Member of the Calvert Formation (Cummins and Mulryan, 1949, p. 295).

<sup>2</sup> Sample from the Monterey Formation, Lompoc, Calif. (Cressman, 1962, p. T6).

The ratio of clay-sized (<2μ) particles to larger grains is approximately 3:1 in a specimen of dark-greenish-gray diatomite obtained in 1959 from the cliffs at Fairhaven. The coarser fraction is made up almost wholly of the opaline silica tests of diatoms, more than half of which are of sand-grain size (>61μ). The rest of this fraction, consisting of silt-sized (<61μ) particles, is made up of smaller diatoms, fragments of diatoms, and a little quartz and other detrital minerals. The clay, as determined by X-ray

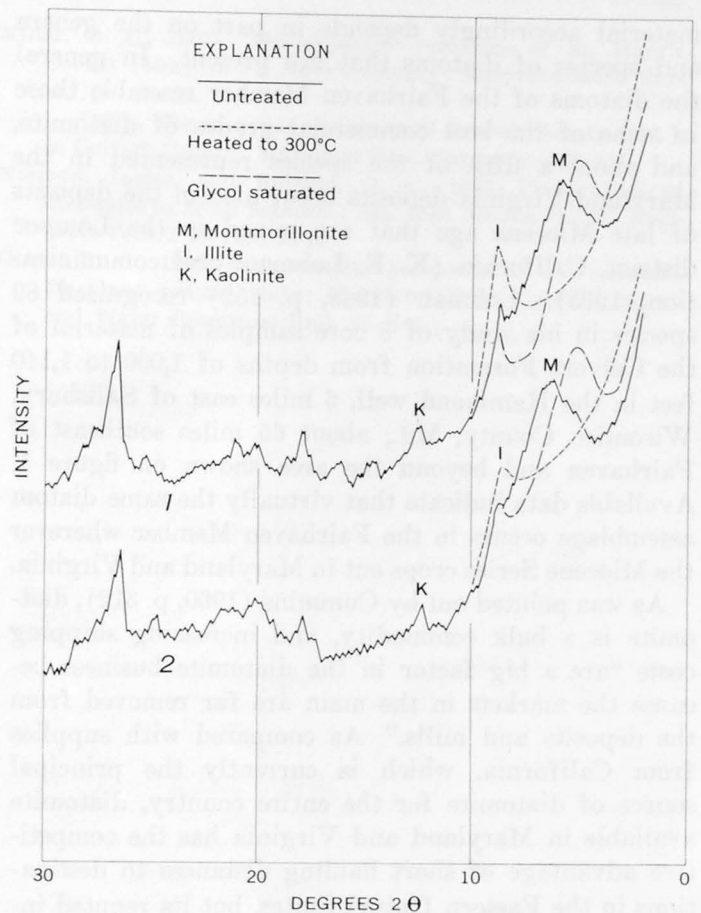


FIGURE 2.—X-ray diffraction traces (CuKα radiation) of clay fractions of diatomite from the Fairhaven Diatomaceous Earth Member of the Calvert Formation (middle Miocene) as exposed in 2 localities: (1) Fairhaven, Anne Arundel County, Md.; and (2) near Ferry Landing, 2 miles southwest of Dunkirk, Calvert County, Md.

diffraction analysis (fig. 2, locality 1), consists chiefly of montmorillonite but includes approximately 15 percent illite and 10 percent kaolinite. Weathered whitish material from a point a few feet away contains virtually the same mineral assemblage plus a small amount of isotropic glass. The approximate bulk density of the unweathered material when dry is 40 pounds per cubic foot; that of the weathered material is 25 pounds per cubic foot. Five specimens of diatomite from an exposure of the Fairhaven Member near Ferry Landing, 2 miles southwest of Dunkirk, Md., including the specimen for which the X-ray diffraction trace of the clay fraction is given in figure 2, were found to have similar grain sizes and mineral content.

Not only the sizes but also the shapes of the opaline silica particles contained in a crude diatomite determine to a large extent some of the uses for which it may be processed and marketed. Evaluation of such



material accordingly depends in part on the genera and species of diatoms that are present. In general the diatoms of the Fairhaven Member resemble those in some of the best commercial grades of diatomite, and about a fifth of the species represented in the Maryland-Virginia deposits occur also in the deposits of late Miocene age that are mined in the Lompoc district, California (K. E. Lohman, oral communication, 1965). Lohman (1948, p. 152) recognized 89 species in his study of 8 core samples of material of the Calvert Formation from depths of 1,000 to 1,140 feet in the Hammond well, 6 miles east of Salisbury, Wicomico County, Md., about 65 miles southeast of Fairhaven and beyond the area shown on figure 1. Available data indicate that virtually the same diatom assemblage occurs in the Fairhaven Member wherever the Miocene Series crops out in Maryland and Virginia.

As was pointed out by Cummins (1960, p. 312), diatomite is a bulk commodity, and increasing shipping costs "are a big factor in the diatomite business because the markets in the main are far removed from the deposits and mills." As compared with supplies from California, which is currently the principal source of diatomite for the entire country, diatomite available in Maryland and Virginia has the competitive advantage of short hauling distances to destinations in the Eastern United States, but its reputed inferior quality, due to its high content of substances other than the opaline silica of diatom tests, has heretofore nullified this advantage. The outlook for resumption of diatomite mining in Maryland and Virginia may nevertheless be expected to improve with further increases in shipping costs and in the demand for diatomaceous materials. Such a result might be hastened by technologic advances, such as the discovery of uses for the diatomaceous material in unbeneficiated form, or the development of economical processes for its beneficiation and of profitable uses for any recoverable byproducts of such processes. Results of tests conducted by the Boone Wood Products Co. of Baltimore in a pilot plant set up in 1961 at Ferry Landing, 2 miles southwest of Dunkirk, suggested that the diatomite is suitable, after being calcined, for preparation of a sweeping powder of a type now used to absorb oil or oil-water mixtures from floors and decks made of concrete, wood, or steel. These experimental results indicate that clay which is present in relatively large amounts in the diatomite and which heretofore has been considered objectionable has adsorptive power generally comparable to that of fuller's earth

and activated bentonite, which are marketed for sweeping materials in large quantities annually.

The feasibility of beneficiating diatomites containing large amounts of clay and sand as impurities was studied, beginning in 1937, in the laboratories of the U.S. Bureau of Mines at College Park, Md. (Norman and Ralston, 1940). After much experimentation with diatomites from Maryland, California, Oregon, and Kansas, a pilot plant was set up at Lyons Creek Wharf, Md., 2 miles northwest of Dunkirk, Md., and several tons of a concentrate rich in diatoms was prepared, using raw material taken from nearby exposures of the Fairhaven Member. It is noteworthy that this material contained considerable sand which had to be removed, whereas 4 of 5 samples that we obtained from the Kaylorite Corp. open pit near Ferry Landing, as well as 2 samples from the cliffs at Fairhaven, contain no grains, other than diatom tests, that are larger than silt particles. Steps in the concentration process were: (1) removal of sand from an aqueous slurry of the raw material; (2) attrition milling to break down clay particles; (3) settling, whereby a slurry containing diatoms and clay was separated from clay left in suspension; and (4) froth flotation to eliminate most of the remaining clay in the diatomaceous slurry. Notwithstanding the demonstrated effectiveness of this process, however, its practical application would presumably involve substantial costs. We accordingly suggest that in efforts to revive the diatomite mining industry of Maryland and Virginia, emphasis be placed on finding uses for the crude diatomaceous material. One property of the crude diatomite that should be especially considered in seeking new uses is the adsorptive power of the large content of montmorillonitic clay.

#### REFERENCES

- Clark, W. B., Shattuck, G. B., and Dall, W. H., 1904, The Miocene deposits of Maryland, in *Maryland Geological Survey, Miocene* [volume]: p. I-CLV.
- Cressman, E. R., 1962, Nondetrital siliceous sediments: U.S. Geol. Survey Prof. Paper 440-T, 23 p.
- Cummins, A. B., 1960, Diatomite, in *Industrial minerals and rocks (nonmetallics other than fuels)*, 3d ed.: New York, Am. Inst. Mining Metall. and Petroleum Engineers, p. 303-319.
- Cummins, A. B., and Mulryan, Henry, 1949, Diatomite, in *Industrial minerals and rocks*: New York, Am. Inst. Mining and Metall. Engineers, p. 294-312.
- Dryden, L., and Overbeck, R. M., 1948, Detailed geology, in *The physical features of Charles County [Md.]*: Maryland

- Dept. Geology, Mines and Water Resources [Rept. 13], p. 29-127.
- Ellertsen, N. A., 1964, The mineral industry of Maryland, in U.S. Bureau Mines, Minerals Yearbook, 1963, v. 3: p. 527-538.
- Ellertsen, N. A., and Dzienis, S. A., 1963, The mineral industry of Maryland, in U.S. Bureau Mines, Minerals Yearbook, 1962, v. 3: p. 525-534.
- Lohman, K. E., 1948, Middle Miocene diatoms from the Hammond well: Maryland Dept. Geology, Mines and Water Resources Bull. 2, p. 151-187, pls. VI-XI.
- Miller, B. L., 1907a, The economic resources of St. Mary's County [Md.], in St. Mary's County: Maryland Geol. Survey, p. 113-124.
- 1907b, The economic resources of Calvert County [Md.], in Calvert County: Maryland Geol. Survey, p. 123-134.
- Norman, James, and Ralston, O. C., 1940, Purification of diatomite by froth flotation: Am. Inst. Mining Metall. Engineers Tech. Pub. 1198, 11 p.
- Otton, E. G., 1955, Ground-water resources of the southern Maryland coastal plain: Maryland Dept. Geology, Mines and Water Resources Bull. 15, 347 p.



## EVALUATION OF THE MARTINSBURG SHALE AND TWO YOUNGER FORMATIONS AS SOURCES OF LIGHTWEIGHT AGGREGATE IN THE DELAWARE RIVER AREA, PENNSYLVANIA-NEW JERSEY

By AVERY ALA DRAKE, JR., M. V. DENNY,<sup>1</sup> and HOWARD P. HAMLIN,<sup>1 2</sup>

Washington, D.C.; Norris, Tenn.

*Work done in cooperation with the U.S. Bureau of Mines*

*Abstract.*—Five samples of slate from different stratigraphic intervals within the Martinsburg Shale and one sample each from the New Scotland Limestone and the Esopus Shale were tested as potential raw materials for production of bloated rotary-kiln-fired lightweight aggregate. The expanded products that formed in the muffle-kiln and rotary-kiln firing tests of the Martinsburg material were found to compare favorably with selected commercial lightweight aggregates. Muffle-kiln firing of shale from the New Scotland Limestone and the Esopus Shale, however, failed to cause it to expand notably, and consequently resulted in products too heavy to be usable as lightweight aggregate.

In a regional geologic study near the Delaware River in western New Jersey and eastern Pennsylvania, samples of shale from the New Scotland Limestone and Esopus Shale and of slate from different stratigraphic intervals of the Martinsburg Shale were collected and tested for possible use in making bloated lightweight aggregate. Similar tests on other raw materials from the Eastern United States have been previously reported by Lodding (1956), Knechtel and Hosterman (1960), Espenshade and Hamlin (1961), and Calver and others (1961). Although material from at least one stratigraphic interval of the Martinsburg has been used previously as raw material for lightweight aggregate, there are no published accounts of testing of New Scotland or Esopus material for this use.

Slate of the Martinsburg Shale has long been quarried for roofing material, blackboards, and other commercial purposes, especially in the Bangor-Pen Argyl

area, in eastern Pennsylvania, where enormous quantities of waste slate have resulted from these operations. Conley (1942), Bates and others (1947), and Conley and others (1948) reported on the suitability of this waste as a potential raw material for manufacture of lightweight aggregate, and in recent years it has been fired for that purpose in a rotary kiln operated by Pennsylvania Lightweight Aggregates, Inc., at East Bangor, Pa. Because the waste slate was quarried from a relatively restricted stratigraphic interval in the upper part of the Martinsburg, we collected samples from four other stratigraphic positions within the main Martinsburg belt. Test results of these samples can be directly compared with those of other samples of Martinsburg materials from the Appalachian Valley that have been subjected to identical firing tests in the U.S. Bureau of Mines laboratory at Norris, Tenn. The results reported here complement the data of Lodding (1956), who used somewhat different techniques in his tests of samples from New Jersey localities. One sample, number 2 in table 1, was taken by us from an outlying mass of Martinsburg that had not previously been sampled. The locations and descriptions of the material sampled for his study are given in table 1, and the locations, together with those of the materials sampled by Bates and others (1947) and by Lodding (1956), are shown also on figure 1.

### DESCRIPTION OF FORMATIONS SAMPLED

The New Scotland Limestone and Esopus Shale are both of Early Devonian age. The New Scotland

<sup>1</sup> U.S. Bureau of Mines.

<sup>2</sup> Deceased.

TABLE 1.—Description of materials tested for suitability as raw material for bloated lightweight-aggregate

Sample	Description
1	Slate of the Martinsburg Shale from outcrop along Mount Vernon Road, about 1.2 miles northwest of its junction with New Jersey Highway 94, Portland quadrangle, Warren County, N.J. Slate occurs interbedded with crossbedded graywacke in the middle graywacke-bearing member of the formation. Field number P-56.
2	Slate of the Martinsburg Shale from outcrops along the Musconetcong River, near the trout hatchery about 2.4 miles southwest of Asbury, Bloomsburg quadrangle, Warren County, N.J. Sample is from a separated mass that is infolded and in-faulted with older rocks. Rock is strongly deformed and has two distinct slaty cleavages. Field number B-G-5-4.
3	Slate of the Martinsburg Shale, verging on phyllite, from outcrops along Delaware, Lackawanna, and Western Railroad, just above U.S. Highway 46, 0.4 mile north of Manunka Chunk, Belvidere quadrangle, Warren County, N.J. This rock occurs stratigraphically in the upper part of the lower claystone member of the formation. It is strongly deformed, and slaty cleavage is folded as well as bedding. Slip cleavage is strongly developed and is paralleled by minor thrust faults. Field number Bv-A-6-1.
4	Slate of the Martinsburg Shale from outcrops along U.S. Highway 46, about 0.8 mile south of Manunka Chunk, Belvidere quadrangle, Warren County, N.J. This material is from the stratigraphically lowest part of the formation in the area. It contains noticeable quantities of calcite and pyrite, and fresh surfaces effervesce slowly in dilute HCl. The outcrop area contains a few 4- to 6-inch interbeds of dolomitic siltstone. The rock is strongly deformed by cascade folds of small amplitude and by small thrust faults that parallel a poorly developed slip cleavage. Field number Bv-C-5-2B.
5	Slate of the Martinsburg Shale from a cut along an unnumbered country road about 1.4 airline miles S. 63° W. from Manunka Chunk, N.J.; locality is in Belvidere quadrangle, Northampton County, Pa. This rock appears to be about 800 feet stratigraphically above sample 4, and is a good hard ribbon slate. Ribbons represent the trace of beds of different composition on the slaty cleavage. Rock contains minor calcite, and effervesces very weakly in dilute HCl. Field number Bv-B-4-2.
6	Shale of the New Scotland Limestone from outcrops along an unnumbered road paralleling Flat Brook, about 3.43 miles southwest of Wallpack Center, Lake Maskenozha quadrangle, Sussex County, N.J. Material is calcareous. Field number LM-1.
7	Esopus Shale from outcrops along an unnumbered road paralleling Flat Brook about 4.44 miles southwest of Wallpack Center, Flatbrookville quadrangle, Sussex County, N.J. Rock is quite siliceous and well cleaved. Field number F-1.

Limestone near the Delaware River consists of 76 feet of fine-grained dark-gray calcareous siliceous shale with interbeds and pods of dark-gray finely crystalline argillaceous limestone. The Esopus Shale in the same general area consists of 180 feet of dark-gray finely arenaceous silt shale, with lesser interbeds of siliceous siltstone. Slaty cleavage is well developed in the Esopus and commonly obscures the bedding.

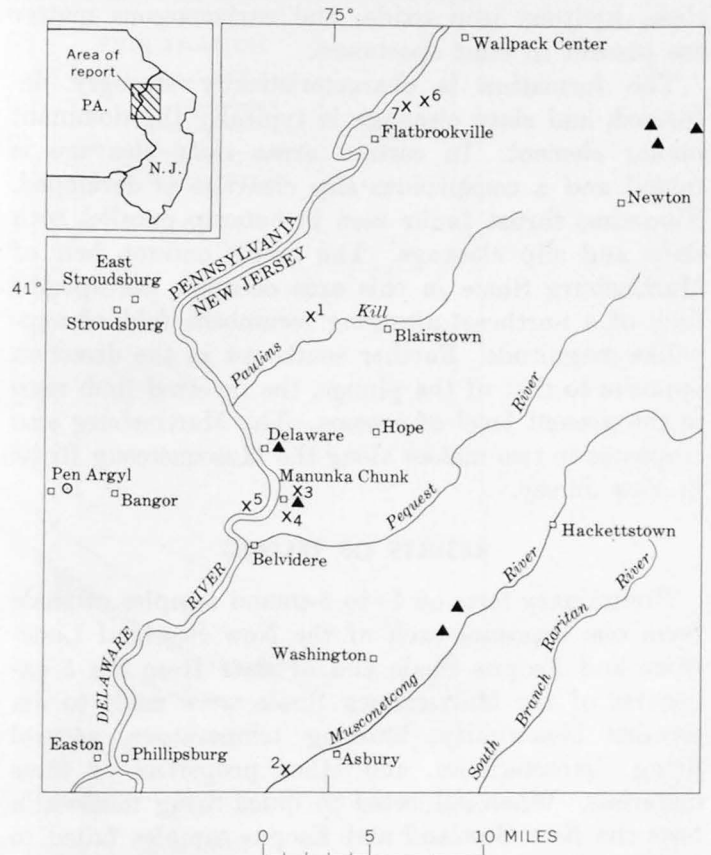


FIGURE 1.—Sketch map of eastern Pennsylvania and western New Jersey, showing localities from which samples were collected for lightweight-aggregate tests. X, this study—numbers refer to table 1; ▲, Lodding (1956); ○, Bates and others (1947).

The Martinsburg Shale of Middle and Late Ordovician age crops out continuously along the Appalachian Valley from Virginia through New Jersey and is the stratigraphic equivalent of rocks that have been called the Hudson (Hudson River) Shales or Schist in New York. Near the Delaware River the formation can be divided into a lower thin-bedded claystone unit, a middle unit of interbedded claystone and graywacke, and an upper unit of thick-bedded claystone. In extreme eastern Pennsylvania and in New Jersey the claystone has been metamorphosed to slate, which in places verges on phyllite. Because of structural complexity and the lack of complete detailed mapping, the exact thickness of the Martinsburg is not known. It is probable, however, that the formation is more than 10,000 feet thick.

Slate of the Martinsburg is mostly dark gray in fresh exposures and weathers medium gray to yellowish brown. Lesser thin beds are black, probably because of their carbonaceous content. Quartz, white mica, illite, and chlorite are the most abundant minerals in the slate. Some calcite, dolomite, pyrite, rutile, plagioclase,

clase, hydrous iron oxide, and carbonaceous matter are present in most specimens.

The formation is characteristically strongly deformed, and slaty cleavage is typically the dominant planar element. In certain areas slaty cleavage is folded and a conspicuous slip cleavage is developed. Numerous thrust faults seen in outcrop parallel both slaty and slip cleavage. The major outcrop belt of Martinsburg Shale in this area occupies the upright limb of a northeast-plunging recumbent fold of nappe-like magnitude. Farther southwest in the direction opposite to that of the plunge, the inverted limb rises to the present level of erosion. The Martinsburg also crops out in two masses along the Musconetcong River in New Jersey.

### RESULTS OF TESTING

Preliminary tests on 3- to 5-pound samples of shale from one exposure each of the New Scotland Limestone and Esopus Shale and of slate from the 5 exposures of the Martinsburg Shale were made to determine bloatability, bloating temperature, general firing characteristics, and other properties of these materials. When subjected to quick-firing muffle-kiln tests the New Scotland and Esopus samples failed to bloat, and materials in these two formations were not tested further. However, the Esopus Shale has a potential use as an ingredient of dark brick or tile if blended with suitable quantities of plastic clay.

Similar tests on the Martinsburg samples were favorable, whereupon duplicate samples weighing approximately 200 pounds each were collected from the same 5 exposures and were tested in a 14-foot rotary kiln. The results show that when fired under controlled conditions the slate expands to produce a lightweight aggregate of good quality. Results of preliminary tests of the Martinsburg samples are given in figure 2 and table 2.

Riley (1951) determined that a bloatable material is one having a chemical composition that balances fluxing agents against silica and alumina to allow the formation of a melt with a viscosity high enough to trap a gas. Some substance must also be contained that will liberate gas at or above the fusion temperature of the material. Riley (1951) also developed a composition diagram that gives the approximate limits beyond which bloating will not occur. The chemical compositions of the 5 Martinsburg samples collected for this study are compared in table 3 with those of 2 sources of commercial lightweight aggregate from other areas and of 1 sample of waste Martinsburg roofing slate. Major oxide data for the Martinsburg samples were calculated from these analyses and

TABLE 2.—Results of preliminary bloating tests of 5 samples of slate from the Martinsburg Shale heated in an electric muffle kiln for 15 minutes

Temperature (degrees Fahrenheit)	Properties		Remarks
	Density (lbs per cu ft)	Absorption <sup>1</sup> (weight percent)	
<b>Sample 1</b>			
1,900-----	100.3	6.5	No bloating.
2,000-----	75.4	6.3	Fair expansion.
2,100-----	38.6	5.9	Excellent bloating.
2,200-----	30.5	14.3	Overbloomed, sticky; slight melting.
<b>Sample 2</b>			
1,900-----	102.8	7.2	No bloating.
2,000-----	69.8	6.8	Good expansion.
2,100-----	42.4	8.2	Excellent expansion; slight sticking.
2,200-----	38.6	7.7	Excellent expansion; very sticky.
<b>Sample 3</b>			
1,900-----	97.8	7.8	No bloating.
2,000-----	77.2	6.9	Good expansion.
2,100-----	44.2	8.0	Excellent expansion.
2,200-----	29.3	10.6	Overbloomed, fragile, and very sticky.
<b>Sample 4</b>			
1,900-----	101.5	9.1	No bloating.
2,000-----	71.0	9.7	Good expansion.
2,100-----	41.7	14.5	Overbloomed, fragile, and very sticky.
2,200-----	34.9	13.2	Overbloomed, fragile, and melting.
<b>Sample 5</b>			
1,900-----	100.9	8.3	No bloating.
2,000-----	56.7	9.2	Good expansion.
2,100-----	36.1	10.8	Overbloomed, very sticky, and melting.
2,200-----	31.8	15.9	Melting, fragile, and sticky.

<sup>1</sup> Water absorption of aggregate, in percent weight increase after soaking for 48 hours.

plotted on Riley's composition diagram (fig. 3). It can be seen that the data fall well within the favorable area and indicate admirable compositions for bloating. Petrographic study and the chemical data suggest that in addition to water, at least two major gas-producing substances, pyrite and dolomite, are present in the Martinsburg. Chemical analyses were not performed on the New Scotland and Esopus samples, as the preliminary bloating tests were unfavorable.

The 200-pound Martinsburg samples were tested by the procedures described by Klinefelter and Hamlin (1957) for evaluating raw materials for manufacture of lightweight aggregate by the rotary-kiln process.

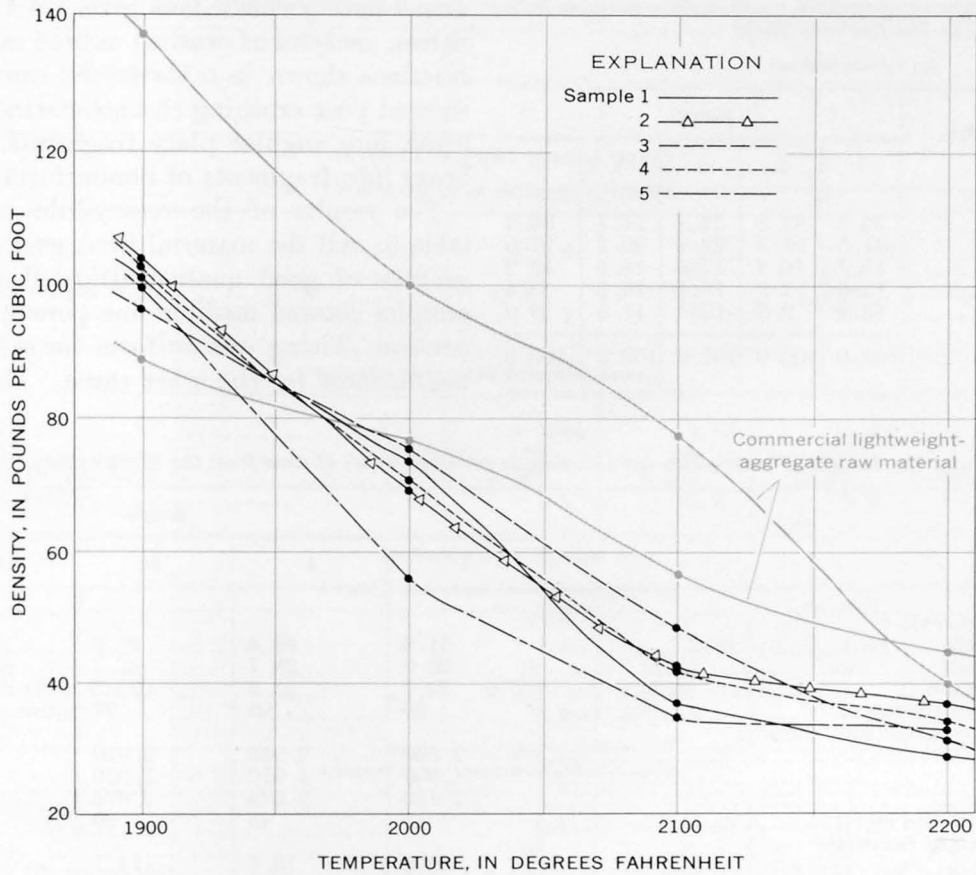


FIGURE 2.—Changes in density of 5 samples of slate from the Martinsburg Shale during 15-minute muffle-kiln bloating tests. Comparable data are also given for two commercial lightweight-aggregate raw materials.

TABLE 3.—Chemical analyses, in weight percent, of 6 samples of slate from the Martinsburg Shale and 2 samples of shale used in manufacture of commercial bloated lightweight aggregate

[Analyses in weight percent]

Constituent	Slate from the Martinsburg Shale						Shale used for commercial bloated lightweight aggregate		
	1 <sup>1</sup>	2 <sup>1</sup>	3 <sup>1</sup>	4 <sup>1</sup>	5 <sup>1</sup>	A <sup>2</sup>	B <sup>3</sup>	C <sup>4</sup>	
SiO <sub>2</sub>	62.0	64.6	64.7	59.1	60.8	57.17	61.70	59.8	
Al <sub>2</sub> O <sub>3</sub>	17.2	15.8	15.2	13.8	14.6	14.04	21.30	19.00	
Fe <sub>2</sub> O <sub>3</sub>	1.5	2.1	2.2	2.8	1.6	8.45	7.80	8.04	
FeO	4.4	4.1	3.8	3.0	4.6				
MgO	3.0	3.2	3.0	2.8	3.8	2.66	2.07	2.09	
CaO	.64	.10	.36	3.4	2.5	3.79	1.30	.39	
Na <sub>2</sub> O	1.1	1.0	1.5	1.1	1.0	1.53	.67	.84	
K <sub>2</sub> O	4.2	3.8	3.7	3.5	3.4	2.83	3.40	3.70	
H <sub>2</sub> O <sup>+</sup>	3.7	3.8	3.6	2.9	3.6	3.18	.26	5.74	
H <sub>2</sub> O <sup>-</sup>	.30	.38	.38	.48	.21				
TiO <sub>2</sub>	.82	.73	.70	.66	.68	.67	1.12	.93	
P <sub>2</sub> O <sub>5</sub>	.18	.16	.15	.17	.15		.01	.21	
MnO	.07	.09	.11	.11	.12	.10			
CO <sub>2</sub>	.42	.07	.15	2.9	2.3	5.54	§.28	§.02	
S as SO <sub>3</sub>				3.6					
Total S						2.73	.14	.015	
Total C						2.17	.25	.30	
Total	99.53	99.93	99.55	100.32	99.36	104.86	100.02	101.15	

<sup>1</sup> Rapid rock analysis by Paul Elmore, Samuel Botts, Gillison Chloe, Lowell Artis, and H. Smith, U.S. Geological Survey.  
<sup>2</sup> Martinsburg ribbon slate from waste pile at Parsons Brothers quarry, Pen Argyl, Pa. (Bates, and others, 1947, p. 43).  
<sup>3</sup> Shale sample from the Western Brick Co. haydite plant, Danville, Ill. (Conley and others, 1948, p. 34).  
<sup>4</sup> Shale sample furnished by the Erath Co., Strawn, Tex., manufacturers of Featherlite aggregate (Conley and others, 1948, p. 34).  
<sup>5</sup> Not included in total.

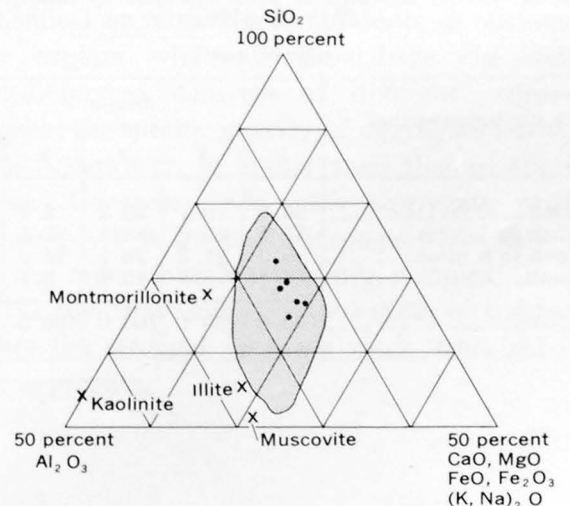


FIGURE 3.—Triangular diagram based on major oxides, showing field (patterned) defined by analyses of clays that fire to a mass viscous enough to insure good bloating (Riley, 1951, p. 123). Dots within patterned area represent analyses of Martinsburg samples given in table 3.

TABLE 4.—Screen analyses of unfired crushed slate samples from the Martinsburg Shale

[In volume percent]

U.S. standard screen size	Sample				
	1	2	3	4	5
+ 3/8 inch	26.5	33.8	24.1	17.7	36.4
- 3/8 inch to 1/4 inch	31.5	27.3	29.8	30.2	27.0
- 1/4 inch to 8 mesh	15.7	16.2	17.6	18.6	15.2
- 8 mesh to 20 mesh	13.5	12.9	16.1	16.2	12.4
- 20 mesh	12.8	9.8	12.4	17.3	9.0
Total	100.0	100.0	100.0	100.0	100.0

These tests yielded data given in tables 4, 5, and 6. Screen analyses of crushed unfired samples yielded size fractions shown in table 4. All samples except No. 1 showed poor crushing characteristics, as they tended to break into angular platy fragments. All the material broke into fragments of nonuniform thicknesses.

The results of the rotary-kiln tests are given in table 5. All the material fired well and produced aggregate of good quality. Bloated material from all samples showed medium-fine pore space and good expansion. Firing was uniform for samples 2 and 5 and nonuniform for the other three. The color of the ag-

TABLE 5.—Results of rotary-kiln test (15-minute retention time) of slate from the Martinsburg Shale

	Sample				
	1	2	3	4	5
Feed size (volume percent):					
- 3/8 inch to 1/4 inch	51.8	48.4	46.9	46.2	49.3
- 1/4 inch to 8 mesh	26.0	28.7	27.7	28.7	27.9
- 8 mesh to 16 mesh	22.2	22.9	22.9	25.1	22.8
Weight of raw material (lb per cu ft)	99	96	97	106	95
Particle temperature (degrees Fahrenheit):					
Minimum	2,000	2,035	2,020	1,990	1,910
Optimum	1,940	1,910	1,960	1,940	1,940
Maximum	2,130	2,075	2,075	2,030	2,065
Weight of aggregate (lb per cu ft)	42	45	50	50	48
Water absorption (weight percent):					
3/4 inch to 1/2 inch	15.9	10.6	14.1	7.4	8.1
1/2 inch to 1/4 inch	16.8	10.2	14.3	8.2	7.9
1/4 inch to 8 mesh	10.7	9.5	12.9	8.3	8.2
Processing characteristics	Good	Good	Good	Good	Good.
Point of material release (minutes)	11	10	11	10	8
Shape of particle in bloated product	Angular to rounded.	Angular to elongated platy.	Angular to platy.	Angular	Angular.

TABLE 6.—Screen analyses of fired aggregate of slate from the Martinsburg Shale

[In volume percent]

U.S. standard screen sizes	Sample				
	1	2	3	4	5
+ 3/8 inch	26.6	19.1	20.2	13.7	7.3
- 3/8 inch to 1/4 inch	57.7	50.9	43.1	52.6	55.8
- 1/4 inch to 8 mesh	9.3	21.3	26.2	25.6	26.3
- 8 mesh	6.4	8.7	10.5	8.1	10.6
Total	100.0	100.0	100.0	100.0	100.0

gregate ranged from light brown through gray to black. Screen analyses of fired aggregate from the five samples are given in table 6.

Standard 2-inch concrete cubes were made with aggregate from all 5 samples, using 2 different mixes and 2 methods of curing. Specific gravity, compressive strength, and absorption data for these cubes are given in table 7. These properties compare favorably with the properties of structural concrete made from samples of commercial lightweight aggregate that normally have a compressive strength of 1,000-5,000

TABLE 7.—Performance tests of concrete made with lightweight aggregate produced from slate from the Martinsburg Shale

Property	Sample				
	1	2	3	4	5
<b>AUTOCLAVE CURE (6 hrs at 150 psi)</b>					
<b>5 bags of cement per cubic yard of concrete</b>					
Bulk specific gravity	1.41	1.45	1.60	1.47	1.47
Density (lb per cu ft)	88	90	100	92	91
Compressive strength (lb per sq in.)	4,788	3,724	4,532	4,089	3,788
Absorption (weight percent)	6.7	6.1	7.2	5.4	7.0
<b>7 bags of cement per cubic yard of concrete</b>					
Bulk specific gravity	1.44	1.53	1.73	1.54	1.49
Density (lb per cu ft)	90	96	108	96	93
Compressive strength (lb per sq in.)	4,565	4,252	5,263	4,288	3,365
Absorption (weight percent)	7.1	7.0	8.4	6.6	5.1
<b>STEAM CURE (28 days)</b>					
<b>5 bags of cement per cubic yard of concrete</b>					
Bulk specific gravity	1.45	1.48	1.64	1.52	1.56
Density (lb per cu ft)	90	92	102	94	97
Compressive strength (lb per sq in.)	3,203	3,061	3,747	3,064	3,845
Absorption (weight percent)	5.8	5.1	6.8	5.1	6.5
<b>7 bags of cement per cubic yard of concrete</b>					
Bulk specific gravity	1.54	1.53	1.69	1.57	1.62
Density (lb per cu ft)	96	96	106	98	101
Compressive strength (lb per sq in.)	4,199	3,658	5,251	3,780	3,495
Absorption (weight percent)	7.5	7.0	8.9	5.6	5.5

pounds per square inch and water absorptions of 5–30 weight percent (Washa, 1956). A comparison of the compressive strength of the 28-day steam-cured samples and the strength of 67 samples of concrete made with commercial, and potentially commercial, expanded-shale aggregate is given on figure 4. These data show that samples of concrete made with Martinsburg bloated aggregate, with one exception, are the strongest of those samples made with the proportion of 5 sacks of cement per cubic yard of concrete and that they compare favorably with concrete made from commercial aggregate.

### CONCLUSIONS

It can be concluded that the slate tested is reasonably representative of the slate from the Martinsburg

Shale near the Delaware River and will make a good-quality lightweight aggregate. In fact, it appears that all the Martinsburg, exclusive of the graywacke, of course, is a potential source of lightweight aggregate. No chemical or mineralogic difference is obvious that might explain why aggregate from the different samples formed concrete of different compressive strengths; the specific gravity of aggregate made from sample 3, however, is higher than that of the other samples. Concrete made with aggregate produced from sample 3 is generally stronger than that made from the other four Martinsburg samples. It seems to be the rule that among various types of lightweight concrete the stronger ones are made from relatively heavy aggregate.



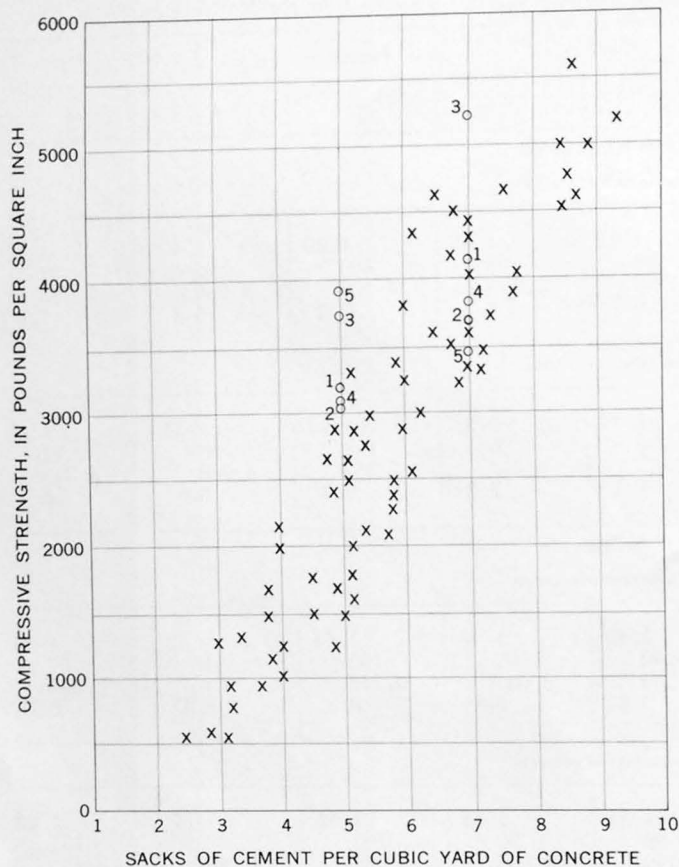


FIGURE 4.—Comparison of compressive strength of 67 samples of concrete made with commercial or potentially commercial expanded-shale aggregate (x) (Kluge, 1956) and 10 samples of concrete made with expanded-slate aggregate from the Martinsburg Shale (o) (this study). All concrete samples were cured for 28 days. Numbers refer to table 1.

## REFERENCES

- Bates, T. F., and others, 1947, Properties and new uses of Pennsylvania slate: Pennsylvania State Coll. Mineral Industries Expt. Sta. Bull. 47, 168 p.
- Calver, J. L., Hamlin, H. P., and Wood, R. S., 1961, Analyses of clay, shale, and related materials—northern counties: Virginia Div. Mineral Resources, Mineral Resources Rept. 2, 194 p.
- Conley, J. E., 1942, Waste slate as a raw material source of lightweight aggregate: Am. Inst. Mining Metal/Petroleum Engineers Trans., v. 148, p. 161–166.
- Conley, J. E., Wilson, Hewitt, Klinefelter, T. A., and others, 1948, Production of lightweight aggregates from clays, shales, slates, and other materials: U.S. Bur. Mines Rept. Inv. 4401, 121 p.
- Espenshade, G. H., and Hamlin, H. P., 1961, Slate from the Greenville quadrangle, Maine, as potential lightweight aggregate material: Art 152 in U.S. Geol. Survey Prof. Paper 424-S, p. C18–C20.
- Klinefelter, T. A., and Hamlin, H. P., 1957, Syllabus of clay testing: U.S. Bur. Mines Bull. 565, 67 p.
- Kluge, R. W., 1956, Structural lightweight-aggregate concrete: Am. Concrete Ins. Proc. v. 53, p. 383–402.
- Knechtel, M. M., and Hosterman, J. W., 1960, Bloating clay in Miocene strata of Maryland, New Jersey, and Virginia: Art. 29 in U.S. Geol. Survey Prof. Paper 400-B, p. B59–B62.
- Lodding, William, 1956, Raw materials for lightweight aggregate production in New Jersey: Rutgers Univ. Bur. Mineral Research Bull. 7, 160 p.
- Riley, C. M., 1951, Relation of chemical properties to the bloating of clays: Am. Ceramic Soc. Jour., v. 34, no. 4, p. 121–128.
- Washa, G. W., 1956, Properties of lightweight aggregates and lightweight concretes: Am. Concrete Inst. Proc., v. 53, p. 375–382.



## LITHIUM-BEARING BENTONITE DEPOSIT, YAVAPAI COUNTY, ARIZONA

By J. J. NORTON, Washington, D.C.

*Abstract.*—Samples of montmorillonitic clay from a deposit in and near the W $\frac{1}{2}$  sec. 12, T. 13 N., R. 6 W., contain 0.3 to 0.5 percent Li<sub>2</sub>O. Chemical and spectrographic analyses show that the clay is characterized by the unusual constituents Li, F, and Mg in amounts intermediate between normal montmorillonite and the end member, hectorite.

The existence of lithium in a deposit of bentonitic montmorillonite, known as the Lyles lithium clay deposit, in Yavapai County, Ariz., has been known for some years but it seems not to have been recorded in the geologic literature. Most of the deposit is in the W $\frac{1}{2}$  sec. 12, T. 13 N., R. 6 W., but some of it extends into secs. 1 and 11 (fig. 1). It is 22 miles S. 80° W. from Prescott and 9 miles N. 60° W. from Kirkland, Ariz. The road from Kirkland to Bagdad passes along the south edge of the area containing exposures of clay.

The discovery that the clay contains lithium in detectable amounts was made by Joseph Lyles of Yarnell, Ariz., in the mid-1950's. He brought the deposit to the attention of E. T. Turley of Phoenix, Ariz., who did a modest amount of exploration by pits and auger holes in 1956 and 1957. W. C. Peters, then of the Westvaco Division of the Food Machinery and Chemical Corp., examined the deposit in 1957. This led to a brief laboratory study of samples from the deposit, but the work was soon stopped because the market outlook for lithium was not encouraging at that time.

The deposit was examined by J. J. Norton in company with E. T. Turley on March 8, 1960, and by Norton alone on March 9 and 11, 1960. Analytical data obtained from samples collected at that time (tables 1 and 2) are sufficiently encouraging to justify returning to the locality to map the geology in and around the deposit and to search for similar deposits elsewhere in the region. Because circumstances have not permitted such work by the author, nor are they likely to in the near future, the data obtained in 1960 have been compiled here for publication in order to

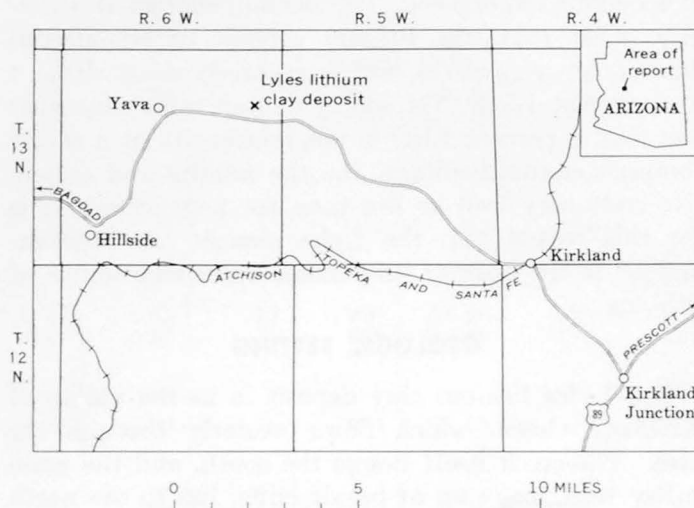


FIGURE 1.—Index map showing location of Lyles lithium clay deposits, Yavapai County, Ariz.

make them available to others.

The Lyles lithium clay deposit is one of a growing list of montmorillonite deposits in the Western United States found to be enriched in lithium. The best known is at Hector, in the Mohave Desert region of California, where a clay mineral of unusual nature was originally reported by Foshag and Woodford (1936). The mineral was named hectorite by Ross and Hendricks (1945, p. 27), who described it as an end member of the montmorillonite group in which magnesium and lithium take the place of aluminum and in which there is more fluorine than OH. An analysis by R. E. Stevens (Ross and Hendricks, 1945, p. 35) shows 0.13 percent Al<sub>2</sub>O<sub>3</sub>, 25.03 percent MgO, 1.05 percent Li<sub>2</sub>O, and 5.96 percent F; another analysis, by S. S. Goldich (Ames and others, 1958, p. 31), shows 0.33 percent Al<sub>2</sub>O<sub>3</sub>, 24.51 percent MgO, 1.14 percent Li<sub>2</sub>O, and 4.75 percent F. Two other lithium-rich clay localities have also been reported in the Mohave Desert region: one of them, 16 miles northeast of Amboy, Calif., has 0.50 percent Li<sub>2</sub>O (Foshag and Woodford, 1936, table 1, p. 241); the other is at Boron, Calif., where the shaly

matrix of borate deposits has 0.5 to 1 percent  $\text{Li}_2\text{O}$  (Kesler, 1960, p. 524). Still another locality is the Roadside beryllium deposit, Spor Mountain, Juab County, Utah, where Shawe and others (1964) found that 18 samples of montmorillonitic tuff have an average of 0.22 percent  $\text{Li}_2\text{O}$  and range from 0.04 to 0.43 percent  $\text{Li}_2\text{O}$ . Clay-rich fractions separated from 2 of these samples contain 0.38 and 0.39 percent  $\text{Li}_2\text{O}$  and 3.10 and 1.88 percent F, respectively.

At the present time, the lithium of such clays is chiefly of geochemical interest, and only potentially of economic importance. The lithium content is generally lower than the lithium content of commercial deposits in pegmatites, which generally range from 1 to 2 percent  $\text{Li}_2\text{O}$ . Yet a clay deposit with somewhat less than 1 percent  $\text{Li}_2\text{O}$  is not necessarily at a severe competitive disadvantage, for the mining and extractive costs may well be less than for pegmatites. It is for this reason that the Lyles deposit has been examined in the light of its possible value as a source of lithium.

#### GEOLOGIC SETTING

The Lyles lithium clay deposit is in the valley of Kirkland Creek, which flows westerly through the area. The creek itself lies to the south, and the main valley wall, made up of basalt cliffs, lies to the north of the deposit (fig. 2). The chief exposures of the clay are on the top and sides of a low north-northeasterly trending hill, shown in figure 2 in the west half of section 12. The largest exposure is in an open pit, 250 feet in diameter, at locality C of figure 2. This pit is a source of bentonite used locally in dams, irrigation ditches, and other water-containing structures. Clay is also exposed in the floor of the arroyos on either side of the hill, and in the pits and auger holes made by E. T. Turley. Throughout most of the area, however, the clay is concealed both by a caliche-cemented caprock and by sandy surficial material. Boulders of basalt from the cliffs to the north are strewn across the surface, and a few outcrops of basalt appear beneath the clay in the floors of arroyos. The geologic map of Yavapai County by the Arizona Bureau of Mines (1958) shows both the basalt and the sediments of this region as Tertiary or Quaternary in age; it also shows Precambrian granites only a few miles away in all directions.

Whether the sediments are younger than the basalt in the cliffs to the north or whether they are interstratified with basalt is by no means certain from existing evidence. Geologic mapping is needed to ascertain the structural and stratigraphic relations of the clay to nearby rocks. Because the clay is not

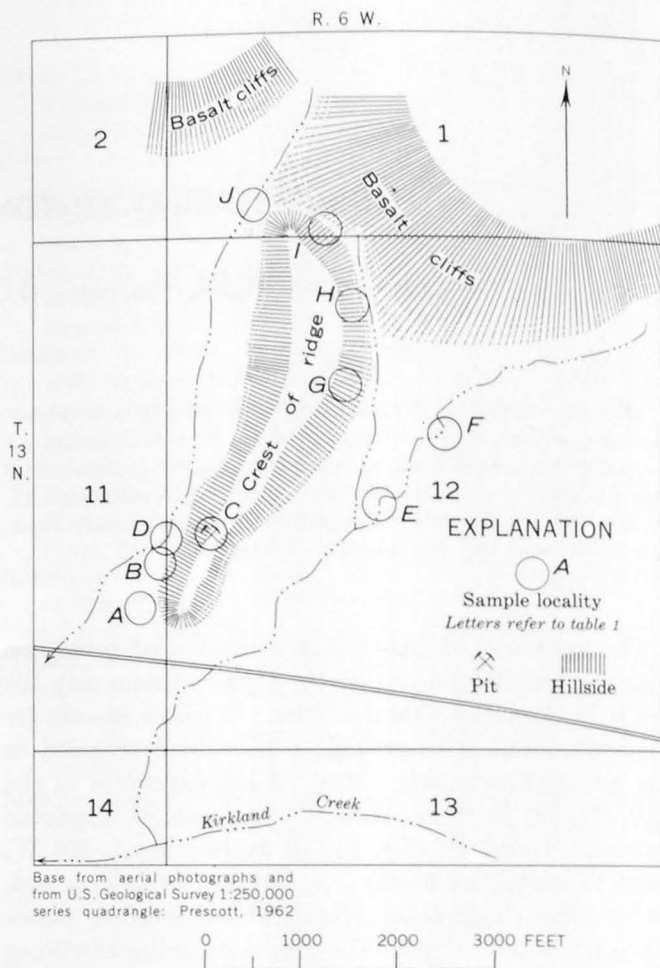


FIGURE 2.—Sketch map of area containing the Lyles lithium clay deposit, T. 13 N., R. 6 W., Yavapai County, Ariz.

widely exposed, the mapping will probably have to be supplemented by auger holes and test pits.

#### DESCRIPTION OF THE BENTONITE

The clay ranges from white to light gray or light green, or even to dark gray or dark green, especially when wet. Some of it is tan. Mottled white and green clay is conspicuous in some exposures. Bedding with a low dip is evident in the larger exposures. The only visible nonclay constituent is opal, pods of which may be several inches across. The high calcium content indicated by the analyses of table 2 presumably reflects a high content of calcite.

The first samples tested in the laboratories of the U.S. Geological Survey were supplied by W. C. Peters. X-ray analysis by A. J. Gude 3d showed that montmorillonite is the dominant clay mineral. Flame photometric analyses by Wayne Mountjoy of two samples, said by W. C. Peters to be especially rich in  $\text{Li}_2\text{O}$ , yielded values of 0.54 and 0.90 percent  $\text{Li}_2\text{O}$ . Analyses of additional samples collected by J. J. Norton in March 1960 are given in tables 1 and 2.

TABLE 1.—Analyses of clay from the Lyles lithium deposit, sections 1, 11, and 12, T. 13 N., R. 6 W., Yavapai County, Ariz.

[In percent; N.D., not determined]

Sample locality (fig. 2) and description	Field No.	Laboratory No.	Li <sub>2</sub> O			<sup>2</sup> Rb <sub>2</sub> O	<sup>2</sup> Cs <sub>2</sub> O	<sup>2</sup> SrO	<sup>4</sup> F
			( <sup>1</sup> )	( <sup>2</sup> )	( <sup>3</sup> )				
A. Bulldozer trench. JJN 1-60, surficial material that forms a hard white caprock; JJN 2-60, 4 to 12 inches below surface; JJN 3-60, 1.5 feet below surface.	JJN 1-60	281065	0.11	0.09	0.1	0.005	N.D.	0.18	N.D.
	JJN 2-60	281076	.35	.32	.4	.014	N.D.	.39	1.07
	JJN 3-60	281077	.45	.43	.4	.015	N.D.	.39	1.20
B. Cuttings from drill hole. JJN 5-60, sandy.	JJN 5-60	281067	.12	.09	N.D.	.020	<.001	.18	N.D.
	JJN 6-60	281068	.37	.37	N.D.	.010	N.D.	.21	N.D.
C. Open pit. JJN 10-60, from east part of pit; JJN 12-60, from north side; JJN 13-, 14-, and 15-60, from 3 separate beds on south side of pit; JJN 13-60, uppermost; JJN 14-60, intermediate; and JJN 15-60, lowermost.	JJN 10-60	281069	.53	.48	N.D.	.013	.001	.28	N.D.
	JJN 12-60	281070	.46	.47	N.D.	<.005	N.D.	.26	N.D.
	JJN 13-60	281078	.46	.50	.4	.009	N.D.	.21	1.36
	JJN 14-60	281079	.29	.28	.2	.009	N.D.	.19	.88
	JJN 15-60	281080	.44	.42	.4	.006	<.001	.14	1.28
D. Gully wall	JJN 17-60	281081	.48	.42	.4	.013	<.001	.21	.96
E. Cuttings from drill hole	JJN 18-60	281071	.31	.28	N.D.	.010	N.D.	.18	N.D.
F. Outcrop and drill hole. JJN 20-60, hard white caprock from exposure in arroyo; JJN 21-60, cuttings from drill hole.	JJN 20-60	281066	.12	.15	.15	.005	N.D.	.80	N.D.
	JJN 21-60	281082	.32	.27	.2	.006	<.001	1.9	.96
G. Cuttings from drill hole	JJN 22-60	281072	.35	.32	N.D.	.014	N.D.	.19	N.D.
H. Prospect pit	JJN 25-60	281074	.24	.19	N.D.	.011	N.D.	<.05	N.D.
I. Drill hole and outcrop. Sandy material. JJN 23-60, cuttings from drill hole; JJN 24-60, from prospect pit.	JJN 23-60	281083	.05	.04	.15	.013	N.D.	N.D.	.21
	JJN 24-60	281073	.03	.02	N.D.	.006	N.D.	.14	N.D.
J. Outcrop near a spring	JJN 27-60	281084	.15	.15	.15	.025	N.D.	N.D.	.33
	JJN 28-60	281075	.08	.07	N.D.	.018	N.D.	N.D.	N.D.

<sup>1</sup> Flame photometric. Analyst: Wayne Mountjoy.<sup>2</sup> Flame photometric. Analyst: J. I. Dinnin.<sup>3</sup> Quantitative spectrographic. Analyst: R. G. Havens.<sup>4</sup> Volumetric. Analyst: W. D. Goss.

The Li<sub>2</sub>O determinations of table 1 indicate that the clay-rich samples at localities A through G generally contain 0.3 to 0.5 percent Li<sub>2</sub>O. Samples from the area to the north, at localities H, I, and J, have less than 0.3 percent Li<sub>2</sub>O.

The fluorine content is also high in the clay-rich samples, ranging from 0.88 to 1.36 percent F. This suggests an affinity with hectorite, yet the fluorine is only about 3 times as abundant as Li<sub>2</sub>O, whereas analyzed hectorite from the type locality has about 5 times as much fluorine as Li<sub>2</sub>O. Lithium-rich samples, according to the semiquantitative spectrographic analyses in table 2, are also high in Mg and low in Al, which suggests similarities to hectorite.

The content of strontium (tables 1 and 2) is high enough to indicate the presence of a strontium mineral, which has not been identified. The content of rubidium and cesium is very low. Unlike these clays, altered tuff described by McAnulty and Levinson (1964, p. 772) in

the Honeycomb Hills, Utah, is enriched not only in lithium but also in rubidium and cesium. Beryllium is conspicuous at the Honeycomb Hills deposit but virtually absent in the Lyles lithium deposit. The beryllium content of three clay samples from localities A, C, and F, determined by D. R. Shawe with photo-neutron activation equipment, is less than 10 ppm.

### ORIGIN

The bedded nature of the clay in the Lyles deposit led both E. T. Turley and W. C. Peters (written communications, 1957) to suppose that it formed originally as a lake sediment. This is an acceptable conclusion for the origin of the main body of material. The abundance of lithium, fluorine, and strontium, however, suggests that the conversion of the sediments to bentonite was at least in part by hydrothermal alteration. In this connection, it is noteworthy that recent papers call for hot springs as the source of some of

TABLE 2.—*Semiquantitative spectrographic analyses of clay from the Lyles lithium clay deposit*  
 [Analysts: R. G. Havens and Nancy Conklin; d, barely detected and concentration uncertain; 0, searched for but not found]

Element	Sample <sup>1</sup>								
	JJN 2-60	JJN 3-60	JJN 13-60	JJN 14-60	JJN 15-60	JJN 17-60	JJN 21-60	JJN 27-20	JJN 23-60
Si	>10	>10	>10	>10	>10	>10	7	>10	>10
Al	3	3	3	.7	.7	3	.7	7	7
Fe	.7	.7	.7	.3	.3	.7	.3	1.5	1.5
Mg	7	7	7	7	>10	7	>10	1.5	3
Ca	>10	7	3	>10	7	7	>10	1.5	7
Na	.7	.7	.7	.7	.7	.7	.3	1.5	3
Ti	.15	.15	.15	.03	.07	.15	.03	.15	.3
Mn	.03	.03	.015	.007	.03	.03	.007	.03	.03
B	.003	.003	.003	d	.003	.007	0	.03	.003
Ba	.015	.03	.015	.007	.007	.015	.007	.07	.07
Ce	0	0	0	0	0	0	0	.03	0
Co	0	0	0	0	0	0	0	.0007	0
Cr	.003	.015	.003	.003	.003	.007	.0015	.007	.007
Cu	.0015	.003	.0015	.0015	.003	.0015	.0015	.007	.003
La	0	0	0	0	0	0	0	.03	0
Nd	0	0	0	0	0	0	0	.015	0
Ni	.0007	.0015	.0007	.0003	.0003	.0015	.0007	.003	.003
Sc	d	.0007	.0007	0	0	.0007	0	.0015	.0015
Sr	.3	.3	.15	.15	.15	.15	1.5	.03	.15
V	.03	.03	.007	.003	.003	.003	.0015	.015	.007
Y	d	d	d	d	0	.0015	0	.0015	.0015
Yb	d	d	d	d	0	.00015	0	.00015	.00015
Zr	.007	.007	.003	.003	.003	.015	.003	.007	.015

Elements searched for but not found in any sample:

P, Ag, As, Au, Be, Bi, Cd, Dy, Er, Eu, Ga, Gd, Ge, Hf, Hg, Ho, In, Ir, Lu, Mo, Nb, Os, Pb, Pd, Pr, Pt, Re, Rh, Ru, Sb, Sn, Sm, Ta, Tb, Te, Th, Tl, Tm, U, W, Zn.

Analytical results are reported to the nearest number in the series 7, 3, 1.5, 0.7, and so forth.

60 percent of the reported results may be expected to agree with results of quantitative analyses.

<sup>1</sup> Location, description, and laboratory number of samples are given in table 1.

the materials at Hector, Calif. (Ames and others, 1958, p. 35), and assign a major role to hydrothermal fluids from magmatic sources at Spor Mountain, Utah (Shawe and others, 1964, p. C87; Staatz, 1963, p. 33-35), and at the Honeycomb Hills, Utah (McAnulty and Levinson, 1964, p. 772-774).

#### REFERENCES

- Ames, L. L., Jr., Sand, L. B., and Goldich, S. S., 1958, A contribution on the Hector, California, bentonite deposit: *Econ. Geology*, v. 53, p. 22-37.
- Arizona Bureau of Mines, 1958, Geologic map of Yavapai County, Arizona: scale 1:375,000.
- Foshag, W. F., and Woodford, A. O., 1936, Bentonitic magnesian clay mineral from California: *Am. Mineralogist*, v. 21, p. 238-244.
- Kesler, T. L., 1960, Lithium raw materials, in *Industrial minerals and rocks*, 3d. ed.: Am. Inst. Mining Metall. and Petroleum Engineers, p. 521-531.
- McAnulty, W. N., and Levinson, A. A., 1964, Rare alkali and beryllium mineralization in volcanic tuffs, Honey Comb Hills, Juab County, Utah: *Econ. Geology*, v. 59, p. 768-774.
- Ross, C. S., and Hendricks, S. B., 1945, Minerals of the montmorillonite group, their origin and relation to soils and clays: U.S. Geol. Survey Prof. Paper 205-B, p. 23-79.
- Shawe, D. R., Mountjoy, Wayne, and Duke, Walter, 1964, Lithium associated with beryllium in rhyolitic tuff at Spor Mountain, western Juab County, Utah, in *Geological Survey Research*, 1964: U.S. Geol. Survey Prof. Paper 501-C, p. C86-C87.
- Staatz, M. H., 1963, Geology of the beryllium deposits in the Thomas Range, Juab County, Utah: U.S. Geol. Survey Bull. 1142-M, 36 p.



## SUBSURFACE STRATIGRAPHY OF GLACIAL DRIFT AT ANCHORAGE, ALASKA

By FRANK W. TRAINER and ROGER M. WALLER, Washington, D.C.

*Abstract.*—Glacial drift at Anchorage, which is situated at an edge of a wide glaciated lowland, reaches a thickness greater than 500 feet. The drift includes till, outwash-stream deposits, and estuarine and lake sediments which represent at least five glacial episodes, and it thickens progressively from the mountain wall on the east toward the deeper, axial part of the valley. Its constitution changes in the same direction, from predominant till near the mountain wall to till, sand and gravel, and clay in an intermediate region and then to till and clay near two estuaries which border the area. These changes are attributed to areal differences in dominant modes of sedimentation. The expression of the same topographic features in several buried surfaces (unconformities) is believed to reflect continuing, indirect influence of the preglacial topography on deposition of the drift. Disastrous slides during the Alaska earthquake of March 27, 1964, were caused by failure of a thick clay unit exposed in bluffs at Anchorage.

Pleistocene deposits at Anchorage, in south-central Alaska, represent at least five episodes of glaciation and include all the types of sediments commonly found in glacial drift. The stratigraphy of the drift is described in this report, and the areal distribution of the separate units is outlined. The distribution of one unit, the Bootlegger Cove Clay, provides background information helpful in the interpretation of why landslides occurred where they did during the Alaska earthquake of March 27, 1964. The results reported in this paper are based upon surface investigations coupled with study of the detailed logs of 21 deep test wells and of the logs of 400 domestic and industrial wells and 93 test borings; and study of samples from many of the wells. The logs studied range from 35 to 540 feet in depth and average 160 feet. A total of 81,500 feet of logs was studied. Criteria for the recognition of different types of glacial drift in the logs are given by Cederstrom and others (1964, p. 16-20).

Anchorage is situated on a triangular tract of lowland that is bounded on the east by high mountains and on the southwest and northwest by two estuaries (fig. 1). The area described in this report is entirely in

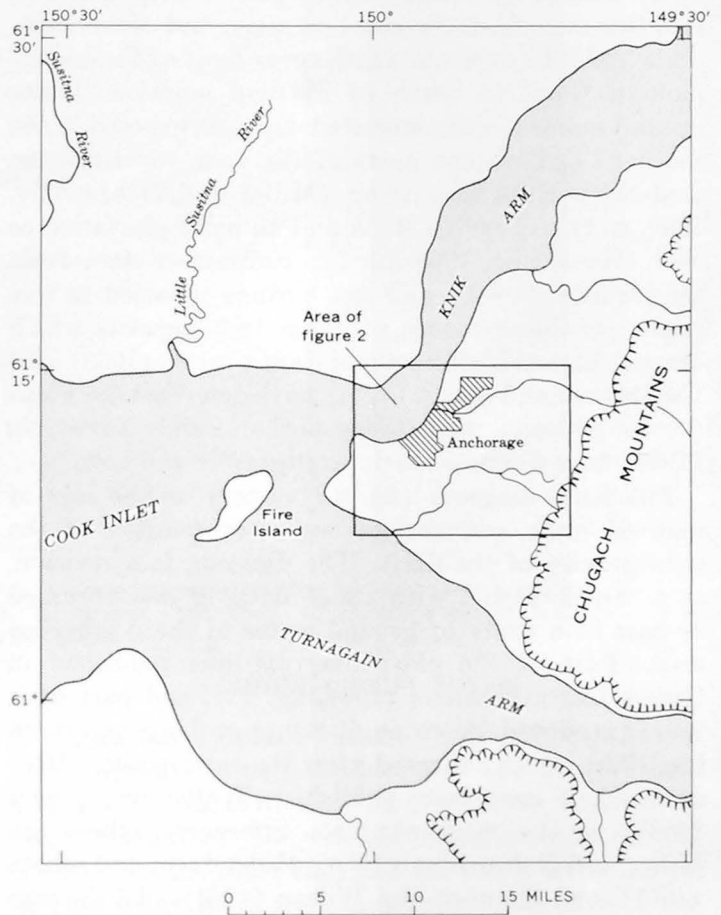


FIGURE 1.—Index map showing approximate boundaries of Anchorage area, Alaska. Diagonal pattern shows Anchorage and heavily settled adjacent areas.

the lowland except at the southeast, where it extends a short distance up the mountain slope. Local relief is less than 100 feet except near some stream valleys and hilly tracts. The land surface is underlain generally by glacial drift. The drift comprises (1) till, and associated till-like sediments believed to have been somewhat sorted during deposition by mudflow, by melt-water streams, or in standing water at glacier margins;

(2) outwash sand and gravel deposited by melt-water streams; and (3) sand, silt, and clay deposited in standing water (fig. 2).

### CHARACTER AND SUBDIVISION OF THE GLACIAL DRIFT

Two sheets of glacial drift are exposed at the land surface (fig. 2). The younger of these was formed during the last glaciation of the upper Cook Inlet lowland, the Naptowne Glaciation of Wisconsin age (Karlstrom, 1964). This drift sheet consists of the Elmendorf end moraine (Miller and Dobrovoly, 1959) formed by a large valley glacier that advanced into this area from the east-northeast, and of outwash-plain and lake deposits which cover most of the central part of the area south of the end moraine. Older ground-moraine and associated deposits, exposed in the southern and eastern parts of the area, represent the next-older Knik Glaciation (Miller and Dobrovoly, 1959, p. 12-14) or the Knik and an older glaciation as well (Karlstrom, 1964, pl. 6). Subsurface data from the records of wells and test borings reported in this paper provide evidence of older drift deposits which are not exposed. Miller and Dobrovoly (1959) and Cederstrom and others (1964) have described the Pleistocene deposits, and these authors and Karlstrom (1964) have discussed their stratigraphy and history.

The fence diagram (fig. 3B), based on the logs of selected wells, summarizes our interpretation of the stratigraphy of the drift. The diagram is a revision, at a new scale and with added data, of one prepared as part of a study of ground water in the Anchorage area. Part of the older diagram was published in Cederstrom and others (1964, fig. 11), and part of it was reproduced in an engineering-geology report on landslides which occurred after the earthquake.<sup>1</sup> Most of the logs have been published: Waller and others (1961) is the most complete reference; others are Miller and Dobrovoly (1959), Cederstrom and others (1964), and Shannon and Wilson (1964). All the logs are in the files of the Water Resources Division of the U.S. Geological Survey at Anchorage.

Problems of identification and of the adequacy of the data affect the reliability of interpretation of the drillers' logs, on which figure 3B is based. The common types of materials can be identified readily from drillers' reports for most wells, and the materials are sufficiently different that the boundaries of till and clay-silt units probably were located within a few feet

of their true positions in one-half to two-thirds of the logs. In most of the remaining logs our error in locating contacts was probably less than 20 to 30 feet. The buried deposits of sand and gravel present a different type of problem. They generally can be identified with confidence, but their thickness is poorly known because most wells do not penetrate them completely. The water wells commonly were drilled into sand and gravel only far enough to obtain the desired yield, and the test borings commonly were terminated in the upper part of the sand and gravel, just below the overlying clay or till.

Figure 3B shows that the deposits at Anchorage form several drift sheets of wide extent. We believe that each of 6 wells (197, 64, 111A, 177, 590, and 291, listed from east to west) penetrates 4 till sheets that are separated by sand and gravel, clay, or a weathered zone (Cederstrom and others, 1964, p. 26). Another well (163) appears to penetrate 4 or 5 till sheets, and several shallower wells penetrate at least 3 tills thought to be part of the same sequence of beds. Because the boundary between each pair of till sheets, as we have correlated them, is marked by a weathered zone that must have required an appreciable ice-free interval for its formation, we believe that the buried till sheets represent at least four glacial episodes. This interpretation, with the additional evidence of the Elmendorf end moraine, implies that the Anchorage area has been glaciated at least five times. Karlstrom (1964) has identified five glaciations in the Cook Inlet region on the basis of surface observations interpreted partly in the light of radiocarbon dates. We believe that the 2 drift sheets exposed in this area represent the 2 youngest members of the sequence — the Knik (older) and Naptowne Glaciations. We hesitate, however, to assign the older tills in the subsurface to the first 3 of his glaciations, because of uncertainty in the correlation of the older tills and because we cannot eliminate the possibility that more than five tills are present.

The composition of the drift section changes progressively with increasing distance from the mountain wall toward the center of the valley. At the wall the drift is largely till. Farther west, near wells 114, 163, and 177, beds of sand and gravel of appreciable thickness, and some of clay, are interbedded with the till. Still farther west (as far as wells 291, 427, and 624, for example) the sand and gravel are thin or absent and the section consists chiefly of clay and till.

The drift also thickens toward the center of the valley. The logs of 9 wells which reach bedrock near Anchorage record total thicknesses of drift of (1) about 100 to 230 feet on and near the slope south and

<sup>1</sup> Engineering Geology Evaluation Group, 1964, Geologic report, 27 March 1964 earthquake in the Greater Anchorage area: Alaska State Housing Authority, 41 p. [Duplicated report]

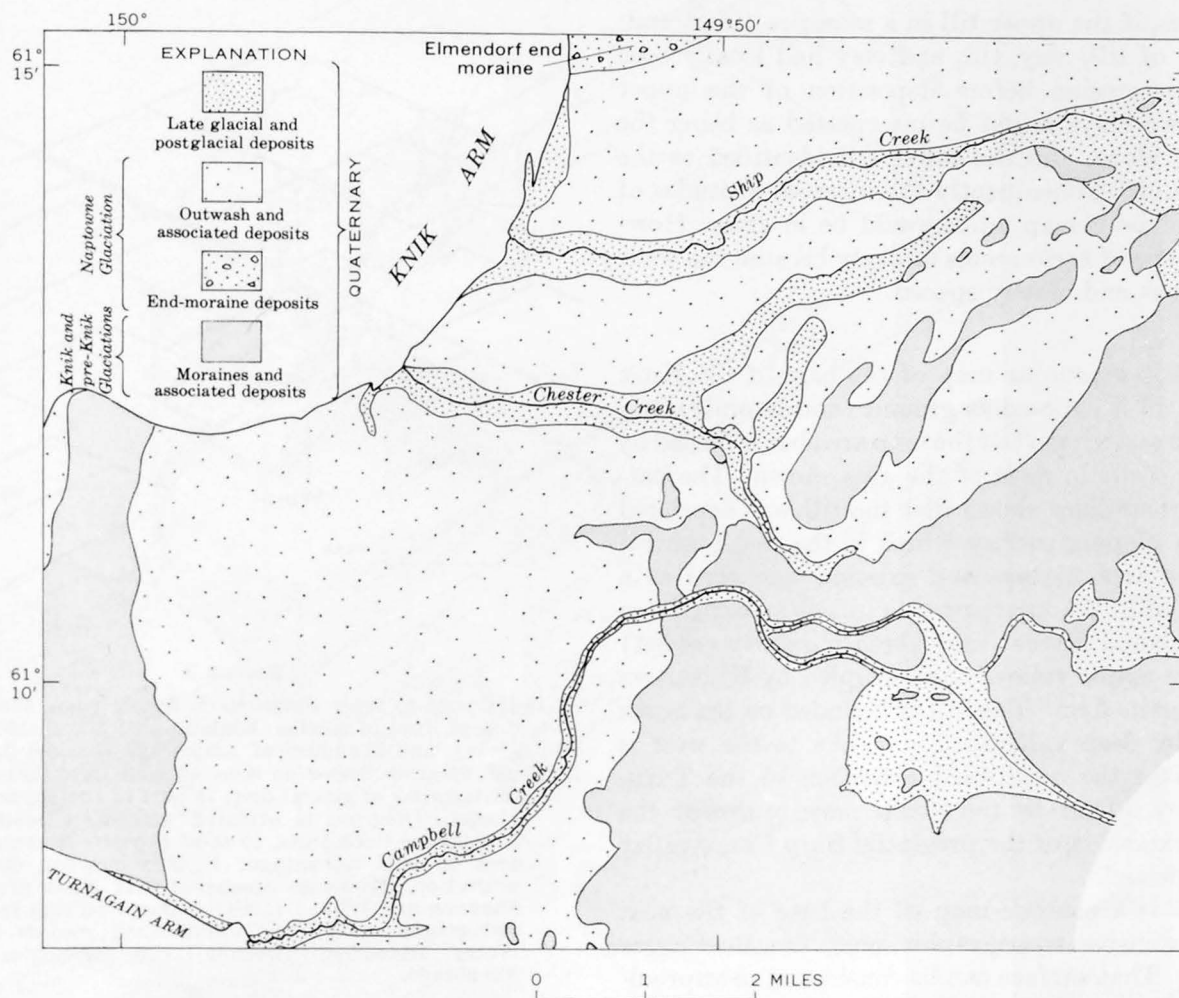


FIGURE 2.—Surficial geology of part of the Anchorage area, Alaska (generalized after Miller and Dobrovoly, 1959, pl. 1, and Cederstrom and others, 1964, pl. 1). Bootlegger Cove Clay, which crops out in bluffs along Knik Arm and Ship Creek and locally elsewhere, is not shown.

east of the region shown in figure 3B; (2) about 350 to 450 feet farther out in the lowland (wells 64 and 197, fig. 3B, and a well northeast of 64 that is not shown on the diagram); and (3) more than 540 feet but less than 700 feet near Knik Arm (well 28; the top of the bedrock is difficult to identify in the log).

These changes in the constitution and thickness of the drift reflect areal differences in the dominant modes of sedimentation. Where the mountain slope and adjacent lowland were not covered by ice, melt-water streams (flowing mainly across the lowland) deposited sand and gravel that represented part of the sediment carried from the glacier. In contrast, much of the deeper part of the valley lay under water during periods when it was not covered by ice, and most of the sediment carried into the standing water was deposited there. Thus, the nontill deposits to the west are much thicker, and contain much more clay and silt, than those to the east.

#### YOUNGEST DRIFT SHEETS

Figure 3B illustrates several drift sheets, each of which appears to be a composite of (1) till, (2) sand and gravel, and (3) clay and silt that represent a single glaciation. The younger deposits are better preserved than the older ones and are much better known because many more wells penetrate them. Two units, the Knik Till and the Bootlegger Cove Clay which overlies the till, are sufficiently well known to be mapped in some detail. Contour maps of the base of the till and of the base of the clay reveal the gross form of the land surface before and after the next-to-last glaciation of the area. The maps agree in their portrayal of several former topographic features (now parts of unconformities), and this agreement lends credence to our interpretation of the subsurface data. It is important to note, however, that the maps are based largely on the same logs, so that if one map is in error at a given place the other probably is also in



error. Thus, if the upper till in a sequence (in ascending order) of till, clay, till, and clay had locally been removed by erosion before deposition of the upper clay, the two clays might be interpreted as being the upper clay alone, and the lower till identified as the upper till unit. Consequently the inferred altitudes of the bases of both map units would be in error. However, this type of error seems unlikely because the wells are numerous and closely spaced.

#### Knik Till

Figure 4 is a contour map of the base of the Knik Till. This till is exposed as ground (and lateral?) moraine in the eastern part of the map area but is buried by younger deposits in most of the area shown. The pattern of contour lines shows that the till was deposited on a gently sloping surface which in the south-central part of the area flattens and extends westward as a broad, low hill. We interpret this hill as an expression of the preglacial divide (undoubtedly greatly eroded) between the major valleys now occupied by Knik Arm and Turnagain Arm. The hill is bounded on the north and west by deep valleys. The valley to the west is thought to be the northward extension of the Turnagain valley. That to the north may represent the westward extension of the preglacial Ship Creek valley into the lowland.

Figure 5 is a contour map of the base of the next younger extensive stratigraphic unit, the Bootlegger Cove Clay. That surface can be considered to approximate the upper surface of the Knik Till because sand and gravel are present between the till and clay only locally. Comparison of figures 4 and 5 shows that the till is commonly about 50 feet thick and that the form of its upper surface is a rather close replica of that of its base. The prominent topographic features of the surface beneath the till—the wide hill in the central part of the area and the valleys north and west of it—are all repeated on its upper surface. Thus, except for small buried hills such as those shown in generalized form at wells 333 and 398, in the northwestern part of figure 3B, and in somewhat more detail in figure 5, the configuration of the till sheet reflects that of the topography on which the till was deposited; it is not due to erosion.

#### Bootlegger Cove Clay

The Bootlegger Cove Clay is a deposit of clay, silt, and subordinate material which underlies the surficial sand and gravel in much of the Anchorage area (Miller and Dobrovolsky, 1959, p. 35-48, pl. 5-6; additional data and discussions of the character, distribution, fossil content, and origin of the clay are given by Schmidt, 1963; Cederstrom and others, 1964; Karlstrom, 1964;

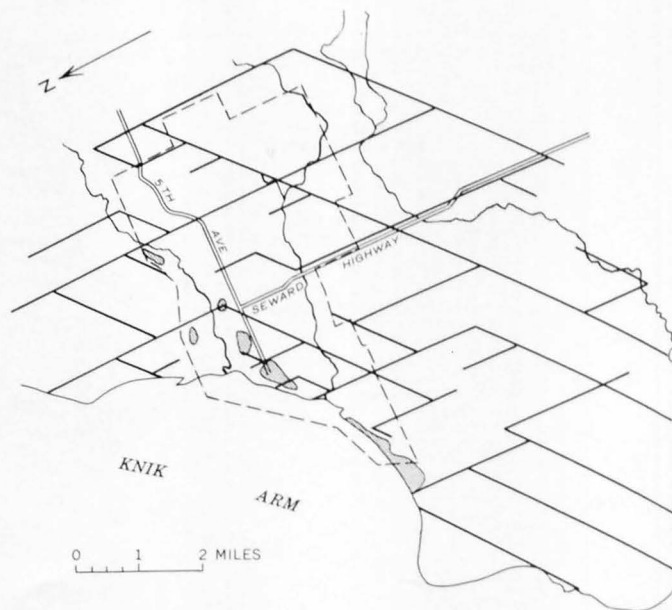


FIGURE 3

- A, Index map to fence diagram on facing page, showing location of lines of section, landslides of March 1964 (shaded areas), and boundary of Anchorage (dashed lines).  
 B, Fence diagram, based on selected well logs, that shows the stratigraphy of glacial drift in part of the Anchorage area, Alaska. Diagram is oriented with view southeastward, from above Cook Inlet, to show deposits in central part of area to best advantage; it is somewhat distorted by projection. Well logs numbered with letter prefixes from Shannon and Wilson (1964); other well logs from Waller and others (1961) and unpublished records in files of Water Resources Division, U.S. Geological Survey, Anchorage.

and Shannon and Wilson, 1964). The clay is younger than part of the Knik drift; in part it extends beneath the Elmendorf end moraine, and, in part, adjacent to the end moraine, it contains what appears to be water-laid till and has been deformed. Evidently the Naptowne glacier advanced into the water body in which the clay was deposited. Karlstrom (1964, p. 37-38) believes that the clay consists of three units. According to his interpretation, which we think reasonable, the lower beds were deposited in a Knik proglacial lake formed when water was ponded in the upper Cook Inlet region by coalescent glaciers to the southwest; the middle beds represent estuarine deposition during the Knik-Naptowne Interglaciation; and the upper beds were laid down in a Naptowne proglacial lake.

In gross form the upper surface of the Bootlegger Cove Clay (fig. 6), with a broad hill in the central part of the area bordered by valleys to the west and north, resembles the form of each of the older unconformities shown in figures 4 and 5. It is inferred that the same strong control operated throughout the separate cycles of sedimentation in this area, giving a simi-

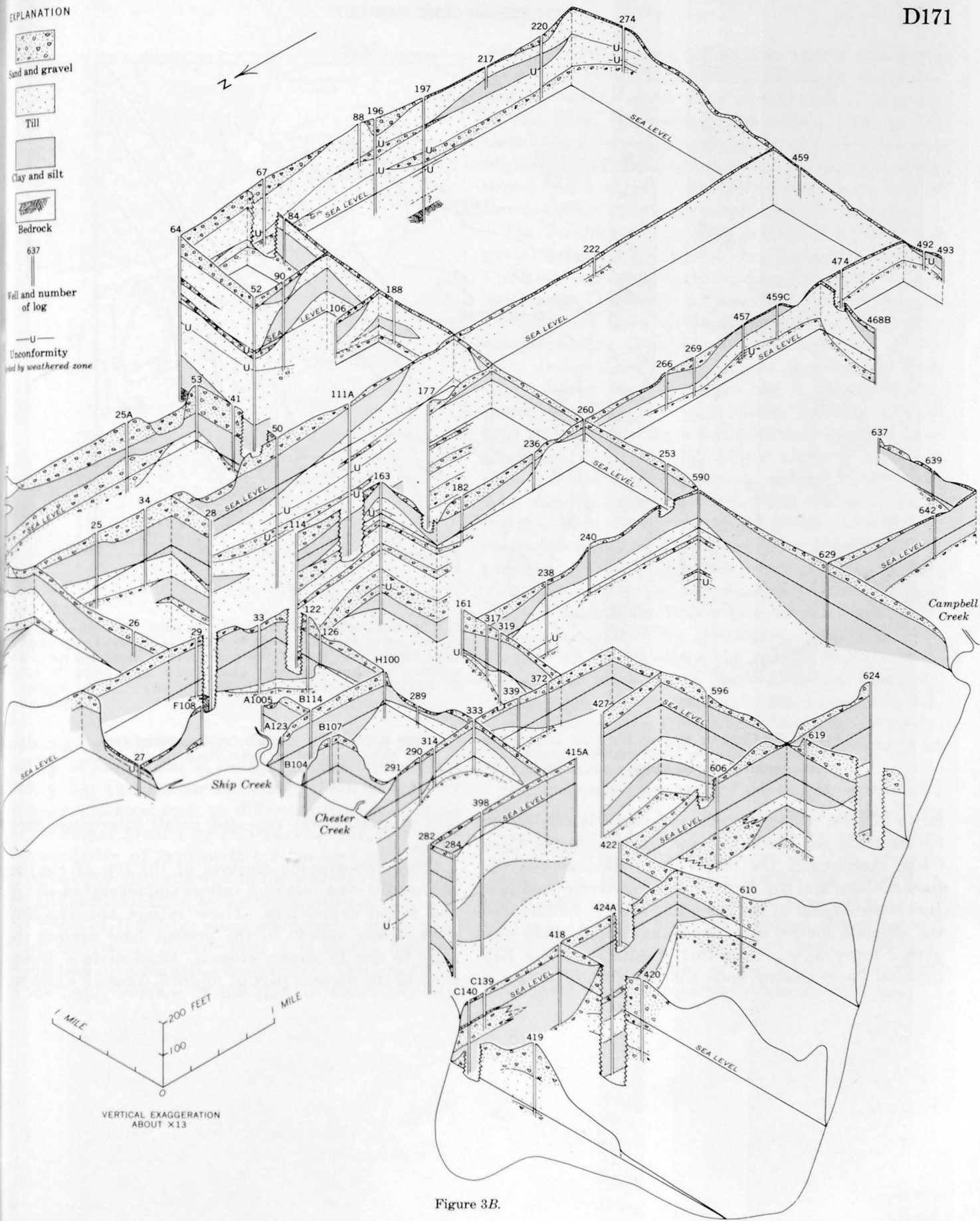


Figure 3B.

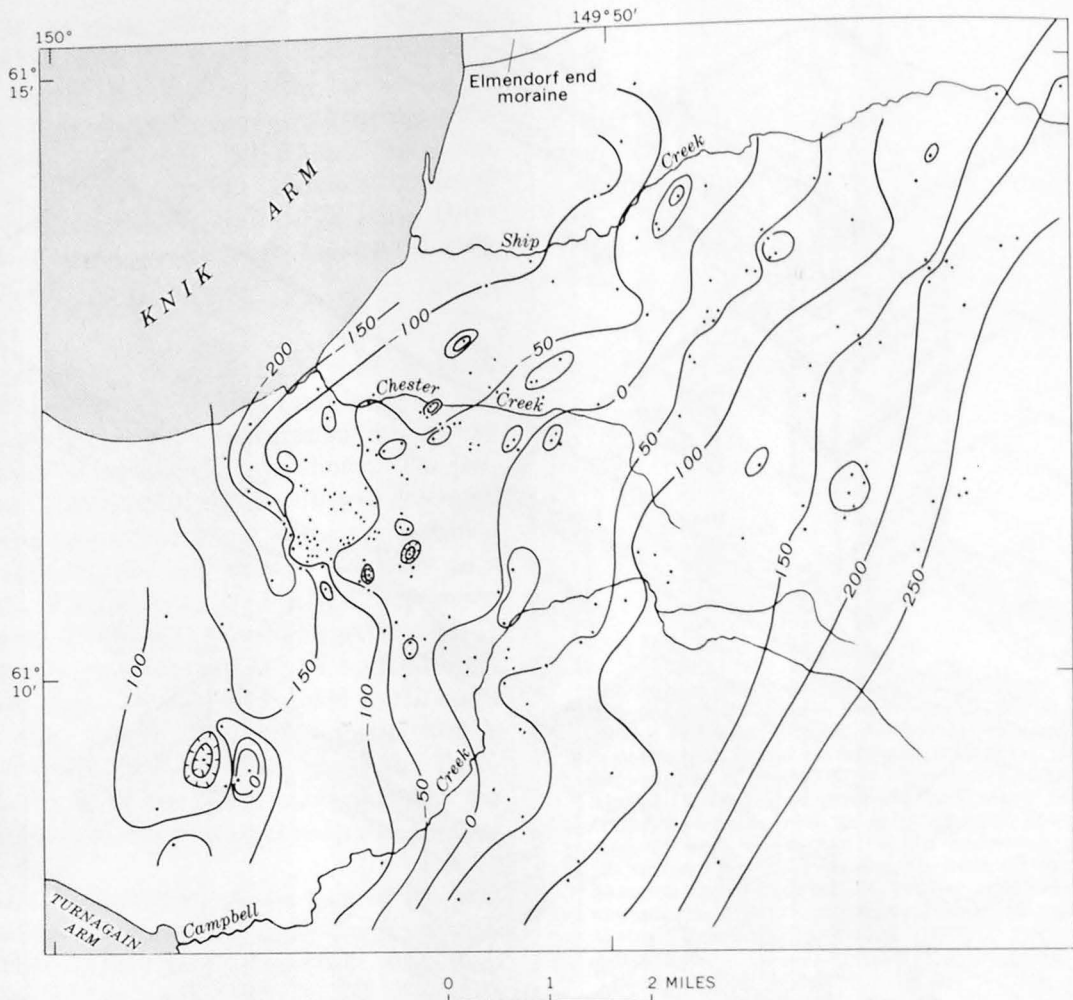


FIGURE 4.—Contour map of the base (unconformity) of the Knik Till in part of the Anchorage area. Datum is mean sea level; contour interval, 50 feet. Dots show location of wells from which data were obtained for drawing contour lines.

larity in form to deposits otherwise quite dissimilar, as for example the Knik Till and the Bootlegger Cove Clay. Apparently the controlling influence was the land surface, and the form of each successive land surface reflected that of the preceding one. It follows that the ultimate control upon deposition would be the preglacial topography. Once this preglacial surface had imposed its symmetry upon the first-formed deposits,

that symmetry was repeated in all subsequent deposition.

Other topographic features of the top of the clay are narrow west-trending valleys and several small hills and closed depressions. These valleys are coincident with stream valleys in the present land surface and must be due to stream erosion. Land-surface depressions in the western part of figure 6, some of which are



FIGURE 5.—Contour map of the base (unconformity) of the Bootlegger Cove Clay in part of the Anchorage area. Datum is mean sea level; contour interval, 50 feet. Dots show location of wells from which data were obtained for drawing contour lines. Dashed lines show inferred boundaries of the clay.

indicated on this map, have been explained by the melting of buried glacial ice (Miller and Dobrovoly, 1959, p. 54; Cederstrom and others, 1964, p. 39) and by other processes such as differential compaction or the melting of ground ice (Karlstrom, 1964, p. 38-39). The similarity of land-surface form here and in the pitted outwash deposits west of the western clay boundary favors explanation by ice-block melting. The fact that some of the depressions on figure 6 are located where the clay is thicker than it is nearby suggests localization by differential compaction. The small hills on the upper surface of the clay, in which the clay

stands 30 feet or more higher than nearby and which are capped by sand and gravel, are chiefly in the central and southwestern parts of the area. During our earlier work (Cederstrom and others, 1964, p. 34) these hills were interpreted as erosional remnants of a higher level of the outwash plain. Comparison of figures 5 and 6 suggests that differential compaction of the clay offers an adequate explanation of the hills.

The Bootlegger Cove Clay is covered by sand and gravel deposited by outwash streams that flowed into this area from the northeast, from mountain valleys outside the Elmendorf end moraine. Toward the west these outwash deposits were deposited in the Naptowne proglacial lake. During westward regression of the lake, streams from the mountains (particularly Ship Creek, which may still have had a glacial source) flowed across the emerging plain, building alluvial fans near the mountains and trenching the plain near the shore. With draining of the lake and return to estuarine conditions the deposits in what is now Knik Arm were also trenched. During this episode of downcutting, Ship Creek flowed in several distributary channels which were abandoned in turn until only the present creek valley contained a through-going stream. Thus, the estuary and the channels of different ages were cut to different depths into the sand and gravel or into the underlying Bootlegger Cove Clay. The presence of the clay near the modern shore, and its exposure in bluffs along Knik Arm and along the deeper stream valleys (especially the deepest one, that of the modern Ship Creek), provided the setting for the disastrous landslides caused by the earthquake of March 27, 1964 (fig. 3A).

During or after drainage of the proglacial lake, and before the postglacial rise of sea level reversed the downcutting trend, the Ship Creek valley was trenched as much as 9 feet below the present sea level. In postglacial time, estuarine water flooded the valley to a level somewhat above present sea level, depositing a relatively thin clay upon the trenched older clay and the alluvial deposits in the valley bottom. Finally, during and after decline of sea level to its present position the clay was covered by modern alluvium.

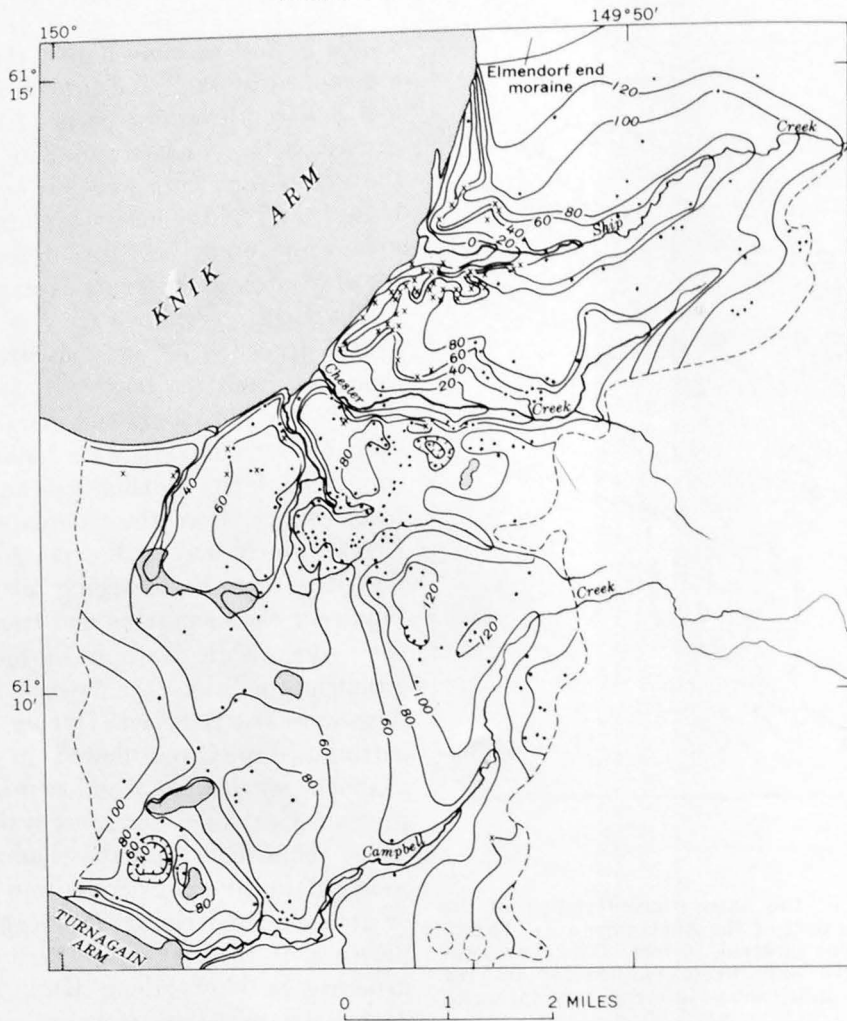


FIGURE 6.—Contour map of the top of the Bootlegger Cove Clay in part of the Anchorage area. Datum is mean sea level; contour interval, 20 feet. Dots show location of wells from which data were obtained for drawing contour lines. Dashed lines show inferred boundaries of the clay. Larger lakes in land area underlain by the clay are shown by stippled pattern.

#### REFERENCES

- Cederstrom, D. J., Trainer, F. W., and Waller, R. M., 1964, Geology and ground-water resources of the Anchorage area, Alaska: U.S. Geol. Survey Water-Supply Paper 1773, 108 p.
- Karlstrom, T. N. V., 1964, Quaternary geology of the Kenai Lowland, and glacial history of the Cook Inlet region, Alaska: U.S. Geol. Survey Prof. Paper 443, 69 p.
- Miller, R. D., and Dobrovlny, Ernest, 1959, Surficial geology of Anchorage and vicinity, Alaska: U.S. Geol. Survey Bull. 1093, 128 p.
- Schmidt, R. A. M., 1963, Pleistocene marine microfauna in the Bootlegger Cove Clay, Anchorage, Alaska: *Science*, v. 141, p. 350-351.
- Shannon and Wilson, 1964, Report on Anchorage area soil studies, Alaska: Seattle, Wash., Shannon and Wilson, Inc., 109 p.
- Waller, R. M., Cederstrom, D. J., and Trainer, F. W., 1961, Data on wells in the Anchorage area, Alaska: Alaska Dept. Health and Welfare Hydrological Data Rept. 14, 124 p.



BASINS OF THE GULF OF MAINE<sup>1</sup>

By ELAZAR UCHUPI, Woods Hole, Mass.

*Abstract.*—Closed depressions occupy about 30 per cent of the floor of the Gulf of Maine and contain about 8 percent of the water in the gulf. In 21 of these depressions the area at sill level ranges from 27 to 10,400 sq km, and the basin floor lies 5 to 135 m below the sills, or 64 to 377 m below sea level. The closed character of the depressions, the lack of seaward gradients, and the presence of sediments similar to glacial drift suggest that glacial erosion and deposition have played significant roles in formation of the present topography of the floor of the Gulf of Maine.

sion that is generally equidimensional. Within the Gulf of Maine there are 21 such basins. There the sill depth (the depth to the low part of the ridge or swell separating one basin from another) ranges from 59 to 242 meters below sea level, and the depth to the sea floor ranges from 5 to 135 m below the sills, or 64 to 377 m below sea level (see accompanying table). The

*Depth, area, and volume of basins in the Gulf of Maine*

Basin	Depth to bottom (meters)	Depth to lowest sill (meters)	Mean depth (meters)	Area of basin at sill (square kilometers)	Volume (cubic kilometers)
Davis	295	188	219	10,400	322.4
Howell					
Murray					
Rodgers					
Sharrer					
Wilkinson	220	165	190	1,100	39.6
Black					
Cashes					
Sigsbee					
Jordan					
Truxton	311	190	214	8,070	193.7
Ammen					
Crowell	221	185	197	760	9.3
Elizabeth	304	212	235	1,310	30.1
Franklin	198	158	178	170	30.4
Georges	243	229	236	340	20.4
Lindenkohl	377	242	286	5,200	228.8
Little	238	223	235	160	1.9
Stellwagen	64	59	62	90	.3
Maces	157	114	129	210	3.2
Manan	211	161	183	1,590	35.0
Matinicus	227	183	205	600	13.2
Murr	119	70	77	190	1.0
Neddick	185	139	149	90	.9
Platts	180	167	174	1,240	8.7
Porpoise	188	154	167	320	4.2
Scantum	139	127	133	30	.2
Stellwagen	102	78	89	350	3.9
Tillies	170	81	105	390	9.4
Tusket	275	201	228	180	4.8

In 1962 the U.S. Geological Survey, in cooperation with the Woods Hole Oceanographic Institution, began a 5-year program to study the sediments, topography, and structure of the continental margin off the east coast of the United States. In the course of this investigation, Uchupi (1965) compiled a set of charts of the continental margin from all available soundings (1,800,000) of the U.S. Coast and Geodetic Survey, the Canadian Hydrographic Service, and Woods Hole Oceanographic Institution. The most striking topographic feature illustrated by these charts is the Gulf of Maine, a rectangular depression with an average depth of about 150 meters (fig. 1). It extends from Massachusetts to Nova Scotia and is bounded on the seaward side by Georges Bank and the Scotian Shelf. Northeast Channel, a U-shaped trough east of Georges Bank, provides a deep-water passageway between the gulf and the open sea. The topography of the floor of the gulf is very complex, consisting of shallow basins separated by low swells and ridges. The basins make up 30 percent of the floor of the gulf, and the swells and ridges the remaining 70 percent. This paper lists and describes the basins and discusses their origin.

## FORM AND SEDIMENTS OF THE BASINS

A submarine basin, according to the usage of the Advisory Committee on Underwater Features of the U.S. Board of Geographic Names, is a sea-floor depres-

area of individual basins, at sill depth, ranges from 27 to 10,400 square kilometers; the volume of water below sill depth ranges from 0.2 to 322 cubic kilometers, and the total volume of the basins, below sill depth, is 906 cu km. This total volume represents about 8 percent of the volume of water in the Gulf of Maine.

<sup>1</sup>Contribution 1652 of the Woods Hole Oceanographic Institution.

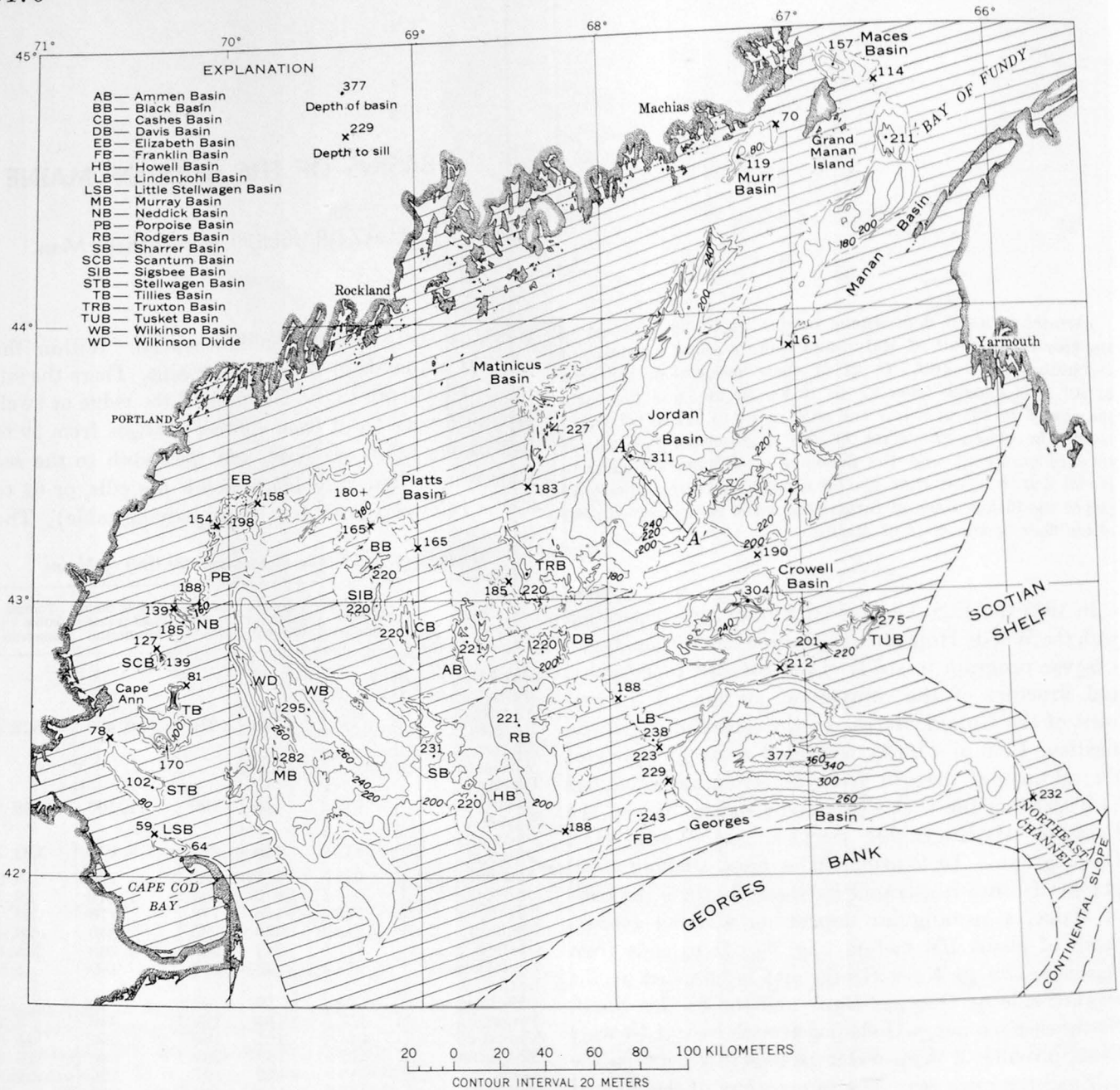


FIGURE 1.—Chart of the Gulf of Maine, showing the outlines (thin dashed lines) and topography (continuous contour lines) of the basins and the interbasin area (diagonal lines) on the floor of the gulf. Numbers indicate depth to basin sill and depth of basin, in meters. Based on soundings by U.S. Coast and Geodetic Survey, Canadian Hydrographic Service, and Woods Hole Oceanographic Institution. Profile along line A-A' is shown on figure 2.

Most of the basins in the gulf are compound — they enclose several areas, each of which is deeper than its surroundings. For example, six such depressions, Murray, Wilkinson, Sharrer, Howell, Rodgers, and Davis Basins, occur within the large basin northeast of the Cape Cod peninsula (fig. 1). The basin floor between these depressions is irregular and gently undulating, and the deeper sections of the basins are occupied by plains (fig. 2). A few of the basins contain small hills

whose crests rise slightly above sill depth. With the exception of Georges Basin and Franklin Basin, which are floored by sand, basin sediments are brown silt and till-like deposits consisting of mixed sand, silt, and gravel. The brown silt deposits, which appear to be restricted to the deeper parts of the basins, transmit sound so readily that the depressions are areas of pronounced sub-bottoms on sections made with a sonic sounder (Murray, 1947).

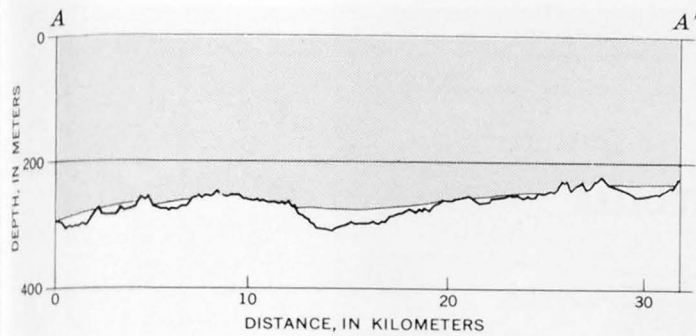


FIGURE 2.—Profile A-A' made with precision depth recorder across part of Jordan Basin, showing reflecting horizon (jagged line) beneath the floor in the deeper parts of the basin. The location of the profile is shown on figure 1.

### ORIGIN OF THE BASINS

In a study of the morphology of the sea floor off New England, Johnson (1925, p. 267) suggested that the Gulf of Maine and Georges Bank are an inner lowland and a cuesta, respectively, that had been eroded subaerially out of the continental-shelf strata and later were drowned. He also suggested that the basins within the gulf are former stream valleys, and that Northeast Channel is the gap associated with this former drainage system. He believed that glacial erosion had played an insignificant part in the formation of the gulf.

Johnson's investigation of the morphology of the sea floor of the Gulf of Maine was based on a few scattered lead-line soundings that outlined the major features of the gulf but were inadequate to portray accurately its diagnostic features. Since then, enough soundings have been collected by the U.S. Coast and Geodetic Survey and the Canadian Hydrographic Service to delineate the topography of the bottom of the gulf in considerable detail. The new sounding data, plus hundreds of sediment samples now available from the floor of the gulf, indicate that the geomorphic evolution of the gulf has been more complex than Johnson believed, and suggest that glacial erosion and deposition have played a significant role in molding its surface. Charts based on the new sounding data clearly show that in detail the floor of the gulf does not resemble drowned fluvial topography: the basins are wider and more irregular than stream channels, they are closed, they lack seaward gradients, and some are deeper than Northeast Channel, the postulated water gap leading from the gulf. These broad depres-

sions, many of which are deeper than 200 m, are typical of glaciated shelves and are absent from nonglaciated shelves (Shepard, 1931, p. 345). Many of the sediment samples from the gulf have textural characteristics similar to those of glacial deposits. These considerations suggest that glacial erosion and deposition have played significant roles in the formation of the gulf. Thus, it is suggested that the origin of the gulf is probably due to a combination of fluvial and glacial erosion, not simply fluvial erosion as Johnson believed.

During the fluvial cycle of Johnson an inner lowland (Gulf of Maine) and cuesta (Georges Bank) are believed to have been cut out of the Mesozoic and Cenozoic strata of the continental shelf. Northeast Channel probably represents the water gap of this drainage system. Cretaceous(?) erosional remnants thought to be present below the Cenozoic strata in Cape Cod Bay (Hoskins and Knott, 1961) may have been formed during this fluvial cycle. At the end of the fluvial cycle the gulf was again submerged and the fluvial topography was partially buried. Later the area was glaciated, and the former fluvial topography was exhumed and reshaped into its present form. The bulk of the sediments removed by fluvial and glacial erosion was transported from the gulf by way of Northeast Channel and deposited on the continental rise. Evidently the volume of material removed and carried seaward from this channel was very large, for the relief of the continental slope in this area is less than 1,000 m, only half that found elsewhere. Degradation within the gulf was so great that large segments of the Paleozoic rocks making up the basement were exposed. To the south and farther west, where erosion of the shelf was negligible, hundreds to thousands of meters of Mesozoic and Cenozoic strata remain on the Paleozoic rocks.

### REFERENCES

- Hoskins, Hartley, and Knott, S. T., 1961, Geophysical investigation of Cape Cod Bay, Massachusetts, using the continuous seismic profiler: *Jour. Geology*, v. 69, p. 330-340.
- Johnson, D. W., 1925, *The New England Acadian shoreline*: New York, John Wiley and Sons, 608 p.
- Murray, H. W., 1947, *Topography of the Gulf of Maine*: *Geol. Soc. America Bull.*, v. 58, p. 153-196.
- Shepard, F. P., 1931, *Glacial troughs of the continental shelves*: *Jour. Geology*, v. 39, p. 345-360.
- Uchupi, Elazar, 1965, *Map showing relation of land and submarine topography, Nova Scotia to Florida*: U.S. Geol. Survey Misc. Geol. Inv. Map I-451.



## AUTOMATIC SAMPLE CHANGER AND CONTROLLER FOR AN X-RAY QUANTOMETER

By LEONARD SHAPIRO and CAMILLO MASSONI,  
Washington, D.C.

*Abstract.*—The automatic sample changer and controller described replaces the manual sample changer of the ARL 10-channel X-ray fluorescence quantometer used in rapid rock analysis. The unit permits exposure of 32 samples to the X-ray beam, in sequence and under vacuum conditions, and automatically controls the various steps of the X-ray analysis up to, and including, the final print-out of characteristic X-ray intensities.

A 10-channel vacuum X-ray fluorescence quantometer, model 25,000 of Applied Research Laboratories, Inc., has been in use in the rapid rock analysis laboratory of the U.S. Geological Survey during the past 2 years. Procedures for preparation of rock samples and for the use of this instrument in rock analysis have been described previously by Rose and others (1963). The instrument comes equipped with a mechanism for manually placing the sample pellet under the X-ray tube and evacuating the air from the sample chamber prior to exposing the sample to the X-ray beam and counting fluorescence intensities. This paper describes a newly designated automatic sample chamber (fig. 1) and control mechanism which replace the manual sample changer and original controller of the instrument.

Advantages of the new sample changer and control for the quantometer include the following: (1) X-ray determinations can be made more quickly, (2) determinations require less time and attention of the operator, and (3) the samples can be kept in a more stable state because a continuous vacuum can be maintained throughout a series of determinations.

The writer is indebted to Ralston Fones, of the U.S. Geological Survey, for helpful suggestions during the development of the working model here described.

### AUTOMATIC SAMPLE CHANGER

The automatic sample changer consists of two components: (1) a sample carrier, and (2) a positioning mechanism.

#### Sample carrier

The sample carrier is made up of a rotatable 16-inch dish-shaped carrier plate enclosed by a metal housing. Thirty-two holes or receptacles along the periphery of the aluminum carrier plate hold the sample pellets,  $1\frac{3}{8}$  inches in diameter and approximately  $\frac{3}{16}$  inch thick (fig. 2). The 16-inch plate diameter is the maximum diameter allowable within the available space in the X-ray unit. The metal housing in which the carrier is positioned (fig. 3) is airtight and air in it can be evacuated by conventional means. A drive shaft (*M*) passes through a Teflon sleeve (*N*) connecting the evacuated side and the air side of the carrier housing. This shaft is offset from the center of the housing and carries a gear (*H*) which meshes with a gear (*I*) around a center post (*O*), which in turn is fastened to the carrier plate. A thin sheet of lead (*G*) on the bottom of the carrier housing functions as an absorber for strong radiation.

In the original construction the drive shaft was centrally located and was fastened to the carrier plate, but it was found that on evacuation of the air from the carrier housing, the housing flexed enough to press upon the shaft and cause it to bind. To eliminate this problem a stainless steel center post (*O*) was constructed to hold the upper and lower walls of the housing apart internally, and the carrier plate was driven by an off-center drive gear.

Samples are inserted into a receptacle in the lower face of the carrier plate through a hatch (*D*) on the

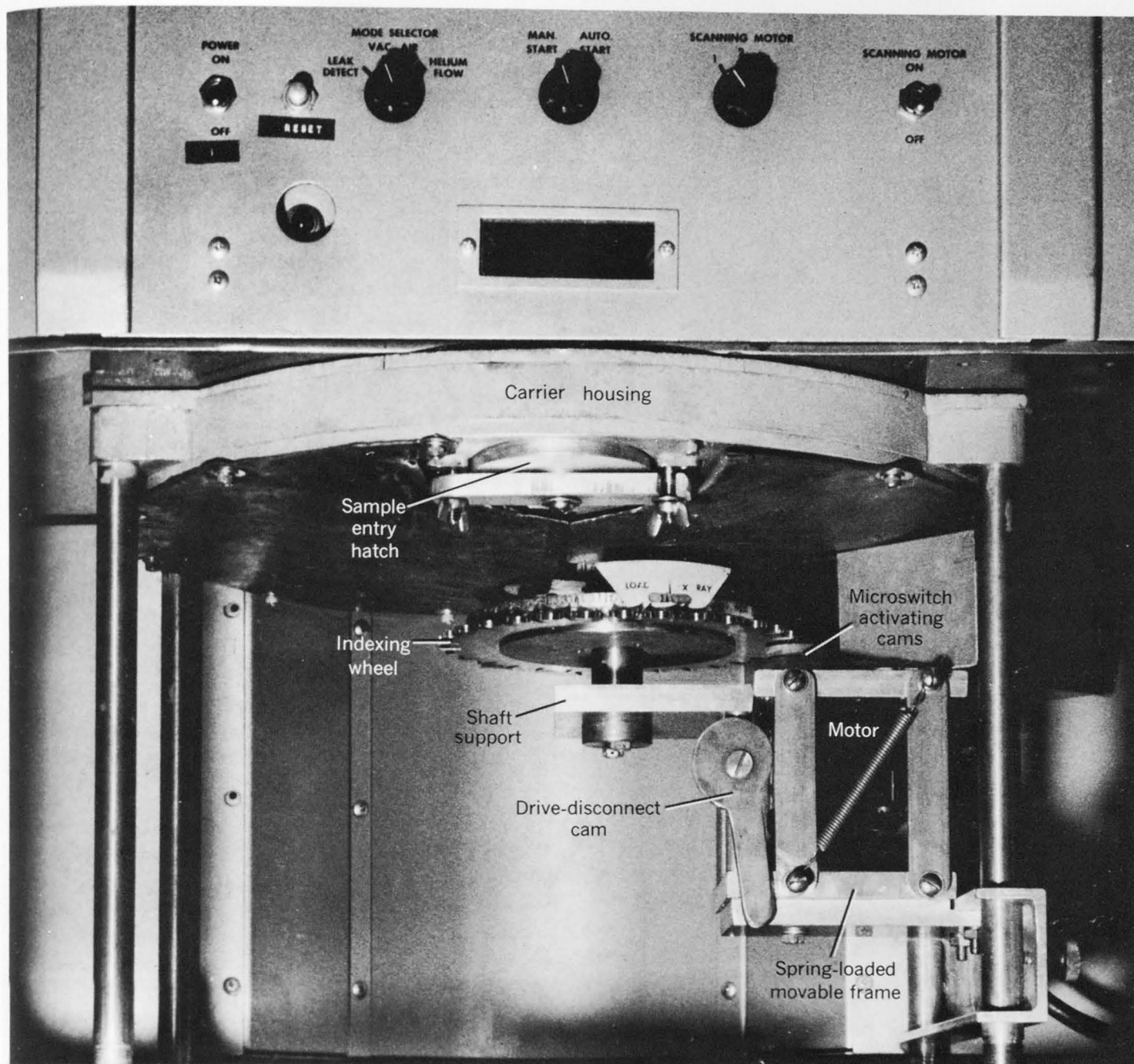


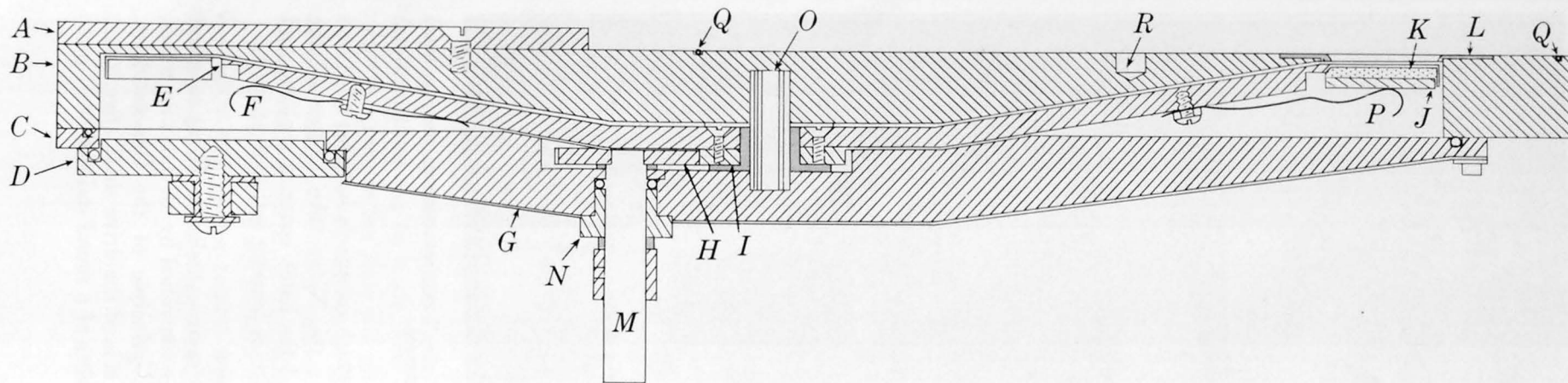
FIGURE 1.—Automatic sample changer in operating position. Some of the controls for the X-ray quantometer, and the RESET button for the sample changer, are shown above the changer.

bottom of the carrier housing. The samples are placed one at a time face up into the receptacles, where they press against a protruding ledge. A brass disk (*J*) slightly less than  $1\frac{3}{8}$  inches in diameter and about  $\frac{1}{8}$  inch thick is placed below the sample, and a spring clip (*P*) is pressed against this disk to support the sample in position. The drive shaft (*M*) is then rotated so that the next receptacle is over the entry hatch, and the loading operation is repeated with the next sample. A numbering indicator fastened to the

drive shaft shows which receptacle is being filled and which one is under the X-ray tube. After all the receptacles are filled the hatch cover is replaced and locked, and the air in the housing is then evacuated.

#### Positioning mechanism

Positioning of the samples under the X-ray tube and at the entry hatch is controlled by an indexing wheel, constructed on the principle of the Geneva drive, fastened on the air side of the drive shaft (figs. 2 and 4). This wheel consists of a round stainless steel plate



- |  |   |
|--|---|
| A, Stainless-steel reinforcement plate bolted and cemented to housing. | J, Brass disk.  |
| B, Carrier housing.  | K, Sample pellet.   |
| C, Cover.  | L, Lead shield.   |
| D, Hatch cover.  | M, Drive shaft.   |
| E, Rotating carrier plate.   | N, Teflon sleeve.   |
| F, Spring-clip sample retainer (pushed in).                            | O, Stainless steel center post.                             |
| G, Lead shield.  | P, Spring-clip sample retainer (pushed out to hold sample). |
| H, Gear on drive shaft.  | Q, O-ring sections.   |
| I, Gear on center post.  | R, Positioning hole.  |

FIGURE 3.—Details of the automatic sample changer.

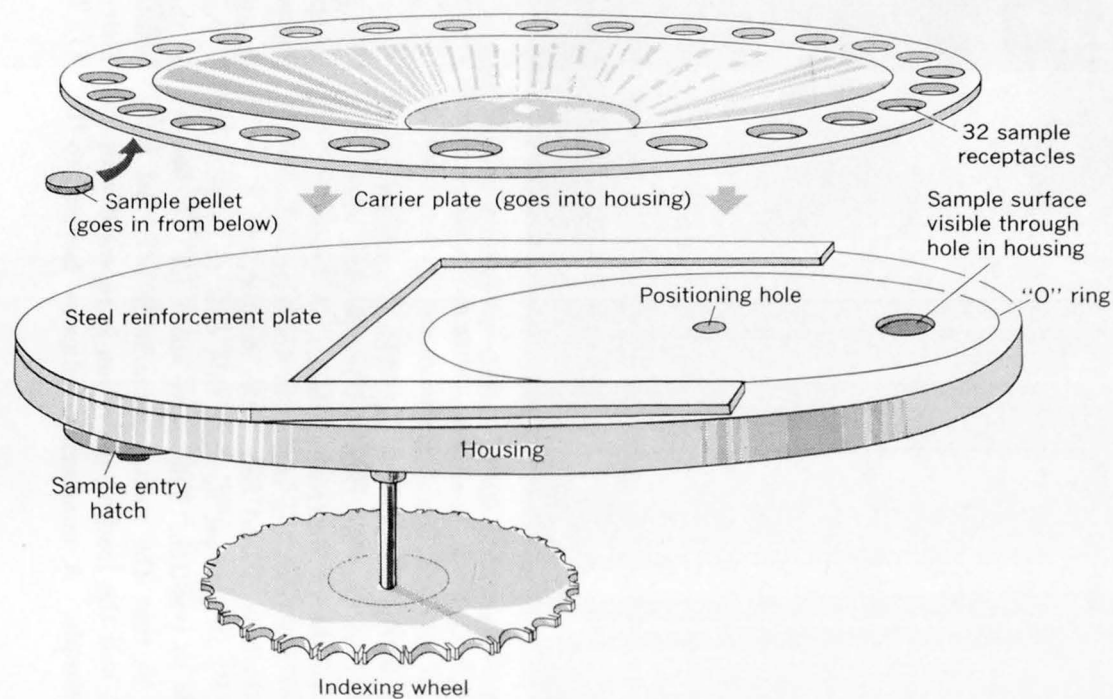


FIGURE 2.—Diagram of carrier plate and housing. (Only 27 of the 32 holes are shown in this diagram.)

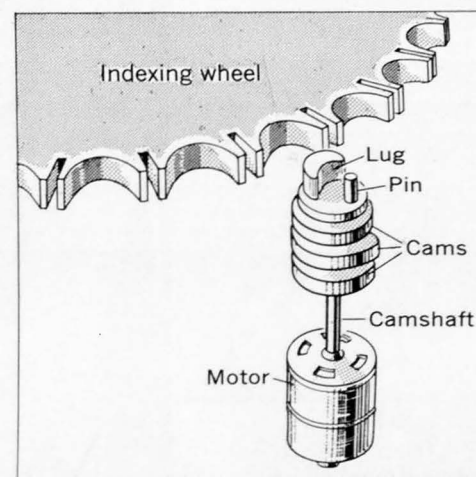


FIGURE 4.—Schematic diagram of pin drive of the Geneva drive mechanism.

7 inches in diameter with a series of semicircles and grooves cut around the periphery. The wheel is driven by a drive pin located off center and at the top of a separate camshaft in such a way that as the camshaft rotates the pin rides into a groove in the indexing wheel and rotates the wheel one sample position ( $1/32$  of a revolution) for each rotation of the camshaft. During the portion of the rotation of the camshaft when the pin is not within the groove of the indexing wheel, the wheel is locked in position by an off-center semicircular lug at the top of the camshaft, in accordance with the principle of the Geneva drive. The camshaft, and three cams attached to it, are driven by a small  $1\frac{1}{2}$ -rpm electric motor which is turned on and off by the control mechanism described later. The whole drive unit (indexing wheel, camshaft, and motor) is mounted on a spring-loaded movable frame (fig. 1), which holds the drive unit against the indexing wheel. When desired, a drive-disconnect cam can be rotated  $90^\circ$  to force the unit away from the indexing wheel, thus allowing the operator to rotate the carrier plate by hand to position any desired sample under the X-ray tube.

#### CONTROL AND RECORDING MECHANISM

The control and recording mechanism consists of four components (1) tandem recycle timer, (2) switching mechanism, (3) X-ray control console, and (4) changer-controller power box (fig. 5).

##### Timer

In the normal manual use of the X-ray quantometer, after the sample pellet has been placed into position and the sample chamber evacuated, a button is pushed which starts the X-ray integration. An external X-ray monitor serves as a timer and provides a pulse at the end of some preselected time period, usually several minutes. This pulse discontinues the integration and causes the quantometer to read out the integrated voltages in each channel in sequence in the form of a pen-and-ink recording. This read-out step takes about 30 seconds. After the vacuum in the sample chamber is eliminated, a new sample is placed in position, and the whole procedure repeated.

When the automatic sample changer is used the internal timer is replaced by an external timer which provides as accurate an integration time as does the internal timer and also allows more flexibility in control. The device used is an Industrial Timer Corp. electric tandem recycle timer containing two adjustable clocks, one calibrated in minutes and the other in seconds. It operates a single-pole single-throw switch which is open for a preset number of minutes and then

is closed for a preset number of seconds. Pairs of wires brought out from the timer paralleling the INTEGRATE and TERMINATE buttons on the X-ray control console can be connected in proper sequence using this timer.

##### Switching mechanism

The switching mechanism is activated by the camshaft which turns the indexing wheel of the automatic sample changer. To the camshaft are fastened 3 brass cams which operate the contact arms of 3 leaf-activated microswitches (fig. 5). These cams and switches provide the electromechanical coordination between the sample changer and the X-ray-unit control.

As the motor on the camshaft receives power the shaft rotates the index wheel of the automatic changer until the next sample has been moved into position. With further rotation of the camshaft, the No. 1 cam (with a short lobe) briefly contacts the No. 1 microswitch (which is connected across the INTEGRATE button and normally is open), and integration by the X-ray equipment commences, simultaneously in all channels. The input to each channel builds up a voltage across a condenser and is there stored for later read-out. A few degrees of rotation later, the No. 2 cam (with a long lobe) contacts the No. 2 microswitch (which connects the tandem recycle timer to the line and normally is open), thus activating the "minutes" clock, which commences to time a preset 2-minute X-ray integration interval.

As the motor continues to operate, the No. 3 cam opens the No. 3 microswitch (which is connected to the motor and normally is closed) and stops the motor. The lobe of the No. 2 cam is sufficiently long to permit the No. 2 microswitch to remain closed and continue channeling power to the timer. The carrier plate of the sample changer remains stationary while integration proceeds for the preset 2 minutes. At the end of this time the timer cuts on an internal switch for 4 seconds to power a relay, with double-pole single-throw contacts, in the power box. One set of contacts connects across the TERMINATE button so that integration stops and the process of read-out commences on the pen-and-ink recorder or the print-out equipment and continues for 30 seconds. The other set of contacts on the relay is connected across the No. 3 microswitch to the motor so that the motor is once again powered and the camshaft starts to rotate. In 4 seconds the motor has rotated the camshaft enough to bring all cams past their microswitches and the motor is then being powered through the closed No. 3 switch. The power to the timer is turned off when the No. 2 cam allows its microswitch to open, which is about 1 second later,

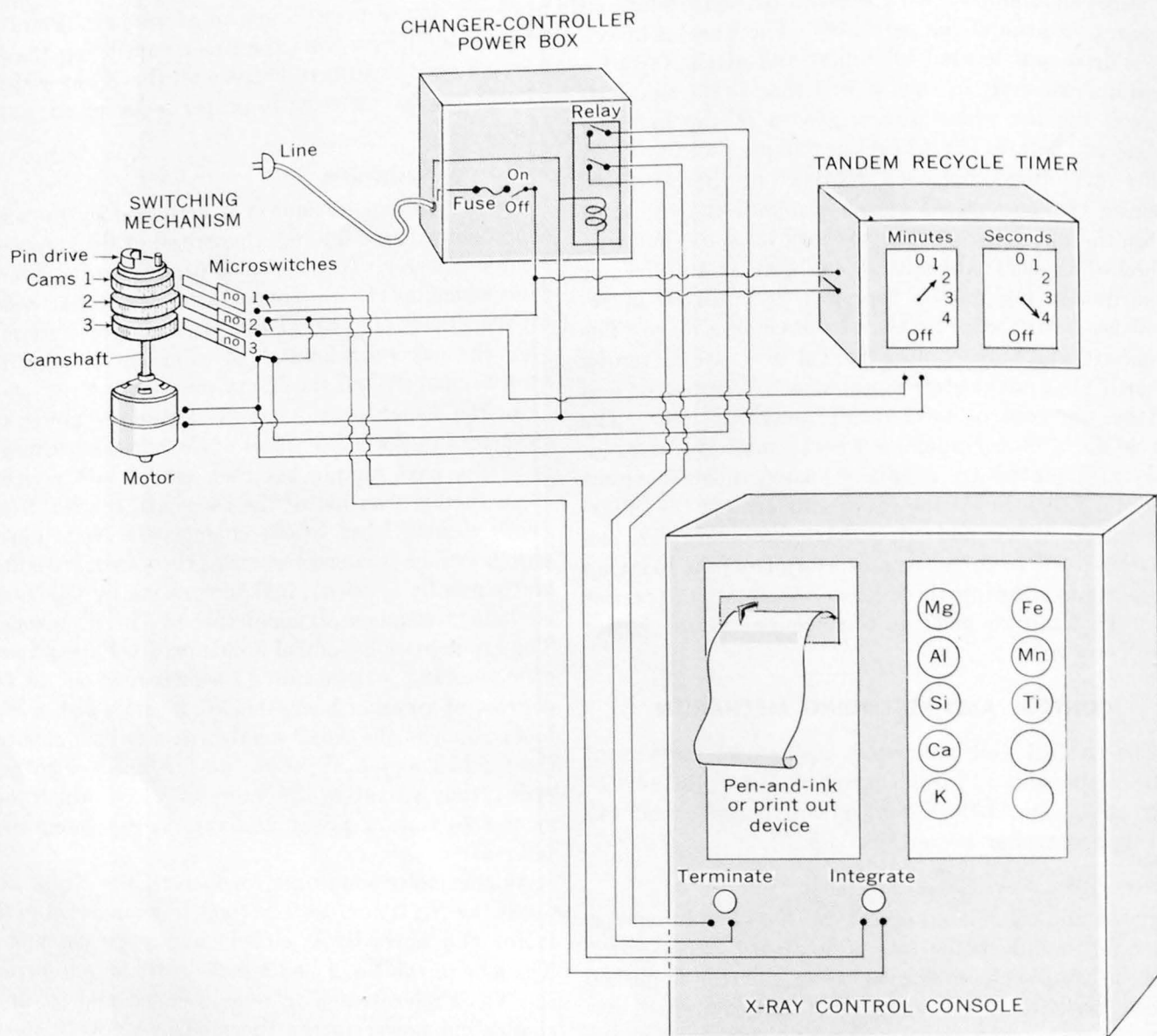


FIGURE 5.—Electrical circuitry of the control mechanism for the automatic sample changer.

and the clocks of the timer snap back to their preset time.

As read-out proceeds, the next sample is being shifted into place by the sample changer. About 15 seconds after completion of read-out and with the next sample in place, the camshaft has rotated to a point where the No. 1 cam with the short lobe presses the No. 1 switch to start the INTEGRATE step, and the entire cycle is repeated. The 32 samples can be passed through a single cycle in about 80 minutes and then recycled so that a duplicate set of data can be obtained without further effort. In fact, the cycle can be repeated any number of times. It is also possible to take advantage of the timing device built into the power

source which feeds the X-ray tube itself. The power-source unit can be set to cut off at some later time, as for example 7 hours later; thus a set of samples can be inserted in the late afternoon and allowed to run during the night. After 7 hours, quadruplicate sets of data will have been obtained and the unit will then shut itself off.

#### Additional recording equipment

For further convenience a print-out device can be used in place of the pen-and-ink recorder in the X-ray console. Commercial equipment is presently available from a number of sources which will convert a d-c voltage into a pulsing voltage the frequency of which

is directly proportional to the voltage. The output from the voltage-to-frequency device is fed to a pulse counter and from there to a printer. The voltage-to-frequency device is attached directly to the pen-and-ink recorder amplifier connections without disconnecting the recorder. The printed numbers are somewhat more accurate than those made by readings from a chart and are not subject to reading error. The print-out represents a considerable time saving during a day's work.

#### OTHER MODIFICATION

Prior to the installation of the sample changer and control mechanism onto the X-ray unit it is necessary to connect a normally closed pushbutton in series with the front safety microswitch. This RESET button (fig. 1) is conveniently mounted on the front of the X-ray unit and is necessary as it is in series with a relay which will prevent the proper operation of the shutter between X-ray tube and sample compartments after vacuum has been eliminated unless the relay is de-energized and then re-energized again. Originally the manual sample changer pushed against the front safety microswitch each time a sample was changed, providing the safety function of ensuring the proper closure of the sample changer. The reset button allows the make-and-break action required by this circuitry.

#### OPERATION

When the X-ray power is on, the operation of the whole X-ray quantometer unit can be briefly described as follows: (1) The 32 samples are placed into the sample receptacles, one at a time, using the brass disks and spring clips to hold them in place. (2) The hatch cover is locked in place with thumbscrews. (3) The RESET button is pushed. (4) The START ANALYSIS button on the X-ray unit is activated, causing the vacuum pump to evacuate the air in the carrier housing and to automatically open the shutter between sample chamber and X-ray tube compartment. Evacuation is allowed to proceed to the desired level or until a constant pressure of about 50 microns is attained. (5) The indexing wheel is rotated by hand until sample 32 is indicated to be under the X-ray tube. (6) The lug at the top of the camshaft is then allowed to rest against the indexing wheel by rotation of the drive-disconnect cam on the spring-loaded movable frame. The force of the spring is sufficient to press the indexing wheel into precise position. (7) The toggle switch on the changer-controller power box is thrown, allowing current to flow. The operator need do no more — all further action is fully automatic.

#### REFERENCE

- Rose, H. J., Jr., Adler, Isidore, and Flanagan, F. J., 1963, X-ray fluorescence analysis of the light elements in rocks and minerals: *Appl. Spectroscopy*, v. 17, no. 4, p. 81-85.



## SELECTIVE REMOVAL OF $Po^{210}$ FROM AGED RADIUM STANDARDS

By KENNETH W. EDWARDS, Denver, Colo.

*Abstract.*—Aged radium standards containing significant amounts of  $Po^{210}$  have been purified by spontaneous deposition of the polonium on 22-kt gold disks. In excess of 80 percent of the polonium in solution is deposited within 48 hours at 27°C and at hydrogen-ion concentrations between 0.11 and 0.21 molar. The maximum polonium deposition (90 percent) took place at an acidity of  $[H^+] = 0.14$  molar. Polonium was determined by measuring its alpha activity with a thin-window alpha-beta counter. Results on several gold disks and on the corresponding solutions were checked with an alpha spectrometer. The method should prove useful not only in purifying radium standards but in providing a basis for measurement of polonium in natural waters.

The analytical method presently used by the Water Resources Division of the U.S. Geological Survey for the determination of radium in natural waters (Barker and Johnson, 1964) makes use of  $Ra^{226}$  standards which contain significant quantities of  $Po^{210}$ . These standards, purchased from the National Bureau of Standards, are prepared for use as gamma sources, for which purpose the presence of  $Po^{210}$  is unimportant. When used as alpha standards, however, the concentration of  $Po^{210}$  must be accurately known or the polonium must be removed.

Radium standards as furnished by the National Bureau of Standards are usually several years old. Thus, even if one assumes the radium to be free of  $Pb^{210}$  (the grandparent of  $Po^{210}$ ) at the time of preparation of the standards, a significant amount of this 20.4-year nuclide will have grown in. The activity of 138-day  $Po^{210}$  is controlled by the activity of  $Pb^{210}$  with which it may be considered to be in transient equilibrium.

The present procedure for radium determinations used in the Survey's quality of water laboratory involves the coprecipitation of radium with barium sulfate. The precipitate is aged for 10–12 days to allow nuclides in the decay series down to, but not including,  $Pb^{210}$  to grow in. The sample is then alpha counted and the activity compared to that of a radium standard prepared in the same way. Figure 1 shows the decay scheme of  $Ra^{226}$  and daughters, together with the appropriate half-lives.

It has previously been assumed that  $Po^{210}$  is present in negligible amounts in both samples and standards. While this approximation appears to be satisfactory for most natural waters, this is not true for radium standards. Examination of the alpha spectra of the barium sulfate precipitates of radium standards clearly indicates the presence of a substantial amount of  $Po^{210}$ . Because of the uncertainty in the degree of coprecipitation of polonium it seemed advisable to remove the polonium before precipitation rather than to attempt to correct for its presence in the final residue. Of the separation methods available — ion exchange, electro-deposition, and spontaneous electrochemical deposition — each has certain advantages. The last method was chosen because of its simplicity.

Spontaneous electrochemical deposition may take place when a metal is brought into contact with a solution containing ions of a more noble metal. The electrochemical displacement occurs by oxidation of the

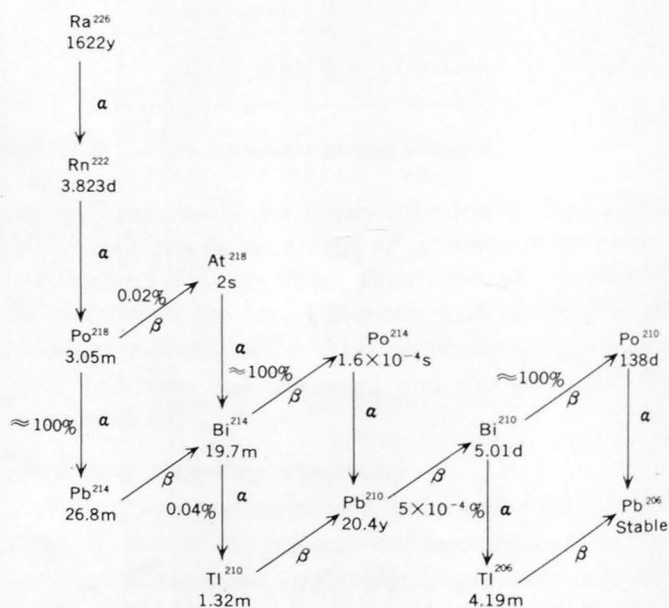


FIGURE 1.—Decay of  $Ra^{226}$  to stable  $Pb^{206}$ .

less noble metal and simultaneous reduction of the more noble metal at the solid-liquid interface. As the metallic ions are reduced at the interface they are simultaneously deposited on the solid surface, and a thin surficial deposit results.

Polonium is a relatively inactive metal, having an oxidation potential of  $-0.8$  volt for the reaction  $\text{Po} \rightarrow \text{Po}^{++} + 4e^{-}$  (Bagnall, 1957, p. 61). It has been frequently deposited on silver, nickel, monel, and copper by electrochemical displacement, and this procedure is often used in the preparation of pure polonium compounds. For present purposes it was desired to remove polonium from the radium standard without removing any radium or contaminating the solution.

The standards received from the National Bureau of Standards contain 0.1 microcuries of radium in 5 milliliters of 5-percent  $\text{HNO}_3$ . These are received in sealed glass ampoules which were prepared by the bureau in May 1947. These standards are diluted with HCl in our laboratory to a concentration of 50 picocuries per milliliter and have a final acid concentration of approximately 0.3 mole per liter.

Although both nickel and monel are efficient in removing polonium from the radium standard, they were both found to be attacked by the acid solution, even with a dilution to an acid concentration of approximately 0.01*M*. Silver is probably the most frequently used metal for spontaneous electrochemical deposition of polonium; however, its use was felt to be undesirable because of the usual formation of silver chloride.

Spontaneous deposition of polonium on pure gold has been studied by several investigators (Bagnall, 1957, p. 13-19) and has been found to be generally unsatisfactory. Erbacher (1932a), however, reported successful deposition on gold from 1*M* HCl in the presence of 0.9*M* thiourea. This complexing agent increases the solubility of gold and raises its oxidation potential above that of polonium. Erbacher (1932b) also reported successful deposition of polonium on gold from 0.1*N* HCl, but details of the procedure were not reported. It is probable, in the latter case, that either the gold contained oxidizable impurities or that the deposition was adsorption rather than an electrochemical process.

Polonium has also been reported to deposit spontaneously on gold alloyed with either copper or silver (Tamman and Rienacker, 1926). The amount of deposition on copper-gold alloys was found to decrease (in the presence of excess polonium) with increasing gold content up to 0.25 mole fraction of gold. Above this amount of gold no deposition was found to occur. The situation was similar with silver-gold alloys, although the polonium deposition did not drop com-

pletely to zero at high gold content.

The present investigation was carried out not only to find a means of removing polonium from radium solutions, but also as a preliminary step in evaluating methods for determination of polonium in natural water samples.

## ANALYTICAL METHOD

### Reagents

Aged radium standard solution — National Bureau of Standards radium gamma-ray standard 4955.

24-kt gold foil, 0.003 in. thick.

22-kt gold foil, 0.003 in. thick, 91.65 percent Au, 6.00 percent Ag, 2.35 percent Cu.

20-kt gold foil, 0.003 in. thick, 83 percent Au, 13.5 percent Ag, 3.3 percent Cu, 0.2 percent Zn.

Gold-silver alloy foil, 0.003 in. thick, 90 percent Au, 10 percent Ag.

Po<sup>210</sup> standard disk (obtained from Atomic Accessories, Valley Stream, N.Y.)

### Apparatus

Sharp Laboratories Wide-Beta low-background simultaneous alpha-beta counter.

Alpha spectrometer consisting of Technical Measurements Corp. 400-channel analyzer, Ortec 300-sq-mm silicon surface-barrier detector, Ortec model-101 preamplifier, Ortec model-201 low-noise amplifier.

Mechanical shaker table.

Constant-temperature bath.

### Procedure

Pure gold and three gold alloys were tested for removal of polonium from the radium standards. All disks were cleaned in a concentrated solution of potassium hydroxide prior to use. Adsorption on pure gold was found to be inefficient and not reproducible. In preliminary studies the three alloys tested appeared to behave identically. The remainder of the measurements were therefore made using 22-kt gold, and the following discussion applies to this alloy only.

Gold disks having a total surface area of 4.0 sq cm were added to 50-ml aliquots of 10 pc/ml (1 pc =  $10^{-12}$  curies = 2.22 disintegrations per minute) radium standard solution in 250-ml Teflon bottles and placed in an agitating water bath at  $27 \pm 0.5^\circ\text{C}$  to attain equilibrium. The rate of deposition of the polonium is shown for a typical sample in figure 2. Although equilibrium appears to be attained after approximately 2 days, a 5-day agitation period was generally used.

After equilibration the solution was poured off and the disks were washed rapidly with distilled water and ethanol, and then air dried. After allowing 3.05-min. Po<sup>218</sup> to decay, both sides of the disks were counted on a thin window proportional counter which had a measured counting efficiency of 30.6 percent for a Po<sup>210</sup> standard under nearly identical counting con-



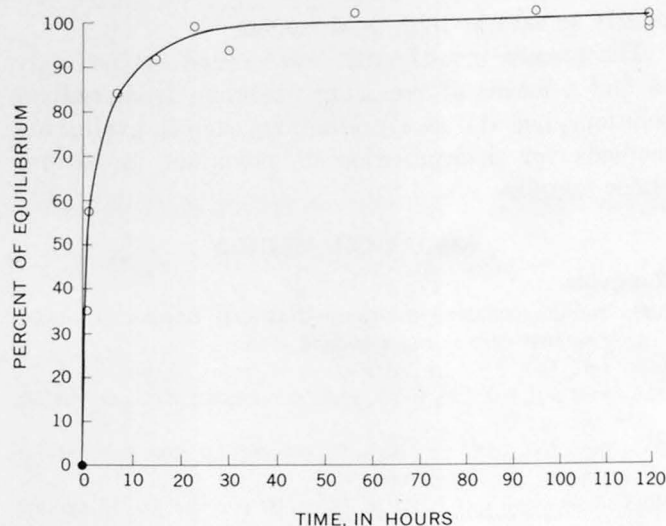


FIGURE 2.—Deposition of  $\text{Po}^{210}$  on 22-kt gold as a function of time at 27°C.

ditions. On a few samples the disks were also counted on an alpha spectrometer to check the purity of the polonium deposit. A portion of the solution remaining after removal of the gold disk was evaporated to dryness on a similar gold disk, and the alpha spectrum similarly measured. A cross-check was thus obtained on the amount of polonium removed from solution.

The experiments were carried out entirely at  $27 \pm 0.5^\circ\text{C}$ . The pH of each solution was adjusted by addition of the appropriate amount of sodium hydroxide or hydrochloric acid. In many instances aliquots of the solutions were titrated to check the calculated hydrogen-ion concentration.

### RESULTS

The effect of hydrogen-ion concentration on the efficiency of polonium deposition on 22-kt gold is shown in the accompanying table and in figure 3. Under no conditions was the polonium found to be completely removed. Maximum recovery is at  $[\text{H}^{+1}] \sim 0.14$ , which gives approximately 90-percent deposition. Greater than 80-percent recovery is obtained over the interval  $0.11 < [\text{H}^{+1}] < 0.21$ .

Figure 4 shows the alpha spectra of the radium standard before purification (4A), after one extraction of the polonium (4B), and after two extractions (4C). In each of the two extractions in this experiment approximately 85 percent of the polonium in solution was removed by the gold disk. The purity of the polonium deposited on the gold disks is shown in figure 5.

It is evident from figure 4A that the initial solution contains a rather large amount of  $\text{Po}^{210}$ , and this may cause significant error in radium determinations if it

is not removed prior to precipitation with barium sulfate. Two separations are sufficient to reduce the polonium activity to a barely detectable level where its interference is negligible.

#### Deposition of $\text{Po}^{210}$ on 22-kt gold at 27°C

$[\text{H}^{+1}]$ (moles per liter)	$\text{Po}^{210}$ deposited (percent)
0.0431	7.2
.0581	15.4
.0819	43.2
.0830	23.8
.1092	86.4
.1321	87.1
.1326	91.5
.1326	92.4
.1336	88.8
.1351	88.2
.1351	87.4
.1370	89.9
.1370	88.7
.1722	84.4
.1913	86.9
.2301	72.8
.3272	66.4
.4691	1.9

Summary of averages from table:

- 92.0 (avg) for  $[\text{H}^{+1}]$  between 0.1326 and 0.1326
- 87.8 (avg) for  $[\text{H}^{+1}]$  between 0.1351 and 0.1351
- 89.3 (avg) for  $[\text{H}^{+1}]$  between 0.1370 and 0.1370

The polonium deposited on the gold disk appears to be completely free of all other radioactive elements. Thus, the deposition does not result in any loss of radium from the solution, and it remains a valid standard for radium determinations. Lead and bismuth were similarly found not to be present in detectable amounts on the disks. This is evidenced by the absence of beta activity in the deposits. The absence of  $\text{Pb}^{210}$  was also shown by agreement of  $\text{Po}^{210}$  activity as a function of time with the theoretical value for a pure  $\text{Po}^{210}$  source. Deposition of polonium on gold under the conditions described thus also gives rise to a pure polonium source for alpha spectrometry and for other uses.

The deposition appears quite definitely to be an equilibrium process. A gold disk with 4 times the surface area, that is, 8 sq cm, was found within counting error to remove the same amount of polonium from solution as the small disks. It was also observed that

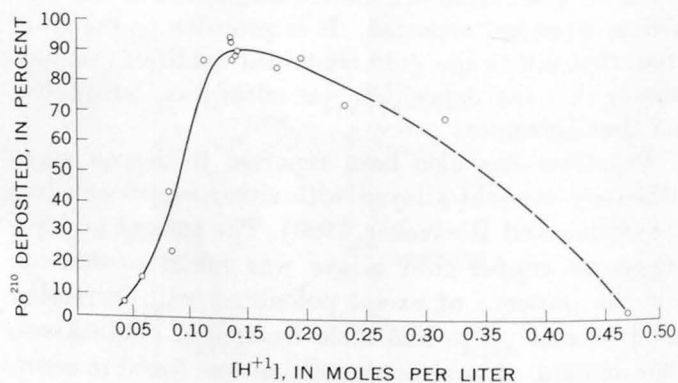


FIGURE 3.—Deposition of  $\text{Po}^{210}$  on 22-kt gold as a function of acidity at 27°C.

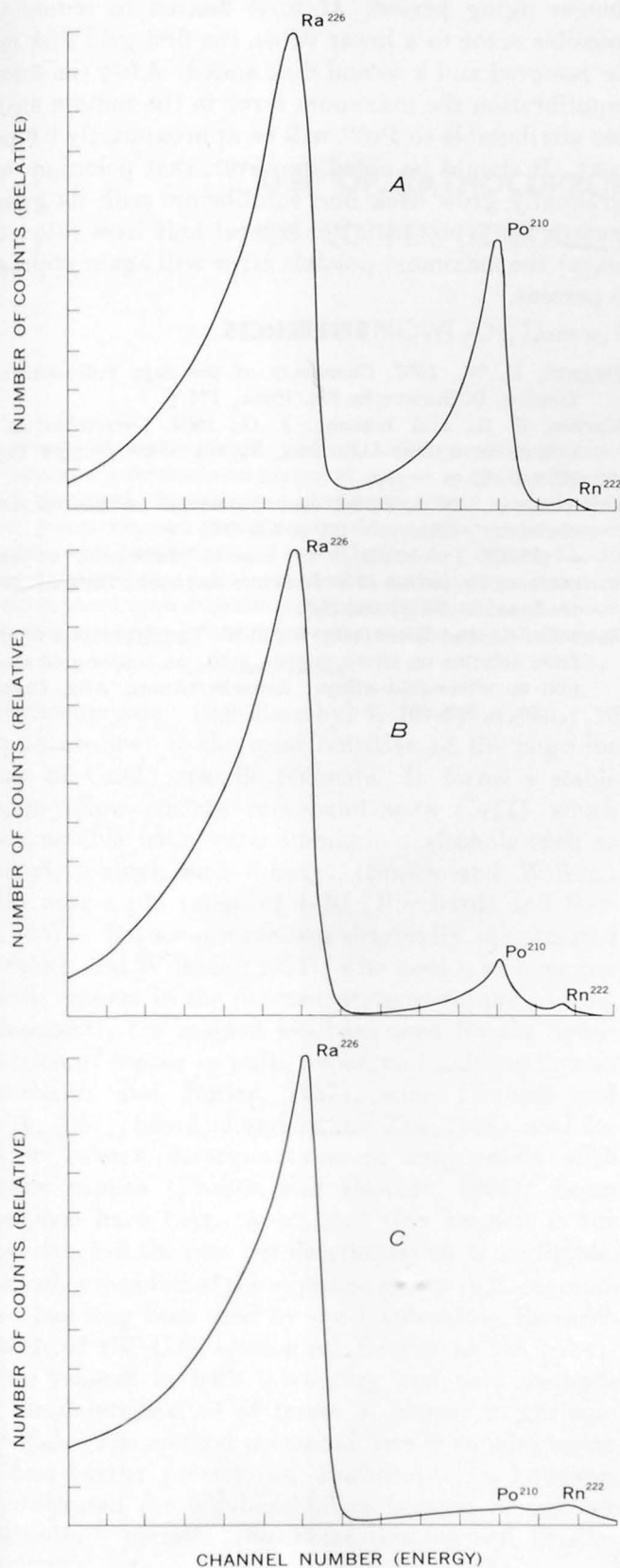


FIGURE 4.—Alpha spectra of diluted National Bureau of Standards radium. *A*, after no purification; *B*, after one  $\text{Po}^{210}$  extraction with 22-kt gold; and *C*, after two successive extractions with 22-kt gold.

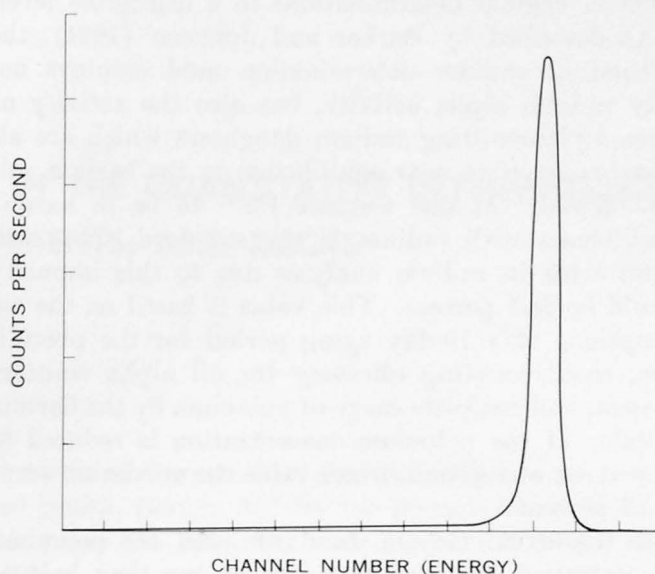


FIGURE 5.—Alpha spectrum of  $\text{Po}^{210}$  spontaneously deposited on 22-kt gold.

the two sides of the disks adsorbed unequal amounts of polonium, but that the total amount adsorbed was constant at a given acidity.

The extent of attack on the gold disks by the acid appears to be quite negligible. A spectroscopic analysis was performed on the residue obtained on evaporation of a solution of 0.13*N* HCl and 0.002*N* HNO<sub>3</sub> in which a 22-kt gold disk had been shaken for 1 week and allowed to stand an additional week. The analysis showed only 15 parts per billion of copper and 6 parts per billion of silver; no gold was detectable.

The dependence of polonium deposition on its concentration was not thoroughly checked, although the fraction removed appears to be independent of concentration for consecutive extractions from the same solution. This will be studied further, together with temperature dependence, in extending this study to development of an analytical method for determining the amount of polonium in natural waters.

#### DISCUSSION

Spontaneous electrochemical deposition of polonium on gold alloys affords a simple and direct method of removal of this impurity from radium standard solutions without contaminating the solution or altering its radium concentration. A 22-kt gold disk allowed to stand, with intermittent agitation, in a radium solution at a hydrogen-ion concentration between 0.11 and 0.21*M* will reduce the polonium concentration to less than 20 percent of its original value. If the polonium activity in the radium standard is not large, a single extraction will be sufficient to reduce polonium

error in radium determinations to a negligible level.

As described by Barker and Johnson (1964), the method of radium determination used employs not only radium alpha activity, but also the activity of three alpha-emitting radium daughters which are allowed to grow to near equilibrium in the barium sulfate deposit. If one assumes  $Po^{210}$  to be in secular equilibrium with radium in the standard, the maximum error in radium analyses due to this impurity would be 28.5 percent. This value is based on the assumptions of a 10-day aging period for the precipitate, equal counting efficiency for all alpha emitters present, and complete carry of polonium by the barium sulfate. If the polonium concentration is reduced to 20 percent of its equilibrium value the maximum error is 5.7 percent.

In the actual radium standards used, the polonium concentration has been found to be less than half of the equilibrium value, so that maximum error will be less than 2.9 percent after polonium deposition on 22-kt gold. In practice it is likely that the error is considerably less than this because of incomplete coprecipitation of the polonium and use of a slightly

longer aging period. If it is desired to reduce the possible error to a lower value, the first gold disk may be removed and a second disk added. After the second equilibration the maximum error in the radium analyses attributable to  $Po^{210}$  will be approximately 0.6 percent. It should be noted, however, that polonium will gradually grow back into equilibrium with its grandparent  $Pb^{210}$ , so that after several half lives ( $t_{1/2}=138$  days) the maximum possible error will again approach 3 percent.

#### REFERENCES

- Bagnall, K. W., 1957, *Chemistry of the rare radioelements*: London, Butterworths Sci. Pubs., 177 p.
- Barker, F. B., and Johnson, J. O., 1964, *Determination of radium in water*: U.S. Geol. Survey Water-Supply Paper 1696-B, 29 p.
- Erbacher, O., 1932a, Novel electrochemical process of radiochemistry: *Nature*, v. 20, p. 390-393.
- 1932b, Investigation of kinetic phenomena at metal surfaces by means of radioactive methods: *Zeitschr. Elektrochem.*, v. 38, p. 532-535.
- Tamman, G., and Rienacker, W., 1926, The deposition of  $RaF$  from solution on silver, copper, gold; on copper-gold alloys, and on silver-gold alloys: *Zeitschr. Anorg. Allg. Chemie*, v. 156, p. 275-287.



## USE OF BATHOCUPROINE IN THE QUANTITATIVE DETERMINATION OF COPPER IN SOILS, SEDIMENTS, AND ROCKS

By G. A. NOWLAN, Denver, Colo.

*Abstract.*—A highly specific and reasonably rapid instrumental method for determining traces of copper in geologic material is presented. The sample is decomposed with a mixture of nitric, perchloric, and hydrofluoric acids; estimation of copper is made with bathocuproine (2,9-dimethyl-4, 7-diphenyl-1, 10-phenanthroline) in an isoamyl alcohol extract. The standard deviation based upon duplicate analyses of 27 samples of stream sediments and rocks is 0.84 ppm copper for the range 5–50 ppm.

Bathocuproine (2,9-dimethyl-4, 7-diphenyl-1, 10-phenanthroline) is the most sensitive of the cuproine group of Cu(I) specific reagents. It forms a stable orange-yellow chelate compound with Cu(I) which is extractable with water-immiscible alcohols such as isoamyl, n-amyl, and n-hexyl (Smith and Wilkins, 1953) over a pH range of 4–10 (Borchardt and Butler, 1957). Bathocuproine was originally investigated by Smith and Wilkins (1953), who used it as a copper specific reagent in the determination of copper in iron. Subsequently the reagent has been used for the determination of copper in pulp, paper, and pulping liquors (Borchardt and Butler, 1957), wine (Banick and Smith, 1957), blood (Landers and Zak, 1958), and for copper valence determinations in conjunction with enzyme studies (Poillon and Dawson, 1963). Some objections have been raised that this reagent is too expensive, but the cost per determination is negligible.

Another member of the cuproine group (2,2'-biquinoline) has long been used by the Exploration Research Branch of the U.S. Geological Survey as the colorimetric reagent in both laboratory and field methods for the determination of traces of copper in geologic materials. The method presented here is an adaptation of these earlier procedures. Bathocuproine, however, is substituted for 2,2'-biquinoline because its greater sensitivity<sup>1</sup> permits the determination of smaller

amounts of copper than does 2,2'-biquinoline (Diehl and Smith, 1958, p. 8). By the procedure described in this paper the lower limit of detection is 5 parts per million.

### REAGENTS AND EQUIPMENT

All reagents are reagent grade. Demineralized water is used throughout the procedure.

Bathocuproine reagent solution, 0.03 percent (W/V): Dissolve 0.300 grams of bathocuproine (2,9-dimethyl-4, 7-diphenyl-1, 10-phenanthroline) in about 900 milliliters of isoamyl alcohol by heating on a steam bath. When the solution has cooled, dilute it to 1,000 ml with isoamyl alcohol. Occasionally some reagent grades of isoamyl alcohol will have a fairly conspicuous yellow color when bathocuproine is dissolved in them, owing to impurities in the alcohol. The use of a different lot of alcohol or even the use of a different brand will solve this problem.

Buffer solution: Dissolve 400 g of sodium acetate ( $\text{NaC}_2\text{H}_3\text{O}_2 \cdot 3\text{H}_2\text{O}$ ), 100 g of sodium tartrate ( $\text{Na}_2\text{C}_4\text{H}_4\text{O}_6 \cdot 2\text{H}_2\text{O}$ ), and 20 g of hydroxylamine hydrochloride ( $\text{NH}_2\text{OH} \cdot \text{HCl}$ ) in 1 liter of water. Adjust the pH to between 6 and 7 with dilute sodium hydroxide or dilute hydrochloric acid, if necessary. If necessary, make this solution copper free by shaking it with successive 50-ml portions of 0.01-percent (W/V) dithizone in carbon tetrachloride ( $\text{CCl}_4$ ) until the carbon tetrachloride layer remains green. Then shake the buffer with successive 50-ml portions of carbon tetrachloride until the carbon tetrachloride layer is colorless.

Ethanol, 95 percent.

Hydrofluoric acid (HF), 50 percent.

Nitric acid, concentrated: Distill concentrated nitric acid ( $\text{HNO}_3$ ) through a Pyrex still. This treatment yields about 68-percent nitric acid.

Nitric acid, 3N: Dilute 200 ml of concentrated distilled nitric acid to 1 liter with water.

Perchloric acid ( $\text{HClO}_4$ ), 70 percent.

Standard copper solution, 100  $\mu\text{g}/\text{ml}$ : Accurately weigh 0.1000 g of pure copper and dissolve it in 10 ml of dilute nitric acid. Evaporate the solution almost to dryness and add 2–3 drops of glacial acetic acid. Transfer the solution quantitatively to a 1-liter volumetric flask, fill to mark with water, and mix thoroughly. More dilute solutions may be prepared just

<sup>1</sup>The molar extinction coefficient is 6,220 for 2,2'-biquinoline and 14,160 for bathocuproine.

prior to use by diluting the proper amounts of this concentrated standard solution with 0.1*N* hydrochloric acid. Transmittance tubes, matched, 2 cm. Beckman model-B spectrophotometer.

### PROCEDURE

Accurately weigh 500 milligrams of -200 mesh material and put it in a 50-ml platinum evaporating dish. If organic material is present or suspected, ash for 1-2 hours at 500° C. After the dish has cooled, moisten the sample with water. Add 2 ml each of concentrated nitric acid and perchloric acid. Place the dish in a fume hood, add 15-20 ml of hydrofluoric acid and stir slightly with a platinum wire if the sample is caked. Cover the dish and allow the dish and contents to stand overnight in the fume hood. Then on a hot plate in the hood slowly evaporate the liquid to incipient dryness over a period of 2½ to 4 hours. Add 10 ml of 3*N* nitric acid to the dish and gently warm to dissolve the residue. After the residue has dissolved, transfer the contents of the dish to a 50-ml volumetric flask, using water to rinse the dish and to dilute to volume in the flask. Mix the contents of the flask well.

Under the conditions of the test a 20-ml aliquot of sample solution is a convenient amount. Should a smaller aliquot be necessary, enough water should be added with the aliquot to make a total volume of about 20 ml. Transfer the aliquot to a 125-ml separatory funnel which contains 25 ml of buffer solution and mix the two solutions. Add 10.0 ml of 0.03-percent bathocuproine solution, stopper the funnel, and shake it for 6 minutes. After the phases have been allowed to separate for several minutes, drain the water layer. Wash the alcohol layer once with 15 ml of water and again discard the water layer. Add 3 drops of 95-percent ethanol and swirl the funnel slightly to clear the alcohol layer. Pour it from the top of the funnel into a transmittance tube and read the percent transmittance at 475  $m\mu$  against isoamyl alcohol.

### STANDARDIZATION

A standard curve was established by adding 0, 1, 2, 5, 7, 10, 15 and 20  $\mu\text{g}$  of copper from standard solutions to 25-ml portions of buffer in 125-ml separatory funnels. The proper amount of water was added with the standard solution in each case to make a total of 20 ml in addition to the buffer. From that point the procedure was the same as for samples. The curve was made from the average of 6 determinations of the 0 and 20  $\mu\text{g}$  standards and 3 determinations of the others.

### DISCUSSION AND RESULTS

Because samples in this laboratory are often analyzed for lead and zinc in addition to copper, this procedure was designed to provide sufficient sample solution to permit the simultaneous determination of copper, lead, and zinc in most samples. The buffer will hold the pH between 5 and 7 when aliquots of 20 ml or less are used. One extraction was found to be sufficient; a second extraction of 16 samples gave blanks in all cases. This agrees with the results obtained by Borchardt and Butler (1957).

Smith and Wilkins (1953) state that the Cu(I) complex is affected by air oxidation at the rate of 0.05 percent per hour under ordinary laboratory conditions. These original investigators did not make a study of cation interferences, as this type of copper chelating agent has been found to be practically free of cation interference. Nor is there a record of any other systematic cation interference study. Smith and Wilkins (1953) did find that the common anions such as chloride, nitrate, perchlorate, phosphate, sulfate, and citrate do not interfere. In this present investigation the following amounts of metals were found not to interfere appreciably under the procedure described: 20 mg of Fe(III), 20 mg of aluminum, 2 mg of Cr(VI), 10 mg of Cr(III), 20 mg of Mn(II), 2 mg of Mo(VI), 2 mg of V(V), 2 mg of Co(II), 2 mg of Ni(II), and 2 mg of zinc.

Although bathocuproine has a greater inherent sensitivity than 2,2'-biquinoline, the eye is not as sensitive to the orange-yellow color of the bathocuproine copper complex as it is to the red-violet color of the 2,2'-biquinoline copper complex. Accordingly, when visual comparison methods are used, 2,2'-biquinoline will generally yield better sensitivities (Diehl and Smith, 1958, p. 7).

In conjunction with this investigation a technique for taking into solution samples with a high content of oxides of manganese was devised. In this study each of 3 samples contained from 6 to 8 percent manganese. Manganese dioxide will dissolve in hydrofluoric acid, giving a maroon-colored solution. However, when the hydrofluoric acid is nearly evaporated the manganese dioxide again forms and will not dissolve in 3*N* nitric acid. If the strong oxidizing action of concentrated nitric acid is not required for a particular sample with a high manganese content, the concentrated nitric acid may be deleted from the procedure; and 0.1 g or less of crystalline hydroxylamine hydrochloride dropped into the hot solution of hydrofluoric and perchloric acids near the beginning of the heating period will put the manganese into solution

TABLE 1.—Replicate analyses of 24 stream sediment samples and 3 rock samples

Sample No.	Copper content (parts per million)	
	1	2
A-462	7.0	7.5
A-512	14.0	13.0
A-738 <sup>1</sup>	21.5	21.5
A-741 <sup>1</sup>	8.5	8.0
A-853	15.5	16.5
A-1008	7.5	6.0
A-1016	7.5	7.5
A-1051	18.0	18.5
A-1055	9.5	8.0
A-1132	9.0	8.0
A-1285	9.0	8.0
A-1362	8.5	10.0
A-1385	12.5	12.0
A-1387	10.0	8.0
A-1392	10.5	9.0
A-1431	12.5	10.5
A-1456	21.0	21.0
A-1477	10.0	8.5
A-1514	7.0	7.5
A-1596	17.5	18.0
A-1606	22.5	23.0
A-1612	5.5	7.0
A-1833	50.5	48.0
A-1914 <sup>1</sup>	45.5	46.0
R-2A	7.0	5.5
R-6A	7.5	9.0
R-8A	5.5	5.5

<sup>1</sup> Contains 6-8 percent manganese and was treated with hydroxylamine hydrochloride as described in text.

smoothly. At this point the concentration of perchloric acid is apparently low enough to prevent its acting as a strong oxidant. Hydroxylamine hydrochloride has been shown to have a powerful solvent effect on oxides of manganese under analytical conditions quite different from these (Canney and Nowlan, 1964).

The precision of the bathocuproine method was calculated from paired analyses by the method described by Youden (1951, p. 17). The precision was

calculated for the entire procedure, using the results of duplicate determinations of 27 samples. Twenty-four of the samples were stream sediments composed of detrital rock and mineral fragments from a wide variety of rock types. Three of the samples, R-2A, R-6A, and R-8A, were rock samples of ferruginous sandstone, granite, and dolomite, respectively. The results of these analyses are shown in the accompanying table. The standard deviation is 0.84 parts per million copper. The samples with footnote references in the table contained 6-8 percent manganese and were treated with hydroxylamine hydrochloride as described above. In addition, the precision of the method, excluding sample preparation and dissolution, was determined by making duplicate determinations on 65 sample solutions. The resulting standard deviation is 0.34 ppm copper.

#### REFERENCES

- Banick, W. M., and Smith, G. F., 1957, The *in situ* determination of iron and copper in wine: *Anal. Chim. Acta*, v. 16, p. 464-472.
- Borchardt, L. G., and Butler, J. P., 1957, Determination of trace amounts of copper: *Anal. Chemistry*, v. 29, p. 414-419.
- Canney, F.C., and Nowlan, G. A., 1964, Solvent effect of hydroxylamine hydrochloride in the citrate-soluble heavy metals test: *Econ. Geology*, v. 59, p. 721, 722.
- Diehl, Harvey, and Smith, G. F., 1958, The copper reagents—cuproine, neocuproine, bathocuproine: Columbus, Ohio, G. Frederick Smith Chemical Co., 48 p.
- Landers, J. W., and Zak, B., 1958, Determination of serum copper and iron in a single small sample: *Am. Jour. Clinical Pathology*, v. 29, p. 590-592.
- Poillon, W. N., and Dawson, C. R., 1963, Copper in ascorbate oxidase: *Biochim. Biophys. Acta*, v. 77, p. 27-46.
- Smith, G. F., and Wilkins, D. H., 1953, New colorimetric reagent specific for copper: *Anal. Chemistry*, v. 25, p. 510, 511.
- Youden, W. J., 1951, *Statistical methods for chemists*: New York, John Wiley and Sons, Inc., 126 p.



## USE OF ARSENAZO III IN DETERMINATION OF THORIUM IN ROCKS AND MINERALS

By IRVING MAY and LILLIE B. JENKINS, Washington, D.C.

*Abstract.*—A method for determining low concentrations of thorium in rocks and minerals, using the reagent arsenazo III, is described. Interference data are given for 29 elements that might affect the determinations. The general procedure includes separation steps with hydrofluoric acid, potassium hydroxide, and potassium iodate. A 1-gram sample is sufficient to determine ThO<sub>2</sub> content as low as 0.5 ppm.

Thorium content of rocks and of mineral separates from rocks has been determined routinely for several years in the Washington laboratory of the Analytical Laboratories Branch of the U.S. Geological Survey. The procedure used has necessarily been long and involved because of the lack of highly selective and sensitive reagents for thorium. This procedure involved decomposition of the sample with hydrofluoric acid and fusion of the residue with potassium pyrosulfate. A series of separations was then made consisting of precipitation with potassium hydroxide using iron as a carrier, extraction of thorium with mesityl oxide (Levine and Grimaldi, 1954), and precipitation of thorium as the iodate from a nitric acid medium containing hydrogen peroxide, *d*-tartaric acid, and 8-quinolinol (Grimaldi and others, 1957). Thorium was then determined with thoron, using *meso*-tartaric acid as a masking reagent for zirconium (Fletcher and others, 1957). To determine concentrations of less than 10 parts per million of ThO<sub>2</sub>, 5-gram samples are required.

A significant simplification in procedures for determining thorium was made possible by the recent introduction of arsenazo III as a reagent for thorium. Arsenazo III (1,8-dihydroxynaphthalene-3,6-disulfonic acid-2, 7-bis [(azo-2)-phenylarsonic acid]) is probably the most sensitive reagent for thorium. It forms a stable complex with thorium in strongly acid solutions even in the presence of complex-forming anions such as sulfate, phosphate, and oxalate (Savvin, 1959, 1961, 1964).

The high sensitivity of arsenazo III for thorium makes it an appealing reagent for determining thorium in rocks. Savvin and Bagreev (1960) proposed determining thorium in rocks with arsenazo III in the presence of oxalate after a separation with hydrofluoric acid. However, they restrict the method to rocks containing a proportion between thorium and interfering elements of no more than 1:10 for titanium, 1:6 for uranium (VI), and 1:50 for some rare-earth elements. Obviously, additional separations would be required for determining low levels of thorium in many rocks.

Volynets (1960) proposed a separation procedure consisting of a peroxide fusion, leaching with water, reprecipitating thorium with ammonia, and finally separating thorium by cationic exchange from titanium, zirconium, and the rare-earth elements.

Abbey (1964) separated thorium by homogeneous precipitation of the oxalate, using calcium as a carrier after decomposing samples with a sodium peroxide sinter. This procedure does not eliminate rare-earth interference and requires the maintenance of fairly uniform calcium levels.

Furtova and others (1964) published a procedure somewhat similar to the one developed in this laboratory and described in this paper. They removed rare-earth elements by using the iodate separation of Grimaldi and others (1957). Samples were decomposed by a sodium peroxide fusion, and a preliminary separation was made by filtering the sodium hydroxide precipitate.

With the aim of simplifying and shortening our procedure for thorium, we undertook a comprehensive study of the arsenazo-III method and the interference levels for 29 elements likely to be found in significant concentrations in rocks and minerals.

The general procedure finally adopted includes separation steps with hydrofluoric acid, potassium hydroxide, and potassium iodate. The mesityl oxide

extraction formerly employed with the thoron method was eliminated. A 1-gram sample is sufficient to determine thorium concentrations as low as 0.5–10 ppm.

The arsenazo-III method is now used routinely in the Washington laboratory of the Analytical Laboratories Branch, replacing the thoron method for determining parts-per-million concentrations of thorium in rocks. Experience gained in the analysis of 300 samples has shown the new method to be more reliable, sensitive, and rapid than the thoron method.

## ANALYTICAL METHOD

### Reagents

When this work was first started, the only arsenazo III available commercially proved to be rather impure and required further purification. Most of this work was done with the reagent synthesized according to the directions of Savvin (1961) and of Zaikovskii and Ivanova (1963). Reagent of good quality is now available from several domestic dealers. The reagent solution is stable enough to keep for about 6 weeks, although there is a gradual decrease in sensitivity to thorium.

The following reagents are used in the arsenazo-III method of thorium determination:

Arsenazo III, 0.05 percent. Dissolve 500 milligrams of arsenazo III in 900 milliliters of water, stirring for several hours with a magnetic stirrer. Filter, wash with water, and dilute to 1 liter.

Calcium carrier solution, 0.5-percent CaO. Suspend 2.5 grams of CaO in about 200 ml of water. Add 100 ml of nitric acid and dilute to 500 ml with water.

Ferric nitrate carrier solution, 0.2-percent  $\text{Fe}_2\text{O}_3$ . Dissolve 0.875 g of  $\text{Fe}(\text{NO}_3)_3 \cdot 6\text{H}_2\text{O}$  in 100 ml of (1+99) nitric acid.

Hydrofluoric acid wash solution, 1 part hydrofluoric acid plus 9 parts of water.

Oxalic acid, 5 percent. Dissolve 100 g of the dihydrate in 2 liters of hot (1+1) hydrochloric acid.

Potassium hydroxide (precipitating solution), 50 percent by weight.

Potassium hydroxide (wash solution). Dilute 2 ml of the 50-percent solution to 500 ml with water.

Potassium iodate, 6 percent.

8-quinolinol, 0.5 percent in (1+99) nitric acid.

*d*-Tartaric acid. Dissolve 600 g of tartaric acid in water and dilute to 1 liter.

Standard thorium solution (1 ml = 4 mg of  $\text{ThO}_2$ ). Dissolve 4.2 g of  $\text{Th}(\text{NO}_3)_4 \cdot 4\text{H}_2\text{O}$  in 500 ml of a solution containing 25 ml of nitric acid. Standardize by precipitating thorium by the peroxy-nitrate procedure and igniting the peroxy-nitrate to form the oxide.

Standard thorium solution (1 ml = 10 micrograms of  $\text{ThO}_2$ ). Deliver from a buret into a beaker an appropriate volume of the concentrated thorium solution equivalent to 20.0 mg of  $\text{ThO}_2$ . Evaporate to dryness 3 times after the addition, each time, of 5 ml of hydrochloric acid. Add 100 ml of hydrochloric acid and dilute to 2 liters.

Preliminary tests confirmed that the medium selected by Savvin (1961) is optimum for determining

thorium, particularly in the presence of zirconium. This medium consists of 2.5*N* to 3*N* hydrochloric acid containing 10 ml of 5-percent oxalic acid and 2 ml of 0.05-percent arsenazo-III solution in a 25-ml volume

### Procedure

Weigh a 1-gram finely ground sample into a platinum dish. Digest on the steam bath with about 20 ml of nitric acid plus 25 ml of hydrofluoric acid. Evaporate finally to a volume of about 20 ml.

If the sample is not completely decomposed by the acid attack, evaporate to dryness. Add 2–3 ml of nitric acid and evaporate to dryness. Repeat twice more. Add 10 ml of nitric acid and 50 ml of water. Warm and filter, washing with hot water. Transfer the residue into a small platinum crucible and ignite. Fuse the residue with a small amount of sodium carbonate or potassium pyrosulfate. If sodium carbonate is used, dissolve the melt in water and add to the main solution. After a pyrosulfate fusion, remove sulfate by dissolving the melt in dilute nitric acid, adding 1 ml of ferric nitrate solution, and precipitating with ammonium hydroxide. Dissolve the ammonium hydroxide group with nitric acid and add to the main solution. Samples which are known to contain more than 10 ppm of  $\text{ThO}_2$  should at this point be diluted to volume and an aliquot taken for further analysis.

To the sample solution or to an aliquot, add 5 ml of the calcium carrier solution and evaporate to dryness in the platinum dish. Add 20 ml of water and 20 ml of hydrofluoric acid. Heat on the steam bath for several minutes, then turn off the steam and let stand for at least 2 hours. Add filter-paper pulp and filter through a fine 9-cm filter which has been pre-washed with hydrofluoric acid wash solution. Return the paper to the platinum dish and ash.

Fuse the residue with 2–3 g of potassium pyrosulfate, cool, and dissolve the melt in 33 ml of (1+4) nitric acid. Transfer to a beaker and dilute to 150 ml. Add methyl-red indicator and 1 ml of ferric nitrate carrier solution. Proceed with the potassium hydroxide precipitation and the iodate separation as described by Grimaldi and others (1957). The potassium hydroxide precipitate can be dissolved readily by transferring the bulk of the precipitate to the beaker prior to the addition of acid to the paper.

When aliquots representing 50 mg or less of sample are taken, the fluoride separation step is omitted. The aliquot is diluted, ferric nitrate carrier is added, and the analysis is continued with the potassium hydroxide precipitation.

The procedure of Grimaldi and others (1957) is followed to the point of evaporating the solution of the iodate precipitate to dryness. No perchloric acid



is added. The dry residue is treated two times with 2-ml portions of hydrochloric acid.

The color development with the arsenazo-III reagent is made after the hydrochloric acid evaporations. Add 1.6 ml of (1+1) hydrochloric acid to the beaker, wetting the wall of the beaker. Add 3-4 ml of water, cover, and warm 3-5 minutes on the steam bath. Cool and transfer to a 25-ml volumetric flask with several small portions of water, not exceeding 7 ml. Add 10 ml of the oxalic acid solution and 2 ml of the arsenazo-III solution. Dilute to volume with water. If the sample solution is expected to contain more than 10  $\mu\text{g}$  of  $\text{ThO}_2$ , dilute to volume without adding the oxalic acid and arsenazo-III reagent. Take an aliquot not exceeding 10  $\mu\text{g}$  of  $\text{ThO}_2$ , adjust the acidity to 1.6 ml of (1+1) hydrochloric acid, and proceed with the addition of oxalic acid and reagent.

Measure the absorbance in a 5-cm DU spectrophotometer cell at 665  $m\mu$  using as a reference solution one containing all the reagents used for the color development. Prepare a calibration curve from solutions containing 1-10  $\mu\text{g}$  of  $\text{ThO}_2$ .

## RESULTS AND DISCUSSION

Linear standardization curves are obtained with thorium levels up to 50  $\mu\text{g}$  of  $\text{ThO}_2$  per 25 ml of the final solution. The sensitivity of the reagent varies somewhat with the source of reagent and ranges between 0.003 and 0.004  $\mu\text{g}$  of  $\text{ThO}_2/\text{cm}^2$  for an absorbance of 0.001.

Excessive amounts of thorium should not be present at the color-formation step, because low results will be obtained due to a precipitation reaction. Moderately high concentrations of thorium (75-100  $\mu\text{g}$  of  $\text{ThO}_2/25$  ml) gave a pronounced Tyndall effect, and higher concentrations gave readily filterable precipitates. Tests with radiothorium tracer showed that thorium was being precipitated. This would indicate the probable formation of a ThR complex instead of the normal  $\text{ThR}_2$  complex (Nemodruk and Kochetkova, 1962; Savvin, 1964).

It is desirable to take at least a 1-g rock sample for analysis even when the thorium content is expected to be sufficiently high to require subsequent aliquoting. Much of the thorium in a rock is commonly present in relatively scarce mineral grains of high thorium content; the use of small samples, therefore, can result in appreciable sampling errors.

Interference studies were made with the elements one would find in rock and mineral analysis. Various amounts of each of the elements were checked with 3 levels of thorium: 0, 2, and 15  $\mu\text{g}$  of  $\text{ThO}_2$ . Absorbance was measured in 5-centimeter cells in a DU spectro-

photometer at 665  $m\mu$ . The results of the interference studies are given in the accompanying table, where the elements are listed as the oxides in order of decreasing interference. These interferences refer to the color-formation step in the final 25-ml volume. These levels, coupled with the acceptable error, set the limits for separation procedures. The values given in the table are the minimum quantities of the element calculated as the oxide which could cause an error of 1  $\mu\text{g}$  of  $\text{ThO}_2$  in the range of 0-15  $\mu\text{g}$   $\text{ThO}_2$  per 25 ml of final solution. The most serious interference is uranium(VI), which has a sensitivity one-tenth that of thorium. Rare-earth elements, titanium, zirconium, and nickel range in sensitivity from one-hundredth to one-thousandth that of thorium. The remaining elements have sensitivities less than one-thousandth of thorium.

### Summary of interference studies

[Elements listed in order of decreasing interference]

Element (as oxide)	Quantity equivalent to 1 $\mu\text{g}$ of $\text{ThO}_2$ (mg)	Element (as oxide)	Quantity equivalent to 1 $\mu\text{g}$ of $\text{ThO}_2$ (mg)
$\text{UO}_3$ -----	0. 01	$\text{Cr}_2\text{O}_3$ -----	7
$\text{Ce}_2\text{O}_3$ -----	. 1	$\text{HgO}$ -----	11
$\text{Sm}_2\text{O}_3$ -----	. 1	$\text{Al}_2\text{O}_3$ -----	13
$\text{Sc}_2\text{O}_3$ -----	. 2	$\text{Fe}_2\text{O}_3$ -----	20
$\text{La}_2\text{O}_3$ -----	. 2	$\text{SnO}_2$ -----	20
$\text{Tb}_2\text{O}_3$ -----	. 2	$\text{CaO}$ -----	40
$\text{Y}_2\text{O}_3$ -----	. 2	$\text{MnO}$ -----	40
$\text{TiO}_2$ -----	. 4	$\text{Bi}_2\text{O}_3$ -----	40
$\text{Lu}_2\text{O}_3$ -----	. 6	$\text{SrO}$ -----	40
$\text{ZrO}_2$ -----	. 7	$\text{BaO}$ -----	40
$\text{NiO}$ -----	. 8	$\text{PtO}_2$ -----	50
$\text{CuO}$ -----	2	$\text{V}_2\text{O}_5$ -----	80
$\text{PbO}$ -----	2	$\text{ZnO}$ -----	60
$\text{CoO}$ -----	2	$\text{MgO}$ -----	140
$\text{Au}_2\text{O}_3$ -----	6		

The interference of a number of the elements varies somewhat with the concentration of thorium; this effect is marked in the case of titanium. Depending upon its concentration and that of thorium, titanium acts either as a positive or a negative interference. The negative effect of titanium was noted by Abbey, who reported that 5 mg of titanium produced, in 30 minutes, a one-third reduction in the absorbance of 20  $\mu\text{g}$  of thorium.

Figure 1 shows the effect of titanium on various levels of thorium. Curve A shows the change in absorbance when titanium is present alone. At the 2- $\mu\text{g}$  of  $\text{ThO}_2$  level there is a positive interference, but the total absorbance is actually less than that of titanium in the absence of thorium. At the 8- $\mu\text{g}$  of  $\text{ThO}_2$  level a negative interference becomes apparent, and at the 15- $\mu\text{g}$  level, there is a marked interference. The absorbance in the presence of 5 mg of  $\text{TiO}_2$  is reduced by half. That this effect is indeed due to titanium and not to sulfate ion introduced with the titanium is shown in curve E. There is but a slight effect on the 15- $\mu\text{g}$  of  $\text{ThO}_2$

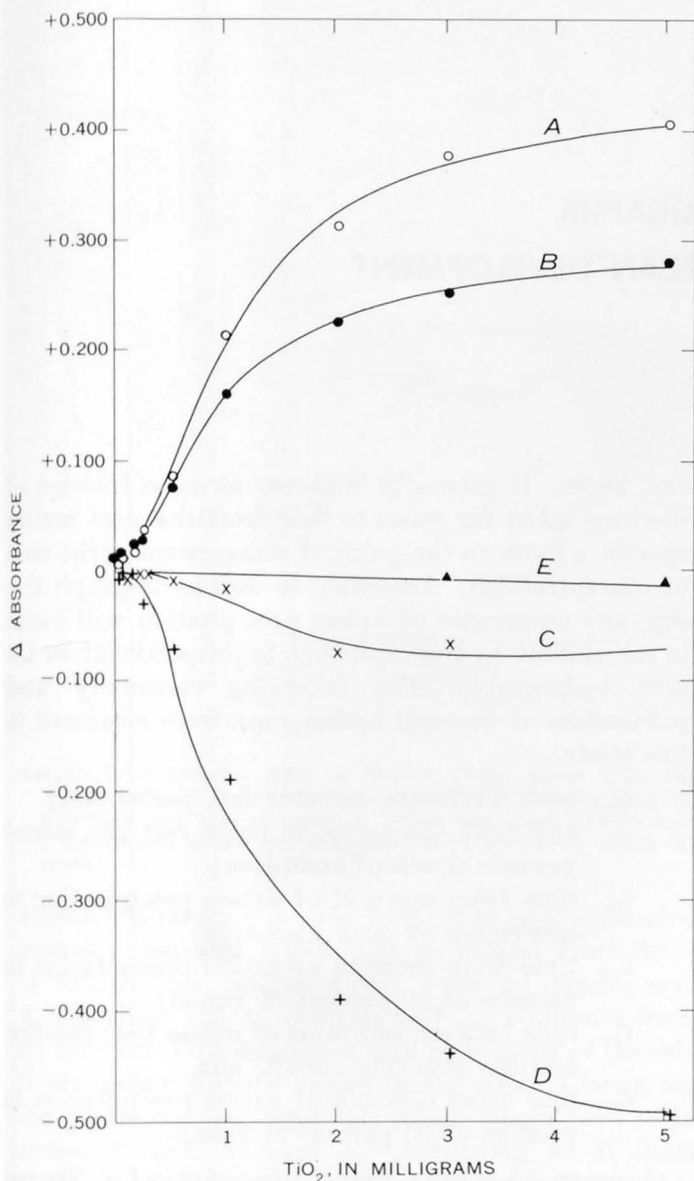


FIGURE 1.—Effect of titanium on absorbance of thorium-arsenazo-III complex: A, absorbance of titanium complex alone; B, 2  $\mu\text{g}$  of  $\text{ThO}_2$  added; C, 8  $\mu\text{g}$  of  $\text{ThO}_2$  added; D, 15  $\mu\text{g}$  of  $\text{ThO}_2$  added; and E, sulfate blank.

level on the addition of sulfate corresponding to concentrations present in the  $\text{TiO}_2$  test solutions (7.5 mg sulfate per milligram of  $\text{TiO}_2$ ).

Along with the analysis of samples, control determinations are made in this laboratory on appropriate standard rock samples. During the past year, 20 de-

terminations were made by the arsenazo-III procedure on the granite, G-1, and 39 determinations on the diabase, W-1, by Esma Campbell and Roosevelt Moore, Geological Survey chemists. The average of the determinations for G-1 is 51.7 ppm of  $\text{ThO}_2$ , with a standard deviation of 1.57 ppm of  $\text{ThO}_2$ . The average value obtained for W-1 is 2.8 ppm of  $\text{ThO}_2$  with a standard deviation of 0.22 ppm of  $\text{ThO}_2$ . The results reported for these samples (Michael Fleischer, written communication, 1965) by investigators using a variety of chemical and physical methods are: average for G-1, 52.5 ppm with a standard deviation of 7.4 ppm; average for W-1, 3.0 ppm with a standard deviation of 0.8 ppm.

#### REFERENCES

- Abbey, Sydney, 1964, Determination of thorium in rocks: *Anal. Chim. Acta*, v. 30, p. 176-187.
- Fletcher, M. H., Grimaldi, F. S., and Jenkins, L. B., 1957, Thoron-*meso*-tartaric acid system for determination of thorium: *Anal. Chemistry*, v. 29, p. 963-967.
- Furtova, E. V., Sadova, G. F., Ivanova, V. N., and Zaikovskii, F. V., 1964, Photometric determination of thorium in natural materials by means of arsenazo III: *Zhur. Anal. Khim.*, v. 19, p. 94-96.
- Grimaldi, F. S., Jenkins, L. B., and Fletcher, M. H., 1957, Selective precipitation of thorium iodate from tartaric acid-hydrogen peroxide medium: *Anal. Chemistry*, v. 29, p. 848-951.
- Levine, Harry, and Grimaldi, F. S., 1954, Mesityl oxide extraction method for thorium analysis, in Grimaldi, F. S., and others, *Collected papers on methods of analysis for uranium and thorium*: U.S. Geol. Survey Bull. 1006, p. 177-184.
- Nemodruk, A. A., and Kochetkova, N. E., 1962, Photometric study of the reaction between thorium and arsenazo III: *Zhur. Anal. Khim.*, v. 17, p. 330-335.
- Savvin, S. B., 1959, Photometric determination of thorium and uranium with arsenazo III reagent: *Doklady Akad. Nauk USSR*, v. 127, p. 1231-1234.
- 1961, Analytical use of arsenazo III: *Talanta*, v. 8, p. 673-685.
- 1964, Analytical applications of arsenazo III: *Talanta*, v. 11, p. 1-19.
- Savvin, S. B., and Bagreev, V. V., 1960, Photometric determination of thorium in rocks with arsenazo III: *Zavodskaya Lab.*, v. 26, p. 412-415.
- Volynets, M. P., 1960, [short note without title]: *Zavodskaya Lab.*, v. 26, p. 1109.
- Zaikovskii, F. V., and Ivanova, V. N., 1963, An improved method for synthesizing arsenazo III: *Zhur. Anal. Khim.*, v. 18, p. 1030.



## CHANGES IN CHARACTER OF UNIT HYDROGRAPHS, SHARON CREEK, CALIFORNIA, AFTER SUBURBAN DEVELOPMENT

By JOHN R. CRIPPEN, Menlo Park, Calif.

*Abstract.*—Unit hydrographs were derived from precipitation and streamflow records collected in a small basin in the coastal region of central California. Hydrographs representing conditions before and after suburban development showed changes similar to those observed elsewhere: runoff was accelerated, and peak flow was increased. However, the magnitude of the hydrograph changes did not correspond closely to the magnitudes reported in some other studies. Much of the difference can be ascribed to the very small size of the Sharon Creek basin. Developments in the basin included typical streets and buildings; they also included an irrigated golf course and channel modifications, which are not always considered in studies of this nature but which occur frequently in the growth of urbanization.

For several years the basin of Sharon Creek near Palo Alto, Calif., has been instrumented in a study of the hydrologic effects of urbanization. The basin (fig. 1) occupies about 245 acres. In its natural state it was grassland with scattered brush and trees. Urban development began in 1961, and by the spring of 1964 about 14 acres was occupied by single-family residences, about 12 acres by office- and apartment-type development, and 85 acres, including the area immediately upstream from the gaging station, by a golf course. The area of roofs, drives, and patios included in the 111 acres of development totaled about 161½ acres, and there were about 81½ acres of streets and roads within the undeveloped part of the basin. The remaining 125 acres of the basin was unchanged.

The relation between excess precipitation and runoff within a basin can be expressed by use of the unit hydrograph, a plot of the time distribution of runoff resulting from a unit of excess precipitation falling evenly throughout the basin during a unit of time. (Excess precipitation is that which leaves the basin as surface flow without being delayed by residence in the ground; its quantity is usually taken, by convention, as 1 inch.) The time unit is usually expressed in minutes or hours and may be a few minutes or sev-

eral hours. It generally is chosen as some fraction of the time taken for water to flow from the most remote spot in a basin to the point of measurement (the time of concentration). According to unit-hydrograph theory, any occurrence of excess precipitation will result in an outflow hydrograph that is proportional to the unit hydrograph. The following commonly used parameters of the unit hydrograph were measured in this study:

- $Q_p$ , peak discharge, in cubic feet per second;
- $q_p$ , unit peak discharge, in cubic feet per second per square mile of basin area;
- $t_p$ , time from centroid of excess precipitation to occurrence of peak discharge;
- $t_{50}$ , time from centroid of excess precipitation to passage of 50 percent of runoff;
- $t_c$ , time between centroids of excess precipitation and the resulting runoff; and
- $t_{90}$ , time from centroid of excess precipitation to passage of 90 percent of runoff.

Average 15-minute unit hydrographs for Sharon Creek have been derived from storms of 1959–60, before development began, and from storms of 1963, after about a year of fairly stable land use with the development described above. The two unitgraphs, with selected parameters, are shown in figure 2.

The parameters of the two unitgraphs reflect basin characteristics under the regime of the stream before and after development, respectively. The magnitude of peak discharge from a small basin usually increases as a result of the construction of paving and drainage facilities that accompanies the urbanization process. This occurred in Sharon Creek;  $Q_p$  increased from 180 cubic feet per second to 250 cfs. Expressed in cubic feet per second per square mile ( $q_p$ ), the increase was from 470 to 653. Snyder (1938, p. 451) related  $q_p$  to  $t_p$  for undeveloped basins in the Appalachian

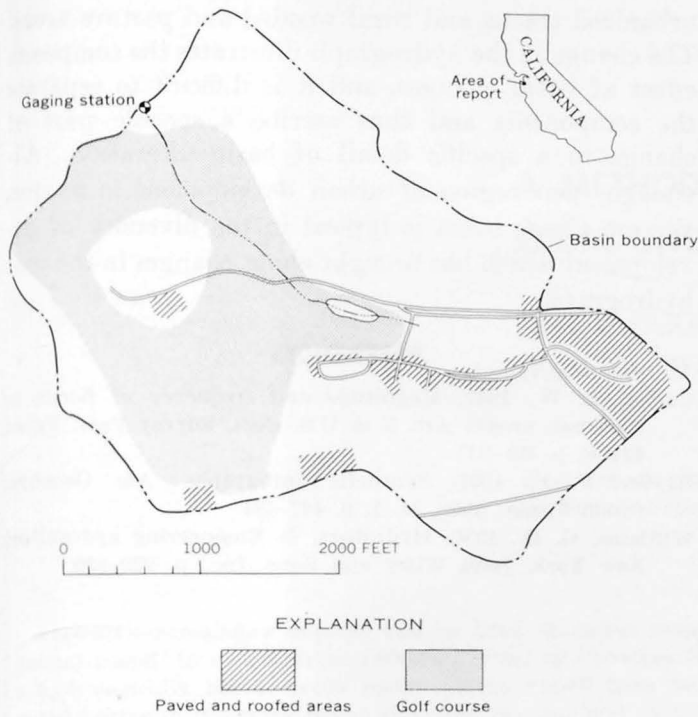


FIGURE 1.—Schematic map of Sharon Creek basin, near Palo Alto, Calif., 25 miles south of San Francisco, showing distribution and size of areas of urban and other development. Unpatterned areas are grassland with scattered brush and trees.

Highlands ranging in area from 10 to several hundred square miles, and found that  $q_p$  ranged from  $360/t_p$  to  $440/t_p$ . For Sharon Creek prior to development,  $q_p$  was about  $170/t_p$ , or about half the minimum found by Snyder. This difference may be because of the relatively gentle hillside slopes in the Sharon basin and the gentle channel gradient, which would tend to increase  $t_p$  and decrease  $q_p$ . According to Williams (1950, p. 302) a small basin would normally produce a relatively larger  $q_p$  than would a larger basin, as a result of the combined differences in  $t_p$  and  $Q_p$  of the unit hydrographs.

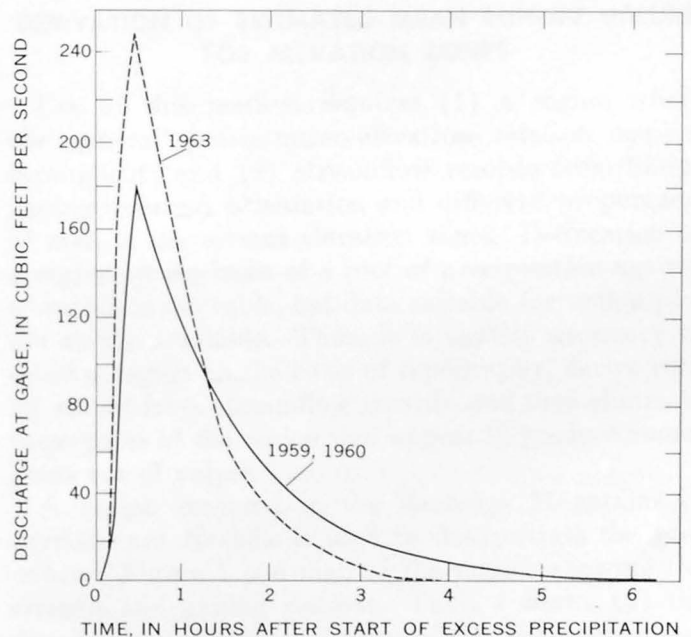
In Sharon Creek basin,  $t_p$  did not change appreciably during basin development, but  $Q_p$  increased and produced a corresponding increase in  $q_p$  of about 40 percent, from  $170/t_p$  to  $240/t_p$ .

Carter (1961, p. B10), studying basins near Washington, D.C., which ranged in area from 4 to 550 square miles, used indexes of channel length ( $L$ ) and slope ( $S$ ) as a measure of  $T_{50}$ . He found that for natural basins  $T_{50} = 3.10 (L \sqrt{S})^{0.6}$ , and for partially sewered basins  $T_{50} = 1.20 (L \sqrt{S})^{0.6}$ . In Sharon Creek before development  $T_{50} = 3.70 (L \sqrt{S})^{0.6}$ , and after development  $T_{50} = 2.60 (L \sqrt{S})^{0.6}$ . The difference between Carter's coefficient for natural basins and that for Sharon Creek before development is no greater than the scatter of points used by Carter in deriving

his relationship, and therefore is not significant. The difference between the coefficients 1.20 and 2.60 has little quantitative meaning, as the definitions of "partially sewered" and of the degree of development in Sharon basin are not precise. The change in the Sharon coefficient accompanying the change in development is consistent with the difference found by Carter.

Flood hydrographs were inspected to determine whether a relation existed between any of the lag times ( $T$ ) and the magnitude of peak flow,  $Q_p$ . The existence of such a relationship has been postulated by some workers upon the basis of data which included a wide range of magnitude. However, the variation in magnitude of peaks available for this study was not great, and no relationship was detected.

In most areas where the hydrologic effect of urbanization has been studied, the process of urban and suburban development has not closely followed the path that was expected beforehand. This is true in Sharon Creek. As in many other basins, development is a complex of the various types of land use which are associated with the working, residential, and recreational needs of a nonrural population. These land uses and their effect on hydrology vary from region to region and even between different parts of the same region.



Hydrograph parameter	1959, 1960	1963
$Q_p$ -----cfs-----	180	250
$t_p$ -----min-----	22	22
$T_{50}$ -----min-----	54	38
$T_c$ -----min-----	69	54
$T_{90}$ -----min-----	145	92

FIGURE 2.—Average 15-minute unit hydrographs of Sharon Creek. Parameters are as defined in text.

In the Sharon basin, the golf course is irrigated by imported water, and the stream which formerly flowed for only a few hours or days after heavy precipitation is now perennial with a constant flow of 0.01 to 0.02 cfs. It is necessary to subtract this artificially induced base flow from the total flood hydrograph in deriving the unit hydrograph. The amount of base flow involved is an insignificant part of the total flood runoff. However, the moist condition of the upper soil horizons resulting from irrigation reduces the infiltration capacity of the golf course and thereby causes a more rapid response of streamflow to precipitation, and produces runoff from light storms which formerly would have had no effect on streamflow.

The unit hydrograph representing conditions in 1963 was derived from storms which caused runoff from the entire basin—golf course, conventionally

urbanized tracts, and rural wooded and pasture areas. The change in the hydrograph illustrates the composite effect of basin changes, and it is difficult to separate the components and thus ascribe a specific part of change to a specific detail of basin alteration. Although each region of urban development is unique, Sharon Creek basin is typical in the diversity of development which has brought about changes in the unit hydrograph.

#### REFERENCES

- Carter, R. W., 1961, Magnitude and frequency of floods in suburban areas: Art. 5 in U.S. Geol. Survey Prof. Paper 424-B, p. B9-B11.
- Snyder, F. F., 1938, Synthetic unit-graphs: Am. Geophys. Union Trans., 1938, pt. 1, p. 447-454.
- Williams, G. R., 1950, Hydrology, in Engineering hydraulics: New York, John Wiley and Sons, Inc., p. 229-320.



## A METHOD OF ESTIMATING MEAN RUNOFF FROM UNGAGED BASINS IN MOUNTAINOUS REGIONS

By H. C. RIGGS and D. O. MOORE,  
Washington, D.C., Carson City, Nev.

*Work done in cooperation with  
the Nevada Department of Conservation and Natural Resources*

*Abstract.*—Streamflow records can be used to define mean annual runoff, in inches, from 1,000-foot zones of elevation in a hydrologically homogeneous region. Mean runoff from ungaged basins in the same region can then be computed on the basis of these derived runoff values. The method is particularly useful in semiarid regions of large relief where the simple relation between mean runoff and total basin drainage area is not well defined. Runoff values derived from one region may be used to estimate the runoff from certain other regions for which available streamflow records are inadequate to define runoff values independently. For the purpose of making such estimates, separate regions which have the same relation of mean annual precipitation to elevation are assumed to be homogeneous.

Mean runoff is closely related to size of drainage area in some regions of little topographic relief (Riggs, 1964), and the relation between runoff and area, as defined by gaging-station records, may be used to estimate mean runoff from ungaged basins in these regions. In mountainous regions, mean runoff may be poorly related to size of drainage area because the magnitudes of precipitation and of losses due to evapotranspiration change substantially with elevation. Thus, mountain drainage basins having equal areas but encompassing different ranges of elevation usually have different mean runoff. Oltman and Tracy (1949) showed the variation of mean runoff on a map of the mountainous Wind River basin in Wyoming. They used records of precipitation and runoff to prepare precipitation-altitude graphs and a graph of the variation of average annual loss with elevation. These graphs and a topographic map formed the basis for their runoff map.

This report describes a method of estimating the mean runoff at ungaged mountain sites, using streamflow records and topographic maps. The mean annual runoff, in inches, is estimated for each of several elevation zones in the region; the sum of the runoff values from the elevation zones in a drainage basin is the total runoff from that basin. Precipitation data are used to extend the runoff-elevation relation to other regions.

### DERIVATION OF ESTIMATED MEAN RUNOFF VALUES FOR ELEVATION ZONES

Use of this method requires (1) a region where one general precipitation-elevation relation applies throughout; and (2) streamflow records from basins having different orientation and different proportions of area in the several elevation zones. Delineation of a region on the basis of a plot of precipitation against elevation is desirable, but data suitable for such a plot are rarely available. Thus, it is usually necessary to select a region on the basis of topography, derive runoff values from streamflow records, and then eliminate those parts of the region that appear to produce anomalous runoff values.

A region centered in the Jarbidge Mountains in northeastern Nevada is used to demonstrate the procedure. Figure 1 is a map of the region, showing the streams and gaging stations. Table 1 shows (1) the distribution of drainage areas above the gaging stations, by 1,000-foot zones of elevation; (2) the total drainage areas; and (3) two values of mean runoff. Some of the values of mean runoff, derived from the streamflow record and shown in the next-to-last col-

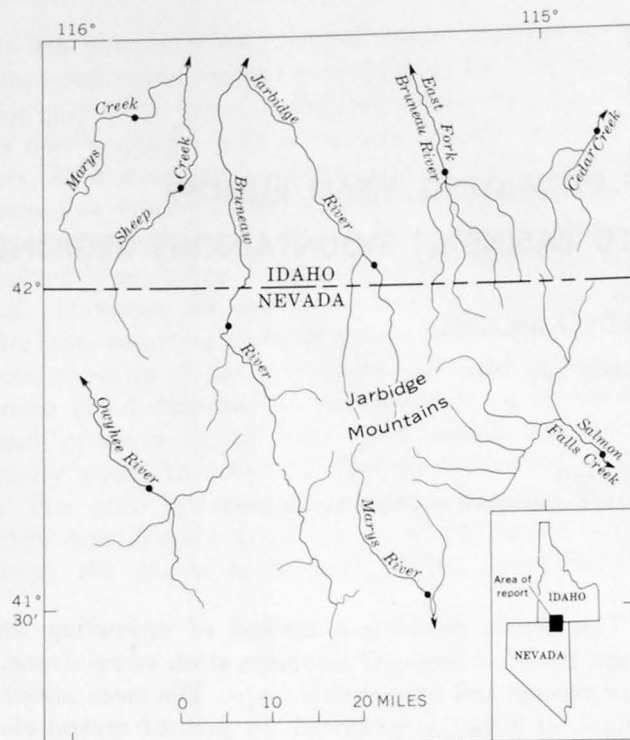


FIGURE 1.—Map of portions of Nevada and Idaho, showing the streams studied in this investigation and the gaging-station sites (dots) used in demonstrating the procedure for estimating runoff values by elevation zones.

umn of table 1, are means for the period of record shown; others in that column (those based on less than 8 years of record) are adjusted to a long-term mean on the basis of the 50-year record for Salmon Falls Creek near San Jacinto, Nev. (Values of mean runoff in the last column of table 1, to be computed, are described in a later section of this report.)

The first problem in the analysis is the selection, for the elevation zones, of values of runoff which increase smoothly with elevation and which produce the best estimates of mean runoff at a gaging station. For this purpose the best estimates are those whose sum approximately equals the mean runoff derived from the streamflow record.

From field observation it was concluded that no appreciable mean runoff occurs where the elevation is less than 5,000 feet. This absence of runoff is attributed largely to the occurrence of precipitation in low amounts and with low intensities. Mean precipitation at the highest elevation in the region is estimated from snow-course data to be about 40 inches; the mean runoff from that elevation probably would not exceed 20 inches. Therefore, mean-runoff values within the 0- to 20-inch range were arbitrarily selected for the 1,000-foot elevation zones and used to compute estimated mean runoff at the gaging stations. Final mean runoff values are defined by the streamflow data; they are not limited to the 0- to 20-inch range. That range only provides a reasonable basis for selection of the first trial values. A typical computation is shown in table 2, in which the mean runoff from each zone is the product of the assumed mean runoff for that zone and the drainage area within that zone.

Similar computations were made for each of the stations shown in table 1, using the same assumed values of mean annual runoff. The assumed values of mean annual runoff listed in column 2 of table 2 are considered the best of several sets tried because they produced the estimates of mean runoff which are closest to the values computed from the streamflow records. Estimated values of mean runoff for the

TABLE 1.—Distribution of drainage area above gaging stations by zone and mean runoff in the region shown in figure 1

Gaging station	Name	Period of record used (water years)	Drainage area (sq mi)					Total	Mean runoff (cfs)	
			Elevation zones (feet)						From stream-flow record	Estimated from runoff values by zones
			5,000-6,000	6,000-7,000	7,000-8,000	8,000-9,000	Over 9,000			
East Fork Jarbidge River near Three Creek, Idaho	1929-32, 1954-60	0	30	26	23	10	89	52	50	
East Fork Bruneau River below Three Creek, near Three Creek, Idaho	1956-60	110	54	42	4	0	210	<sup>1</sup> 29	38	
Cedar Creek near Roseworth, Idaho	1911-14	54	49	25	0	0	128	<sup>2</sup> 21	24	
Marys River at Marys River cabin, near Deeth, Nev.	1914	0	51	25	17	7	100	<sup>2</sup> 50	44	
Bruneau River near Rowland, Nev.	1914-18	37	260	45	43	0	385	<sup>2</sup> 120	112	
Owyhee River near Gold Creek, Nev.	1918-25	0	171	38	0	0	209	<sup>2</sup> 47	55	
Sheep Creek near Tindall, Idaho	1912	64	93	22	0	0	180	<sup>2</sup> 41	33	
Marys Creek near Tindall, Idaho	1911-13	68	36	6	0	0	110	<sup>2</sup> 22	14	
Salmon Falls Creek above upper Vineyard ditch, near Contact, Nev.	1949-60	49	282	94	30	6	461	<sup>1</sup> 89	136	

<sup>1</sup> Many diversions for irrigation; record not used to derive runoff values.

<sup>2</sup> Adjusted on basis of 50-year record of Salmon Falls Creek.

TABLE 2.—Computation of estimated mean runoff for East Fork Jarbidge River near Three Creek, Idaho

Range in elevation of zone (feet)	Assumed mean annual runoff		Drainage area (sq mi)	Mean runoff (cfs)
	Inches/yr	Cfs/sq mi		
5,000-6,000-----	0.5	0.037	0	0
6,000-7,000-----	3	.221	30	7
7,000-8,000-----	6	.442	26	12
8,000-9,000-----	11	.810	23	19
9,000-10,000-----	16	1.18	10	12
Total-----			89	50

basins, computed as described above, are shown in the last column of table 1. Mean runoff computed from the streamflow record is shown in the next-to-last column. Agreement between the two is considered close enough to indicate the homogeneity of the region with respect to this type of analysis.

**APPLICATION TO UNGAGED BASINS**

To compute the mean runoff from an ungaged basin in the region shown in figure 1, determine the area of the basin that lies within each of the elevation zones and compute runoff as shown in table 2, using the assumed values of mean annual runoff shown in the table. For another region, different runoff values may have to be derived. For example, the 5 sets of runoff values shown in table 3 were derived for 5 different regions in Nevada by Lamke and Moore (1965).

TABLE 3.—Runoff values by elevation zones for five regions in Nevada

Range of elevation of zone (feet)	Runoff (inches per year) in region—				
	A	B	C	D	E
5,000-6,000-----	0	0	0.5	0.5	1.6
6,000-7,000-----	0	0	1.2	3.0	5.5
7,000-8,000-----	.4	.5	3.0	6.0	10
8,000-9,000-----	2.5	3.2	5.5	11	16
9,000-10,000-----	5.6	7.0	9.5	16	21
10,000-11,000-----	9.4	12	14	21	26
11,000-12,000-----	16	18			
12,000-13,000-----		26			

In some parts of Nevada there are not sufficient streamflow records to define a set of runoff values. For those areas one of the derived sets of runoff values may be used. The following procedure, used to select the appropriate set, is based on one followed by Lamke and Moore (1965).

For each region for which runoff values had been defined, a relation of precipitation to elevation was prepared from available information. Figure 2 shows the relations derived for the numbered regions of table

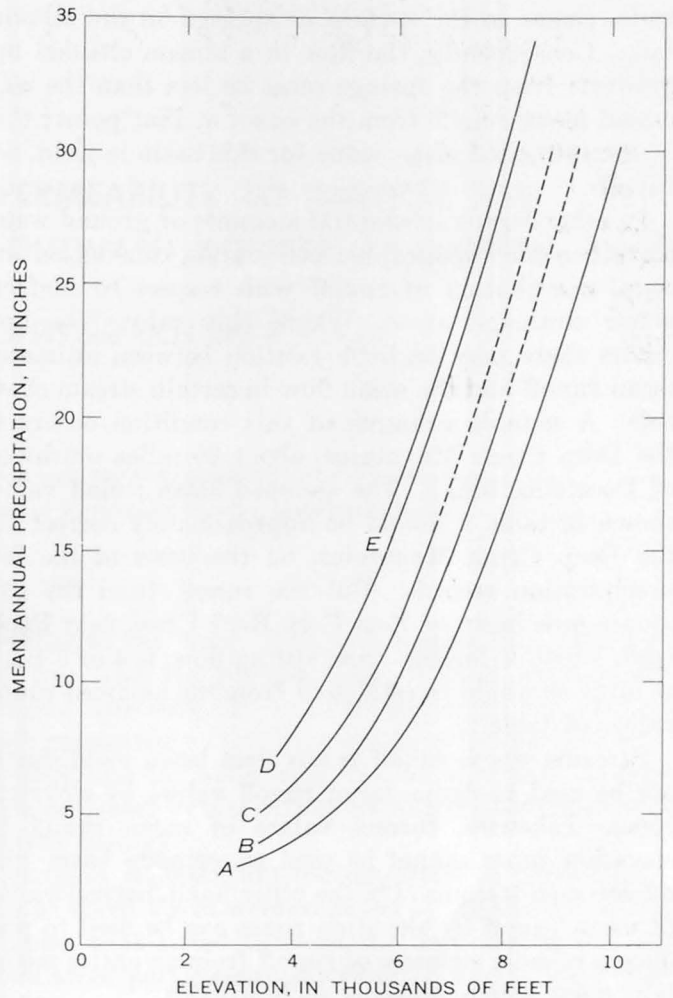


FIGURE 2.—Relation of precipitation to elevation for the regions listed in table 3.

3. For a basin widely separated from the regions of table 3, and in which a precipitation record is available, the mean annual precipitation was plotted against elevation on figure 2. The curve nearest which the plotted point fell identified the region of similarity and the appropriate set of runoff values.

**EVALUATION OF THE METHOD**

Runoff and yield are used synonymously in this paper, although runoff is defined as flow in stream channels, whereas yield may include ground-water outflow that bypasses the stream channels (Langbein and Iseri, 1960). In deriving runoff values by elevation zones it is assumed that all the yield from the basin passes down the stream channels. If this assumption is correct, application of the method gives the total yield from the basin. Field information may indicate that yield and runoff are not equal in some basins. For example, part of the yield of certain areas on the western side of Snake Valley, in eastern Ne-



vada, comes to the surface as springs on the alluvial fans. Consequently, the flow in a stream channel up-gradient from the springs must be less than the estimated mean runoff from the basin at that point; that is, the estimated mean value for this basin is yield, not runoff.

In other basins substantial amounts of ground water move beneath topographic boundaries, causing an unequal distribution of runoff with respect to surface-water drainage areas. Where this subsurface flow occurs there may be little relation between estimated mean runoff and the mean flow in certain stream channels. A notable example of this condition occurs in the Deep Creek Mountains, about 30 miles southwest of Pocatello, Idaho. The assumed mean runoff values shown in table 2 should be approximately correct for the Deep Creek Mountains, on the basis of the few precipitation records. But the runoff from the 13.7 square-mile basin of East Fork Rock Creek near Rockland, which is largely from spring flow, is 4 or 5 times as large as would be estimated from the assumed runoff values of table 2.

Streams whose runoff is less than basin yield should not be used to define mean runoff values by elevation zones. Likewise, correct values of mean runoff by elevation zones cannot be used to estimate basin runoff for such streams. On the other hand, correct values of mean runoff by elevation zones can be used to produce a reliable estimate of runoff from an entire mountain mass which contains such streams.

In addition to the effects of geology, errors in the estimated mean runoff are caused at some places by large areal variations in precipitation. These variations, which have not been adequately mapped, probably are caused by the location of mountains with respect to the prevailing paths of storms. If the effect of such a variation is large and occurs on a gaged basin, that basin may be rejected as nonhomogeneous with respect to nearby basins and would not be used in defining runoff values. The identification of a basin as nonhomogeneous restricts the ability of the analyst to estimate mean runoff reliably in the vicinity of that basin; but on the other hand it should lead, through a more detailed investigation, to a better understanding of the hydrology of the region.

The reliability of estimated mean runoff varies from region to region. One method of evaluation is the comparison of estimated and measured mean runoff from individual streams. Table 4 shows such a comparison for streams draining the Wallowa Mountains of Oregon and the Jarbidge Mountains of Nevada.

Also shown are estimates made from the relation of discharge to drainage area alone, although such estimates are known to be unreliable in semiarid mountainous regions.

The method described in this report is potentially most useful in the Great Basin and in other regions of similar topography and climate where there are few large streams but a great many small ones. Here, although water is valuable and should be inventoried, it is impracticable to gage more than a small percentage of the streams. An adequate inventory may be provided by the method described if sufficient gaging-station and storage-precipitation gage records are obtained at representative locations. Discharge measurements may be used as an aid in determining the distribution of flow in the various channels and springs in those regions where the distribution is different than that expected on the basis of the topography.

TABLE 4.—Comparison of estimated mean runoff with mean runoff based on streamflow record and on drainage area

Stream and location	Mean runoff (cfs)		
	By estimation method of this report	From streamflow record	From relation with drainage area only
Wallowa Mountains, Oregon:			
Hurricane Creek.....	75	73	65
East Fork Wallowa River.....	29	21	30
Bear Creek.....	111	113	130
Lostine River.....	159	194	135
Catherine Creek.....	132	120	192
Jarbidge Mountains, Nevada-Idaho:			
East Fork Jarbidge River.....	50	52	27
East Fork Bruneau River.....	38	29	59
Cedar Creek.....	24	21	36
Marys River.....	44	50	30
Bruneau River.....	112	120	100
Owyhee River.....	55	47	58
Sheep Creek.....	33	41	52
Marys Creek.....	14	22	33

## REFERENCES

- Lamke, R. D., and Moore, D. O., 1965, Interim inventory of surface-water resources of Nevada: Nevada Dept. Conserv. and Nat. Resources Bull. 30. [In press]
- Langbein, W. B., and Iseri, K. T., 1960, Manual of hydrology: General introduction and hydrologic definitions: U.S. Geol. Survey Water-Supply Paper 1541-A, 29 p.
- Oltman, R. E., and Tracy, H. J., 1949, Average annual runoff in the Wind River basin in Wyoming: U.S. Geol. Survey Circ. 66, 9 p.
- Riggs, H. C., 1964, The relation of discharge to drainage area in the Rappahannock River basin, Virginia, in U.S. Geological Survey Research 1964: U.S. Geol. Survey Prof. Paper 501-B, p. B165-B168.

## RELATION OF PERMEABILITY TO PARTICLE SIZE IN A GLACIAL-OUTWASH AQUIFER AT PIKETON, OHIO

By STANLEY E. NORRIS and RICHARD E. FIDLER,  
Columbus, Ohio

*Work done in cooperation with the U.S. Atomic Energy Commission  
and the Ohio Department of Natural Resources, Division of Water*

**Abstract.**—Significantly different types of particle-size distribution curves characterize two suites of sandy glacial-outwash materials that have relatively lower and higher permeability, respectively. The material of lower permeability is well sorted medium to coarse sand for which the uniformity coefficient averages 6; the more permeable material ranges from coarse sand to coarse gravel and has an average uniformity coefficient of 13.9. The uniformity coefficients of the materials are reasonably good indexes of their respective permeabilities, whereas the 60-percent-finer sizes and the effective particle sizes are poor indexes.

parallel to the river. The well nearest the river was 340 feet from the pumped well; the end wells on the parallel line were 150 and 350 feet from the pumped well, respectively. Drilling was done by the cable-tool method, and all wells were "bailed in" (that is, they were deepened by alternately bailing the hole and driving the casing).

Samples representing the materials in depth intervals of about 5 feet were collected by the driller. These samples were sifted through standard sieves, and accumulative particle-size distribution curves were prepared.

### ANALYSIS AND RESULTS

On a single plot the particle-size distribution curves for all samples from one well form two distinct families of curves. For example, all the curves for observation well W-1 lie within 1 of the 2 regions shown on figure 1. The family that lies farther to the left (that is, in the direction of finer grain size) represents materials that the driller described as "tight" or "dirty" and which are referred to in this paper as materials of relatively low permeability. The other family, which is generally less steep and farther to the right, is for materials of relatively high permeability. Two families of curves having ranges almost identical with those in figure 1 characterize the materials penetrated in the drilling of all the other wells at the Piketon site.

The material of relatively low permeability consists of gray sand that is of remarkably uniform appearance from well to well at the Piketon site and contrasts markedly in both color and texture with the brown,

The hydraulic characteristics and related physical properties of a glacial-outwash aquifer near Piketon, in southern Ohio, were investigated by the U.S. Geological Survey in collaboration with the Ohio Department of Natural Resources. The study, which was made at the request of the U.S. Atomic Energy Commission, included an aquifer test and particle-size analysis of the water-bearing materials at the Piketon site. The aquifer in the vicinity of the site is 80 to 85 feet thick; it consists in larger part of coarse sand and medium gravel and in smaller part of medium to coarse sand. The saturated thickness is about 65 feet. Because the Piketon site (lat 39°04'12" N., long 83°01'47" W.) is about 20 miles south of the glaciated area in the State, no part of the aquifer in the vicinity of Piketon consists of till.

A discharge well 12 inches in diameter and 83 feet deep was drilled at a spot 450 feet from the south bank of the Scioto River. Ten 6-inch observation wells were drilled at intervals along two lines, one of which extended from the pumped well toward the river and the other through the pumped well approximately

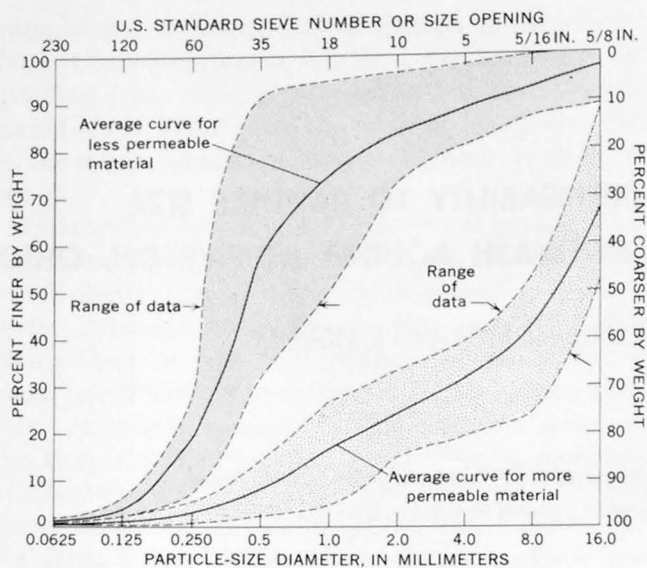


FIGURE 1.—Graphs showing particle-size analyses of samples collected in the drilling of observation well W-1 for an aquifer test at Piketon, Ohio.

coarser grained and more heterogeneous appearing sand and gravel that composes the more permeable part of the aquifer. The finer grained and less permeable material constitutes two discrete zones, a thinner one lying a few feet above the bedrock and another, 10 to 20 feet thick, separating the coarser grained material into lower and upper zones of about equal thicknesses. Generally the two zones of fine-grained material comprise about a third of the saturated thickness, but very locally they comprise as much as half.

Although the zone of fine-grained material near the middle of the aquifer functioned in slight degree as a confining bed, water-level data obtained from both deep and shallow observation wells during a 9-day aquifer test indicated that the aquifer responded hydraulically as a unit. Moreover, after development, all wells at the Piketon site responded about the same to water-level changes in the aquifer, even though some wells were screened above the lowermost poorly permeable zone, others were screened below this zone, and still others were screened partially in this lowermost zone. Thus, the permeability of the fine-grained and coarser grained materials is assumed not to be greatly different. This assumption is strengthened by the curves shown in figure 1, which indicate that the fine-grained material is more uniform and better sorted than the coarser grained material.

The coefficient of transmissibility, determined from the aquifer test, is about 215,000 gallons per day per foot; divided by the saturated thickness of 65 feet, this value implies an average coefficient of permeability

of the aquifer of about 3,300 gpd per sq ft. Several parameters were considered in an effort to find "reasonable" empirical values of the coefficient of permeability with which to tag the materials of relatively low and relatively high permeability.

One factor commonly used in application of particle-size analyses to hydrologic and hydraulic studies is the effective size, which is defined by Hazen (1893, p. 553) as the particle diameter such that 10 percent of the particles are of smaller diameter. On the particle-size distribution curves (fig. 1) the effective size, expressed in millimeters, is indicated by the point near the bottom of the plot at which the curve crosses the horizontal line designated on the left-hand margin as 10 percent finer by weight and on the right hand margin as 90 percent coarser by weight. A factor used to indicate the degree of sorting is the uniformity coefficient, which is defined as the ratio of the 60-percent-finer size to the effective size (10-percent-finer size). Wenzel (1942, p. 52) states that the uniformity coefficient indicates whether the sand particles are chiefly of the same size or whether there is a great range in their diameters. A small uniformity coefficient, denoted by a steeply sloping particle-size curve, indicates a well-sorted mixture. A large uniformity coefficient, denoted by a flatter curve, indicates a poorly sorted mixture.

Wenzel (1942, p. 50-55) gives formulas developed by Hazen, Slichter, and other early workers which show that the permeability of certain sands is proportional to the square or to some slightly lower power of the effective size. Rose and Smith (1957), working with glacial-outwash deposits in Illinois, also found that permeability could be correlated closely with the effective particle size of the samples tested.

The effective size does not appear to be a good index of the relative permeability of the Piketon samples, however. The average effective size of the material of relatively low permeability at the Piketon site is 0.22 mm, which is classed as fine sand in the classification system used by the Water Resources Division of the U.S. Geological Survey. The average effective size of the more permeable parts of the aquifer is 1.05 mm, which is classed as very coarse sand. Thus, the effective size of the more permeable material is nearly 5 times that of the less permeable material, and if permeability were related directly to the square of effective size, the permeability of the more permeable parts of the aquifer would be more than 20 times as great as that of the less permeable material. This seems unlikely in view of the hydraulic response of the aquifer and of the substantial thickness of the less permeable material relative to the remainder of the aquifer.

As with effective size, the ratio of the averages of the 60-percent-finer sizes for the two materials also seems too large to serve as an index of relative permeability. The average 60-percent-finer size for the less permeable material is 1.29 mm (very coarse sand), and the average 60-percent-finer size for the more permeable material is 8.42 mm (medium gravel), or about 6.5 times greater.

Of the parameters studied, the uniformity coefficient could be correlated best with the estimated permeability of the Piketon samples. However, nowhere in the literature could the writers find reference to studies specifically relating permeability and the uniformity coefficients of samples of sand and gravel, nor of studies showing the significance of uniformity coefficients as high—more than 30—as those determined for some of the samples at the Piketon test site.

The accompanying table presents the driller's log and the values for the effective particle size and the uniformity coefficient of the materials sampled in the drilling of observation well W-1. The zones of relatively low permeability (indicated in the table) have uniformity coefficients ranging from 1.6 to 6.5. (The uniformity coefficients of a few samples that the driller described as "tight" or "dirty" proved to be significantly larger than average and so may reflect observational errors.) For all wells, the uniformity coefficient of the material of low permeability averages about 6. The average value of the uniformity coefficient for the more permeable material is 13.9, or about double that of the less permeable material; a few values larger than 30 were found. The small uniformity coefficient of the less permeable material contrasts sharply with the very much larger values for the more permeable material.

It seemed likely that an empirical constant could be found, for each of the Piketon samples, with which the uniformity coefficient could be converted into a reasonable value for the permeability coefficient. By trial and error it was found that multiplying the uniformity coefficients of the samples by a constant ranging between about 250 and 275, depending upon the well to which it was applied, yielded values for the coefficient of permeability that appeared reasonable. For example, if 250 is used as the empirical constant for well W-1 the coefficient of permeability of the less permeable material obtained by this method ranges from 400 to 1,625 gpd per sq ft and that of the more permeable material ranges from 1,975 to 11,250 gpd per sq ft. These values, except perhaps the highest one given, appear reasonable. Moreover, when these empirical values for permeability are weighted by the respective thicknesses of the material, the resulting

*Driller's lithologic description, thickness, and depth, together with effective particle size and uniformity coefficient, of materials sampled in the drilling of observation well W-1.*

[Well drilled Sept. 17, 1963; depth to water, 20 feet]

	Thick- ness (feet)	Depth (feet)	Effective particle size (mm)	Uniformity coefficient
Sandy soil.....	4	4	0.054	18.1
Sandy clay and river silt.....	8	12	.158	3.9
Clay and medium gravel.....	4	16	.076	43.4
Fine to medium gravel with about 25 percent medium to coarse sand and heavy silt...	5	21	1.40	10.7
Do.....	5	26	.82	12.2
Medium to coarse gravel with about 20 percent fine to me- dium sand and heavy silt...	5	31	.40	45.0
Medium to coarse gravel with about 20 percent fine to me- dium sand and heavy silt, tight; bailed fairly hard.....	1 2	33	-----	-----
Gray silty fine sand and scat- tered medium gravel, tight; bailed fairly hard.....	1 3	36	.20	3.0
Do.....	1 5	41	.15	2.1
Do.....	1 5	46	.17	1.6
Do.....	1 5	51	.18	3.8
Do.....	1 5	56	.16	2.9
Do.....	1 5	61	.18	6.5
Do.....	3	64	.51	33.3
Gray medium to coarse gravel with about 35 percent me- dium to coarse sand and scat- tered boulders and heavy silt...	5	69	.71	16.3
Do.....	5	74	.44	38.6
Fine to medium sand and scat- tered medium gravel and heavy silt, firm, dirty.....	1 7	81	.29	2.2
Fine to medium gray gravel, pieces of shale, fine to me- dium sand, and heavy silt...	3	84	.39	24.9
Gray shale.....	2	86	-----	-----

<sup>1</sup> Zones of relatively low permeability.

value for the coefficient of transmissibility is 218,000 gpd per ft, or about the same as that determined from the aquifer test.

Application of the same empirical method to data from all the wells at the Piketon site indicated that the average coefficient of permeability of the less permeable material is 1,500 to 1,650 gpd per sq ft and that of the more permeable material is 3,475 to about 3,825 gpd per sq ft. If computed from data from all the wells, the average coefficient of transmissibility closely approximates the value obtained from the pumping test.

### CONCLUSIONS

A simple and direct relation appears to exist between permeability and the uniformity coefficient of the samples of glacial-outwash material from Piketon.

However, it is conjectural whether a similar relation would apply to another aquifer, or even to the same aquifer at another site. After very extensive studies of particle-size analyses of natural sand and gravel from various parts of the United States, the Edward E. Johnson Co. (1959) sums up the problem by stating: "Many attempts have been made to calculate permeability from the results of grain-size tests of sand samples—from the sand analysis. Some success has been attained in dealing with formation materials in a given locality. However, no formula has as yet been devised that will give reasonably accurate values for permeability that can be applied to a wide range of sand types." The results obtained from the Piketon data and the potential usefulness of a method of determining permeability from particle-size analysis under-

score the need for more experiments with samples from sand and gravel aquifers at other sites.

#### REFERENCES

- Hazen, Allen, 1893, Some physical properties of sands and gravels with special reference to their use in filtration: Massachusetts State Board of Health 24th Ann. Rept., p. 541-556.
- Edward E. Johnson Co., 1959, Factors affecting permeability: The Johnson Natl. Drillers' Jour., v. 31, no. 1, p. 1-3.
- Rose, H. G., and Smith, H. F., 1957, A method for determining permeability and specific capacity from effective grain size: Illinois State Water Survey Div. Circ. 59, 2 p.
- Wenzel, L. K., 1942, Methods for determining permeability of water-bearing materials, with special reference to discharging-well methods, *with a section on* Direct laboratory methods and bibliography on permeability and laminar flow, by V. C. Fishel: U.S. Geol. Survey Water-Supply Paper 887, 192 p.



## COMPUTATION OF GROUND-WATER DISCHARGE TO STREAMS DURING FLOODS, OR TO INDIVIDUAL REACHES DURING BASE FLOW, BY USE OF SPECIFIC CONDUCTANCE

By GEORGE R. KUNKLE, Iowa City, Iowa

*Work done in cooperation with the Iowa Geological Survey*

*Abstract.*—Relations between stream discharge and the chemical quality of the water as determined by specific-conductance measurements are used to analyze streamflow that consists of water from two sources. The contribution from each source is computed after measurement of the discharge and quality of the mixed streamflow water and after determination of representative quality values for each of the two kinds of water. The method is illustrated by two studies made of small streams in Iowa: (1) separation of a stream hydrograph into surface-runoff and ground-water components; and (2) verification and computation of ground-water discharge from an aquifer into a particular reach of a stream.

Two of the basic problems in hydrology are (1) the separation, on the stream hydrograph, of ground-water runoff and surface runoff or direct overland flow; and (2) the determination of the presence, site, and magnitude of ground-water discharge from a particular aquifer to a stream. Under favorable conditions, approximate solutions for these problems can be obtained by determination of representative values for the chemical quality of the water from the two sources to be differentiated and by measurement of the discharge and quality of the mixed water in the stream. This paper illustrates the solution of these problems through use of data from two small streams in Iowa.

For the purpose of this discussion, specific electrical conductance, which is used as a descriptive measure of chemical quality, is a simple, rapid, and economical test which adequately characterizes the water. Specific conductance, a measure of the resistivity of the ionized material in the water, is related to total dissolved solids by the following relation (Hem, 1959, p. 40):

(Specific conductance, in micromhos, at 25°C) ( $A$ )  
= Dissolved solids, in parts per million.

The value of coefficient  $A$  can differ among waters that are greatly different in chemical composition; however, in the examples considered here the waters are of similar composition (bicarbonate and bicarbonate sulfate), and the variation in  $A$  is insignificant.

### SEPARATION OF THE STREAM HYDROGRAPH

Data on the discharge and chemical quality of water in Four Mile Creek near Traer, in east-central Iowa, were used to differentiate the ground-water and surface-water components of the streamflow.

The part of the Four Mile Creek basin studied consists of 19.5 square miles above the gaging station near Traer. Detailed geologic investigations show that the upland areas are underlain by loess that rests on till, whereas the bottomlands are underlain by permeable alluvium, as much as 30 feet thick, that also rests on till. Only the loess and the alluvium contribute appreciable amounts of ground water to the creek. Much of the water in the till is lost from the basin as vertical leakage to underlying bedrock aquifers. Pressure head in the bedrock is too low to cause water from this aquifer to enter Four Mile Creek.

Records obtained from a recording conductance meter installed at the gaging station for a period of 5 months show that when streamflow is composed entirely of ground-water runoff the specific conductance of the creek water is uniformly 520 micromhos  $\pm 1$  percent. This value corresponds closely to those for 24 samples of ground water collected from the loess and alluvium (range, 418 to 635 micromhos, average 545; 66 percent of the values are in the range of 475 to 580 micromhos).

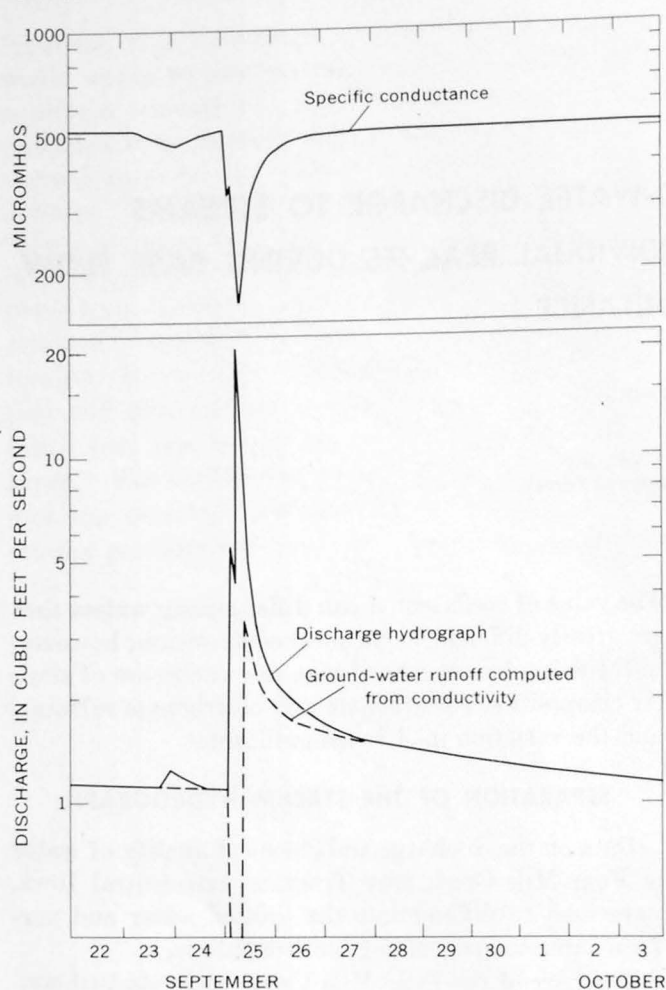


FIGURE 1.—Hydrographs showing water discharge, specific conductance, and computed ground-water runoff in Four Mile Creek near Traer, Iowa, September and October 1963.

The discharge peak shown on figure 1 is the result of a 1.10-inch rainstorm which occurred early on September 25, 1963. As surface runoff entered the creek channel, the conductance of the creek water at the gage decreased at a nearly constant rate until it reached a minimum value of 160 micromhos that coincided in time with the peak discharge. After the flood wave passed the gage, decrease in discharge was accompanied by increase in the conductance of the water, denoting a greater percentage of ground-water runoff. This general inverse relation between the magnitude of flood discharge and that of the specific conductance of the water has been noted by numerous workers (for example, Durum, 1953; Hendrickson and Krieger, 1960 and 1964; and Toler, 1965a).

In determining a representative conductance value for surface runoff, the 160 micromhos recorded during the peak rate of runoff must be considered a maximum for water derived from overland flow. Because of the

rapid change in specific conductance associated with the peak flows, it seems doubtful that the creek channel was completely flushed of ground water in channel storage; had that occurred, the minimum conductance values would probably have been sustained for a longer period of time. Other flood flows recorded at the Four Mile Creek gage had minimum values of specific conductance of 180–210 micromhos, while samples of water in surface detention, collected during storm events, had values of 120–250 micromhos. The high value of 250 micromhos was obtained from ponded water draining from a roadway graveled with limestone chips. Values of 120–150 micromhos, obtained from running water in grassed ditches draining open fields, are felt to be more representative of drainage conditions in the basin.

For the storm of September 25 the value of 160 micromhos is selected to represent surface-runoff water, and discharge values of ground-water runoff for selected times are computed by simultaneous solution of equations 1 and 2 below. These equations are similar to ones used by Corbett and others (1943, p. 89). Hem (1959, p. 231), and Toler (1965b).

$$520x + 160y = Cq \quad (1)$$

$$x + y = q, \quad (2)$$

where

$x$  = ground-water discharge,

$y$  = surface-water discharge,

$C$  = specific conductance of streamflow water, and

$q$  = total discharge.

The dashed curve on figure 1 shows ground-water discharge to the stream as computed by the equations. Although the creek channel gains water from surface runoff during the period of rising stage, it loses water to bank storage at the same time, and the equations are invalid until the creek stage drops sufficiently to permit ground water to flow into the creek again. Undoubtedly, the computed discharge values, even then, include a high percentage of water from bank storage.

At present there is no quantitative way to check the hydrograph separation obtained. Several errors caused by channel storage and peak attenuation are known to exist. Also, the selection of a representative conductance value for surface-runoff water introduces uncertainty. For the storm of September 25, the maximum conductance value for surface runoff water has purposely been used in order to compute minimum values of ground-water discharge. Despite this conservative approach, it will be noted that the computed ground-water discharges are considerably greater than would commonly be predicted using standard methods of hy-

hydrograph separation (see, for example, Hursh and Brater, 1941). However, the separation as shown depicts instantaneous discharges. If both the streamflow and ground-water hydrographs had been converted to daily averages, the ground-water separation would more closely resemble the more commonly used separation.

### MEASUREMENT OF GROUND-WATER INFLOW

Wolf Creek, in east-central Iowa, has a drainage area of 325 square miles. The creek drains morainic terrain underlain by till that is 50 to 400 feet or more thick. Bedrock in the area is mostly limestone but includes some shale. The valley of Wolf Creek is infilled with permeable alluvium averaging about 40 feet in thickness.

A piezometric-surface map for the limestone aquifer, constructed from water-well information collected from drillers, indicates that the stream and the aquifer are not hydraulically connected except in a reach of about 5 miles within the downstream portion of the basin. Upstream from this reach, pressure levels in the limestone aquifer are below the elevation of the streambed and base flow is maintained primarily by discharge from alluvium. Within the 5-mile reach, base flow is derived from the limestone aquifer and from the alluvium. Downstream the piezometric surface again falls beneath the streambed and base flow is derived from alluvium.

Because the specific conductance of water in the alluvium is significantly different from that of water in the limestone, the conductance of water in the stream should change within any reach where the stream receives an appreciable quantity of water from the limestone. In the Wolf Creek basin these natural changes in water quality will not be unduly influenced by man, as the entire basin is used for agriculture, and the stream during most periods of the year is free from irrigation withdrawals and return flows.

To verify that the reach receives discharge from the limestone and to determine the magnitude of inflow, water samples were collected and discharge measurements made at a point 8 miles upstream from the reach, midway within the reach, and at a point 7 miles downstream from the reach. Additional water samples were collected at intervals between these measuring stations to determine whether any unusual changes in quality occurred.

The data obtained at the three measuring stations are shown in the accompanying table.

At the time that the discharge measurements were made, streamflow was composed entirely of ground-

water runoff. Water flowing into the reach, representing discharge from the alluvium upstream, had a specific conductance of 475 micromhos. Because a weighted average of 19 samples collected from bedrock wells in the reach area was 1,330 micromhos, the conductance of the creek water within the reach would be expected to increase if the stream receives discharge from the bedrock. Observation shows that the conductance did increase and verifies that the reach is a discharge outlet for the limestone aquifer.

*Relation between quantity and chemical quality of base flow in Wolf Creek, Iowa, June 21, 1963*

Station location, relative to reach studied	Drainage area, $DA$ (sq mi)	Discharge, $Q$ (cfs)	$\Delta Q$ (cfs)	$\Delta Q/\Delta DA$ (cfs/sq mi)	Conductivity (micromhos/cm at 25°C)
8 miles upstream-----	190	16.4	-----	-----	475
Midway within reach-----	299	29.8	-----	-----	560
7 miles downstream-----	325	37.0	-----	-----	550

The quantity of water discharged from the limestone can be estimated by using the following equations:

$$475Q_i + 475Q_a + 1,330Q_b = CQ_o \quad (3)$$

$$Q_i + Q_a + Q_b = Q_o, \quad (4)$$

where

- $Q_i$  = discharge from upstream (inflow),
- $Q_a$  = discharge from alluvium in reach,
- $Q_b$  = discharge from bedrock in reach,
- $Q_o$  = discharge downstream (outflow), and
- $C$  = conductance of outflow water.

Simultaneous solution of equations 3 and 4, using data in the table, gives a discharge from the limestone aquifer of 3.2 cubic feet per second. Because of probable errors in the discharge measurements and of the possible additive effect of these errors in determining the gain in the reach, it is more reasonable to conclude that the limestone aquifer contributed about 3 to 4 cfs to the stream.

### REFERENCES

- Corbett, D. M., and others, 1943, Stream-gaging procedure: U.S. Geol. Survey Water-Supply Paper 888, 245 p.
- Durum, W. H., 1953, Relationship of the mineral constituents in solution to stream flow, Saline River near Russell, Kans.: Am. Geophys. Union Trans., v. 34, p. 435-442.



- Hem, J. D., 1959, Study and interpretation of the chemical characteristics of natural water: U.S. Geol. Survey Water-Supply Paper 1473, 269 p.
- Hendrickson, G. E., and Krieger, R. A., 1960, Relationship of chemical quality of water to stream discharge in Kentucky: Internat. Geol. Cong., 21st, Copenhagen 1960, *Geochem. Cycles*, pt. 1, p. 66-75.
- 1964, Geochemistry of natural waters of the Blue Grass region, Kentucky: U.S. Geol. Survey Water-Supply Paper 1700, 135 p.
- Hursh, C. R., and Brater, E. F., 1941, Separating storm hydrographs from small drainage areas into surface and sub-surface flow: *Am. Geophys. Union Trans.*, pt. 3, p. 863-870.
- Toler, L. G., 1965a, Relation between chemical quality and water discharge in Spring Creek, southwestern Georgia, in *Geological Survey Research 1965*: U.S. Geol. Survey Prof. Paper 525-C, p. 209-213.
- 1965b, Use of specific conductance to distinguish two base-flow components in Econfinia Creek, Florida, in *Geological Survey Research 1965*: U.S. Geol. Survey Prof. Paper 525-C, p. 206-208.



## RELATION OF GROUND-WATER INFLOW AND OF BANK AND CHANNEL STORAGE TO STREAMFLOW PICKUP IN THE SANTA FE RIVER, FLORIDA

By WILLIAM E. CLARK, Tallahassee, Fla.

*Work done in cooperation with the Florida Geological Survey*

*Abstract.*—The pickup in flow of the Santa Fe River in the 8-mile reach between gaging stations near High Springs and near Fort White, in north-central Florida, averages about 800 cfs and is provided entirely or almost entirely by ground-water runoff. The magnitude of streamflow pickup in this reach changes slowly, or is almost uniform, except during times of flood. At those times part of the floodwater derived from surface runoff in the region upstream goes into channel and bank storage while passing through this reach. During succeeding periods of resumed base flow, this water drains back into the stream.

Streamflow records for a reach of the Santa Fe River near High Springs, in north-central Florida (fig. 1), show features that are difficult to identify in records for most streams. The flow of the Santa Fe River, a tributary of the Suwannee River, is measured at gaging stations near High Springs and near Fort White; the Fort White station is approximately 8 miles downstream from the High Springs station. Between these stations the stream occupies a channel which has been cut into the highly permeable limestone of the Floridan aquifer. Little or no overland flow enters the river between these stations because all or nearly all the rainfall either returns directly to the atmosphere by evaporation and transpiration or infiltrates the cover of sand and clayey sand that overlies the limestone. A few miles upstream from the gaging station near High Springs, the river, responding rapidly to rainfall, receives overland flow at a high rate during storms and recedes rapidly to a low base flow after storms (Clark and others, 1964, p. 53). The flow of the river at these stations, in a reach of the river that receives no overland flow, is therefore more variable than would otherwise be expected. The result is

that the effects of changing river stages are more apparent in the records from these stations than from most other stations because these effects are not masked by the effects of local overland runoff.

Figure 2 shows hydrographs of the flow at the gaging stations near High Springs and near Fort White and of streamflow pickup between these stations. The pickup was computed by subtracting the flow at the High Springs station from the flow at the Fort White station. As is shown by 30 years of record, the increase in flow between the two stations—the streamflow pickup—averages about 800 cubic feet per second or about 100 cfs per mile of river. As a matter of interest and comparison, this pickup is approximately equal to the flow of Silver Springs, one of the largest springs in the United States, and is only slightly less than the rate of withdrawal of water for all public supplies in Florida in 1960 (MacKichan and Kammerer, 1961, p. 13).

As shown on figure 2 the streamflow pickup, which is largely ground-water inflow, for the most part changes slowly. Similarly, in an earlier study of Pond Creek, in Oklahoma, Clark (1956) found after accounting for the loss of water by evaporation and transpiration from the bottom lands near the creek that ground-water inflow to the creek for the most part changed slowly. Both Pond Creek and the Santa Fe River drain extensive aquifers.

Streamflow pickup does not continue to change slowly, however, during periods when the stage of the river is changing comparatively rapidly. When surface runoff upstream from the gaging station near High Springs raises the river level rapidly, pickup decreases and at times even becomes negative (that is, the stream

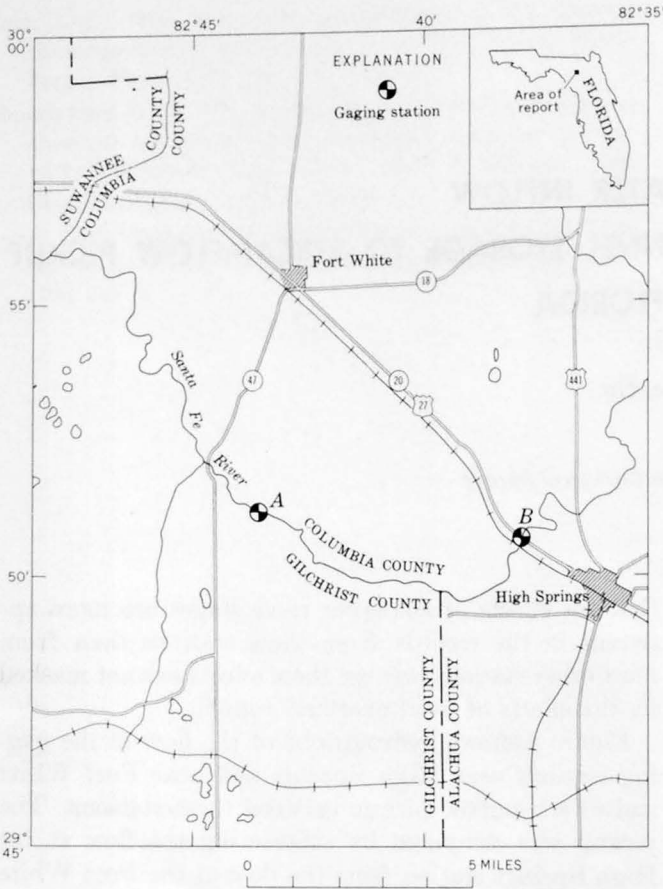


FIGURE 1.—Map showing location of the gaging stations on the Santa Fe River near Fort White and near High Springs in Florida. A, Fort White station; B, High Springs station.

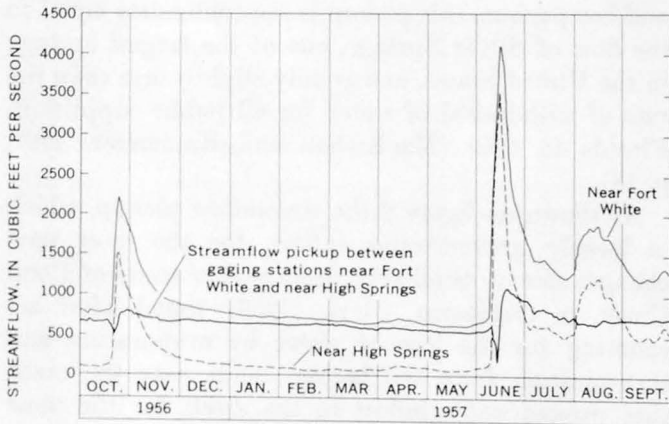
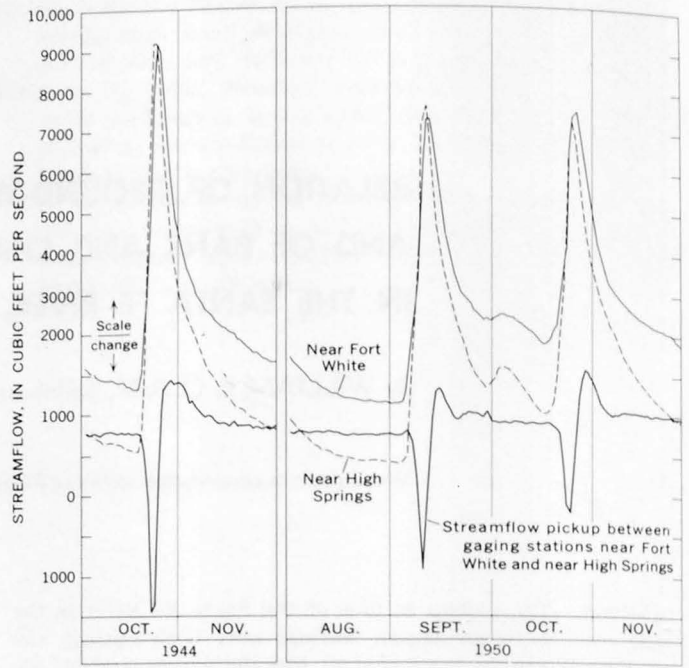
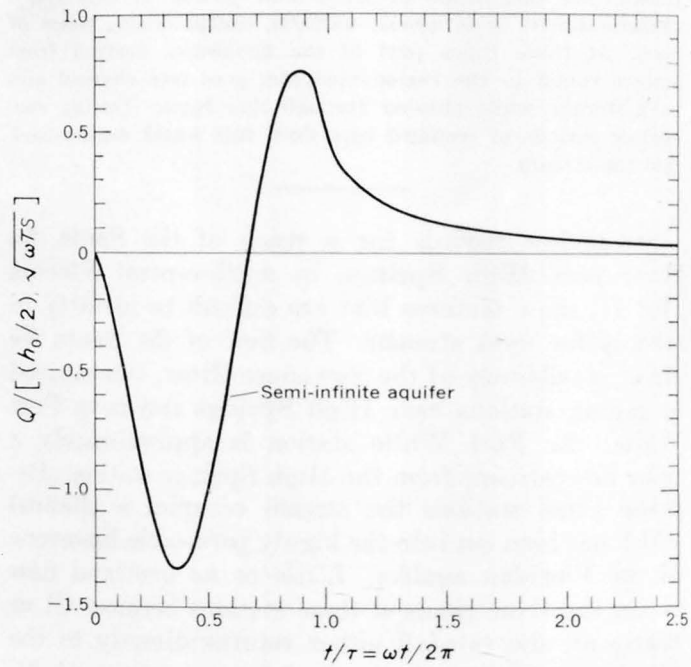


FIGURE 2.—Hydrographs of the Santa Fe River for the 1957 water year, at gaging stations near High Springs and near Fort White, Fla., showing streamflow at these stations and streamflow pickup between the stations.



A



B

FIGURE 3.—A, Hydrographs of the Santa Fe River at gaging stations near High Springs and near Fort White, Fla., showing water discharge at these stations and streamflow pickup between the stations. B, Theoretical ground-water flow from a semiinfinite aquifer into a stream (from Cooper and Rorabaugh, 1963a, fig. 102; 1963b, fig. 53.3).

loses water in the reach between the stations; see fig. 3A). When the river stage subsequently subsides, pickup increases, even reaching for a time a rate higher than its rate before the rise in stage.

The examples of streamflow pickup shown in figure 3A are provided by daily discharge data for periods in 1944 and 1950 when surface runoff from the area upstream from the High Springs gaging station was very high. As can be seen in this figure, streamflow pickup for a few days in October 1944 was negative by almost 1,500 cfs (a decrease in flow of almost 2,300 cfs). Change in the rate of streamflow pickup is attributed to: (1) time of travel of the water between the gaging stations near High Springs and near Fort White, (2) addition of water to, and release from, channel storage, and (3) flow of water into and out of bank storage. As the time of travel between the two stations is only a few hours, it can account for only a small part of the change in the rate of streamflow pickup. Therefore, the remainder must be attributed to changes in channel storage and bank storage—both of which are related to river stage.

The flow of water into and out of bank storage has predictable characteristics. Cooper and Rorabaugh (1963a, b) derived equations for the flow of water into and out of bank storage for a variety of stream-stage hydrographs simulating the passing of a flood and for finite and semiinfinite aquifers. The similarity between the hydrographs of the pickup in the Santa Fe River and of the theoretical ground-water flow into and out of a stream is shown on figure 3. Ground-water flow into a stream, shown on figure 3B, was computed ac-

ording to the formula of Cooper and Rorabaugh (1963a, b) for a semiinfinite aquifer.

Bank storage in the reach of the Santa Fe River consists partly of ground water that would have been discharged into the stream if the river stage had not risen, and at times partly of river water that seeped into the limestone aquifer as a result of the rise in river stage. When the river stage declines after a flood, the water held in channel and bank storage in the reach between the stations is released and pickup within the reach temporarily increases to a rate greater than that before the river rise. Then, unless another rise in river stage intervenes, both the river stage and pickup between stations gradually decline to a level about the same or slightly higher than that before the rise in river stage.

#### REFERENCES

- Clark, W. E., 1956, Forecasting the dry-weather flow of Pond Creek, Oklahoma; a progress report: *Am. Geophys. Union Trans.*, v. 37, no. 4, p. 442-450.
- Clark, W. E., Musgrove, R. H., Menke, C. G., and Cagle, J. W., Jr., 1964, Water resources of Alachua, Bradford, Clay, and Union Counties, Florida: *Florida Geol. Survey Rept. Inv.* 35, 170 p.
- Cooper, H. H., Jr., and Rorabaugh, M. I., 1963a, Ground-water movements and bank storage due to flood stages in surface streams: *U.S. Geol. Survey Water-Supply Paper* 1536-J, p. 343-366.
- 1963b, Changes in ground-water movement and bank storage caused by flood waves in surface streams: *Art. 53 in U.S. Geol. Survey Prof. Paper* 475-B, p. B192-B195.
- MacKichan, K. A., and Kammerer, J. C., 1961, Estimated use of water in the United States, 1960: *U.S. Geol. Survey Circ.* 456, 44 p., 10 figs.



## CHANGES IN QUALITY OF WATER IN THE PASSAIC RIVER AT LITTLE FALLS, NEW JERSEY, AS SHOWN BY LONG-TERM DATA

By PETER W. ANDERSON and SAMUEL D. FAUST, Trenton, N.J.

*Work done in cooperation with the New Jersey State Departments of Health,  
Conservation and Economic Development, and Agriculture,  
and the Passaic Valley Water Commission*

*Abstract.*—Preliminary analysis of 17 years (1947–64) of chemical-quality and streamflow data shows a general increase in content of dissolved solids per unit volume of water and a 20-percent decrease in dissolved-oxygen content. Similar analysis of seasonal variations in these water-quality parameters indicates that these trends occur during all months of the year, and not only during months having low streamflow conditions. The deterioration of quality of this water supply is attributed to the disposal of increasing volumes of municipal- and industrial-waste waters in the river basin.

The use of streams in the Passaic River basin (fig. 1) above Little Falls, N.J., as sources of water supply and as means of disposing of waste waters has become increasingly heavy during recent years. Diversions of water for domestic and industrial supplies above Little Falls exceeded 280 million gallons per day during 1963 (New Jersey Dept. of Health, written communication, 1964), an increase of more than 30 percent since 1950. Returns of industrial- and municipal-waste waters into the basin exceeded 30 mgd in 1963, or slightly more than 10 percent of the withdrawal. Increases of 20 percent in population and 50 percent in employment within the basin during the next 20 years, projected on the basis of population- and employment-growth data (U.S. Corps of Engineers, 1960), imply a continued rapid expansion in the demand for water.

Efficient and prudent water-resources management is a necessity in an area of such rapid and extensive development. One requirement for improved water management is a knowledge of the nature and magnitude of changes in water quality. This article describes the preliminary findings of an analysis of long-term and seasonal trends in the concentration of dissolved solids

and dissolved oxygen in the Passaic River at Little Falls, N.J. This basin and location were chosen for the study because the basin is one of large diversion for water supply, the drainage area at this site (about 760 square miles or approximately 80 percent of the total area of the basin) provides a good sample of the basin, and long-term data are available.

All chemical-quality data used in the preparation of this article were kindly provided by Messrs. Frank J. DeHooze and Richard E. Roby, of the Passaic Valley Water Commission.

### LONG-TERM CHANGES IN DISSOLVED LOAD

The relation between content of dissolved solids and water discharge in a natural stream that is unaffected by man's activities should remain fairly consistent, with time, at a particular sampling site. The dissolved solids (solutes) originate mainly from the weathering or dissolution of soils and rocks through which and over which the water passes. The water discharge (solvent) comes from precipitation, directly as overland runoff and indirectly as ground-water inflow to the stream. The chief changes in the solute-solvent relation that are likely to occur under natural conditions are due to relatively slow changes in climate. However, many manmade changes in the natural regimen of a stream produce measurable changes in the solute-solvent relation. For example, industrial- and municipal-waste waters are artificial sources of dissolved solids which commonly increase the dissolved load carried by a stream while the amount of water in the stream is being decreased by regulation of streamflow by impoundment and diversion.

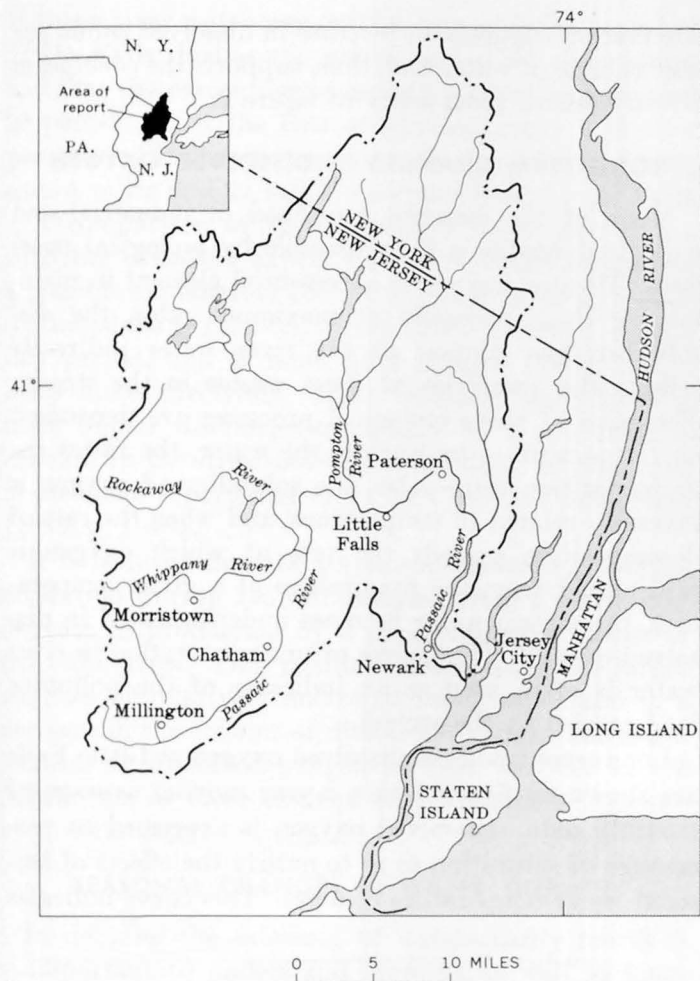


FIGURE 1.—Map showing location of the Passaic River basin.

Changes in the relation between dissolved solids and water discharge at Little Falls are demonstrated by linear-regression analyses of data collected during the period 1947-64 (fig. 2). The graphs indicate that the dissolved-solids content of the water has been increasing since 1947. For example, at a streamflow of 500 cubic feet per second the river carried 132 parts per million of dissolved solids in 1948, 144 ppm in 1955, and 187 ppm in 1963. This is a 40-percent increase between 1947 and 1963. Furthermore, a proportionately greater increase in dissolved solids is shown for the period 1955-64 than for the period 1948-54.

A regression analysis of one set of data with two variables considers the frequency distribution of a dependent variable when an independent variable is held fixed at each of several levels or values. This analysis usually leads to a linear relation between the dependent ( $Y$ ) and independent ( $X$ ) variables, described by the equation

$$\bar{Y}_x = \bar{Y} + b(X - \bar{X}),$$

where  $\bar{Y}_x$  is the estimate of the mean of the dependent variable at a given value of  $X$ ,  $\bar{Y}$  is the mean of all

values of the dependent variable,  $b$  is the slope of the regression line,  $\bar{X}$  is the mean of all values of the independent variable, and  $X$  is any given value of the independent variable. The objective is to derive a linear-regression equation and to solve for  $\bar{Y}_x$  at various levels of  $X$  (Dixon and Massey, 1957, p. 189-196). In this analysis (fig. 2), water discharge was taken as the independent variable ( $X$ ) and concentration of dissolved solids was taken as the dependent variable ( $Y$ ). Computation produced the following linear-regression equations:

Year	Equation
1948	$\bar{Y}_x = 113.25 - 56.98 (\log X - 3.021)$
1955	$\bar{Y}_x = 145.58 - 51.66 (\log X - 2.674)$
1963	$\bar{Y}_x = 189.00 - 86.51 (\log X - 2.680)$

A "t" distribution test (Dixon and Massey, 1957, p. 196) for independence of the dissolved solids ( $Y$ ) and water discharge ( $X$ ) was applied at the 95-percent level of significance for the years 1947-64 inclusive. It indicated that the variance about the mean value of dissolved solids was not influenced by water discharge for 95 percent of the observations. Evidently some other variable, such as discharge of industrial and municipal wastes, was responsible for an increase in the variance around a mean dissolved-solids content, per unit volume of discharge, from 1947 to 1964.

A second graphical analysis of the dissolved-solids and streamflow data collected at Little Falls is shown on figure 3. The lower curve shows the 2-year moving average of monthly average streamflow data for the period 1947-64. The upper curve is a similar plot of the monthly average dissolved solids during the same

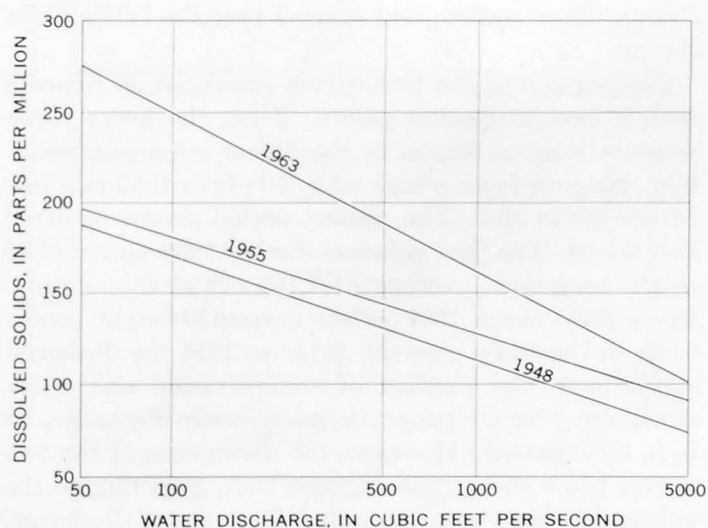


FIGURE 2.—Relation between water discharge and content of dissolved solids in the Passaic River at Little Falls, N.J., derived by linear-regression analysis of data for the period 1947-64.

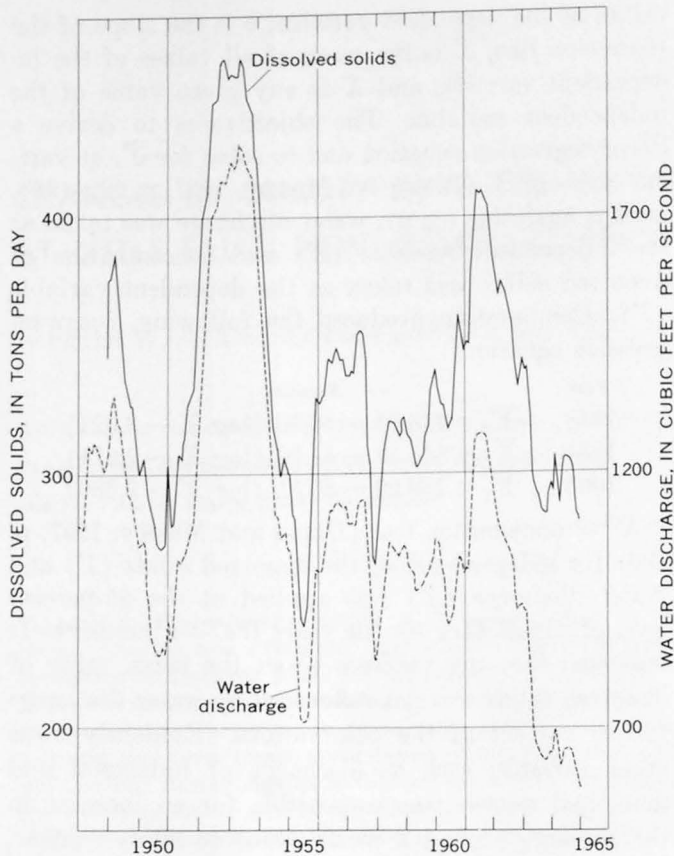


FIGURE 3.—Two-year moving averages of monthly average dissolved-solids load and of monthly streamflow in the Passaic River at Little Falls, N.J.

period. Dissolved solids are expressed in tons per day so as to relate them to streamflow. Streamflow data have been adjusted to fit the composite periods of the chemical data. This upper curve, therefore, shows the average load of dissolved material accumulated in the Passaic River system and carried past the Little Falls station.

Comparison of the two curves presented on figure 3 reveals two interesting points. First, the lower curve shows a wide variation in the 2-year average streamflow, ranging from a high of 1,850 cfs in 1953 to a low of 587 cfs in 1964. The wettest period shown occurred in 1951–54. The flow patterns during 1955–60 are close to the long-term average of 1,182 cfs at this station. River flows since 1961 reflect current drought conditions in the basin. Second, prior to 1955 the dissolved solids load—the product of concentration and water discharge—varied proportionately with discharge, as is to be expected. However, the divergence of the two curves after about 1955 suggests that, even though the values for load were computed from water discharge, concentration of dissolved material increased so markedly with time that the graphs diverge. This latter

observation suggests an increase in dissolved solids per unit volume of water and, thus, supports the conclusion already drawn from study of figure 2.

#### LONG-TERM CHANGES IN DISSOLVED OXYGEN

Much of the material contained in industrial and municipal wastes is decomposable by biological processes. Because oxygen is an essential element in maintaining these processes at maximum rates, the dissolved-oxygen content of the river water indirectly reflects the quantities of these wastes in the stream. The rates of these biological processes are dependent on temperature—the warmer the water, the faster the decomposition rate. Also, the solubility of oxygen is inversely related to temperature, and when the rate of decomposition exceeds the rate at which oxygen is replenished from the atmosphere at a given temperature, the stream water becomes undersaturated in dissolved oxygen. The degree of undersaturation in river water is often used as an indicator of the pollutant load carried by the stream.

Long-term trends in dissolved oxygen at Little Falls are shown on figure 4 as a 2-year moving average of monthly data. Dissolved oxygen is expressed as percentage of saturation so as to nullify the effects of seasonal water-temperature changes. This curve indicates

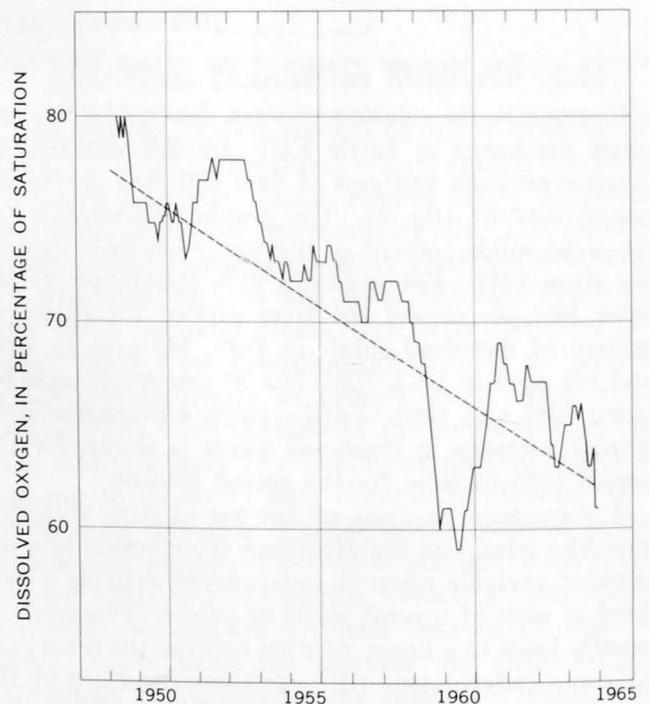


FIGURE 4.—Two-year moving average of monthly concentration of dissolved oxygen in water in the Passaic River at Little Falls, N.J. Dashed line reflects the general trend in oxygen content.

that the river water was consistently undersaturated at Little Falls during the entire period of observation, and that the percentage of oxygen saturation decreased 20 percent or at the rate of approximately 1 percent per year. Similar curves were obtained for sampling sites 4 miles and 22 miles upstream from Little Falls.

A comparison of the streamflow curve on figure 3 with the dissolved-oxygen curve on figure 4 provides a possible explanation for the slight increase in oxygen content during 1952-53. Streamflow increased during this period, and it must have diluted the pollutant loads more effectively. Also, increased turbulence at these higher discharge rates may have produced an increase in the dissolved-oxygen content, as happened in instances reported recently by Churchill and others (1962, p. 1-46).

It is believed that the 10-percent decrease in oxygen saturation during 1959-61 resulted from a substantial increase in production by a paper industry on one of the tributaries. This resulted in the inflow of larger volumes of relatively untreated waste water and in a decrease in the content of dissolved oxygen. The slight increase in dissolved oxygen in 1961 was due to the installation of more efficient waste-treatment facilities by this industry.

#### SEASONAL CHANGES IN WATER QUALITY

In defining the existence of water-quality trends it is important to understand seasonal as well as long-term effects. The range of fluctuation in monthly dissolved-solids concentration is greater for the 5-year period 1958-62 than for the 1948-52 period (fig. 5), despite the fact that streamflow did not differ greatly during the two periods. Also, the overall dissolved-solids concentration is significantly higher during the more recent period. In both periods these seasonal variations were more pronounced during times of low flow than during times of high flow. This inverse relation between the concentration of dissolved solids and the streamflow in the Passaic River is typical of streams in northern New Jersey. Thus, these curves (fig. 5) indicate that the dissolved-solids content has increased from one period to the other, and that this increase has occurred for all periods of the year, but especially during the summer and fall.

The curves on figure 6, which are based on monthly averages, show seasonal fluctuations in dissolved oxygen and water temperature during the same two 5-year periods. Since average streamflow (fig. 5) and water temperature differed only slightly during the two periods illustrated, their effect on the percentage of saturation of oxygen is thought to be insignificant. The

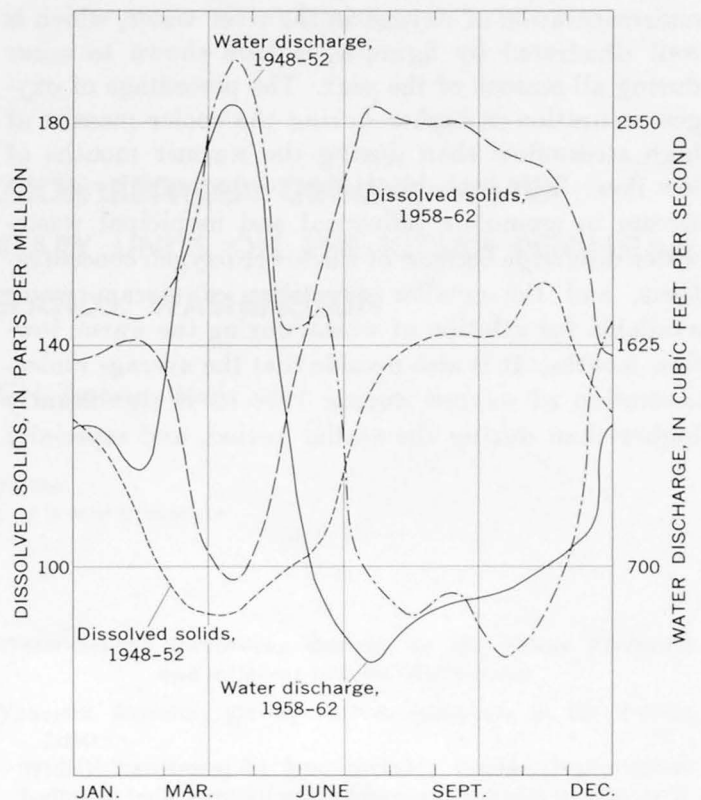


FIGURE 5.—Average monthly streamflow and concentration of dissolved solids in the Passaic River at Little Falls, N.J.

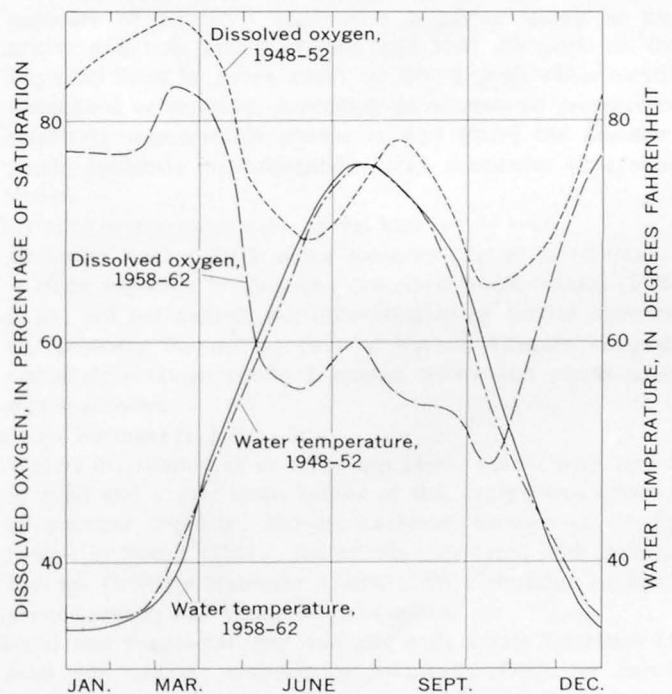


FIGURE 6.—Average monthly water temperature and concentration of dissolved oxygen in the Passaic River at Little Falls, N.J.



undersaturation of oxygen in the river water, which is well illustrated by figure 4, is here shown to occur during all seasons of the year. The percentage of oxygen saturation is higher during the cooler months of high streamflow than during the warmer months of low flow. This probably is due to the inability of the stream to assimilate industrial and municipal wastewater discharge because of the lower oxygen concentrations, and the smaller quantities of stream water available for dilution of waste, during the warm, low-flow months. It is also notable that the average undersaturation of oxygen during 1958-62 is significantly higher than during the earlier period, and especially

in the warmer months. These last observations are consistent with the increased discharge of waste waters into the river systems and are further evidence of their detrimental effect on water quality.

#### REFERENCES

- Churchill, M. A., Elmore, H. L., and Buckingham, R. A., 1962, The prediction of stream reaeration rates: *Jour. Sanitary Eng. Div., Am. Soc. Civil Engineers*, v. 88, SA4, p. 1-46.
- Dixon, W. J., and Massey, F. J., 1957, *Introduction to statistical analysis*, 2d ed.: New York, McGraw-Hill Book Co. Inc., 488 p.
- U.S. Corps of Engineers, 1960, Passaic River basin flood control study: U.S. Army Engineer District, New York, Inf. Bull., 39 p.



## CHEMICAL DISTINCTION BETWEEN GROUND WATER OF FOUR SEDIMENTARY UNITS ON THE KITSAP PENINSULA AND ADJACENT ISLANDS, WASHINGTON

By A. S. VAN DENBURGH, Tacoma, Wash.

*Work done in cooperation with the  
State of Washington Division of Water Resources*

*Abstract.*—Although ground water from a sequence of four units of Pleistocene glacial and fluvial sediments exhibits noticeable differences in the average amount of dissolved constituents, almost all the constituents have wide ranges in concentration that overlap from one unit to another. However, amounts of potassium, orthophosphate, and dissolved solids show distinctive variations and thus serve to identify the source of an individual ground-water sample with reasonable accuracy. The most pronounced differences are between water from the Salmon Springs(?) Drift and older formations, in which the contents of potassium, orthophosphate, and dissolved solids characteristically are equal to or greater than 1.4, 0.20, and 104 ppm, respectively, and water from the Colvos Sand and younger sediments, in which concentrations generally are less than these values.

The analysis of 37 ground-water samples from the Kitsap Peninsula and adjacent islands in Puget Sound, Wash. (fig. 1), as part of an evaluation of the water resources of the area, has allowed definition of the characteristic chemical qualities of water from the several principal productive rock formations in the area (Van Denburgh, 1965, p. 156). The accompanying table summarizes the character of the water-bearing deposits. The water samples used in this study represent four units in the thick sequence of sedimentary deposits. Two of these units are named: the Salmon Springs(?) Drift (older), and the Colvos Sand. One unnamed unit lies beneath the Salmon Springs(?) Drift, and one unnamed unit lies above the Colvos Sand. The thicknesses of the deposits are not given in the table because they differ from place to place. In the area as a whole the thickness of each unit ranges from 0 to 300 feet.

### *Water-bearing Pleistocene deposits on the Kitsap Peninsula and adjacent islands, Washington*

Youngest deposits; glacial-outwash sediments in the Vashon Drift:

Widely distributed at land surface; include discontinuous bodies of both advance and recessional deposits of silt, sand, and gravel; contain unconfined ground water and locally yield moderately large water supplies.

Colvos Sand Member of the Vashon Drift (Molenaar, 1965, p. 32; Noble and Wallace, 1965):

Widely distributed beneath younger units of the Vashon Drift or, where they are absent, at land surface; a thick sequence of stratified sand with irregular lenses of fine gravel and thin strata of clay and silt; discussed as the Puyallup Sand by Sceva (1957, p. 19); ground water locally unconfined or confined, depending on absence or presence of relatively impermeable phases in and above the member; yields moderate to moderately large quantities of ground water.

Fluviatile or glaciofluviatile gravel and coarse sand:

Underlies Vashon Drift along southern part of Hood Canal; a thick sequence of deposits, described by Molenaar (1965, p. 31) but not named; not differentiated by earlier workers, but probably mapped as part of Vashon advance outwash material; contains confined ground water and yields some water supplies.

Salmon Springs(?) Drift:

Widely distributed at or below sea level; gravel with lenses of sand and a few small bodies of till, everywhere covered by younger deposits; mapped as lower member of Orting Gravel by Sceva (1957); tentatively correlated with Salmon Springs Drift by Molenaar (1965, p. 28); contains confined ground water, and yields large supplies.

Glacial and nonglacial clay and silt with a few interbeds of sand and gravel; mapped as Admiralty Drift by Sceva (1957) and as undifferentiated pre-Salmon Springs(?) deposits by Molenaar (1965, p. 27); yields little ground water.

The Pleistocene deposits are underlain by the Blakeley Formation, a thick sequence of folded well-indurated marine shale, sandstone, and conglomerate of Tertiary age that yields little water.

The ground water is derived entirely from precipitation. The water table and most piezometric surfaces stand high in hills on the Kitsap Peninsula and on the adjacent islands. Ground-water movement is generally downward in these hills and laterally toward valleys and the coast. The paths followed by the water are complex, however, because of the presence of interbedded impervious materials which impede downward movement. Natural discharge, through seeps and springs, occurs in streams and lakes, and offshore.

Thirty-six of the ground-water samples were collected from wells, which range in depth from 18 to 832

feet; one sample was obtained from a spring on Vashon island. With one exception, each well produces from a single perforated or screened interval that generally is from 5 to 20 feet in thickness. Water analyses were made by standard methods in use in the U.S. Geological Survey (Rainwater and Thatcher, 1960). On the basis of well logs, surficial geology, and physiographic relations the samples are grouped according to probable geologic source as follows:

- 4 samples from pre-Salmon Springs(?) deposits,
- 13 samples from the Salmon Springs(?) Drift,
- 15 samples from the Colvos Sand, and
- 5 samples from post-Colvos deposits.

Most ground water on the Kitsap Peninsula and adjacent islands, regardless of its geologic source, is of the silica calcium bicarbonate type and has a dissolved-solids content in the range from 50 to 180 parts per million. (Water derived from marine sedimentary rocks of the Blakeley Formation, or affected by seawater encroachment adjacent to Puget Sound, is an exception; such water is likely to contain objectionable amounts of dissolved solids, chiefly sodium and chloride.) The average amount of many constituents in the ground water differs considerably from unit to unit. However, most of the concentration ranges are wide and overlapping, as exemplified by the distribution of silica values in figure 2. Nonetheless, three chemical characteristics—potassium concentration, orthophosphate concentration, and dissolved-solids content—can be used to help distinguish among waters of the four units. These three characteristics provide good criteria for the distinction of waters of the Colvos Sand and younger sediments from those of the Salmon Springs(?) Drift and older formations. In addition, a sharp boundary exists between orthophosphate concentrations in ground water above the Colvos Sand and those in water of the Colvos Sand itself, as is shown in figure 2.

Identification of a water-bearing unit by hydrochemical characteristics can be accomplished also by plotting one chemical parameter against another. A plot of the potassium concentration in a water versus its orthophosphate concentration provides a generally successful means of distinguishing among ground waters of the four units, as is shown in figure 3. Water from each unit is segregated into a reasonably distinct area of the graph. This technique has proved useful in the subsequent correlation of water-bearing zones in wells for which no reliable geologic information is available, both on the Kitsap Peninsula and in adjacent parts of the Puget Sound region.

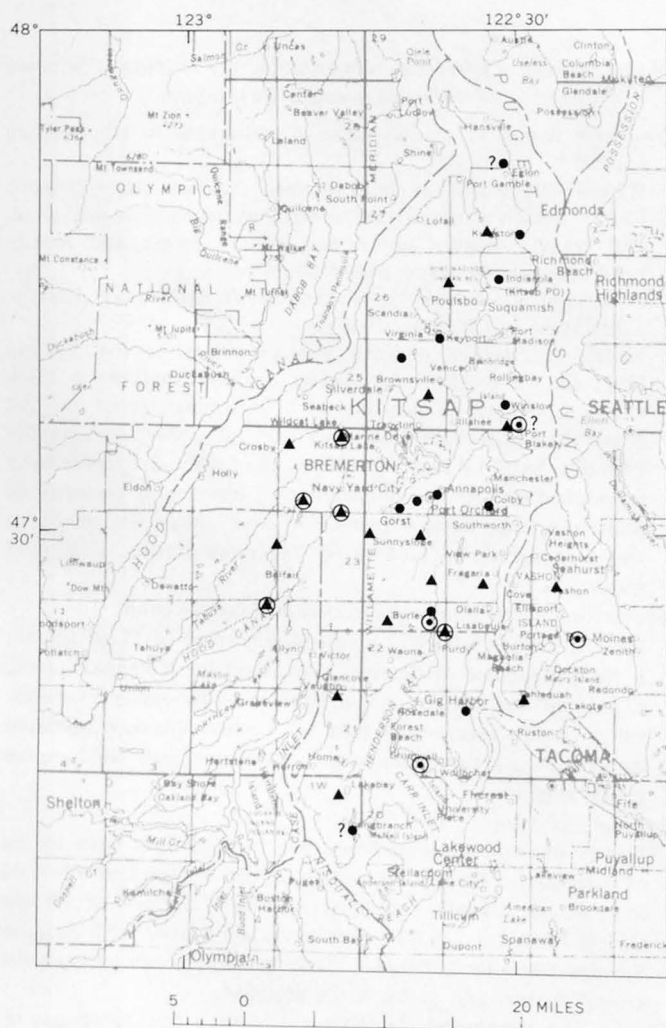


FIGURE 1.—Location and geologic sources of ground-water samples used in this study. Circled triangle, post-Colvos sediments; triangle, Colvos Sand; dot, Salmon Springs(?) Drift; circled dot, pre-Salmon Springs(?) sediments. Question mark denotes uncertain geologic source.

Reasons for the chemical variations doubtless are many and complex. In general, however, the parallel between increasing amounts of many dissolved constituents in ground water and increasing geologic age of the host aquifer is a common, though not universal, characteristic in many parts of the United States. Normally, the water in older formations is deeper and has spent a longer period in contact with the rock materials. Hence, it has had more time to dissolve the

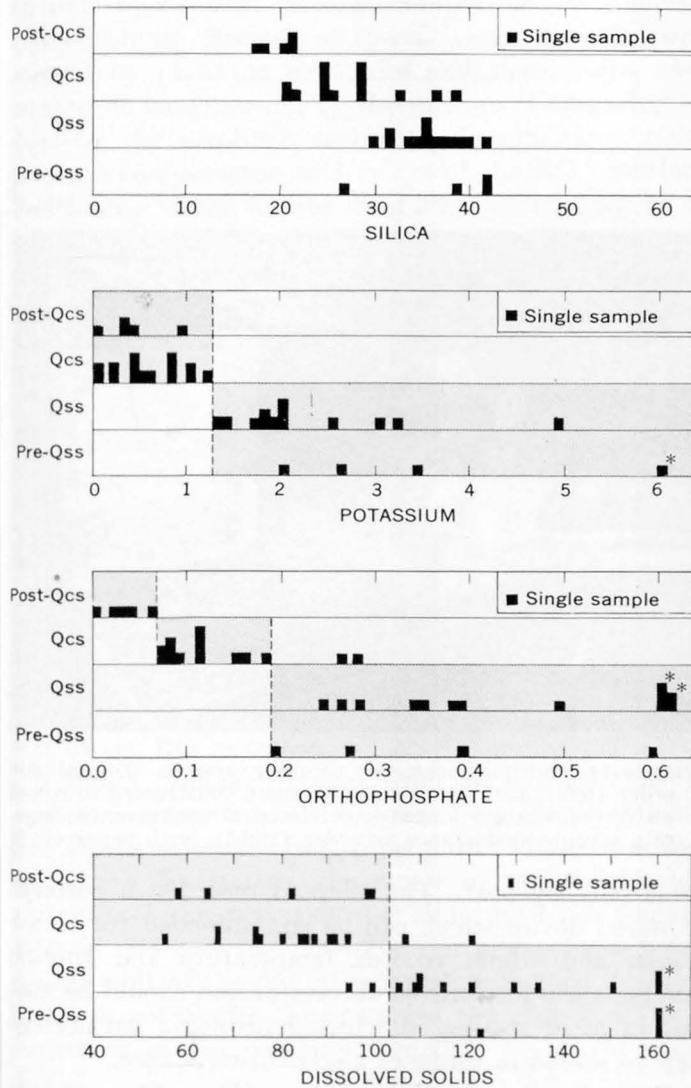


FIGURE 2.—Graphs showing concentration, in parts per million, of silica, potassium, orthophosphate, and dissolved solids in the ground water, relative to the geologic source of the water. Geologic units: Pre-Qss, pre-Salmon Springs(?) sediments; Qss, Salmon Springs(?) Drift; Qcs, Colvos Sand; Post-Qcs, Post-Colvos Sand Sediments. Stippled pattern emphasizes differences in concentration among units. Values of starred (\*) samples are equal to or greater than the amounts shown (6, 0.6, and 160 ppm for potassium, orthophosphate, and dissolved-solids content, respectively).

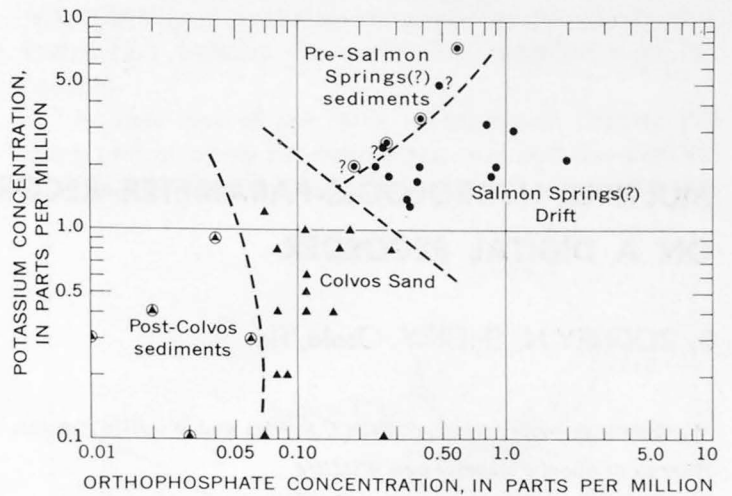


FIGURE 3.—Relations between potassium concentration and orthophosphate concentration and the geologic source of the ground water. Circled triangle, post-Colvos sediments; triangle, Colvos Sand; dot, Salmon Springs(?) Drift; circled dot, pre-Salmon Springs(?) sediments. Question mark denotes uncertain geologic source.

slightly soluble mineral constituents of the host rocks. Conversely, water in the younger, generally shallower formations has had less residence time, and it is also subject to the diluting effects of downward-percolating surface water. Figure 2 shows examples of generally increasing concentration with increasing geologic age and increasing depth of burial of the aquifer, which is characteristic of most constituents of ground water on the Kitsap Peninsula and adjacent islands. More specific reasons for the relations shown on figures 2 and 3 cannot be given until a detailed geochemical study has been made.

REFERENCES

Molenaar, Dee, 1965, Geology and ground-water resources, in Garling, M. E., Molenaar, Dee, and others, Water resources and geology of the Kitsap Peninsula and certain adjacent islands: Washington Div. Water Resources Water-Supply Bull. 18, 309 p.

Noble, J. B., Wallace, E. F., 1965, Geology and ground-water resources of Thurston County, Washington: Washington Div. Water Resources Water-Supply Bull. 10, v. 2. [In press]

Rainwater, F. H., and Thatcher, L. L., 1960, Methods for collection and analysis of water samples: U.S. Geol. Survey Water-Supply Paper 1454, 301 p.

Sceva, J. E., 1957, Geology and ground-water resources of Kitsap County, Washington: U.S. Geol. Survey Water-Supply Paper, 1413, 178 p.

Van Denburgh, A. S., 1965, Water quality, in Garling, M. E., Molenaar, Dee, and others, Water resources and geology of the Kitsap Peninsula and certain adjacent islands: Washington Div. Water Resources Water Supply Bull. 18, 309 p.



## MULTIPLE HYDROLOGIC-PARAMETER RECORDING ON A DIGITAL RECORDER

By RODNEY N. CHERRY, Ocala, Fla.

*Work done in cooperation with the U.S. Fish and Wildlife Service,  
Bureau of Sport Fisheries and Wildlife*

*Abstract.*—A multiple-parameter modification of a digital recorder measures and records hydrologic parameters that can be sensed as electrical resistance. The digital recorder collects data on tape for processing by electronic computer and is therefore especially useful where large volumes of data are to be collected and analyzed. The modified apparatus is portable and battery powered, and it can be left untended for 3 to 4 weeks. The multiple-parameter recorder described measures and records 4 parameters (2 values of water temperature and 2 values of specific electrical conductance) on punched tape, and also records one of these parameters in visible form on a paper chart.

The increasing complexity of many types of hydrologic studies and the importance of continuous or frequent periodic measurements of some hydrologic parameters have led to increasing use of recording devices in field studies. Because the data can be processed by electronic computer, the digital recorder was developed for use in field studies where large volumes of data are to be collected and analyzed. The recorder is a battery-operated paper-tape punch which periodically, and at a preselected time interval, records data as 4-digit numbers on a 16-channel paper tape. The record is translated later to a 7-channel digital tape suitable for use in automatic data-processing equipment. (See discussions of the digital recorder by Carter and others, 1963, and by Isherwood, 1964.)

Various modifications and attachments have been devised to record different parameters on the digital recorder. The adaptation discussed in this paper was developed in connection with a study of salinity and temperature of surface water at several places in the Everglades National Park, in southern Florida. The observation sites in the park are as much as 25 miles from the nearest habitation, and are generally acces-

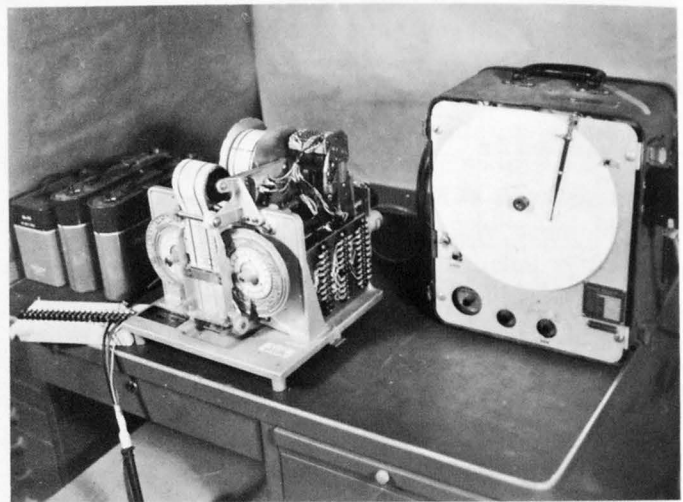


FIGURE 1.—Multiple-parameter recorder system. Digital recorder (left), with electrical-data input, constructed to record water temperature and specific electrical conductance; separate specific-conductance recorder (right), with paper chart.

sible only by boat. The adapted recorder, a battery-powered device which can be left untended for 3 to 4 weeks and which records temperature and specific conductance, has proved successful and should be useful in other studies in which hydrologic parameters can be sensed in terms of electrical resistance.

Basically, the adaptation is a coupling of two recording devices, the Fischer-Porter digital recorder and the Industrial Instruments RQ electrolytic-conductivity recorder (fig. 1). The input mechanism of the digital recorder is a shaft which rotates a coded disk. The position of the disk with respect to a punching mechanism determines which values will be punched on the tape. The RQ recorder utilizes a wheatstone bridge in which a sensing element (conductivity cell) constitutes

one segment of the bridge and a potentiometer constitutes the other. A signal from the sensing element is electrically compared with a signal from the potentiometer; if there is imbalance a motor is activated and moves the slide of the potentiometer until the signals balance (that is, the bridge is balanced). Movement of the potentiometer slide moves the recording pen, which is geared to it, thus making a graphic record of the values indicated by the sensing element.

The multiple-parameter recording process consists of four operations: sensing, comparing, positioning, and punching. Sensing of specific conductance is performed by platinum electrodes and thermistors, and sensing of temperature, by thermistors. Comparing is done by the amplifier, oscillator, discriminator, temperature compensator, and relays of the RQ recorder. Positioning in the digital recorder is carried out by a unit made up of a 3-turn 5,000-ohm potentiometer and a 6-volt direct-current motor; the potentiometer slide is mechanically coupled to the input shaft of the recorder, and the motor is geared to drive the potentiometer slide. Positioning in the RQ recorder is carried out by a unit consisting of the motor and potentiometer which are standard for this recorder. Punching is done by the digital recorder, equipped with a Chelsea timer.

During the recording process, the sensing element for either specific conductance or temperature is selected by a stepping switch and connected to the comparing unit, which is connected through a latch relay (5-pole, double-throw) to either the positioning unit mounted on the digital recorder or the positioning unit of the RQ recorder.

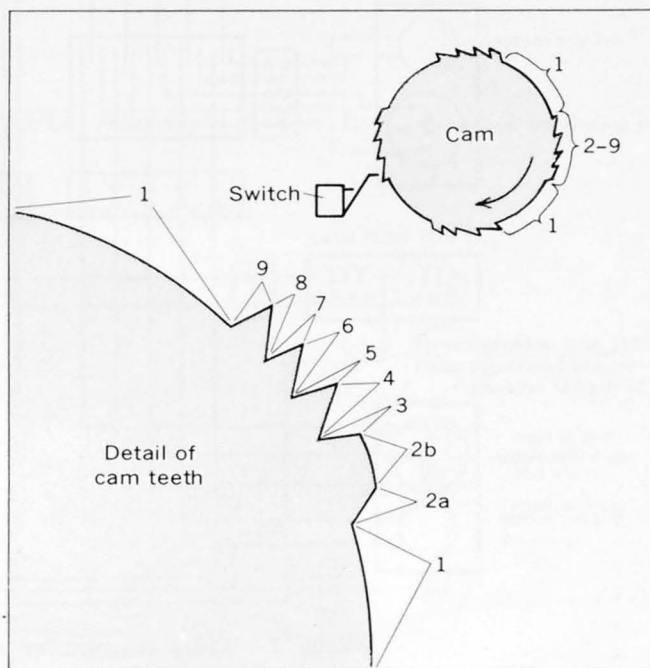
A signal (voltage change) from the selected sensing element is compared with a signal from the potentiometer of the selected positioning unit. If there is imbalance in the signals, the motor of the positioning unit rotates the potentiometer slide until the signals balance. Because the potentiometer slide of the positioning unit of the digital recorder is coupled directly to the input shaft which rotates the code disk, any movement of the potentiometer slide moves the code disk.

A modifier cam on a Chelsea timer controls the frequency and the time during which the positioning units operate for each parameter punched or recorded. Using the modified cam (fig. 2) on the timer, the digital recorder punches values for 4 parameters in close succession at the beginning of each 15-minute period and records 1 parameter on the RQ circular chart for the remainder of the 15-minute period.

The stepping switch mounted on the digital recorder is advanced during the punching process by a rod

which is linked to the rocker arm (see Fischer-Porter instruction bulletin for series-1540 punched-tape recorder).

The first coil of the latch relay, which throws the relay and connects the comparing unit and the digital-recorder positioning unit, is energized when (1) the



SEQUENCE OF STEPS CONTROLLED BY CAM ON CHELSEA TIMER DURING RECORDING CYCLE:

1. Bottom conductivity is recorded on circular chart of RQ recorder.
2. a. Circuits are switched by latch relay from positioning unit (motor and potentiometer) of RQ recorder to positioning unit of digital recorder. Relay is activated by switch in motor circuit when stepping switch is in step 1 and when the switch operated by the locking cam is closed.  
b. Bottom conductivity is positioned on digital recorder for 30-35 seconds.
3. Bottom conductivity is recorded on tape; stepping switch is advanced to bottom temperature (stepping switch, step 2).
4. Bottom temperature is positioned on digital recorder for 30-35 seconds.
5. Bottom temperature is recorded on tape. Stepping switch is advanced to surface conductivity (stepping switch, step 3).
6. Surface conductivity is positioned on digital recorder for 30-35 seconds.
7. Surface conductivity is recorded on tape. Stepping switch is advanced to surface temperature (stepping switch, step 4).
8. Surface temperature is positioned on digital recorder for 30-35 seconds.
9. Surface temperature is recorded on tape. Stepping switch is advanced to bottom conductivity (stepping switch, step 1). Circuits are switched by latch relay from positioning unit of digital recorder to positioning unit of RQ recorder. Relay is activated by switch in motor circuit when the stepping switch is in step 1 and when the switch operated by the locking cam is closed.

FIGURE 2.—Modified cam for Chelsea timer. Numbers on teeth show sequence of steps in recording cycle, as listed above. The cam makes 1 complete rotation per hour, and thus activates 4 recording cycles per hour.

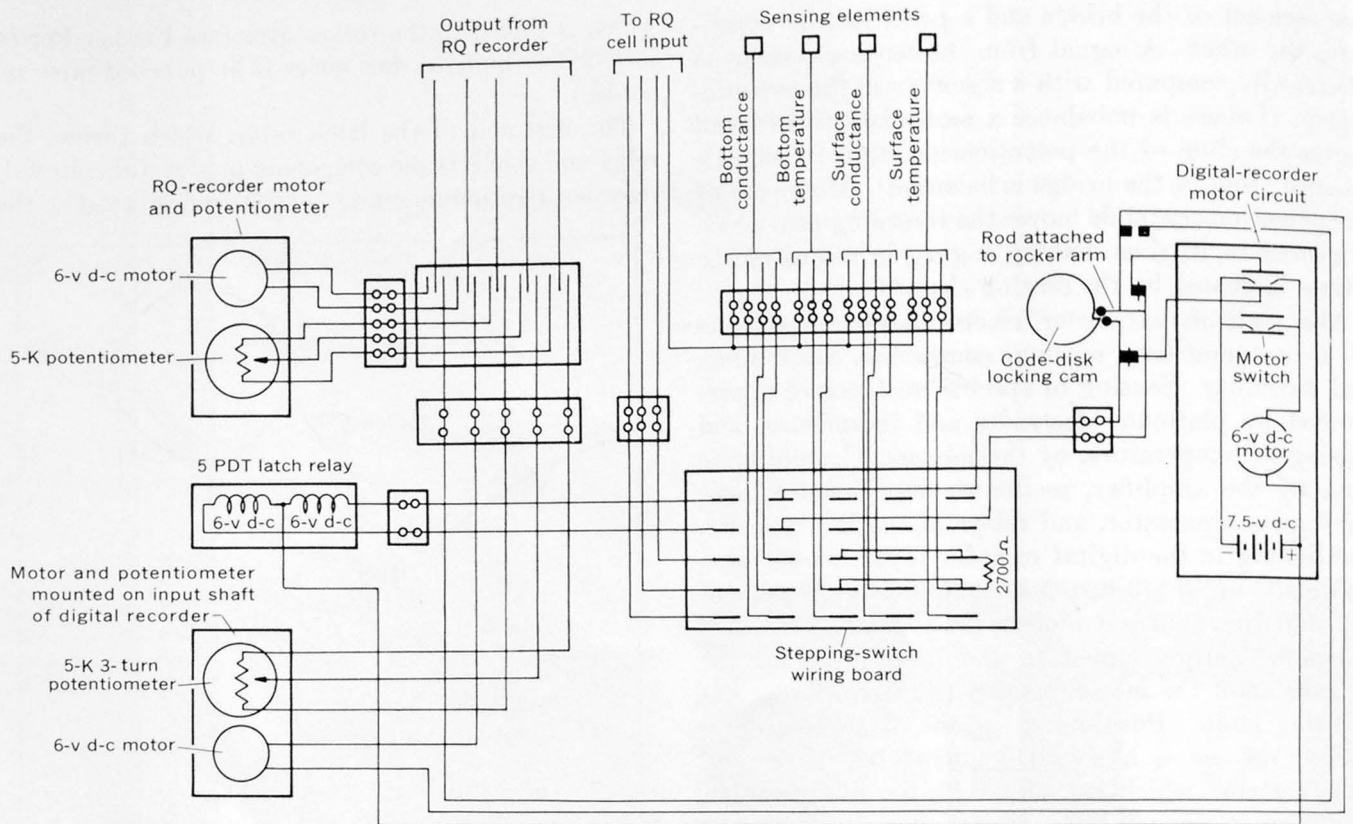


FIGURE 3.—Wiring diagram for multiple punching on the digital recorder.

modified cam of the Chelsea timer lifts the switch blade to the "up" position (point 2a in fig. 2), (2) the stepping switch is in step 1, and (3) a switch mounted in a position to operate on the code-disk locking cam (see Fischer-Porter manual) of the digital recorder is in a closed position. Simultaneously, the motor of the digital-recorder punching mechanism rotates the cam about  $\frac{1}{8}$  revolution, allowing the switch blade to drop off the cam, opening the switch, and de-energizing the first coil of the latch relay. This switch is positioned so as to allow current (about 300 milliamperes) to flow through the coil for less than 1 second.

The second coil of the latch relay, which throws the relay and connects the comparing unit and the RQ positioning unit, is energized when (1) the cam of the Chelsea timer drops the switch blade to the "down" position (point 9 in fig. 2) (2) the stepping switch is in step 1, and (3) a switch mounted on the tape-support spool is closed by forward motion of the rocker arm during the punching operation. This switch is positioned in such a manner as to allow current to flow through this coil for about 1 second.

Figure 3 is a wiring diagram for an instrument now in operation in the Everglades National Park. This

instrument records values for the specific conductance and temperature at the surface and near the bottom of the stream. If only a punched-tape record is desired, the latch relay and its related wiring, and the motor and potentiometer of the RQ recorder, can be omitted. The manufacturer of the RQ recorder can provide a comparing unit like that described in this paper for about half the price of a standard recorder. If additional parameters are desired, additional steps of the stepping switch are utilized.

Modified recorders have been in operation in the park for about 3 years. The punched tape from the digital recorder is being programmed for compilation of data. The visual record being obtained from the RQ recorder until the programming has been completed is especially useful as a check on operation of the digital recorder and on the need for, and nature of, maintenance.

#### REFERENCES

- Carter, R. W., chm., and others, 1963, Automation of stream-flow records: U.S. Geol. Survey Circ. 474, 18 p.  
 Isherwood, W. L., 1964, Data acquisition systems in hydrology, in Valid data and logical interpretation, symposium [on] environmental measurements: U.S. Public Health Service, p. 170-185.

## EFFECTS OF SAMPLE AND FLUOROMETER-COMPARTMENT TEMPERATURES ON FLUOROMETER READINGS

By BERNARD DUNN and DONALD E. VAUPEL, Albany, N.Y.

*Work done in cooperation with the New York State Department of Health*

**Abstract.**—Sample temperature and fluorometer-compartment temperature influence determination of the concentration of dye in water by means of fluorescence readings on the Turner Model-111 fluorometer. A procedure for the preparation of correction curves for these temperature effects has been developed for field use of the fluorometer where sample and compartment temperatures cannot be controlled.

In time-of-travel studies of streams, results obtained by use of a Turner Fluorometer (Model 111) and Rhodamine-B dye have been found to be affected by variations in both sample and instrument-compartment temperatures. In a succession of measurements it is necessary either to stabilize sample and fluorometer-compartment temperatures, or to make corrections for the variations in these temperatures, in order to obtain consistent values of relative fluorescence. Correction curves for sample and fluorometer-compartment temperatures were developed by the writers because field use of the fluorometer makes stabilization of temperatures impractical. Although the current literature describes the variation of fluorescence with sample temperature (Feuerstein and Selleck, 1963, p. 16, and Pritchard and Carpenter, 1960, p. 39) it does not express the relationship in a form suitable for field use. The purpose of this paper is to consider the variation of fluorescence-dial readings with fluorometer-compartment temperature and to describe the procedure used for developing the correction curves. The procedure for developing the instrument correction curve is stressed, rather than the curve itself, because the curve probably changes whenever significant electronic changes, such as the replacement of a tube or lamp, are made in the fluorometer. It may also change from instrument to instrument. A sample-temperature

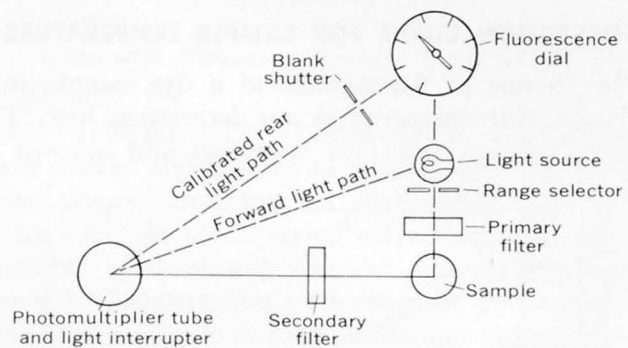


FIGURE 1.—Optical system of the fluorometer.

correction curve probably remains unchanged as long as the same type of fluorescent dye is used.

### GENERAL PROCEDURE

All quantitative fluorescence measurements were made with a Turner Model 111 Fluorometer. The fluorometer is basically an optical bridge which is analogous to the wheatstone bridge used in measuring electrical resistance. The optical bridge measures the difference between light emitted by the sample and that from a calibrated rear light path (fig. 1). A single photomultiplier tube surrounded by a mechanical light interrupter sees light alternately from the sample and from the rear light path. The quantity of light required in the rear light path to balance that from the sample is indicated by the fluorescence dial.

Two color-filter systems are used in the fluorometer. The primary filter passes only those spectra shorter than the fluorescent wavelengths, while the secondary filter passes only the desired fluorescence spectrum. The primary filter was a combination of 2 Corning glass color filters of Color Specification No. 1-60 and



1 Kodak Wratten No. 58 filter. The secondary filter was a Kodak Wratten No. 23A.

The instrument has four operating ranges to give it a large range of sensitivity. Each range is determined by the size of aperture emitting light to the sample from the light source.

Engraved-stem thermometers with a range of 20° to 110°F were used to determine the sample and instrument-compartment temperatures.

The fluorescent dye used in all tests was Rhodamine B. It is obtained in a 40-percent color by weight solution in acetic acid. This solution was mixed with distilled water to obtain dye concentrations of approximately 10, 20, and 30 parts per billion to simulate the concentrations that are common in field investigations.

### CORRECTION CURVE FOR SAMPLE TEMPERATURE

The change in fluorescence of a dye sample with variation of its temperature was determined first. The fluorometer was put into operation and allowed to

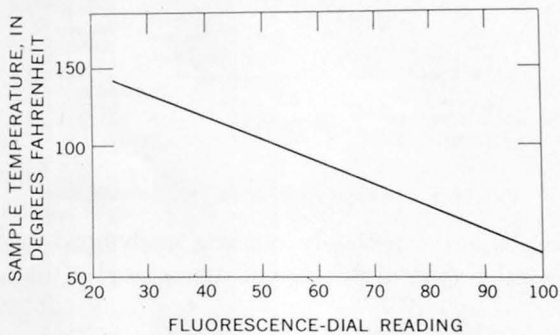


FIGURE 2.—Relation of sample temperature to fluorescence-dial reading.

warm up until the instrument compartment reached equilibrium temperature, which at the time was 103.5° F. The sample was cooled to 45°F and placed into the instrument. The fluorescence-dial reading and sample temperature were recorded at 5-minute intervals until the sample had reached the temperature of the instrument compartment. The sample was then removed from the instrument, placed in an oven, heated to 150°F, and replaced in the fluorometer. Dial readings and sample temperatures were recorded at 1-minute intervals as the sample cooled to the temperature of the instrument. From these data the relation of fluorescence-dial reading to sample temperature was plotted (fig. 2).

A sample-temperature correction curve was determined from the relation of sample temperature to fluorescence-dial reading in figure 2 by using a sample-temperature base of 80°F with a corresponding fluorescence-dial reading of 70 units. The difference be-

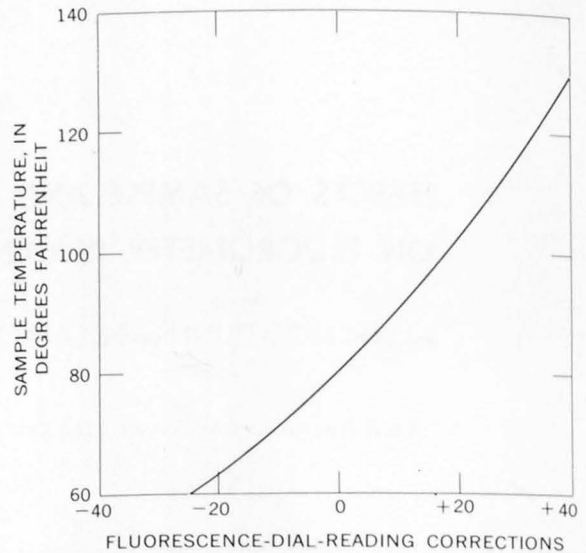


FIGURE 3.—Sample-temperature correction curve (base 80°F).

tween fluorescence-dial reading and 70 was then determined for sample temperatures between 60°F and 130°F in 5-degree intervals. For example, the fluorescence-dial reading at 80°F (base) is 70, and the correction at 80°F is  $70 - 70 = 0$ . The correction for a sample temperature of 60°F with a fluorescence-dial reading of 84.5 is  $70 - 84.5 = -14.5$ . The correction curve prepared on the basis of these measurements is shown in figure 3.

### CORRECTION CURVE FOR FLUOROMETER TEMPERATURE

The fluorometer-compartment correction curve was prepared in a similar fashion. The fluorometer was allowed to warm up for 5 minutes. A sample at room

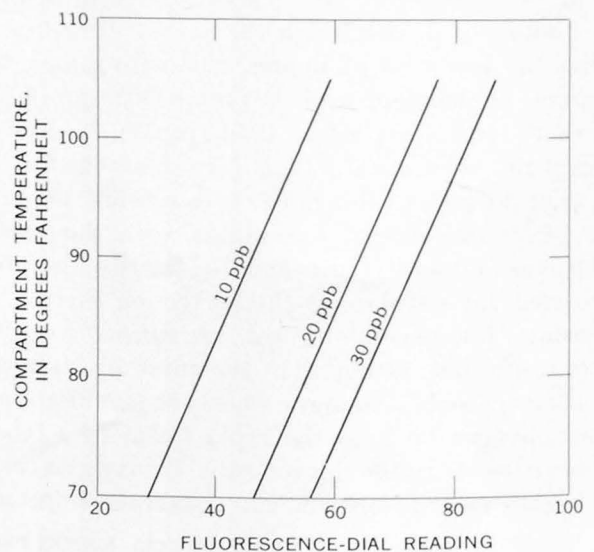


FIGURE 4.—Relation of compartment temperature to fluorescence-dial reading.

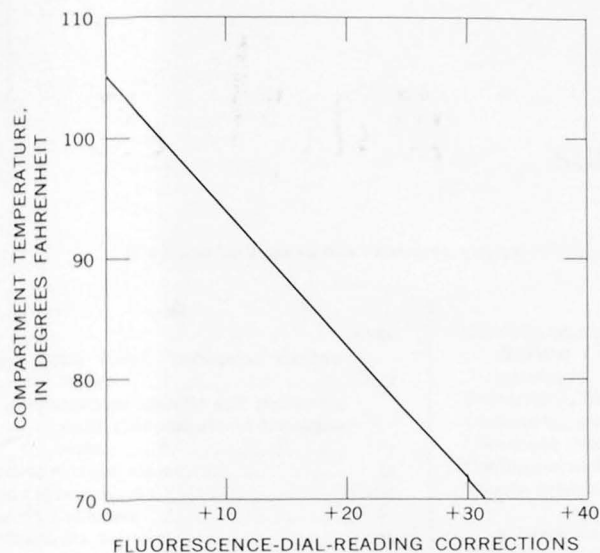


FIGURE 5.—Fluorometer-compartment correction curve (base 105°F).

temperature was placed in the instrument, the fluorescence-dial reading was recorded, and the sample was removed. This process was repeated at 5-minute intervals. The slight variation in sample temperature was corrected for by use of the sample-temperature correction curve developed earlier. The readings were stopped when the compartment temperature reached its equilibrium. Three runs were made in this manner with sample concentrations of 10, 20, and 30 parts per billion, and a graph showing the relation of compartment temperature to fluorescence-dial reading was plotted for each concentration (fig. 4).

Using temperatures at 5-degree intervals, within the range from 70° to 105° to simulate probable field conditions and a base of 105°F, the instrument correction for each temperature was determined in the same manner as that described for the sample correction curve. The fluorometer-compartment correction curve is shown in figure 5.

It should be noted here that the correction curves for all three runs were the same. This shows that dye concentration had no significant effect on the instrument-temperature correction.

After the temperature correction curves for a sample and for the instrument compartment had been determined, corrections were applied to the initial data obtained for the sample solution of 20 parts per billion

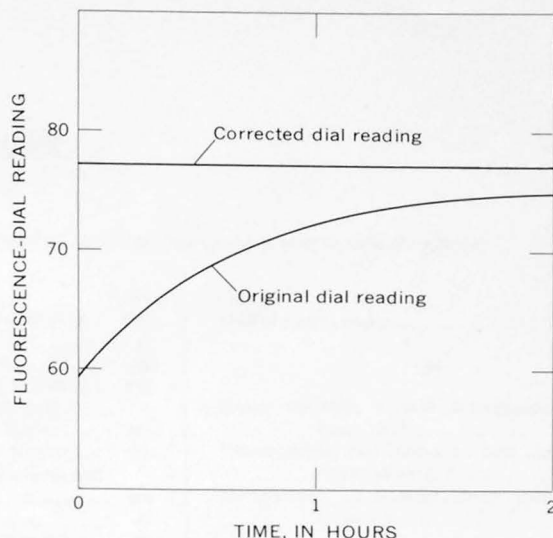


FIGURE 6.—Graphical summary of original and adjusted data.

to show the reliability of these curves. The fluorometer was started and allowed to operate until the compartment temperature reached equilibrium. During this time a sample was inserted periodically into the fluorometer compartment and the dial reading was recorded. Temperatures were taken in the compartment and in the sample as soon as the fluorescence dial was read. The data, with the corrections applied for sample and compartment temperatures, are presented graphically in figure 6.

It is clear from the foregoing discussion that both sample and fluorometer-compartment temperatures influence instrument fluorescence-dial readings. Actually, sample temperature affects the fluorescence of the tracer while fluorometer-compartment temperature appears to affect the efficiency of the fluorometer to measure sample fluorescence. The concentration of the sample has no apparent effect on instrument efficiency, as is shown by the three curves of figure 4 (each of which has the same slope,  $dy/dx = 1.1$ ).

#### REFERENCES

- Feuerstein, D. L., and Selleck, R. E., 1963, Tracers for dispersion measurements in surface waters: Calif. Univ., Sanitary Eng. Research Lab. Rept. 63-1.  
 Pritchard, D. W., and Carpenter, J. H., 1960, Measurements of turbulent diffusion in estuarine and inshore waters: Internat. Assoc. Sci. Hydrology Bull. 20.



# SUBJECT INDEX

[For major headings such as "Economic geology," "Geophysics," "Paleontology," see under State names or refer to table of contents]

## A

	Page
Abrams Mica Schist, California, geochronology.....	D27
Age determinations, granitic and pegmatitic rocks, Connecticut and Massachusetts.....	1
intrusive rocks, Alaska.....	16
lake terrace, Alaska.....	34
schist, California.....	27
silicic rocks, Nevada.....	11
zircon in sandstone, Wyoming.....	22
<i>See also</i> Carbon-14 age, Lead-alpha age, Potassium-argon age, Strontium-rubidium age.	
Alaska, geochronology, Cook Inlet area.....	16
geochronology, southwestern part.....	34
paleontology, east-central part.....	120
Pleistocene geology, Anchorage area.....	167
Alkalic rocks, composition of magnetite in.....	82
Antarctica, stratigraphy and structural geology, Neptune Range.....	112
Alluvium, geochemical prospecting for fluorine.....	59
Aquifers, relation of permeability to particle size.....	203
Arizona, lithium-bearing bentonite, Yavapai County.....	163
Arsenazo III, use in determining thorium content of rocks and minerals.....	192

## B

Basins, continental. <i>See</i> Bighorn Basin, Green River Basin.	
submarine, continental shelf off New England.....	175
Bathocuproine, use in copper determination.....	189
Batholiths, age determination, Alaska.....	16
mineralogy, Colorado.....	55
Beach sand, heavy-mineral and other constituents.....	37
Bentonite, lithium-bearing, Arizona.....	163
Bighorn Basin, Wyoming, paleontology.....	133
Bootlegger Cove Clay, Alaska, stratigraphy.....	167
Boulder Creek Granodiorite, Colorado, mineralogy.....	55
Breathitt Formation, Kentucky, flint clay.....	52

## C

Caballo Mountains, New Mexico, radioactive orthoclase-rich rocks.....	48
California, petrology, El Paso Mountains.....	44
stratigraphy, Salinas Valley.....	106
southern Klamath Mountains.....	27
structural geology, Salinas Valley.....	106
surface water, Palo Alto area.....	196
Cambrian, Alaska, paleontology.....	120
Carbon-14 age, Pleistocene-Recent lake terrace, Alaska.....	34
Carbonatite, composition of magnetite in.....	82
Carboniferous, California, geochronology.....	27
<i>See also</i> Mississippian, Pennsylvanian.	
Clay, lithium-bearing, Arizona.....	163
<i>See also</i> Flint clay.	

	Page
Colorado, crustal studies, north-central part.....	D85
fluorspar, Chaffee County.....	59
mineralogy, north-central part.....	55
Colvos Sand, Washington, quality of water.....	219
Connecticut, geochronology, eastern part.....	1
Conodonts, Oklahoma, Woodford Shale.....	125
Continental shelf, basins, off New England.....	175
Copper, determination in soils, sediments, and rocks.....	189
in beach sand, Massachusetts.....	37
Corundum, in beach sand, Massachusetts.....	37
Cretaceous, Dakotas-Montana-Wyoming, organic content of shale and marlstone.....	73
Wyoming, zircon in sandstone.....	22
Crustal studies, southern Rocky Mountains.....	85

## D

Delaware River area, Pennsylvania-New Jersey, lightweight-aggregate raw material.....	156
Devonian, Oklahoma, Woodford Shale.....	125
Pennsylvania-New Jersey, economic geology.....	156
Diagenesis, zeolitic, of vitric tuffs.....	44
Diatomite, occurrence, Maryland and Virginia.....	151
Digital recorder, multiple hydrologic-parameter modification.....	222

## E

Eocene, Wyoming, stratigraphy.....	133
Esopus Shale, Pennsylvania-New Jersey, lightweight-aggregate raw material.....	156

## F

Fairhaven Diatomaceous Earth Member, Calvert Formation, Maryland and Virginia, diatomite.....	151
Faulting, strike-slip, California.....	106
Flint clay, postulated volcanic origin.....	52
Florida, surface water, north-central part.....	211
Fluorine, as an indicator element in geochemical prospecting.....	59
Fluorometers, effect of sample and instrument-compartment temperatures.....	225
Fluorspar, geochemical prospecting.....	59

## G

Gahnite, in beach sand, Massachusetts.....	37
Geochemical prospecting, fluoride.....	59
Glacial deposits, relation of permeability to particle size in outwash.....	203
seismic studies, Massachusetts.....	101
Glacial transport, Massachusetts, Martha's Vineyard.....	37
Gold, in beach sand, Massachusetts.....	37
under ash flows, Nevada.....	144
Green River Basin, Wyoming, stratigraphy.....	139
Green River Formation, Luman Tongue, Wyoming, stratigraphy.....	139

	Page
Gulf of Maine, basins.....	D175

## H

Heavy minerals, natural concentrations in beach sand.....	37
Herzenbergite, new values for heat and free energy of formation.....	65
Hydrogarnet, in Boulder Creek batholith, Colorado.....	55

## I

Infrared surveys, volcanoes.....	93
Instrumentation, digital recorder, multiple hydrologic-parameter modification.....	222
sample changer for X-ray quantometer.....	178
Iowa, ground-water, east-central part.....	207

## J

Jurassic, Alaska, age of Aleutian Range batholith.....	16
--	----

## K

Kentucky, flint clay, Hazard area.....	52
Klamath Mountains, California, geochronology.....	27
Knik Till, Anchorage area, Alaska, stratigraphy.....	167

## L

Lead-alpha age, Cretaceous sandstone, Wyoming.....	22
early-middle Paleozoic granitic and pegmatitic rocks, Connecticut and Massachusetts.....	1
Mesozoic-Tertiary silicic rocks, Nevada.....	11
Lightweight aggregate, made from slate.....	156
Lithium, in montmorillonitic clay, Arizona.....	163

## M

Magnesite, new values for heat and free energy of formation.....	65
Magnetic spherules, in beach sand, Massachusetts.....	37
Magnetite, composition, relation to type of occurrence.....	82
Marlstone, extractable organic material.....	73
Martinsburg Shale, Pennsylvania-New Jersey, lightweight-aggregate raw material.....	156
Maryland, diatomite, southern part.....	151
Massachusetts, geochronology, eastern part.....	1
heavy minerals in beach sand, Martha's Vineyard.....	37
seismic studies, Cape Cod.....	101
stratigraphy, Cape Cod.....	101
Mesozoic. <i>See</i> Jurassic, Cretaceous.	
Miocene, Maryland and Virginia, diatomite.....	151
Mississippian, Oklahoma, Woodford Shale.....	125
Montana, geochemistry, eastern part.....	73
Mount Rainier, Washington, infrared surveys.....	93

<b>N</b>		Page
Neptune Range, Antarctica, stratigraphy and structural geology.....	D112	
Nevada, geochronology, Elko County.....	11	
gold and silver, Nye and Esmeralda Counties.....	144	
New England. <i>See</i> Connecticut, Massachusetts.		
New Jersey, lightweight-aggregate raw material, western part.....	156	
quality of water, Passaic River.....	214	
New Mexico, petrology, Caballo Mountains...	48	
New Scotland Limestone, Pennsylvania-New Jersey, lightweight-aggregate raw material.....	156	
North Dakota, geochemistry, northeastern part.....	73	
<b>O</b>		
Ohio, ground-water hydraulics, Scioto River valley.....	203	
Oil shale, Wyoming, Green River Basin.....	139	
Oklahoma, paleontology and stratigraphy, Woodford shale.....	125	
<i>Oldhamia</i> , Cambrian, Alaska.....	120	
Ordovician, Pennsylvania-New Jersey, economic geology.....	156	
Outwash deposits, relation of permeability to particle size.....	203	
<b>P</b>		
Paleozoic, Antarctica, stratigraphy and structural geology.....	112	
Connecticut and Massachusetts, geochronology.....	1	
<i>See also</i> Cambrian, Ordovician, Devonian, Carboniferous, Mississippian, Pennsylvanian.		
Pancho Rico Formation, California, structural geology.....	106	
Particle size, effect on permeability, in outwash deposits.....	203	
Passaic River, New Jersey, quality of water..	214	
Pennsylvania, lightweight-aggregate raw material, eastern part.....	156	
Pennsylvanian, Kentucky, flint clay.....	52	
Permeability, relation to particle size, in outwash deposits.....	203	
Pierre Shale, Dakotas-Montana-Wyoming, organic content.....	73	
Pleistocene, Alaska, age of lake terrace.....	34	
Alaska, Anchorage area, subsurface stratigraphy.....	167	
Washington, quality of water.....	219	
Pliocene, California, diagenesis of tuffs.....	44	
Plutons, silicic rock, Nevada.....	11	
<i>See also</i> Batholiths.		
Polonium, selective removal from radium standards.....	184	
<b>Potassium-argon age, Jurassic intrusive rocks,</b>		Page
Alaska.....	D16	
Mesozoic-Tertiary silicic rocks, Nevada..	11	
Paleozoic granitic and pegmatitic rocks, Connecticut and Massachusetts....	1	
Pennsylvanian schist, California.....	27	
<b>Precambrian, Antarctica, stratigraphy and structural geology.....</b>		112
Colorado, mineralogy.....	55	
New Mexico, petrology.....	48	
Prehnite, in Boulder Creek batholith, Colorado.....	55	
Provenance, black sandstone, Wyoming.....	22	
<b>Q</b>		
Quaternary, California, structural geology....	106	
<i>See also</i> Pleistocene, Recent.		
<b>R</b>		
Radioactive rocks, orthoclase-rich, New Mexico.....	48	
Radiocarbon age. <i>See</i> Carbon-14 age.		
Radium standards, selective removal of polonium.....	184	
Recent, Alaska, age of lake terrace.....	34	
Recorder, digital, multiple hydrologic-parameter modification.....	222	
Remote sensing. <i>See</i> Infrared surveys.		
Rhodochrosite, new values for heat and free energy of formation and entropy..	65	
Ricardo Formation, California, petrology....	44	
Rivers, change in quality of water, New Jersey.....	214	
Rocky Mountains, southern, crustal study....	85	
Runoff, estimation, in mountain areas.....	199	
relation to precipitation, in suburban basin.	196	
<b>S</b>		
Salmon Hornblende Schist, California, geochronology.....	27	
Salmon Springs Drift, Washington, quality of water.....	219	
Sample changer, for X-ray quantometer.....	178	
Santa Fe River, Florida, surface-water-ground-water relations.....	211	
Santa Margarita Formation, California, structural geology.....	106	
Seismic studies, crustal structure, Rocky Mountains.....	85	
depth to bedrock, Massachusetts.....	101	
Shale, extractable organic material.....	73	
Siderite, new value for entropy.....	65	
Silver, possible occurrence under ash flows, Nevada.....	144	
Slate, use in making lightweight aggregate....	156	
Soils, determination of copper content.....	189	
geochemical prospecting for fluorine.....	59	
South Dakota, geochemistry, southern part... 73		
Specific conductance, use in computing ground-water runoff.....	207	
Streamflow, effect of ground water on.....	211	
<b>Streamflow records, use in estimating runoff in ungaged basins.....</b>		D199
<b>Strontium-rubidium age, Paleozoic granitic and pegmatitic rocks, Connecticut and Massachusetts.....</b>		1
<b>Submarine basins, off New England.....</b>		175
<b>T</b>		
Tertiary, California, structural geology.....	106	
Nevada, gold and silver.....	144	
<i>See also</i> Eocene, Miocene, Pliocene.		
Thermochemistry, heat and free energy of formation of herzenbergite, troilite, magnesite, and rhodochrosite....	65	
Thirsty Canyon Tuff, Nevada, relation to underlying gold and silver deposits..	144	
Thorium, determination in rocks and minerals, arsenazo-III method.....	192	
in orthoclase-rich rocks.....	48	
Trace fossils, Cambrian, Alaska.....	120	
Trap rock, basaltic, composition of magnetite in.....	82	
Troilite, new values for heat and free energy of formation.....	65	
Tuffs, vitric, zeolitic diagenesis.....	44	
<b>U</b>		
Ungaged drainage basins, estimation of mean runoff.....	199	
Urbanization, effect on quality of river water, New Jersey.....	214	
effect on runoff, California.....	196	
<b>V</b>		
Virginia, diatomite, eastern part.....	151	
Volcanoes, infrared surveys.....	93	
<b>W</b>		
Wasatch Formation, Niland Tongue, Wyoming, stratigraphy.....	139	
Washington, infrared surveys, Mount Rainier. quality of water, Kitsap Peninsula.....	93	
stratigraphy, Kitsap Peninsula.....	219	
Willwood Formation, Wyoming, faunal zones..	133	
Woodford Shale, Oklahoma, paleontology and stratigraphy.....	125	
Wyoming, crustal studies, southeastern part... 85		
faunal zones of the Willwood Formation, Bighorn Basin.....	133	
geochemistry, eastern part.....	73	
geochronology, zircon in sandstone.....	22	
petrology, zircon in sandstone.....	22	
stratigraphy, Green River Basin.....	139	
<b>X</b>		
X-ray quantometer, automatic sample changer for.....	178	
<b>Z</b>		
Zircon, age and distribution, as a guide to provenance.....	22	

## AUTHOR APPENDIX

<b>A</b>					
Adams, J. W.....	D48	Hamlin, H. P.....	D156	Pakiser, L. C.....	D85
Anderson, P. W.....	214	Hass, W. H.....	125	<b>R</b>	
Anderson, R. E.....	144	Healey, D. L.....	144	Reed, B. L.....	16, 34
<b>B</b>					
Brabb, E. E.....	120	Hosterman, J. W.....	151	Riggs, H. C.....	199
Bucknam, R. C.....	1	Houston, R. S.....	22	Robie, R. A.....	65
<b>C</b>					
Cherry, R. N.....	222	Huddle, J. W.....	125	Rohrer, W. L.....	133
Churkin, Michael, Jr.....	120	<b>I</b>			
Clark, W. E.....	211	Irwin, W. P.....	27	Rubin, Meyer.....	34
Coats, R. R.....	11	<b>J</b>			
Conklin, N. M.....	48	Jackson, W. H.....	85	<b>S</b>	
Crandell, D. R.....	93	Jenkins, L. B.....	192	Schmidt, D. L.....	112
Crippen, J. R.....	196	<b>K</b>			
Culbertson, W. C.....	139	Kaye, C. A.....	37	Seiders, V. M.....	52
<b>D</b>					
Denny, M. V.....	156	Knechtel, M. M.....	151	Shapiro, Leonard.....	178
Detterman, R. L.....	16, 34	Kunkle, G. R.....	207	Sheppard, R. A.....	44
Drake, A. A., Jr.....	156	<b>L</b>			
Dunn, Bernard.....	225	Lanphere, M. A.....	16, 27	Snyder, George.....	1
Durham, D. L.....	106	<b>M</b>			
<b>E</b>					
Edwards, K. W.....	184	Marlatt, W. E.....	93	Staatz, M. H.....	48
Ege, J. R.....	112	Marvin, R. F.....	1, 11	Stern, T. W.....	1, 11
Ekren, E. B.....	144	Massoni, Camillo.....	178	<b>T</b>	
<b>F</b>					
Faust, S. D.....	214	May, Irving.....	192	Tourtlot, H. A.....	73
Fidler, R. E.....	203	Moore, D. O.....	199	Trainer, F. W.....	167
Fleischer, Michael.....	82	Moxham, R. M.....	93	Tuttle, C. R.....	101
Frost, I. C.....	73	Mrose, M. E.....	37	<b>U</b>	
<b>G</b>					
Gazin, C. L.....	133	Murphy, J. F.....	22	Uchupi, Elazar.....	175
Gude, A. J., 3d.....	44	<b>N</b>			
<b>H</b>					
Nelson, W. H.....	112	<b>O</b>			
Norris, S. E.....	203	Oldale, R. N.....	101	<b>V</b>	
Norton, J. J.....	163	<b>P</b>			
Nowlan, G. A.....	189	<b>Q</b>			
<b>I</b>					
<b>J</b>					
<b>K</b>					
<b>L</b>					
<b>M</b>					
<b>N</b>					
<b>O</b>					
<b>P</b>					
<b>Q</b>					
<b>R</b>					
<b>S</b>					
<b>T</b>					
<b>U</b>					
<b>V</b>					
<b>W</b>					
<b>X</b>					
<b>Y</b>					
<b>Z</b>					
Zartman, Robert.....	1				